SYNTHESIS AND PROCESSING OF NANOCRYSTALLINE ZIRCONIUM CARBIDE FORMED BY CARBOTHERMAL REDUCTION

A Thesis
Presented to
The Academic Faculty

By

ANUBHAV JAIN

In Partial Fulfillment
Of the Requirements for the Degree
Master of Science in Materials Science and Engineering

Georgia Institute of Technology

August 2004

SYNTHESIS AND PROCESSING OF NANOCRYSTALLINE ZIRCONIUM CARBIDE FORMED BY CARBOTHERMAL REDUCTION

Approved:

Dr. Michael D. Sacks, Advisor

Dr. Joe K. Cochran

Dr. Robert F. Speyer

Date Approved

August 20th, 2004

ACKNOWLEDGEMENTS

I would like to thank Dr. Michael Sacks for his help towards completing this thesis. I would like to thank Dr. Joe Cochran and Dr. Robert Speyer for serving as committee members. I would also like to thank Mr. Greg Staab, Dr. Zhaohui Yang, and Ms. Yanli Xie for their experimental contributions.

This work was supported by the Air Force Office of Scientific Research (Grant No. F49620-01-1-0112).

TABLE OF CONTENTS

LIST OF TABLES

LIST OF FIGURES

CHAPTER I

INTRODUCTION

Zirconium carbide (ZrC) is among the hardest known compounds with micro-hardness value of ~ 2600 kg/mm^2.[1,2,3] This property has been utilized in producing cutting tools and in wear-resistant coatings. ZrC is a candidate material for ultrahigh temperature applications because of its high melting point ~3550ºC, solid-state phase stability, and good thermomechanical and thermochemical properties.[4,5] Besides high hardness and high melting temperature ZrC exhibits high emissivity and high current capacity at elevated temperatures. Thus, zirconium carbide is a promising material for use in thermophotovoltaic radiators and field emitter tips and arrays.[3-8] ZrC also has low neutron cross-section and thus can be used as a nuclear reactor core material.[9]

Generally, powder mixtures of carbon (C) and zirconium metal (Zr), zirconium hydride (ZrH_2) or zirconium oxide ZrO_2) are reacted to synthesize zirconium carbide powders.[1,10-12] Because of relatively coarse-scale mixing of starting materials (starting materials are in micrometer range) high temperatures are required for carbide formation during carbothermal reduction reaction. This also leads to zirconium carbide powders with relatively large particle sizes. Hence, hot pressing is usually necessary to produce dense bulk ZrC parts.

Recent studies have shown that zirconium carbide can be synthesized at lower temperatures by using precursors that have been prepared by solution-based processing methods.[13-21] Solution-based processing also has the advantage of fine-scale (molecular-level) mixing of carbon-rich and zirconia-rich precursors that can be used to

produce thin films, powders and fibers. Fine-scale mixing of the reactants helps in reducing the carbothermal reduction temperature to produce zirconium carbide and it also helps in restricting the crystallite size of zirconium carbide.

The studies reported so far have concentrated on producing ZrC fibers and powders with varying chemical composition and have determined their stoichiometry but the characteristics of powders/fibers produced have not been discussed in detail. The effects of solution-based variables on the final composition of ZrC-based powders/fibers have also not been discussed in detail. No attempt has been made to understand the pressureless sintering behavior of ZrC-based powders produced by solution-based processing.

The objective of this research study was to use solution-based processing and carbothermal reduction heat treatments to produce fine-sized ZrC-based powders that would be suitable for fabrication of bulk samples via pressureless sintering.

The solution-based processing method consisted of using soluble metal-organic (zirconium-bearing) precursors and organic carbon-bearing precursors in order to produce fine-scale zirconia/carbon mixtures. The processing steps used to produce these mixtures included: (i) modifying the starting organozirconium compound, (ii) mixing the soluble precursors, (iii) carrying out controlled hydrolysis/condensation reactions, (iv) removing solvent from the processed solutions, and (v) carrying out pyrolytic decomposition of the dried products that were prepared by the solution-processing steps. The resulting fine-scale zirconia/carbon mixtures were used to produce ZrC by carrying out carbothermal reduction reactions at elevated temperature in an inert atmosphere.

A variety of processing variables were investigated in order to produce ZrC-based powders with fine particle size and controlled chemical and phase composition. The solution-processing variables that were investigated included the: concentrations of starting materials, conditions used to modify the metal-organic precursor (e.g., concentration of the modifying compound used and refluxing temperature), concentrations of water and acid used in hydrolysis/condensation reactions, etc. The heat treatment processing variables included: temperature, time, gas flow rate, etc.

ZrC-based powders were characterized to determine particle/aggregate size, crystallite size, specific surface area, phases present, compositional information (carbon and/or oxygen content), and lattice parameter.

Powder compacts were prepared from ZrC powders using uniaxial dry pressing. The compacts were pressureless sintered and the densification behavior was investigated.

CHAPTER II

LITERATURE REVIEW

2.1 Zirconium Carbide Properties and Applications

Zirconium carbide, chemical formula of ZrC, has a cubic close packed NaCl-type structure (fcc B1).[1,2,3,23] The properties of ZrC depends on a number of factors like chemical composition, defect structure, sample homogeneity, grain size, porosity, etc.[23] Thus, variations in the reported values of various properties have been observed in the literature. Zirconium carbide is readily produced with a wide range of stoichiometries (i.e., from carbon-deficient ZrC_{1-x} to stoichiometric ZrC). Therefore, in reporting the properties and characteristics, the zirconium carbide stoichiometry was specified whenever this information was evaluated. Table 2.1 lists some characteristics and properties of zirconium carbide as reported in the literature.

Many studies have been done to determine the feasibility of using ZrC for various applications. Mackieet al.[11] and Charbonnier et al.[7] studied ZrC as a possible material to be used in field-emission cathodes. Single crystal ZrC wire was grown using floating-zone technique[24] and was subsequently used to deposit coatings of ZrC on molybdenum (Mo) and tungsten (W) substrates by physical vapor deposition. Mo field-emission arrays (FEAs) had random sharp micro- or nano-protrusions on the surface that limited the emission, as the total array emission was limited by the current limit of the sharpest tip. The threshold temperature for surface migration, that eventually destroyed the emitter, was 927^{o}C and 677^{o}C for W and Mo, respectively. The threshold temperature for surface migration in ZrC was not measured, but was expected to exceed 1227^{o}C.

Table 2.1 Characteristics and properties of ZrC as reported in literature.

Structure	Cubic close pack (fcc, B1) [1,2,3,23]
Color	Silver gray [1], Gray [23]
Space group	Fm3m [1]
Lattice parameter (nm)	0.4698 [1], 0.47017[a] [2], 0.4689[3], 0.4698 [23]
Density (g/cm^3)	6.59 [1,2,23], 6.9 [3]
Melting temperature (^oC)	3420 [1,23], 3530 [3]
Hardness	25.5 Gpa Vickers hardness [1], 2600-2900 kg/mm^2 [2], 2600 kg/mm^2 (50g load) [3]
Thermal conductivity	0.049 cal/cm.sec^oC [3], 20.5 W/m^oC [1]
Thermal expansion (x $10^{-6}/^oC$)	6.7 [1,23]
Electrical resistivity (microohm-cm)	45 ± 10 [1], 63-75 [3]
Modulus of elasticity	350-440 GPa [1]
Magnetic susceptibility	-23 x 10^{-6} emu/mol [1]

Reference [1]: The ZrC composition was close to stoichiometric and the reported properties were determined at 20^{o}C. The values for lattice parameter, density, melting temperature, hardness, thermal conductivity, electrical resistivity, thermal expansion and magnetic susceptibility were averages of the values reported by other authors.

Reference [2]: The lattice parameter and density values were reported for zirconium carbide with composition of $ZrC_{0.83}$. The range of hardness value was cited from several references.

Reference [3]: The values reported were from several references. The composition of zirconium carbide was not specified.

Reference [23]: The values reported were for zirconium carbide of composition $ZrC_{0.97}$.

FEAs with ZrC coatings were more resistant to surface migration and had smoother surfaces (no micro- or nano-protrusions). Thus, it could be used for stable high current emissions.

Minato et al.[10] studied the use of a ZrC coating layer as a replacement for silicon carbide (SiC) coatings for nuclear fuel particles. SiC coating layers lost their mechanical integrity at temperatures >1700^{o}C and were chemically attacked by the fission product palladium (Pd). In contrast, ZrC coating layers had much higher temperature stability[25,26] and were more resistant to the chemical attack by the Pd fission product.[27,28]

Reynolds et al.[5] also tested zirconium carbide coatings under high-temperature irradiation for various fuel particle designs in order to replace SiC. ZrC was selected because of its high melting point of ~3540^{o}C (versus 2700^{o}C for SiC), reduced affinity to form eutectic phases with metallic fission products, and its relatively low neutron-absorption cross sectional area. ZrC was found to have excellent resistance to the fission products generated in the carbide fuel system. There was no irradiation-induced coating failure in the material system that was tested which indicated that the ZrC had excellent mechanical integrity.

He et al.[4] studied the corrosion resistance of ZrC films synthesized by ion-beam-assisted deposition on A3 steel substrates. The hardness of ZrC films was 2200 kgf mm^{-2}. A3 steel with ZrC coatings showed greatly enhanced corrosion resistance compared to uncoated A3 steel and compared to A3 steel with ZrN or Teflon^{TM} coatings. The results of electrochemical measurements performed on various coatings and uncoated A3 steel substrate are reproduced in Table 2.2.

Table 2.2 Corrosion resistant properties of A3 steel and coated A3 steel samples.

Material	Film Thickness (nm)	Corrosion current ($\mu A\ cm^{-2}$)	Polarization resistance ($K\Omega\ cm^2$)	Corrosion potential (mV/SCE)
A3 steel	-	-22.5	1.60	-610
Teflon	190	-11.1	4.27	-540
ZrN	190	-10.5	3.14	-465
ZrC	190	- 1.0	33.4	-430

Cockeram et al.[8] evaluated the vacuum plasma spray coatings of ZrC as a means to increase the emissivity of molybdenum, niobium, and Haynes 230 (nickel-base alloy) that were candidate materials for a thermophotovoltaic (TPV) radiator. As-deposited coatings and coatings annealed for 500 h in vacuum at 1100^{o}C had emittance values that were $\geq$0.8. The coatings exhibited acceptable stability during vacuum annealing at 1100^{o}C and excellent resistance to thermal cycling. ZrC coating could potentially be used to improve the surface emittance of molybdenum, niobium, or nickel base metals for at least 500 h at 1100^{o}C.

ZrC has high hardness in the range of 2700 – 2900 kg/mm^2 for $ZrC_{1.0}$[2] and can potentially be used in cutting tool applications.[23] Kyocera Inc. currently manufactures hot-pressed ZrC knives (see Figure 2.1) with sharp edges that are extremely hard (8.2 Mohs scale vs. 5-6 for steel and 10 for diamond), wear resistant, and chemically inert[29].

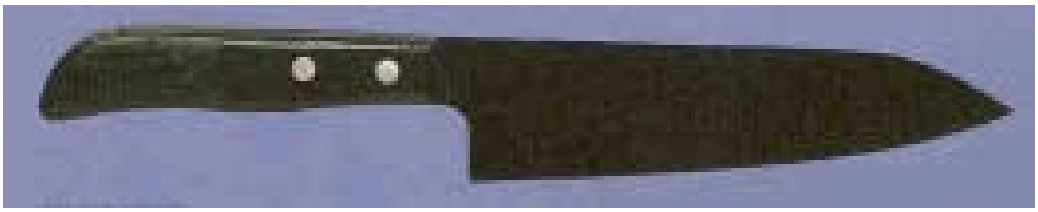

Figure 2.1 Hot pressed ZrC knife manufactured by Kyocera Inc. (This figure is reproduced exactly from reference 29.)

2.2 Synthesis

2.2.1 Carbothermal Reduction

2.2.1.1 Powder Mixtures

The most common industrial process for the synthesis of zirconium carbide is by carbothermal reduction in which the reactants are zirconium dioxide (ZrO_2) and carbon (C) powders.[2,3,23] These powders are mixed and subsequently reduced carbothermally by reactions as shown below:

$$ZrO_{2\,(s)} + 3C_{(s)} = ZrC_{(s)} + 2CO_{(g)} \qquad (2\text{-}1)$$

Ruff et al.[30] produced ZrC powders by carbothermal reduction reaction between ZrO_2 and C at temperatures in the range of 1900 to 2100^{o}C. Friederich et al.[31] produced ZrC by carbothermal reduction of ZrO_2 and C under hydrogen at 1900^{o}C.

Sarkar et al.[13] thoroughly mixed reactor-grade ZrO_2 and spectrographic-grade natural graphite and then heat treated the mixture in a graphite tube resistance furnace

which allowed the CO pressure to be varied. The carbothermal reduction reaction between ZrO_2 and carbon was carried out at temperatures in the range of 1400°C to 1800°C under CO pressures from 100 to 760 torr with a hold at maximum temperature from 4 to 75 h. The carbothermally reduced powders contained zirconium oxycarbide (ZrC_xO_y) phase with varying amounts of unreacted ZrO_2 and C. The lattice parameters calculated for the ZrC_xO_y phase are reproduced in Table 2.3 along with the various heat treatment temperatures and hold times.

Maitre et al.[11] synthesized ZrC powder by solid-state reaction between ZrO_2 (particle size of 3.1 μm; BET surface area of 2 m^2/g) and C (particle size of 0.2-0.3 μm; BET surface area of 35 m^2/g) powders. 77.4 wt% ZrO_2 and 22.6 wt% C, corresponding to a C/Zr molar ratio of 3, were mixed with a mortar and pestle. The mixtures were placed in carbon crucibles that were heat treated in flowing argon in a graphite furnace at temperatures in the range of 1350°C to 1550°C. The samples were held at temperature for times in the range of 0.5 to 24h. The reaction was nearly complete in samples heat treated at 1550°C for 4h or 1530°C for 12 h. The extent of reaction was monitored by weight loss and lattice parameter measurements. The samples heat treated under the conditions indicated had weight losses consistent with the theoretical yield expected from the CTR reaction in equation 2-1 and had lattice parameters similar to those reported for near-stoichiometric ZrC.

Dong et al.[32] synthesized ZrC which was encapsulated with graphite layers. Natural graphite was milled with ZrO_2 media in a high-energy planetary mill for 24 h. The milled powder was heat treated at 1800°C. XRD showed sharp peaks of ZrC. The crystallite size was reported to be “several hundred nanometers.”

Table 2.3 Chemical and lattice parameter data for ZrC_xO_y specimens.

Temp. (^oC)	Time (h)	Initial comp. (wt%)		CO pressure (torr)	Amount of ZrC_xO_y formed (wt%)*	Lattice parameter of ZrC_xO_y (nm)	Chemical formula of ZrC_xO_y**
		ZrO_2	Carbon				
1400	24	79.0	21.0	100	0	-	-
1500	20	79.0	21.0	100	30	0.4676	-
1600	7	79.0	21.0	100	35	0.4674	-
1600	12	79.0	21.0	100	60	0.4673	-
1700	7	77.5	22.5	100	97	0.4683	-
1700	8	79.0	21.0	100	97	0.4675	-
1800	7	79.0	21.0	100	98	0.4676	-
1800	18	79.0	21.0	100	-	0.4678	-
1800	6	80.0	20.0	100	97	0.4674	-
1800	6	80.0	21.0	100	97	0.4675	-
1800	18	80.0	20.0	100	-	0.4674	-
1800	4	84.0	16.0	100	85	0.4673	-
1800	8	77.5	22.5	120	-	0.4688	$ZrC_{0.831}O_{0.039}$
1800	8	77.5	22.5	120	-	0.4688	$ZrC_{0.856}O_{0.041}$
1800	12	79.0	21.0	120	-	0.4678	$ZrC_{0.754}O_{0.108}$
1800	12	79.0	21.0	120	-	0.4679	$ZrC_{0.825}O_{0.098}$
1800	16	80.0	20.0	120	-	0.4674	$ZrC_{0.707}O_{0.134}$
1800	16	80.0	20.0	120	-	0.4674	$ZrC_{0.696}O_{0.144}$
1800	17	81.0	19.0	120	-	0.4674	$ZrC_{0.697}O_{0.149}$
1800	17	82.0	18.0	120	-	0.4673	$ZrC_{0.695}O_{0.148}$
1800	18	79.0	21.0	400	-	0.4681	-
1800	18	80.0	20.0	400	-	0.4677	-
1800	18	79.0	21.0	700	-	0.4684	-
1800	75	79.0	21.0	700	-	0.4686	-
1800	18	80.0	20.0	700	-	0.4681	-
1800	8	79.0	21.0	760	-	0.4683	$ZrC_{0.775}O_{0.085}$
1800	8	79.0	21.0	760	-	0.4681	$ZrC_{0.750}O_{0.099}$

* Determined by quantitative X-ray diffraction techniques.
** Determined by elemental analysis.

The use of powder mixtures for forming ZrC generally has the following advantages: (1) The processing method is relatively simple. (2) The cost of the raw materials may be relatively low. (3) It is relatively easy to control the composition, i.e., the Zr/C ratio in the final product.

However, these methods generally require relatively high reaction temperatures for ZrC formation, i.e., typically in the range of 1800-2200^{o}C with hold times of several hours or more[23]. This is because the reactants are not mixed on a fine scale (e.g., molecular-scale mixing), so diffusion distances are relatively long. The product particle sizes tend to be relatively large due to the large starting particle sizes and the high temperatures that are required for the reaction. In addition, there may be a need for extensive grinding/milling to reduce the particle sizes of the relatively coarse product. The latter step tends to be expensive (energy-intensive) and may lead to contamination problems. Even with milling, the powders still tend to be in a size range that may be unsuitable for preparing bulk objects by pressureless sintering. (Pressureless sintering is the preferred method to produce dense objects because it is considerably less expensive than hot pressing.)

2.2.1.2 Solution-based processing

The most common methods of solution-based synthesis involve preparing solutions with Zr-containing and C-containing precursors. The precursors are often metal(Zr)-organic Zr compounds and organic C-containing compounds which are solubilized in a commom solvent in order to achieve molecular-scale solution mixing. This is often followed by hydrolysis/condensation reactions. The solutions are dried to remove the solvent and the solid product (usually a gel, powder, or fiber) is pyrolyzed to form a fine-scale mixture of C and ZrO_2. These mixtures are subsequently carbothermally reduced to form ZrC.

Sham et al.[18] synthesized ZrC using mixed solutions of zirconium n-propoxide (as a zirconia source) and either ethylene glycol or 1,4 benzenediol (as a carbon source). The reactants were mixed with a wide range of ratios in order to produce products wih varying C/Zr molar ratios. Homogeneous gels were formed when an ethylene glycol or 1,4 benzendiol solution was added to a zirconium n-propoxide solution of 40 wt% in n-propanol. The gel was heated and refluxed at the boiling temperature for 24 h to continue the reaction. After the refluxing step, the solid was separated from the solvent by centrifugation and the product was washed several times with acetone. Fine white powders (henceforth referred to as "ZrOEG" powders) were obtained after drying the solid at 60^{o}C when ethylene glycol was used. Dark brown, very fine powders (henceforth referred to as "ZrOBD" powders) were obtained after drying at 60^{o}C when 1,4 benzendiol was used.

The carbon content of the ZrOEG samples after 60^{o}C drying increased from 19 wt% to 30 wt% as the C/Zr molar ratio in starting material increased from 1 to 3. The ZrOBD samples had carbon contents ≈ 30 wt% for samples with an initial C/Zr molar ratio of 3. Dried powders were X-ray amorphous. Thermogravimetric analysis of a ZrOEG revealed a two-step decomposition process, while a multi-step decomposition process was observed for ZrOBD. The pyrolytic decomposition was mostly complete at ~650^{o}C for a ZrOEG sample and at ~700^{o}C for a ZrOBD sample. XRD showed the presence of tetragonal zirconia (t-ZrO_2) in a ZrOEG sample heat treated at 600^{o}C for 30min. XRD showed t-ZrO_2 in a ZrOBD sample heat treated at 800^{o}C for 90 min.

The powder samples were heat treated under vacuum at 1200^{o}C with varying heating rates (0.5^{o}C, 1^{o}C, and 2^{o}C per minute) and varying hold times (up to 360

minutes). It was assumed that slow heating rate (0.5^{o}C) was best suited for formation of the ZrC phase. XRD showed that ZrOEG samples (with different initial C/Zr molar ratios) had ZrC contents in the range of ~7 – 26 wt% after heat treatments at 1200^{o}C for 0.05 to 6 h. The authors claimed that full conversion to ZrC was observed for a ZrOBD sample (initial C/Zr molar ratio of 4) that was heat treated at 1200^{o}C for 6 h.

Preiss et al.[17] used chelated derivatives of zirconium n-propoxide and various soluble carbon-bearing compounds having two or more reactive OH groups, such as ethylene glycol, saccharose, tartaric acid or dihydroxybenzenes, to form ZrC fibers, films, and powders. These organic groups were believed to act as bridging ligands for transesterification and condensation polymerization reactions.

0.01 mole of zirconium n-propoxide was dissolved in 5 ml of butanol and heated to 50^{o}C for 30 min. 0.022 mole of acetylacetone or ethyl acetoacetate was then drop-wise added at 50^{o}C under constant stirring for 30 min. The sensitivity to hydrolysis of the starting alkoxides was reduced and further operations were done in open atmosphere. Solutions were then heated to 80^{o}C and the carbon-bearing compounds with reactive OH groups were added. (The amounts were adjusted in order to vary the C/Zr molar ratio.) The solutions were heated at temperatures up to 130^{o}C and then they were concentrated to remove solvent.

Thermal gravimetric analysis (TGA) of the precursors could be roughly divided into three stages. There was a large weight loss (~50 wt%) in the range ~100^{o}C – 550^{o}C due to decomposition of the precursors. This was followed by a small weight loss (~2 wt%) in the range of ~550^{o}C – 1100^{o}C. The rest of the weight loss (mostly >1300^{o}C) was due to the carbothermal reduction reaction. XRD showed the presence of cubic ZrO_2 after

heat treatment at 700°C (1 h). Raman spectroscopy for the latter sample showed a broad band centered at ~620 cm^{-1} that was assigned to cubic ZrO_2. The metastable zirconia phase transformed into monoclinic ZrO_2 at temperatures in the range of 1000 - 1100°C. The formation of ZrC phase was observed only at temperatures >1300°C. The carbon contents for samples heated at 1550°C (1 h) were in the range of 13 - 16 wt%. The carbon content for stoichiometric ZrC is 11.6 wt%. Hence, the samples contained unreacted ("free") carbon.

Hasegawa et al.[16] used mixtures of zirconium 2,4,-pentanedionate (ZTP) and phenolic resins to produce ZrC fibers with diameter ≥ 60 μm. ZTP and phenolic resins were dissolved in a mixture of ethanol (10 ml) and 2,4 pentanedione (10 ml), followed by the addition of distilled water and H_2SO_4. The initial C/Zr molar ratio was 4.0, where the carbon content indicated in this ratio was derived only from the phenolic resin. The solutions were stirred at room temperature for 30 min and then "aged" at 65°C. The viscosity of the solutions increased with time and fibers were hand drawn. They were left to dry at room temperature overnight. The spinnability of the solutions varied with amount of water and H_2SO_4 that were added. The optimum concentrations for drawing long fibers were an H_2O/Zr molar ratio of 0.45 and an H_2SO_4/Zr ratio of 0.66. The dried fibers were heat treated at 1100 – 1500°C for 4 h in argon. A sample heat treated at 1500°C showed only ZrC in the XRD pattern.

Kurokawa et al.[14,15] produced large-diameter (~100 μm) ZrC fibers by feeding cellulose acetate-based solutions into zirconium n-butoxide. Dehydrated acetone was used as a solvent. A 10wt% cellulose acetate (acetyl content 38.8 wt%) was slowly injected (using a syringe) into a 10 wt% zirconium n-butoxide solution. The fibers were

allowed to stand for 30 min before ethanol and water were used to wash away the entrapped acetone. Gel fibers were then dried at room temperature and pyrolyzed at various temperatures in argon. A sample pyrolyzed at 700°C (1 h) was X-ray amorphous. The XRD pattern for a sample heat treated at 800°C (1 h) showed tetragonal zirconia (t-ZrO_2). A sample heat treated at 1000°C (1 h) showed both t-ZrO_2 and monoclinic ZrO_2 (m-ZrO_2) in the XRD pattern. The XRD pattern for a sample heat treated at 1600°C (1 h) showed only ZrC. However, this sample still contained free carbon (XRD-amorphous) and residual oxygen, as indicated from the elemental analysis in Table 2.4. (Note that a pure stoichiometric ZrC would have a Zr content of 88.4 wt% and a C content of 11.6 wt%.)

The above studies indicate that "ZrC" can be formed at moderate temperatures by using precursors that have been prepared by solution-based processing methods. Some of the precursors (e.g., carbon-bearing compounds) are relatively inexpensive. However, the metal (Zr)-organic compounds are relatively expensive. The processing methods are relatively simple. Environmental and safety concerns are usually not too significant for the materials used during processing. Although not indicated in the above review, small crystallite sizes can be produced by these methods.

Table 2.4 Elemental analysis of ZrC fibers heat-treated at various temperatures.

Heat Treatment Temperature (°C)	Zr (wt%)	C (wt%)	O_2 (wt%)
800	42.2	36.8	20.2
1200	45.7	33.3	20.6
1600	61.4	30.0	8.0

2.2.2 Direct Reaction of Zr Metal or Zr Hydride (ZrH_2) with Carbon

"The direct reaction of Zr and ZrH_2 with C is often the most common laboratory method for the formation of ZrC."[23] The overall reaction to produce ZrC can be given by the following equations:

$$Zr + C = ZrC \quad (2\text{-}2)$$

$$ZrH_2 + C = ZrC + H_2 \quad (2\text{-}3)$$

Ando and Uyeda[33] synthesized fine ZrC particles using a block of zirconium and a carbon rod which were in contact and which were heated (under vacuum conditions) by passing a large electric current ("a few hundred amperes") through the materials. After the materials reached red-heat, Ar or He was introduced into the chamber and the electric current was increased. (The current was not specified, but it was indicated that the carbon rod became white hot.) The zirconium melted and, after a few minutes, a smoke was observed to develop surrounding the carbon rod. Most of the smoke was amorphous carbon particles, but some ZrC particles were present. It was unclear if the mechanism for forming ZrC involved the direct exothermic reaction between molten Zr metal and sputtered carbon particulates or if the reactants (one or both) were molecular vapor species.

Norton and Lewis[34] formed ZrC by reacting ZrH_2 with C at temperatures as high as 2200^{o}C for 3 h.

Many refractory ceramics (including some carbides, borides, nitrides, etc.) can be synthesized by a method known as self-propagating synthesis, or combustion

synthesis.[35] The method makes use of highly exothermic reactions. The exothermic reactions can be initiated by conventionally heating a powder mixture in a furnace, but the reactions can also be initiated by locally heating one part of the sample (such as by using an electrically heated wire coil). Once the reaction is initiated, a combustion (or synthesis) wave propagates through the material. In other words, the reaction continues spontaneously once initiated and heat is released during the reaction. The reaction between Zr and C is exothermic, but preparation of ZrC using coarse powder mixtures usually requires relatively high temperatures for the reaction to be initiated. However, the reaction can be accelerated by several methods, such as using fine-sized Zr particles, adding "accelerant" additions, and applying mechanical energy (e.g., through milling/grinding processes).

Tsuchida et al.[12] used mechanical activation or “mechanosynthesis” to produce ZrC from Zr-C powder mixtures. Zr metal (<150 μm) and natural graphite (5 μm) were first mixed in various atomic fractions (5-75 at% of C) using an agate mortar and pestle. The mixture was loaded in a planetary ball mill and ground for 30 min with tungsten carbide (WC) media. The ground mixtures were transferred to a graphite crucible and briefly exposed to air at room temperature. This initiated an exothermic oxidation reaction which was believed to be the oxidation of disordered carbon. (The other possibility was oxidation of some of the Zr.) This reaction was exothermic and was accompanied by the emission of red light. The sample was covered as soon as the reaction was initiated to prevent further of oxidation of the sample. The heat generated from this reaction then initiated a second exothermic reaction which was believed to be the self-propagating synthesis of ZrC via the reaction of Zr and C. This reaction was

accompanied by the emission of white light, thus indicating that the local temperature reached during the second reaction was much higher.

The phases present in the final products are listed in Table 2.5. A trace of ZrO_2 was also observed in samples with initial C contents of 25 at% or less. The lattice parameter of the zirconium carbide increased from 0.4637 to 0.4693 nm with increasing C content as shown in the Figure 2.2. The amounts of the different phases formed were not determined.

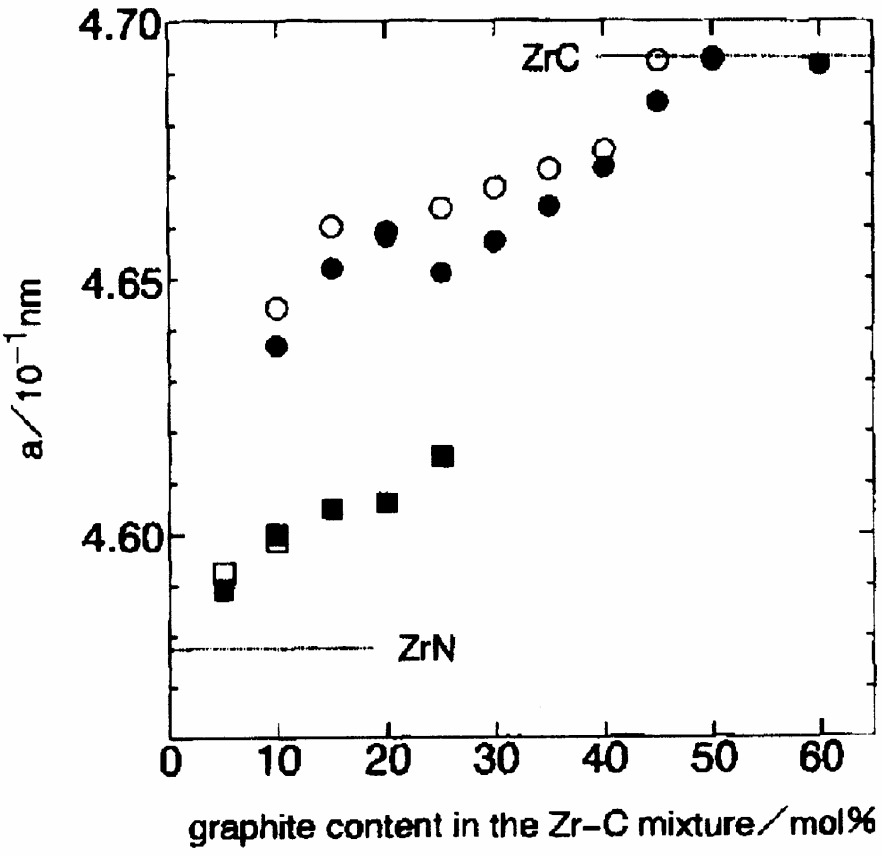

Figure 2.2 Plot of lattice parameter vs. graphite content in Zr-C mixture. (The figure is reproduced exactly from reference 12.)

Table 2.5 Phases of the final product obtained in Zr-C powder mixtures with different C amount.

Graphite content (at.%)	Grinding time (min)	Phase*
75	30	α-Zr
67	30	ZrC
50	25	ZrC
45	25	ZrC
40	25	ZrC
35	25	ZrC, α-Zr
30	25	ZrC, α-Zr
25	25	ZrC, α-Zr, ZrN
20	25	ZrC, α-Zr, ZrN
15	25	ZrC, α-Zr, ZrN
10	25	ZrC, α-Zr, ZrN
5	35	ZrC, α-Zr, ZrN

* Traces of ZrO_2 were present in some samples. The amount of ZrO_2 was not determined.

2.2.3 Methods Involving Alkali Metal or Alkaline Earth Metal Reduction of $ZrCl_4$ or ZrO_2

Li et al.[36] synthesized ZrC by a method that was referred to as a "co-reduction-carburization" route. $ZrCl_4$ (zirconium source) and CCl_4 (carbon source) were heated in autoclave at temperatures in the range of 500-650^{o}C (12 h) along with sodium (Na) metal that acted as a reducing agent. The pressure in the autoclave was estimated to be 4 MPa. The overall reaction to produce ZrC is given by the following equation:

$$ZrCl_4 + CCl_4 + 8Na = ZrC + 8NaCl \quad (2\text{-}4)$$

However, the sodium metal reduces the $ZrCl_4$ to Zr and the CCl_4 to C, so the reaction to produce ZrC is presumably between Zr and C. The product was washed with

0.1 M hydrochloric acid and water in order to remove NaCl and other impurities. XRD of the washed product showed ZrC phase with very weak peaks of ZrO_2 phase. The measured lattice parameter value was 0.4686 nm and the average crystallite size was 18 nm. High-resolution electron microscopy (HREM) images showed that ZrC particles were covered with graphite. The presence of graphite was also confirmed by Raman spectroscopy.

Shen et al.[37] synthesized hollow nanospheres of ZrC by a very similar method. $ZrCl_4$, C_6Cl_6, and Na were mixed together and heated in an autoclave at 600^oC (20 h). The solid product was washed several times with ethanol and water to remove sodium chloride (NaCl) and other impurities. XRD of the washed and dried sample showed ZrC with a measured lattice parameter of 0.4861 nm. The crystallite size was 6 nm.

Chang et al.[38] reduced $ZrCl_4$ by adding it to an n-butyllithium (C_4H_9Li)/hexane solution at 273K. The product consisted of colloidal particles that were air-sensitive, so drying and heat treatment of the colloids was done under vacuum conditions. Samples were given heat treatments at 973-1273K for 2-12 h in order to crystallize the product to ZrC and to remove (by sublimation) the LiCl by-product formed when the $ZrCl_4$ was reduced by the n-butyllithium. XRD results showed the formation of ZrC with lattice parameter of 0.4688 nm and crystallite of 7 nm. (The specific heat treatment conditions associated with these values were not given.)

Kobayashi et al.[39] synthesized ZrC by the following overall reaction:

$$ZrO_{2(s)} + 2Mg_{(s)} + CH_{4(g)} = ZrC_{(s)} + 2MgO_{(s)} + 2H_{2(g)} \qquad (2\text{-}5)$$

ZrO_2 and Mg powder mixtures (Mg/ZrO_2 molar ratios 2-5) were placed in a graphite boat that was placed in quartz reaction tube. Samples were heated at 750°C (0.5 h) under a flowing CH_4 (100 cm^3/min) atmosphere. The authors proposed that Mg acted as the carbon source through the Mg-Mg_2C_3-Mg cyclic reactions shown in equations 2-6 and 2-7. Mg also reduced ZrO_2 to form α-Zr, as shown in equation 2-8. Subsequently, α-Zr reacted with C to form ZrC as shown in equation 2.9.

$$3CH_4 + 2Mg = Mg_2C_3 + 6H_2 \quad (2\text{-}6)$$

$$Mg_2C_3 = 2Mg + 3C \quad (2\text{-}7)$$

$$ZrO_2 + 2Mg = \alpha\text{-}Zr + 2MgO \quad (2\text{-}8)$$

$$\alpha\text{-}Zr + C = ZrC \quad (2\text{-}9)$$

The MgO in the product was removed by repeated washing with 1 M hydrochloric acid (HCl) solution. SEM indicated that the ZrC primary particle sizes were on the order of 50 nm. BET specific surface areas were in the range of 44 – 63 m^2/g. The measured lattice parameter was 0.4699 nm.

2.2.4 Vapor Phase Methods

Motojima et al.[40] synthesized micro-coiled ZrC fibers by a gas-solid reaction with micro-coiled carbon fibers. Zr sponge was chlorinated at 700°C to form $ZrCl_4$. The $ZrCl_4$ was carried by argon to a reaction chamber. The micro-coiled carbon coils were heated at temperatures in the range 1100-1250°C (for 0.25 – 2 h) in an atmosphere containing $ZrCl_4$, H_2, and Ar. No ZrC peaks were observed in the XRD pattern of a

sample heat treated at 1100°C (1 h). XRD of samples heat treated at 1200-1250°C (1 h) showed the presence of ZrC and $ZrCl_2$ phases. Very weak peaks of $ZrCl_2$ were observed in the XRD pattern for a sample heat treated at 1250°C for 2 h.

Baklanova et al.[41] synthesized ZrC coatings on silicon carbide fibers by gas-phase transport reactions. Zirconium metal, iodine crystals, and carbon tetrafluoride were heated to temperatures in the range of 927-1027°C for 1 - 40 h. XRD of the coatings showed ZrC as the only crystalline phase present. No further characterizations of the coatings were reported.

Chemical vapor deposition (CVD) of ZrC can be carried out by the reaction between zirconium halide (as the Zr source) and a hydrocarbon (as the C source) in a H_2-containing atmosphere at temperatures ≥1000°C. The zirconium halide vapor was obtained either by a reaction between a halide vapor and zirconium metal[58] or by sublimation of $ZrCl_4$.

Reynolds[42] coated nuclear fuel particles with CVD ZrC coatings. Argon (Ar) gas was initially bubbled through reagent grade dichloromethane (CH_2Cl_2) that was maintained at 0°C. The Ar- CH_2Cl_2 gas mixture was then passed over heated (600°C) zirconium (Zr) "sponge" to produce $ZrCl_4$ vapors. Methane (CH_4) and hydrogen (H_2) gases, preheated to 600°C, were then mixed with the $ZrCl_4$ vapors inside a graphite tube and heated to 1100°C (3 h) to produce ZrC coatings. Chemical analysis of the coating gave a C/Zr ratio of 1.01 which indicated that some free carbon was present in the coatings.

Wagner et al.[43] and Hollabaugh et al.[44] studied the effect of varying the composition of gas mixtures on the properties of ZrC coatings. Chemical vapor

deposition of ZrC coatings was achieved by reacting gaseous mixtures of CH_4, H_2, $ZrCl_4$, and Ar (used as carrier gas). The overall reaction is given by:

$$xCH_4 + ZrCl_4 + 2(1-x)H_2 = ZrC_x + 4HCl \qquad (2\text{-}10)$$

where $x \leq 1$. Increasing the amount of CH_4 in the coating gas mixture (i.e., increasing C/Zr molar ratio) resulted in ZrC coatings with increased amounts of carbon as shown in Table 2.6. The chemical analysis of the coating showed the presence of free carbon when the C/Zr molar ratio in the coating gas mixture was > 0.21.

Hanko et al.[45] prepared CVD ZrC coatings using an organometallic precursor. (Cyclopentadienyl)zirconium was used to deposit ZrC coatings at temperatures in the range of 300-600^{o}C. The chemical composition of the films synthesized at 600^{o}C, as determined by x-ray photoemission spectroscopy (XPS) and electron probe microanalysis methods (EPMA), showed presence of zirconium carbide.

Healy et al.[46] used the complex organometallic precursor, $Zr[CH_2C(CH_3)_3]_4$, to deposit ZrC films on silicon (Si) substrates. The substrate was maintained at 560-570^{o}C in a reaction chamber with a pressure of ~10^{-6} torr. XRD showed the presence of ZrC phase in the coated films. The ZrC coatings contained excess of carbon and hydrogen (15 wt%) as determined by x-ray photoemission spectroscopy (XPS) for carbon and elastic recoil detection (ERD) for hydrogen.

Table 2.6 Effect of coating gas composition on chemical vapor deposited ZrC coatings.

Mol fraction				Coating gas C/Zr	Carbon analysis	
Ar	H_2	CH_4	$ZrCl_4$		$C_{combined*}$	$C_{total**}$
0.82	0.14	0.007	0.034	0.21	0.87	0.87
0.81	0.14	0.016	0.034	0.47	0.84	0.89
0.80	0.14	0.034	0.033	1.00	0.89	1.18
0.78	0.13	0.049	0.032	1.50	0.63	1.88
0.77	0.13	0.060	0.032	1.90	0.45	2.40

* $C_{combined}$ is the amount of C in zirconium carbide lattice.
** C_{total} is the sum of $C_{combined}$ and "free" C in the sample.

2.2.5 Solid State Metathesis Method

Nartowski et al.[47] produced ZrC by solid-state metathesis reactions between zirconium chloride ($ZrCl_4$) and either CaC_2 or Al_4C_3. $ZrCl_4$ and CaC_2 or Al_4C_3 were ground together and heated in an evacuated ampoule to initiate the reaction. The temperatures were increased to 500°C in case of CaC_2 and to 1000°C for Al_4C_3. The reactions that were used to synthesize ZrC are shown below:

$$ZrCl_4 + 2CaC_2 = ZrC + 2CaCl_2 + 3C \quad (2\text{-}11)$$

$$3ZrCl_4 + Al_4C_3 = 3ZrC + 4AlCl_3 \quad (2\text{-}12)$$

The $AlCl_3$ by-product was removed by sublimation. The $CaCl_2$ by-product was removed by dissolution in methanol and water. (The excess carbon apparently remained with the ZrC product.) XRD of the final product showed a single crystalline phase of ZrC. The lattice parameter value was reported as 0.4690 nm.

2.3 Lattice Parameter, ZrC Stoichiometry and Oxygen Solubility

A wide range of lattice parameters have been reported for "ZrC." There are two primary reasons for this observation: (1) The cubic zirconium carbide phase can be produced with a wide range of C/Zr molar ratios, ranging from stoichiometric ZrC to highly carbon-deficient ZrC_{1-x}.[48,49,50] (2) Many studies have shown that there is considerable solid solubility of ZrO_2 in the ZrC lattice.[11,13,48,51] The amount of oxygen (y) dissolved and the amount of combined carbon (x) in the ZrC lattice affects the lattice parameter of the resulting zirconium oxycarbide (ZrC_xO_y).

Sarkar et al.[13] studied the effect of oxygen content on the lattice parameters of zirconium oxycarbide. Figure 2.3 shows that the lattice parameter of ZrC_xO_y decreased with increased amount of oxygen dissolved in ZrC lattice.[13]. (It should be noted that the lattice parameters were "normalized" to a fixed C/Zr molar ratio of 0.75. The actual C/Zr molar ratios of the samples varied in the range of ~0.695 to ~0.856.) Table 2.3 lists the composition of the various ZrC_xO_y samples along with their lattice parameters.

Alyamovskii et al.[48] also studied the variation of lattice parameter of ZrC_xO_y with varying amounts of oxygen (y) and carbon (x). Table 2.7 lists the composition of various ZrC_xO_y samples and their measured lattice parameters. The data in Table 2.7 for "x + y" = 0.99-1.00 and "x + y" = 0.92-0.93 were used to understand the effects of the amounts of oxygen and carbon on the lattice parameter. Line 3 ("x + y" = 0.92-0.93) and line 4 ("x + y" = 0.99-1.00) in Figure 2.4 shows plots of the measured lattice parameter vs. the carbon content x. The lattice parameter decreases with decreasing amount of carbon in the ZrC_xO_y. Line 1 ("x + y" = 0.99-1.00) and line 2 ("x + y" = 0.92-0.93) in

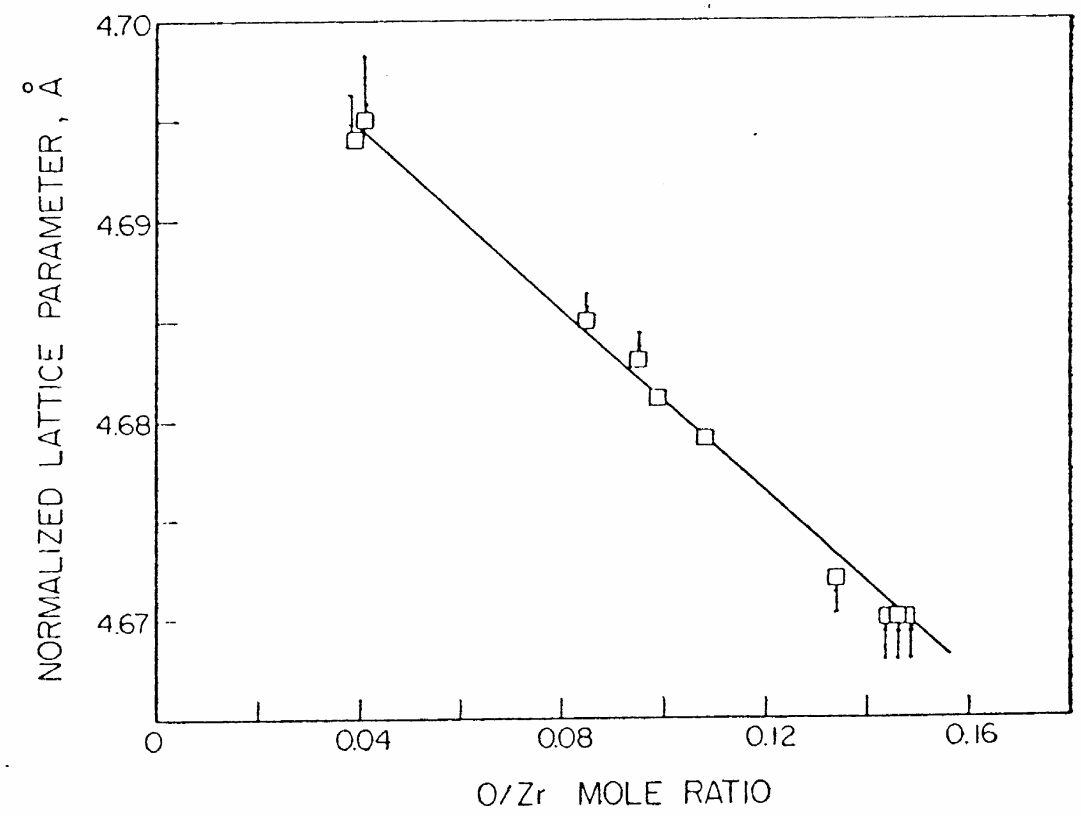

Figure 2.3 Plot of lattice parameter vs. oxygen content in ZrC (This figure is reproduced exactly from reference 13).

Figure 2.4 shows plots of the measured lattice parameter vs. the oxygen content y. The lattice parameter decreases with increasing amount of oxygen in ZrC_xO_y.

Figure 2.5 shows that the lattice parameter decreases with decreasing carbon content for ZrC_{1-x} samples. The data for three independent studies are shown in the figure.[48,49,50] Figure 2.6 combines the lattice parameter data from four different studies of ZrC_xO_y samples.[13,48,49,50] As previously indicated, the lattice parameter decreases with increasing oxygen content for ZrC_xO_y samples. Figure 2.7 shows a compilation of lattice parameter data (similar to the ones shown in Figs. 2.5 and 2.6).[11]

Table 2.7. Chemical composition, lattice parameter and densities for ZrC_xO_y of various compositions. (This table is reproduced from reference 48).

Number	Composition of ZrC_xO_y		x + y	*a* (nm)	Density (ρ) g/cm^3
	x	y			
1	0.83	0.18	1.01	0.4680	6.62
2	0.79	0.21	1.00	0.4676	6.60
3	0.74	0.26	1.00	0.4671	6.55
4	0.84	0.16	1.00	0.4681	6.62
5	0.85	0.15	1.00	0.4692	6.62
6	0.75	0.24	0.99	0.4672	6.56
7	0.75	0.24	0.99	0.4673	6.54
8	0.69	0.30	0.99	0.4667	6.52
9	0.64	0.30	0.94	0.4660	6.46
10	0.69	0.25	0.94	0.4666	6.52
11	0.70	0.24	0.94	0.4667	6.54
12	0.68	0.25	0.93	0.4664	6.52
13	0.59	0.34	0.93	0.4655	6.40
14	0.60	0.33	0.93	0.4655	6.40
15	0.65	0.28	0.93	0.4661	6.50
16	0.73	0.19	0.92	0.4667	6.56
17	0.79	0.13	0.92	0.4672	6.53
18	0.79	0.19	0.98	0.4674	6.58
19	0.62	0.36	0.98	0.4661	6.42
20	0.72	0.24	0.96	0.4669	6.56
21	0.63	0.33	0.96	0.4661	6.45
22	0.64	0.31	0.95	0.4661	6.46
23	0.50	0.21	0.71	0.4643	6.18

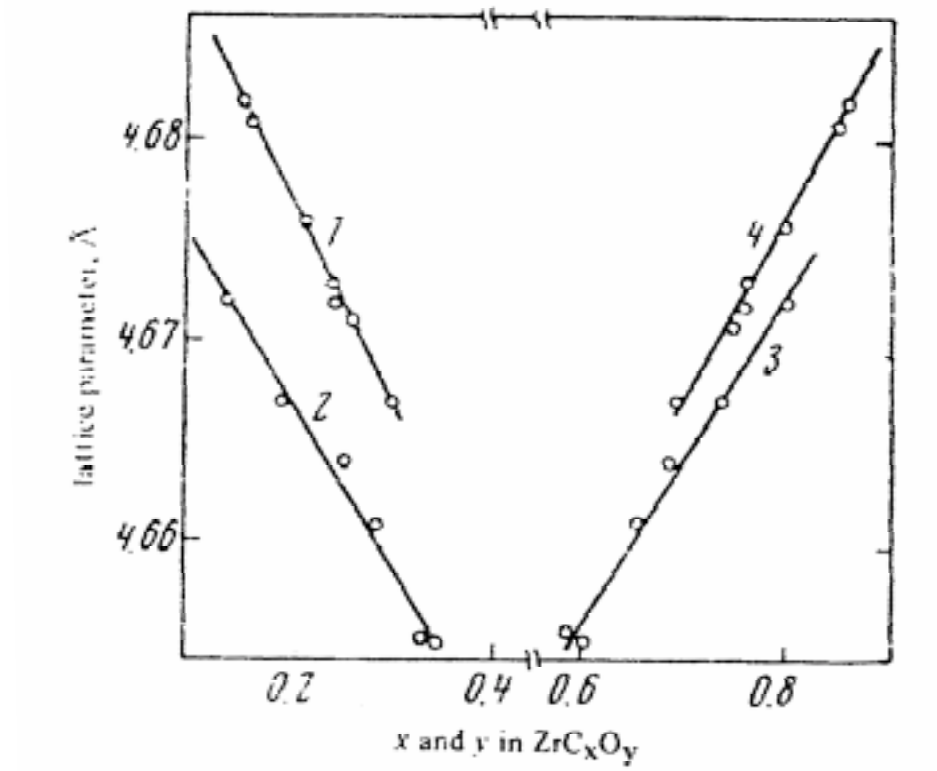

Figure 2.4 Plot of lattice parameter vs. oxygen (y) and carbon (x) contents in ZrC. Variation of the lattice parameter with oxygen content is shown by lines 1 and 2. Variation of the lattice parameter with carbon content is shown by lines 3 and 4. (This figure is reproduced exactly from reference 48).

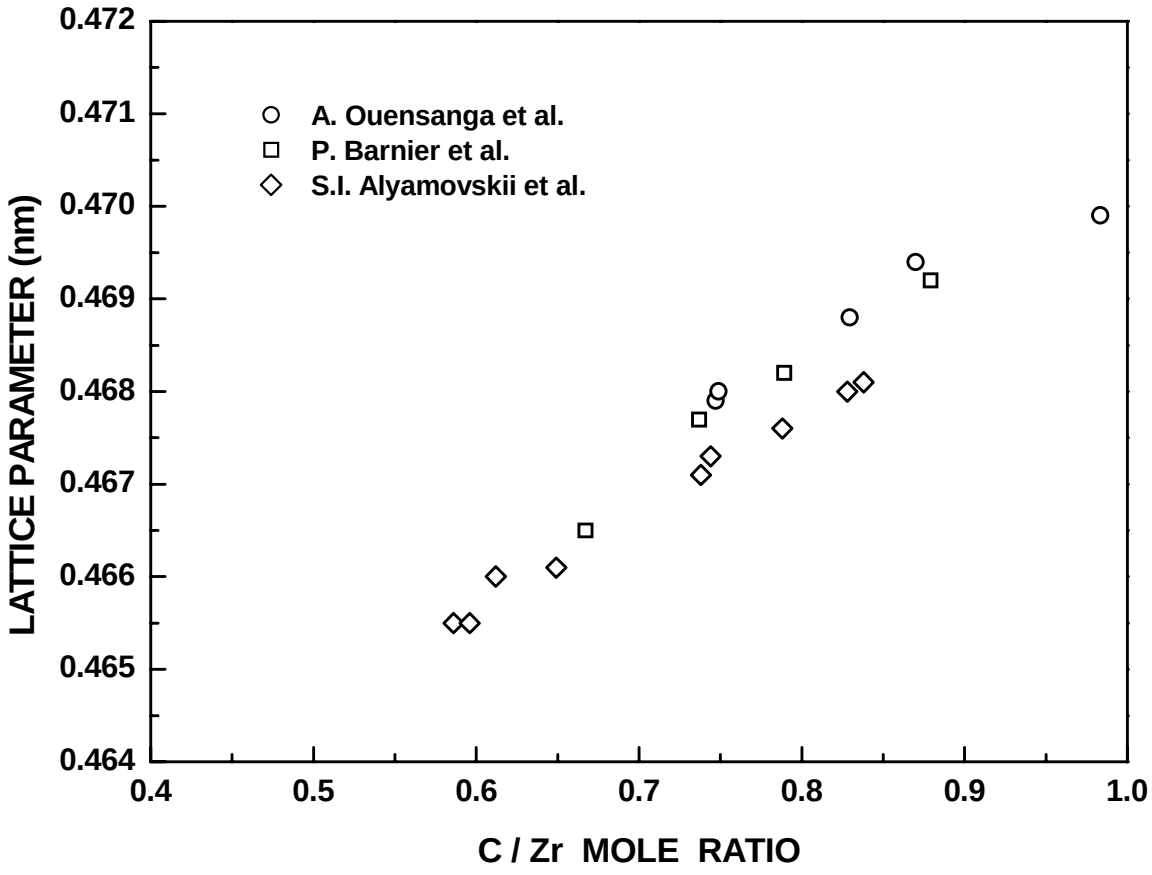

Figure 2.5 Plot of lattice parameter vs. carbon/zirconium molar ratio from previous studies.

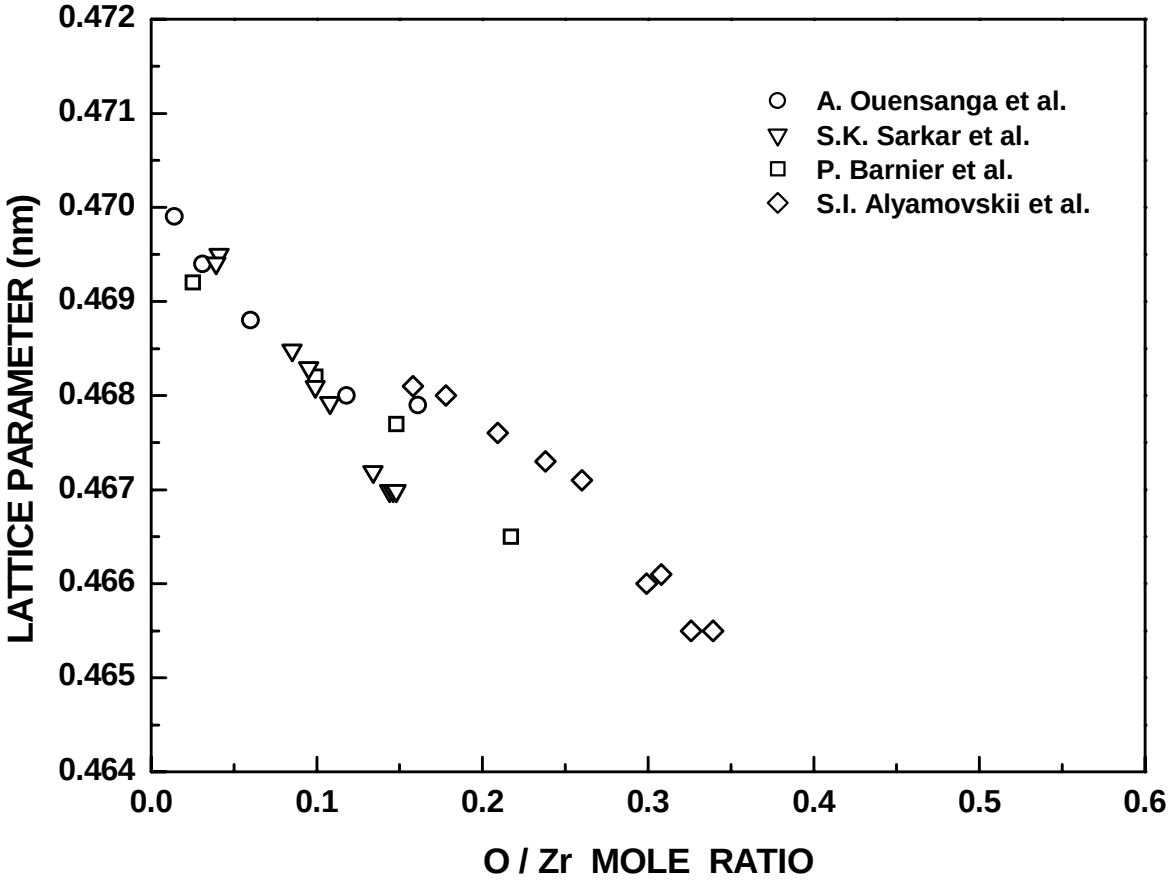

Figure 2.6 Plot of lattice parameter vs. oxygen/zirconium molar ratio from previous studies.

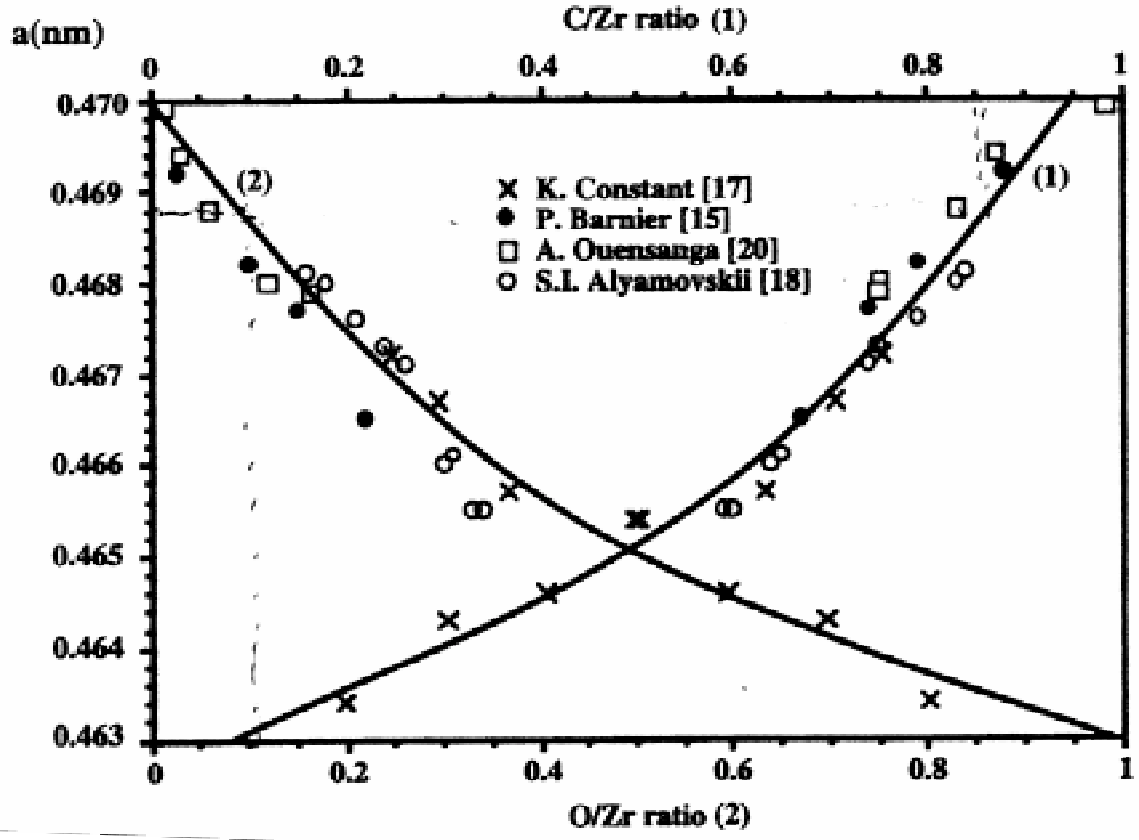

Figure 2.7 Plot of lattice parameter vs. oxygen and carbon contents in ZrC. (This figure is reproduced exactly from reference 11).

2.4 Mechanism of carbothermal reduction reaction

Maitre et al.[11] studied the reaction mechanism of carbothermal reduction of ZrO_2 and carbon. ZrO_2 and carbon (C/Zr molar ratio = 3) were carbothermally reduced at various temperatures in the range of 1350 to 1550^{o}C with hold times of 0.5 to 24 h under flowing argon. The percentage relative weight loss defined as $(\Delta m/m_o) \times 100$, where m_o was the initial weight and Δm was the change in weight for the reaction at a given temperature and time. The maximum weight loss observed in the study did not exceed the

theoretical maximum of 35.17 wt% that would be expected for the ideal reaction (equation 2-1). This result suggested that no Zr-containing volatile formed during CTR and that only the removal of CO was responsible for the observed weight losses.

Scanning electron microscopy (SEM) micrographs of the powders before and after CTR showed that the carbon particles disappeared as the reaction proceeded and that the reaction product retained the morphology of the original zirconia particles. The lattice parameters of the zirconium carbide product were essentially constant (see Figure 2.7) with values of ~0.4688 nm, for relative weight losses ($\Delta m/m_o$) up to ~ 32%. These lattice parameter values indicated that the reaction product was zirconium oxycarbide. The composition of oxycarbide was $ZrC_{0.84}O_{0.06}$ as determined by comparing the 0.4688 nm lattice parameter value with values reported by previous investigators.[48,49,50,51] Hence, the reaction thus far could be represented by the following equation:

$$ZrO_2 + 2.78C = ZrC_{0.84}O_{0.06} + 1.94CO \qquad (2\text{-}13)$$

Figure 2.8 shows that the lattice parameter increased sharply during the late stages of the reaction, i.e., $\Delta m/m_o > 32\%$. This increase in lattice parameter value was assumed to be related to the transformation of the oxycarbide into a near stoichiometric ZrC, as represented by the following equation:

$$ZrC_{0.84}O_{0.06} + 0.22C = ZrC + 0.06CO \qquad (2\text{-}14)$$

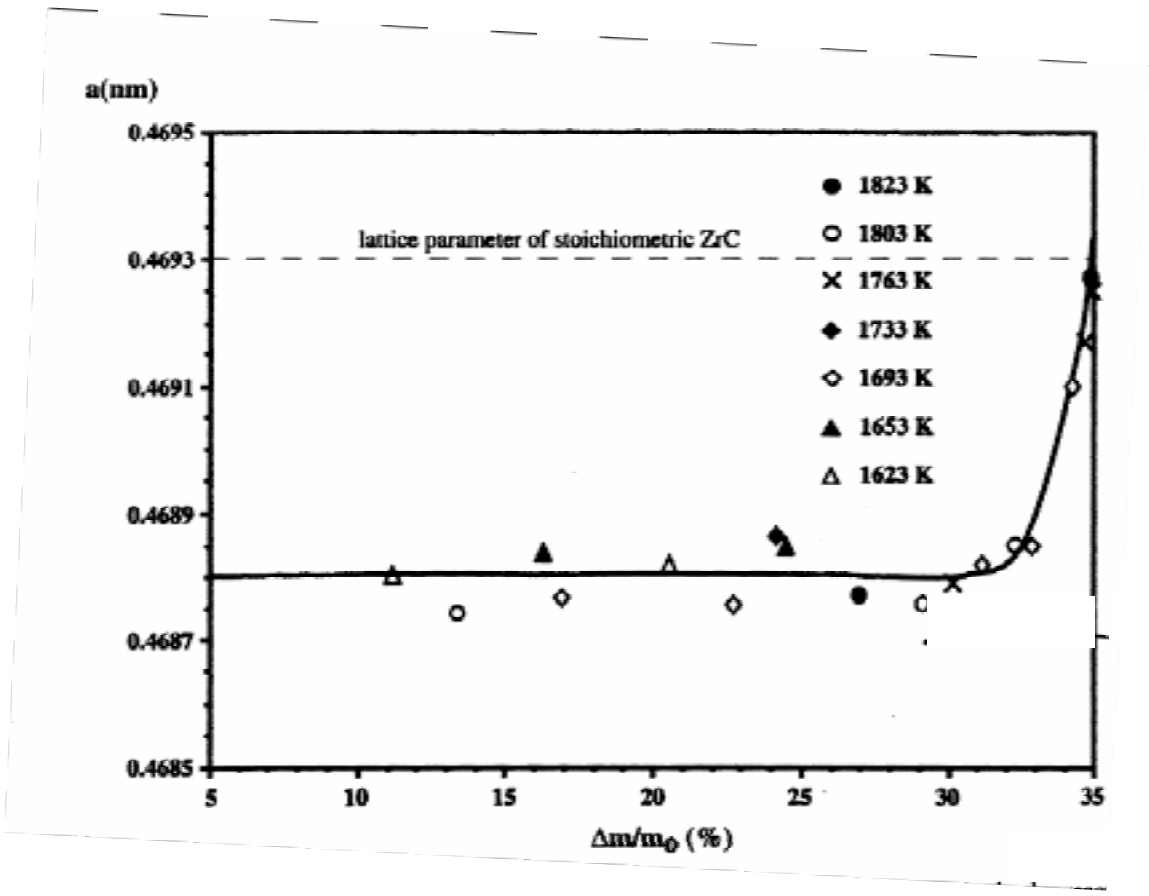

Figure 2.8 Plot of lattice parameter vs. relative weight loss in the reaction. (This figure is reproduced exactly from reference 11).

2.5 Sintering Study

Nezhevenko et al.[52] studied the sintering behavior of ZrC (near-stoichiometric composition) and ZrC-C composites. The specific surface area of the ZrC powder was 2.7 m^2/g, the calculated particle diameter was 5 μm, and the lattice parameter was 0.4697 nm. Cylindrical powder compacts (10 mm diameter, 20 mm height) were prepared with relative densities in the range of 47.5 – 57%. A ZrC powder compact with 56% green density was sintered at 10°C/min in argon to 2500°C. The relative density after sintering was 97%. Densification was significantly inhibited in samples containing carbon

(graphite or diamond) particles. The sintered densities tended to decrease as the (i) volume fraction of the carbon particle increased (for a fixed carbon particle size) and (ii) the size of the carbon particles decreased (for a fixed volume fraction of carbon particles).

Bulychev et al.[53] studied the sintering behavior of a ZrC powder produced by carbothermal reduction reaction carried out at 2100^{o}C. The lattice parameter of the ZrC powder was 0.4700 nm and its elemental analysis is shown in Table 2.8. The ZrC powder was ground using a mill lined with ZrC plates in order to reduce the contamination. The BET specific surface area of the milled powder was 4.35 m^2/g. Specimens were produced by extrusion and sintered for 0, 15, 30, 60, and 120 min in a furnace with graphite heating elements under various atmospheres (vacuum, H_2, and Ar) using temperatures in the range of 1400 - 2800^{o}C. Samples sintered at 2600^{o}C reached relative densities as high as 98%. Samples sintered at 2000^{o}C for 100 min only reached relative densities of ~85%, ~92%, and ~94% in sintering atmospheres of vacuum, argon, and hydrogen, respectively.

Table 2.8 Elemental analysis of ZrC powder produced by carbothermal reduction reaction.

Element	Wt%
Zr	87.80
C (total)	11.40
C (free)	0.15
N	0.02
O	0.62

Min-haga et al.[54] studied the sintering behavior of ZrC-ZrO_2 powder compacts. Two types of ZrO_2 powders were used. "Type A" powder was a pre-reacted yttria-stabilized (3 mol% Y_2O_3) ZrO_2 with specific surface area of 17 m^2/g and particle size of 24 nm. "Type B" powder was a physical mixture of ZrO_2 and Y_2O_3 with specific surface area of 13.6 m^2/g and particle size of 75 nm. The as-received zirconium carbide had average particle size of 3.5 μm and a near-stoichiometric composition ($ZrC_{0.97}$). Powder mixtures were prepared using up to 40 wt% of the yttria-containing ZrO_2. Two types of powder mixtures were used to prepare samples. In one case (Type B samples), Type B ZrO_2 and as-received ZrC were initially balled milled for 16 h to reduce the particle size to <2 μm. Green bodies were prepared by slip casting followed by isostatic pressing. A relative packing density of 58% was obtained. In the other case (Type A samples), the as-received ZrC was first fractionated by sedimentation and the portion of powder <1 μm was used. The submicrometer ZrC and Type A ZrO_2 were mixed and green bodies were prepared by slip casting. The green density was 45%. One factor responsible for the higher green density of the Type B samples was a broader size distribution for particle mixture. Another possible factor may have been the application of isostatic pressing after slip casting. Also, there may have been better particulate dispersion of the suspensions during slip casting. In general, it usually becomes more difficult to achieve high packing densities in green bodies as the particle size is reduced (especially in the submicrometer range) because of more difficulties with agglomeration and/or flocculation of the particles. The Type A samples were prepared with smaller particles for both the ZrC and the ZrO_2.

Figure 2.9 shows a plot of bulk density vs. sintering temperature (1 h hold time) for 80 wt% ZrC - 20 wt% ZrO_2 samples which were heated at 30°C/min in an argon atmosphere using a graphite tube furnace. The following observations are noted: (i) A small amount of densification occurred at 1200°C. This presumably reflects some sintering that was primarily associated with the fine zirconia particles. (ii) The Type A samples sintered to a maximum relative density (~95%) at 2000°C, while the Type B samples reached a similar relative density at 2100°C. Although the green relative density was lower, it is presumed that the Type A samples had more rapid densification because of the finer particle size.

Figure 2.10 shows a plot of lattice parameter vs. sintering temperature for Type A samples with 30 wt% ZrO_2. (Some of the samples were sintered in an atmosphere with CO.) The figure shows that the lattice parameter decreased at temperatures above ~1450°C. This observation is consistent with the occurrence of dissolution of some ZrO_2 in the ZrC lattice, i.e., the formation of ZrC_xO_y. The lowest value of the lattice parameter (~0.4655 nm) corresponded to a composition of $ZrC_{0.75}O_{0.21}$ (as determined by using Sarkar's data in reference 13). This composition also indicates that the samples must have been losing "oxide" during the heat treatments. Indeed, a significant weight loss was observed in samples sintered at and above 1600°C. Figure 2.11 shows plots of weight loss vs. sintering temperature and bulk density vs. sintering temperature (1 h hold time) for Type A samples with 30 wt% ZrO_2. The authors attributed the weight loss to the reaction of ZrO_2 with ZrC, the evaporation of ZrO_2, or both. At least for the lower temperatures, however, evaporation of ZrO_2 seems unlikely. Instead, carbothermal reduction reactions would be expected.

Figure 2.12 shows a comparison of the bulk densities obtained for both ZrC and 70 wt% ZrC - 30 wt% ZrO_2 samples sintered at 2000°C and 2200°C in different atmospheres. (The method for preparing the ZrC green compacts was not described by the authors.) The ZrC samples had lower sintered densities in each case. The maximum relative density achieved for the ZrC samples was only ~87%. Figure 2.13 shows the lattice parameters for the same samples shown in Figure 2.12. As expected, lower lattice parameters were observed for the ZrC/ZrO_2 samples, presumably due to dissolution of ZrO_2 in the ZrC lattice. The authors attributed the higher densities in the ZrC/ZrO_2 samples to enhanced diffusion in the zirconium oxycarbide samples. Although this is a plausible explanation, the authors did not isolate and study all the factors that may have been responsible for the higher densities. (The differences in particle size and green density were not reported for these samples. In addition, it was not possible to separate the effect on densification of the ZrO_2 phase alone vs. the effect of the ZrC_xO_y phase.)

Lanin et al.[55] studied the ZrC sintering process under non-isothermal conditions. The ZrC powder was obtained by carbothermal reduction of zirconium dioxide and carbon at 2027°C, followed by ball milling to reduce the particle size. The milled powder had BET specific surface area of 4.9 m^2/g and a "calculated diameter" of 2.6 μm. Cylindrical compacts (2.4 mm in diameter and 60-80 mm in length) were prepared by extrusion and the binder was removed at 307°C in vacuum. The samples were then initially sintered at 1027, 1527, 1827, and 2527°C (1 h hold) by heating and cooling at 0.2°C/sec. The densities achieved after initial sintering are listed in Table 2.9. The chemical formula of the zirconium carbide was $ZrC_{0.95}$, as determined from

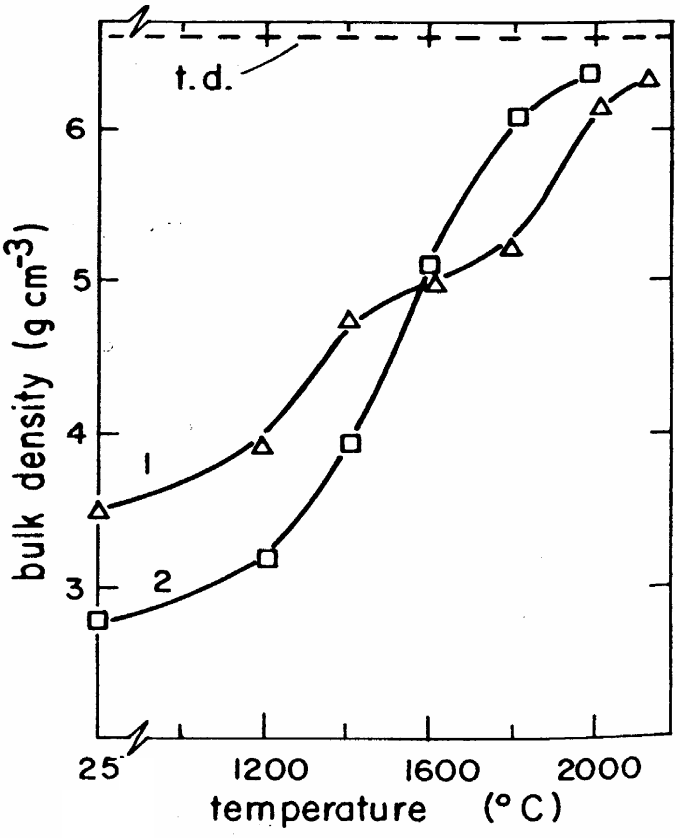

Figure 2.9 Plot of bulk density vs. sintering temperature for ZrC samples (1) with Type B ZrO_2 and (2) with Type A ZrO_2. (This figure is reproduced exactly from reference 54).

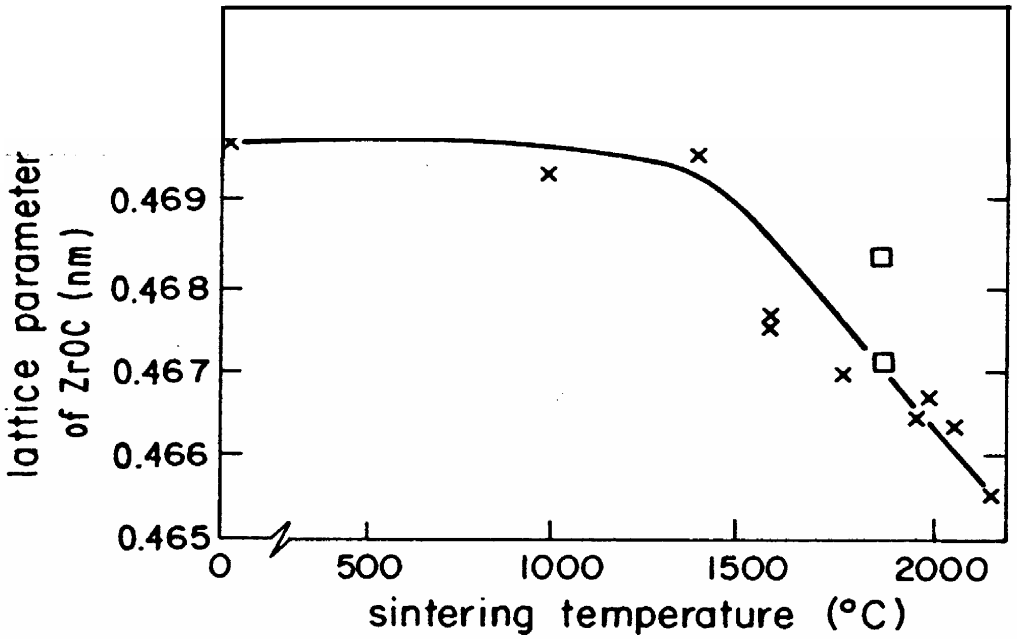

Figure 2.10 Plot of lattice parameter vs. sintering temperature of ZrC/ZrO_2 samples. (x) sintering in Ar atmosphere, (□) sintering in CO atmosphere. (This figure is reproduced exactly from reference 54).

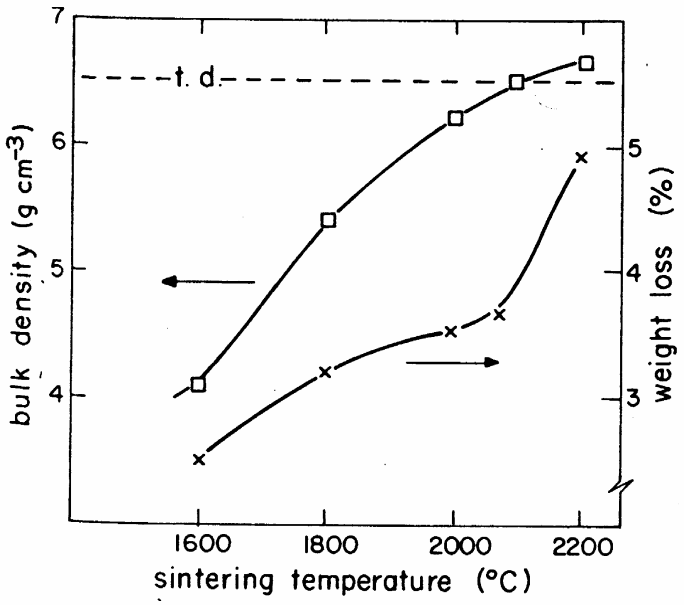

Figure 2.11 Plot of weight loss and bulk density vs. sintering temperature for 30 wt% Type A ZrO_2 samples. (This figure is reproduced exactly from reference 54).

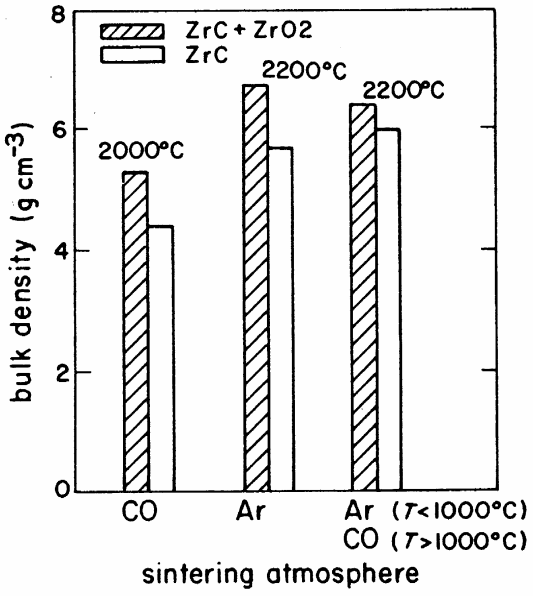

Figure 2.12 A comparison of fired density obtained for pure ZrC and ZrC + 30% Type A ZrO_2 at different temperatures and firing atmospheres. (This figure is reproduced exactly from reference 54).

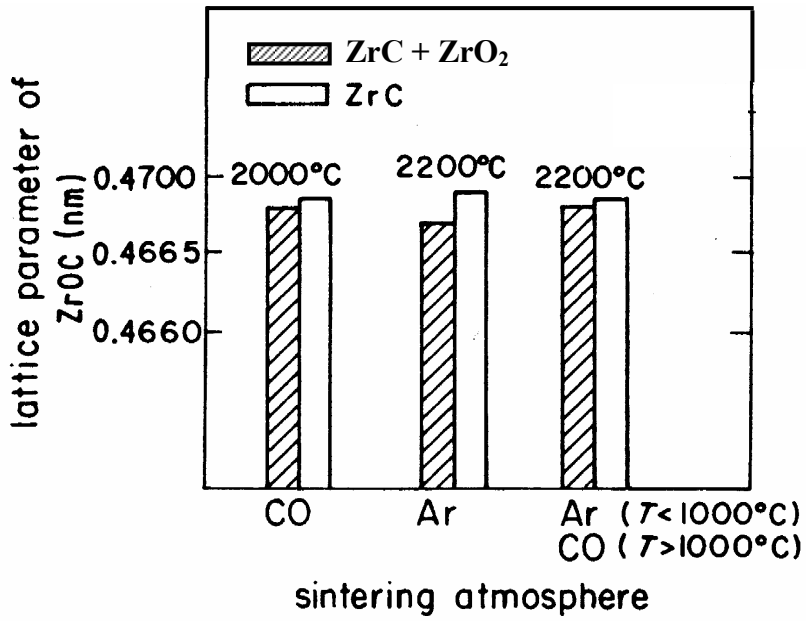

Figure 2.13 The lattice parameter of pure ZrC and ZrC with 30% Type A ZrO_2 sintered samples. (This figure is reproduced exactly from reference 54.)

elemental analysis (C_{free} 0.04%, N 0.03%, O 0.33%). Pre-sintered samples with different initial densities (Table 2.9) were then used to study the sintering process under non-isothermal conditions in the temperature range of 2327 to 2927°C. The samples were placed and withdrawn from a pre-heated furnace at a rate such that heating and cooling rates of 600°C/s were achieved. The number of heating cycles to which the specimens were exposed was in the range of 1 to 20. The non-isothermal densification data for samples with relative density of 71% (initially heat treated at 1527°C) are listed in Table 2.10.

Table 2.9 Relative densities of ZrC samples after initial sintering.

Temperature (^{o}C)	Relative density (%)
1027	59
1527	71
1827	87
2527	96

Table 2.10 Relative densities of ZrC samples after non-isothermal sintering.

Temperature (^{o}C)	Number of cycles	Relative density (%)
2327	10	86
2527	10	92
2727	10	94
2927	10	96

Barnier et al.[49] studied the hot-pressing kinetics of ZrC powder formed by carbothermal reduction reaction between zirconium dioxide and carbon. The chemical formula for the zirconium carbide was $ZrC_{0.963}$ as determined from elemental analysis (by weight: 88.16% Zr, 11.47% C (total), 0.28% C (free), 0.25% N, 0.11% O, 0.01% Fe). The measured lattice parameter was 0.4698 nm which corresponds to a calculated solid density of 6.58 g/cm^3. SEM indicated that the particles had sizes in the range of 3 to 5 μm. The BET specific surface area was 0.5 m^2/g.

The powders were hot pressed using graphite die and punches. Samples were heated in vacuum up to 1000^{o}C and in argon at higher temperatures, under a constant

load of 8 MPa. At maximum temperatures in the range of 1700 to 2400°C, a pressure of 40 MPa was applied and held for 1 to 2 h. Table 2.11 lists the density values for ZrC samples prepared under various hot pressing conditions. The relative density reached ~95% and ~98% after hot pressing at 1900°C and 2300°C, respectively.

Table 2.11 Density results for hot-pressed ZrC bulk ceramics.

Temperature (°C)	Time (min)	Bulk Density (g/cm^3)	Relative density (6.58 g/cm^3)
1700	120	4.92	74.7
1800	60	5.26	79.9
1800	120	5.47	83.2
1900	60	6.07	92.2
1900	120	6.29	95.5
2000	60	6.35	96.5
2000	120	6.40	97.2
2100	60	6.38	96.9
2200	60	6.40	97.3
2300	60	6.45	98.1
2400	60	6.43	97.8

CHAPTER III

Research Approach

This section describes the research approach used to synthesize nanocrystalline ZrC-based powders and the rationale behind the approach.

Solution-based processing was chosen for this study because of its advantages mentioned in Chapter II: (i) Starting materials can be mixed on a molecular-scale using solution methods. Under appropriate processing conditions, this can produce fine-scale mixtures of the reactants that are used for carbothermal reduction (CTR) reactions. In turn, the CTR reactions can be carried out at lower temperatures and the resulting ZrC product can have finer crystallite sizes. In addition, there may be less need for grinding (milling) of the reacted powders. (ii) The processing methods are relatively simple and do not require expensive equipment. (iii) The starting materials have moderate costs.

The research approach for this study involved using soluble Zr-bearing and C-bearing compounds as starting materials in order to first form fine-scale mixtures of zirconia and carbon. These mixtures were subsequently used to carry out carbothermal reduction reactions to form the ZrC-based powders. The specific approach used for most of the synthesis experiments is illustrated in the flow chart in Figure 3.1. A metal alkoxide (i.e., zirconium n-propoxide, ZP) was used as an alcohol-soluble precursor for the formation of the metal oxide reactant (i.e., zirconia, ZrO_2) needed for the carbothermal reduction reaction. (The precursor is also a source for some of the carbon that develops upon pyrolysis.) This precursor was selected for the following reasons: (i) There is substantial knowledge in the literature concerning the processing of metal oxides from

metal alkoxides precursors. (ii) The potential yield of ZrO_2 from ZP is reasonable. (iii) ZP is soluble in relatively benign and inexpensive solvents. (iv) ZP is neither extremely sensitive nor extremely resistant to hydrolysis. In addition, ZP can be modified readily in order to alter its hydrolysis resistance. (v) ZP is readily available from commercial sources and it has a relatively moderate cost.

Zirconium n-propoxide was refluxed with 2,4-pentanedione (also known as acetylacetone and often referred to as "acacH") in order to partially or fully convert the metal alkoxy groups to a chelated metal diketonate structure (i.e., zirconium pentandionate, $Zr(O_2C_5H_7)_4$). Replacement of one propoxy group is shown in Figure 3.2. The primary reason for carrying out the replacement reaction was to produce a soluble metal-organic precursor that allowed for greater control over the hydrolysis and condensation reactions that were carried out in a subsequent processing step. In general, zirconium alkoxides would be expected to undergo more rapid hydrolysis/condensation reactions compared to chelated zirconium diketonates.[56] Rapid hydrolysis/condensation reactions may sometimes result in uncontrolled precipitation of relatively large precursor particles. The replacement reaction also allowed for more control over the C/ZrO_2 molar ratio in the pyrolyzed powders that were subsequently produced and used for carbothermal reduction (CTR) reactions. For example, pyrolyzed material with higher carbon content can be obtained by using precursors with a higher degree of replacement of the alkoxide groups. (The acac-modifed ZP is the source for some or all of the carbon that develops upon pyrolysis.) The extent of the replacement of the propoxide groups can be varied by factors such as the acacH/ZP molar ratio and the heating conditions (temperature/time) used during refluxing.

The next solution-processing step was to hydrolyze the acac-modified ZP precursor through the addition of water. Hydrolysis was required to initiate condensation reactions which, in turn, resulted in the build-up of sol species with three-dimensional structure. The latter development was important in order to obtain a reasonable ceramic yield upon subsequent pyrolytic decomposition. Hydrolysis and condensation reactions are illustrated in Figure 3.3. The extent of the hydrolysis/condensation reactions depended on variables such as the water/ZP ratio and the solution pH.

The flow chart in Figure 3.1 also shows that the C/Zr ratio in the pyrolyzed product can be varied by combining the Zr-bearing precursor with a soluble carbon-bearing source in a mutually compatible solvent. The carbon-bearing source can be introduced at different stages of the process. Phenolic resin and glycerol were used as carbon-bearing source in this study. These precursors were selected for the following reasons: (i) They have low molecular weight which is useful for achieving intimate mixing with the Zr-bearing precursor. (ii) They are soluble in the solvents of interest in this study (i.e., alcohols and water). (iii) They have relatively low cost. (iv) They are polyhydroxy compounds and, thus, there is potential for these compounds to participate in condensation reactions with the hydroxyl groups from the hydrolyzed organozirconium precursors. (This possibility has been suggested by previous researchers.[17] Such reactions might be beneficial in maintaining an intimate mixing of the Zr-bearing source and the external C-bearing source during subsequent processing when the solvent is evaporated.)

The next processing step was to remove solvent from the solution by rotary evaporation. The solution became increasingly concentrated and eventually transformed to a powder or a gel as solvent was removed. Rotary evaporation allows for more control

over the solvent removal process and helps to reduce segregation of the Zr-bearing and carbon-bearing precursors as drying occur. The powder/gel material was then dried at higher temperature in an oven to remove the residual solvent. This was followed by a pyrolysis heat treatment in order to decompose the Zr-bearing and C-bearing precursors and to form the fine-scale ZrO_2/C mixture desired for the CTR reaction. The CTR heat treatment resulted in the formation of a ZrC-based powder. The characteristics of the CTR powders (e.g., crystallite size, particle/aggregate size, phase composition, etc.) were dependent on factors such as the heat treatment temperature/time schedule, gas flow rate, batch size, etc.

As discussed in Chapter II, solution-based processing has been used in several previous studies to prepare ZrC-based powders and fibers.[14,15,16,17,18] The present investigation differs from those earlier studies in several ways: (1) A more extensive investigation was carried out concerning the effects of selected processing variables on powder characteristics. This included studies of selected variables for the solution-processing steps that produced the ZrO_2/C powder precursors used for the CTR reactions and studies of selected variables for the CTR heat treatments used to produce the ZrC-based powders. (2) The synthesized materials were characterized more extensively compared to previous studies. A variety of powder characteristics were evaluated for selected samples (e.g., phases present, crystallite size, particle size, specific surface area, carbon content, weight loss, etc.). In addition, these characteristics were determined in selected samples that had been heat treated over a fairly broad range of temperatures. (3) Processing behavior (i.e., milling, dry pressing, and pressureless sintering) was also

investigated for selected powders. This type of study has not been reported previously for other powders produced by solution-based synthesis methods.

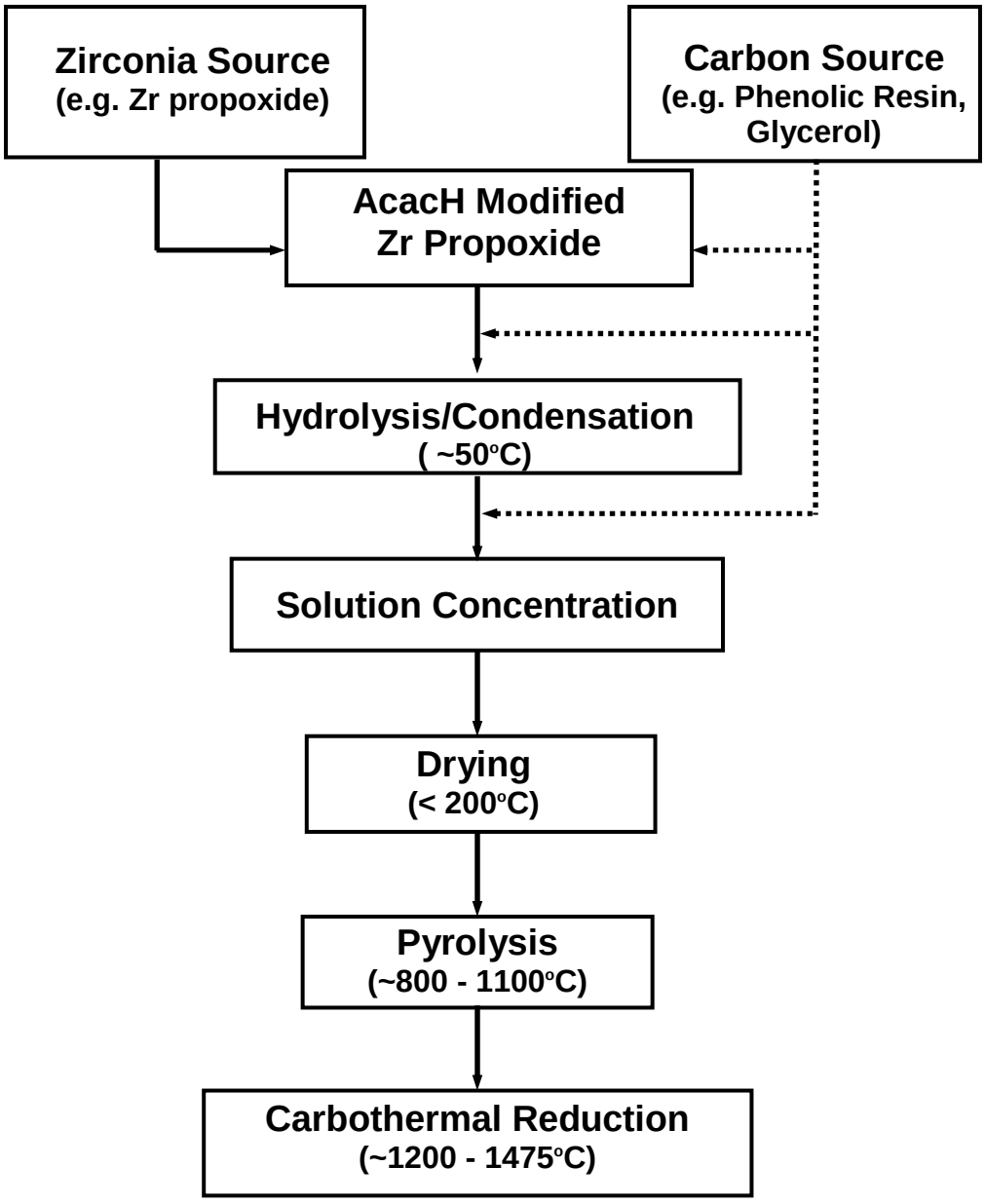

Figure 3.1 Flowchart showing various steps involved in the synthesis of ZrC-based powders.

Zirconium Diketonate Synthesis

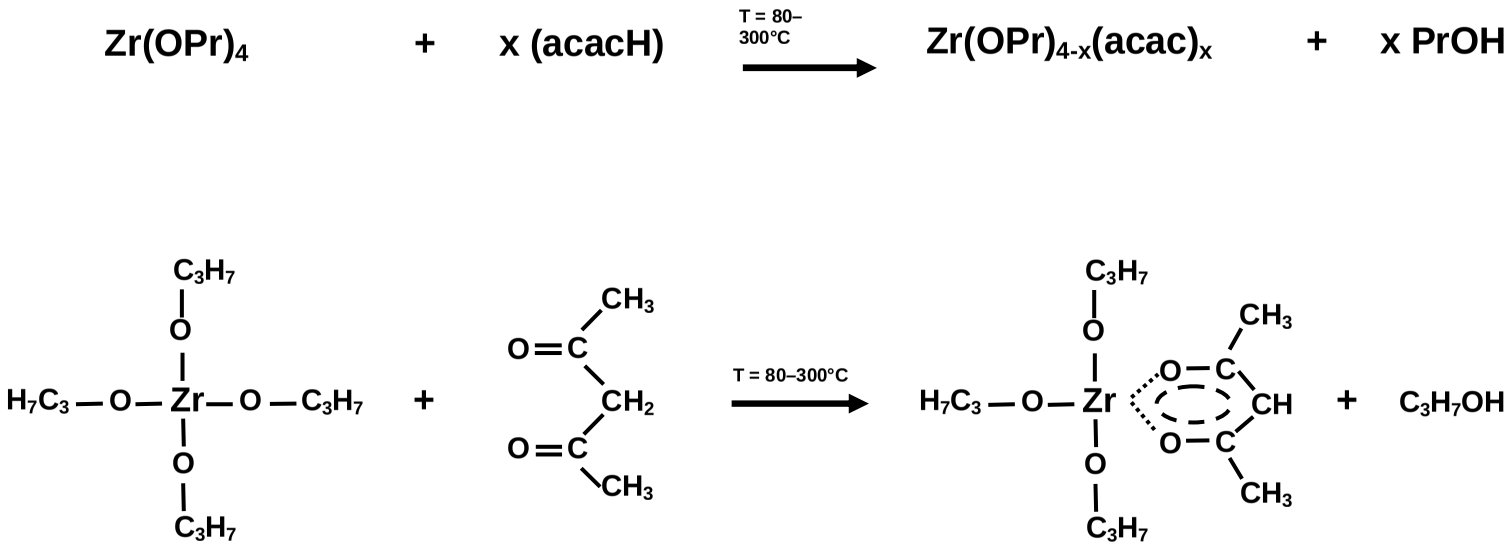

Figure 3.2 Alkoxy replacement reactions involved in the synthesis of ZrC-based powders.

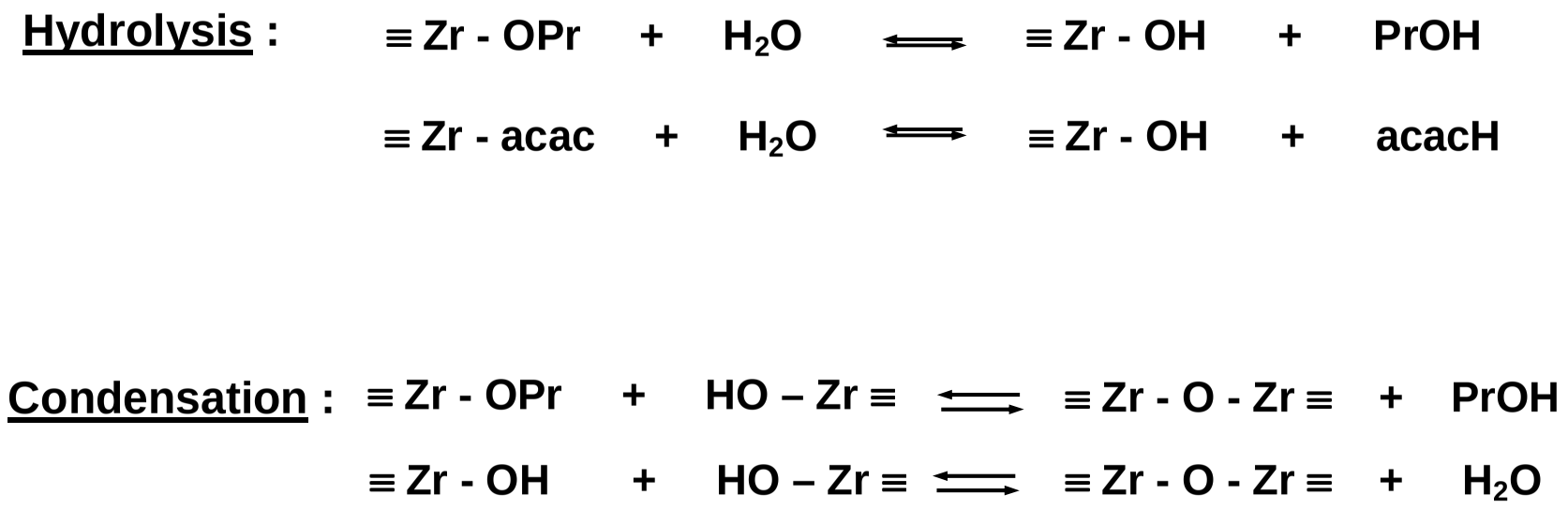

Figure 3.3 Hydrolysis and condensation reactions involved in the synthesis of ZrC-based powders.

CHAPTER IV

EXPERIMENTAL PROCEDURES

4.1 Synthesis of Nanocrystalline Zirconium Carbide Powder

4.1.1 Starting Materials

This section will describe the starting materials used in this study and their characteristics.

4.1.1.1 Zirconium Source

The zirconium precursor used in this study for most experiments was a zirconium n-propoxide/n-propanol solution (i.e., 70 wt% $Zr(OC_3H_7)_4$ in n-propanol, Alfa Aesar, Ward Hill, MA). The chemical structure of zirconium n-propoxide is shown in Figure 4.1. Zirconium n-propoxide is a moisture-sensitive solid. This means that hydrolysis reactions occur when the propoxide is exposed to water (see Figure 3.3). The propoxide was dissolved in propanol to reduce its tendency for hydrolysis to occur as a result of exposure to atmospheric water vapor. The choice of this precursor was based on moderate cost, relatively low molecular weight (327.62 g/mol), and solubility in various solvents considered. Zirconium n-propoxide will be abbreviated as ZP in this thesis.

In some experiments, zirconium 2,4-pentanedionate (Fisher Scientific, Fair Lawn, NJ) (also known as zirconium tetra-pentanedionate (ZTP) or zirconium acetylacetone (Zr acac) was used as the zirconium precursor. The choice of this precursor was based on its low molecular weight (487.66 g/mol), relatively low cost, and solubility in various solvents considered. ZTP is a less moisture-sensitive solid material when compared to ZP. The chemical structure of ZTP is shown in Figure 4.1.

Zirconium Propoxide (ZP)

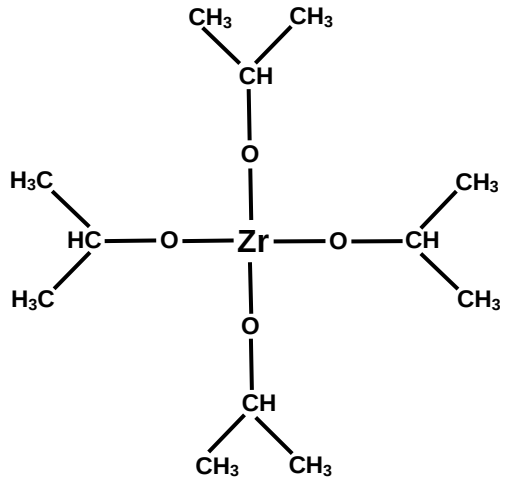

Zirconium 2,4-pentanedionate (ZTP)

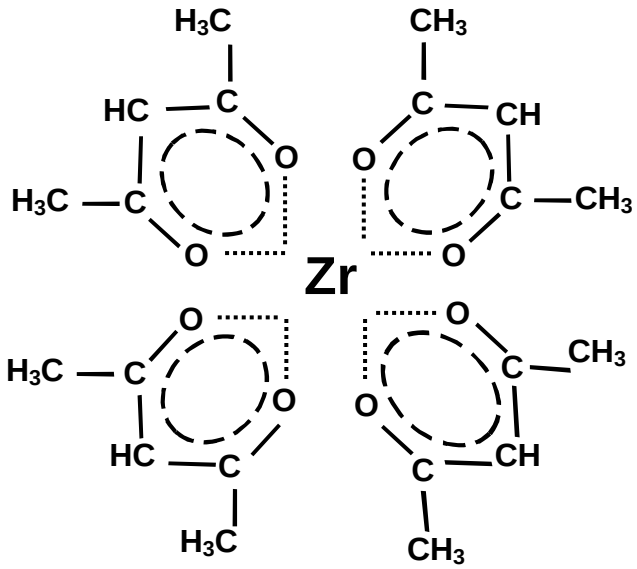

Figure 4.1. Chemical structures of zirconium n-propoxide (top) and zirconium 2,4 pentanedinate (bottom).

4.1.1.2 External Carbon Sources

Glycerol ($C_3H_8O_3$, Fisher Scientific, Fair Lawn, NJ) was used as an additional source of carbon to synthesize some ZrC-based powders batches. Glycerol has low molecular weight and, thus, "intimate mixing" (i.e., molecular-scale) with ZP (and modified ZP) was obtained in solutions. The chemical structure of glycerol is shown in Figure 4.2.

Phenol-formaldehyde resin (GP 775D69 "novolac" type, Georgia Pacific, Atlanta, GA) was also used as additional source of carbon to synthesize some ZrC-based powder batches. Information concerning this resin is provided in Table 4.1. The phenolic resin is comprised of oligomers with low molecular weight. Figure 4.2 shows an idealized structure of an oligomer with four phenol units.

Table 4.1 Details of phenolic resin.

Resin Name	Form	Solubility	Free Phenol	Free Aldehyde	Softening Point (^oC)	Water Absorption
GP 775D69 (Ga. Pac.)	Pellet solid	alcohols, ketones, 20 wt% water/EtOH	0.3 wt%	< 0.1 wt%	102-105	2.0 wt%

Phenolic Resin

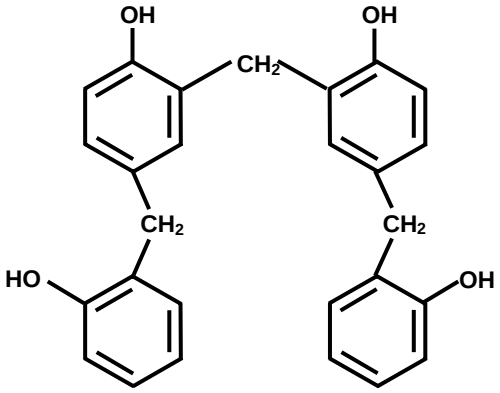

Oligomer of 4 phenol units

Glycerol

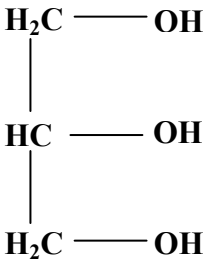

Figure 4.2. Chemical structures of phenolic resin (top) and glycerol (bottom).

4.1.1.3 Solvents

The primary solvent used in the study was ethanol (absolute, Chemical Stock Room, Georgia Institute of Technology). The density of ethanol is 0.789 g/cm^3 and its boiling point is 78.3^{o}C.[57] The vapor pressures of ethanol are ~44 and ~134 mm Hg at 20 and 40^{o}C, respectively.[57,58] Ethanol was first distilled to remove any water absorbed. Ethanol was poured into a 1 liter round bottom flask (Flask A), which was then placed on a heating mantle as shown in Figure 4.3. A few boileezers (Fisher Scientific, Fair Lawn, NJ) were added to the flask to prevent violent boiling of the ethanol. Flask A was connected to a distillation column, which was in turn attached to another 1 liter round-bottom flask (Flask B) via a condenser (to collect the condensed ethanol vapors). The temperature of the mantle was adjusted to obtain ~1-2 drops per second of distilled ethanol. (The temperature of the mantle was not recorded.) The distillation was stopped when ~100 ml of ethanol was left in flask "A". Flask "B" with distilled ethanol was then sealed with a glass stopper. Thermoplastic tape (Parafilm®, Pechiney Plastic Packaging, Chicago, IL) was used as a secondary sealant to make sure that no water was absorbed during storage.

Two other solvents, 1-butanol (Fisher Scientific, Fair Lawn, NJ) and n-propanol (Fisher Scientific, Fair Lawn, NJ), were used as received without any further treatment. The densities of 1-butanol and n-propanol are 0.81 g/cm^3 and 0.8 g/cm^3, respectively,[57] and their boiling points are 118^{o}C and 97^{o}C, respectively.[57] The vapor pressures of 1-butanol are ~6 and ~20 mm Hg at 20 and 40^{o}C, respectively.[59] The vapor pressure of n-propanol is 21 mm Hg at 25^{o}C.[57]

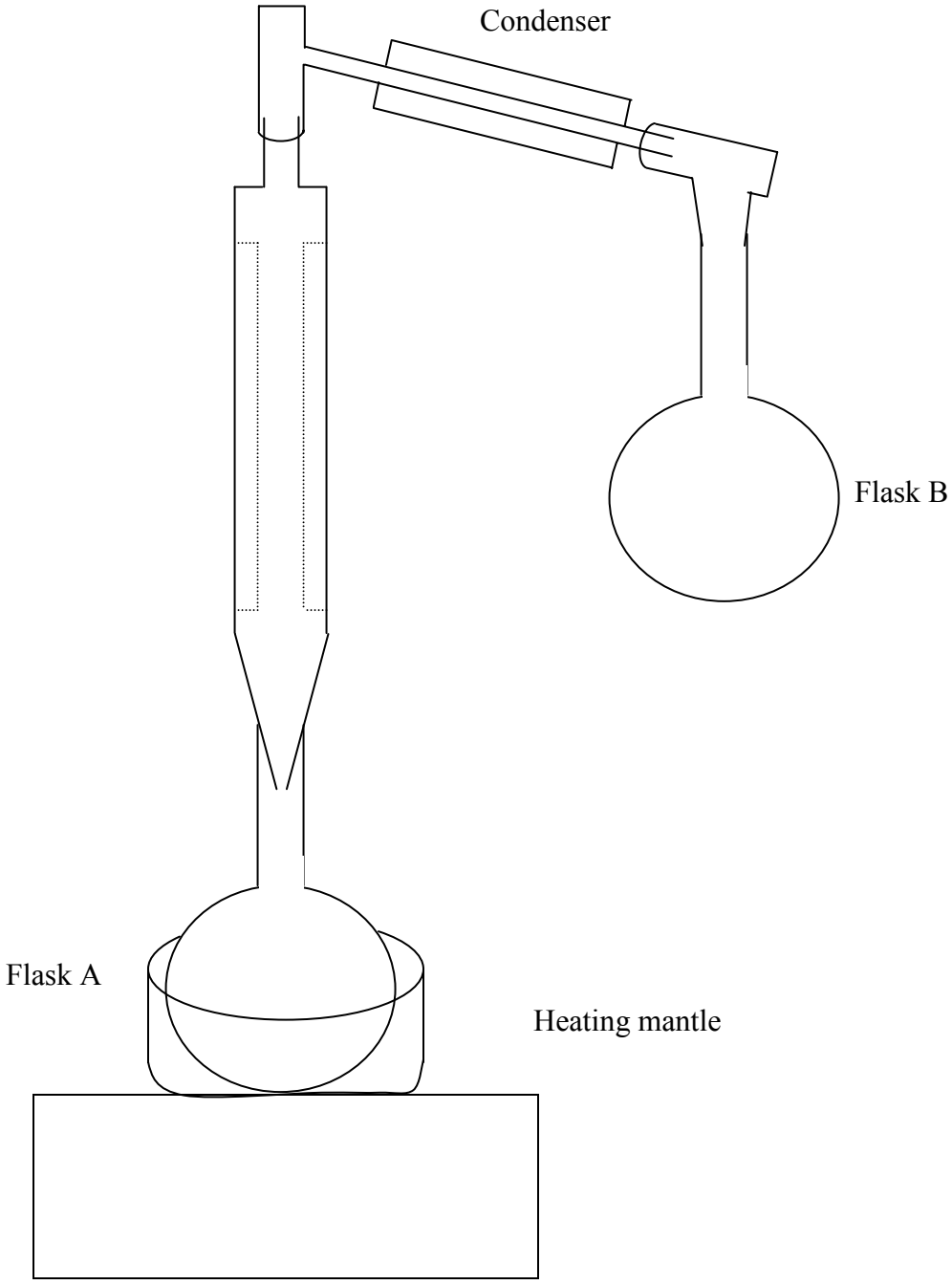

Figure 4.3 Schematic of set-up for ethanol distillation.

Table 4.2 Physical properties of various solvents and acacH.

	Boiling point (^oC)	Density (g/cm^3)	Vapor pressure (mm Hg)	
			at 20^oC	at 40^oC
ethanol	78.3	0.789	44	134
1-butanol	118	0.81	6	20
n-propanol	97	0.80	21 (at 25^oC)	-
acacH	138	0.97	7.5 (at 25^oC)	-

The boiling points, vapor pressures, and densities of the various solvents used in this study are summarized in Table 4.2 for comparison. Properties for 2,4-pentanedione ("acacH") are also listed.

4.1.1.4 Other materials

2,4-pentanedione (molecular weight of 100.3 g/mol, Alfa Aesar, Ward Hill, MA), also known as acetylacetone and abbreviated as "acacH" was used to modify zirconium n-propoxide. The density of acacH is 0.97 g/cm^3 and its boiling point is 138^oC.[57] The vapor pressure value is 7.5 mm Hg at 25^oC.[57] The chemical structure of acacH is shown in Figure 4.4.

De-ionized (DI) water and nitric acid (HNO_3, 69 - 70 wt% in water, J. T. Baker, Philipsburg, NJ)) were used in the hydrolysis/condensation step (section 4.1.2.3). Tap water was passed through carbon filter cartridges (CF-300, Pureflow Ultraviolet Inc., Lawrenceville, GA) and ion exchange cartridges (HP-100, Pureflow Ultraviolet Inc., Lawrenceville, GA) in order to obtain DI water. The conductivity of DI water varied in the range of 0.29 - 0.36 μS/cm.

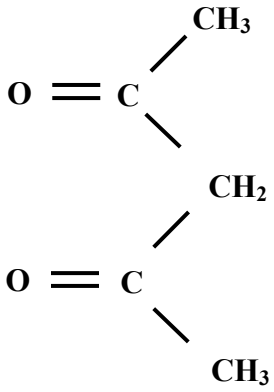

Figure 4.4 Chemical structure of 2,4-pentandione (acetylacetone, “acacH”).

4.1.2 Solution-Based Processing

4.1.2.1 General Considerations

The primary objective of this study was to produce fine-sized ZrC-based powders that would be suitable for fabrication of bulk samples via pressureless sintering. As described in Chapter III, this objective was pursued using solution-based processing in order to produce fine-scale precursors containing Zr and C; the solution-derived precursors were given heat treatments (pyrolytic decomposition and carbothermal reduction reactions) that ultimately resulted in the formation of ZrC. The solution-processing steps were important for controlling the (i) C/Zr ratio, (ii) crystallite size, and (iii) homogeneity of the final powder.

The C/Zr ratio was varied using three solution-processing steps illustrated in Figure 3.1: modification of the zirconium n-propoxide, hydrolysis/condensation, and addition of "external" carbon sources (glycerol or phenolic resin). For each of these

steps, there were specific processing variables that affected the C/Zr ratio: (i) The concentration of acacH (i.e., acacH/Zr propoxide ratio) and the solution heat treatment (refluxing) conditions (i.e., temperature/time) were used to vary the extent of the conversion of the zirconium n-propoxide (ZP) to zirconium 2,4-pentanedionate (ZTP). This, in turn, affected the C/Zr ratio. (ii) The concentrations of water (i.e., H_2O/Zr propoxide ratio) and acid (i.e., HNO_3/Zr propoxide ratio) were used to vary the extent of the hydrolysis and condensation reactions. This, in turn, affected the C/Zr ratio. (iii) The concentration of the external carbon source (glycerol or phenolic resin) was used to directly vary the C/Zr ratio in the precursor.

The effects of solution-processing variables on the particle or crystallite sizes in the pyrolyzed or carbothermally-reduced powders were not systematically investigated in this study. Instead, conditions were pre-selected which were expected to avoid or minimize extensive precipitation of large particles during solution processing (i.e., prior to solvent removal). As described in Chapter III, the approach used in this study involved the preparation of relatively hydrolysis-resistant chelated organozirconium derivatives in order to avoid rapid hydrolysis and condensation reactions. (Such rapid reactions might lead to the formation of relatively large precipitate particles.) In addition, pH adjustments were made using only acid additions for the same reason.

Batch "homogeneity" was assessed only qualitatively in this study and this was based on visual observations that were made during solution-processing studies that were focused primarily on varying the C/Zr ratio. Specific observations concerning the effect of solution processing variables on "homogeneity" of the dried material will be discussed in Chapter V.

The assessment of batch "homogeneity" was based on several considerations: (1) Solutions were inspected for the occurrence of precipitation, either during processing in the dilute state or during concentration to remove solvent. The occurrence of precipitation was distinguished from cases in which the solution is concentrated to form a gel-like material. (2) Powders were inspected for uniformity in texture and color after they were oven-dried and, in some cases, after they were crushed up. (3) Some organozirconium precursors did not undergo direct pyrolytic decomposition of the solid product, but instead melted (or partially melted) at some stage in the heat treatment (i.e., either during drying or pyrolysis). Hence, the product after heat treatment was not a homogeneous powder. (4) Batches would be considered inhomogeneous if the "external" carbon source (glycerol or phenolic resin) segregated from the organozirconium precursor during concentration and drying. This type of problem was observed in a previous study involving the preparation of SiC-based powders using phenolic resin as a carbon source and silicon tetra-ethoxide as a silica source.[60] The problem was associated with carrying out the concentration and drying steps too rapidly. Hence, precautions were taken from the initial batch of this study by using low-temperature rotary evaporation to concentrate and to partially dry the batches.

The detailed procedures used to prepare most of the batches are described in sections 4.1.2.2 and 4.1.2.3. There were some batches in which there were some minor deviations from the procedures described in these sections. The differences in those batches are described in section 4.1.2.4.

Some batches were prepared with more significant differences. In particular, some batches were prepared with zirconium 2,4-pentatanedionate (ZTP) as the starting

material (instead of zirconium n-propoxide). In these batches, there was no need to carry out a refluxing step with acacH. However, acid and water addition steps were carried out for most of the batches. The detailed procedures are described in section 4.1.2.5.

4.1.2.2 Modification of Zirconium n-Propoxide (Including Method Using "External" Carbon Precursor)

4.1.2.2.1 Introduction

As indicated in section 4.1.1.1, the source of zirconium for most synthesis experiments was a zirconium n-propoxide (ZP) solution (70 wt% propoxide in 1-proponol).

Based on previous work in the literature, it was hypothesized that the extent of the conversion from the zirconium alkoxide (i.e., zirconium n-propoxide in this case) to the zirconium diketonate (i.e., zirconium 2,4-pentanedionate in this case) could be controlled by varying the acacH/Zr molar ratio and the temperature/time schedule for the reflux operation.[56] The specific ranges used in this investigation were as follows:

(i) AcacH/Zr molar ratios were varied over the range of 2-50.

(ii) Reflux temperatures and times were varied in the range of 80 - 300^{o}C and 1- 3 h, respectively.

4.1.2.2.2 Detailed Procedure

ZP solution was transferred to a flask in a glove box (Labmaster 130, M. Braun, Stratham, NH) under an inert atmosphere (argon, 99.999% purity). The transfer was done in an inert atmosphere because ZP is moisture-sensitive. (Precautions were taken because of the concern that atmospheric water vapor would be absorbed into the concentrated propanol-based solution. This could initiate uncontrolled hydrolysis/condensation

reactions.) The amount of solution transferred was in the range of 0.469 - 75 g. These amounts were equivalent to 0.001 – 0.1602 mol of ZP (i.e., based on a molecular weight of 327.62 g/mol for the zirconium n-propoxide and an assumed concentration of 70 wt% in the propanol solution.) Smaller amounts (i.e., usually 0.001 - 0.032 mol) were used mostly to investigate the effects of some solution-synthesis processing variables on the dried and/or pyrolyzed powder characteristics (e.g., the C/Zr ratio of pyrolyzed material and the "powder homogeneity" of dried and/or pyrolyzed material). Larger amounts (i.e., usually 0.156 - 0.1602 mol) were used mostly to produce batch of sufficient size to carry out more detailed investigations of either the CTR (carbothermal reduction) reaction and/or the sintering behavior. The flask sizes used for smaller batches were in the range of 100 - 250 ml, while the flask sizes for larger batches were in the range of 2000 – 3000 ml. Table 4.3 lists the amount of ZP used in 100 different batches that were produced. The earliest-produced batches (identified with asterisks) were prepared by Greg Staab of the Georgia Institute of Technology.

The ZP solution was diluted by adding alcohol to the flask in the glove box. The reasons for diluting the ZP solutions with alcohol were as follows: (1) Dilution would reduce the moisture sensitivity of the ZP when the solutions were subsequently handled outside the glove box. (2) Dilution would result in more gradual mixing when acacH was subsequently added to the ZP solution.

The amount of alcohol diluent that was added to the ZP solution was in the range of 5.9 – 675 g (see Table 4.3). Most of earlier experiments (batch numbers ZrPM-1 - 44, ZrPM-46 - 57) were carried out using 92.5 - 95 wt% diluent. The amount of diluent was reduced when some of the first larger-size batches (e.g., batch numbers ZrPM-45, 58, 59)

were prepared. This was done because there were limitations in the available flask sizes and heating mantle sizes. It was then decided that the lower amount of diluent could be used for the rest of the batches (i.e., ZrPM-60 – ZrPM-100) because the solutions (and the dried powders eventually produced) were visually homogeneous. The weight percent of diluent was calculated on the basis of ZP weight as shown in the equation below:

$$wt\%\ of\ diluent = \frac{weight\ of\ diluent}{weight\ of\ diluent + weight\ of\ ZP}\ x\ 100 \qquad (4\text{-}1)$$

The alcohol used for dilution for most experiments was ethanol. In some of the earlier batches (see Table 4.3), propanol or butanol was used as the diluent. The reasons for selecting the latter solvents in the initial experiments were as follows: (1) It was thought that the ZP and the acacH (which was added later to the solution) might have higher solubility in propanol or butanol, i.e., compared to the solubility in ethanol. The actual solubilities of ZP and acacH in the various alcohols were never determined. However, subsequent qualitative observations indicated that both ZP and acaH were "highly soluble" in ethanol. (2) There was some concern that ethanol additions would cause the ZP solutions to be more moisture sensitive. However, there were no obvious visual observations during synthesis experiments that suggested this was a problem. (Specifically, it was observed that solutions remained transparent during the early stages of synthesis. If the solutions had developed any haziness or if the formation of precipitates had been observed, then the occurrence of uncontrolled hydrolysis/condensation reactions might have been suspected.) The reasons for ultimately selecting ethanol as the diluent for most of the experiments were: (1) The removal of this solvent (via evaporation) during

subsequent concentration and drying operations could be carried out more quickly at lower temperatures. (2) It had been previously determined that the grade of phenolic resin that was to be used in this study (as an externally added source of carbon) had good solubility in ethanol. (3) Ethanol had lower cost than propanol and butanol.

After adding the alcohol diluent, the flask was then sealed inside the glove box using a glass stopper and then the flask was removed from the glove box. The flask (item C in Figure 4.5) was quickly attached to the Schlenk apparatus shown in Figure 4.5. The flask was opened and exposed to the atmosphere only for the time (≤ 1 second) that it took to attach it to the apparatus. Prior to attaching flask C, the entire Schlenk setup was purged with N_2 (99.999% purity) for at least 5 min. This purge was carried out to remove any residual moisture in the apparatus that could have resulted in uncontrolled hydrolysis/condensation reactions in the ZP solution. After flask C was attached to the Schlenk apparatus, vacuum was pulled to 5 torr using a mechanical pump (Model 2022B-01, Welch Vacuum, Thomas Industries, East Hanover, NJ). The apparatus was then back filled with N_2. This cycle was repeated at least 4 times to make sure that no traces of moisture remained in the setup.

The next step in the synthesis was to prepare acacH/alcohol solutions. The acacH was diluted in alcohol for the same reasons stated above regarding the dilution of the ZP solution with alcohol. The dilution was carried out in a fume hood. 1-butanol was used as the diluent for batch numbers 1 and 2 (33 wt% acaH/ 67 wt% 1-butanol and 60 wt% acaH/ 40 wt% 1-butanol, respectively.). 1-propanol was used as the diluent for batch number ZrPM-3 and batch numbers ZrPM-5 – ZrPM-9 (60 wt% acaH/ 40 wt% 1-propanol and 45 wt% acaH/ 55 wt% 1-propanol, respectively). Ethanol was used as the diluent for all other

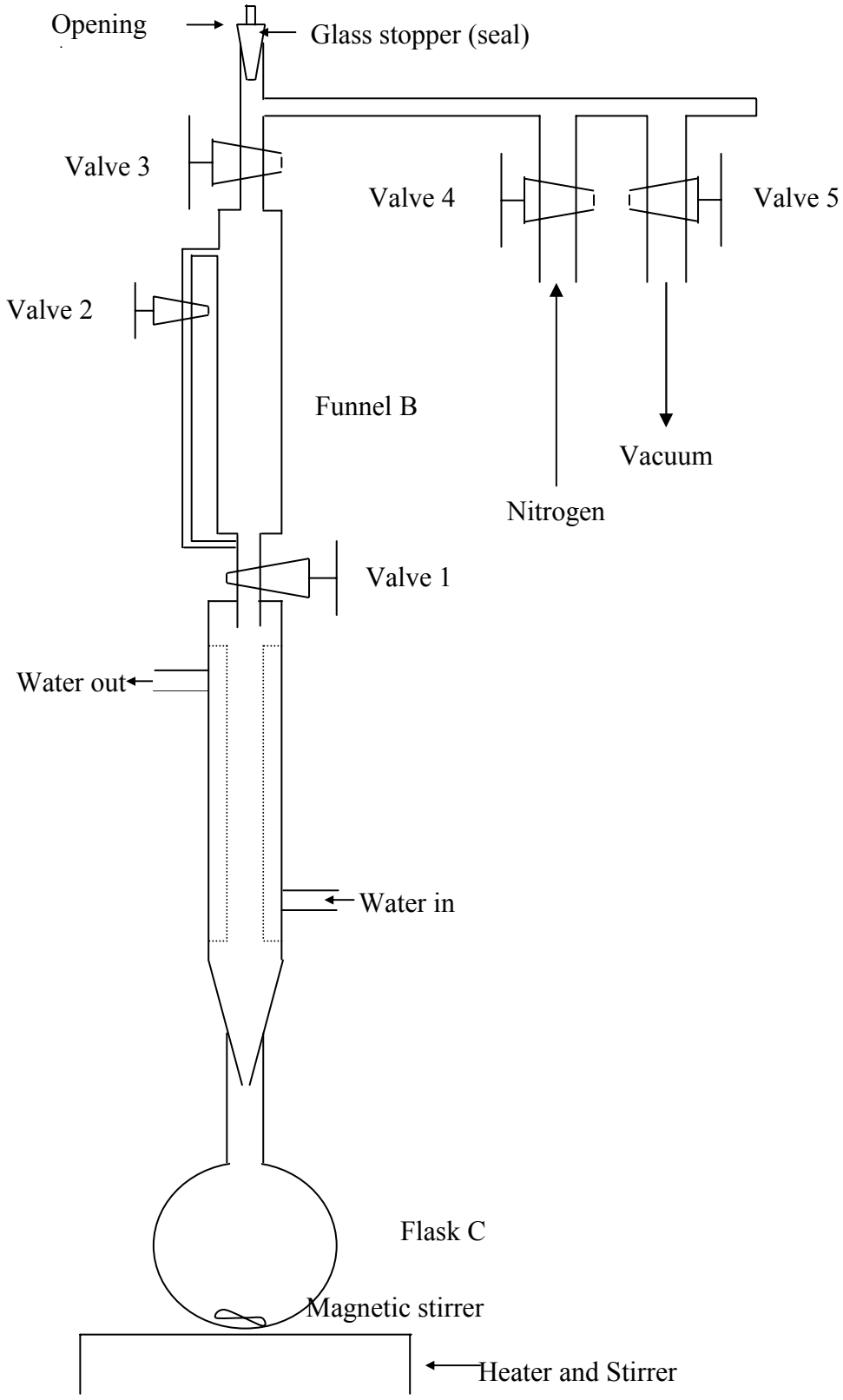

Figure 4.5 Schematic of schlenk apparatus.

batches (range of 5 wt% acaH/ 95 wt% ethanol - 20 wt% acaH/ 80 wt% ethanol). The amounts of alcohol used for dilution are listed in Table 4.3.

The acacH/alcohol solution was then added to funnel B (Figure 4.5) through opening A. This was done with valve 3 open and all other valves closed. Opening A was then sealed and valve 3 was closed. Vacuum was pulled and the Schlenk setup was purged with nitrogen to remove any traces of moisture that entered during addition of the acacH/alcohol solution to funnel B. The cycle was repeated at least 4 times. Valves 4 and 5 were closed and then valve 2 was opened. Valve 2 served the purpose of equalizing the pressure between the top and bottom nozzles of funnel B. The acacH/alcohol solution was then added to the ZP/alcohol solution in flask C by opening valve 1 and adjusting the flow rate to approximately 1-2 drops per second (i.e., ~50 – 100 ml/min). The solution was stirred during the addition using a magnetic stir plate. (A magnetic stir bar had been placed inside flask C during the initial preparation of the ZP/alcohol solution.) After the acacH/alcohol solution had been drained out of funnel B and transferred to flask C, valves 1 and 2 were closed. The next step was to add 5 ml of alcohol to funnel B in the same way that was used to add the acacH/alcohol solution. The alcohol used in this step was the same type as used to prepare the acacH/alcohol solution (i.e., ethanol for most experiments). The purging of the apparatus and the addition of the 5 ml of alcohol to the solution in flask C were carried out in the same way as before. This last addition of alcohol was used to rinse acacH/alcohol solution that had remained attached to the walls of funnel B after it had been drained.

The solution in flask C was then refluxed using a heating mantle with a variac. This was carried out with valves 1, 2, and 3 open and valves 4 and 5 closed. Solutions

were heated at temperatures in the range of 80 – 300^{o}C for times in the range of 1-3 h (see Table 4.3). The temperature was measured by using a K-type thermocouple (Model 600-1040, Barnant Co., Barrington, IL) that was placed under the bottom center of flask C. For some large samples (final yield > 60 g dried powder), there was a pressure build-up inside the apparatus which forced the stopper at opening A to pop out. This exposed the refluxed solution to atmospheric moisture and, therefore, may have resulted in uncontrolled hydrolysis/condensation reactions in the solution. Therefore, a one-way check valve (Part No. 902209, 3-50 psi pressure range, Swagelok Co., Solon, OH) was attached at opening A in order to relieve the pressure when a preset limit (5 psi) was reached. The check valve was used in the preparation of batches ZrPM-60 – ZrPM-100.

For most of the larger batches (including ZrPM-58 – ZrPM-100), the next processing step was not carried out until approximately ~0.5-1 days (but usually 14-18 hours) after the refluxing step was complete. In contrast, processing was continued without a delay for most of the small batches.

After refluxing, flask C was removed from the apparatus and quickly sealed with a glass/teflon stopper. The solution was exposed to the atmosphere for ≤ 1 second during this operation. The weight of the solution inside flask C was recorded and then flask C was quickly attached to a vacuum rotary evaporator (Model R-114, Büchi Laborator-Technik, Switzerland), as shown in Figure 4.6.

Solvent was removed from the refluxed solution under rotary evaporation conditions. Flask C was kept in constant contact with a water bath (Figure 4.6) that had the temperature maintained at approximately 40 to 45^{o}C. For most of the earlier batches (i.e., numbers ZrPM-1 – ZrPM-30, ZrPM-32, ZrPM-39, and ZrPM-40), essentially all liquids

were removed from the solution by rotary evaporation and the acac-modified ZP product was a solid. (Some batches, discussed in section 4.1.2.4, were directly concentrated using the rotary evaporator and then dried. There were no acid addition, water addition (hydrolysis/condensation), or aging steps.) The liquid removal step was carried out for two reasons: (1) It was intended to remove most of the "excess" acacH, i.e., acacH that did not react with the ZP. Based on the boiling point and vapor pressure information in Table 4.2, it was presumed that the alcohols would be mostly removed during the earlier stage of rotary evaporation and that this would be followed by the removal of most of the excess acacH. Thus, it would be necessary to remove essentially all the liquid in order to remove the excess acacH. (2) It was convenient for determining the amount of acac-modified ZP formed in flask C if essentially all the liquid was removed.

A different rotary evaporation procedure was used for other batches (numbers ZrPM-31, ZrPM-33 – ZrPM-38, and ZrPM-41 – ZrPM-100) in which only some of the solvent was removed from the refluxed solution. Hence, the product after this step was a solution of the acac-modified ZP in a solvent of unknown composition. (The percentages of residual alcohol (ethanol, propanol, and/or butanol) and unreacted acacH were not known.) The change in procedure was instituted because of concerns that uncontrolled hydrolysis/condensation might have occurred due to exposure of the dried acac-modified ZP precursor to the ambient air atmosphere during the time after the flask was removed from the apparatus in Fig. 4.5 and before it was subsequently attached to the rotary evaporator. Table 4.3 shows the approximate percentage of concentration, n, that was carried out on the various batches. If the solvent was removed completely (or nearly completely), no calculation was made and the table entry simply states "To Solid." This

was the case for batches ZrPM-1 - ZrPM-30, ZrPM-33, ZrPM-39, and ZrPM-40. For the rest of the batches, the extent of concentration was calculated as a percentage based on the weights of the refluxed solution prior to concentration and after concentration. The extent of concentration, n, is given by:

$$n = \frac{weight\ of\ solution\ after\ concentration}{weight\ of\ solution\ before\ concentration} x\ 100 \qquad (4\text{-}2)$$

After evaporation of solvent to the desired extent, the flask was removed from the rotary evaporator and quickly (~1 second) sealed.

Prior to carrying out hydrolysis/condensation reactions (section 4.1.2.3), distilled ethanol was added back to the acac-modified ZP product obtained from the previous steps. (The acac-modified ZP product was either a solid or a solution depending on the particular batch, as indicated in Table 4.3.) The purpose of the ethanol addition was to have a relatively dilute (mostly alcohol-based) solution for the hydrolysis/condensation reactions. Dilution would allow for more gradual mixing when water and acid were subsequently added to the acac-modified ZP solution.

The amount of ethanol added for different batches is listed in Table 4.3. The amount varied in the range of 13-80 ml ethanol per gram of the starting amount of ZP solution (i.e., 70 wt% zirconium n-propoxide in 1-propanol). Most of earlier experiments (batch numbers ZrPM-16 – ZrPM-44 and ZrPM-47 – ZrPM-57) were carried out using larger amounts of ethanol per gram of starting ZP solution (i.e., 80 ml/g). The amount of diluent was reduced substantially when the first larger batches (e.g., ZrPM-45, 58, 59) were prepared. This was done because there were limitations in the available flask sizes and

heating mantle sizes. It was then decided that the lower amount of diluent could be used for the rest of the batches (i.e., batches ZrPM-60 – ZrPM-100) because the solutions (and the dried powders eventually produced) were visually homogeneous.

The addition of the distilled ethanol to the flask containing the acac-modified ZP was carried out quickly in order to minimize the occurrence of uncontrolled hydrolysis/condensations reactions that might result from exposure of the solid or concentrated solution to atmospheric water vapor. The amount of time required to add the ethanol depended on the batch size, but it was typically in the range of 5 - 20 sec. After the ethanol addition, the solution was shaken manually for approximately 30 sec. The solution was also mixed by a magnetic stirrer for an additional ~5 min.

When the material was a solid product (i.e., acac-modified ZP), the dissolution time was usually in the range of 1 – 3 min depending on the batch size. For all batches, the product after sufficent mixing time was a homogeneous solution with greenish-yellow color.

4.1.2.2.3 Glycerol Additions

As discussed in Chapter III, the final C/Zr ratio in synthesized batches was sometimes varied by adding an "external carbon source," i.e., glycerol or phenolic resin. In some cases, the external carbon source was added to the batch during the preparation of the acac-modified ZP. This method will be referred to as Case #1 to distinguish it from other methods discussed below in section 4.1.2.3.1.

The overall procedure described above was modified for three batches (i.e., batch numbers ZrPM-80, 82, 84). The only change was that glycerol ($C_3H_8O_3$) amounts in the

range of 0.011 – 0.02 g (0.343 – 0.63 mol) were added to the acacH/ethanol solutions described earlier (see Table 4.4). After the addition, the solution was shaken manually for approximately 30 sec. The rest of the procedure was identical to that described above. (The acacH/ethanol/glycerol solution was added to the ZP solution and the resulting solution was refluxed.)

4.1.2.3 Hydrolysis/Condensation (Including Methods Using "External" Carbon Precursors)

4.1.2.3.1 Introduction

As discussed earlier (Chapter III), the zirconium n-propoxide starting material was partially or fully converted to zirconium 2,4-pentanedionate in order to achieve better control over the hydrolysis/condensation reactions that would be subsequently carried out. The extent and rate of the hydrolysis/condensation reactions was also controlled by varying the amount of water and the pH used for these reactions. The pH was changed by using nitric acid (HNO_3) additions. The H_2O/Zr and HNO_3/Zr molar ratios used in this investigation were as follows:

(i) H_2O/Zr molar ratios were varied over the range of 8 – 24.

(ii) HNO_3/Zr molar ratios were varied over the range of 0.04 - 0.462.

In section 4.1.2.2.3, it was noted that some batches were prepared by adding glycerol to the acacH/ethanol solutions that were used to modify the ZP solutions. This method of varying the C/Zr ratio with an external carbon source was referred to as Case #1. In this section, three more cases will be described: (1) Case #2 refers to batches which contain no external carbon source. The detailed procedure used to prepare these batches is

described below in section 4.1.2.3.2. (2) Case #3 refers to batches in which the external carbon source was added after the modification of the ZP solution, but prior to carrying out the hydrolysis/condensation reactions. The detailed procedure used to prepare these batches is described below in section 4.1.2.3.3. (3) Case #4 refers to batches in which the external carbon source was added after carrying out the hydrolysis/condensation reactions. The detailed procedure used to prepare these batches is described in section 4.1.2.3.3.

4.1.2.3.2 Batches with no External Carbon Addition (Case #2)

As-received concentrated nitric acid (70 wt% of HNO_3 in water) was combined with distilled ethanol in a 250 ml vial to produce a 10 wt% HNO_3/90 wt% ethanol solution. The solution was shaken manually for ~30 sec. The purpose of diluting the acid with ethanol was to allow for more gradual mixing when the acid was subsequently added to the acac-modified ZP solution. The pH of the acac-modified ZP solution was measured approximately 1 min before adding the acid solution by a pH meter (Orion 320 PerpHecT, Thermo Electron Corporation, Woburn, MA). The acid was added to the former solution (in flask C) using a 10 ml pipette. The rate of addition was approximately 10 ml/min. The solution in flask C was stirred continually (using a magnetic stirrer) during the addition and for approximately 1 min after the addition was complete. The pH of the solution in flask C was measured approximately 1 min after the mixing step was completed. Table 4.5 gives the measured pH values for each batch.

The amount of acid added to the batch was based on reaching a targeted pH value. For batches prepared before ZrPM-65, the amount of acid solution added to the batch was not explicitly measured by volume or weight. However, the number of drops of acid added

to the solution was recorded for these batches. Subsequently, "calibration" measurements were made in order to determine the average weight per drop of added acid solution.* This average value was then used to convert the number of added drops of acid solution in each batch to a total weight of added acid solution. This, in turn, was used to determine the number of moles of HNO_3 that was added to the batch. For batch numbers ZrPM-65 – ZrPM-100, the weight of acid solution added to the batch was measured directly. Table 4.5 gives the number of moles of acid added to each batch. This table also gives the HNO_3/Zr molar ratio. This ratio was calculated based on the initial number of moles of ZP in the batch. (Hence, it was assumed that there was no loss of the ZP or the acac-modified ZP during the refluxing or other batch preparation steps.) The number of moles of water in the acid solution that were added to each batch are also listed in Table 4.5.

Water was used to promote hydrolysis and condensation reactions in the acac-modified ZP precursor solution. Deionized water was first mixed with distilled ethanol in weight ratios in the range of 10% water/90% ethanol to 20% water/80% ethanol (see Table 4.5). Dilution was carried out to allow more gradual addition of the water to the acac-modified ZP solution.

---

* The weight of 140 drops of 20 wt% acid/80 wt% ethanol solution was measured to be ~2 g. The same pipette size was used for this experiment as used for acid additions in previous batch preparations. The weight per drop was calculated and used to calculate the amount of acid added.

The water/ethanol solution was transferred to a funnel (with a valve) that was attached to flask C (which contained the acac-modified ZP solution). The water/ethanol solution was then added to flask C at a rate of approximately ~100 ml/min under constant stirring (using a magnetic stirrer). Table 4.5 gives the number of moles of water added to each batch. This table also gives the H_2O/Zr molar ratio. This ratio was calculated based on the initial number of moles of ZP in the batch and it was assumed that there were no losses of Zr during the previous batch preparation steps.

Flask C was then sealed and placed in an air-oven (Isotemp 500 series, Fisher Scientific, Fair Lawn, NJ) at temperatures in the range of 50 - 66^{o}C for 1-2 h (see Table 4.5). The solutions after this stage were essentially the same color (greenish-yellow) as described for solutions after the acacH refluxing and ethanol re-dissolution steps (see section 4.1.2.2.2). The only difference was that the color was lighter due to the dilution with ethanol and water that occurred during hydrolysis/condensation.

The sealed flask C was taken out of the air-oven after the heat treatment period and then left to cool for ~0.5 h at room temperature. The pH of the solution in flask C was measured after the cooling period. Table 4.5 gives the measured pH for each batch. Solvent was then removed from the solution using rotary evaporation. Flask C was kept in constant contact with a water bath that was maintained at approximately 35 - 40^{o}C (Figure 4.6). The rate of solvent removal was ~100 - 400 ml/h. The solution was concentrated until solvent loss was no longer obvious.

The flask was then sealed with aluminum foil that was perforated in order to allow removal of small amounts of residual solvent during the subsequent drying step. The flask

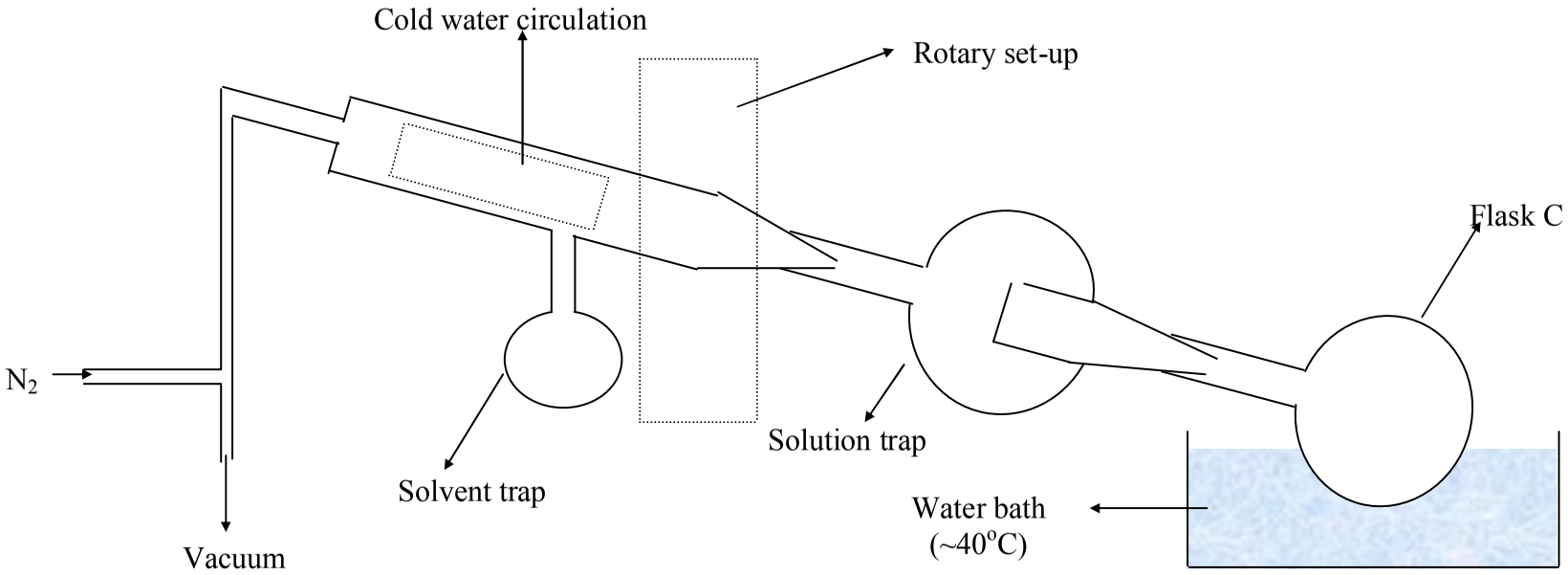

Figure 4.6. Schematic of rotary evaporator.

was then placed in a vacuum oven (see Figure 4.7) (Model 5831, National Appliance Company, Portland, OR) and heated to 120^{o}C for 3h.

It should be noted that hydrolysis and condensation reactions might continue for relatively long periods of time (i.e., days, weeks, or longer) after water is added to solutions with organometallic compounds.[61] The reactions will continue to produce changes not only in the molecular structure of the condensed species in the solution, but also in various bulk properties of the sols (e.g., rheological properties). The collective changes in the solution characteristics are often referred to as "aging" phenomena. The processing conditions used in the present study may have been helpful in minimizing batch-to-batch differences in aging. This is suggested based on the following considerations:

(1) Relatively high water concentrations were used in most experiments. (Table 4.5 shows that most experiments were carried out using moles H_2O/Zr molar ratios ≈24, while several experiments were carried using molar ratios in the range of ~8-16.) The high water concentrations would tend to drive the hydrolysis reactions toward their maximum extent in a more rapid manner.

(2) The "aging" treatment carried out at elevated temperature (i.e., 50 - 66^{o}C) accelerated the hydrolysis/condensation reactions under controlled conditions. This treatment may have minimized differences in aging that may have occurred because of differences in processing time after the water addition was made. It was inevitable that there would be differences in the time required to process the batches because the batch sizes varied significantly. For example, the time to remove solvent during the subsequent rotary evaporation step was highly dependent on batch size.

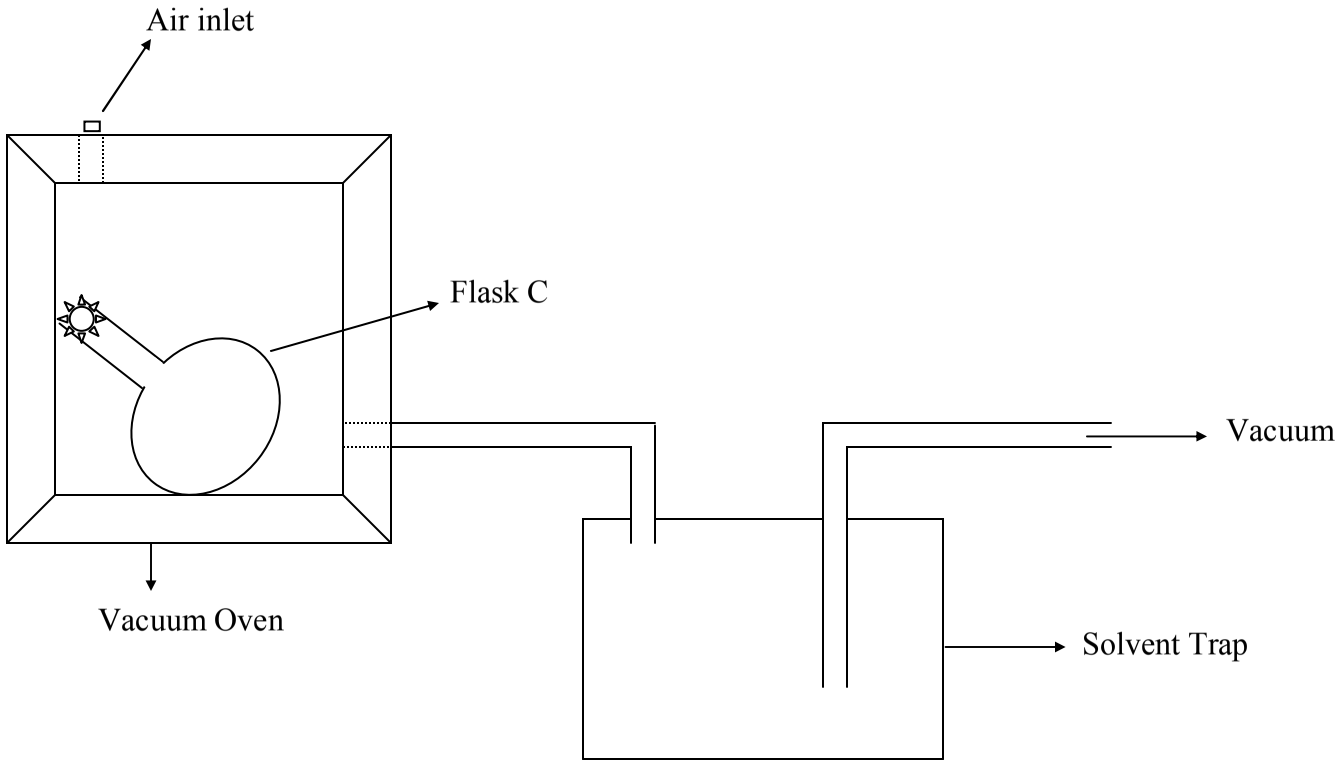

Figure 4.7 Schematic for vacuum oven with solvent trap.

(3) Solvent was removed from the batches soon after the aging heat treatment in order to minimize the time for additional aging. Also, solvent removal via rotary evaporation was carried out at a lower temperature (~35-40^{o}C) than the aging heat treatment.

(4) Samples were oven-dried soon after the rotary evaporation step was complete.

Except as noted in section 4.1.2.2.2, the processing was usually carried out without delays between the specific steps that have been identified. In other words, solutions were not left standing between steps. The solutions were exposed to the ambient atmosphere only for the time it took to make acid and water additions and to measure the pH.

4.1.2.3.3 Batches with External Carbon Addition

Case #3

The procedure was exactly same as described above for Case #2 except that the external carbon precursor was added to the acac-modified ZP solution prior to the addition of the HNO_3 solution. The external carbon source was either phenolic resin or glycerol.

Phenolic resin additions were made using ethanol-based solutions. 20 wt% phenolic resin was mixed with 80 wt% distilled ethanol in a flask under continuous stirring (with a magnetic stirrer) until the resin was completely dissolved at room temperature. (The dissolution time was usually < 10 min.) The phenolic resin/ethanol solution was added to the acac-modified ZP solution (in Flask C) under continuous stirring (with a magnetic stirrer) at a rate of ~100 ml/min. The solution was exposed to the ambient atmosphere only for the time (~10-30 sec) that it took to add the desired amount of phenolic resin. The solution was stirred another 5 min after the phenolic resin addition was completed. The amounts of phenolic resin added to each batch are shown in Table 4.4.

Glycerol additions were made by direct additions (without dilution) into the acac-modified ZP solution under continuous stirring (with a magnetic stirrer). The rate of addition was ~ 5 g/min. The solution was exposed to the ambient atmosphere only for the time (~10–30 sec) that it took to add the desired amount of glycerol. The solution was stirred another 5 min after the glycerol addition was completed. The amounts of glycerol added to each batch are shown in Table 4.4.

Case #4

The procedure was exactly same as described above for Case #3 except that the external carbon precursor (phenolic resin or glycerol) was added after the water addition, but before subsequent "aging" heat treatment at 50 - 66^{o}C. The mixed solution was allowed to stand for ~5 min prior to the “aging” heat treatment.

Case #5

The procedure was exactly same as described above for Case #3 except that the external carbon precursor (phenolic resin or glycerol) was added after the water addition and subsequent "aging" heat treatment at 50 - 66^{o}C. The carbon precursor was added to flask C after it had been removed from the oven and allowed to cool for ~0.5 h at room temperature. The mixed solution was allowed to stand for ~0.5 h prior to the rotary evaporation step.

4.1.2.4 Procedural Differences Associated with Certain Specific Batches

ZrPM-1a, 1b, 1c, and 1d were the same batch through the stage in which the ZP solution was refluxed with acacH at 103^{o}C (1 h). After that stage, the solution was divided into four parts. One part (ZrPM-1a) was directly concentrated using the rotary evaporator and then dried. There were no acid addition, water addition (hydrolysis/condensation), or aging steps. Other parts (ZrPM-1b, 1c, and 1d) were processed in the standard way.

Batches ZrPM-2 and ZrPM-5 – ZrPM-14 were directly concentrated, after acacH-reflux step, using the rotary evaporator and then dried. There were no acid addition, water addition (hydrolysis/condensation), or aging steps.

ZrPM-3a, 3b, and 3c were the same batch through the stage in which the ZP solution was refluxed with acacH at 98^{o}C (1 h). After that stage, the solution was divided into three parts. All the parts (ZrPM-3a, 3b, and 3c) were then processed in the standard way.

ZrPM-4a, 4b, and 4c were the same batch through the stage in which the ZP solution was refluxed with acacH at 80^{o}C (1 h). After that stage, the solution was divided into three parts. All the parts (ZrPM-4a, 4b, and 4c) were then processed in the standard way.

ZrPM-24a and ZrPM-24b were the same batch through the stage in which the ZP was refluxed with acacH at 145^{o}C (1 h). Batch ZrPM-24a was directly concentrated using the rotary evaporator and then dried. There were no acid addition, water addition (hydrolysis/condensation), or aging steps. The procedure used for batch ZrPM-24b was different from the standard method in that hydrolysis was carried out before the acid addition. The rest of the processing followed the standard procedure.

ZrPM-25a and 25b were the same batch through the stage in which the solution was aged at 45°C (1 h). After that stage, the solution was divided in two parts. One part (ZrPM-25a) was processed in the standard way. Phenolic resin was added to the other part (ZrPM-25b) (Case #5). The rest of the processing followed the standard procedure.

ZrPM-27a, 27b, and 27c were the same batch through the stage in which the solution was aged at 45°C (1 h). After that stage, the solution was divided into three parts. One part (ZrPM-27a) was processed in the standard way. Phenolic resin was added to a second portion (ZrPM-27b) (Case #5). The third portion (ZrPM-27c) was aged at 65°C (2 h), instead of at 45°C (1 h). The rest of the processing followed the standard procedure.

ZrPM-35 and ZrPM-36 were the same batch through the stage in which the ZP solution was refluxed with acacH at 170°C (3 h). After that stage, the solution was divided in two parts. One part (ZrPM-35) was processed in the standard way. The other part (ZrPM-36) was refluxed for an additional 3 h at 185°C and then processed in the standard way.

ZrPM-39 and ZrPM-40 were the same batch through the stage in which the water addition was made to the acac-modified ZP solution. After that stage, the solution was divided in two parts. One part (ZrPM-39) was aged at 65°C (3 h), while the other part (ZrPM-40) was aged at 50°C (2 h). The rest of the processing followed the standard procedure.

ZrPM-41 and ZrPM-42 were the same batch through the stage in which the water addition was made to the acac-modified ZP solution. After that stage, the solution was divided in two parts. One part (ZrPM-41) was aged at 50°C (2 h), while the other part

(ZrPM-42) was aged at 65°C (3 h). The rest of the processing followed the standard procedure.

ZrPM-46, ZrPM-49, and ZrPM-63 were discontinued because of extensive precipitation after the acacH-reflux step.

ZrPM-51, ZrPM-52, and ZrPM-53 were the same batch through the stage in which the ZP solution was refluxed with acacH (275°C, 3 h), partially concentrated, and had ethanol added back to the partially concentrated solution. The solution was then divided into three parts. The batches were prepared with three different amounts of water. The H_2O/Zr molar ratios were 8:1, 16:1, and 24:1 for batches ZrPM-51, ZrPM-52, and ZrPM-53, respectively. The rest of the processing followed the standard procedures.

ZrPM-54a and 54b were the same batch through the stage in which the solution was aged at 50°C (2 h). After that stage, the solution was divided in two parts. One part (ZrPM-54a) was processed in the standard way. Glycerol was added to the other part (ZrPM-54b) (Case #5). The solution was stored for 15 h before next processing step (i.e., concentration/solvent removal). The rest of the processing followed the standard procedure.

ZrPM-55a and 55b were the same batch through the stage in which the solution was aged at 50°C (2 h). After that stage, the solution was divided into two parts. One part (ZrPM-55a) was processed in the standard way. Glycerol was added to a second portion (ZrPM-55b) (Case #5). The rest of the processing followed the standard procedure.

ZrPM-56a, b, c, and d were the same batch through the stage in which the water addition was made to the acac-modified ZP solution. The solution was then divided into four parts. One part (ZrPM-56a) was processed in the standard way. Glycerol was added to two different portions (ZrPM-56b and 56d) before the 50°C (2 h) aging step (Case # 4).

Glycerol was added to another portion (ZrPM-56c) after the 50°C (2 h) aging step (Case # 5).The rest of the processing followed the standard procedures.

ZrPM-57a, b, and c were the same batch through the stage in which the water addition was made to the acac-modified ZP solution. The solution was then divided into three parts. The batches were prepared with three different amounts of glycerol which were added before the aging treatment (Case #4). The glycerol/Zr molar ratios were 1.03:1, 1.72:1, and 1.03:1 for batches ZrPM-57a, b, and c, respectively. The rest of the processing followed the standard procedures.

ZrPM-64a, 64b, and 64c were the same batch through the stage in which the ZP solution was refluxed with acacH (195°C, 2 h), partially concentrated, and had ethanol added back to the partially concentrated solution. The solution was then divided into three parts. The three parts were processed separately following the standard procedures.

4.1.2.5 Batches Prepared with ZTP

ZTP powder was transferred to a flask in a glove box (Labmaster 130, M. Braun, Stratham, NH) under an inert atmosphere (argon, 99.999% purity). The amount of ZTP transferred was ~1 g. This amount was equivalent to 0.00205 mol of ZTP (i.e., based on a molecular weight of 487.66 g/mol for the ZTP). The flask size used was in the range of 50 - 100 ml.

30 ml (~23.5 g) of distilled ethanol was used to dissolve the ZTP powder (i.e., 4 wt% ZTP/96 wt% ethanol). The ethanol was added to the flask in glove box. The flask was sealed with a glass stopper and the solution was mixed with a magnetic stirrer for ~30 min. Some amount of ZTP remained un-dissolved in the ethanol.

The sealed flask was taken out of the glove box. The acid solution was prepared as described in section 4.1.2.3.2 and was diluted for the same reason specified in that section. The acid was added to the ZTP solution using a 10 ml pipette. The rate of addition was approximately 10 ml/min. The solution was stirred continually (using a magnetic stirrer) during the addition and for approximately 1 min after the addition was complete. The pH of the solution was measured approximately 1 min after the mixing step was completed. Table 4.6 gives the measured pH values for each batch. The amount of acid added to the batch was based on reaching a targeted pH value and achieving complete dissolution of the ZTP. The amount of acid solution added was not explicitly measured by volume or weight but was later calculated by the method described in section 4.1.2.3.2. Table 4.6 gives the number of moles of acid added to each batch. This table also gives the HNO_3/Zr molar ratio. This ratio was calculated based on the initial number of moles of ZTP in the batch.

For most batches, water was used to promote hydrolysis and condensation reactions in the ZTP solution. Deionized water was first mixed with distilled ethanol in weight ratio of 10% water/90%. Dilution was carried out for the same reasons described in section 4.1.2.3.2. The water/ethanol solution was then added to the ZTP solution at a rate of approximately ~100 ml/min under constant stirring (using a magnetic stirrer). The solutions were transparent with no color. Table 4.6 gives the number of moles of water added to each batch. This table also gives the H_2O/Zr molar ratio. This ratio was calculated based on the initial number of moles of ZTP in the batch. The pH of the solution was measured ~1 min after the mixing step. Table 4.6 gives the measured pH values for each batch which had a water addition.

The flask was then sealed and placed in an air-oven (Isotemp 500 series, Fisher Scientific, Fair Lawn, NJ) at 45^{o}C for 1 h. The sealed flask was taken out of the air-oven after the heat treatment period and then left to cool for ~0.5 h at room temperature. The pH was measured for some batches (Table 4.6). Solvent was then removed from the solution using rotary evaporation. The flask was kept in constant contact with a water bath that was maintained at approximately 35 - 40^{o}C (Figure 4.6). The rate of solvent removal was ~100 - 200 ml/h. The solution was concentrated until solvent loss was no longer obvious. The flask was then sealed with aluminum foil that was perforated in order to allow removal of small amounts of residual solvent during the subsequent drying step. The flask was then placed in a vacuum oven and heated to 120^{o}C for 2h.

Table 4.3 Information on the batch component compositions and the refluxing and post-refluxing processing conditions for the synthesis of the ZrPM batches.

ZrPM Batch #	Zr Amount		Alcohol Diluent for ZP			AcacH (g)	Alcohol Diluent for AcacH			AcacH /Zr Molar Ratio	Reflux		Extent of conc. (n) (%)	Ethanol after conc.[b]
	(g)	(mol)		(g)	(Wt %)[a]			(g)	(Wt%)[a]		Temp .(°C)	Time (h)		
1a[c]	0.543	0.0060	1-butanol	35	7.5	1.20	1-butanol	2.4	33	2.0	103	1	To solid	-
1b[c]	0.120	0.0013	1-butanol	7.8	7.5	0.30	1-butanol	0.5	33	2.0	103	1	To solid	80
1c[c]	0.124	0.0014	1-butanol	8.0	7.5	0.30	1-butanol	0.5	33	2.0	103	1	To solid	80
1d[c]	0.125	0.0014	1-butanol	8.1	7.5	0.30	1-butanol	0.5	33	2.0	103	1	To solid	80
2[c]	0.912	0.01	1-butanol	59	7.5	6.00	1-butanol	4.0	60	6.0	100	1	To solid	-
3a[c]	0.141	0.0016	1-propanol	9.1	7.5	0.93	1-propanol	0.6	60	6.0	98	1	To solid	80
3b[c]	0.164	0.0018	1-propanol	11	7.5	1.10	1-propanol	0.7	60	6.0	98	1	To solid	80
3c[c]	0.146	0.0016	1-propanol	9.4	7.5	0.96	1-propanol	0.6	60	6.0	98	1	To solid	80
4a[c]	0.093	0.0010	ethanol	9.1	5.0	0.41	ethanol	0.9	32	4.0	80	1	To solid	80
4b[c]	0.086	0.0009	ethanol	8.4	5.0	0.38	ethanol	0.8	32	4.0	80	1	To solid	80
4c[c]	0.09	0.001	ethanol	8.8	5.0	0.40	ethanol	0.8	32	4.0	80	1	To solid	80
5[c]	0.602	0.0066	1-propanol	40	7.0	4.00	1-propanol	4.8	45	6.0	110	1	To solid	-
6[c]	0.602	0.0066	1-propanol	40	7.0	2.60	1-propanol	4.0	39	4.0	-	1	To solid	-
7[c]	0.611	0.0067	1-propanol	40	7.0	4.00	1-propanol	76	5	6.0	113	1	To solid	-
8[c]	0.611	0.0067	1-propanol	40	7.0	3.40	1-propanol	64	5	5.0	110	1	To solid	-
9[c]	0.091	0.001	1-propanol	5.9	7.5	0.40	1-propanol	7.6	5	4.0	101	1	To solid	-
10	0.091	0.001	ethanol	5.9	7.5	0.40	ethanol	7.6	5	4.0	94	1	To solid	-
11	0.098	0.0011	ethanol	5.9	7.5	0.40	ethanol	7.6	5	3.5	-	1	To solid	-
12[c]	0.098	0.0011	ethanol	5.9	7.5	0.30	ethanol	4.0	7	3.0	95	1	To solid	-
13[c]	0.091	0.001	1-butanol	5.9	7.5	0.30	1-butanol	4.0	7	3.0	110	1	To solid	-

Table 4.3 continued.

ZrPM Batch #	Zr Amount		Alcohol Diluent for ZP			AcacH (g)	Alcohol Diluent for AcacH			AcacH /Zr Molar Ratio	Reflux		Extent of conc. (n) (%)	Ethanol after conc.[b]
	(g)	(mol)		(g)	(Wt %)[a]			(g)	(Wt%)[a]		Temp .(°C)	Time (h)		
14[c]	0.091	0.001	ethanol	5.9	7.5	0.40	ethanol	7.6	5	3.5	111	1	To solid	-
15	0.091	0.001	ethanol	5.9	7.5	0.40	ethanol	7.6	5	3.5	111	1	To solid	80
16	0.091	0.001	ethanol	6.0	7.5	0.40	ethanol	7.6	5	4.0	115	1	To solid	80
17	0.091	0.001	ethanol	6.0	7.5	0.80	ethanol	15	5	8.0	117	1	To solid	80
18	0.091	0.001	ethanol	6.0	7.5	1.20	ethanol	23	5	12.0	113	1	To solid	80
19	0.195	0.0021	ethanol	19	5.0	5.10	ethanol	97	5	24.0	143	1	To solid	80
20	0.390	0.0043	ethanol	38	5.0	0.90	ethanol	8.1	10	2.0	120	1	To solid	80
21	0.195	0.0021	ethanol	19	5.0	4.30	ethanol	39	10	2.0	120	1	To solid	80
22	0.195	0.0021	ethanol	19	5.0	4.30	ethanol	39	10	2.0	129	1	To solid	80
23	0.195	0.0021	ethanol	19	5.0	4.30	ethanol	39	10	2.0	122	1	To solid	80
24a[c]	0.522	0.0057	ethanol	51	5.0	13.7	ethanol	124	10	24.0	145	1	To solid	-
24b[c]	0.195	0.0021	ethanol	19	5.0	5.14	ethanol	46	10	24.0	145	1	To solid	80
24c[c]	0.195	0.0021	ethanol	19	5.0	5.14	ethanol	46	10	24.0	145	1	To solid	80
25a	0.196	0.0021	ethanol	19	5.0	7.35	ethanol	66	10	34.0	125	1	To solid	80
25b	0.194	0.0021	ethanol	19	5.0	7.35	ethanol	66	10	34.0	125	1	To solid	80
26	0.195	0.0021	ethanol	19	5.0	10.7	ethanol	9.0	10	50.0	140	1	To solid	80
27a	0.16	0.0044	ethanol	16	5.0	4.19	ethanol	37	10	24.0	125	1	To solid	80
27b	0.158	0.0044	ethanol	16	5.0	4.14	ethanol	37	10	24.0	125	1	To solid	80
27c	0.079	0.0022	ethanol	7.8	5.0	2.07	ethanol	19	10	24.0	125	1	To solid	80
28	0.195	0.0021	ethanol	19	5.0	10.9	ethanol	44	20	50.0	145	3	To solid	80
29	0.195	0.0021	ethanol	19	5.0	10.9	ethanol	44	20	50.0	155	3	To solid	80

Table 4.3 continued.

ZrPM Batch #	Zr Amount		Alcohol Diluent for ZP			AcacH (g)	Alcohol Diluent for AcacH			AcacH /Zr Molar Ratio	Reflux		Extent of conc. (n) (%)	Ethanol after conc.[b]
	(g)	(mol)		(g)	(Wt %)[+]			(g)	(Wt%)[a]		Temp .(°C)	Time (h)		
30	0.195	0.0021	ethanol	19	5	5.2	ethanol	21	20	24.0	126	2.5	To solid	80
31	0.196	0.0022	ethanol	19	5	5.2	ethanol	21	20	24.0	125	2.5	30-35	80
32	0.195	0.0021	ethanol	19	5	10.7	ethanol	43	20	50.0	170	3	30-35	80
33	0.200	0.0022	ethanol	19	5	5.3	ethanol	21	20	24.0	127	2.5	To solid	80
34	0.198	0.0022	ethanol	19	5	5.2	ethanol	21	20	24.0	127	2.5	30-35	80
35	0.311	0.0034	ethanol	30	5	17.1	ethanol	68	20	50.0	170	3	30-35	80
36	0.180	0.0020	ethanol	18	5	9.9	ethanol	40	20	50.0	170 and 185	3 + 3	30-35	80
37	0.091	0.001	ethanol	9	5	0.4	ethanol	1.6	20	4.0	180	3	30-35	80
38	0.301	0.0033	ethanol	29	5	2.7	ethanol	11	20	8.0	186	3	30-35	80
39	0.294	0.0032	ethanol	28	5	1.3	ethanol	5.2	20	4.0	180	3	To solid	80
40	0.294	0.0032	ethanol	28	5	1.3	ethanol	5.2	20	4.0	180	3	To solid	80
41	0.584	0.0064	ethanol	57	5	2.6	ethanol	10	20	4.0	180	3	30-35	80
42	0.584	0.0064	ethanol	57	5	2.6	ethanol	10	20	4.0	180	3	30-35	80
43	0.296	0.0033	ethanol	29	5	1.3	ethanol	5.2	20	4.0	195	3	30-35	80
44	0.210	0.0023	ethanol	20	5	1.8	ethanol	7.2	20	8.0	185	3	30-35	80
45	14.23	0.156	ethanol	657	10	62.4	ethanol	249	20	4.0	130	3	30-35	13
46[d]	14.23	0.156	ethanol	657	10	62.4	ethanol	249	20	4.0	130	3	30-35	13
47	0.201	0.0022	ethanol	20	5	1.3	ethanol	5.2	20	6.0	225	3	30-35	80
48	0.198	0.0022	ethanol	19	5	1.7	ethanol	6.8	20	8.0	254	3	30-35	80

Table 4.3 continued.

ZrPM Batch #	Zr Amount		Alcohol Diluent for ZP			AcacH (g)	Alcohol Diluent for AcacH			AcacH /Zr Molar Ratio	Reflux		Extent of conc. (n) (%)	Ethanol after conc.[b]
	(g)	(mol)		(g)	(Wt %)[a]			(g)	(Wt%)[a]		Temp .(°C)	Time (h)		
49[e]	0.198	0.0022	ethanol	19	5	1.7	ethanol	6.8	20	8.0	284	3	-	-
50	0.593	0.0065	ethanol	58	5	2.6	ethanol		20	4.0	254	3	30-35	80
51	0.198	0.0022	ethanol	19	5	0.9	ethanol	3.6	20	4.0	275	3	30-35	80
52	0.196	0.0022	ethanol	19	5	0.9	ethanol	3.6	20	4.0	275	3	30-35	80
53	0.194	0.0021	ethanol	19	5	0.9	ethanol	3.6	20	4.0	275	3	30-35	80
54a	0.196	0.0022	ethanol	19	5	1.7	ethanol	6.8	20	8.0	250	3	30-35	80
54b	0.196	0.0022	ethanol	19	5	1.7	ethanol	6.8	20	8.0	250	3	30-35	80
55a	0.192	0.0022	ethanol	19	5	0.9	ethanol	3.4	20	8.0	195	3	30-35	80
55b	0.192	0.0022	ethanol	19	5	0.9	ethanol	3.4	20	8.0	195	3	30-35	80
56a	0.212	0.0023	ethanol	21	5	0.7	ethanol	2.8	20	3.0	195	3	30-35	80
56b	0.184	0.0020	ethanol	18	5	0.6	ethanol	2.4	20	3.0	195	3	30-35	80
56c	0.196	0.0021	ethanol	19	5	0.6	ethanol	2.6	20	3.0	195	3	30-35	80
56d	0.193	0.0021	ethanol	19	5	0.6	ethanol	2.6	20	3.0	195	3	30-35	80
57a	0.262	0.0029	ethanol	25	5	0.9	ethanol	3.5	20	3.0	195	3	30-35	80
57b	0.262	0.0029	ethanol	25	5	0.9	ethanol	3.5	20	3.0	195	3	30-35	80
57c	0.262	0.0029	ethanol	25	5	0.9	ethanol	3.5	20	3.0	195	3	30-35	80
58	14.23	0.156	ethanol	657	10	46.8	ethanol	187	20	3.0	195	3	30	13
59	14.23	0.156	ethanol	657	10	46.8	ethanol	187	20	3.0	195	3	30	13
60	14.23	0.156	ethanol	657	10	46.8	ethanol	187	20	3.0	195	3	30	13
61	14.23	0.156	ethanol	657	10	46.8	ethanol	187	20	3.0	195	3	30	13
62	2.924	0.0321	ethanol	135	10	9.6	ethanol	38	20	3.0	195	2	40-45	20

Table 4.3 continued.

ZrPM Batch #	Zr Amount		Alcohol Diluent for ZP			AcacH (g)	Alcohol Diluent for AcacH			AcacH /Zr Molar Ratio	Reflux		Extent of conc. (n) (%)	Ethanol after conc.[b]
	(g)	(mol)		(g)	(Wt %)[a]			(g)	(Wt%)[a]		Temp .(°C)	Time (h)		
63[e]	14.23	0.156	ethanol	657	10	46.8	ethanol	187	20	3.0	195	3	-	-
64a	1.949	0.021	ethanol	90	10	6.4	ethanol	26	20	3.0	195	2	40-45	20
64b	1.949	0.021	ethanol	90	10	6.4	ethanol	26	20	3.0	195	2	40-45	20
64c	1.949	0.021	ethanol	90	10	6.4	ethanol	26	20	3.0	195	2	40-45	20
65	2.924	0.0321	ethanol	135	10	9.6	ethanol	39	20	3.0	195	2	40-45	20
66	2.924	0.0321	ethanol	135	10	9.6	ethanol	39	20	3.0	195	2	40-45	20
67	2.924	0.0321	ethanol	135	10	9.6	ethanol	39	20	3.0	195	2	45-50	20
68	2.924	0.0321	ethanol	135	10	9.6	ethanol	39	20	3.0	195	2	40-45	20
69	2.924	0.0321	ethanol	135	10	9.6	ethanol	39	20	3.0	195	2	40-45	20
70	2.924	0.0321	ethanol	135	10	9.6	ethanol	39	20	3.0	195	2	40-45	20
71	2.924	0.0321	ethanol	135	10	9.6	ethanol	39	20	3.0	195	2	40-45	20
72	2.924	0.0321	ethanol	135	10	12.8	ethanol	51	20	4.0	195	2	40-45	20
73	2.924	0.0321	ethanol	135	10	9.6	ethanol	39	20	3.0	195	2	40-45	20
74	2.924	0.0321	ethanol	135	10	9.6	ethanol	39	20	3.0	195	2	40-45	20
75	2.924	0.0321	ethanol	135	10	9.6	ethanol	39	20	3.0	195	2	40-45	20
76	2.924	0.0321	ethanol	135	10	9.6	ethanol	39	20	3.0	195	2	40-45	20
77	2.924	0.0321	ethanol	135	10	9.6	ethanol	39	20	3.0	195	2	40-45	20
78	2.924	0.0321	ethanol	135	10	9.6	ethanol	39	20	3.0	195	2	40-45	20
79	2.924	0.0321	ethanol	135	10	9.6	ethanol	39	20	3.0	195	2	45-50	20
80	2.924	0.0321	ethanol	135	10	9.6	ethanol	39	20	3.0	195	2	40-45	20
81	2.924	0.0321	ethanol	135	10	9.6	ethanol	39	20	3.0	195	2	40-45	20

Table 4.3 continued.

ZrPM Batch #	Zr Amount		Alcohol Diluent for ZP			AcacH (g)	Alcohol Diluent for AcacH			AcacH /Zr Molar Ratio	Reflux		Extent of conc. (n) (%)	Ethanol after conc.[b]
	(g)	(mol)		(g)	(Wt %)[a]			(g)	(Wt%)[a]		Temp .(°C)	Time (h)		
82	2.924	0.0321	ethanol	135	10	9.6	ethanol	39	20	3.0	195	2	40-45	20
83	2.924	0.0321	ethanol	135	10	9.6	ethanol	39	20	3.0	195	2	40-45	20
84	2.924	0.0321	ethanol	135	10	9.6	ethanol	39	20	3.0	195	2	40-45	20
85	2.924	0.0321	ethanol	135	10	9.6	ethanol	39	20	3.0	195	2	40-45	20
86	14.61	0.1602	ethanol	675	10	48.1	ethanol	193	20	3.0	195	2	40-45	13
87	14.61	0.1602	ethanol	675	10	48.1	ethanol	193	20	3.0	195	2	35-40	13
88	14.61	0.1602	ethanol	675	10	48.1	ethanol	193	20	3.0	195	2	40-45	13
89	14.61	0.1602	ethanol	675	10	48.1	ethanol	193	20	3.0	195	2	40-45	13
90	14.61	0.1602	ethanol	675	10	48.1	ethanol	193	20	3.0	195	2	40-45	13
91	14.61	0.1602	ethanol	675	10	48.1	ethanol	193	20	3.0	195	2	40-45	13
92	14.61	0.1602	ethanol	675	10	48.1	ethanol	193	20	3.0	195	2	40-45	20
93	14.61	0.1602	ethanol	675	10	48.1	ethanol	193	20	3.0	195	2	40-45	20
94	14.61	0.1602	ethanol	675	10	48.1	ethanol	193	20	3.0	195	2	40-45	20
95	14.61	0.1602	ethanol	675	10	48.1	ethanol	193	20	3.0	195	2	40-45	20
96	14.61	0.1602	ethanol	675	10	48.1	ethanol	193	20	3.0	195	2	40-45	20
97	14.61	0.1602	ethanol	675	10	48.1	ethanol	193	20	3.0	195	2	35-40	20
98	14.61	0.1602	ethanol	675	10	48.1	ethanol	193	20	3.0	195	2	40-45	20
99	14.61	0.1602	ethanol	675	10	48.1	ethanol	193	20	3.0	195	2	40-45	20
100	14.61	0.1602	ethanol	675	10	48.1	ethanol	193	20	3.0	195	2	40-45	20

[a] Wt% is defined by amount of ZP or acacH divided by total solution weight (i.e., wt. of ZP or acacH plus wt. of diluent).
[b] Amount of ethanol added per gram of starting ZP solution.

Table 4.3 continued.

[c] Batches prepared by Greg Staab.
[d] Batch was discontinued after addition of ethanol after initial concentration. (Precipitates were formed in the solution because undistilled ethanol was used.)
[e] Batch was discontinued after acacH-reflux step because precipitates were formed in the solution. (Due to exposure to atmospheric moisture.)

Table 4.4 Amounts and types of external carbon sources added and their point of addition during processing.

ZrPM Batch Number	Phenolic (g)	Ethanol Diluent for Phenolic		Glycerol			Case #*
		(g)	(Wt. %)	(g)	(moles)	Glycerol/Zr molar ratio	
20	-	-	-	1.00	0.011	5.10	5
25 b	0.056	0.22	20	-	-	-	5
27 b	0.022	0.09	20	-	-	-	5
45	4.21	16.84	20	-	-	-	5
54 b	-	-	-	0.44	0.005	1.11	5
55 b	-	-	-	0.44	0.005	1.11	5
56 b	-	-	-	0.10	0.001	0.52	4
56 c	-	-	-	0.10	0.001	0.52	3
56 d	-	-	-	0.05	0.001	0.26	4
57 a	-	-	-	0.82	0.009	1.03	4
57 b	-	-	-	1.36	0.015	1.72	4
57 c	-	-	-	0.82	0.009	1.03	4
58	-	-	-	14.78	0.161	1.03	3
59	-	-	-	24.66	0.268	1.72	3
79	-	-	-	1.86	0.020	0.63	3
80	-	-	-	1.86	0.020	0.63	1
81	-	-	-	1.86	0.020	0.63	3
82	-	-	-	1.01	0.011	0.34	1
83	-	-	-	1.01	0.011	0.34	3
84	-	-	-	1.05	0.011	0.36	1
85	-	-	-	0.50	0.005	0.17	3
86	-	-	-	4.00	0.044	0.27	3
87	-	-	-	3.50	0.038	0.24	3

Table 4.4 continued.

ZrPM Batch Number	Phenolic (g)	Ethanol Diluent for Phenolic		Glycerol			Case #*
		(g)	(Wt. %)	(g)	(moles)	Glycerol/Zr molar ratio	
88	-	-	-	2.53	0.028	0.17	3
89	-	-	-	1.80	0.020	0.12	3
90	-	-	-	1.01	0.011	0.07	3
91	-	-	-	4.23	0.046	0.29	3
92	-	-	-	4.23	0.046	0.29	3
93	-	-	-	2.21	0.024	0.15	3
94	-	-	-	7.45	0.081	0.51	3
95	-	-	-	11.04	0.120	0.70	3
96	5.03	20.12	20	-	-	-	3
97	4.66	18.64	20	-	-	-	5
98	4.01	16.04	20	-	-	-	5
99	4.25	17.00	20	-	-	-	5
100	-	-	-		0.073	0.45	3

* Case #s are defined in section 4.1.2.3.

Table 4.5 Information on the batch component compositions, the aging conditions, and the pH values at different processing stages for the synthesis of the ZrPM batches.

ZrPM Batch Number	pH before acid addition	HNO_3 addition				pH after acid addition	H_2O addition			pH after water addition	Aging		pH after aging treatment
		Acid / ethanol (wt%)	Moles of acid added	HNO_3/Zr molar ratio	Moles of water from acid		Water/ ethanol (wt%)	Moles of water added	H_2O/Zr molar ratio		Temp. (^oC)	Time (h)	
1a	-	-	-	-	-	-	-	-	-	-	-	-	-
1b	9.3	10	0.0070	5.303	0.0120	3.2	10	0.0317	24	4.75	45-50	1	-
1c	8.0	10	0.0015	1.103	0.0025	6.0	10	0.0327	24	-	45-50	1	-
1d	8.0	10	0.0001	0.073	0.0002	6.9	10	0.0328	24	7.3	45-50	1	-
2	-	-	-	-	-	-	-	-	-	-	-	-	-
3a	6.6	10	0.0074	4.787	0.0122	3.5	10	0.0371	24	-	45-50	1	-
3b	6.6	10	0.0011	0.613	0.0018	5.8	10	0.0430	24	-	45-50	1	-
3c	6.9	10	0.0002	0.125	0.0004	7.3	10	0.0384	24	-	45-50	1	-
4a	8.2	10	0.0023	2.255	0.0038	3.2	10	0.0245	24	-	45-50	1	-
4b	7.2	10	0.0005	0.534	0.0008	5.7	10	0.0225	24	-	45-50	1	-
4c	7.5	10	0.0001	0.101	0.0002	7.7	10	0.0238	24	-	45-50	1	-
5	-	-	-	-	-	-	-	-	-	-	-	-	-
6	-	-	-	-	-	-	-	-	-	-	-	-	-
7	-	-	-	-	-	-	-	-	-	-	-	-	-
8	-	-	-	-	-	-	-	-	-	-	-	-	-
9	-	-	-	-	-	-	-	-	-	-	-	-	-
10	-	-	-	-	-	-	-	-	-	-	-	-	-
11	-	-	-	-	-	-	-	-	-	-	-	-	-
12	-	-	-	-	-	-	-	-	-	-	-	-	-
13	-	-	-	-	-	-	-	-	-	-	-	-	-
14	-	-	-	-	-	-	-	-	-	-	-	-	-

Table 4.5 continued.

ZrPM Batch Number	pH before acid addition	HNO_3 addition				pH after acid addition	H_2O addition			pH after water addition	Aging		pH after aging treatment
		Acid / ethanol (wt%)	Moles of acid added	HNO_3/Zr molar ratio	Moles of water from acid		Water/ ethanol (wt%)	Moles of water added	H_2O/Zr molar ratio		Temp. (°C)	Time (h)	
15	8.6	10	0.0005	0.45	0.001	6.0	10	0.024	24	6	45-50	1	-
16	9.4	10	0.0005	0.5	0.001	5.9	10	0.024	24	5.8	45-50	1	-
17	8.1	10	0.0013	1.27	0.002	4.4	10	0.024	24	4.6	45-50	1	-
18	7.6	10	0.0012	1.22	0.002	4.3	10	0.024	24	4.6	45-50	1	-
19	7.8	10	0.0022	1.005	0.004	4.5	10	0.051	24	4.02	45-50	1	-
20	10.3	10	0.0028	0.656	0.005	-	10	0.103	24	4.9	45-50	1	-
21	10.1	10	0.0043	2.009	0.007	2.9	10	0.051	24	3.5	45-50	1	-
22	8.0	10	0.0001	0.047	0.000	7.2	10	0.051	24	6.8	45-50	1	-
23	8.8	10	0.0005	0.21	0.001	7.9	10	0.051	24	-	45-50	1	-
24a	-	-	-	-	-	-	-	-	-	-	-	-	-
24b	7.2	10	0.006	2.804	0.0102	4. 5	10	0.0514	24	-	45-50	1	-
24c	7.2	10	0.005	2.336	0.0083	4.5	10	0.0514	24	-	45-50	1	-
25a	7.0	10	0.0016	0.748	0.0025	4.6	10	0.0514	24	4.5	45-50	1	-
25b	7.0	10	0.0016	0.748	0.0025	4.6	10	0.0514	24	4.5	45-50	1	-
26	7.5	10	0.0022	1.005	0.004	4.6	10	0.0514	24	4.56	45-50	1	-
27a	7.4	10	0.0016	0.368	0.0028	4.5	10	0.104	24	4.6	45-50	1	-
27b	7.4	10	0.0016	0.368	0.0028	4.5	10	0.104	24	4.6	45-50	1	-
27c	7.4	10	0.0008	0.369	0.0014	4.5	10	0.052	24	4.6	65	2	-
28	7.5	10	0.0019	0.888	0.003	4.5	10	0.0514	24	4.3	45-50	1	-
29	7.0	10	0.0014	0.654	0.002	4.5	10	0.0514	24	4.5	66	3	-
30	7.4	10	0.0024	1.121	0.004	4.5	10	0.0514	24	4.3	50	2	-

Table 4.5 continued.

ZrPM Batch Number	pH before acid addition	HNO_3 addition				pH after acid addition	H_2O addition			pH after water addition	Aging		pH after aging treatment
		Acid / ethanol (wt%)	Moles of acid added	HNO_3/Zr molar ratio	Moles of water from acid		Water/ ethanol (wt%)	Moles of water added	H_2O/Zr molar ratio		Temp. (^oC)	Time (h)	
31	6.9	10	0.0011	0.512	0.002	4.6	10	0.0516	24	4.5	50	2	-
32	6.8	10	0.0010	0.467	0.002	4.6	10	0.0514	24	4.6	65	3	-
33	7.0	10	0.0018	0.822	0.003	4.5	10	0.0526	24	-	50	2	-
34	7.0	10	0.0013	0.598	0.002	4.5	10	0.0522	24	4.5	50	2	-
35	6.9	10	0.0018	0.513	0.003	4.5	10	0.082	24	4.5	50	2	-
36	7.0	10	0.0011	0.558	0.002	4.5	10	0.0473	24	4.5	50	2	-
37	8.6	10	0.0012	1.22	0.002	5.9	10	0.024	24	5.9	50	2	-
38	7.2	10	0.0003	0.076	0.000	5.9	10	0.0788	24	6.1	50	2	-
39	8.5	10	0.0012	0.356	0.002	5.8	10	0.0775	24	5.9	65	3	-
40	8.5	10	0.0012	0.356	0.002	5.8	10	0.0775	24	5.9	50	2	-
41	8.6	10	0.0022	0.344	0.004	5.9	10	0.1536	24	-	50	2	-
42	8.6	10	0.0022	0.344	0.004	5.9	10	0.1536	24	-	65	3	-
43	9.2	10	0.0015	0.462	0.003	5.8	10	0.052	16	5.5	50	2	-
44	7.1	10	0.0005	0.217	0.001	5.5	10	0.0552	24	5.8	50	2	-
45	8.9	20	0.0062	0.04	0.010	6.9	20	3.744	24	-	50	2	-
46	-	-	-	-	-	-	-	-	-	-	-	-	-
47	7.3	10	0.0005	0.227	0.001	5.9	10	0.0533	24	6.15	50	2	-
48	7.6	10	0.0005	0.23	0.001	5.9	10	0.052	24	-	50	2	-
49	-	-	-	-	-	-	-	-	-	-	-	-	-
50	7.6	10	0.0005	0.077	0.001	5.9	10	0.156	24	-	50	2	-
51	8.1	10	0.0020	0.922	0.003	5.9	10	0.0174	8	-	50	2	-

Table 4.5 continued.

ZrPM	pH before acid addition	HNO_3 addition				pH after acid addition	H_2O addition			pH after water addition	Aging		pH after aging treatment
		Acid / ethanol (wt%)	Moles of acid added	HNO_3/Zr molar ratio	Moles of water from acid		Water/ ethanol (wt%)	Moles of water added	H_2O/Zr molar ratio		Temp. (^oC)	Time (h)	
52	8.6	20	0.0016	0.744	0.003	5.9	10	0.0347	16	-	50	2	-
53	8.5	20	0.0015	0.723	0.003	5.9	10	0.051	24	-	50	2	-
54a	7.4	20	0.0005	0.233	0.001	5.9	10	0.0345	16	6.1	50	2	-
54b	7.4	20	0.0005	0.233	0.001	5.9	10	0.0345	16	6.1	50	2	-
55a	8.1	20	0.0010	0.463	0.002	5.9	10	0.035	16	6.15	50	2	-
55b	8.1	20	0.0010	0.463	0.002	5.9	10	0.035	16	6.15	50	2	-
56a	10.1	20	0.0001	0.047	0.0003	5.9	10	0.056	24	6.7	50	2	-
56b	10.1	20	0.0001	0.047	0.0002	5.9	10	0.048	24	6.7	50	2	-
56c	10.1	20	0.0001	0.045	0.0003	5.9	10	0.051	24	6.7	50	2	-
56d	10.1	20	0.0001	0.047	0.0003	5.9	10	0.051	24	6.7	50	2	-
57a	10.1	20	0.0005	0.174	0.0007	5.9	10	0.069	24	6.7	50	2	-
57b	10.1	20	0.0005	0.174	0.0007	5.9	10	0.069	24	6.7	50	2	-
57c	10.1	20	0.0005	0.174	0.0007	5.9	10	0.069	24	6.7	50	2	-
58	-	20	0.0120	0.077	0.020	-	20	3.744	24	-	50	2	-
59	-	20	0.0136	0.087	0.023	-	20	3.744	24	-	50	2	-
60	-	20	0.0128	0.082	0.0215	-	20	3.744	24	-	50	2	-
61	-	20	0.0128	0.082	0.0215	-	20	3.744	24	-	50	2	-
62	10	10	0.0070	0.218	0.012	5.4	10	0.77	24	6	50	2	5.4
63	-	-	-	-	-	-	-	-	-	-	-	-	-
64a	9.3	10	0.0013	0.062	0.0023	6.2	10	0.5	24	6.43	50	2	5.3
64b	9.6	10	0.0013	0.062	0.0023	6.2	10	0.5	24	6.38	50	2	5.3

Table 4.5 continued.

ZrPM Batch Number	pH before acid addition	HNO_3 addition				pH after acid addition	H_2O addition			pH after water addition	Aging		pH after aging treatment
		Acid / ethanol (wt%)	Moles of acid added	HNO_3/Zr molar ratio	Moles of water from acid		Water/ ethanol (wt%)	Moles of water added	H_2O/Zr molar ratio		Temp. (^oC)	Time (h)	
64c	9.5	10	0.0013	0.062	0.0023	6.3	10	0.5	24	6.50	50	2	5.3
65	10.5	10	0.0070	0.218	0.012	5.5	10	0.77	24	6.11	50	2	4.6
66	9.7	10	0.0040	0.124	0.007	7.0	10	0.77	24	7.3	50	2	7.0
67	9.5	10	0.0087	0.27	0.015	4.4	10	0.77	24	5.26	50	2	4.4
68	9.5	10	0.0112	0.35	0.019	4.0	10	0.77	24	4.38	50	2	-
69	9.6	10	0.0087	0.27	0.015	4.5	10	0.77	24	5.27	50	2	4.3
70	9.6	10	0.0112	0.35	0.019	4.1	10	0.77	24	4.37	50	2	3.8
71	9.6	10	0.0087	0.27	0.015	4.8	10	0.512	16	5.56	50	2	4.6
72	8.4	10	0.0087	0.27	0.015	4.2	10	0.77	24	5.06	50	2	4.3
73	9.5	10	0.0087	0.27	0.015	4.6	10	0.512	16	5.31	50	2	4.2
74	9.1	10	0.0071	0.22	0.012	4.6	10	0.256	8	5.05	50	2	4.3
75	9.4	10	0.0137	0.421	0.023	3.8	10	0.77	24	3.62	50	2	3.4
76	9.6	10	0.0112	0.35	0.019	4.1	10	0.77	24	4.29	50	2	3.7
77	9.6	10	0.0137	0.421	0.023	3.6	10	0.385	12	3.39	50	2	3.4
78	9.4	10	0.0137	0.421	0.023	3.7	10	0.77	24	3.46	50	2	3.4
79	9.5	10	0.0087	0.272	0.015	5.8	10	0.77	24	5.39	50	2	5.0
80	9.7	10	0.0087	0.272	0.015	4.3	10	0.77	24	4.5	50	2	4.5
81	9.0	10	0.0087	0.272	0.015	5.6	10	0.77	24	5.3	50	2	4.9
82	9.8	10	0.0087	0.272	0.015	4.3	10	0.77	24	4.4	50	2	4.6
83	9.4	10	0.0087	0.272	0.015	5.4	10	0.77	24	5.6	50	2	-
84	9.9	10	0.0087	0.272	0.015	4.4	10	0.77	24	4.8	50	2	4.4

Table 4.5 continued.

ZrPM Batch Number	pH before acid addition	HNO_3 addition				pH after acid addition	H_2O addition			pH after water addition	Aging		pH after aging treatment
		Acid / ethanol (wt%)	Moles of acid added	HNO_3/Zr molar ratio	Moles of water from acid		Water/ ethanol (wt%)	Moles of water added	H_2O/Zr molar ratio		Temp. (^oC)	Time (h)	
85	9.4	10	0.0087	0.272	0.015	5.2	10	0.77	24	5.6	50	2	4.7
86	10.4	10	0.0440	0.272	0.073	5.3	20	3.845	24	6.0	50	2	5.4
87	10.3	10	0.0440	0.272	0.073	5.3	20	3.845	24	6.2	50	2	5.3
88	10.3	10	0.0440	0.272	0.073	5.4	20	3.845	24	6.5	50	2	-
89	10.1	10	0.0440	0.272	0.073	5.1	20	3.845	24	6.0	50	2	4.9
90	10.3	10	0.0440	0.272	0.073	5.3	20	3.845	24	6.2	50	2	5.1
91	10.2	10	0.0440	0.272	0.073	5.6	20	3.845	24	6.4	50	2	5.6
92	10.5	10	0.0440	0.272	0.073	5.2	10	3.845	24	5.9	50	2	4.8
93	10.1	10	0.0440	0.272	0.073	4.9	10	3.845	24	5.8	50	2	4.7
94	9.9	10	0.0440	0.272	0.073	5.8	10	3.845	24	6.0	50	2	5.2
95	10.0	10	0.0440	0.272	0.073	5.8	10	3.845	24	5.6	50	2	5.2
96	10.0	10	0.0440	0.272	0.073	4.7	10	3.845	24	5.2	50	2	4.3
97	9.9	10	0.0440	0.272	0.073	4.9	10	3.845	24	5.3	50	2	4.4
98	9.7	10	0.0440	0.272	0.073	4.6	10	3.845	24	5.3	50	2	4.3
99	9.9	10	0.0440	0.272	0.073	5.1	10	3.845	24	5.8	50	2	4.6
100	9.9	10	0.0440	0.272	0.073	5.7	10	3.845	24	6.1	50	2	5.3

Table 4.6 Amounts of acid and water added and the pH values during various stages of synthesis from ZTP precursor.

Batch number	pH before acid addition	Acid		pH after acid addition	Water		pH after water addition	pH after 45°C/1h treatment
		Mol	HNO_3/Zr molar ratio		Mol	H_2O/Zr molar ratio		
ZTP-H1	-	0.011	5.5	3.9	0.626	16	3.9	n.a.
ZTP-H2	-	0.022	10.5	4.5	0.843	24	3.6	n.a.
ZTP-H4	-	0.025	12.2	4.6	0.000	0	n.a.	n.a.
ZTP-H5	-	0.020	10.0	3.7	0.074	2	3.6	4.0
ZTP-H6	-	0.019	9.4	3.7	0.884	24	-	3.6
ZTP-H7	-	0.019	9.4	4.5	0.890	24	4.4	4.3
ZTP-H8	-	0.041	19.9	3.0	0.890	24	2.9	3.0
ZTP-H9	-	0.018	8.6	4.5	0.074	2	4.6	n.a.
ZTP-H10	-	0.016	7.7	4.5	0.000	0	n.a.	n.a.

4.1.3 Drying and Sieving

After rotovapping to remove solvent, samples were dried at 120^{o}C for 2 h under vacuum. The consistency and extent of agglomeration of the dried samples varied widely. Some samples would flow somewhat freely like a powder, while others were in the form of a powder "cake." To obtain powders with more uniform consistency, all of the dried samples were first manually ground up using a quartz mortar and pestle (SPI Supplies, West Chester, PA) and then screened through a sieve (Fisher Scientific, Fair Lawn, NJ) with 150 mesh-size openings. The force applied during grinding was relatively small in order to minimize the possibility of contamination from the mortar and pestle.

4.1.4 Pyrolysis

The sieved powders (from section 4.1.3) were transferred into alumina “boats” (Vesuvius McDanel, Beaver Falls, PA) for pyrolysis in a tube furnace (Model 55031, Lindberg, Watertown, WI). The alumina boats used for pyrolysis were 6 x 0.5 x 0.5 inches in dimensions for larger sample sizes (10 – 16 g). For smaller batch sizes (0.1 – 0.3 g), cylindrical alumina crucibles (0.4 inches diameter, 0.4 inches high) were used for pyrolysis. The heating rate for all the pyrolysis experiments was 2^{o}C/min to the desired temperature with a hold of 2 h at the maximum temperature. The pyrolysis experiments were done in flowing (100 ml/min) argon (Ar, >99.999%, Airgas, Randor, PA) atmosphere. The temperature range for most pyrolysis experiments was 800^{o}C to 1100^{o}C. (However, lower temperatures were used in several experiments.) The temperature was controlled using a Type K thermocouple. The furnace was allowed to cool naturally by switching off the power supply. The weights of alumina boats and powder samples were

recorded before and after the pyrolysis to determine the powder yields. For the rest of this thesis, powders that were given a pyrolysis heat treatment will be referred to as "pyrolyzed powders."

C/Zr molar ratios in 1100°C-pyrolyzed samples were estimated by oxidative combustion of the carbon in the samples. The heating rate for all experiments was 5°C/min to 1100°C with a hold of 1 h at the maximum temperature. These experiments were done in a flowing air (100 ml/min, moisture-free) atmosphere. The weight losses that occurred during oxidative combustion of pyrolyzed samples were determined by measuring the sample weight (using an analytical balance) before and after the heat treatment. The C/Zr molar ratios were then estimated from the weight losses by assuming that the (pyrolyzed) material consisted of only ZrO_2 and C.

4.1.5 Carbothermal Reduction Reaction

Pyrolyzed samples were heat treated in argon at temperatures in the range of 1100°C to 2000°C. In most cases, these heat treatments were carried out so that carbothermal reduction reactions would occur in the pyrolyzed zirconia/carbon mixtures. For some samples, the heat treatments carried out at the highest temperatures (usually ≥1800°C) were above that required to complete the carbothermal reduction reactions.

Most heat treatments at temperatures <1500°C were carried out in a three-zone furnace (Model 54259, Lindberg, Watertown, WI) under flowing argon (Ar, >99.999%, Airgas, Randor, PA) atmosphere. The flow rate of Ar was in the range of 100 – 500 ml/min. Trace amounts of water and/or oxygen in the as-received argon were reduced by passing the argon through a gettering furnace (Model 2-3200, Supelco Carrier Gas Purfier,

Sigma Aldrich, St. Louis, MO). Silicon carbide (SiC) heating elements (SE016x05x0.05, Starbar, Akron, NY) were used to heat the furnace. The mullite furnace tube (MV0161830060000, Vesuvius Mcdanel, Beaver Falls, PA) was 60 inches in length and had internal and external diameter of 1.75 and 2.0 inches respectively. The samples were placed in the center of the furnace tube. Table 4.7 shows temperatures measured at three locations in the furnace. The measurements were made using a static air atmosphere. The "control temperature" was measured by a thermocouple that was interfaced with the furnace controller and was used to control the furnace temperature. The thermocouple used was a Type B (94%Pt/6%Rh vs. 70%Pt/30%Rh); (Omega Engineering, Stamford, CT). This thermocouple was not located inside of the furnace tube where the samples had been placed for heat treatment. Instead, the thermocouple was in the surrounding region of the furnace where the insulation and the heating elements were located. The temperatures reported at various positions inside the furnace tube were recorded using a separate thermocouple (also Type B, Omega Engineering, Stamford, CT). The values listed are average values obtained from measurements that were recorded by inserting the thermocouple from both ends of the furnace. These measurements were carried out under conditions in which both ends of the furnace tube were open. During the sample heat treatments, however, the ends of the furnace tube were sealed, so it might be expected that these temperatures would show a "flatter profile" along the length of the tube. The temperatures reported in this study for the sample heat treatments carried out in this furnace are those from the "control thermocouple." The temperatures were not corrected for the offset between the temperature recorded by the "control thermocouple" and the temperature

Table 4.7 Temperature profile of three-zone Lindberg furnace.

Control Temperature	Thermocouple reading at various positions inside the furnace tube		
	Upstream side (- 5 inches)	Center (0 inches)	Downstream side (+ 5 inches)
1450°C	1445°C	1465°C	1455°C
1300°C	1318°C	1313°C	1308°C
1200°C	1218°C	1213°C	1214°C

recorded for the thermocouple placed in the center of the furnace tube. Table 4.7 indicates that the offset is approximately on the order of 15°C.

For temperatures >1500°C heat treatments were done in an "M-11" furnace (Model M11, Centorr Furnace, Nashua, NH) under flowing argon (Ar, >99.999%, Airgas, Randor, PA) atmosphere. The flow rate of Ar was ~500 ml/min. Trace amounts of water and/or oxygen in the as-received argon were reduced by passing the argon through a gettering furnace with a Ti charge (Model 2B200 120V, Centorr Associates Inc., Nashua, NH). The heating element was made of graphite and also served as the furnace tube. The temperature was measured at the center of the furnace tube by a Type C (95%W/5%Re vs. 74%W/26%Re) thermocouple (W5-.01-125-M-H-U-LP-16, Flow Autoclave System Inc., Columbus, OH) with a Mo sheath. The samples were placed in the center of the furnace tube, i.e., the temperature was measured essentially at the top of the samples. The thermocouple had an offset of +5°C as determined by melting of pure copper metal pieces. Thus, the furnace was heated to 5°C above the desired temperature. (For example, if

1800°C was the desired temperature, then the furnace was heated to 1805°C to compensate for the offset of the thermocouple.)

The ramping rate for the heat treatments was usually 5°C/min to the desired temperature with a hold of 2 h at the maximum temperature. Some samples were given additional heat treatments after an initial CTR treatment at temperatures in the range of 1200–1500°C. If the additional heat treatment was carried out in the M11 furnace, then heating rate was increased to 20°C/min for heating to the temperature of the first heat treatment and this was followed by 5°C/min to the desired temperature with a hold of 2 h at the maximum temperature.

Graphoil® (Electrical conductive grade, Graphoil®, UCAR Carbon Company Inc., Cleveland, OH) was used to form containers for all powder heat treatments at temperatures <1500°C. The Graphoil® was shaped in the form of an open rectangular tray or box (with no top cover). The containers are referred to as "graphoil boats." The dimensions of the graphoil boats varied depending upon the size of sample used in the heat treatment. Larger trays (7" x 1.5" x 0.25") were used for large samples (~6-8 g). Smaller trays (1" x 0.75" x 0.25") were used for small samples (<2 g). In most cases, the graphoil boats were of sufficient size such that the powder sample could be loosely spread to form a layer ~1–2 mm in thickness. The channels were made in the powder to promote the gas flow, as shown in Figure 4.8.

The weights of graphoil boat and powder sample were recorded before each experiment. The powder was placed in the boat and then the boat was placed inside the tube furnace. The position of the boat in the furnace tube was always kept the same so that similar conditions could be obtained for different heat treatment experiments.

"ZrC" substrates were used for some experiments in which samples were heat treated at temperatures ≥1600^{o}C. These substrates were prepared in-house using powder from batch ZrPM-61. The samples were made by dry pressing the powder and by subsequent sintering at 1800^{o}C for 4 h. (The detailed procedures are described in section 4.3.1.1.) These samples were not pure ZrC, but also had some free carbon. This was indicated from analyses of the carbon content by the "LECO method." The results of these analyses are given in section 5.6.1.3.1.

For cooling, the power to the three-zone furnace was switched off and the furnace was allowed to cool naturally. The M-11 furnace was programmed to cool at a rate of 50^{o}C/min to room temperature. (However, cooling slowed to less than 50^{o}C/min after the temperature decreased ~400^{o}C below the isothermal hold temperature.) The samples were then taken out of the furnace and the weights for the substrate and powder samples were recorded.

For the rest of this thesis, powders which were given a carbothermal reduction heat treatment will be referred to as either "CTR powders" or "carbothermally-reduced powders."

4.1.6 Milling of Powder Samples

Some of the carbothermally-reduced powder samples were milled to break down “soft” agglomerates using a Spex mill (Model 8000, Spex Certiprep, Metuchen, NJ). In the spex mill, the “vial is swung back and forth in a shallow arc, its ends are displaced laterally in a “figure-8”; this distributes the grinding-ball impact over wide areas of the caps”.[62]

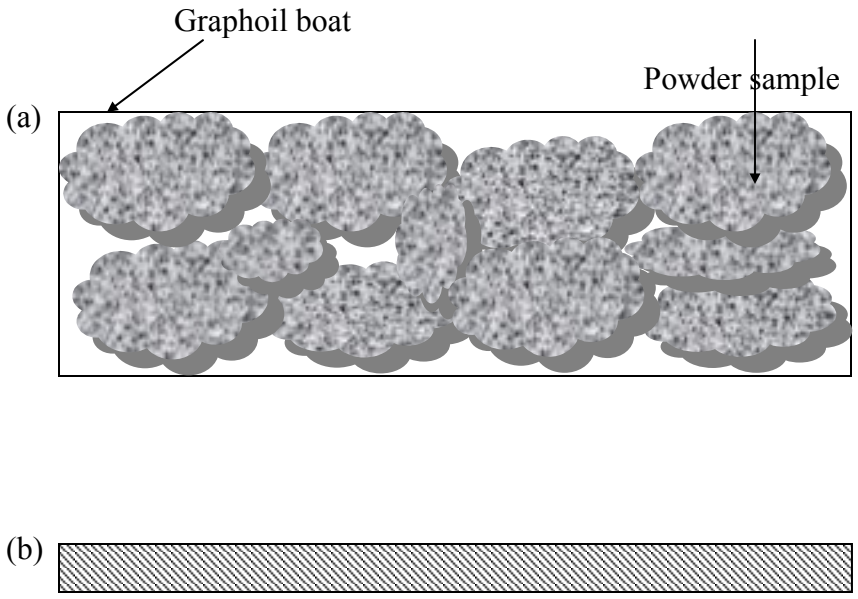

Figure 4.8 a) Top view of the Graphoil boat with powder sample b) Front view of the Graphoil boat.

The powder samples were milled in a methacrylate vial (cylinder shaped with 1.5 cm diameter and 5 cm in length). The amount of powder samples used was in the range of 1.5 – 1.6 g. The vial had Derlin® slip-on end caps that were lined with tungsten carbide (WC) inserts. The grinding media for most millings was single zirconia ball (Spex Certiprep, Metuchen, NJ) (10.5 mm in diameter). For some samples two WC balls (Spex Certiprep, Metuchen, NJ) (~8 mm in diameter) were used for milling. The time of milling was in the range of 10 – 40 min.

In most of the samples, to ensure proper milling, powder was scratched off the walls of milling vial after every 2 minutes of milling. For larger sample size, the milling

procedure was repeated and different milled powder batches were mixed and the mixed batch was used for subsequent characterization of the particle size distribution. The milled powders were mixed using a procedure similar to the mixing procedure that is described later in section 4.2.3.3.1.

4.2 Techniques for powder characterization

4.2.1 Thermogravimetric Analysis Measurements

Thermogravimetric analysis was done on powder samples using TGA (Model STA 409, Netzsch, Exton, PA). In-situ measurements of the weight change as a function of temperature were made using as-dried unpyrolyzed powders, pyrolyzed powders, and CTR powders. The former samples were heat treated in a flowing argon atmosphere in order to study the pyrolytic decomposition behavior of the precursors (The argon was passed through a getter furnace (Model 2-3200) as described in section 4.1.5). Experiments with the pyrolyzed and CTR powders were carried in a flowing air atmosphere in order to remove carbon (i.e., via oxidative combustion) from the samples. Based on the weight loss during such a heat treatment, it was possible to obtain an estimate of the weight percent carbon that was originally in the sample.

TGA experiments were carried out using 100 – 200 mg of powder. Samples were initially dried at 120^{o}C (3 h) in vacuum. Powder was placed in an alumina crucible and the crucible was then placed in the TGA head. For the experiments carried out in flowing argon, the furnace chamber was sealed and initially evacuated at a controlled rate using an evacuation valve. The evacuation rate was critical because if the rate was too high then the powder in the crucible spilled out making the weight change measurements useless. For all the measurements, the evacuation valve was opened such that it took about 5 min to get to the desired vacuum level (~10 torr). The valve was then opened fully and the chamber was left to evacuate for 1 min before the valve was closed. Argon gas was used to refill the chamber and the rate of argon addition was also controlled. After the pressure inside the chamber reached slightly above the atmospheric pressure, the leak valve was

opened to allow extra argon to flow out of the chamber. The flow of argon gas was then continued in order to purge the chamber for another 30 min. The TGA experiment was then started. The argon gas flow in the chamber during the TGA experiments was kept constant at ~100 ml/min. The heating rate for most weight loss measurements in argon was 10^{o}C/min to 150^{o}C, 5^{o}C/min to 175^{o}C, 2.5^{o}C/min to 550^{o}C, 10^{o}C/min to 1100^{o}C and hold of 1h at 1100^{o}C. One experiment was carried out to get information on weight loss that occurred during CTR. In this experiment, the starting material was an 800^{o}C-pyrolyzed powder. The sample was heated at 10^{o}C/min to 800^{o}C, then 1^{o}C/min to 1425^{o}C, and then held at 1425^{o}C for 2 h.

For TGA experiments carried out using air, the chamber was purged with flowing air (100 ml/min, moisture-free) for 30 min before heating was started. The heating rate was 5^{o}C/min to 1100^{o}C with a hold of 1 h. The TGA had two thermocouples; one was used to control the furnace temperature ("control thermocouple") and one was used to measure the temperature close to the sample ("sample thermocouple"). The reported temperatures in this study were those determined with the sample thermocouple. In order to obtain the desired sample temperature, it was necessary to program the furnace controller such that the reading for the "control thermocouple" was approximately 25^{o}C higher than the reading for the "sample thermocouple."

In addition to the in-situ weight losses measured by TGA, the weight losses that occurred during oxidative combustion of pyrolyzed and CTR samples were checked via ex-situ weight measurements made (using an analytical balance) on samples before and after they were heat treated. The alumina crucibles were weighed using an analytical balance (Model AX205, Mettler Toledo, Switzerland) both before and after the TGA

analysis was performed. The difference between the weights determined by the external analytical balance and the TGA balance were generally in the range of 1-1.5 mg.

C/Zr molar ratios in pyrolyzed samples were estimated by oxidative combustion of the carbon in the samples. The pyrolyzed samples were heated in the TGA furnace at 5^{o}C/min to 1100^{o}C with a hold of 1 h at the maximum temperature. The atmosphere was flowing air (100 ml/min, moisture-free). The C/Zr molar ratio in the starting (pyrolyzed) material was estimated from the weight loss which was assumed to be entirely due to oxidative combustion of the carbon. It was also assumed that the original sample consisted only of ZrO_2 and C.

4.2.2 Surface Area Measurements by Gas Adsorption

Surface area measurements on heat-treated powders was carried out using the nitrogen gas adsorption method (Model ASAP 2000, Micromeritics, Norcross, GA).

The powder samples were degassed (out-gassed) at temperatures ranging from 300^{o}C to 400^{o}C for 2-3 h to remove any volatiles (i.e., mostly adsorbed water). The gas absorbate used for the measurements was nitrogen (99.999% pure). The carrier (dilution) gas was helium (99.999% pure). The adsorption measurements were done at liquid nitrogen temperature (-196^{o}C). Adsorption isotherms were collected at nitrogen relative pressures in the range of 0.05 to 0.25 at increments of 0.05.

A description of some theoretical aspects of the gas adsorption method for determining specific surface area is given below. This description below was written by Zhe Cheng of the Georgia Institute of Technology.[63]

"From the adsorption isotherm, the specific surface area can be obtained based on either the BET or Langmuir equation as shown below:

BET equation

$$\frac{P/P_0}{V(1-P/P_0)} = \frac{1}{V_m C} + \frac{C-1}{V_m C}\frac{P}{P_0} \tag{4-3}$$

Langmuir equation

$$\frac{P/P_0}{V} = \frac{b}{V_m} + \frac{P/P_0}{V_m} \tag{4-4}$$

in which P/P_0 is the relative pressure (P is the equilibrium pressure and P_0 is the saturation pressure), V is the total amount of gas (in cm^3/g STP) adsorbed at P, V_m is the monolayer capacity (in cm^3/g STP) which is the gas volume (reduced to STP) that is sufficient to form a complete adsorbed monolayer on the sample surface, and C and b are constants in the two models.[16]

For both BET and Langmuir equations, the specific surface area, SA (in m^2/g), is calculated by the following equation:

$$SA = \frac{V_m}{22414} A_m N_A \tag{4-5}$$

in which V_m is the monolayer capacity (in cm^3/g STP) from the BET of the Langmuir equation; N_A is the Avagadros constant, $N_A = 6.023 \times 10^{23}$; A_m is the cross-sectional area of the analysis gas. $A_m = 0.162$ nm^2 for N_2.

To obtain V_m, C, and b in the BET and Langmuir equations, the data from the adsorption isotherm (i.e., P, V values) in the relative pressure range from ~0.05 to 0.25 ($0.05 < P/P_o < 0.25$) are fitted to those equations. (The BET and Langmuir models are

generally only applicable at pressures within this range.) Linear regression is then carried out on the $(\frac{P/P_o}{V(1-P/P_o)}, P/P_o)$ data pairs for the BET model (based on equation 4-3) and on the $(\frac{P/P_o}{V}, P/P_o)$ etc. data pairs for the Langmuir model (based on equation 4-4). From the results of the linear regressions, the value of V_m (from the BET and/or Langmuir models) is calculated and then the specific surface areas are determined from the equation 4-5. In addition, the values of C in the BET model, b in the Langmuir model, and the correlation coefficients of the linear regression, r_L, for each model are obtained. The C value in the BET equation should be positive to have physical meaning. Actually, it is desirable that the C value be in the range of 80-120 [64]. For the Langmuir model, the b value should also be a positive value to have physical meaning, and it is desirable that the b value be less than 0.02. The parameters, i.e. C, b, and r_L, are used to determine whether the BET surface area or the Langmuir surface area is more representative of the actual specific surface area of the sample tested."

The specific surface areas were reported using both the BET and Langmuir models. If the BET model gave a positive C value and the Langmuir model gave a positive b value, then measurements which gave the better correlation coefficient (r_L) value was considered more reliable. (In most cases, the r_L values were at least 0.9999.) If the Langmuir model gave a positive b value and the BET model gave a negative C value, then the surface area from Langmuir model was adopted if the r_L values were good. (If r_L value was low, the measurement was repeated.) Conversely, if the BET model gave a positive C value and Langmuir model gave a negative b value, then the surface area from

the BET model was adopted. In most cases, the measurements were repeated (two times) for each sample to verify the results and check the reproducibility of data.

4.2.3 X-ray Diffraction (XRD)

4.2.3.1 Phase Analysis

X-ray Diffraction (XRD) analysis (Model PW1800, Philips Analytical, Netherlands) was used to determine phases present in powders (as-prepared and heat treated) and in sintered samples.

4.2.3.1.1 Sample Preparation

4.2.3.1.1.1 Powders

The sample holders used for XRD analysis on powders were fabricated using glass slides. The holders were made in house in order to minimize the amount of material required for analysis. (The amount of material available was limited in many cases.) The holders were fabricated from two glass slides. A 1 cm-diameter hole was drilled through one slide and the slide was then ground to 500-600 microns in thickness. This slide was glued to a second slide that served as the base. A schematic of XRD holder is shown in Figure 4.9. The cylindrical cavity formed by the two glass slides had a volume of ~3.9 - 4.7 x 10^{-2} cm^3. The amount of powder required to fill the cavity was ~70 - 200 mg. There was a significant variation in the amount of powder required to fill the cavity. The main reason for this variation was because the solid density of the powders varied significantly. (For example, consider the difference between the oven-dried powders, pyrolyzed powders, and the carbothermally-reduced powders. CTR powders consisted mostly of

ZrC. Stoichiometric ZrC has a solid density of ~6.63 g/cm^3. Pyrolyzed powders consisted mostly of zirconia (ZrO_2) and carbon and had approximate solid densities in the range of ~3.7 – 4.4 g/cm^3. The solid densities of the oven-dried powders were not estimated, but they would be expected to be considerably less than the pyrolyzed powders.) The amount of powder required to fill the cavity in the glass sample holder may also have varied because of differences in the packing densities for the different powders.

The cavity of the sample holder was initially overfilled with powder to a slight extent. The top (open) surface of the powder was then lightly compacted and leveled with the top glass surface of the holder. This was done by using a smooth glass slide to apply a light pressure. The glass slide was also used to lightly scrape away any excess powder that was present (i.e., powder that remained on the top glass surface of the holder). The sample holder was then placed on metal sample support with the help of plasticene. The glass surface (of the sample holder) was leveled with that of metal support as shown in Figure 4.10.

a) b)

Figure 4.9 a) Top view of the sample holder b) Front view of the sample holder.

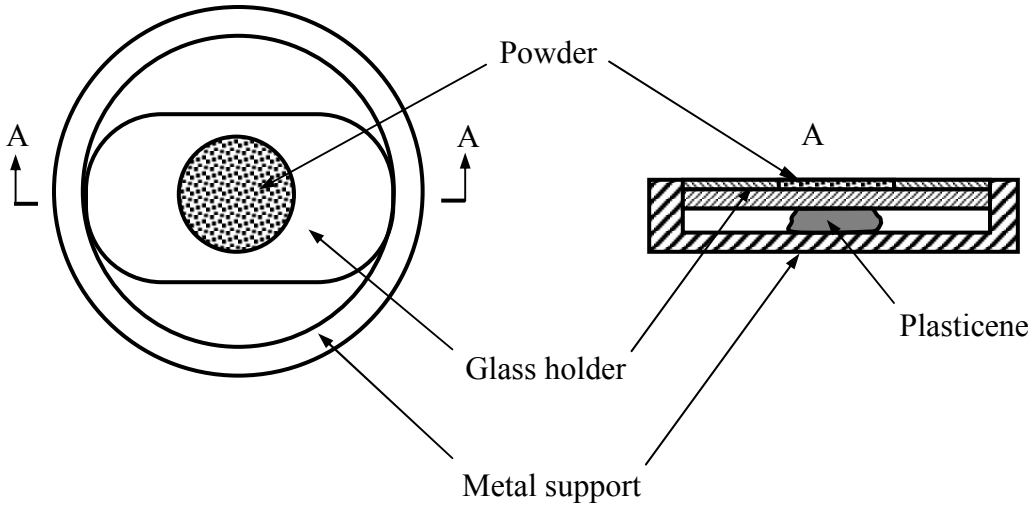

Figure 4.10 Illustration of glass sample holder with metal support for XRD measurements. (This figure is reproduced exactly from the reference 63.)

4.2.3.1.1.2 Bulk Samples

The surfaces of sintered samples were smoothed using a grinding machine (Ecomet® III, Buehler, Lake Bluff, IL) with a 12 μm diamond particle-embedded metal disk (TBW Industries Inc., Furlong, PA). Light pressure was applied manually during grinding. The sample was then placed on the same metal sample support shown in Figure 4.10. The sample was attached to the support using plasticene and was then leveled as shown in Figure 4.10.

4.2.3.1.2 Measurement Conditions and Analysis

The sample were placed in the XRD instrument for phase analysis. The radiation used for the XRD analysis was the Cu K_α line with an average wavelength of 1.54184Å, which was comprised of the $K_{\alpha1}$ and $K_{\alpha2}$ double lines ($\lambda_{\alpha1}$ = 1.54056Å and $\lambda_{\alpha2}$ = 1.54439Å). The radiation was passed through a monochromator that precluded the use of filter. Data was collected using a "continuous scan" mode with a step size of 0.02^o and scan speed of 0.4 sec/step. (In the "continuous scan" mode, the sample and the detector move continuously and the intensity counts are integrated over the small angular step.) The scanning range for 2θ angles was between 10º and 100º.

In most cases, the phases in the XRD patterns were automatically identified using the instrument software (Philips PC-APD software, version 3.6, Philips Analytical, Netherlands). Some peaks in the XRD pattern were manually analyzed by comparing measured 2θ values (and d-spacings) with information on the relevant JCPDS cards. This was done for cases in which phase identification was difficult due to low-peak intensity and/or the overlap of peaks from more than one phase.

4.2.3.2 Crystallite Size

4.2.3.2.1 Sample Preparation

The crystallite sizes were determined only on heat-treated powder samples (pyrolyzed and CTR). The sample preparation conditions were same as described in section 4.2.3.1.1.1.

4.2.3.2.2 Measurement Conditions and Analysis

Crystallite sizes were determined using XRD data that was collected for phase analysis. The scanning conditions were same as described in section 4.2.3.1.2.

The crystallite sizes of tetragonal zirconia (t-ZrO_2), monoclinic zirconia (m-ZrO_2), and zirconium carbide were determined from the broadening of the XRD diffraction lines using the Scherrer equation :

$$D_{hkl} = \frac{0.9\lambda}{\beta_{hkl} \cos\theta} \tag{4-6}$$

where D_{hkl} is the thickness of the crystal measured in a direction perpendicular to the (hkl) reflecting planes, λ is the radiation wavelength, θ is the Bragg angle, and β_{hkl} is the true width of the diffraction line at a height where the intensity is one-half of the maximum intensity. Because the Cu K_α double line was the radiation source, α_2 stripping must be performed first to obtain the true line shape contributed by the Cu $K\alpha_1$ line. The wavelength of the Cu $K\alpha_1$ line is 1.5406Å (0.15406 nm). Background subtraction was also necessary to obtain the true height of the diffraction line.

If the XRD diffraction lines have Cauchy shape, the value of β_{hkl} can be obtained from the following equation:

$$\beta_{hkl} = B - b \tag{4-7}$$

where B is the measured width of the diffraction line (or Full Width at Half Maximum, FWHM) and b is the portion of the measured width that is due to instrumental broadening. Therefore, the crystallite size D_{hkl} (in nm) is given by:

$$D_{hkl} = \frac{0.9 \times 0.15406}{(B - b) \times \cos\theta} nm \tag{4-8}$$

in which B, b and θ are all in radians.

The α_2 stripping and the background subtraction were performed on XRD patterns using Powder 2.0 software [65]. Figure 4.11 illustrates an example of an XRD pattern before (a) and after (b) the automated background subtraction.

To determine the FWHM (*B*), a lorentzian fit was performed on each individual peak using Origin® software (version 6.1, OriginLab Corporation, Northampton, MA). The angle range for each peak was chosen as two points where the peak started to flatten out and form the baseline shown in Figure 4.12a. The Lorentzian fitted curve was then used to determine the maximum intensity (*M*) and the peak position at *M*, as shown in Figure 4.12b. The FWHM (*B*) was the difference in the points of intersection (i.e., I_2 - I_1) of the Lorentzian curve with a line drawn parallel to x-axis at an intensity value (y-coordinate) that was half of the maximum intensity (i.e., at *M*/2), as shown in Figure 4.11b.

Peak broadening (*b*) resulting from the instrument was determined from the peak broadening that occurred using a single crystal silicon (Si) wafer. The Si single crystal diffraction peak was very sharp, but it was not an ideal vertical line. There was some peak width due to instrumental factors. This width was determined and then used to correct the instrument-related broadening that contributed to the broadening in the powder samples. The Si XRD pattern was obtained using same conditions as used for powder samples. The results for peak width are listed in Table 4.8.

Table 4.8. XRD peak widths of single crystal Si.

2θ (degree)	28.667	47.524	56.331	69.346	76.570
Width (degree)	0.058	0.069	0.089	0.093	0.123

Linear interpolation was used to obtain the *b* values for any angles within the different 2θ ranges. Since no data was available for angles greater than ~77°, the width was assumed to be same as of ~77° i.e., 0.123°. The interpolation equations are listed below:

$$28.667^{o}<2\theta<47.524^{o} \qquad b = [0.000583 \times (2\theta - 28.667)] + 0.058 \qquad (4\text{-}9)$$

$$47.524^{o}<2\theta<56.331^{o} \qquad b = [0.002270 \times (2\theta - 47.524)] + 0.069 \qquad (4\text{-}10)$$

$$56.331^{o}<2\theta<69.346^{o} \qquad b = [0.000307 \times (2\theta - 56.331)] + 0.089 \qquad (4\text{-}11)$$

$$69.346^{o}<2\theta<76.570^{o} \qquad b = [0.004150 \times (2\theta - 69.346)] + 0.093 \qquad (4\text{-}12)$$

The crystallite size was then calculated using equation 4-8 for all diffraction peaks observed in the XRD pattern. It was assumed that crystallites had an equidimensional shape and the average values were reported as the average crystallite sizes for the m-ZrO_2, t-ZrO_2, and ZrC.

4.2.3.3 Lattice parameter

4.2.3.3.1 Sample Preparation

The samples for lattice parameter analysis were prepared by mixing powders with 15wt% National Bureau of Standards (NBS) standard silicon. The powder samples and silicon were first weighed separately on a weighing papers (Fisher Scientific, Fair Lawn, NJ) and then transferred to a 5 ml glass vials. The vials were sealed by screw-on caps. The vials were then wrapped with Parafilm® (Fisher Scientific, Fair Lawn, NJ) to protect them from breaking during the subsequent mixing operation. Up to four vials were then

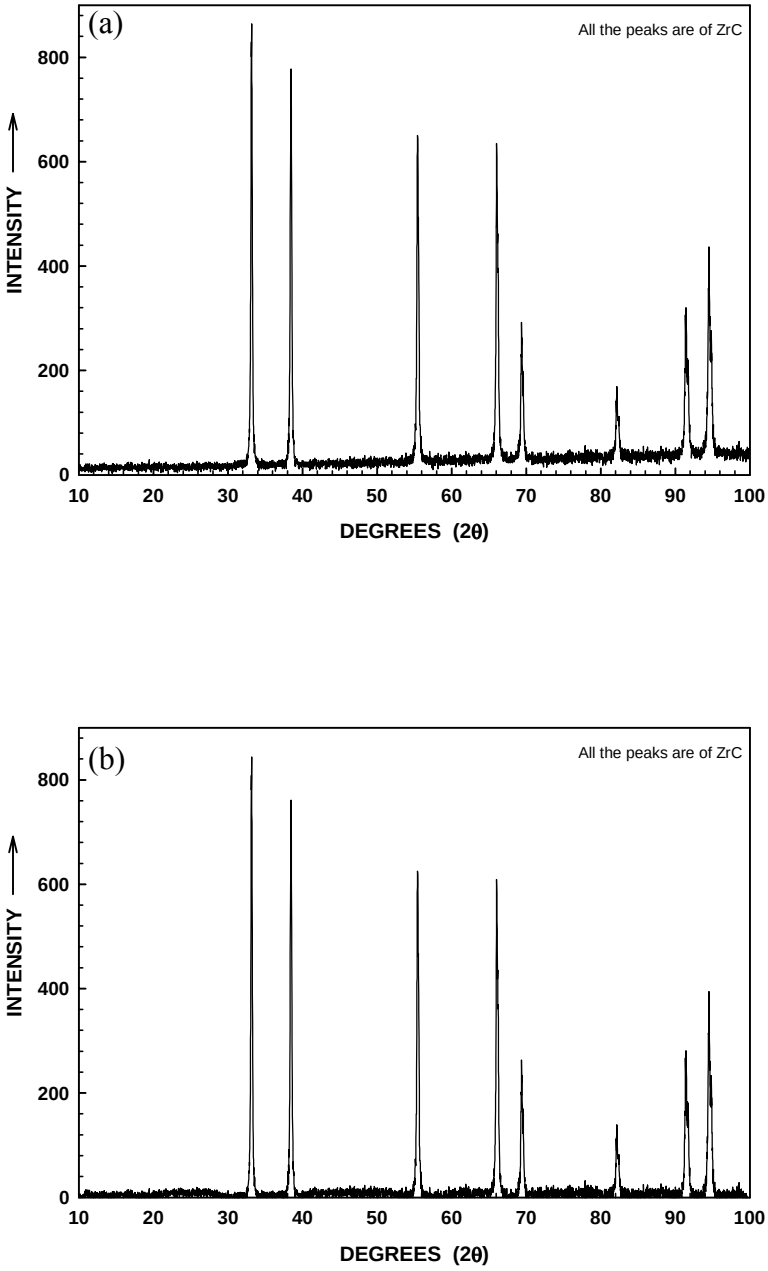

Figure 4.11. a) XRD pattern of ZrC sample with background intensity b) XRD pattern after background subtraction.

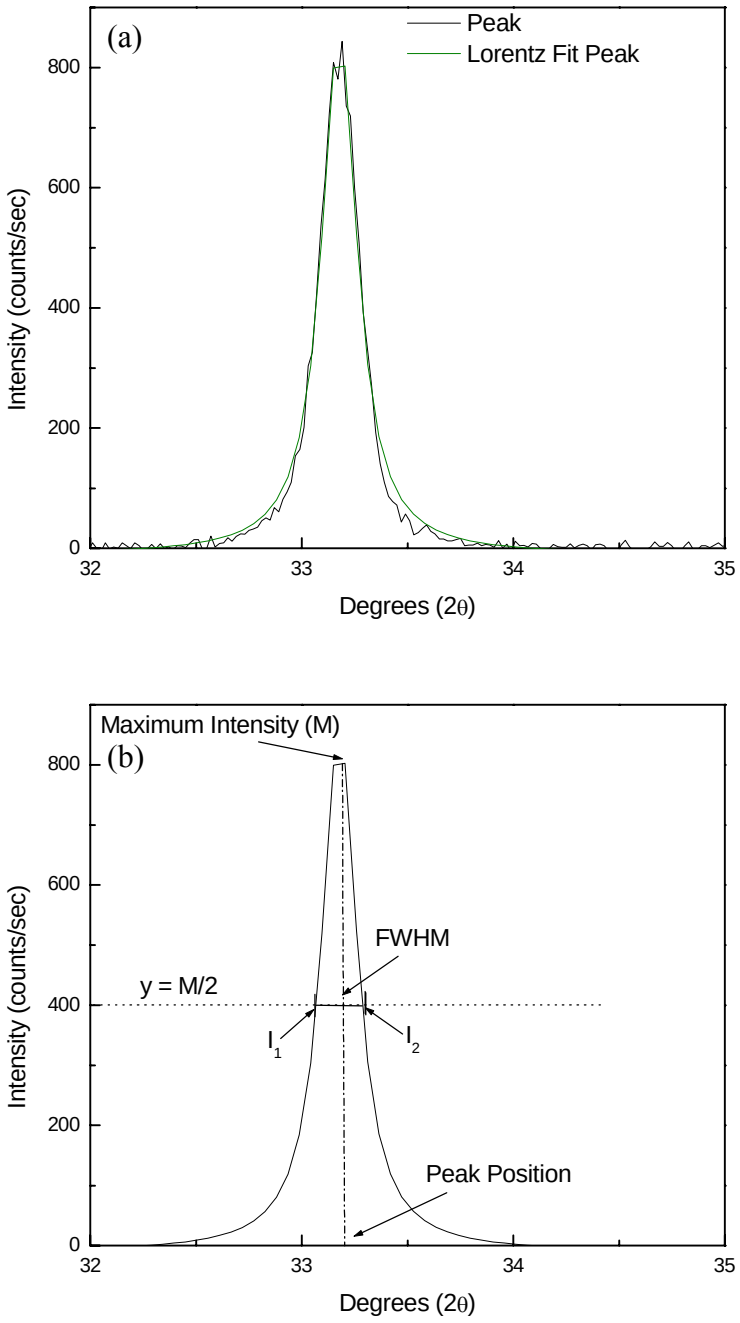

Figure 4.12 a) Single ZrC peak along with Lorentzian fitted peak b) Lorentzian fitted peak analyzed for FWHM.

placed in 500 ml polyethylene (PE) bottle (Fisher HDPE round bottles). The PE bottle was stuffed with Kimwipe® (Kimberly-Clark, Roswell, GA) paper to hold the glass vials in their position and prevent them (glass vials) from colliding with each other. The PE bottle was then placed on a tumbling machine (CV-79450, Norton Chemical Process Product Div.) for at least 2 h to achieve proper mixing of powders.

After mixing, the powder samples were loaded onto the XRD sample holder as described in section 4.2.3.1.1.1.

4.2.3.3.2 Measurement Conditions and Analysis

The measurement conditions were same as described in section 4.2.3.1.2 except for the scanning conditions. Data was collected using a "step scan" mode with a step size of 0.02^{o} and scan speed of 2.5 sec/step. (In the "step scan" mode, the sample and the detector move at fixed steps and the intensity counts are only recorded at each step for a specified time, i.e., 2.5 sec in this study.) The scanning range for 2θ angles was between 10º and 100º.

Lattice parameters were calculated from the raw XRD data using two different procedures which will be referred to as the "Extrapolation Method" and "Cohen's Method."[66] Each calculation method is described below. This is followed by an example of applying each method to a set of XRD data collected in this study.

Extrapolation Method

Bragg's law is given by:

$$\lambda = 2d\sin\theta \tag{4-13}$$

where λ is the wavelength (1.5406Å) for Cu $K_{\alpha 1}$ radiation, d is the distance between adjacent planes or the "d-spacing", and θ is the peak position.

Displacement error is caused by displacement of the specimen from the diffractometer axis. For a cubic crystal, an extrapolation curve based on the displacement error is given by :

$$\frac{\Delta d}{d} = \frac{\Delta a}{a_0} = b\frac{\cos^2\theta}{\sin\theta} \tag{4-14}$$

where a_0 is the lattice parameter, b is a constant, and Δa is given by :

$$\Delta a = a - a_0 \tag{4-15}$$

where a is the apparent lattice parameter.

Substituting the value of Δa from equation 4-15 into equation (4-14) and rearranging the terms we have:

$$a = a_0 + a_0 b\frac{\cos^2\theta}{\sin\theta} \tag{4-16}$$

This yields $a = a_0$ at $\theta = 90$. In a cubic system, a is given by:

$$a = d\sqrt{h^2 + k^2 + l^2} \tag{4-17}$$

where h, k, l are the plane indices.

Thus, values of d and a can be calculated for all the diffraction peaks observed in the XRD pattern using the equations (4-14) and (4-17) respectively. According to equation 4-16, a plot of a versus $\cos^2\theta/\sin\theta$ should yield a straight line, and the lattice parameter a_0 can be obtained by extrapolating the values to $\theta = 90^o$.

Cohen's Method

Bragg's law is given by equation (4-13). Squaring both sides of this equation, rearranging terms, and taking the natural logarithms of each side results in the following equation :

$$\ln \sin^2 \theta = \ln(\frac{\lambda^2}{4}) - 2 \ln d \tag{4-18}$$

Differentiation gives

$$\frac{\Delta \sin^2 \theta}{\sin^2 \theta} = -\frac{2\Delta d}{d} \tag{4-19}$$

For a cubic material, we have

$$\frac{\Delta d}{d} = \frac{\Delta a}{a} = K \cos^2 \theta \tag{4-20}$$

where K is a constant.

$$\Delta \sin^2 \theta = \sin^2 \theta(Observed) - \sin^2 \theta(True) \tag{4-21}$$

where $sin^2\theta(Observed)$ is calculated from the measured peak position in the XRD pattern and $sin^2\theta(True)$ is the ideal value.

Combining Eq. (4-19) and (4-20), we have:

$$\Delta \sin^2 \theta = \sin^2 \theta(Observed) - \sin^2 \theta(True) = -2K \sin^2 \theta \cos^2 \theta = D \sin^2 2\theta \tag{4-22}$$

where D is a new constant.

By squaring equations (4-13) and (4-17), and then rearranging the terms, the true value of $\sin^2\theta$ for any diffraction line is given by :

$$\sin^2 \theta(True) = \frac{\lambda^2}{4a_0^{\,2}}(h^2 + k^2 + l^2) \tag{4-23}$$

Combining Eq. (4-22) and Eq. (4-23) gives :

$$\sin^2\theta(Observed) = \frac{\lambda^2}{4a_0^{\,2}}(h^2 + k^2 + l^2) + D\sin^2 2\theta \qquad (4\text{-}24)$$

Therefore a plot of $\sin^2\theta$ versus $(h^2+k^2+l^2)$ should yield a straight line, and the lattice parameter a_0 can be obtained from the slope of the straight line by using the equation given below:

$$a_0 = \frac{\lambda}{2\sqrt{slope}} \qquad (4\text{-}25)$$

Examples

In this example, the lattice parameter measurements were made using a CTR sample consisting mostly of ZrC. The sample was given the name "ZrPM-45-1600-2".

1. Extrapolation Method

Table 4.9. Measured and NBS 2θ values of Si standard.

2θ (NBS values)	Measured 2θ	Δ 2θ
28.443	28.555	0.112
47.303	47.4	0.097
56.123	56.21	0.087
76.377	76.46	0.083
88.032	88.11	0.078
94.954	95.005	0.051

Table 4.9 shows the measured 2θ values obtained for the Si peaks in the sample. Also, listed in the table are the 2θ values provided by NBS for the Si standard. Figure 4.13 shows a plot of the difference between these 2θ values (y-axis values) versus the measured 2θ values (x-axis values). The two data points were fit with a linear equation; the correlation coefficient (R) and the equation are given below:

$$y = 0.13473 - (7.95967e\text{-}4x) \qquad (4\text{-}26)$$

$$R = -1$$

As seen in Table 4.9 the measured 2θ values of Si standard shifted to higher values as compared to values provided by NBS. This shift may be caused by the difference in sample positions during analysis. Thus, equation 4-26 was used to correct the measured 2θ values of ZrC peaks in the XRD pattern that were in the 2θ range used for the linear fit in equation 4-26 (For example, equation 4-26 was used to correct the 2θ values in ZrC peaks that were measured (see Table 4.10) at 33.145 and 38.425). This procedure was repeated over the entire range of measured 2θ values for ZrC. Table 4.10 lists the measured and corrected 2θ values for the ZrC peaks observed in the XRD pattern. Table 4.10 also lists the *d* (d-spacing), *hkl* (indices of plane) and *a* (apparent lattice parameter) values that were calculated by using the corrected 2θ values.

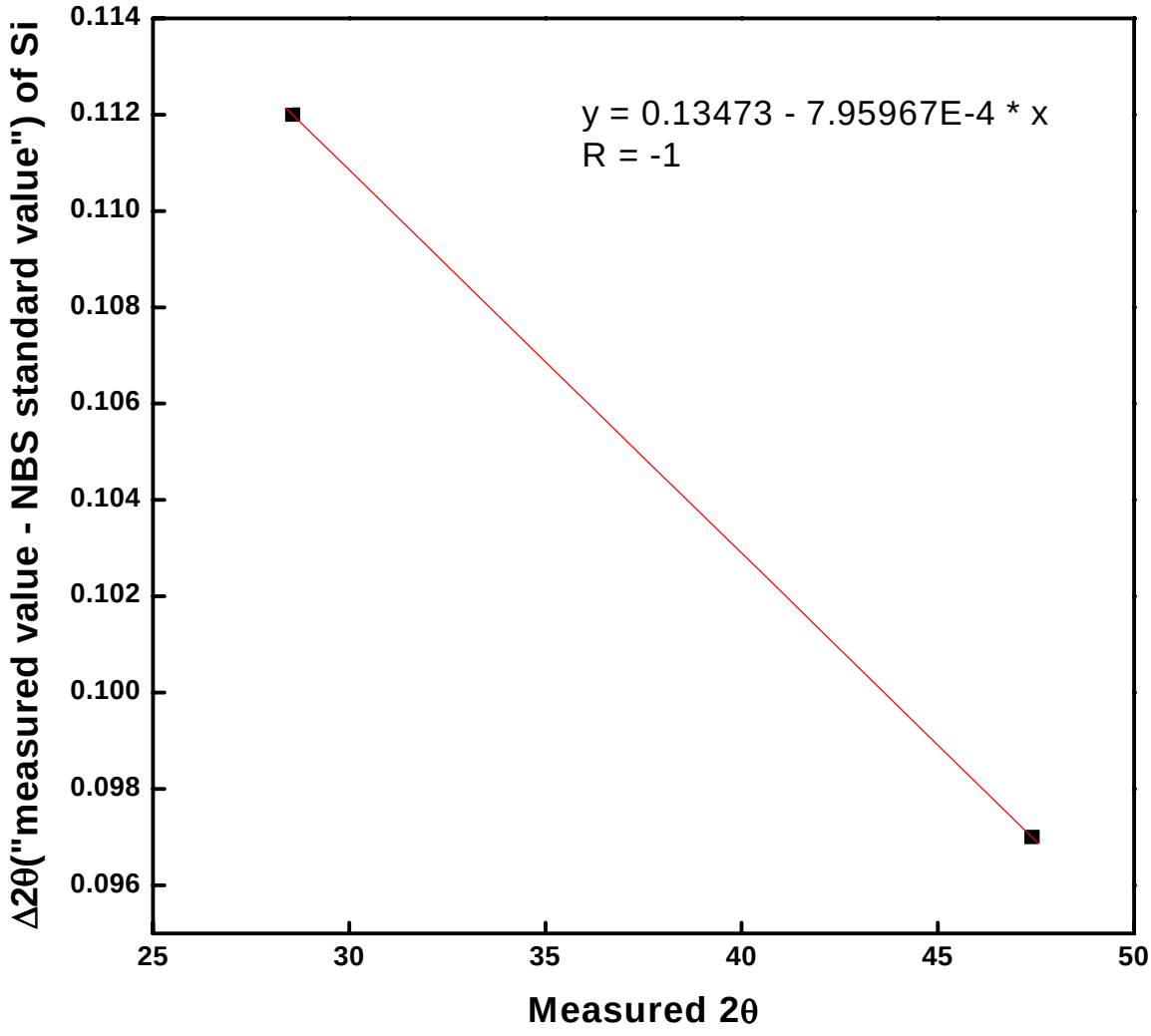

Figure 4.13 Plot of Δ2θ vs. 2θ of Si standard.

Table 4.10. Measured and corrected ZrC peak positions and their corresponding *d* and *hkl* values.

Measured 2θ	Corrected 2θ	*d*	*h*	*k*	*l*	*a*
33.145	33.0367	2.70979	1	1	1	4.69349
38.425	38.3209	2.34737	2	0	0	4.69475
55.405	55.3174	1.65937	2	2	0	4.69341
66.035	65.9499	1.41521	3	1	1	4.69372
82.125	82.0444	1.17365	4	0	0	4.69459
91.405	91.3403	1.07687	3	3	1	4.69398
94.48	94.4273	1.04962	4	2	0	4.69405

Figure 4.14 shows the plot of the apparent lattice parameter, *a*, (y-axis values) vs. $\cos^2\theta/\sin\theta$ (x-axis values). The data were fit by the least-squares method. The equation and correlation coefficient (R) are given below:

$$y = 4.69411 - 6.75082e^{-5}x \qquad (4\text{-}27)$$

$$R = 0.13508$$

As noted earlier, the lattice parameter, a_0, is given by the y-intercept value at x = 0 (i.e., θ = 90°). In this case, the value is 0.4695 nm.

2. Cohen's Method

The method used to correct the measured 2θ values for the Si standard and ZrC peaks observed in the XRD pattern was the same as described for the Extrapolation Method. Table 4-11 lists the measured and corrected 2θ values for the ZrC peaks observed in the

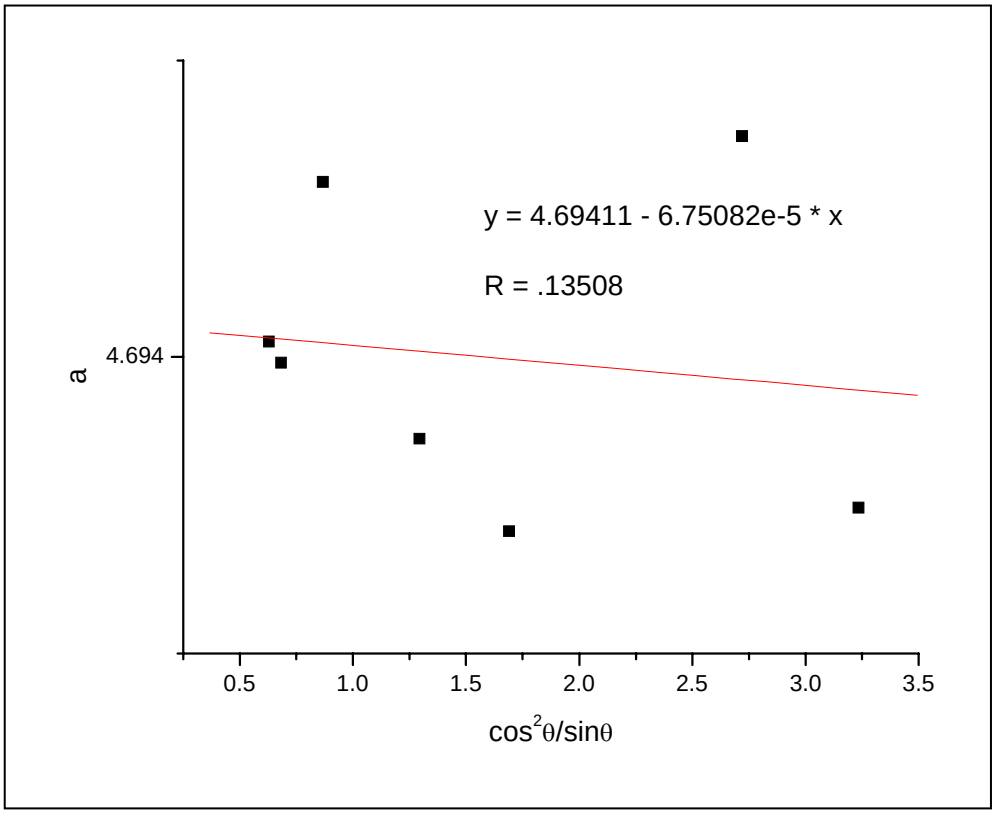

Figure 4.14 Plot of "a" vs. $\cos^2\theta/\sin^2\theta$ to determine the lattice parameter.

XRD pattern. Table 4-11 also lists the $\sin^2\theta$, *hkl* (indices of plane) and $h^2+k^2+l^2$ values that were calculated by using the corrected 2θ values.

Table 4.11. Measured and corrected ZrC 2θ values and their corresponding $sin^2\theta$ and *hkl* values.

Measured 2θ	Corrected 2θ	$\sin^2\theta$	*h*	*k*	*l*	$h^2+k^2+l^2$
33.145	33.0367	0.080807	1	1	1	3
38.425	38.3209	0.107685	2	0	0	4
55.405	55.3174	0.215492	2	2	0	8
66.035	65.9499	0.296263	3	1	1	11
82.125	82.0444	0.430769	4	0	0	16
91.405	91.3403	0.511671	3	3	1	19
94.48	94.4273	0.538585	4	2	0	20

Figure 4.15 shows the plot of $\sin^2\theta$ (y-axis values) vs. $h^2+k^2+l^2$ (x-axis values). The data were fit by the least-squares method. The equation and correlation coefficient (R) are given below:

$$y = 3.85056e^{-5} + 0.02693x \qquad (4\text{-}28)$$

$$R = 1.0000$$

As noted earlier, the lattice parameter, a_0, is calculated from the slope of the equation (4-24). In this case, the value of slope is 0.02693 and the calculated lattice parameter value using equation (4-25) is:

$$\frac{1.54056}{2\sqrt{0.02693}} = 0.4694\,nm \qquad (4\text{-}29)$$

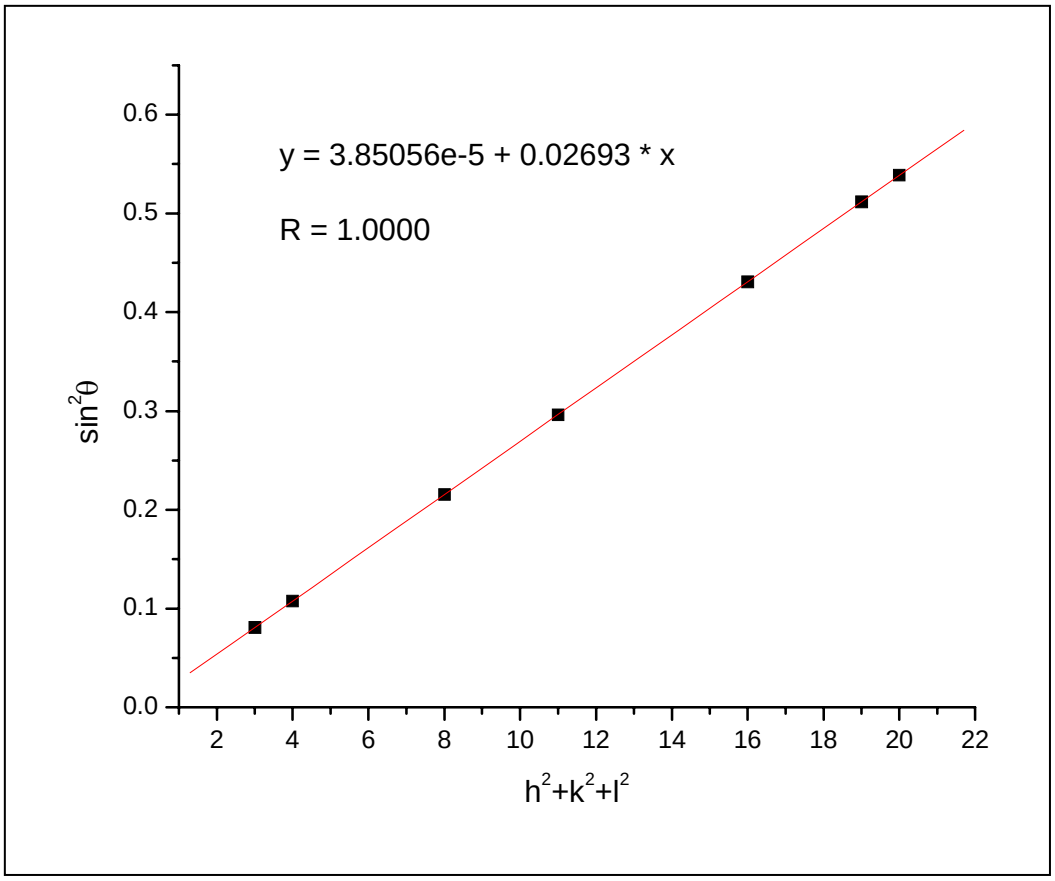

Figure 4.15 Plot of $\sin^2\theta$ vs. $h^2+k^2+l^2$ for measuring the lattice parameter.

The "Extrapolation Method" consistently showed poor R values compared to values obtained by "Cohen's Method". Therefore, it was decided that the lattice parameter values from only "Cohen's Method" will be reported in this thesis.

4.2.4 Scanning Electron Microscopy

Scanning electron microscopy was used to observe the particle sizes and morphologies of carbothermally-reduced powder samples. The initial step in the sample preparation process was to put some double-sided adhesive-coated graphite tape (S T R

Tape, Shinto Paint Company, Japan) onto a cylindrical aluminum-mounting block. A spatula containing the powder sample of interest was held over the tape and then the spatula was lightly tapped in order to deposit a thin layer of powder. The whole sample mount was then coated with a thin layer of gold-palladium by sputtering with a gold-palladium target. The sputter coater (Sputter Coater, International Scientific Instruments, England) chamber was evacuated to 0.07 torr pressure. The coater was operated at ~20 mA current (1.2 kilovolts) for ~1.5 min in order to coat the sample. The gold-palladium coating prevented the accumulation of charge on the sample during SEM observations. The experiments were performed by using a field emission SEM (Model 1530, LEO, Thornwood, NY). The acceleration voltage used for observation was in the range of 10-20 kV.

4.2.5 Electrophoretic Mobility Measurements

Electrophoretic mobilities of ZrC-based CTR powders were determined using the method of microelectrophoresis (Beckman Coulter, Delsa 440SX, FL). This information was used to determine the optimum conditions for the preparation of electrostatically-stabilized suspensions that were used for measurements of particle size distributions (section 4.2.6).

When an electric field is applied to particles suspended in a liquid, the particles accelerate until they reach the terminal velocity. At the terminal velocity, the viscous drag force acting on the particles moving through the liquid equals the motive force of the applied electric field. The terminal velocity is typically reached in μsec.[67] The

electrophoretic mobility is calculated by the equation given below:

$$U = \frac{v}{E} \tag{4-30}$$

where U is the electrophoretic mobility (μm·cm/V·s), v is the terminal velocity (μm/s), and E is the applied electric field (V/cm).

With certain restrictions, the zeta potential can be calculated from the electrophoretic mobility using the Helmholtz-Smoluchowski equation :

$$\zeta = \frac{\eta U}{\varepsilon} \tag{4-31}$$

where ζ is the zeta potential (volts x 10^{-10}), η is the viscosity of the liquid (N·s/m^2), and ε is the permittivity (farad/cm) of the liquid.

Electroosmosis tends to be a major source of error in measuring U. It occurs because of the difference in the electrical potential of glass walls of the sample cell used for the measurements and the bulk solution. (The sample chamber is a channel with a rectangular cross-section (see Figure 4.16).) This difference in electrical potential causes non-uniform distribution of ions in the liquid in the channel, i.e., the potential varies with the distance from the channel wall. At the application of external electric field, the liquid in the channel moves with a speed that depends on the electrical potential which, in turn, depends on the position in the channel. However, the electrophoresis cell chamber is a closed system during the measurement, so that the liquid displaced by electroosmotic flow must circulate back in the opposite direction by Poisseuille flow (i.e., so that the total liquid flow rate in the closed chamber is zero). A parabolic “flow profile” (see Figure 4.17) is observed in a channel with a rectangular cross-section, provided the

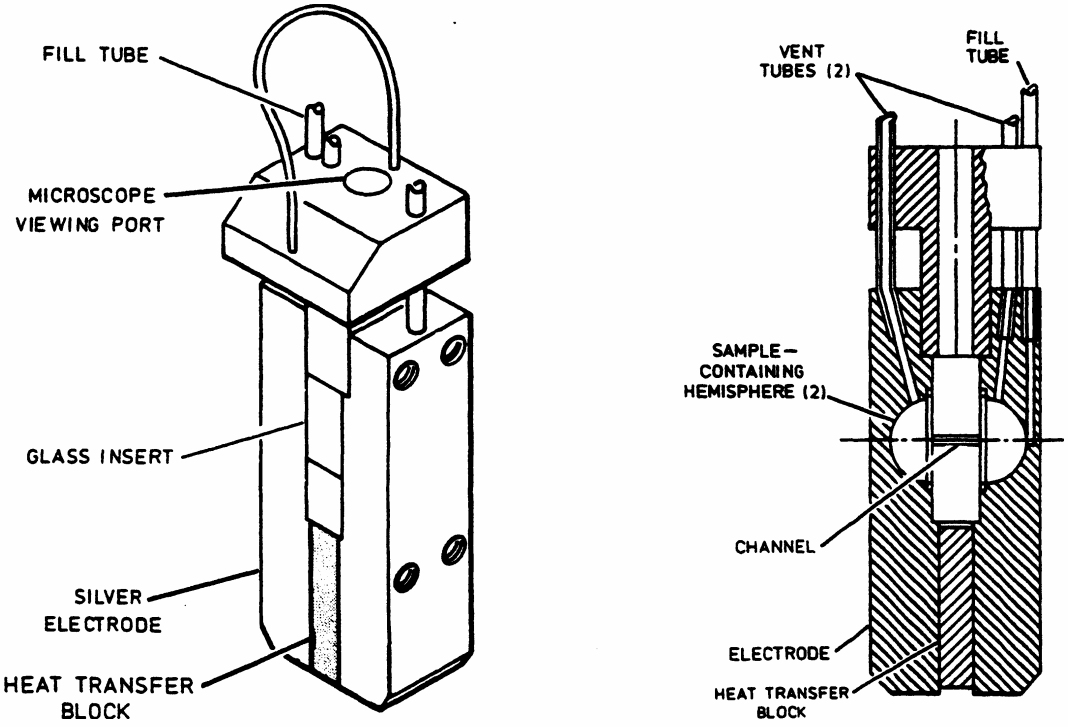

Figure 4.16 Schematic of sample cell used for mobility measurements. (The figure is reproduced exactly from reference 67.)

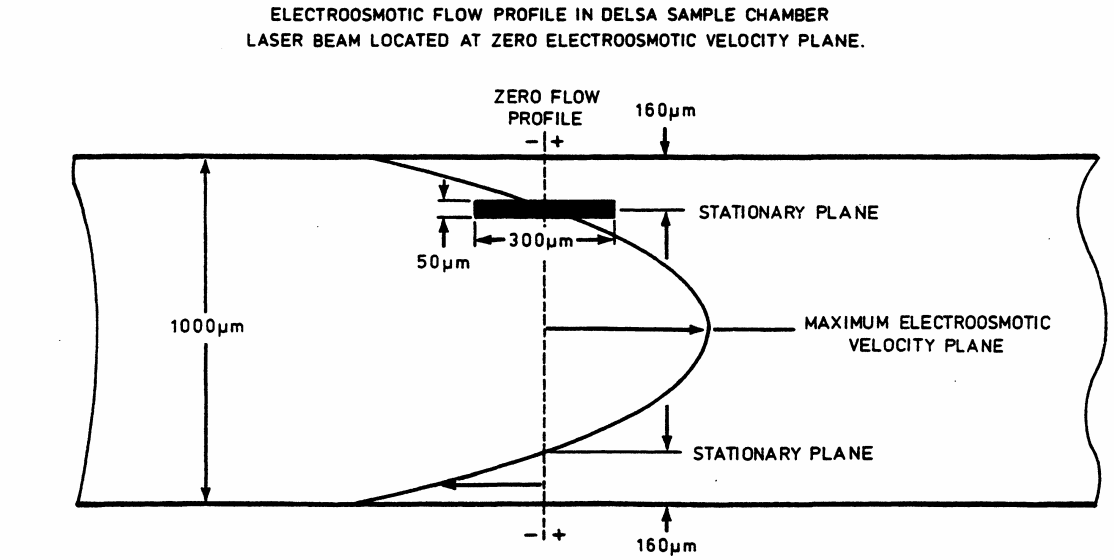

Figure 4.17 Electroosmotic flow profile. (The figure is reproduced exactly from reference 67.)

potential is uniform on the cell walls. As shown in Figure 4.17, there are two locations in the cell chamber in which the liquid flow rates in the forward and backward directions are equal in magnitude (but opposite in direction). The two locations are referred to as the "upper stationary level" and the "lower stationary level" of the cell chamber. For accurate determination of the particle velocity (and, therefore, the particle electrophoretic mobility), measurements are made at either or both of these two locations where the liquid has a net zero velocity. In this study, measurements were made at both the upper and lower stationary level.

All particles do not move with the same velocity during an electrophoresis experiment. A light scattering method is used in the Delsa 440SX instrument to determine distributions of the particle velocities (and, hence, distributions of the particle electrophoretic mobilities). Measurements of the velocity distributions were made at four different scattering angles.

The samples were prepared by first dispersing about 1-5 mg of powder sample in 20 ml of deionized water (DI). The pH of the water was varied in the range of 2.9 to 10. The suspension was then sonicated ultrasonically for about 15-20 minutes to break any “soft” or “weak” powder agglomerates.

The sample holder was cleaned using DI water at least three times prior to measurements. The DI water used had the same pH as that of suspension to be analyzed. The sample holder was filled with the sample suspension by using a 5 ml syringe. The sample holder was then wiped and dried with a Kimwipe® paper tissue (Kimberly-Clark, Roswell, GA). Special glass wipes (KP 62647-B, Kodak, Rochester, NY) were used to clean the glass chamber of the sample holder to prevent the formation of scratches. It was

important to wipe off all water from the sample holder surfaces, prior to placing the holder in the instrument chamber, in order to achieve good temperature equilibration. The instrument manufacturer recommended that sample measurements be carried out only when temperatures differences between the two sides of the sample holder were ≤ 0.2^{o}C.

To ensure the validity of the data, measurements for solution conductivity and particle electrophoretic mobility were periodically checked using standards. The solution conductivity standard was a 10 mS/cm KCl conductivity standard (YSI 3128, Fisher Scientific, Fair Lawn, NJ). A suspension of polystyrene latex particles (EMPSL7, Beckman Coulter, Miami, FL) was used as a standard for the electrophoretic mobility.

4.2.6 Particle Size Distribution Measurements

Particle size distributions were determined using a light scattering method (Model LS 13320, Beckman Coulter, Miami, FL). A schematic of the instrument used in this study is shown in Figure 4.18. The basic components of the systems are a monochromatic source of illumination, a spatial filter to focus the light beam, a sample chamber which holds the sample and allows the particles to interact with the light beam, and an array of photodetectors that record the intensity patterns for the light scattered by the particles.

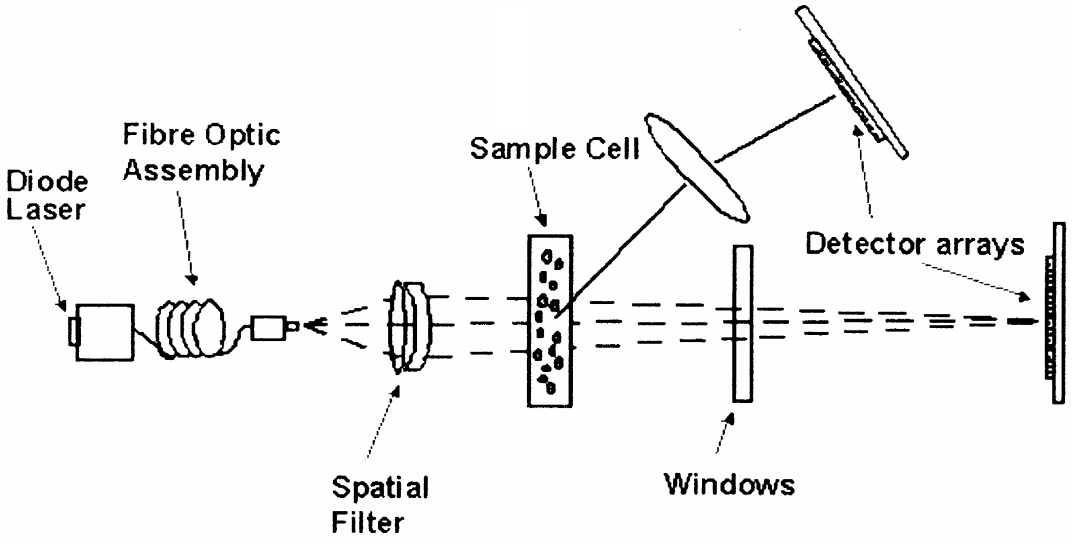

Figure 4.18 Schematic of optical system for particle size analysis. (The figure is reproduced exactly from reference 68.)

In the general case, the intensity pattern for the scattered light is rather complex and depends on the properties of the light source (wavelength and polarization), properties of the particles (sizes, shapes, concentration, and complex refractive index), and the angle of scattering. Experimentally, scattered light intensities are measured at known scattering angles using light sources with known properties and using suspensions with fixed particle concentration. The scattering pattern is deconvoluted using theoretical equations which relate the scattering intensity to the scattering angle, particle size, and particle shape. Mie theory is usually applied when particles are smaller than the wavelength of the incident light. The theory requires knowledge of the particle complex refractive index. In addition, the theory is based on the assumption that particles have a spherical shape. Fraunhofer diffraction theory can be used when particles are much

larger than the wavelength of the incident light. Fraunhofer theory is easier to apply because the particle refractive index is not needed. (For large particles (or highly absorptive particles), most of the scattered intensity is concentrated at very small angles in the forward direction (i.e., "forward diffraction"), so it is not necessary to know the refractive index.) The Mie theory was required for most of the powders characterized in this study. For example, fully-converted CTR samples which had been milled (ground) had particles that were mostly submicrometer, with the smallest particles extending to the lower limit of detection of the instrument (~40 nm).

Measurements of particle size distributions via light scattering are carried out using dilute particle/liquid suspensions. The concentration is sufficient to provide enough scattered light to reach the detectors with adequate signal-to-noise ratio, but low enough to minimize particle-particle interactions and multiple light scattering. In the LS 13320 instrument, the suspensions are loaded into a "liquid module" which consists of a sample cell and a circulation system. The sample cell allows the particles in the suspension to be exposed to the illuminating source. The circulation system has a pump which allows the cell to be filled and rinsed automatically. It also serves the function of keeping particles suspended in the liquid. This becomes increasingly important as the size of the particles increases because the rate of particle sedimentation is proportional to the diameter squared.

The light scattering method used to determine the particle size distributions required the use of dilute particle/liquid suspensions. The starting materials were dry powders, which consisted of agglomerates (porous clusters of particles). "Soft" agglomerates were broken down by first mixing the powder with the suspending liquid

and then applying ultrasonication to the suspension. (Mechanical mixing and ultrasonication are generally effective in breaking down most "soft" agglomerates, but will usually be ineffective in breaking down "hard" agglomerates (i.e., aggregates). The latter agglomerates refer to particle clusters in which particles are held together by strong chemical bonds, in contrast to the weaker bonds arising from "surface forces" (e.g., van der Waals, capillary forces, etc.) that hold particles together in "soft" agglomerates.) Although mixing and ultrasonication can be used to break down powder soft agglomerates and to disperse particles in a liquid, the dispersed particles often have a tendency to re-agglomerate in the liquid (i.e., to flocculate) when the mechanical forces are no longer applied. (This tendency usually becomes increasingly more important as the particle size decreases.) Therefore, it is often necessary to ensure that repulsive forces are operative between particles in order to maintain a dispersed state. A common method of producing interparticle repulsive forces is to impart a net surface charge of similar sign (either positive or negative) on all of the particles. This method of stabilizing a suspension against particle flocculation is known as "electrostatic stabilization." In this study, a surface charge (sufficient to maintain good particulate dispersion) was imparted on the ZrC-based particles by adjusting the pH of the suspension. (See Appendix A for details.) Suspensions were prepared using deionized (DI) water in which the pH was adjusted to ~9.5 by adding dilute ammonium hydroxide solution. The ammonium hydroxide (Fisher Scientific, Fair Lawn, NJ) was diluted to 10 wt% in DI water. About 7 – 20 mg of powder sample was then put in a 20 ml polyethylene vial. Approximately 20 ml of DI water, whose pH was adjusted to 9.5, was then added to the vial (with powder). The pH of the solution was adjusted to 9.5 if it varied because of the powder addition.

The solution was then sonicated (Model VC600, Sonics and Materials Inc., Danbury, CT) for about 30 min. The sonicator was operated at 600 watts and 20 kHz frequency.

Prior to the measurements, the liquid module was first rinsed with pH 9.5 DI water and then filled with pH 9.5 DI water. A "de-bubbling" step was used to remove the air bubbles from the DI water in the liquid module prior to a "background" measurement. Bubbles need to be eliminated because they produced a light scattering pattern that causes incorrect analysis of the particle size distribution for the samples. The "background" measurement recorded the light scattering pattern from the liquid and glass sample cell (i.e., with no particles present). It was automatically subtracted from the light scattering pattern of the samples. The concentrated powder suspension was then added to the liquid module by using a pipette. The suspension was added drop by drop until the desired amount was added, as indicated from the instrument software. The conditions used for different measurements are listed in Table (4-12). The measurements were repeated and the average data of two results were reported.

Table 4.12. Typical steps followed before particle size analysis was performed.

Condition		Comments
De-bubbling	Yes	Used for each measurement
Background Measurement	Yes	Used for each measurement
Pump Speed	40 to 70%	Depends upon the particle size of samples. Larger particles required higher pump speed.
Detectors Alignment	Yes	Used for each measurement

To determine the particle size distribution accurately, it was of primary importance to have the sample material's optical constants (i.e., real component of the refractive index and extinction coefficients) at the specific wavelengths of light that were used in the LS 13320 instrument to collect the light scattering data. Unfortunately, this information was not available for ZrC. The closest material to ZrC, in terms of structure and chemistry, for which the complex refractive index data were available, was titanium carbide (TiC). Table 4.13 shows refractive index (real component) and extinction coefficient values, at the wavelengths of interest, that were obtained by Koide et al.[69] for $TiC_{0.95}$. The real component values of the refractive index were used in this study for the following reasons: (1) As mentioned above, ZrC and TiC have similar structure and chemistry. (2) Refractive index (real component) values were reported by the same authors for VC[69] (another refractory transition metal carbide) and the values were very similar to those obtained for $TiC_{0.95}$. (3) The calculated particle size distributions showed only moderate differences for samples in this study when the input values for the refractive index (real component) were significantly varied (while maintaining the same extinction coefficient values). This is illustrated in Figures 4.19 – 4.21 in which particle size distribution data is plotted for a ZrPM-99-800-1475 sample (milled 10 min) using the optical constants reported for $TiC_{0.95}$ (Figure 4.19) and refractive index values that were decreased by 1 (Figure 4.20) or increased by 1 (Figure 4.21). (The values used for Figures 4.20 and 4.21 are listed in Table 4-14 as "self-defined 1" and "self-defined 2.") Although there were some obvious changes in the shape of the particle size distributions in Figures 4.19 – 4.21, the mean diameter values, as well as the d_{10}, d_{50}, and d_{90} values, were quite similar (Table 4-15). (The d_{10}, d_{50}, and d_{90} values are the diameters at the ten-

percentile, 50-percentile, and 90-percentile points in the volume-based cumulative particle size distribution plot.) Therefore, it was concluded that it would be reasonable to use the refractive index (real component) values reported by Koide et al. for $TiC_{0.95}$ for the materials used in this study.

The choice of the extinction coefficients to use in this study was more problematic for the following reasons: (1) Figure 4.19 shows that the calculated particle size distribution contains four modes if the values reported by Koide et al. for $TiC_{0.95}$ are used. This is a concern because it is unusual for a milled powder to show four modes when the overall range of particle sizes in the distribution is relatively narrow. (In this case, essentially all the particles in the distribution in Figure 4.19 are in the range of ~0.1-2.6 μm.) (2) Figure 4.19 shows that all the particles in the distribution were greater than 0.1 μm and 90% of the particles were greater than the 0.18 μm (i.e., the d_{10} value). This is a concern because SEM observations (Figure 4.22) indicate that there are a substantial number of primary particles with sizes close to 0.1 μm (or less). However, it should be noted that this is not conclusive proof that the particle size distribution measurements are in error. It is possible that most of the primary particles remained clustered together in the form of aggregates of various sizes in the suspensions that were used for the particle size distribution measurements. (The term "aggregates" refers to clusters of primary particles which are held together by strong bonding forces. Hence, such particles do not break down (to any significant extent) under suspension preparation conditions of the type used in this type (i.e., using ultrasonication). Although the suspensions in this study were prepared using electrostatic stabilization, the particles that would be dispersed under those conditions could be primary particles and/or aggregates.) (3) Calculated particle

size distributions varied significantly when the extinction coefficient values were changed. This is illustrated by comparing the results in Figure 4.19 to particle size distributions calculated (for the same 10-min milled ZrPM-99-800-1475 sample) using extinction coefficients that varied in the range of 0.01 to 0.5, while maintaining constant refractive index (real component) values (Figures 4.23-4.26). (The values used for Figures 4.23-4.26 are listed in Table 4.14 as "self-defined-3" - "self-defined-6," respectively.) Table 4.15 shows the mean diameter, d_{10}, d_{50}, and d_{90} values for these distributions. Clearly, the calculated particle size distributions are highly dependent upon the choice of the extinction coefficient values. (4) The extinction coefficients reported for SiC [70,71,72] were much lower than the values obtained by Koide et al.[69] for $TiC_{0.95}$ and VC. Figure 4.27 shows the particle size distribution calculated for the 10-min milled ZrPM-99-800-1475 sample using the SiC refractive index and extinction coefficient values reported in reference 71 (see Table 4.13). It is apparent that the much lower extinction coefficients used in this case (i.e., compared to the values used in Figure 4.19) once again changed the calculated particle size distribution significantly. (5) There is some concern regarding the extinction coefficients reported by Koide et al. because their measurements were carried out on mechanically-polished bulk samples (disks with ~1 mm thickness). In contrast, the materials in this study were dispersed particles with sizes that were mostly in the submicrometer range (i.e., for most samples). The concern with using extinction coefficients obtained from bulk samples is that processing defects might have caused scattering and absorption effects in the optical range of the spectrum that were not representative of the inherent material properties. As indicated above, the extinction coefficients are much lower in the visible range (<0.02) for the cubic form of

SiC.[71] In addition, a limited survey of the literature showed that several ceramic materials (i.e., Y_2O_3-stabilized ZrO_2, HfO_2, TiO_2, SiO_2, Al_2O_3), in the form of sputtered or vapor-deposited thin (submicrometer) films, all had very low extinction coefficients (always <0.03, but usually less than <0.01) in the visible range of the spectrum.[73,74,75,76] In contrast, extinction coefficients reported for ZrN thin films [77] were ~1-2 in the visible range. (This ZrN material clearly showed semiconductor characteristics, as indicated by relatively low electrical resistivities and a gold color of the films.)

In summary, it is evident that there is not a clear basis for selecting specific extinction coefficient values to use for the particle size analysis in this study. Therefore, a decision was made to choose an arbitrary, but intermediate, value of the extinction coefficient in hopes that this would not excessively bias the data toward larger or smaller sizes. A value 0.05 of was used for all wavelengths.

Table 4.13. Refractive index and extinction coefficient for various metal carbides.

Metal Carbide	Wavelength (nm)	*n*	*k*
TiC	450	2.86	2.4000
	600	3.03	2.6000
	750	3.40	2.9000
	900	3.59	3.2000
VC	450	2.80	2.1900
	600	3.00	2.5000
	750	3.20	2.7000
	900	3.40	2.9000
SiC	450	2.69	0.0011
	600	2.62	0.0002
	750	2.62	0.0003
	900	2.55	0.0004

Table 4.14 Self defined refractive index and extinction coefficient values.

	Wavelength (nm)	*n*	*k*
Self-defined-1	450	1.86	2.40
	600	2.03	2.60
	750	2.40	2.90
	900	2.59	3.20
Self-defined-2	450	3.86	2.40
	600	4.03	2.60
	750	4.40	2.90
	900	4.59	3.20
Self-defined-3	450	2.86	0.50
	600	3.03	0.50
	750	3.40	0.50
	900	3.59	0.50
Self-defined-4	450	2.86	0.10
	600	3.03	0.10
	750	3.40	0.10
	900	3.59	0.10
Self-defined-5	450	2.86	0.05
	600	3.03	0.05
	750	3.40	0.05
	900	3.59	0.05
Self-defined-6	450	2.86	0.01
	600	3.03	0.01
	750	3.40	0.01
	900	3.59	0.01

Table 4.15 Particle size distribution data for the milled ZrPM-99-800-1475 powder sample.

	Mean	**D_{90}**	**D_{50}**	**D_{10}**
TiC	0.64	1.77	0.35	0.80
Self-defined-1	0.65	1.75	0.35	0.18
Self-defined-2	0.66	1.81	0.35	0.17
Self-defined-3	0.44	0.91	0.25	0.16
Self-defined-4	0.11	0.22	0.07	0.05
Self-defined-5	0.09	0.19	0.06	0.05
Self-defined-6	0.08	0.18	0.06	0.05
SiC	0.11	0.24	0.07	0.05

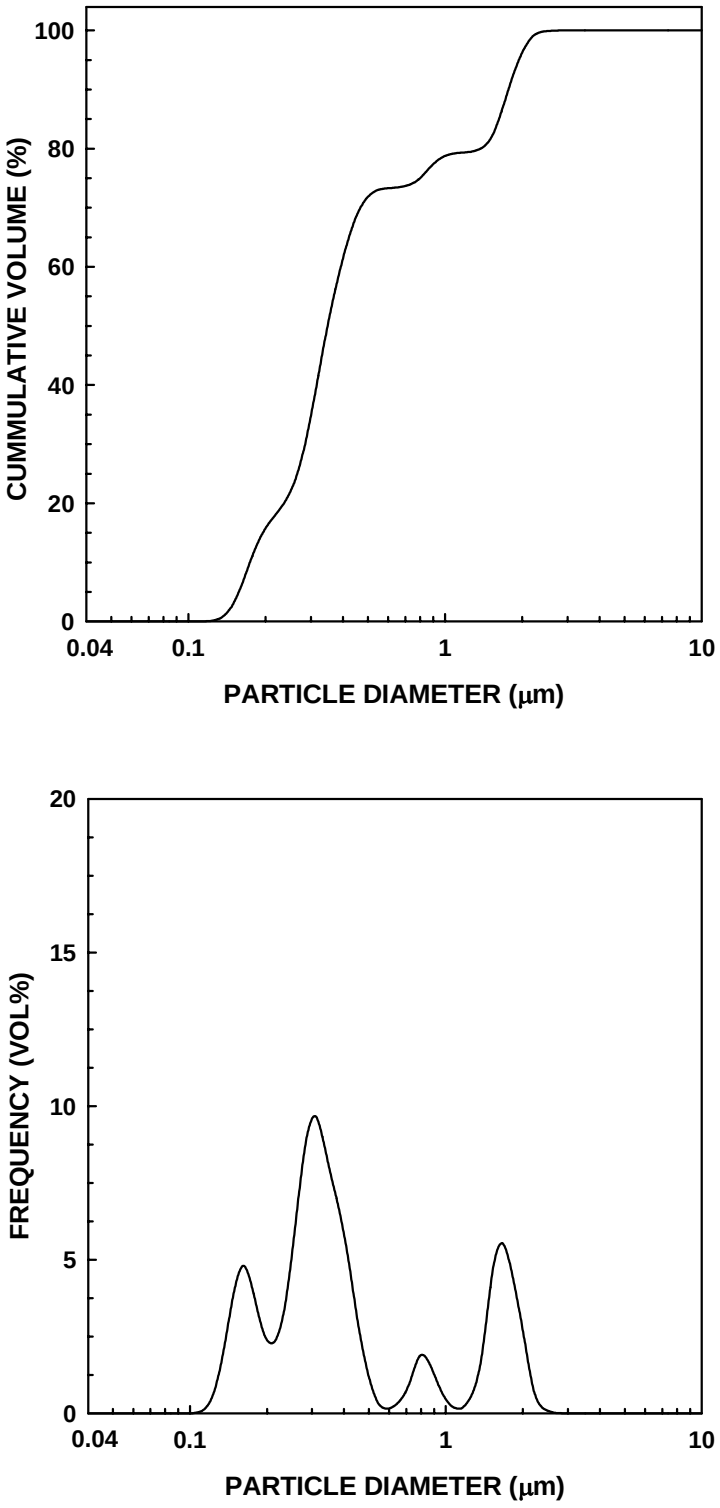

Figure 4.19 Particle size distribution of milled ZrPM-99 powder samples using TiC data a) cumulative distribution plot b) relative frequency plot.

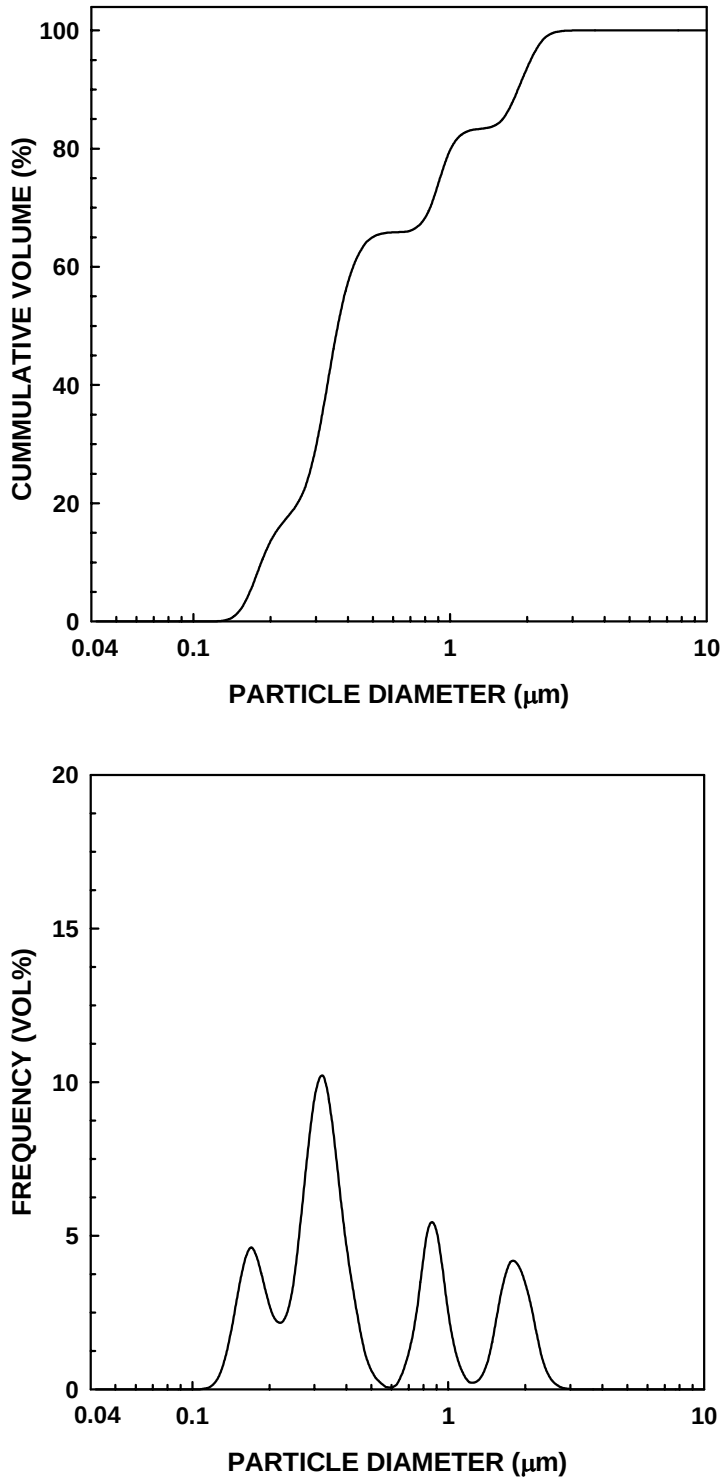

Figure 4.20 Particle size distribution plots for the milled ZrPM-99–800-1475 powder using self-defined-1 data: cumulative distribution plot (top) and relative frequency plot (bottom).

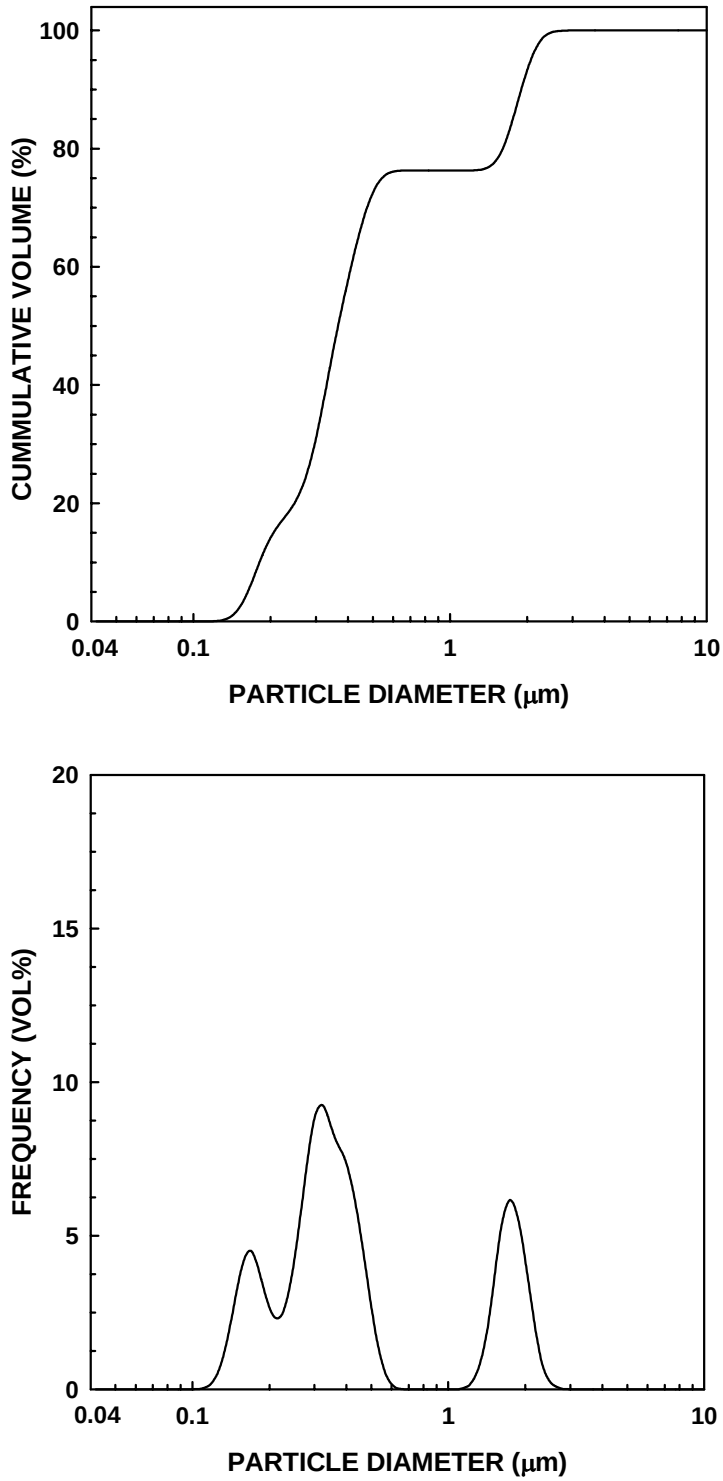

Figure 4.21 Particle size distribution plots for the milled ZrPM-99–800-1475 powder using self-defined-2 data: cumulative distribution plot (top) and relative frequency plot (bottom).

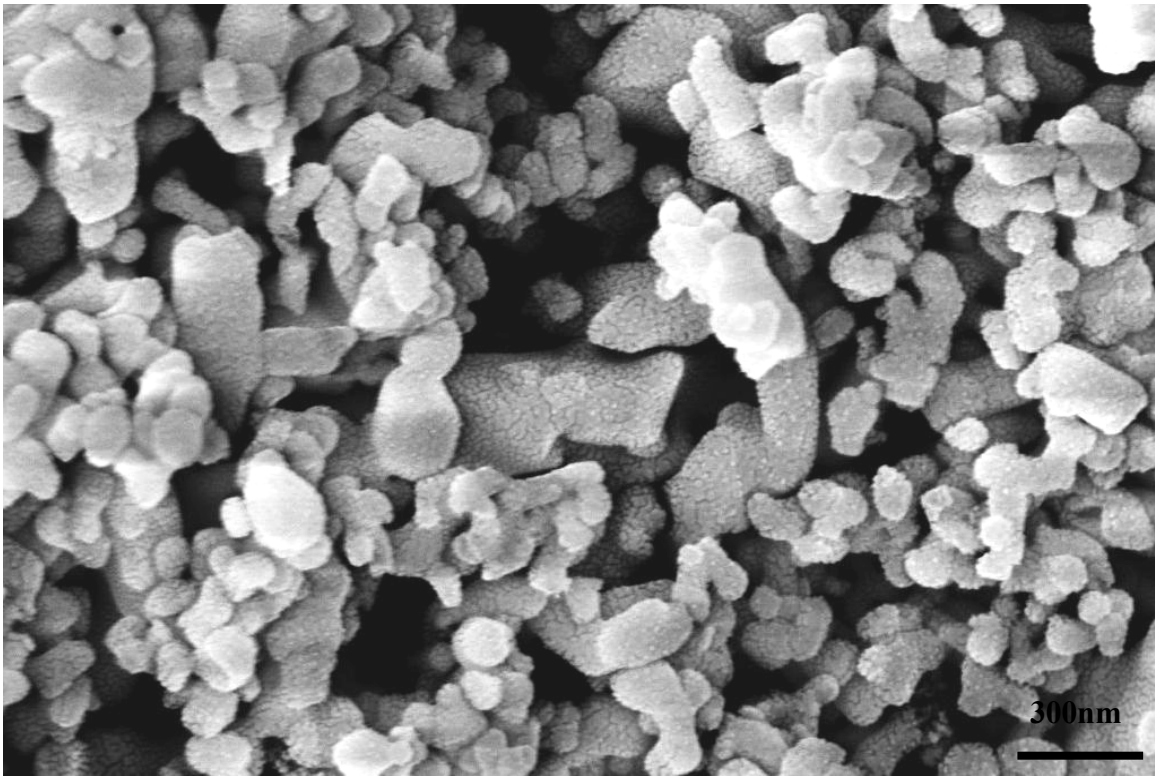

Figure 4.22 SEM micrograph of milled ZrPM-99-800 powder sample heat treated at 1475^{o}C for 2 h.

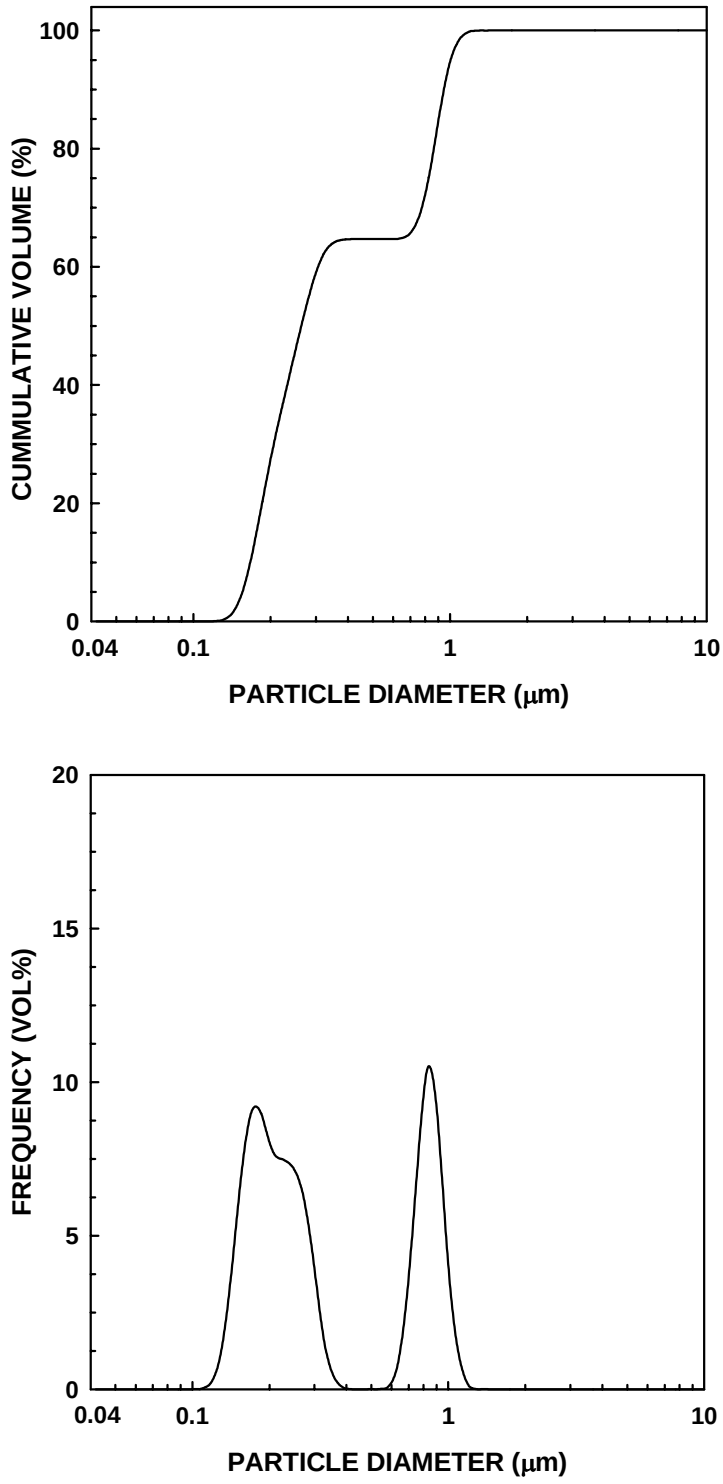

Figure 4.23 Particle size distribution plots for the milled ZrPM-99–800-1475 powder using self-defined-3 data: cumulative distribution plot (top) and relative frequency plot (bottom).

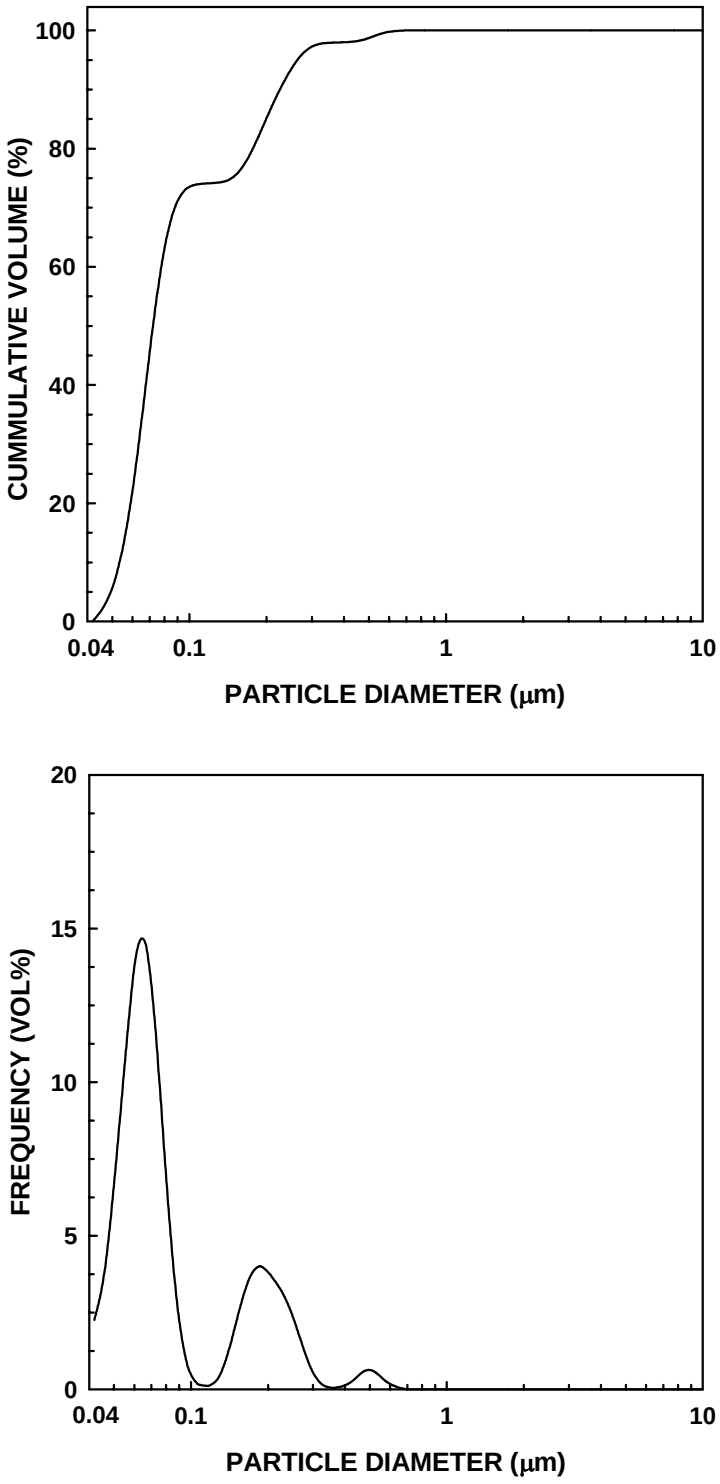

Figure 4.24 Particle size distribution plots for the milled ZrPM-99–800-1475 powder using self-defined-4 data: cumulative distribution plot (top) and relative frequency plot (bottom).

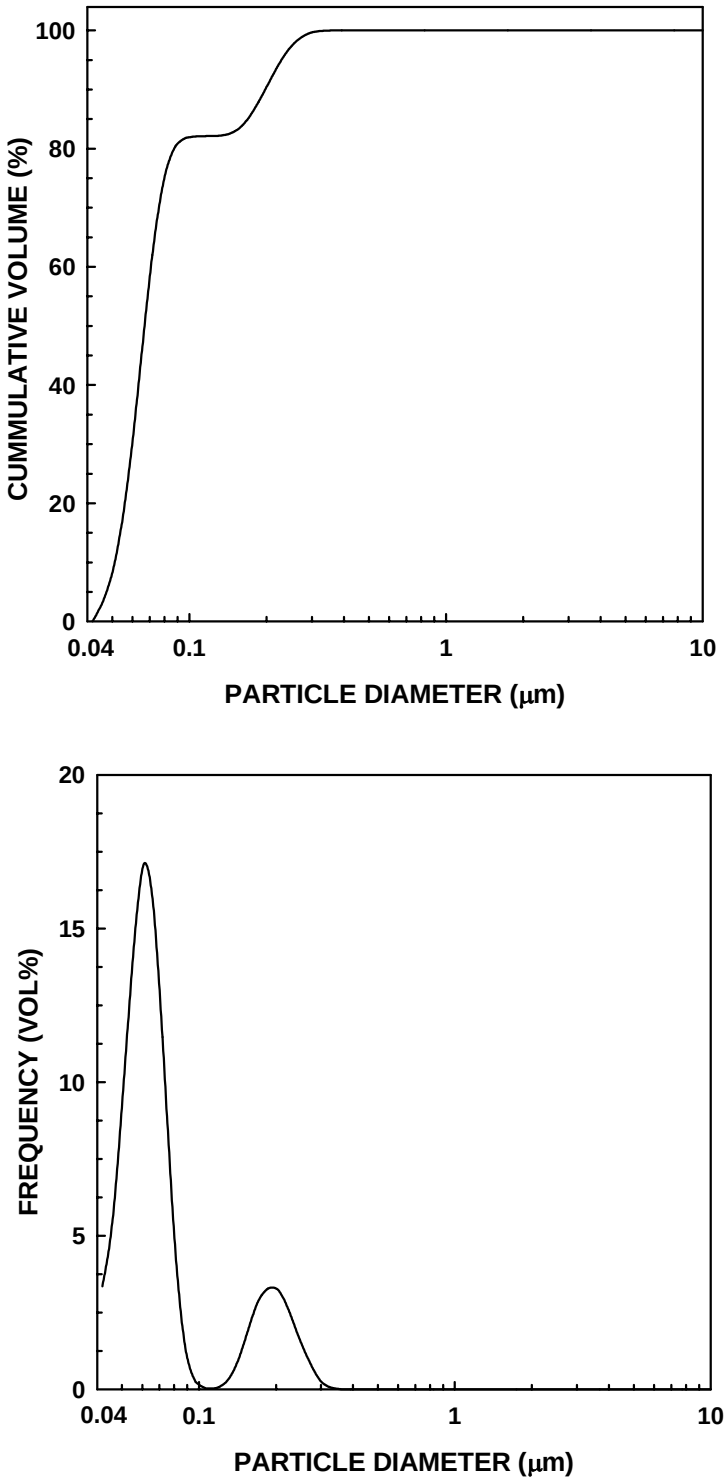

Figure 4.25 Particle size distribution plots for the milled ZrPM-99–800-1475 powder using self-defined-5 data: cumulative distribution plot (top) and relative frequency plot (bottom).

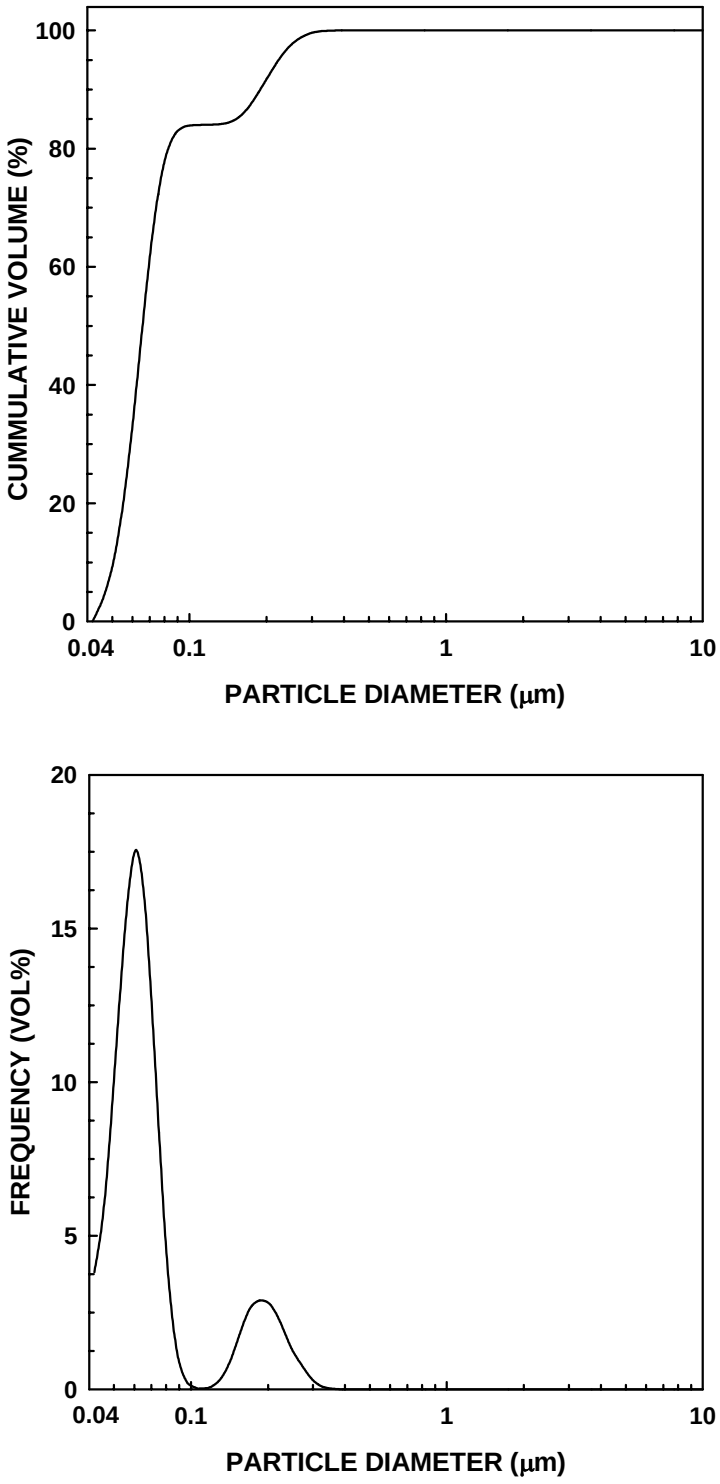

Figure 4.26 Particle size distribution plots for the milled ZrPM-99–800-1475 powder using self-defined-6 data: cumulative distribution plot (top) and relative frequency plot (bottom).

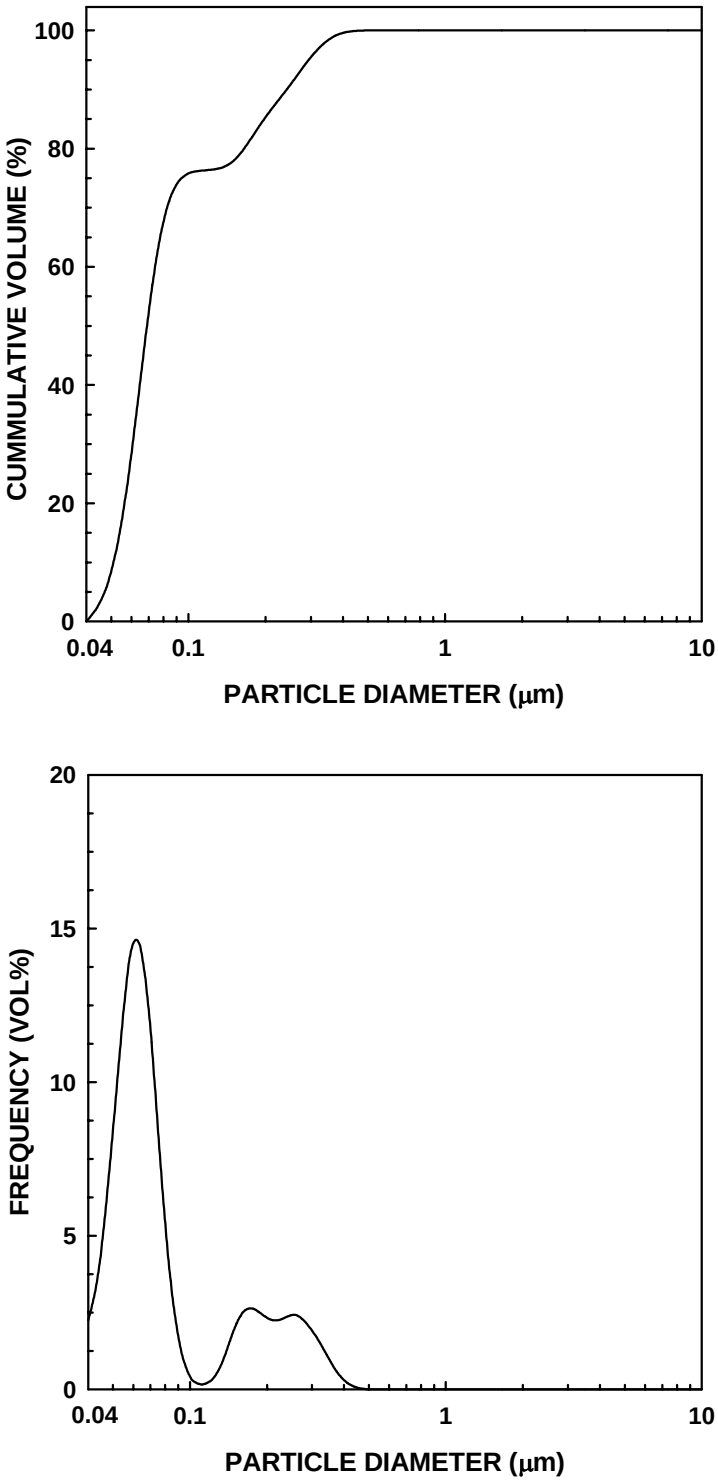

Figure 4.27 Particle size distribution plots for the milled ZrPM-99–800-1475 powder using SiC data: cumulative distribution plot (top) and relative frequency plot (bottom).

4.3 Pressureless Sintering of ZrC

4.3.1 Sample Preparation and Sintering Conditions

4.3.1.1 Green Body Preparation

Powder compacts were prepared from the ZrC-based powders by dry pressing. A conventional polymeric "binder system" was used to facilitate the dry pressing operation.[78] Binder systems used in dry pressing of powders usually contain a higher-molecular-weight polymer (i.e., the "binder" which is used mostly to improve strength) and a low-molecular-weight polymer (i.e., the "plasticizer" which is used mostly to improve plasticity). In this study, the binder was a polyvinyl alcohol-polyvinyl acetate copolymer ("PVA", 88% hydrolyzed, grade 205 polyvinyl alcohol, 11,000-31,000 molecular weight, Air Products and Chemicals Inc., Allentown, PA) and the plasticizer was polyethylene glycol ("PEG", 1000 molecular weight, 1000NF, FCC grade polyethylene glycol, Union Carbide Chemicals and Plastics Company Inc., Danbury, CT). The ratio of binder to plasticizer for this study was 85:15 by weight. Binder solutions were prepared by adding PVA and PEG, one by one, to deionized water to make up a 5 wt% solution. The water was heated to 60^{o}C prior to addition of PVA/PEG in order to increase the dissolution rate. The solution was continuously stirred using a magnetic stirrer for ~20 min.

Powder samples used for dry pressing were prepared with approximately 10 vol% polymer. The required amount of polymer solution was ~0.37 ml per gram of ZrC-based powder. This amount was calculated using the following assumptions: solid density of ZrC-based powder = 6.6 g/cm^3, solid density of binder/plasticizer = 1.15 g/cm^3. The binder solution was added to the powder sample drop by drop using a 1 ml syringe and

was simultaneously mixed the powder using a spatula. The time of adding the binder/plasticizer solution varied with the powder sample size (~1.6–4.8 g) and was in the range ~45–100 sec. Extreme care was taken to add the solution slowly and thoroughly mix it with the powder sample using the spatula. The mixture was then dried in an air oven (Isotemp oven, Fisher Scientific, Fair Lawn, NJ) at 70°C for at least three hours to evaporate the water. The coarse powder chunks were first broken up using a spatula and then lightly ground using a quartz mortar and pestle. The powder was then sieved through a 150-mesh screen.

The sieved powders were used to form powder compacts by uniaxial dry pressing. Samples were prepared using stainless steel die sets with diameters of 6.4 mm and 14 mm. The die sets were first cleaned using Kimwipe® paper tissue. The inside surfaces of the dies were lubricated using a stearic acid/toluene solution which was applied by using a cotton swab. (The stearic acid/toluene solution was prepared by adding ~5 g of stearic acid (Fisher Scientific, Fair Lawn, NJ) to 100 ml of toluene (Fisher Scientific, Fair Lawn, NJ).) The toluene was allowed to evaporate and a lubricating film of stearic acid remained on the die surfaces. ~0.7 g and ~0.4 g of powders were used for pressing in the 14 mm and 6.4 mm dies, respectively. Most of the dry powders were compacted at ~250 MPa using a manually-operated hydraulic press (Model #3925, Carver Inc., Wabash, IN). Some powder samples were compacted at pressures in the range of 140 – 210 MPa. The time to reach the maximum pressure was in the range of 10 – 20 sec and the hold time at maximum pressure was ~1 min.

4.3.1.2 "Pre-Sintering" Heat Treatments

4.3.1.2.1 Binder Burnout

After pressing, pellets were heat treated in a flowing argon (100 ml/min) atmosphere to remove the organic binder. The pellets were placed on an alumina substrate and heated to 1150^{o}C (5^{o}C/min to 150^{o}C, 2^{o}C/min to 600^{o}C, 5^{o}C/min to 1150^{o}C) with a hold of 2 h at the maximum temperature in a tube furnace (Model 55031, Lindberg, Watertown, WI). The dimensions and weights of the pellets before and after the binder burnout were recorded by using a vernier caliper (smallest measured division = 10 μm). The measurements were made at different points on the sample and data were averaged for at least 5 readings.

4.3.1.2.2 "Pre-Sintering"

Some of the samples, after binder burnout, were given a "pre-sintering" heat treatment. The samples were heated in the 3-zone furnace (Model 54259, Lindberg, Watertown, WI) under a flowing (100 ml/min) argon atmosphere. The samples were heated at 5^{o}C/min to 1490^{o}C and held at temperature for 4 h. The furnace was allowed to cool naturally by switching off the power.

Pre-sintering was carried out for two reasons: (1) The samples produced after the binder burnout did not have high strength. There was some concern that samples might fracture due to differential stresses that could arise because of the rapid heating rates used in many of the sintering experiments. The "pre-sintering" heat treatment would give the samples improved strength. (2) CTR reactions, with accompanying weight loss, were not complete in the powders used to form the powder compacts. (Results concerning the

weight losses that occur during high temperature heat treatment of samples are described in Chapter V.) There was some concern that the evolution of gaseous volatiles during rapid heating might damage the samples. A "pre-sintering" heat treatment would allow for more CTR weight losses to occur in the samples prior to higher temperature sintering experiments.

As discussed in Chapter V (section 5.6.1), the "pre-sintering" heat treatment actually resulted in some densification/sintering of the samples, so the term "pre-sintering" was not an accurate description of the process. Furthermore, it was subsequently determined that the "pre-sintering" heat treatment was unnecessary. This was because the high heating rates used in the sintering experiments did not have any obvious adverse effect on the samples. None of the samples fractured during sintering. Hence, a "pre-sintering" heat treatment was not used for samples prepared later in the study.

4.3.1.3 Sintering

4.3.1.3.1 Studies Based on Only Post-Sintering Shrinkage/Densification Measurements

The 1150^{o}C heat treated and “pre-sintered” samples were placed in the M11 furnace tube on “ZrC” substrates. The furnace chamber was evacuated and heated to 300^{o}C under vacuum. This was done in order to remove any water adsorbed on the sample and the interior parts of the furnace. The chamber was initially evacuated to pressures in the range of 50–100 millitorr prior to heating to 300^{o}C. The furnace was then

heated at 300°C and vacuum was pulled until vacuum levels in the range of 25–35 millitorr were obtained.

Argon gas was then back-filled in the furnace chamber and a flow rate of 500 ml/min was maintained for sintering experiments. The samples which had been initially "pre-sintered" at 1490°C were sintered with the following schedule: (i) heating rate of 50°C/min to 1450°C, 20°C/min to 1470°C, 10°C/min to 1480°C, 5°C/min to 1485°C, 2°C/min to 1489°C, 1°C/min to 1490°C and 5°C/min to sintering temperatures in the range of 1600 – 1950°C and (ii) hold at the maximum temperature for times in the range of 1-16 h. Other samples (without the "pre-sintering" treatment) were heated at ~5°C/min to temperatures in the range 1600-1950°C and held at the maximum temperature for 1 h. The furnace was programmed to cool at 50°C/min to room temperature. (However, cooling slowed to less than 50°C/min after the temperature decreased ~600-900°C below the isothermal hold temperature.)

The weight and linear dimensions of each sample were recorded before and after each heat treatment in order to determine the sample weight loss, linear shrinkage, and bulk density.

4.3.1.3.2 Studies Based on In-Situ and Post-Sintering Shrinkage Measurements

A high-temperature dilatometer system was used to determine linear dimensional changes in samples during sintering at temperatures up to 2200°C. A description of some design aspects of the dilatometer, reproduced mostly from reference 79 is given below:

"The dilatometer furnace (Model 1000-2560-FP, Thermal Technology, Inc., Santa Rosa, CA) used for the heat treatments was comprised of graphite heating elements

and fibrous insulation. Temperature was monitored using an optical pyrometer (Model MA1SC, Raytek Co., Santa Clara, CA), which was sighted on the graphite casing (which surrounded the dilatometer) near the sample. Measurements were made at a wavelength of 1.0 μm through a fused silica viewing port mounted on the furnace radial wall. The calibration readings of the pyrometer were within $\pm 10^{o}C$ of a tungsten-rhenium thermocouple for temperatures over the range of 750 to $2200^{o}C$."[79]

A vertical double-pushrod dilatometer (Theta Industries, Inc., Port Washington, NY) extended into the furnace. A cylindrical casing that covered/surrounded the dilatometer and the dilatometer pushrods was made of graphite (Poco Graphite Inc., Decatur, TX). A counterweight was applied to the sample pushrod to minimize the load on the sample (i.e., the load due to the weight of the pushrod). The advantage of the two-pushrod dilatometer over a single-pushrod dilatometer was that the measurements were more precise and more accurate. In single-pushrod dilatometers, the expansion behavior of the sample may be affected by expansion of the pushrod/casing material. In two-pushrod dilatometers, the expansion of pushrod/casing material has no affect on the measurements because they are recorded with respect to a reference material.

The dilatometer used a linear variable differential transformer (LVDT) position transducer to measure specimen expansion/shrinkage. The voltage output of the LVDT was converted to units of length via a calibration constant. The electrical output of the LVDT was compared to that of micrometer displacement readings and a least-squares fit was done to obtain an optimum fit between the voltage output and the change in length.

Dilatometry measures the overall linear dimensional changes in the sample. For a dense sample, the dimensional changes are due to the thermal expansion or contraction

that occur upon heating or cooling, plus the dimensional changes associated with any phase changes/chemical reactions that occur within the sample. For a sample undergoing sintering, there is also the shrinkage that occurs as a result of densification process.

To separate out the dimensional changes due to sintering (densification), an almost 100% dense sample of ZrC was first heated in the dilatometer and its expansion data was recorded. The heating rate used to collect this data was same as used for sintering measurements. The expansion data was then subtracted, automatically by using the computer software, from the expansion/contraction data collected during the sintering experiments.

The samples were carefully placed below the pushrod and were lowered into the furnace chamber. It was of primary importance that sample did not move or fall off into the furnace chamber while being lowered into the furnace; this was verified by noting the reading of LVDT before and after the sample was lowered inside the furnace chamber. The chamber was then sealed, evacuated, and backfilled with helium gas. This step was repeated to ensure that all the air had been removed from the furnace chamber. The flow rate of helium gas was 1 standard cubic feet per hour (scfh) for all the sintering experiments. The heating schedule used for the experiments was 50^{o}C/min to 1400^{o}C, 10 min hold at 1400^{o}C, and 2-10^{o}C/min to 1900 - 2200^{o}C. The pyrometer could only record temperatures above 750^{o}C, so no data was collected below 750^{o}C.

4.3.2 Characterization of Sintered Samples

4.3.2.1 Linear Shrinkage Measurements (Axial and Radial)

The diameter and thickness of green and sintered samples were measured using vernier calipers. The measurement conditions were the same as described in section 4.3.1.2.1. The density was calculated by using the equation:

$$Density = \frac{Weight}{Volume} \tag{4-32}$$

The volume was calculated by following equation:

$$Volume = \pi \times (Radius)^2 \times Thickness \tag{4-33}$$

Determination of volume was, by far, the bigger source of error (i.e., compared to the weight measurement which was done using an analytical balance). This was because the sintered samples were not perfect cylinders. Furthermore, in some cases, some very small pieces were lost from the edges or faces of the samples.

The percent shrinkages in the axial and radial directions were calculated by the equations given below.

Axial Shrinkage:

$$\%shrinkage_a = \frac{t_o - t}{t_o} \times 100 \tag{4-34}$$

where t is sample thickness after sintering and t_o is sample thickness before sintering.

Radial Shrinkage:

$$\%shrinkage_r = \frac{r_o - r}{r_o} \times 100 \tag{4-35}$$

where r is sample radius after sintering and r_o is sample radius before sintering.

4.3.2.2 Bulk Density and Open Porosity Measurements by the Archimedes Method

The Archimedes method was used to determine density and open porosity of the sintered samples. The pellet was first dried in an air oven at 70^{o}C for at least 1 h. The dried weight was measured and this step was repeated to check for reproducibility of data. The pellet was placed in a beaker and the beaker was put in a vacuum chamber. This chamber was evacuated for ~2 min by using a vacuum pump (Model #8890, Welch Vacuum Technology Inc., Skokie, IL). Under vacuum, the beaker in the chamber was filled with DI water by using the set-up shown in Figure 4.28.

The chamber was then kept under vacuum for ~2 h to promote complete infiltration of water into the pores, if any were present. The pellet was then taken out of the vacuum chamber, taking care that it remained submerged completely under water in the beaker. The "suspended weight" was recorded by using the set-up shown in Figure 4.29. The sample was then taken out of water and the sample surfaces were wiped off by using a Kimwipe® "delicate task" wiper (Kimberly-Clark, Roswell, GA). The pellet was then immediately placed in a previously weighed vial and the vial was quickly sealed. The vial (with the sample) was weighed and the "saturated weight" of the sample was determined. This procedure was used in order to minimize changes in the "saturated weight" of the sample as a result of evaporation of water from the near-surface region of the sample.

The temperature of the water was recorded to the nearest 0.1^{o}C. The sample was then dried in an oven in air at 70^{o}C until it gave a constant value for the "dry weight." The bulk volume (*BV*), percentage open porosity (%*OP*), and the bulk density (*BD*) for the pellet were then calculated by using the following equations:

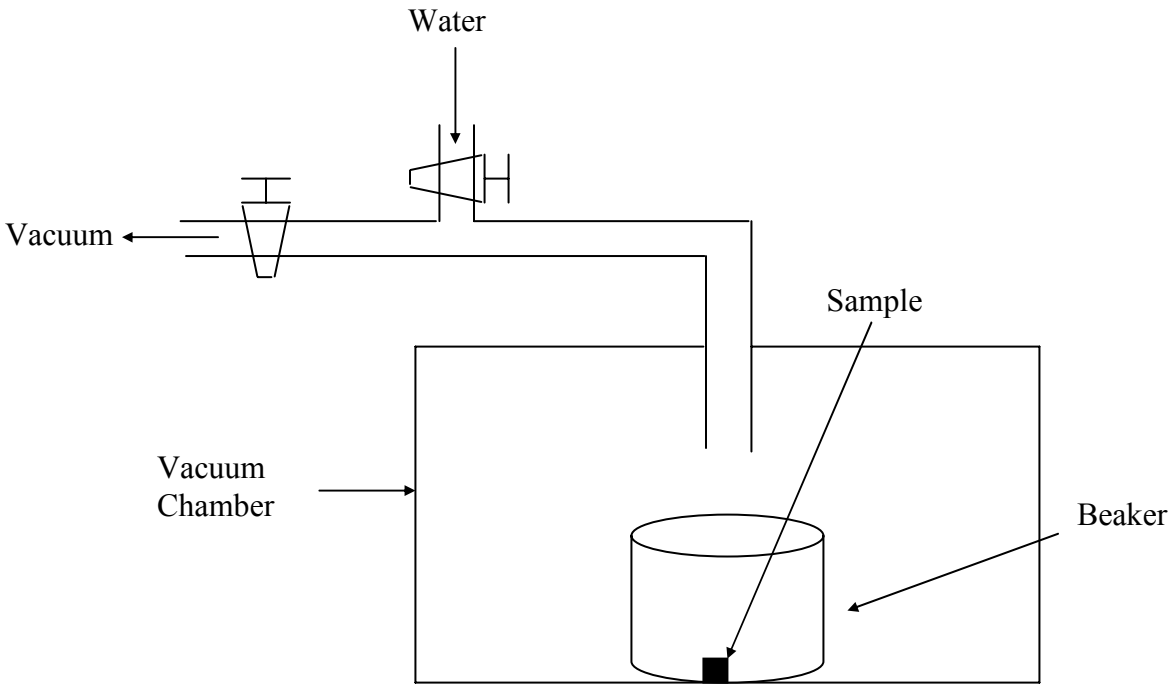

Figure 4.28 Set-up for evacuating and back filling water into a beaker.

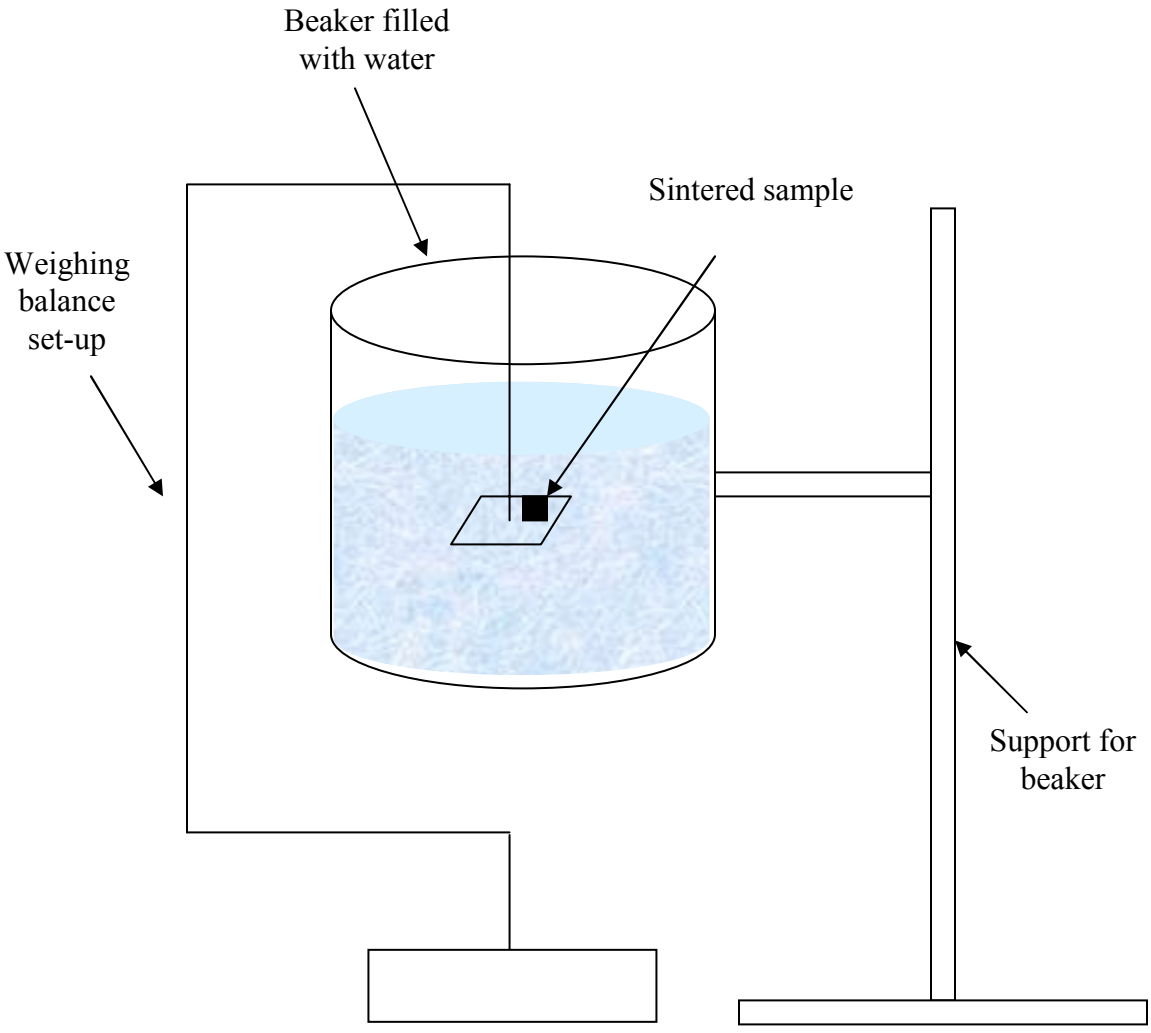

Figure 4.29 Set-up to obtain the suspended weight using an analytical weighing balance.

$$BV = \frac{SaW - SuW}{DL} \tag{4-36}$$

$$\%OP = \left(\frac{SaW - DW}{SaW - SuW} \right) * 100 \tag{4-37}$$

$$BD = \frac{DW}{BV} \tag{4-38}$$

where SaW is the saturated weight, SuW is the suspended weight, DL is the density of liquid, and DW is the dry weight.

4.3.2.3 Relative Density Calculations

Relative density, RD, (i.e., percentage of the theoretical density of the solid material) were calculated by using the following equation:

$$RD = \frac{BD}{TD} \times 100 \tag{4-39}$$

where BD is the bulk density and TD is the true (theoretical) density of the pore-free solid.

The bulk density was obtained using the measurement methods described in section 4.3.2.2, i.e., by using the geometric dimensions of the sample and/or the Archimedes method. The true density of the solid was estimated based on the phase composition and the true densities of each phase that was present in the solid. However, the true densities

were estimated values because the phase compositions and true densities of some of the phases were estimated. Depending on the particular sample, the phases present included zirconium carbide, monoclinic zirconia (m-ZrO_2), tetragonal zirconia (t-ZrO_2), and/or carbon. Futhermore, the "zirconium carbide" often was not stoichiometric ZrC, but instead was either a zirconium oxycarbide (ZrC_xO_y) or a carbon-deficient zirconium carbide (ZrC_{1-x}). The assumptions made in estimating the true density values for specific samples are given in individual sections in Chapter 5. However, some general procedural considerations that were used in making the estimates are given here:

(1) The composition and density of the "zirconium carbide" phase were estimated by using measured lattice parameters and by sometimes using available compositional information (i.e., measured carbon contents for the overall sample).

(2) The amounts of t-ZrO_2 and m-ZrO_2 in samples were estimated based on the integrated peak areas in the XRD patterns. The procedure is described in more detail in Appendix G.

(3) The amount of "free" carbon in samples was estimated from the overall carbon content in the sample. The density of the "free" carbon was estimated based on the following considerations. Bulk density values are typically reported in the range of ~1.4-1.6 g/cm^3 for relatively coarse "glassy carbon" samples prepared by heat treatment of phenolic-based resins at various temperatures.[80,81,82] However, these values are for samples that contained substantial amounts of closed porosity.[80,81,82] Furata et al. [83] reported true (solid) densities for carbons derived from phenolic resins by using measured d-spacings obtained from X-ray diffraction analysis. The density values

increased gradually in the range of 2.12 - 2.26 g/cm^3 as the heat treatment temperature increased from 1000^{o}C to 3000^{o}C. This was due to increasing crystallinity of the carbons with increasing heat treatment temperature. The highest density value (i.e., 2.26 g/cm^3) is the true density for well-crystallized graphite. Density values in the range of 1.9-2.1 g/cm^3 have been reported for submicrometer vapor-grown carbon fibers.[84,85] The higher values in the aforementioned density range were associated with fibers which had a higher degree of graphitization.

The "free" carbon regions in the "carbon-rich" CTR samples in this study are believed to be have fine-scale dimensions (i.e., <0.1 μm). (This is suggested because the sizes of the ZrC primary particle for most CTR samples were roughly on the order of ~0.1 μm.) Therefore, the carbon regions in the CTR samples are not expected to have any significant amount of closed porosity. Hence, it was assumed that a true (solid) density for carbon should be used in calculating the overall solid density of the ZrPM material. The carbon true density was expected to be considerably less than the value for graphite (2.26 g/cm^3) because the carbon present in the samples in this study was not well-crystallized. This conclusion was reached because well-defined peaks for graphite were not observed in any of the XRD patterns. (In addition, it is also known from the literature [refs] that carbons derived from phenolic resins usually do not shown extensive graphitization at the temperatures used in this study.) Therefore, considering the glassy nature of the carbon in this study, it was decided that a value of 2 g/cm^3 would be used as a rough estimate for the carbon true density. The same value was used for all samples regardless of the heat treatment temperature.

4.3.2.4 Polishing

Some sintered samples were polished in order to observe the microstructure under SEM. A hollow aluminum cylinder (2.5 mm diameter and 15 mm high) was placed on a flat glass piece. The sintered sample was then centrally placed inside the aluminum cylinder. Quickmount® resin (Buehler Ltd., Lake Bluff, IL) solution was then poured into the cylinder and was allowed to cure for ~30 min. The mounted sample was separated from the aluminum cylinder. The surface of the mounted sample was ground (by the same method described in section 4.2.3.1.1.2) in order to obtain a flat surface that would subsequently be used for polishing. The mounted sample was then polished (~3 – 4 days) with a 6 μm diamond suspension (Metadi® Diamond Suspension, Buehler Ltd., Lake Bluff, IL) using a vibratory polisher (Vibromet® I, Beuhler Ltd., Lake Bluff, IL).

CHAPTER V

RESULTS AND DISCUSSION

5.1 Solution-Based Synthesis of Zirconium Carbide

In this section, the effects of various solution synthesis variables on the C:Zr molar ratio and other characteristics of pyrolyzed powder are described.

5.1.1 Processing-Related Observations for Synthesized Batches

Table 5.1 gives processing-related qualitative observations, measured yields upon pyrolysis, and calculated C/Zr molar ratios (based on oxidation weight loss measurements) for all ZrPM batches. The table lists qualitative observations concerning the following: the occurrence of precipitation during processing of solutions, the color of the solution-processed powder after oven drying, the homogeneity of the oven-dried powders, and the occurrence of melting during pyrolysis.

The color of the dried powder for almost all batches ranged from light yellow to dark brown. It is not known why a few batches (ZrPM-13 and ZrPM-24b) showed some different colors (i.e., other than yellow/brown) after drying. The batches had similar color after the final concentration step, so the color differences in the dried powders were caused by the drying process. The variations in color may have been related to small differences in the oven temperature, differences in sample and flask sizes, differences in phase composition of the batches, etc. It is speculated (with no supporting evidence) that the darker colors (more brown) may indicate that some very early stage decomposition reactions had been initiated in the precursors for some batches.

The term "precipitation" was used when precipitates were observed throughout the solution. As a result, the solution was no longer transparent and, instead, became hazy. (In some cases, settling of particles was observed if solutions were allowed to stand (without mixing) for an extended period. This observation was made on a few batches in which processing was discontinued because the precipitation was very extensive.) The precipitation that occurred during the acacH addition is referred to as "Type-1." The precipitation that occurred during cooling of the solution after the acacH refluxing step is referred to as "Type-2." The precipitation that occurred during the initial concentration after the refluxing step is referred to as "Type-3." (Unless the processing was discontinued due to extensive precipitation, the Types 1-3 precipitation were reversed (i.e., the precipitates re-dissolved) when one of the subsequent processing steps (ethanol, acid, or water additions) was made.) The precipitation that occurred after the water addition is referred to as "Type-4." The precipitation that occurred during the final concentration is referred to as "Type-5." The author was unable to identify any relationships between the occurrence of a type of precipitation and any of the solution processing variables. The product after the final concentration step had the appearance of a highly viscous liquid or a more solid-like gel.

There were two types of inhomogeneity observed in some of the oven-dried batches: (1) Two or more colors could be observed throughout the dried powder. This type of inhomogeneity is referred to as "inhomogeneous-1." This type of inhomogeneity was only developed in some batches after the drying step. (The material obtained after the final concentration step was homogeneous in color for all batches.) Some batches that were directly concentrated after the acacH-refluxing step (i.e., without any acid

addition, water addition, or aging steps) exhibited "inhomogeneous-1" characteristics. (2) Partial melting was observed in some samples during the oven drying step (at 120oC) and, as a result, the dried material was an inhomogeneous mixture of powder and solid chunks of "melted material." This type of inhomogeneity is referred to as "inhomogeneous-2." Batches with high acacH/Zr molar ratio (i.e., >6) exhibited "inhomogeneous-2" characteristics.

The term "melting" refers to samples that melted extensively during pyrolysis in a flowing argon atmosphere. The samples that melted were essentially one solid mass and did not retain the characteristics of a powder after pyrolysis. The term "slight melting" refers to samples in which some sharp edges of the powders became rounded or formed a bead-like shape during pyrolysis. However, the overall sample retained the characteristics of a powder. Melting was usually observed in batches which were directly concentrated after the acacH refluxing step and in batches that had high acacH/Zr molar ratio (i.e., >6).

Table 5.1 Processing-related observations, yields upon pyrolysis, and C/Zr molar ratios in the pyrolyzed material for batches synthesized.

ZrPM Batch Number	Precipitation	Color	Powder Homogeneity	Melting During Pyrolysis	Pyrolysis Yield (wt%)*		C/Zr Molar Ratio	
					TGA	Pyro Furnace	TGA**	Pyro Furnace**
1a	None	Uniform dark brown	Homogeneous	Yes	46.7	N.A.	1.6	N.A.
1b	None	Uniform dark brown	Homogeneous	No	N.A.	N.A.	1.4	N.A.
1c	None	Uniform pale yellow	Homogeneous	No	56.1	N.A.	2.0	N.A.
1d	None	Uniform yellow	Homogeneous	No	59.0	N.A.	1.7	N.A.
2	Type-2	N.A.	N.A.	N.A.		N.A.	-	N.A.
3a	Type-2	Uniform dark yellow	Homogeneous	Yes	49.0	N.A.	3.6	N.A.
3b	Type-2	Light and dark brown	Inhomogeneous-2	Yes	N.A.	N.A.	1.9	N.A.
3c	Type-2	Uniform pale yellow	Homogeneous	Yes	N.A.	N.A.	1.8	N.A.
4a	None	Dark yellow and brown	Inhomogeneous-1	Yes	N.A.	N.A.	3.5	N.A.
4b	None	Dark brown	Inhomogeneous-2	No	48.8	N.A.	2.8	N.A.
4c	None	Uniform brown	Homogeneous	No		N.A.	2.7	N.A.
5	Type-1	Uniform dark yellow	Homogeneous	Yes	41.9	N.A.	4.9	N.A.
6	None	Dark brown	Inhomogeneous-2	Yes	41.7	N.A.	4.3	N.A.
7	Type-1	Uniform yellow	Homogeneous	No	N.A.	N.A.	N.A.	N.A.
8	Type-1	Uniform light yellow	Homogeneous	No	N.A.	N.A.	N.A.	N.A.
9	None	White and yellow	Inhomogeneous-1	No	N.A.	N.A.	N.A.	N.A.

Table 5.1 continued.

ZrPM Batch Number	Precipitation	Color	Powder Homogeneity	Melting During Pyrolysis	Pyrolysis Yield (wt%)*		C/Zr Molar Ratio	
					TGA	Pyro Furnace	TGA**	Pyro Furnace**
10	None	Uniform pale yellow	Homogeneous	Yes	51.1	N.A.	2.3	N.A.
11	N.A.	N.A.	N.A.	N.A.	N.A.	N.A.	N.A.	N.A.
12	None	Dark yellow and brown	Inhomogeneous-1	No	N.A.	N.A.	N.A.	N.A.
13	None	Dark orange with pink tinge	Inhomogeneous-1	No	N.A.	N.A.	N.A.	N.A.
14	None	Uniform pale yellow	Homogeneous	Yes	45.1	N.A.	4.2	N.A.
15	None	Uniform light yellow	Homogeneous	No	58.2	N.A.	1.5	1.3
16	None	Uniform light yellow	Homogeneous	No	56.9	56.5	1.3	1.3
17	None	Uniform pale brown	Homogeneous	Yes	55.2	N.A.	2.0	N.A.
18	None	Uniform pale brown	Homogeneous	Yes	N.A.	47.9	N.A.	2.2
19	None	Uniform pale brown	Homogeneous	Yes	44.8	50.3	2.0	1.9
20	None	Uniform dark brown	Homogeneous	No	59.2	57.7	2.1	1.7
21	None	Uniform dark brown	Homogeneous	No	N.A.	56.7	1.4	2.8
22	None	Uniform dark yellow	Homogeneous	No	59.0	59.7	2.0	2.1
23	None	Uniform brown	Homogeneous	No	N.A.	N.A.	1.8	N.A.
24a	None	Uniform pale amber	Homogeneous	Yes	N.A.	39.0	N.A.	6.1
24b	None	Brown	Inhomogeneous-2	Yes	40.0	41.6	5.9	5.0

Table 5.1 continued.

ZrPM Batch Number	Precipitation	Color	Powder Homogeneity	Melting During Pyrolysis	Pyrolysis Yield (wt%)*		C/Zr Molar Ratio	
					TGA	Pyro Furnace	TGA**	Pyro Furnace**
24c	None	Red and brown	Inhomogeneous-2	Yes	43.3	43.3	5.2	6.1
25a	None	Dark brown	Inhomogeneous-2	Yes	53.5	54.6	2.9	3.6
25b	None	Dark brown	Inhomogeneous-2	Yes	N.A.	54.6	N.A.	4.8
26	None	Dark brown	Inhomogeneous-2	Yes	53.5	51.9	2.4	2.4
27a	None	Brown	Inhomogeneous-2	Yes	55.7	56.9	2.6	3.2
27b	None	Uniform light brown	Homogeneous	Yes	N.A.	53.6	N.A.	3.6
27c	None	Brown	Inhomogeneous-2	Yes	N.A.	51.5	N.A.	3.9
28	None	Dark brown	Inhomogeneous-2	Yes	49.2	48.7	1.9	2.4
29	None	Dark brown	Inhomogeneous-2	Yes	52.3	51.9	2.6	3.2
30	None	Dark brown	Inhomogeneous-2	Yes	52.2	49.0	2.5	2.3
31	None	Dark yellow and brown	Inhomogeneous-2	Yes	N.A.	58.7	N.A.	3.0
32	None	Dark brown	Inhomogeneous-2	Yes	53.0	53.1	3.0	3.2
33	None	Dark brown	Inhomogeneous-2	Yes	45.1	44.0	3.8	3.5
34	None	Dark brown	Inhomogeneous-2	Yes	46.4	46.6	4.6	4.7
35	None	Dark brown	Inhomogeneous-2	Yes	48.4	49.3	4.9	5.2
36	None	Dark brown	Inhomogeneous-2	Yes	53.8	55.1	2.8	3.2
37	None	Uniform yellow	Homogeneous	No	60.7	61.4	2.2	2.4
38	None	Uniform pale yellow	Homogeneous	Yes	42.5	41.8	5.1	5.6
39	None	Uniform yellow	Homogeneous	No	N.A.	61.7	N.A.	2.2
40	None	Uniform yellow	Homogeneous	No	N.A.	59.7	N.A.	2.4
41	Type-4	Uniform yellow	Homogeneous	No	60.3	61.6	2.1	2.4
42	Type-4	Uniform yellow	Homogeneous	Slight melting	N.A.	62.3	N.A.	2.0
43	None	Uniform light yellow	Homogeneous	No	59.6	60.9	2.5	2.9

Table 5.1 continued.

ZrPM Batch Number	Precipitation	Color	Powder Homogeneity	Melting During Pyrolysis	Pyrolysis Yield (wt%)*		C/Zr Molar Ratio	
					TGA	Pyro Furnace	TGA**	Pyro Furnace**
44	None	Uniform light yellow	Homogeneous	Yes	N.A.	N.A.	N.A.	N.A.
45	None	Uniform dark yellow	Homogeneous	No	61.0	62.0	3.4	3.7
46	N.A.	N.A.	N.A.	N.A.	N.A.	N.A.	N.A.	N.A.
47	None	Uniform light yellow	Homogeneous	Yes	52.2	54.1	2.6	2.7
48	None	Uniform light yellow	Homogeneous	Slight melting	53.6	54.2	2.4	2.5
49	Type-3	Discontinued	Discontinued	Discontinued	N.A.	N.A.	N.A.	N.A.
50	None	Uniform light yellow	Homogeneous	No	N.A.	N.A.	N.A.	N.A.
51	Type-5	Dark brown and yellow	Inhomogeneous-2	No	N.A.	58.4	N.A.	2.7
52	Type-5	Uniform brown	Homogeneous	No	N.A.	59.4	2.0	2.4
53	None	Uniform yellow	Homogeneous	No	N.A.	58.2	N.A.	1.8
54a	None	Uniform dark yellow	Homogeneous	Slight melting	56.6	N.A.	1.1	N.A.
54b	None	Uniform dark yellow	Homogeneous	No	N.A.	58.2	N.A.	4.0
55a	None	Dark brown and yellow	Inhomogeneous-2	No	60.6	61.1	2.5	3.0
55b	None	Dark brown and yellow	Inhomogeneous-2	No	N.A.	58.5	N.A.	4.1
56a	None	Uniform yellow	Homogeneous	No	N.A.	63.3	N.A.	1.9
56b	None	Uniform dark yellow	Homogeneous	No	N.A.	61.0	N.A.	2.5

Table 5.1 continued.

ZrPM Batch Number	Precipitation	Color	Powder Homogeneity	Melting During Pyrolysis	Pyrolysis Yield (wt%)*		C/Zr Molar Ratio	
					TGA	Pyro Furnace	TGA**	Pyro Furnace**
56c	None	Uniform dark yellow	Homogeneous	No	N.A.	66.7	N.A.	2.6
56d	None	Uniform dark yellow	Homogeneous	No	N.A.	60.1	N.A.	2.5
57a	None	Uniform brownish yellow	Homogeneous	No	N.A.	60.1	N.A.	3.2
57b	None	Uniform yellow	Homogeneous	No	49.2	50.5	3.10	3.4
57c	None	Uniform brownish yellow	Homogeneous	No	N.A.	58.4	N.A.	3.4
58	None	Uniform brownish yellow	Homogeneous	No	57.2	59.2	2.50	3.0
59	None	Uniform brownish yellow	Homogeneous	No	56.6	57.0	2.7	3.1
60	N.A.	N.A.	N.A.	N.A.	N.A.	N.A.	N.A.	N.A.
61	N.A.	N.A.	N.A.	N.A.	N.A.	50.8	N.A.	3.8
62	None	Uniform dark yellow	Homogeneous	No	61.5	62.3	1.7	2.0
63	N.A.	N.A.	N.A.	N.A.	N.A.	N.A.	N.A.	N.A.
64a	Type-2	Uniform light yellow	Homogeneous	No	N.A.	59.2	N.A.	1.9
64b	Type-2	Uniform light yellow	Homogeneous	No	N.A.	64.1	N.A.	2.5
64c	Type-2	Uniform yellow	Homogeneous	No	N.A.	59.5	N.A.	2.5
65	None	Uniform light yellow	Homogeneous	No	59.5	59.4	2.0 (2.0, 1.9)	2.1 (1.9, 2.4, 2.2, 2.1, 2.1, 2.1, 2.0, 2.0)
66	None	Uniform dark brown	Homogeneous	No	61.9	62.2	1.60 (1.6, 1.60)	1.7 (1.6, 1.6, 1.8, 1.7, 1.7, 1.6)
67	None	Uniform yellow	Homogeneous	No	60.1	59.3	2.3 (2.4, 2.4, 2.2)	2.23 (2.6, 2.3, 2.2, 2.4, 2.2, 2.2, 2.2)

Table 5.1 continued.

ZrPM Batch Number	Precipitation	Color	Powder Homogeneity	Melting During Pyrolysis	Pyrolysis Yield (wt%)*		C/Zr Molar Ratio	
					TGA	Pyro Furnace	TGA**	Pyro Furnace**
68	None	Uniform dark yellow	Homogeneous	No	59.3	59.0	2.2 (2.2, 2.2)	2.3 (2.0, 2.7, 2.2, 2.3, 2.3, 2.2, 2.2, 2.2)
69	None	Uniform yellow	Homogeneous	No	60.6	59.4	2.2	2.5 (2.6, 2.4, 2.1, 2.2, 2.2)
70	None	Uniform dark yellow	Homogeneous	No	59.8	59.4	2.3	2.4 (2.6, 2.5, 2.4, 2.3, 2.2, 2.2)
71	None	Uniform light yellow	Homogeneous	No	58.7	59.2	1.9 (1.9, 1.8)	2.1 (2.2, 2.2, 1.9)
72	None	Uniform dark brown	Homogeneous	No	57.9	56.9	2.3	2.3 (2.2, 2.3)
73	None	Uniform dark yellow	Homogeneous	No	57.9	59.1	2.3	2.3 (2.4, 2.3, 2.3)
74	Type-3	Uniform dark yellow	Homogeneous	No	57.0	56.5	2.8	2.6 (2.7, 2.6)
75	None	Uniform dark yellow	Homogeneous	No	60.0	60.1	2.3 (2.3, 2.4)	2.4 (2.3, 2.5, 2.4)
76	None	Uniform dark yellow	Homogeneous	No	60.2	60.2	2.5 (2.5, 2.4)	2.4 (2.4, 2.4, 2.4, 2.3, 2.4)
77	None	Yellow and blackish yellow	Inhomogeneous-1	No	59.7	59.3	2.6	2.6
78	None	Uniform dark yellow	Homogeneous	No	58.9	59.0	2.0	2.3 (2.2, 2.2, 2.3, 2.3)
79	None	Uniform dark yellow	Homogeneous	No	56.7	57.0	3.4	3.5 (3.5, 3.5, 3.5, 3.5, 3.4)
80	None	Uniform dark yellow	Homogeneous	No	56.1	56.5	3.3 (3.3, 3.3)	3.4 (3.4, 3.5, 3.4)
81	None	Uniform dark yellow	Homogeneous	No	56.0	57.1	3.2 (3.3, 3.1)	3.4 (3.4, 3.4, 3.5, 3.4)

Table 5.1 continued.

ZrPM Batch Number	Precipitation	Color	Powder Homogeneity	Melting During Pyrolysis	Pyrolysis Yield (wt%)*		C/Zr Molar Ratio	
					TGA	Pyro Furnace	TGA**	Pyro Furnace**
82	None	Uniform dark yellow	Homogeneous	No	56.6	56.9	3.3	3.4 (3.4, 3.4, 3.3, 3.3, 3.4)
83	None	Uniform dark yellow	Homogeneous	No	55.9	56.6	3.1 (3.1, 3.1)	3.2 (3.2, 3.3, 3.2, 3.2, 3.2)
84	None	Uniform dark yellow	Homogeneous	No	57.6	58.1	3.1 (3.1, 3.1)	3.2 (3.3, 3.3, 3.2, 3.2, 3.2)
85	None	Uniform dark yellow	Homogeneous	No	58.7	59.0	2.8 (2.7, 2.8)	2.80 (2.8, 2.9, 2.8, 2.7)
86	None	Uniform dark yellow	Homogeneous	No	62.4	62.5	3.1	3.2 (3.2, 3.1, 3.2, 3.2, 3.1)
87	None	Uniform dark yellow	Homogeneous	No	59.1	59.9	3.3 (3.4, 3.2)	3.32 (3.3, 3.3, 3.3, 3.3, 3.5, 3.2, 2.9)
88	None	Uniform dark yellow	Homogeneous	No	62.1	63.1	3.0 (3.0, 3.0)	3.1 (3.1, 3.1, 3.2, 3.1, 3.1)
89	None	Uniform dark yellow	Homogeneous	No	56.9	57.6	2.7 (2.7, 2.7)	2.9 (2.9, 3.1, 2.8, 2.9, 2.9)
90	None	Uniform dark yellow	Homogeneous	No	57.4	58.1	2.6 (2.6, 2.7)	2.7 (2.7, 2.9, 2.7, 2.6, 2.7)
91	None	Uniform dark yellow	Homogeneous	No	55.1	56.0	3.2 (3.1, 3.2)	3.34 (3.3, 3.3, 3.4, 3.5, 3.4)
92	None	Uniform dark yellow	Homogeneous	No	54.8	55.8	3.2	3.3 (3.4, 3.3, 3.3, 3.3, 3.3, 2.7)
93	None	Uniform dark yellow	Homogeneous	No	55.8	56.2	2.9	2.9 (2.9, 3.0)
94	None	Uniform dark yellow	Homogeneous	No	N.A.	55.4	N.A.	3.6 (3.6, 3.8,3.6, 3.5)
95	None	Uniform dark yellow	Homogeneous	No	55.8	55.3	2.9	3.7 (3.7, 3.7, 3.6, 3.6)
96	None	Uniform dark yellow	Homogeneous	No	N.A.	59.5	N.A.	4.2

Table 5.1 continued.

ZrPM Batch Number	Precipitation	Color	Powder Homogeneity	Melting During Pyrolysis	Pyrolysis Yield (wt%)*		C/Zr Molar Ratio	
					TGA	Pyro Furnace	TGA**	Pyro Furnace**
97	None	Uniform dark yellow	Homogeneous	No	N.A.	62.4	N.A.	3.8 (3.8, 3.8, 3.9)
98	None	Uniform dark yellow	Homogeneous	No	N.A.	58.5	N.A.	3.4 (3.1, 3.5, 3.4)
99	None	Uniform dark yellow	Homogeneous	No	N.A.	60.6	N.A.	3.5 (3.3, 3.6, 3.5)
100	None	Uniform dark yellow	Homogeneous	No	N.A.	53.7	N.A.	3.1 (3.2, 3.1, 3.0)

* The samples were pyrolyzed at 1100^{o}C for 1 h.

** The values in parentheses are individual measurements. The number in the larger font is the average value.

5.1.2 Effect of Water Amount on Powder Characteristics

The effect of the concentration of water on powder characteristics (especially C/Zr molar ratio) was investigated. Table 5.2 shows the synthesis conditions for samples in which the water concentration was varied, but most other processing conditions remained constant.

The extent of hydrolysis in the modified zirconium precursor was reduced with lower amount of water. Thus, the samples with lower water/Zr molar ratio gave higher C/Zr molar ratio after pyrolysis. However, there tended to be more processing problems (e.g., inhomogeneity, precipitation, melting) with samples prepared with lower water/Zr molar ratios. Some samples with lower water ratio tend to form inhomogeneous solutions during drying (see Table 5.1). For example, after drying at 120^{o}C, ZrPM-77 was blackish yellow in color and inhomogeneous, while ZrPM-78 was light yellow in color and homogeneous. For batches ZrPM-51 and 52, there was some precipitation observed during concentration (see Table 5.1). In addition, melting was also observed in batch ZrPM-51 during drying (see Table 5.1). No precipitation or melting was observed in the batch (ZrPM-53) with the highest water concentration.

Based on the above observations, it was concluded that all subsequent batches (after batch ZrPM-78) would be prepared using an H_2O/Zr molar ratio of 24. Although, higher water concentrations produced batches with lower C/Zr molar ratios, it was decided that it was more important to maintain good batch homogeneity and avoid precipitation and/or melting during processing. The C/Zr molar ratio was instead controlled by making changes in other synthesis variables.

Table 5.2 Composition of batches synthesized with varying H_2O/Zr molar ratio.

Batch Number	AcacH/Zr Molar Ratio	Reflux Temp. (^oC)	Carbon Source/Zr Molar Ratio	Acid/Zr Molar Ratio	pH*	H_2O/Zr Molar Ratio	C/Zr+ Molar Ratio
ZrPM-51	4	275	0	0.002	5.9	8	2.7
ZrPM-52	4	275	0	0.002	5.9	16	2.4
ZrPM-53	4	275	0	0.002	5.9	24	1.8
ZrPM-74	3	195	0	0.200	4.6	8	2.6
ZrPM-65	3	195	0	0.200	5.5	24	2.1
ZrPM-73	3	195	0	0.271	4.6	16	2.3
ZrPM-67	3	195	0	0.271	4.4	24	2.3
ZrPM-77	3	195	0	0.421	3.6	12	2.6
ZrPM-78	3	195	0	0.421	3.7	24	2.3

* pH of the solution was measured after acid addition step during processing.
+ Estimated from the "pyrolysis furnace" method.

5.1.3 Effect of Acid Amount on Powder Characteristics

The effect of the concentration of acid on powder characteristics (especially C/Zr molar ratio) was investigated. Table 5.3 shows the synthesis conditions for samples in which the acid concentration was varied, but most other processing conditions remained constant.

Table 5.3 Composition of batches synthesized with varying acid/Zr molar ratio.

Batch Number	AcacH/Zr Molar Ratio	Reflux Temp. (^{o}C)	Carbon Source/Zr Molar Ratio	H_2O/Zr Molar Ratio	pH*	Acid/Zr Molar Ratio	C/Zr+ Molar Ratio
ZrPM-66	3	195	0	24	7.0	0.12	1.7
ZrPM-65	3	195	0	24	5.5	0.20	2.1
ZrPM-67	3	195	0	24	4.4	0.27	2.3
ZrPM-70	3	195	0	24	4.1	0.35	2.4
ZrPM-75	3	195	0	24	3.8	0.42	2.4

* pH of the solution was measured after acid addition step during processing.
+ Estimated from the "pyrolysis furnace" method.

Figure 5.1 shows the effect of acid/Zr molar ratio on the C/Zr molar ratio in the pyrolyzed powders. The C/Zr molar ratio increased from 1.65 to 2.4 as the acid/Zr molar ratio increased from 0.12 to 0.42. The C/Zr molar ratios listed in Table 5.3 (and plotted in Figure 5.1) are average values determined from multiple oxidation heat treatments using the methods described in section 4.1.4. There was considerable scatter in the data for individual determinations of the C/Zr molar ratio. This is illustrated in Figure 5.2.a for measurements carried out using both the "in-situ TGA method" and the "ex-situ pyrolysis furnace" method. Figure 5.2.b shows a plot of the average values (from the individual data points in Figure 5.2.a) for both measurement methods. The average values from the "pyrolysis furnace" method were usually higher than those obtained from TGA furnace.

Table 5.3 and Figure 5.1 show that the maximum C/Zr molar ratio (i.e., 2.4) was well below the desired molar ratio of 3. Hence, it was concluded that other synthesis variables would need to be investigated to increase the C/Zr molar ratio.

5.1.4 Effect of Acetylacetone (acacH) Amount on Powder Characteristics

The effect of the concentration of acacH on powder characteristics (especially C/Zr molar ratio) was investigated. Table 5.4 shows the synthesis conditions for samples in which the acacH concentration was varied. The water/Zr molar ratio was the same for these batches, but the acacH reflux temperature and acid/Zr molar ratio were not kept constant.

Table 5.4 shows that there was a trend toward higher C/Zr molar ratios (in the pyrolyzed powders) for samples prepared with higher acacH/Zr molar ratios during synthesis. (It is not known why the C/Zr molar ratio was so high (5.1) for the sample with an acacH/Zr molar ratio of 8.) However, the samples prepared with higher acacH/Zr molar ratio melted upon pyrolysis. This was considered undesirable in terms of the ultimate objective of producing a highly-sinterable ZrC-based powder. (The concern was that using a material which had melted during pyrolysis would eventually result in a highly aggregated powder after the carbothermal reduction reaction.)

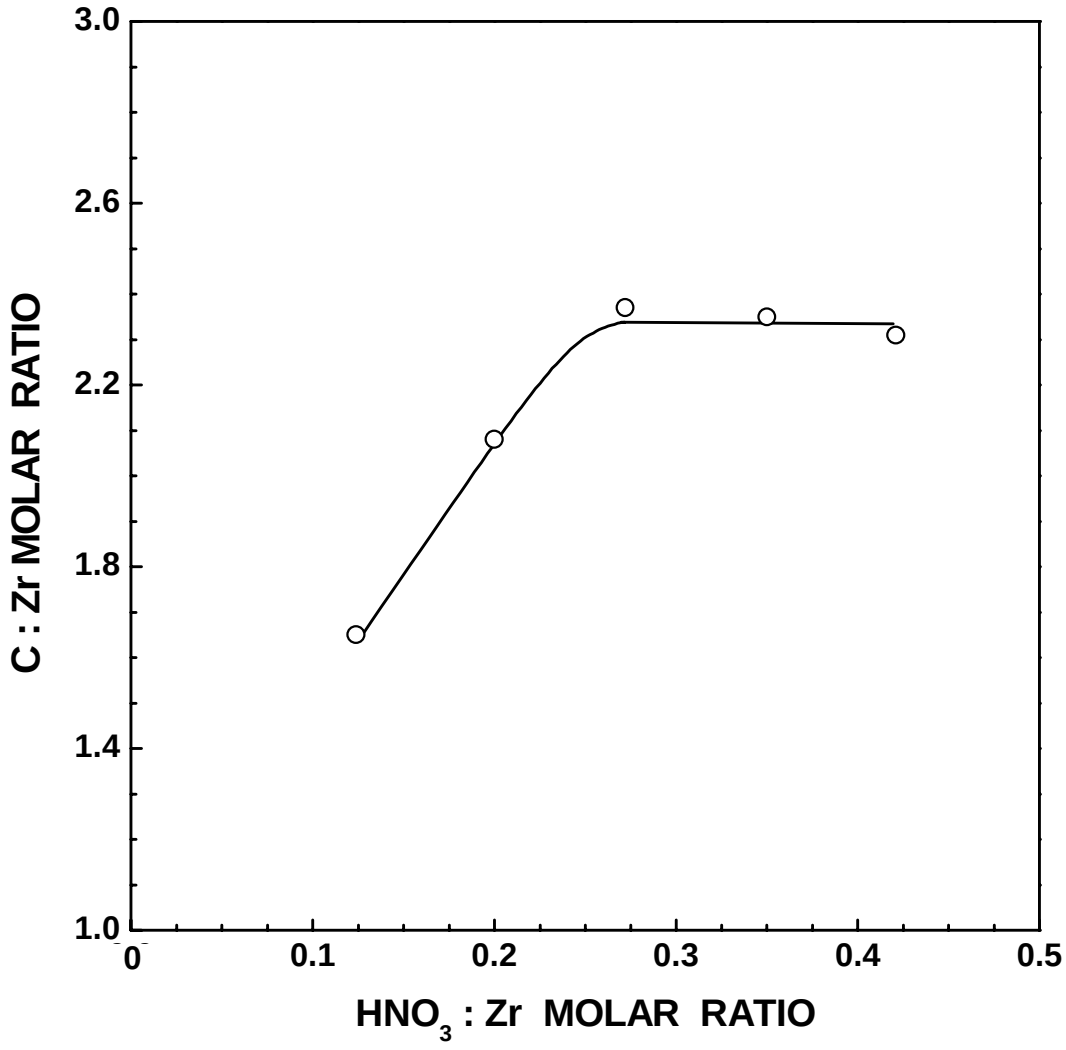

Figure 5.1 Plot of C/Zr molar ratio vs. HNO_3/Zr molar ratio for samples pyrolyzed at 1100°C.

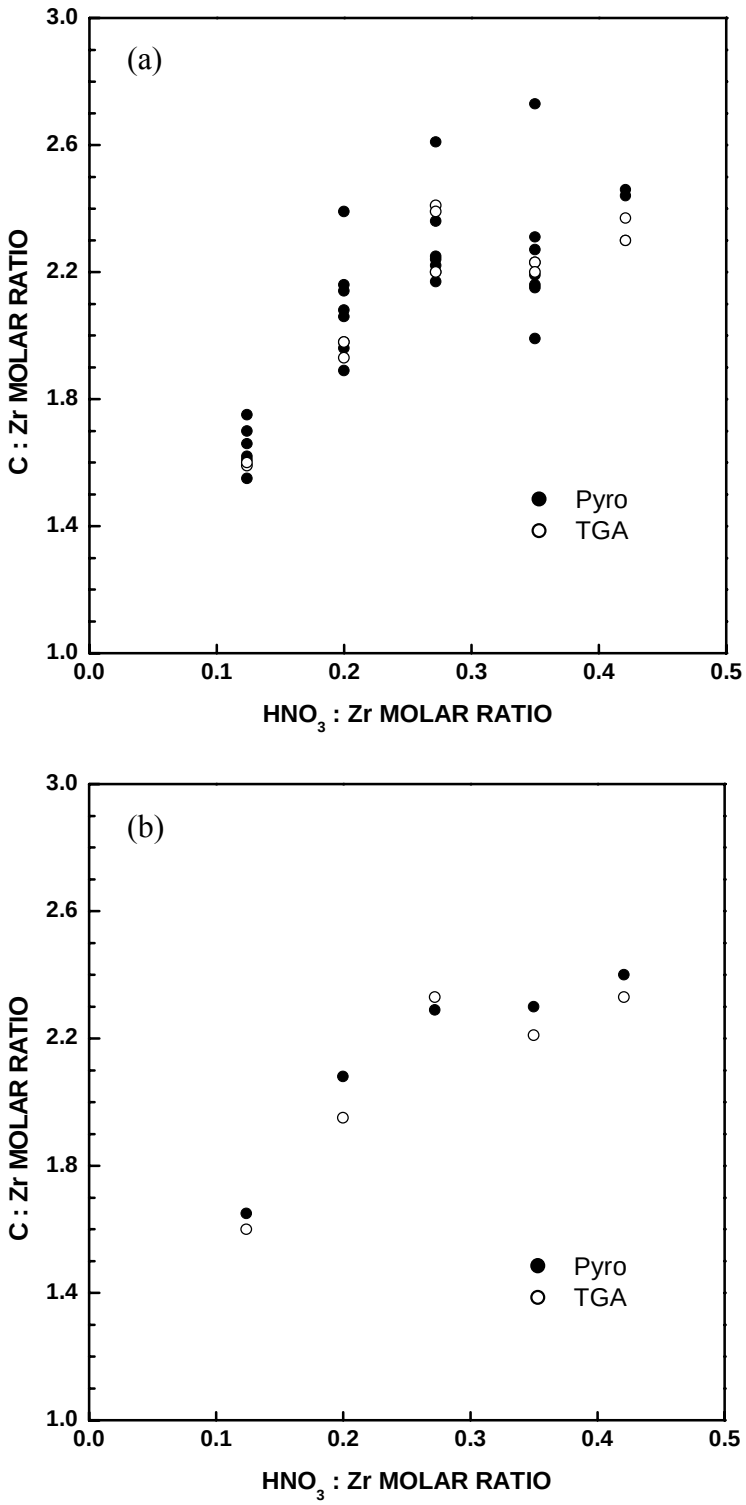

Figure 5.2 Plots of C/Zr molar ratio vs. HNO_3/Zr molar ratio for samples pyrolyzed at 1100°C in the pyrolysis furnace and the TGA furnace: a) data for individual runs for each sample and b) average values for each sample.

Table 5.4 Composition of various batches synthesized with varying amount of acacH/Zr molar ratio.

Batch Number	Reflux Temp. (^{o}C)	Acid/Zr Molar Ratio	pH*	H_2O/Zr Molar Ratio	AcacH/Zr Molar Ratio	C/Zr+ Molar Ratio	Pyrolysis
ZrPM-67	195	0.27	4.5	24	3	2.3	Did not melt
ZrPM-47	225	0.23	5.9	24	6	2.6	Melted
ZrPM-38	186	0.08	5.9	24	8	5.1	Melted
ZrPM-31	125	0.51	4.5	24	24	3.0	Melted
ZrPM-32	170	0.47	4.5	24	50	3.0	Melted

* pH of the solution was measured after acid addition step during processing.
+ Estimated from the "pyrolysis furnace" method.

Melting always occurred in samples prepared with acacH/Zr molar ratios >6, regardless of the concentrations of the other components. Melting also occurred in some samples prepared with a acacH/Zr molar ratio of 4. For example, as discussed in section 5.1.1, melting occurred during drying in samples with lower H_2O/Zr molar ratio. In contrast, melting did not occur in some samples with acacH/Zr molar ratio of 4 if the acid/Zr molar ratio was in the range of 0.22 to 0.36 and H_2O/Zr molar ratio was 24, as in batches ZrPM-39, ZrPM-40, ZrPM-45, and ZrPM-72. Nevertheless, to ensure that melting was avoided, all batches produced after batch ZrPM-56 (except for batch ZrPM-72) were produced using an acacH/Zr molar ratio of 3.

5.1.5 Zirconium Tetra-Pentanedionate (ZTP)

Experiments were carried out with ZTP for two reasons: (1) The overall powder preparation process would be simplified by using ZTP because the steps associated with acacH-refluxing would not be necessary. (2) It might be possible to obtain high C/Zr ratios (i.e., ≥3) without using an external carbon source.

Figure 5.3 shows a thermogravimetric analysis (TGA) plot of percentage residual weight vs. temperature for an as-received ZTP powder sample. The sample was heated at 2°C/min to 100°C and 1°C/min to 1050°C with a hold of 2 h at the maximum temperature. Most of the decomposition was completed by ~300°C, although continued small weight losses were observed throughout the rest of the heat treatment. The final yield was 41.1 wt%. The C/Zr molar ratio in the pyrolyzed material was 5.8. (This was determined via the TGA oxidation method discussed in section 4.2.1.) This high value for the C/Zr molar ratio provided support for one of rationales listed above for using ZTP, i.e., it might be possible to prepare near-stoichiometric ZrC batches without using an external carbon source.

Table 5.5 shows that it was possible to produce pyrolyzed powders with C/Zr ratios >3. As expected, a high value was obtained (5.2) for a batch (ZTP-H4) that was processed without using a hydrolysis step (i.e., no acid or water was added). In addition, C/Zr ratios near or greater than 3 were obtained in batches (ZTP-H5 and ZTP-H9) prepared with relatively low H_2O/Zr molar ratio (i.e., 2). As expected, most batches prepared with relatively high H_2O/Zr molar ratios (i.e., 16-24) resulted in pyrolyzed material with lower C/Zr molar ratios (i.e., usually ≤3). However, the pyrolyzed ZTP-H6 sample unexpectedly

showed a C/Zr molar of 4.6. The reason for this high value is not known, but it is believed that the result is due to some significant experimental error.

Table 5.5 shows that all the batches prepared with ZTP melted during pyrolysis. This observation was consistent with the results discussed in section 5.1.4 in which melting was observed during pyrolysis for samples prepared with relatively high acacH/Zr molar ratios (i.e., ≥6).

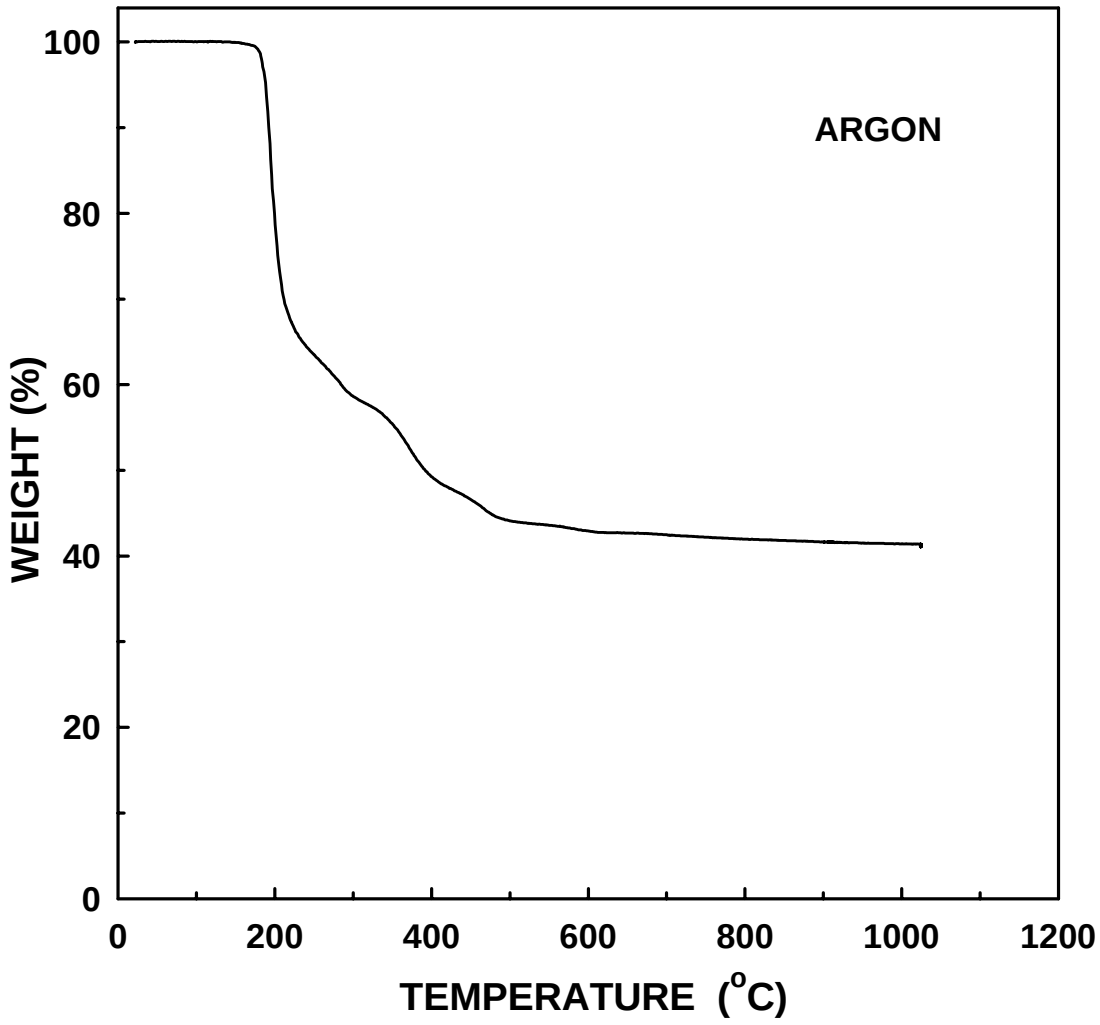

Figure 5.3 Plot of weight loss vs. temperature for an as-received ZTP powder sample.

Table 5.5 Processing-related observations and C/Zr molar ratios in the pyrolyzed material for batches prepared with ZTP.

ZTP Batch Number	Precipitation	Powder Color	Powder Homogeneity	Melting During Pyrolysis	C/Zr Molar Ratio	
					TGA	Pyro Furnace
H1	None	Uniform brown	Homogeneous	Yes	2.0	1.9
H2	None	Amber	Inhomogeneous-2	Yes	n.a.	2.8
H4	None	Uniform amber	Homogeneous	Yes	n.a.	5.2
H5	None	Dark brown	Inhomogeneous-2	Yes	3.1	3.8
H6	None	Dirty yellow	Inhomogeneous-2	Yes	n.a.	4.6
H7	None	Orange and yellow	Inhomogeneous-1	Yes	1.6	2.2
H8	None	Dark brown	Inhomogeneous-2	Yes	2.4	2.6
H9	None	Dark brown	Inhomogeneous-2	Yes	2.8	3.8
H10	None	Dark brown	Inhomogeneous-2	Yes	n.a.	n.a.

5.1.6 Effect of Glycerol Amount on Powder Characteristics

The effect of the concentration of glycerol on powder characteristics (especially C/Zr molar ratio) was investigated. Table 5.6 shows the synthesis conditions for samples in which the glycerol concentration was varied, but most other processing conditions remained constant. Table 5.6 shows that the C/Zr molar ratio in the pyrolyzed samples increased with increasing amount of glycerol. The C/Zr molar ratio increased from ~2.3 to ~3.5 as the glycerol/Zr molar ratio increased from 0 to 0.63. The C/Zr molar ratios listed in Table 5.6 (and plotted in Figure 5.4) are average values determined from multiple oxidation heat treatments using the methods described in section 4.1.4. There was considerable scatter in the data for individual determinations of the C/Zr molar ratio. This is illustrated in Figure 5.5.a for measurements carried out using both the "in-situ TGA method" and the "ex-situ pyrolysis furnace" method. Figure 5.5.b shows a plot of average values (from the individual data points in Figure 5.5.a) for both measurement methods. The average values from the "pyrolysis furnace" method were usually higher than those obtained from TGA furnace.

Experiments were also carried out to determine if the C/Zr molar ratio was affected by the order of addition of the components during synthesis. In one case, the glycerol was added just before the acacH refluxing step. In the other case, glycerol was added after the water addition (which was used for hydrolysis/condensation), but prior to the 50^{o}C aging heat treatment. Table 5.7 shows the results for two different comparison experiments. It is evident that the order of addition of the glycerol did not have any significant effect on the C/Zr molar ratio.

Table 5.6 Composition of batches synthesized with varying glycerol/Zr molar ratio.

Batch Number	AcacH/Zr Molar Ratio	Reflux Temp. (^{o}C)	Acid/Zr Molar Ratio	pH*	H_2O/Zr Molar Ratio	Glycerol/ Zr Molar Ratio	C/Zr+ Molar Ratio
ZrPM-67	3	195	0.27	4.4	24	0.00	2.3
ZrPM-85	3	195	0.27	5.2	24	0.17	2.8
ZrPM-83	3	195	0.27	5.4	24	0.34	3.2
ZrPM-79	3	195	0.27	5.8	24	0.63	3.5

* pH of the solution was measured after acid addition step during processing.
+ Estimated from the "pyrolysis furnace" method.

Figure 5.4 shows a plot of the C/Zr molar ratio in the pyrolyzed samples vs. the glycerol/Zr molar ratio used during synthesis. The plotted C/Zr molar ratios for the samples with glycerol/Zr molar ratios of 0.34 and 0.63 were the average values obtained from the two samples of each composition that are listed in Table 5.7. It is evident from Figure 5.4 (and from Tables 5.6 and 5.7) that the C/Zr molar ratio increased with increasing amount of glycerol used during synthesis. By using an external carbon source, it was possible to achieve (or exceed) the desired C/Zr ratio of 3.

Table 5.7 Composition of batches synthesized with the glycerol addition made at different stages of processing.

Sample Name	Glycerol or Resin/Zr molar ratio	C/Zr molar ratio	Glycerol added before
ZrPM-84	0.34	3.23	AcacH Reflux
ZrPM-83	0.34	3.23	50^{o}C heat treatment
ZrPM-80	0.63	3.44	AcacH Reflux
ZrPM-79	0.63	3.48	50^{o}C heat treatment

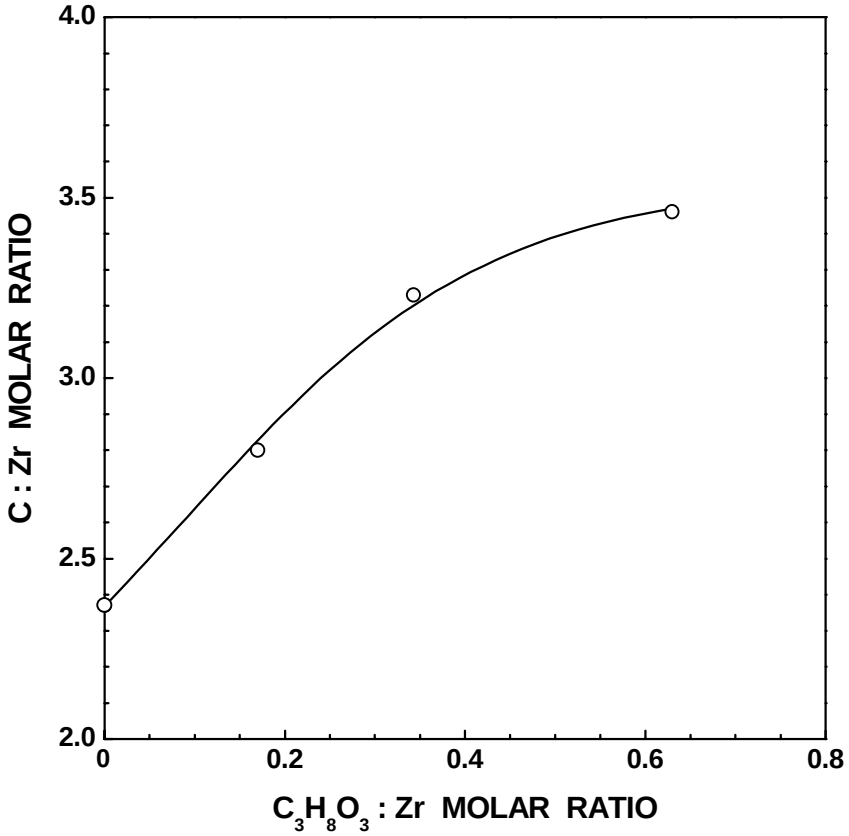

Figure 5.4 Plot of C/Zr molar ratio vs. glycerol($C_3H_8O_3$)/Zr molar ratio for samples pyrolyzed at 1100^{o}C.

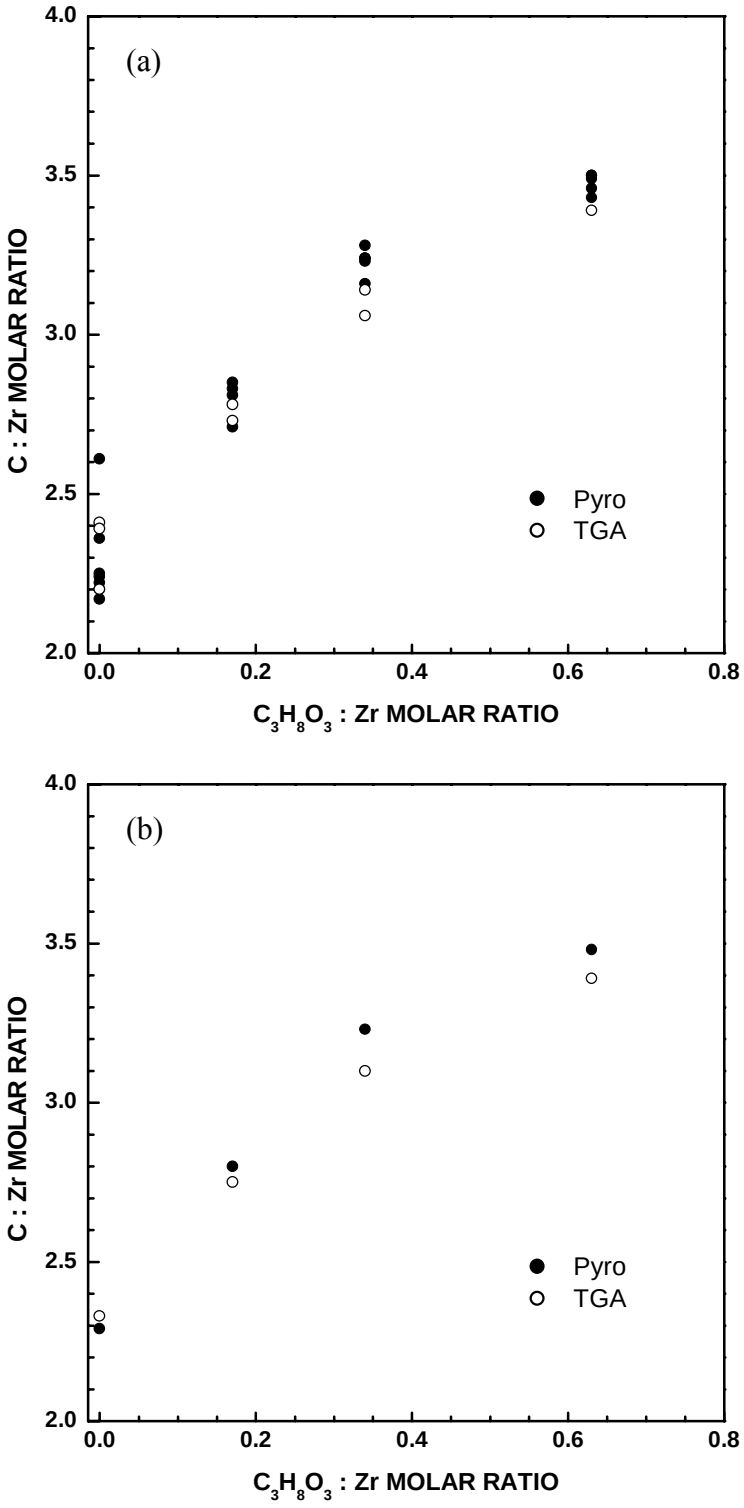

Figure 5.5 Plots of C/Zr molar ratio vs. $C_3H_8O_3$/Zr molar ratio for samples pyrolyzed at 1100°C in the pyrolysis furnace and the TGA furnace: a) data for individual runs for each sample and b) average values for each sample.

5.1.7 Effect of Hydrolysis/Condensation Reactions on Pyrolysis Yield

Figure 5.6 shows a thermogravimetric analysis (TGA) plot of residual weight vs. temperature for sample ZrPM-1a heat treated at 1100^{o}C for 1 h. This sample was prepared by concentrating an acacH-refluxed (103^{o}C, 1 h) solution. The acacH/Zr molar ratio was 2. The solution had no acid or water additions, so essentially no hydrolysis/condensation reactions would have occurred during processing. The sample was then dried at 120^{o}C for 3 h. Figure 5.7 shows the thermogravimetric analysis (TGA) plot of residual weight vs. temperature for sample ZrPM-1b heat treated at 1100^{o}C for 1 h. The initial processing through acacH-refluxing and concentration were same as for the ZrPM-1a sample. After concentration, the precipitate was processed according to the method described in section 4.1.2.2.2 using an acid/Zr molar ratio of 5.3 and a H_2O/Zr molar ratio of 24. The solution was then concentrated and material was dried at 120^{o}C for 3 h. (See Tables 4.3 and 4.5 for other information concerning the synthesis of batches ZrPM-1a and 1b.)

The yields after the 1100^{o}C (1 h) treatment were ~49 wt% and ~59 wt% for the ZrPM-1a and ZrPM-1b samples, respectively. Thus, it was evident that hydrolysis/condensation reactions during synthesis were useful in giving increased yield in the pyrolyzed product.

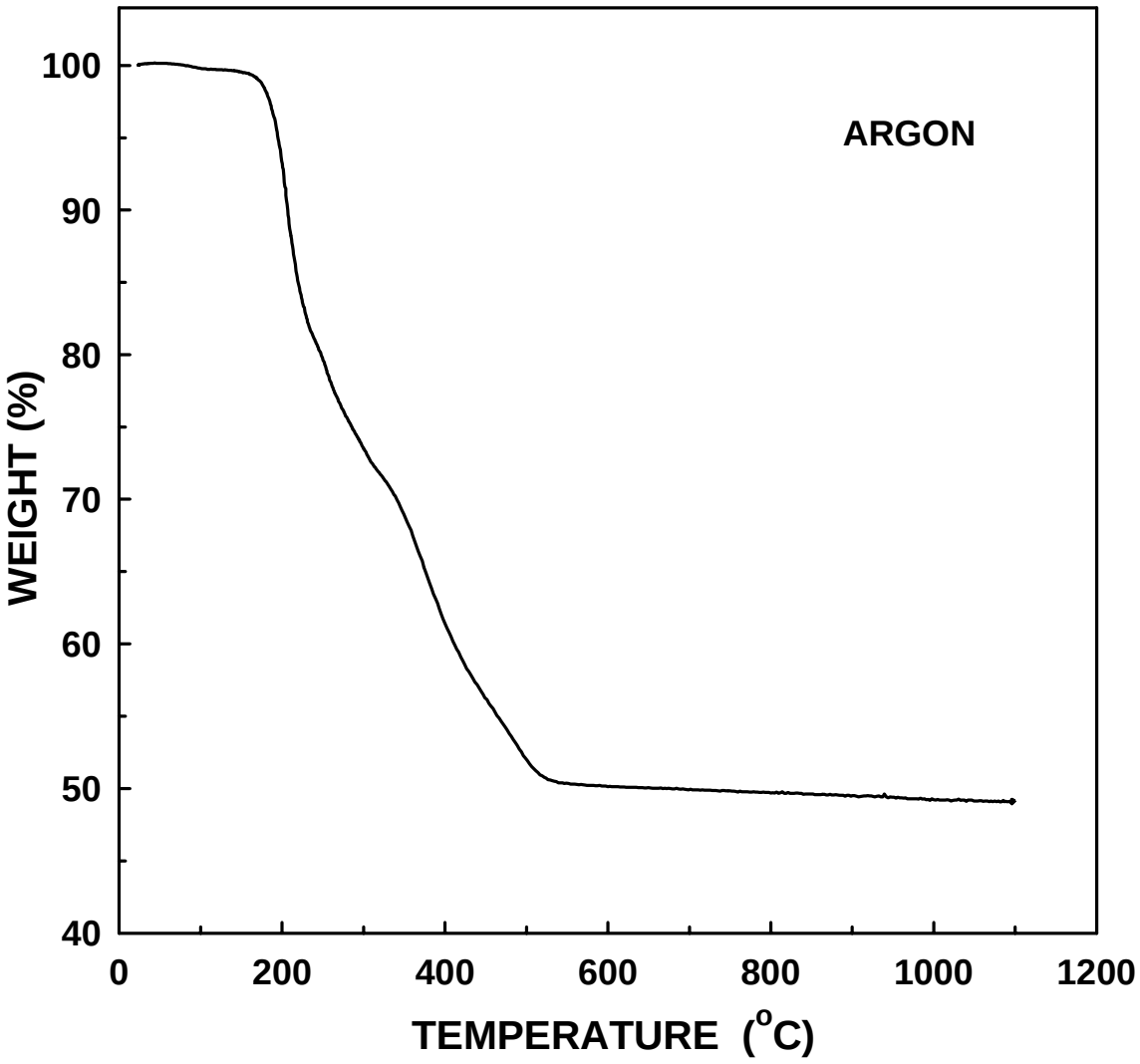

Figure 5.6 Plot of weight loss vs. temperature for ZrPM-1a sample dried at 120°C for 3 h.

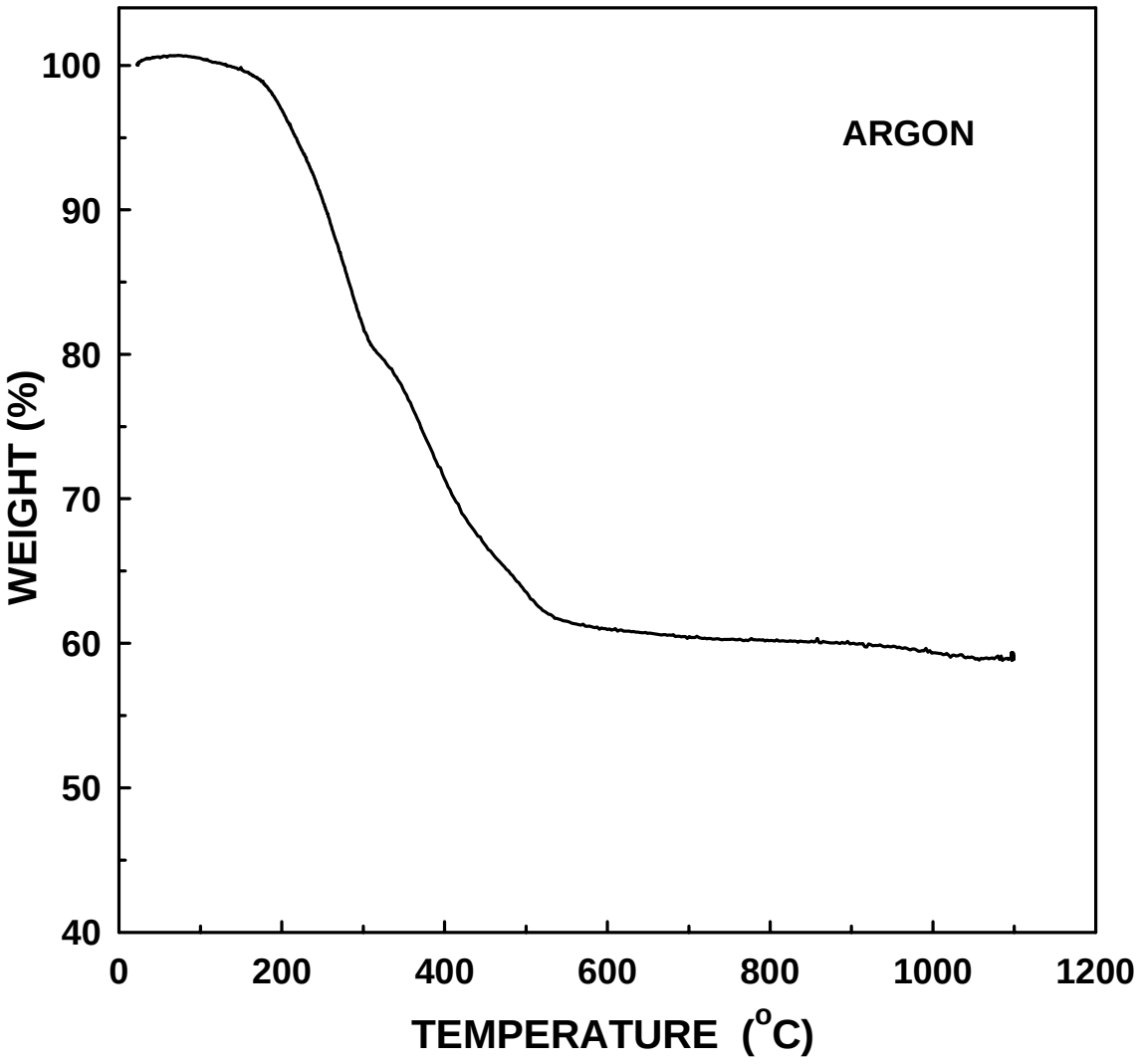

Figure 5.7 Plot of weight loss vs. temperature for ZrPM-1b sample dried at 120°C for 3 h.

5.2 Effect of Heat Treatment Temperature on Phase Development and Powder Characteristics for Two Batches with Different C/Zr Molar Ratios

5.2.1 ZrPM-45

5.2.1.1 Synthesis

The synthesis procedure for ZrPM-45 is given in Appendix B.

5.2.1.2 Low Temperature Heat Treatments (≤1100°C)

Figure 5.8 shows a thermogravimetric analysis (TGA) plot of residual weight vs. temperature for a ZrPM-45 sample (initially dried at 120°C, 3 h) heat treated at 1100°C for 1 h. The pyrolytic decomposition of the mixed precursor started around ~180°C and was mostly completed by ~550°C, although small weight losses were observed throughout the rest of the heat treatment. There was also a small weight loss of ~0.4% observed during the 1 h hold at 1100°C. The final yield was 60.9 wt%. The yields for samples heat treated at temperatures in the range of 800-1100°C for 2 h are shown in Table 5.8. (The yields were determined by measurement of sample weights before and after heat treatment in a tube furnace.)

Table 5.8 Pyrolysis yield of ZrPM-45 samples heat treated at various temperatures for 2 h.

Temperature (°C)	Yield (%)
800	59.5
1025	60.0
1100	57.0

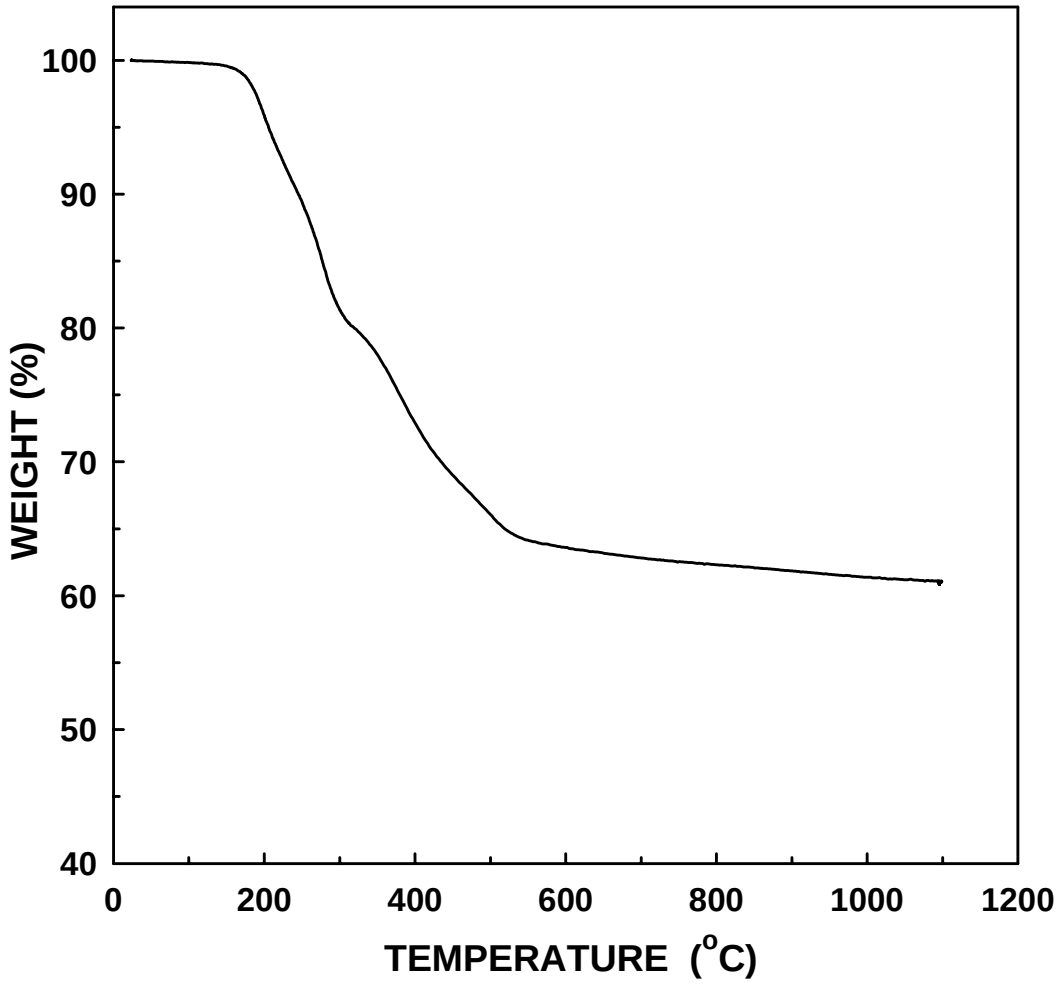

Figure 5.8 Plot of weight loss vs. temperature for the as-dried (120°C) ZrPM-45 material.

Table 5.9 shows the carbon content for a sample heat treated at 1025°C for 2 h. The measured carbon content of the sample (analyzed by Sherry Laboratories) was 23.3 wt% which was equivalent to a C/Zr molar ratio of 3.1, i.e., assuming that the pyrolyzed material contained only ZrO_2 and C. The measured oxygen content of the sample (analyzed by Leco Corp.) was 16.3 wt%.

Suppose the 1025°C materials contained only C and ZrO_2. If the measured C content of 23.3 wt% is correct, then the calculated amount of oxygen (O) should be 19.9 wt% (i.e., higher than the measured amount). In contrast, if the measured O content of 16.3 wt% is correct, then the calculated amount of C should be 37.2 wt% (i.e., higher than the measured amount). These results suggest that the 1025°C material did not consist of ZrO_2 and C only. This is not an unreasonable conclusion considering that some additional weight loss was observed (see Table 5.12) upon heat treatment at higher temperature (i.e., 1100°C). Furthermore, mass spectroscopy analysis of the gas species formed during heat treatment of a related ZrO_2/C sample (ZrPM-67) showed that hydrogen was still being evolved at temperatures above 1000°C.[86]

Table 5.9 Carbon and oxygen contents of a ZrPM-45 sample heat treated at 1025°C for 2 h.

Temperature (°C)	Carbon Content[a] (wt%)	Oxygen Content[b] (wt%)
1025	23.3	16.3

[a] Measured by Sherry Laboratories.
[b] Measured by Leco Corp.

Figure 5.9 shows the XRD patterns for samples heat treated at temperatures in the range of 600-1100^{o}C for 2 h. The as-dried powder was X-ray amorphous. The XRD pattern for the sample pyrolyzed at 600^{o}C (2 h) showed weak and broad diffraction peaks that were due to tetragonal zirconia (t-ZrO_2). With further heat treatment at higher temperatures (800-1100^{o}C), the only significant change in the XRD patterns were that the t-ZrO_2 peaks increased in intensity and became sharper. Thus, it was concluded that the only crystalline phase formed in these samples was tetragonal zirconia and that the carbon present in the samples remained X-ray amorphous for all heat treatment conditions.

Table 5.10 shows the average crystallite sizes (determined by XRD line broadening) for the tetragonal ZrO_2 for samples heat treated at temperatures in the range of 600-1100^{o}C for 2 h. (See Appendix C for details.) The crystallite size increased from ~3 nm to ~17 nm as the heat treatment temperature increased from 600 to 1100^{o}C. The relatively small crystallite sizes indicated that a fine scale of mixing between zirconia and carbon was obtained after pyrolysis.

Table 5.10 Crystallite sizes for tetragonal ZrO_2 in ZrPM-45 samples heat treated at various temperatures for 2 h.

Heat treatment Temperature (^{o}C)	Crystallite Size (nm)
600	3
800	6
900	10
1100	17

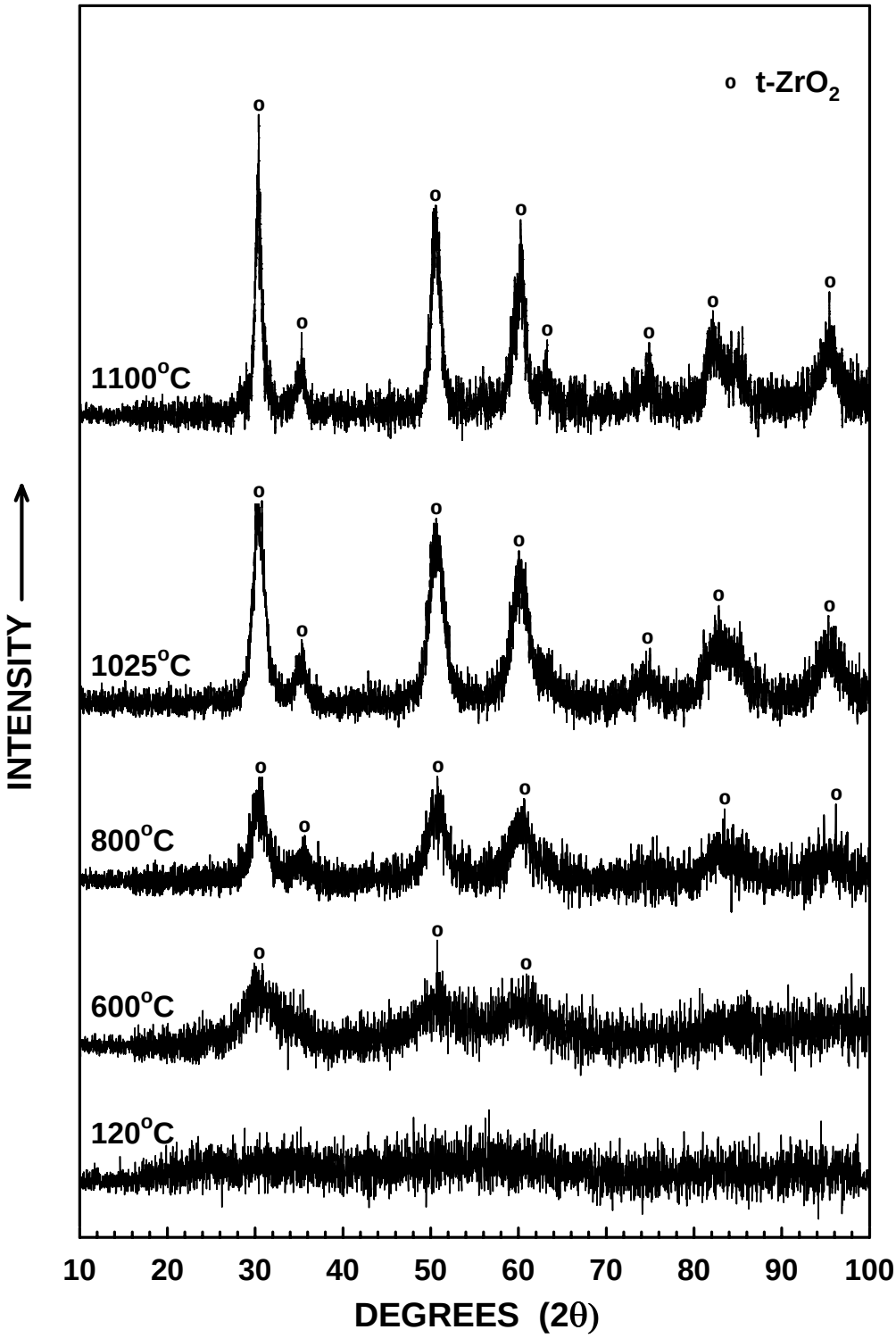

Figure 5.9 X-ray diffraction patterns for as-dried (120°C) and heat treated (600-1100°C) ZrPM-45 samples.

Table 5.11 shows the specific surface area values of samples heat treated at temperatures in the range of 800-1100°C for 2 h. (See Appendix D for details.) The values from both the BET and Langmuir models have been reported along with the constants C and b and the correlation coefficients (r_L). The specific surface area of the 800°C (2 h) pyrolyzed sample was only ~4 m^2/g, even though the sample contained ZrO_2 with very small crystallite sizes (~ 6 nm). It should be noted that the pyrolyzed powder consisted of relatively large particles (i.e., mostly larger than 10 μm). (The dried powder obtained after solution processing was sieved through a relatively coarse-mesh (150-mesh) sieve prior to pyrolysis. The pyrolyzed particle sizes were presumably related in some way to the sieve size.) The pyrolyzed particles were essentially large agglomerates of the fine zirconia/amorphous carbon mixture. The reasons for the low measured specific surface area for the 800°C-pyrolyzed sample might include one or both of the following: (i) The large pyrolyzed particles may have been relatively dense (i.e., relatively pore-free), either throughout the entire particle or at the surface. (ii) The pores of the pyrolyzed particles were too fine to be penetrated by nitrogen gas.

The specific surface area for the 900°C-pyrolyzed sample increased to 149 m^2/g. Although there was essentially no weight loss observed upon heat treatment from 800°C to 900°C (see Table 5.12), the large increase in the specific surface area indicates that accessible porosity developed at the higher heat treatment temperatures (i.e., accessible to penetration by nitrogen gas). The crystallite size of the t-ZrO_2 in the 900°C sample was 9.5 nm (Table 5.10). Consider the following relationship between specific surface area and crystallite size (assuming monosized spheres) :

$$SA = \frac{6}{c.\rho} \tag{5-1}$$

where *SA* is the specific surface area, *c* is the crystallite size, and ρ is the density (ρ = 5.95 g/cm^3 for t-ZrO_2).[87] The calculated specific surface area for the 900°C sample is 106.1 m^2/g. This calculated value is less than the measured value of ~149 m^2/g. However, the material did not contain only t-ZrO_2 crystallites, but instead was a mixture of amorphous carbon and t-ZrO_2. The size of the carbon "particles" (or carbon regions) was not known. However, the higher measured specific surface area could be attributed to: (1) the presence of carbon "particles" between the zirconia crystallites that resulted in smaller porosity than expected for zirconia crystallites alone and/or (2) the presence of fine pores within the carbon regions. The specific surface area for the 1100°C-pyrolyzed sample increased to 206 m^2/g. (The calculated value using equation 5-1 was 60.4 m^2/g. The crystallite size of the t-ZrO_2 (1100°C sample) was 16.7 nm (Table 5.10).) In this case, there was some additional weight loss upon heat treatment. The increase in surface area (compared to the value for the 900°C sample) indicates that additional porosity became accessible during the heat treatment.

Table 5.11 Specific surface areas and other gas adsorption results for ZrPM-45 samples heat treated at various temperatures for 2 h.

Temperature (°C)	BET (m^2/g)	*C*	r_L	Langmuir (m^2/g)	*b*	r_L
800	1.2	4.2	0.9883	4.1	0.87	0.9347
900	106	-96	0.9981	**149**	**0.012**	**0.9999**
1100	**206**	**244**	**0.9995**	297	0.027	0.9985

Table 5.12 Weight loss of ZrPM-45 samples heat treated at various temperatures for 2 h.

Temperature (^{o}C)	Weight Loss (wt%)
800	0.0
900	0.0
1025	2.4
1100	3.3

5.2.1.3 High Temperature Heat Treatments (>1100^{o}C)

Figure 5.10 shows the XRD patterns for samples heat treated at temperatures in the range of 1100 to 1400^{o}C for 2 h. The initial formation of ZrC was observed in the sample that was heat treated at 1200^{o}C (2 h). The XRD pattern for this sample (Figure 5.10) also showed that some t-ZrO_2 had transformed to monoclinic ZrO_2 (m-ZrO_2). ZrC became the predominant phase after heat treatment at 1300^{o}C (2 h), although a substantial amount of m-ZrO_2 and t-ZrO_2 were still present. ZrC was the only crystalline phase observed in the samples heat treated for 2 h at 1400^{o}C (Figure 5.10) and at higher temperatures (shown in Figure 5.11). Although the only phase observed in the XRD patterns (for samples heat treated at 1400^{o}C or higher) was that of zirconium carbide, further characterization results (discussed below) showed that it was not phase pure and had some oxygen dissolved in the lattice.

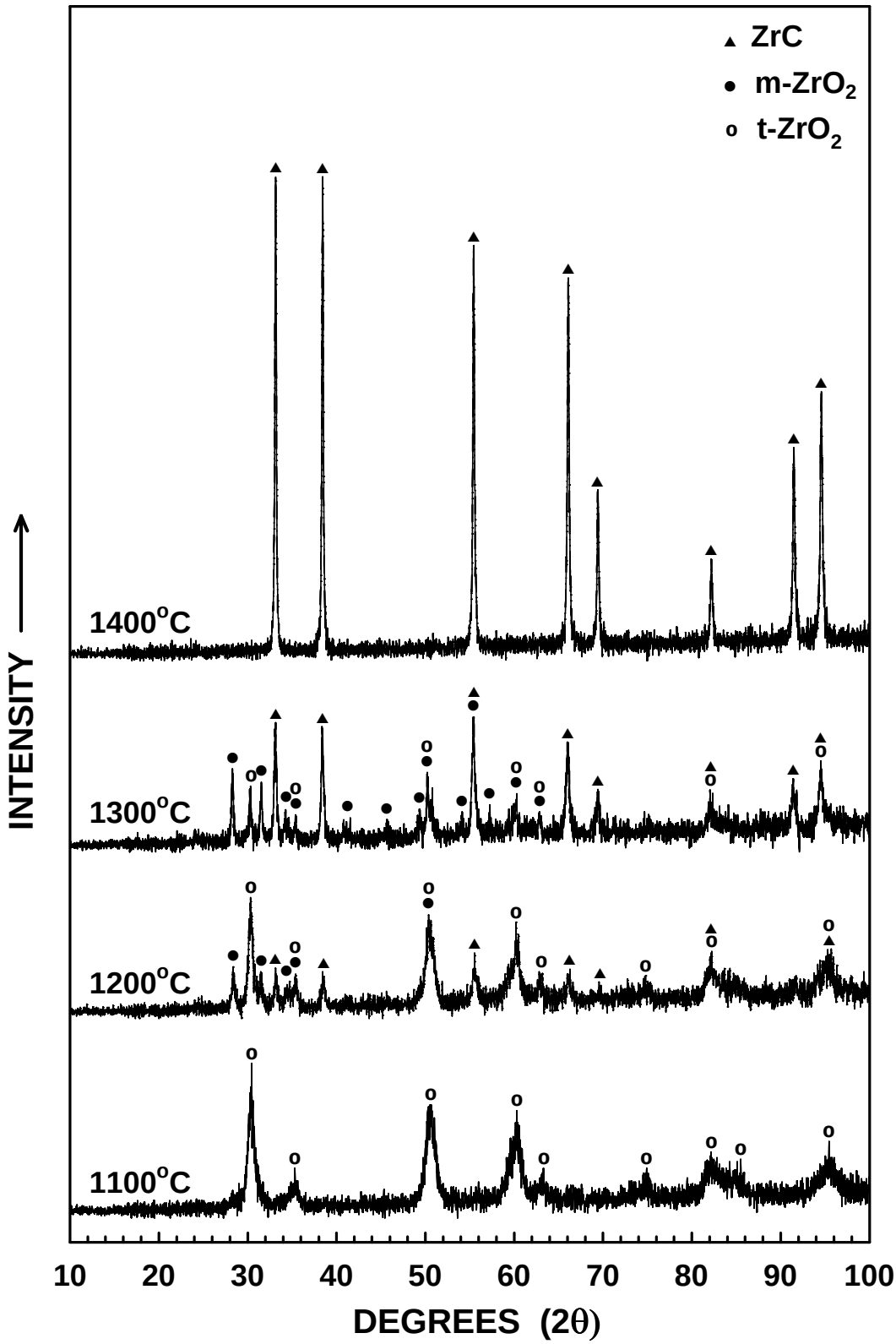

Figure 5.10 X-ray diffraction patterns for carbothermally reduced (1100-1400°C) ZrPM-45 samples.

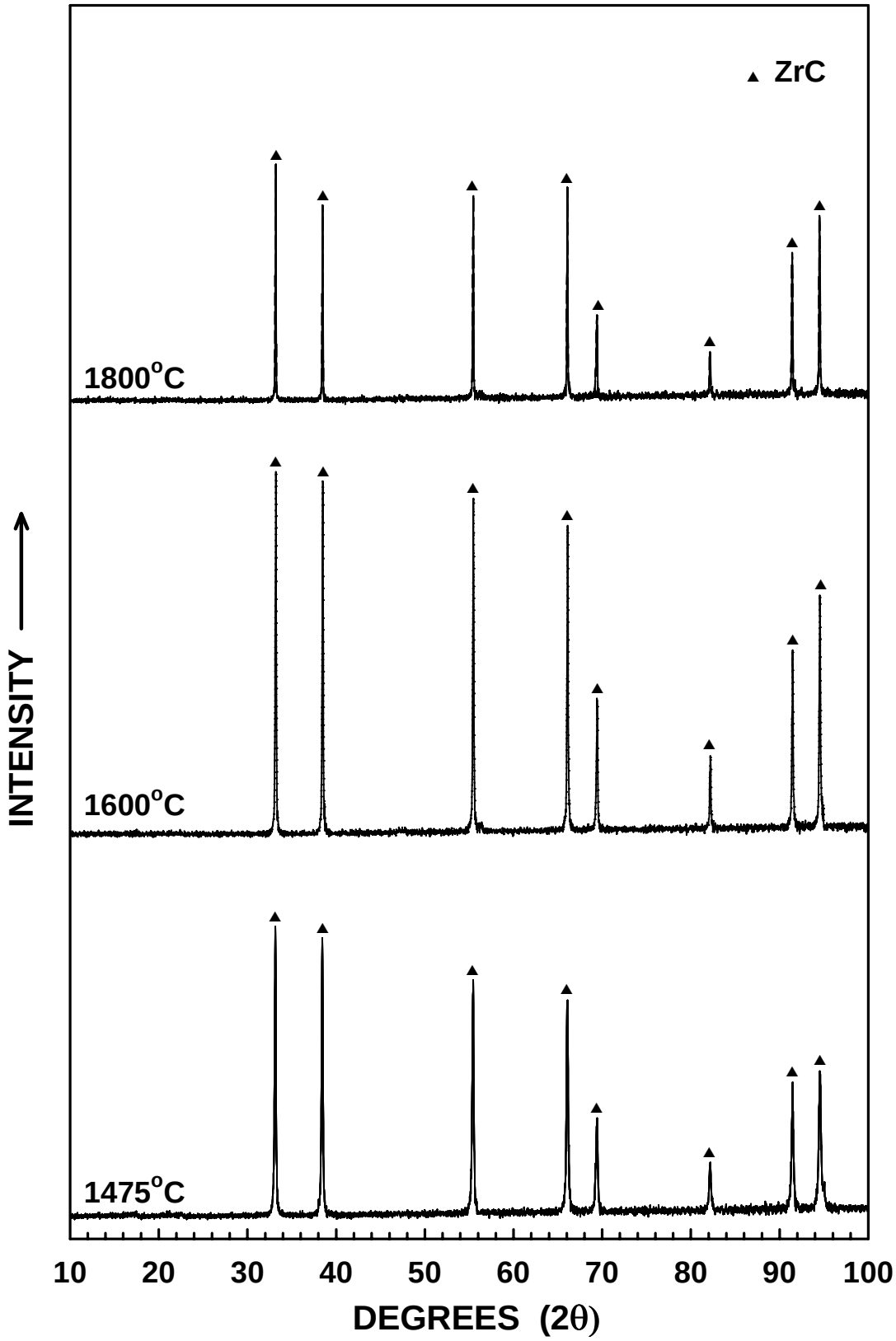

Figure 5.11 X-ray diffraction patterns for carbothermally reduced (1475-1800°C) ZrPM-45 samples.

Table 5.13 shows the carbon (analyzed by Sherry Laboratories) and oxygen (analyzed by Leco Corp.) contents for samples heat treated at temperatures in the range of 1025 to 1800°C for 2 h. (See Appendix E for details.) (The data for the 1025°C sample are the same as shown previously in Table 5.9.) The sample carbothermally reduced at 1475°C (2 h) had a carbon content of 13.3 wt%. This carbon content was greater than the value of 11.6 wt% that would be expected if the sample was phase-pure stoichiometric ZrC. Hence, it was apparent that the sample retained some free carbon (XRD-amorphous) after the heat treatment. Table 5.13 also shows that the amount of oxygen in 1475°C CTR sample was ~3.3 wt%. Since the XRD pattern for samples heat treated at temperatures ≥1400°C did not show the presence of ZrO_2 phase, it is evident that the oxygen present in the samples was dissolved in zirconium carbide lattice.

Table 5.13 also shows that further heat treatment at 1800°C (2 h) produced a sample with carbon concentration of 11.3 wt%. This is very close to the value of 11.6 wt% for stoichiometric ZrC (i.e., the values are the same within experimental error of the measurement for the 1800°C sample.) The oxygen content of the sample also reduced to a very low value of 0.1 wt%. The decrease in carbon and oxygen contents for the 1800°C sample are consistent with the weight losses observed upon heat treatment above 1475°C (see Table 5.14). Figure 5.12 shows a plot of weight loss vs. heat treatment temperature (in the range of 900-1800°C) using the data in Tables 5.12 and 5.14. Figure 5.12 shows that there was still a significant weight loss (~7 wt%; see Table 5.14) upon heat treatment from 1400°C to 1800°C, even though samples heat treated at (or above) this temperature showed no residual ZrO_2 in the XRD patterns (see Figure 5.10). (Almost all of this weight loss occurred between 1400°C and 1600°C.) The weight loss

(Figure 5.12) and the decrease in carbon and oxygen contents (Table 5.13) upon heat treatment to 1800°C are attributed to a carbothermal reduction reaction in which the reactants were zirconium oxycarbide and free carbon:

$$ZrO_yC_{(1+y-x)} + xC = ZrC + yCO \quad (5\text{-}2)$$

Table 5.13 Carbon and oxygen contents of a ZrPM-45 sample heat treated at various temperatures for 2 h.

Temperature (°C)	Carbon Content[a] (wt%)	Oxygen Content[b] (wt%)
1025	23.3	16.3
1300	n.d.	n.d.
1400	n.d.	n.d.
1475	13.3	3.3
1800	11.3	0.1

[a] Measured by Sherry Laboratories.
[b] Measured by Leco Corp.

Table 5.14 Weight loss of ZrPM-45 samples heat treated at various temperatures for 2 h.

Temperature (°C)	Weight Loss (wt%)
1200	8.0
1300	16.8
1350	22.7
1400	30.0
1475	32.1
1600	36.6
1800	37.1

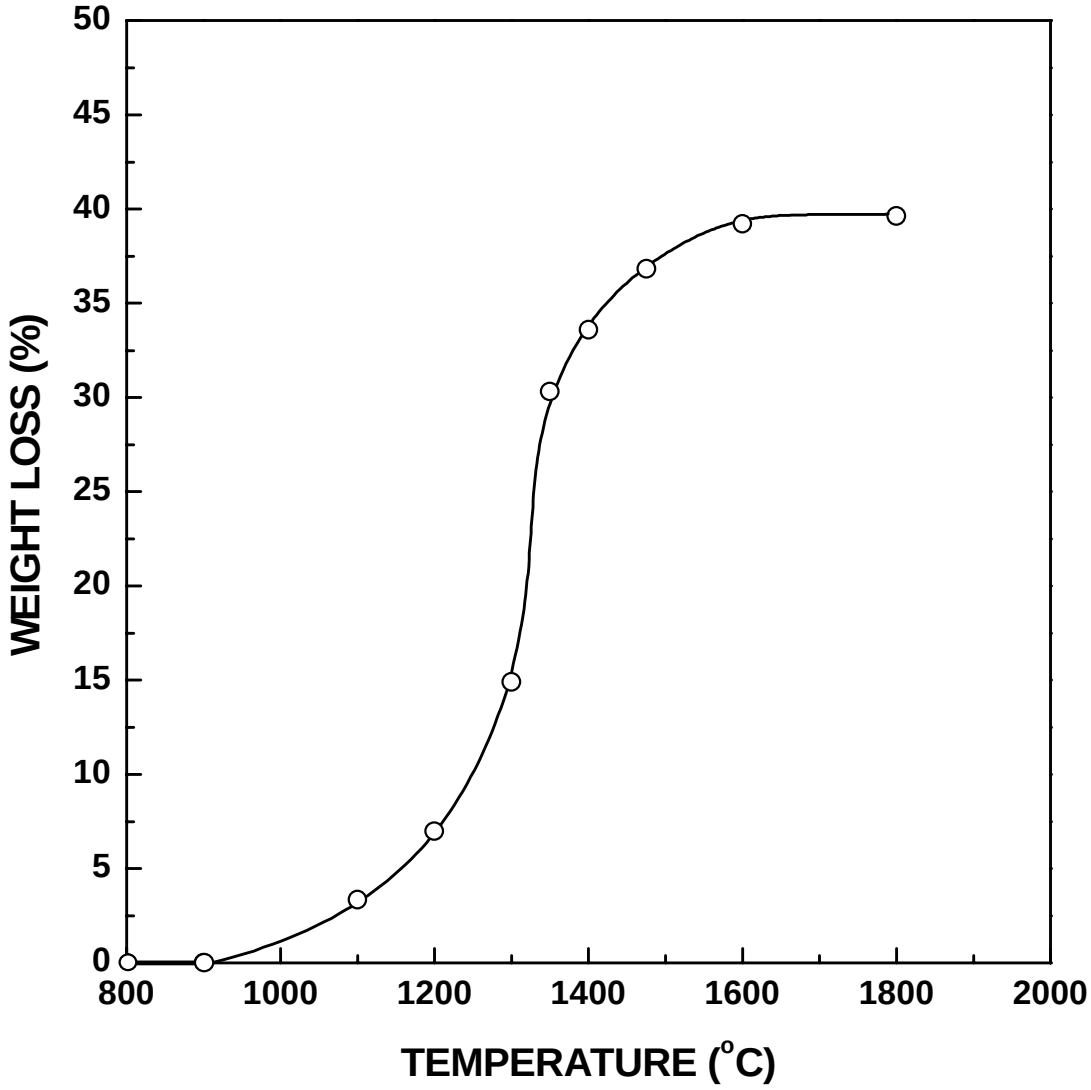

Figure 5.12 Plot of weight loss vs. temperature using the 800°C-pyrolyzed ZrPM-45 sample as the starting material.

Table 5.15 shows the zirconium carbide lattice parameters for samples heat treated at temperatures in the range of 1300°C to 1800°C for 2 h. (See Appendix F for details.) Figure 5.13 shows a plot of lattice parameter vs. heat treatment temperatures for above samples. The lattice parameter value for 1300°C CTR sample was 0.4693 nm. This value is slightly smaller than some lattice parameter values reported for stoichiometric ZrC (see section 2.3[11]). This suggests that a small amount of oxygen had already dissolved in the zirconium carbide lattice after the 1300°C heat treatment. The lattice parameter value decreased slightly to 0.4691 nm for the CTR samples prepared at 1400°C. This decrease indicated that either some additional zirconia dissolved in the zirconium carbide lattice or that direct formation of an oxycarbide composition (instead of stoichiometric ZrC) was more favorable. There was no change in lattice parameter for the 1475°C sample. The lattice parameter increased to 0.4696 nm for the 1600°C and 1800°C samples. The lattice parameter value of 0.4696 nm is close to values reported for stoichiometric ZrC.[11] This increase in lattice parameter value (from 0.4691 to 0.4696 nm) is consistent with the removal of oxygen from the zirconium carbide lattice by the reaction shown in equation 5-2. The increase in lattice parameter from 1475°C to 1600°C was also consistent with the weight loss (~5 wt%) observed in Table 5.14 and Figure 5.10. The weight loss was very small above 1600°C and this was consistent with the lack of change in the lattice parameter between 1600°C and 1800°C. Therefore, the results indicated that most of the dissolved oxygen had been removed after 1600°C heat treatment.

Table 5.15 Lattice parameters of ZrPM-45 samples heat treated at various temperatures for 2 h.

Temperature (^{o}C)	Lattice Parameter (nm)
1300	0.4693
1350	0.4693
1400	0.4691
1475	0.4691
1600	0.4696
1800	0.4696

Figure 5.14 shows the average crystallite sizes for each phase (i.e., ZrC, t-ZrO_2, and m-ZrO_2) as a function of heat treatment temperature. (Data from Tables 5.10 and 5.16 have been combined for these plots.) The crystallite size increased rapidly with the onset of carbothermal reduction reaction at temperatures >1100^{o}C. The crystallite sizes for both t-ZrO_2 and m-ZrO_2 increased from ~35-40 nm at 1200^{o}C to ~110-130 nm at 1350^{o}C during carbothermal reduction reaction. The crystallite size of ZrC also increased from ~40 nm at 1200^{o}C (from onset of carbothermal reduction reaction) to ~120 nm in a sample heat treated at 1400^{o}C (which contained no ZrO_2 phase).

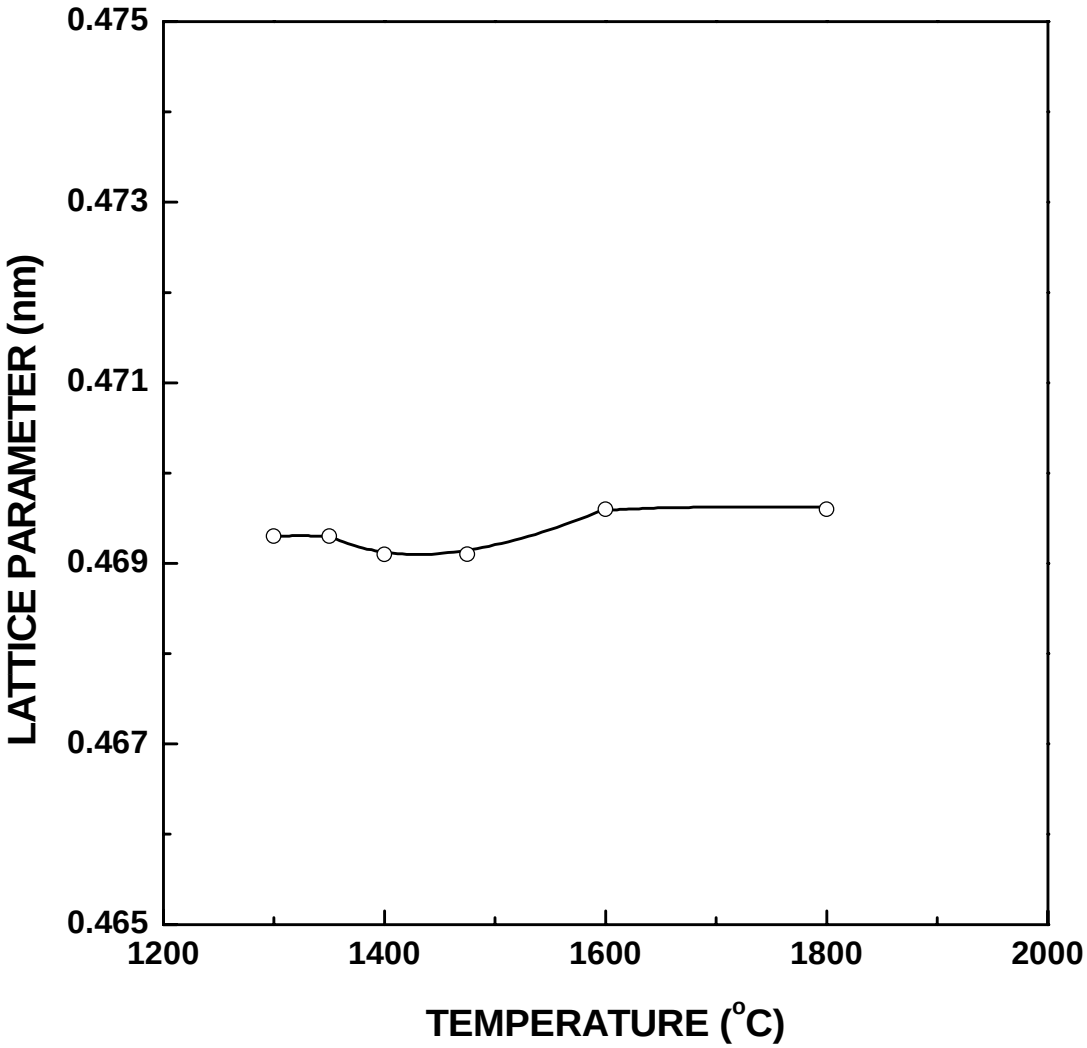

Figure 5.13 Plot of lattice parameter vs. temperature for carbothermally reduced ZrPM-45 samples.

The close correspondence in crystallite size growth of the ZrC and the two ZrO_2 phases was consistent with certain aspects of the reaction mechanism suggested by Maitre et al.[11] in a solid-state carbothermal reduction study carried out using mixtures of ZrO_2 and C powders. In particular, they proposed that the transformation occurred by the "contracting-volume" ("shrinking-core") mechanism in which growth of ZrO_xC_y proceeded from the surface to the interior of the ZrO_2 particles.

Figure 5.15 shows an SEM micrograph of a powder that had been carbothermally reduced at 1475°C (2 h). Zirconium carbide crystallites with diameters in the range of ~100-200 nm are observed in the micrograph.

Table 5.16 Crystallite sizes for the phases observed by XRD in ZrPM-45 samples after heat treatment at various temperatures for 2 h.

Heat treatment Temperature (°C)	Crystallite Size (nm)		
	t-ZrO_2	m-ZrO_2	ZrC
1200	30	45	42
1300	69	91	56
1350	127	115	96
1400	-	-	115
1475	-	-	127

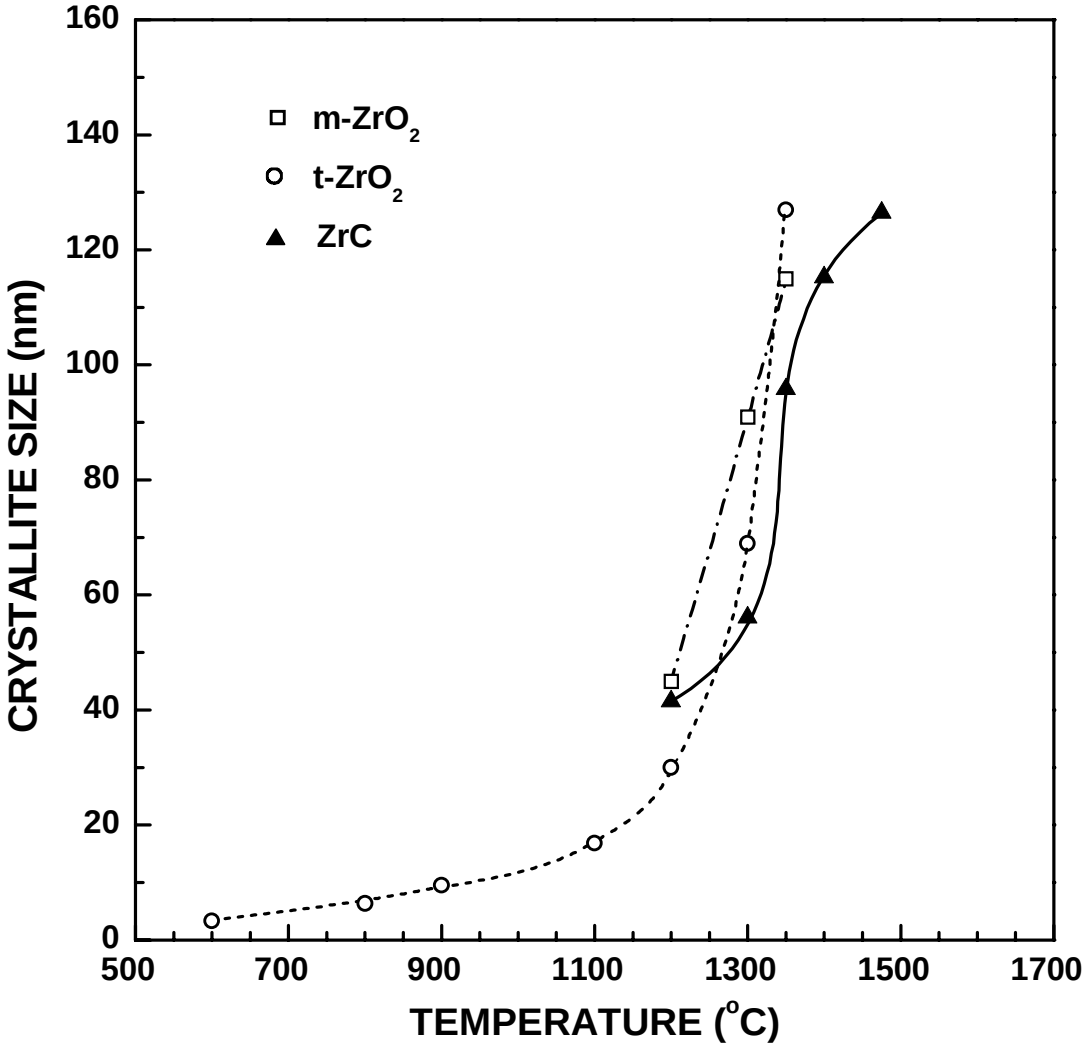

Figure 5.14 Plot of the t-ZrO_2, m-ZrO_2, and ZrC crystallite sizes (determined from XRD line broadening measurements) vs. heat treatment temperature for ZrPM-45 samples.

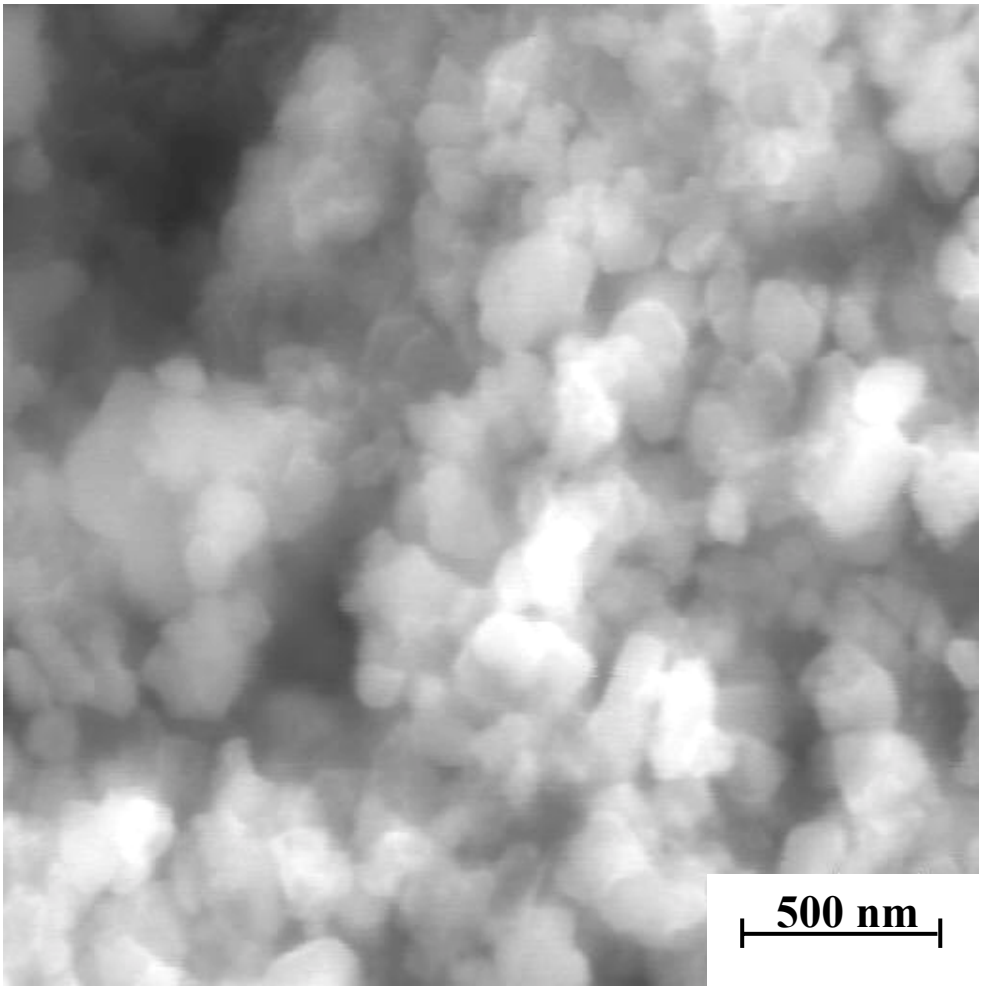

Figure 5.15 SEM micrographs of ZrPM-45 powder heat treated at 1475^{o}C for 2 h.

Figure 5.16 shows a plot of specific surface area vs. temperature for samples heat treated in the range of 800 to 1475°C for 2 h. (Tables 5.11 and 5.17 show the data used to plot Figure 5.16.) The specific surface area initially increased with increasing heat treatment temperature and reached a maximum value of ~231 m^2/g for the 1200°C sample. The calculated specific surface area using equation 5-1 would be in the range of ~22 to ~33 m^2/g. This range of specific surface areas was determined by using the following crystallite sizes and densities: 30 nm and 5.95 g/cm^3 for t-ZrO_2, 45 nm and 5.82 g/cm^3 for m-ZrO_2[88], and 41.5 nm and 6.6 g/cm^3 for ZrC. (See Tables 5.10 and 5.16 for the crystallite sizes.) As discussed previously, the fact that the measured specific surface area is higher than the values calculated from equation 5-1 indicates that fine porosity (i.e., finer than the ZrC and ZrO_2 crystallite sizes) is present in the sample.

Figure 5.16 shows that the specific surface area decreased with increasing temperature above 1200°C. This indicates that finer pores underwent coarsening and/or were eliminated. Based on equation 5-1 and the crystallite sizes in Table 5.16, specific surface areas of 8 m^2/g and 7 m^2/g were calculated for the 1400°C and 1475°C samples. The measured values were ~39 m^2/g and ~23 m^2/g, respectively. XRD patterns (Figure 5.11) showed that these samples do not have any ZrO_2 present. The samples are comprised of zirconium carbide (with some dissolved oxygen) and some residual carbon. Hence, the higher measured specific surface areas (compared to the calculated values) may be attributed to fine pores associated with presence of the residual carbon.

The specific surface area that was associated with residual "free" carbon in the ZrPM-800-1475 sample was estimated. First, the amount of the residual carbon was estimated. The Zr content was determined by difference to be 83.4 wt%. (The sample was

assumed to contain only Zr, C, and O. The C and O amounts are shown in Table 5.13.) It was then assumed that all the oxygen was dissolved in the zirconium carbide lattice and that the Zr:C molar ratio in the oxycarbide was 1:1. With these assumptions, the weight of "free" carbon was determined to be 2.32 wt%. The next step was to determine the portion of measured specific surface area (22.6 m^2/g, Table 5.17) that was "contributed" by the "free" carbon. This was determined by difference by assuming that the specific surface area due to the zirconium oxycarbide was 7 m^2/g. (The latter value was calculated using the measured crystallite size and equation 5-1, as discussed earlier in this section.) Therefore, the specific surface area "contributed" by the "free" carbon (2.32 wt%) was 14.6 m^2/g. Hence, the estimated specific surface area of the carbon phase alone is 629 m^2/g.

Table 5.17 Specific surface areas and other gas adsorption results for ZrPM-45 samples heat treated at various temperatures for 2 h.

Temperature (°C)	BET (m^2/g)	C	r_L	Langmuir (m^2/g)	b	r_L
1200	**232**	**232**	**0.9998**	337	0.032	0.9979
1300	**184**	**208**	**0.9999**	268	0.035	0.9971
1350	**124**	**127**	**0.9999**	180	0.038	0.9963
1400	**39**	**100**	**0.9999**	55	0.034	0.9983
1475	**23**	**65**	**0.9999**	33.8	0.051	0.9950

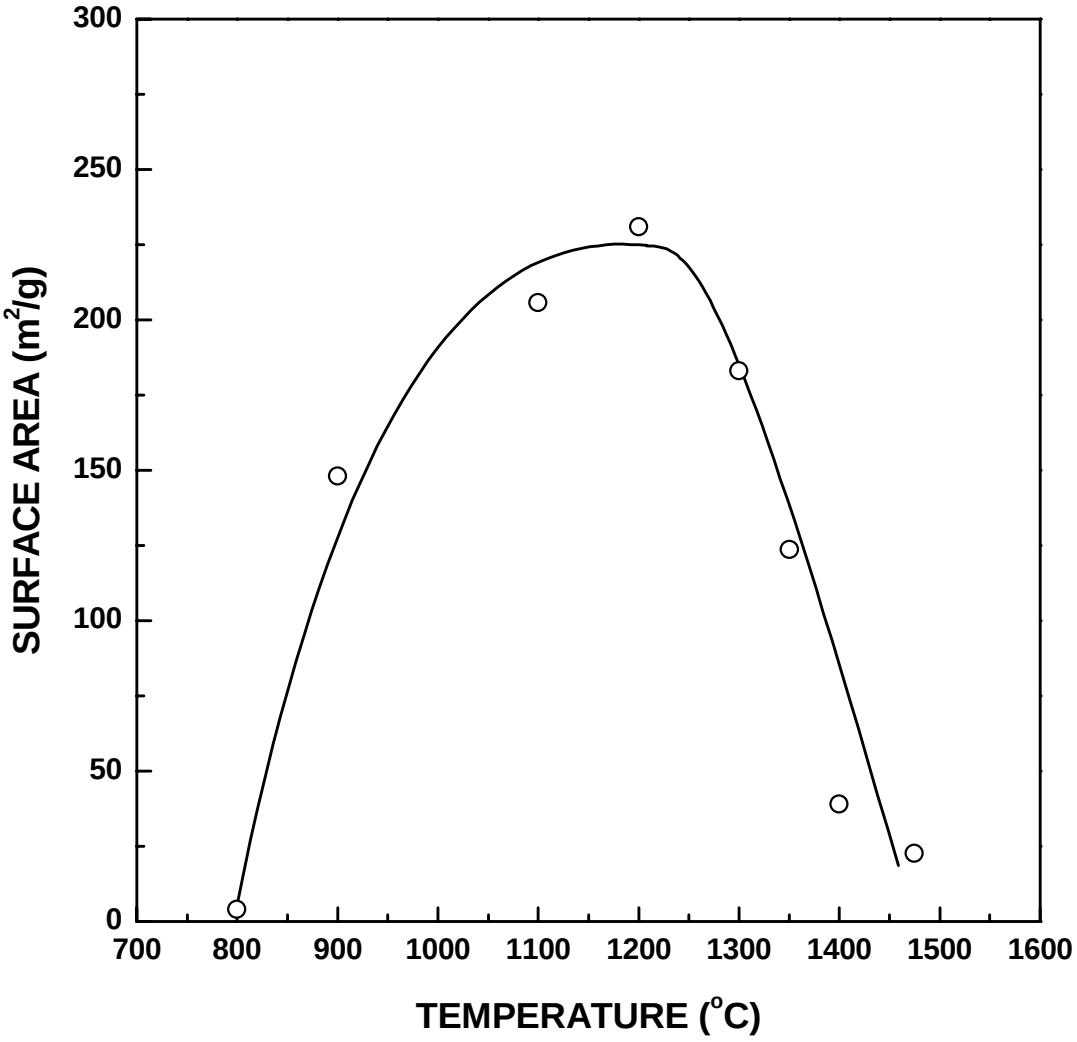

Figure 5.16 Plot of surface area vs. temperature for pyrolyzed and carbothermally reduced ZrPM-45 samples.

Figure 5.17 shows the particle size distribution for a sample which was heat treated at 1475°C for 2 h and then ground (using the Spex mill) for 10 min. Table 5.18 shows some statistical data from the particle size distribution data. The mean particle size was ~0.1 μm and essentially all the particles were less than 1 μm. It should be noted that the mean particle size obtained by the light scattering method was smaller than crystallite size determined by XRD line broadening (~127 nm). This discrepancy is even more significant if the aggregated portion of the distribution in Figure 5.17 is neglected. (The XRD line broadening measurement reflects the crystallite size and would not be affected by the presence of aggregates.) The results suggest that there may be a significant error associated with the choice of the optical constants that were used to convert the light scattering data to a particle size distribution. (The main error is presumably in the choice of the extinction coefficients.)

Table 5.18 Particle size distribution data for the 10 min-milled 1475°C ZrPM-45 powder sample.

	Diameter (μm)
Mean	0.09
Modes*	0.06, 0.19
D_{90}	0.19
D_{50}	0.07
D_{10}	0.05
Standard Deviation	0.38

* Mode values are listed for each distinct peak in the accompanying relative frequency plot.

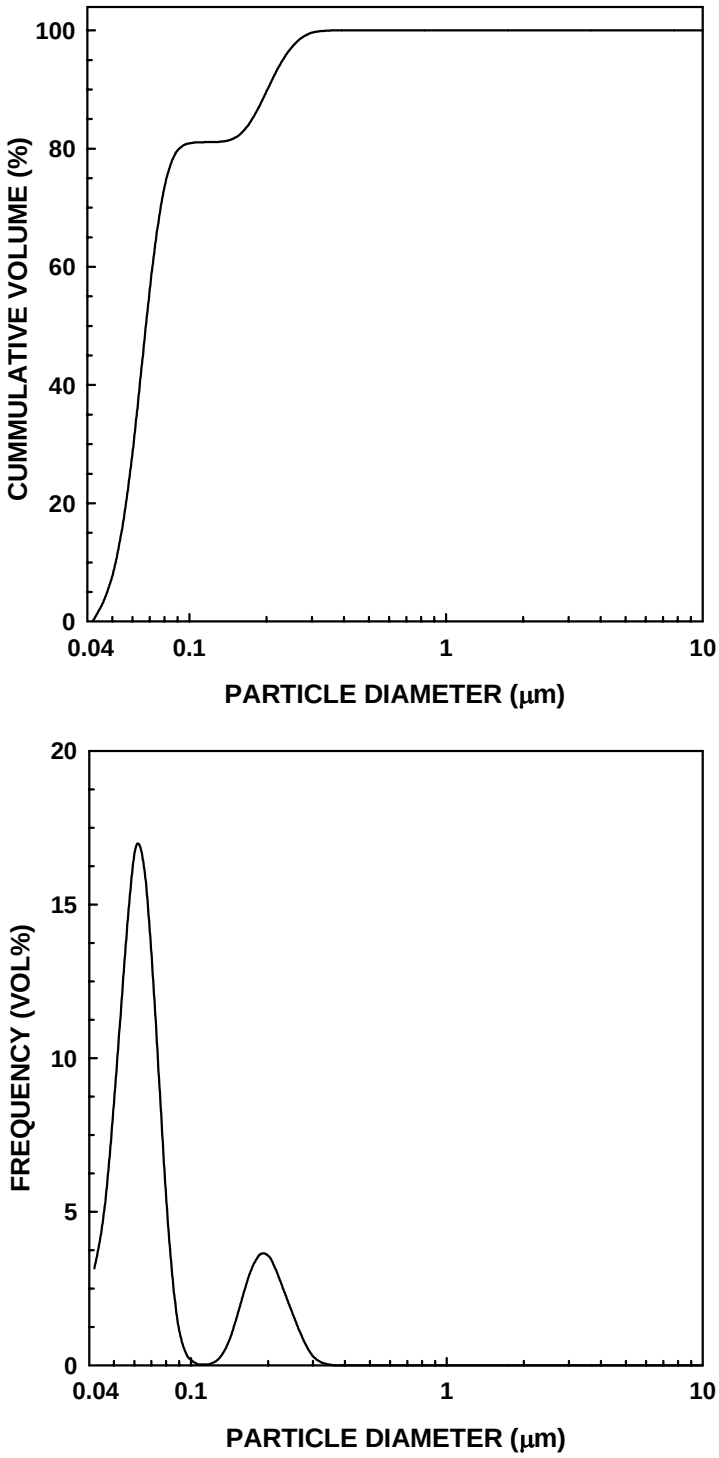

Figure 5.17 Particle size distribution plots for the 10 min-milled 1475°C ZrPM-45 powder: cumulative distribution plot (top) and relative frequency plot (bottom).

5.2.2 ZrPM-59

5.2.2.1 Synthesis

The synthesis procedure for ZrPM-59 is given in Appendix B. This batch differed from ZrPM-45 in the following ways: (i) The external carbon source was glycerol for ZrPM-59, while it was phenolic resin for ZrPM-45. (ii) The acacH/Zr molar ratio in ZrPM-59 was 3, while it was 4 for ZrPM-45. (iii) The acacH-reflux was done at 195^{o}C (3 h) in ZrPM-59, while it was done at 130^{o}C (3 h) for ZrPM-45. (iv) The acid/Zr molar ratio in ZrPM-59 was 0.087, while it was 0.04 in ZrPM-45.

5.2.2.2 Low Temperature Heat Treatments (≤1100^{o}C)

Figure 5.18 shows a thermogravimetric analysis (TGA) plot of residual weight vs. temperature for a ZrPM-59 sample (initially dried at 120^{o}C, 3 h) heat treated at 1100^{o}C for 1 h. The pyrolytic decomposition of the mixed precursor started around ~160^{o}C and was mostly completed by ~500^{o}C. However, small weight losses were observed throughout the rest of the heat-treatment. There was also a small weight loss of ~0.2% observed during the 1 h hold at 1100^{o}C. The final yield was 56.5 wt%. The total weight loss observed for ZrPM-59 was 4.4 wt% more than that observed for ZrPM-45. The yields for samples heat treated at temperatures in the range of 800-1025^{o}C for 2 h are shown in Table 5.19. (The yields were determined by measurement of sample weights before and after heat treatment in a tube furnace.) The yields are ~3-4 wt% lower than those observed in the ZrPM-45 sample (Table 5.8).

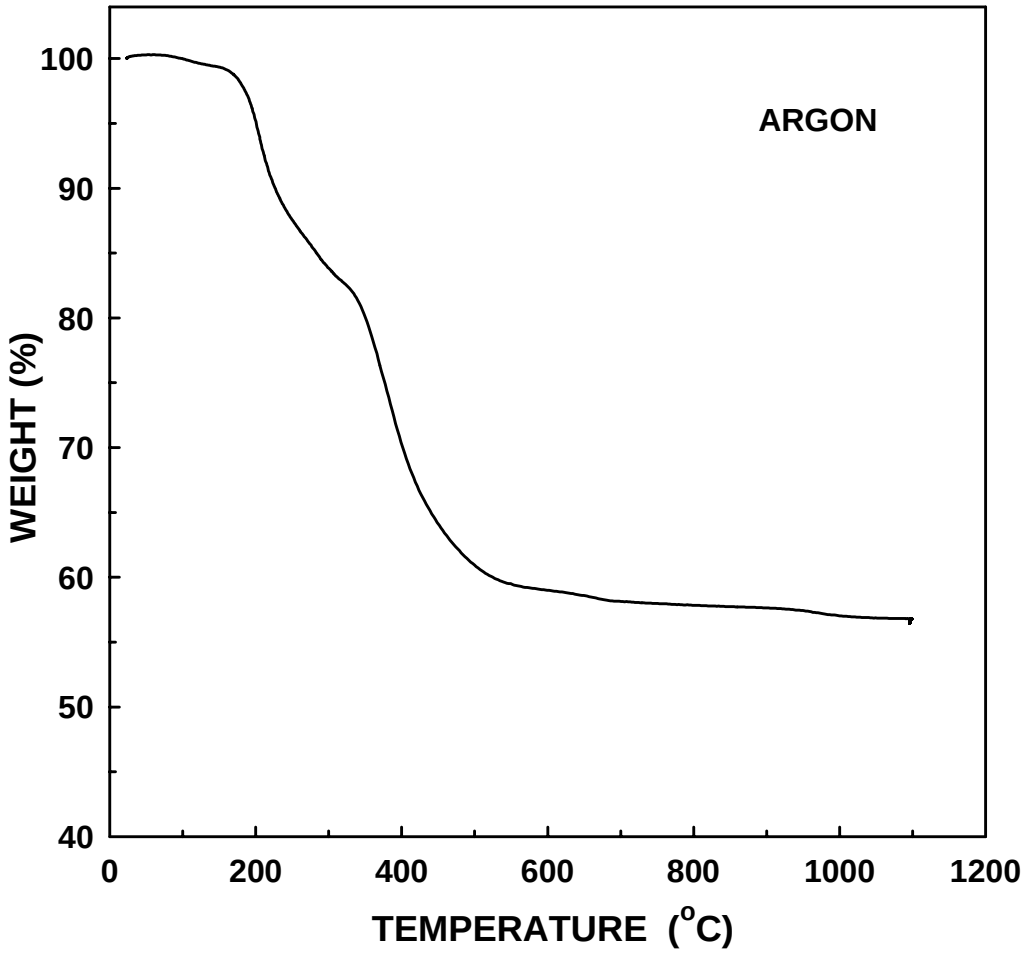

Figure 5.18 Plot of weight loss vs. temperature for the as-dried (120°C) ZrPM-59 material.

Table 5.19 Pyrolysis yield of ZrPM-59 samples heat treated at various temperatures for 2 h.

Temperature (^{o}C)	Yield (%)
800	57
1025	56

The measured carbon content of the sample heat treated at 1025^{o}C (2 h) (analyzed by Sherry Laboratories) was 19.4 wt% which was equivalent to a C/Zr molar ratio of 2.5, i.e., assuming that the pyrolyzed material contained only ZrO_2 and C.

Figure 5.19 shows the XRD patterns for samples heat treated at temperatures in the range of 800-1100^{o}C for 2 h. The as-dried powder was X-ray amorphous. The XRD pattern for the sample pyrolyzed at 800^{o}C (2 h) showed weak and broad diffraction peaks that were due to tetragonal zirconia (t-ZrO_2). The XRD patterns for the samples heat treated at 1025^{o}C and 1100^{o}C showed some small peaks due to monoclinic zirconia (m-ZrO_2) in addition to the major peaks due to t-ZrO_2. Very weak zirconium carbide (ZrC) peaks were observed in the XRD pattern of the 1100^{o}C-pyrolyzed sample. The carbon present in the samples remained X-ray amorphous for all heat treatment conditions.

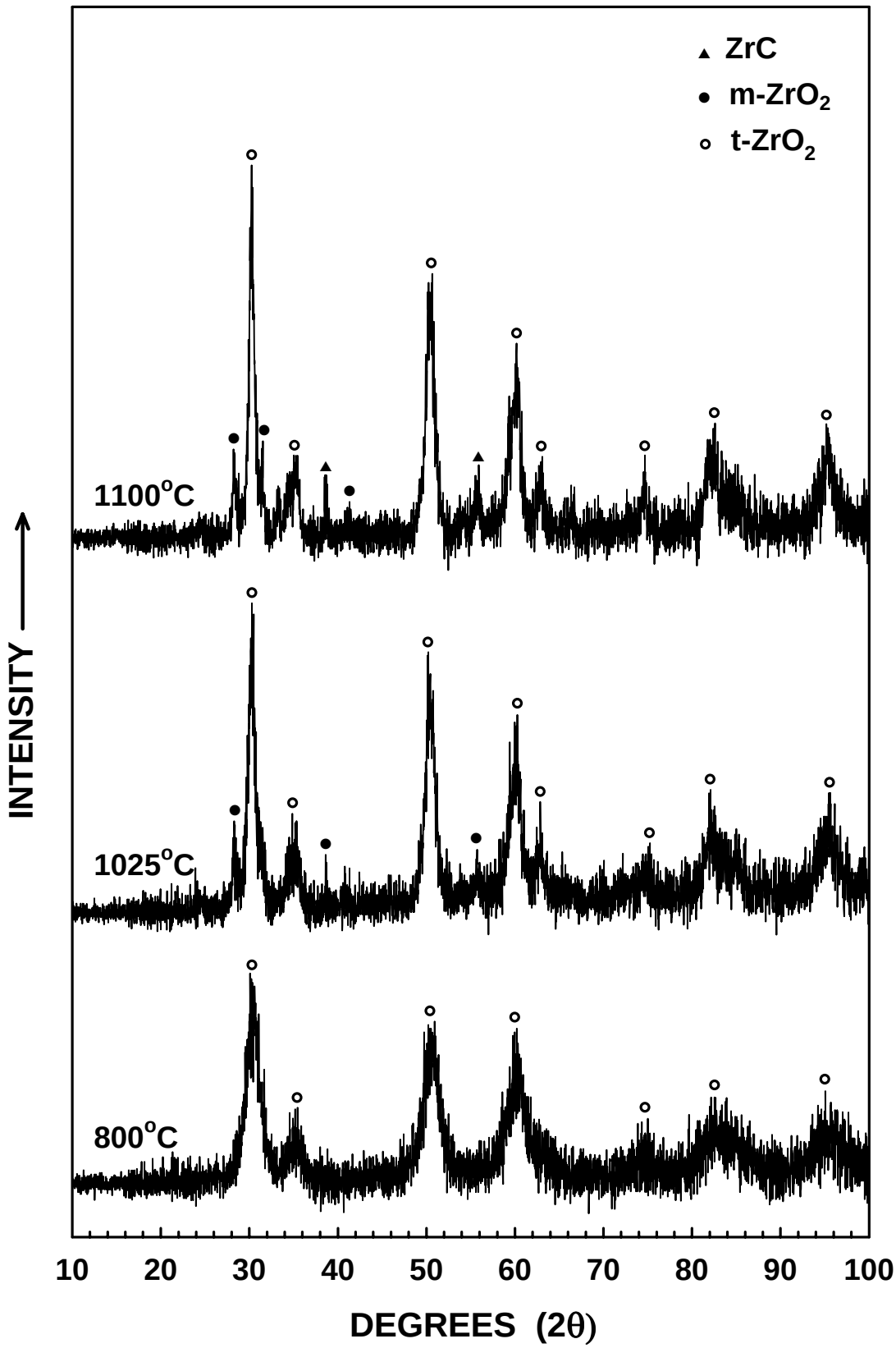

Figure 5.19 X-ray diffraction patterns for heat treated (800-1100°C) ZrPM-59 samples.

Table 5.20 shows the average crystallite sizes (determined by XRD line broadening) for the t-ZrO_2, m-ZrO_2, and zirconium carbide for samples heat treated at temperatures in the range of 800-1100^{o}C for 2 h. (See Appendix C for details.) The crystallite size for t-ZrO_2 increased from ~10 nm to ~27 nm as the heat treatment temperature increased from 800^{o}C to 1100^{o}C. The relatively small crystallite sizes indicated that a fine scale of mixing between zirconia and carbon was obtained after pyrolysis.

Table 5.20 Crystallite sizes for tetragonal zirconia, monoclinic zirconia, and zirconium carbide in ZrPM-59 samples heat treatment at various temperatures for 2 h.

Heat treatment Temperature (^{o}C)	Crystallite Size (nm)		
	t-ZrO_2	m-ZrO_2	ZrC
800	10	-	-
1025	20	-	-
1100	27	37	40

Table 5.21 shows the specific surface area values of samples heat treated at 800^{o}C and 1100^{o}C for 2 h. (See Appendix D for details.) The values from both BET and Langmuir models have been reported along with the constants *C* and *b* and the correlation coefficients (r_L). The specific surface area for the 800^{o}C (2 h) pyrolyzed sample was ~4 m^2/g, even though the sample contained ZrO_2 with small crystallite sizes (~10 nm). The possible reasons for the low specific surface area of the 800^{o}C-pyrolyzed sample are the same as discussed for the corresponding ZrPM-45 sample.

The specific surface area for the 1025°C (2 h) pyrolyzed sample increased to 159 m^2/g. (There was a slight weight loss observed upon heat treatment from 800°C to 1025°C (2 h) (Table 5.22).) As discussed in section 5.2.1 for the 900°C ZrPM-45 sample, the large increase in the specific surface area indicates that accessible porosity developed at the higher heat treatment temperature. The crystallite sizes for the t-ZrO_2 in the 1025°C and 1100°C samples were 20 and 28 nm, respectively (Table 5.20). The corresponding calculated specific surface areas (using equation 5-1) are 50.4 and 36 m^2/g, respectively. The calculated values are less than the measured values of ~159 and ~186 m^2/g, respectively. As noted in section 5.2.1.2, this discrepancy is attributed to the presence of fine pores that are in some way associated with the amorphous carbon in the samples.

Table 5.21 Specific surface areas and other gas adsorption results for ZrPM-59 samples heat treated at various temperatures for 2 h.

Temperature (°C)	BET (m^2/g)	C	r_L	Langmuir (m^2/g)	b	r_L
800	4.5	2	0.7734	-108	-3.01	-0.4489
1025	**159**	**135**	**0.9997**	229	0.028	0.9985
1100	**186**	**475**	**0.9998**	270	0.031	0.9980

Table 5.22 Weight loss data of ZrPM-59 samples heat treated at various temperatures for 2 h.

Temperature (^{o}C)	Weight Loss (%)
800	0.0
1025	2.4

5.2.2.3 High Temperature Heat Treatments (>1100^{o}C)

Figures 5.20, 5.21 and 5.22 show XRD patterns for samples heat treated at temperatures in the range of 1200 to 2000^{o}C for 2 h. As noted earlier, the initial formation of ZrC was observed (Figure 5.19) in a sample that was heat treated at 1100^{o}C (2 h). The ZrC peak intensities increased significantly for the 1200^{o}C sample, but tetragonal zirconia and monoclinic zirconia were still the predominant phases (Figure 5.20). It is also noted that the monoclinic zirconia peak intensities increased significantly compared to the 1100^{o}C sample. ZrC became the predominant phase in the sample that was heat treated at 1300^{o}C (2 h), although Figure 5.20 shows that there was still a significant amount of m-ZrO_2 and a small amount of t-ZrO_2. The amount of ZrC continued to increase and the amount of ZrO_2 continued to decrease in the samples as the heat treatment temperature increased over the range of 1350^{o}C - 1475^{o}C (Figures 5.20 and 5.21). The XRD pattern for the 1475^{o}C sample showed no t-ZrO_2 and only a trace amount of m-ZrO_2 (Figure 5.21). The sample heat treated at 1600^{o}C had only ZrC in the XRD pattern (Figure 5.21).

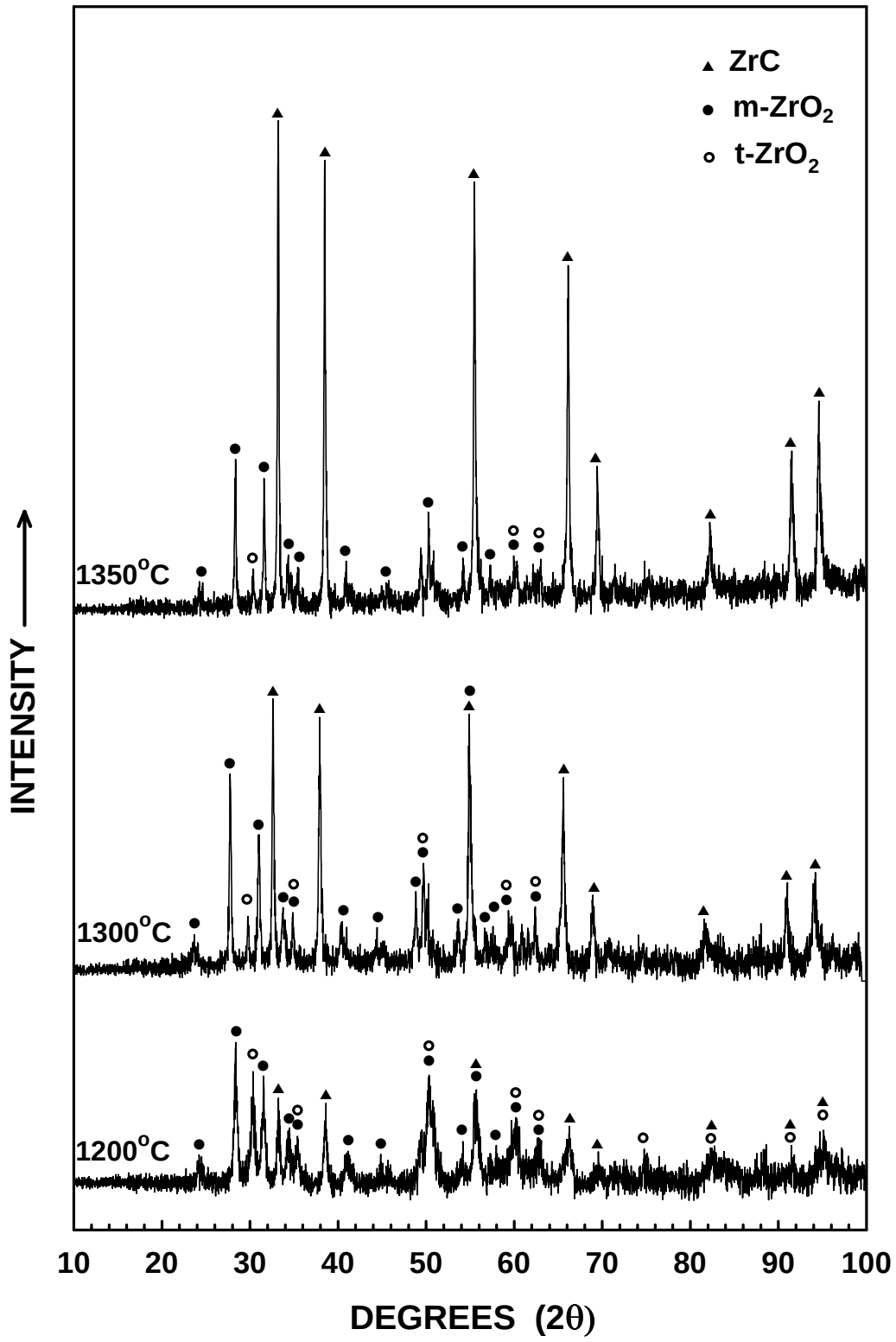

Figure 5.20 X-ray diffraction patterns for carbothermally reduced (1200-1350°C) ZrPM-59 samples.

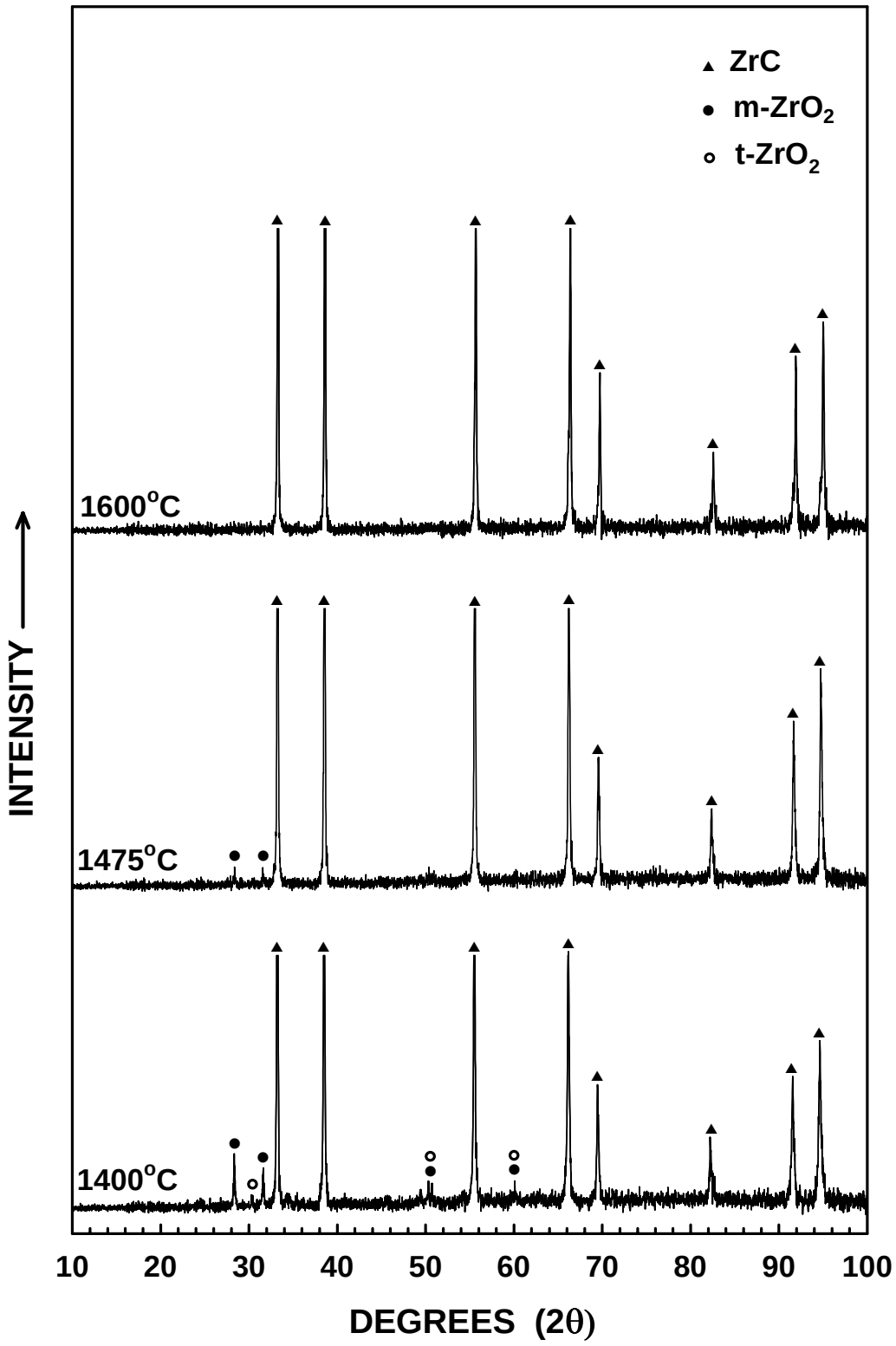

Figure 5.21 X-ray diffraction patterns for carbothermally reduced (1400-1600°C) ZrPM-59 samples.

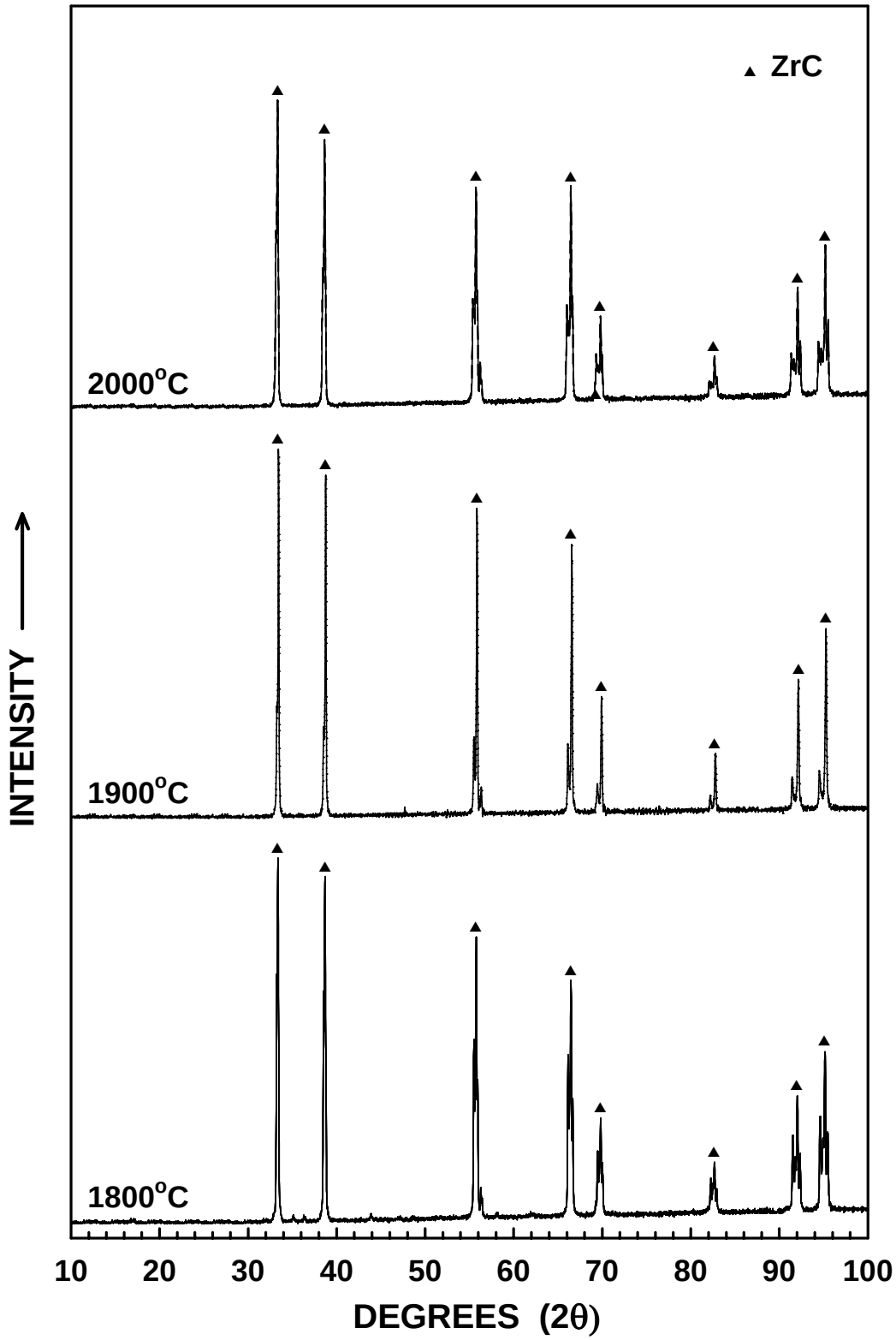

Figure 5.22 X-ray diffraction patterns for carbothermally reduced (1800-2000°C) ZrPM-59 samples.

The phase evolution for the ZrPM-59 samples was different from that described in section 5.2.1 (Figures 5.9 - 5.11) for the ZrPM-45 samples in that zirconia persisted to higher temperatures in the former samples. Recall that the ZrPM-45 samples showed only zirconium carbide in the XRD patterns (Figures 5.10 and 5.11) for samples heat treated at or above 1400°C. This difference in phase development is consistent with the lower starting carbon content in the ZrPM-59 samples (i.e., a C/Zr molar ratio of 2.5 in the 1025°C-pyrolyzed material) compared to the ZrPM-45 samples (i.e., a C/Zr molar ratio of 3.1 in the 1025°C-pyrolyzed material).

In section 5.2.1.3, it was shown that the ZrPM-45 1400°C and 1475°C samples were zirconium oxycarbides, i.e., oxygen was dissolved in the ZrC lattice. (This was proven by elemental analysis. Lattice parameter measurements were also consistent with the formation of zirconium oxycarbide.) Elemental analysis also showed that a zirconium oxycarbide phase had formed in the 1475°C ZrPM-59 sample. Table 5.23 shows the carbon concentrations (analyzed by Sherry Laboratories) and the oxygen concentrations (analyzed by Leco Corp.) for ZrPM-59 samples heat treated at temperatures in the range of 1025 to 2000°C for 2 h. The sample heat treated at 1475°C had an oxygen content of ~4.5 wt%. Since this sample only showed a trace amount of m-ZrO_2 in the XRD pattern (Figure 5.21), it is apparent that some oxygen must have been dissolved in the ZrC lattice. Oxygen analysis was not carried out on ZrPM-59 samples heat treated at temperatures below 1475°C. However, based on the XRD results for the ZrPM-45 sample, it is presumed that zirconium oxycarbide formation also occurred at lower temperatures (e.g., at least 1300-1400°C) in the ZrPM-59 samples. Table 5.23 also shows that the 1475°C ZrPM-59 sample had a carbon content of 9.0 wt%. This is

Table 5.23 Carbon and oxygen contents for ZrPM-59 samples heat treated at various temperatures for 2 h.

Temperature (^{o}C)	Carbon Content[a] (wt%)	Oxygen Content[b] (wt%)
1025	19.4	n.d.
1300	n.d.	n.d.
1400	n.d.	n.d.
1475	9.0	4.50
1600	9.4	n.d.
1800	8.9	1.00
2000	n.d.	0.56

[a] Measured by Sherry Laboratories.
[b] Measured by Leco Corp.

considerably smaller than the carbon content in the 1475^{o}C ZrPM-45 samples (13.3 wt%) and it is also smaller than the carbon content of 11.6 wt% in phase-pure stoichiometric ZrC. Hence, the 1475^{o}C ZrPM-59 sample had a "carbon-deficient" oxycarbide composition, ZrC_xO_y, in which x is <1.

Figure 5.22 shows the XRD patterns for ZrPM-59 samples which were heat treated at temperatures in the range of 1800-2000^{o}C. As in the 1600^{o}C ZrPM-59 sample, the only phase present in these samples was zirconium carbide. However, Figure 5.22 shows that extensive peak splitting occurred in the XRD patterns for these samples. This is illustrated more clearly in Figures 5.23a and 5.23b which show the portion of each XRD pattern from 30-60 degrees (2θ) and 65-95 degrees (2θ), respectively. The peak splitting was apparently caused by reaction of the powder samples with the Graphoil® substrates that were used in the heat treatments. As noted above, the ZrPM-59 samples

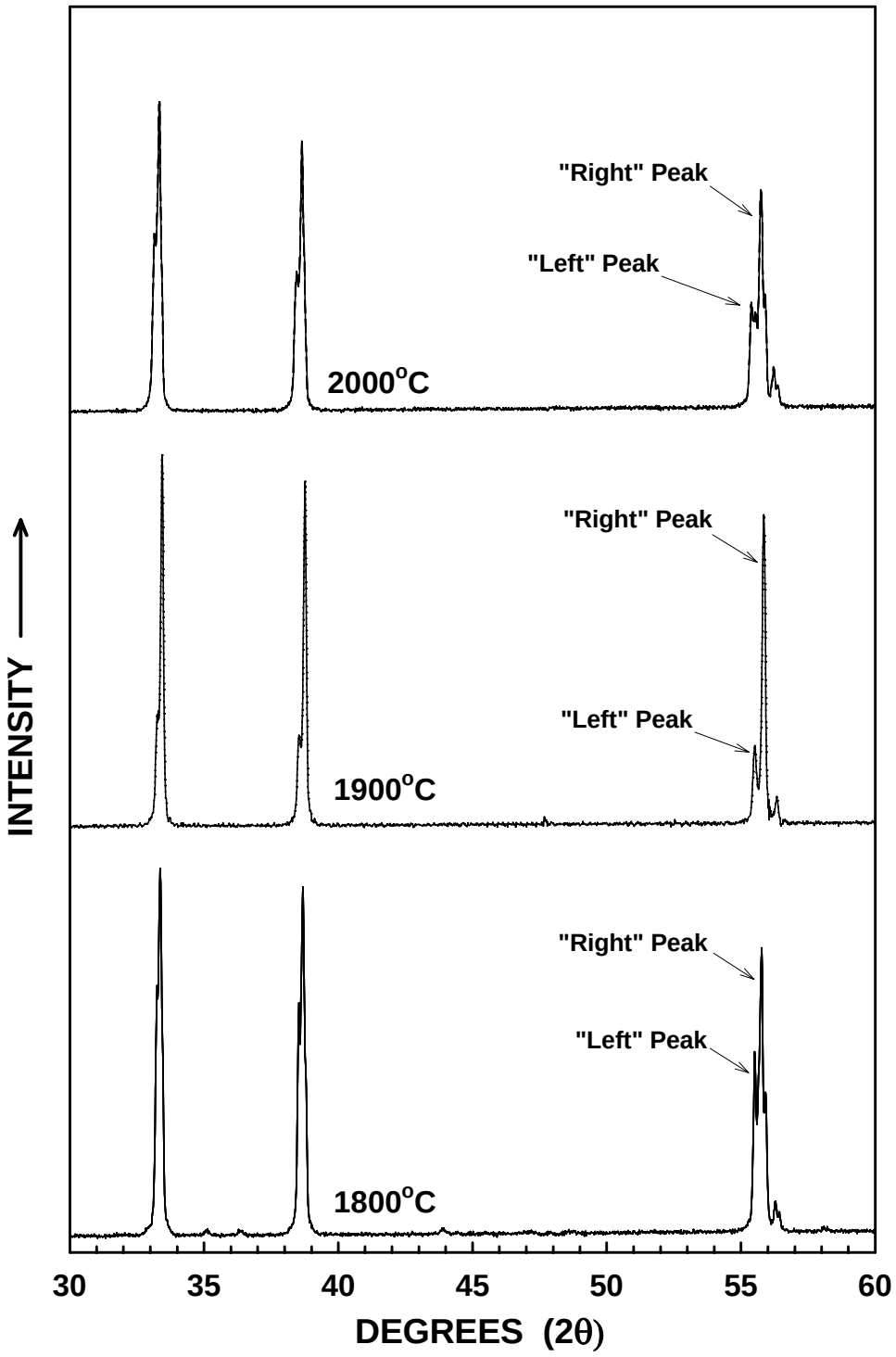

Figure 5.23a Peak splitting (30-60°) observed in X-ray diffraction patterns for carbothermally reduced (1800-2000°C) ZrPM-59 samples.

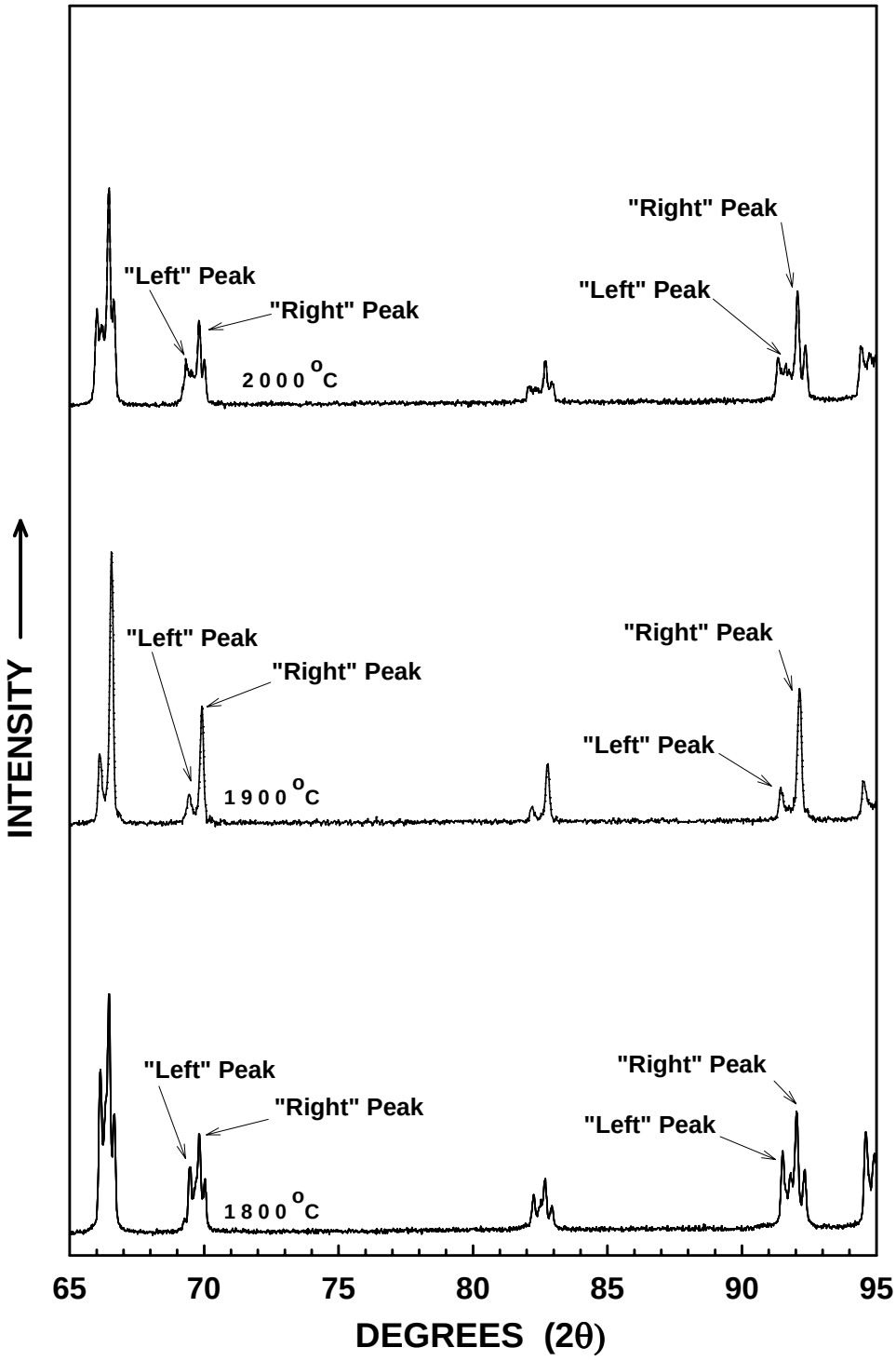

Figure 5.23b Peak splitting (65-95°) observed in X-ray diffraction patterns for carbothermally reduced (1800-2000°C) ZrPM-59 samples.

have dissolved oxygen in the ZrC lattice at lower temperatures. At elevated temperatures (e.g., >1475^{o}C), the "carbon-deficient" zirconium oxycarbide apparent reacted with the carbon (Graphoil®) substrate according to the reaction shown in equation 5-2. This would have resulted in the formation of some stoichiometric (or near-stoichiometric) ZrC at the interface between the ZrPM-59 powder and the carbon substrate. However, in regions far away from the powder/substrate interface, there was no carbon source for the reaction (equation 5-2) and the powder would have remained carbon-deficient. It is expected that a compositional gradient would have developed from the interface to the outer portions of the powder sample. Experimentally, each heat-treated powder sample was mixed (after being collected from the carbon substrate) in order to have a homogenized sample for subsequent powder characterization measurements. Therefore, the XRD patterns shown in Figure 5.22 were carried out on powders which had a mixture of phases, i.e., stoichiometric ZrC and carbon-deficient zirconium carbide (or carbon-deficient zirconium oxycarbide). Hence, peak splitting was observed in the XRD patterns because more than one "zirconium carbide" phase was present in each sample. To confirm this explanation, the lattice parameters were calculated using both the "right-side" peaks and "left-side" peaks in Figure 5.22 for the 1800^{o}C - 1900^{o}C ZrPM-59 samples. (See Appendix F for the detailed results.) The lattice parameters obtained from the "left-side" peaks for these samples (1800^{o}C - 2000^{o}C) were all in the range of 0.4693 – 0.4699 nm (Tables F13, F15, and F17, Appendix F), i.e., close to the values expected for stoichiometric ZrC. In contrast, much lower lattice parameters (in the range of 0.4668 – 0.4673, Table 5.24) were obtained when the "right-side" peaks were used. This would be expected for a carbon-deficient zirconium carbide, as discussed in section 2.3. This

Table 5.24 Lattice parameter values of ZrPM-59 samples heat treated at various temperatures for 2 h.

Temperature (^{o}C)	Lattice Parameter (nm)
1300	0.4690
1350	0.4692
1400	0.4690
1475	0.4686
1600	0.4675
1800	0.4673
1900	0.4669
2000	0.4668

overall explanation for the peak splitting was further confirmed by the ZrPM-87 and ZrPM-94 results discussed in Appendix F.

Figure 5.24 shows a plot of weight loss vs. heat treatment temperature (in the range of 800-1900^{o}C) for the ZrPM-59 samples using the data in Tables 5.22 and 5.25. This figure shows that there was still a significant weight loss (~6 wt%; see Table 5.25) upon heat treatment from 1475^{o}C to 1900^{o}C, even though the 1475^{o}C sample had only a trace of ZrO_2 in the XRD pattern (Figure 5.21). This is consistent with the previous conclusion that carbothermal reduction reactions continue at higher temperatures due to the presence of dissolved oxygen in the ZrC lattice. The removal of oxygen from the lattice as a result of carbothermal reduction reactions was confirmed by elemental analysis. Table 5.23 shows that the oxygen concentration decreased to ~1.0 wt% and ~0.6 wt% in the 1800^{o}C and 2000^{o}C ZrPM-59 samples, respectively. (It should

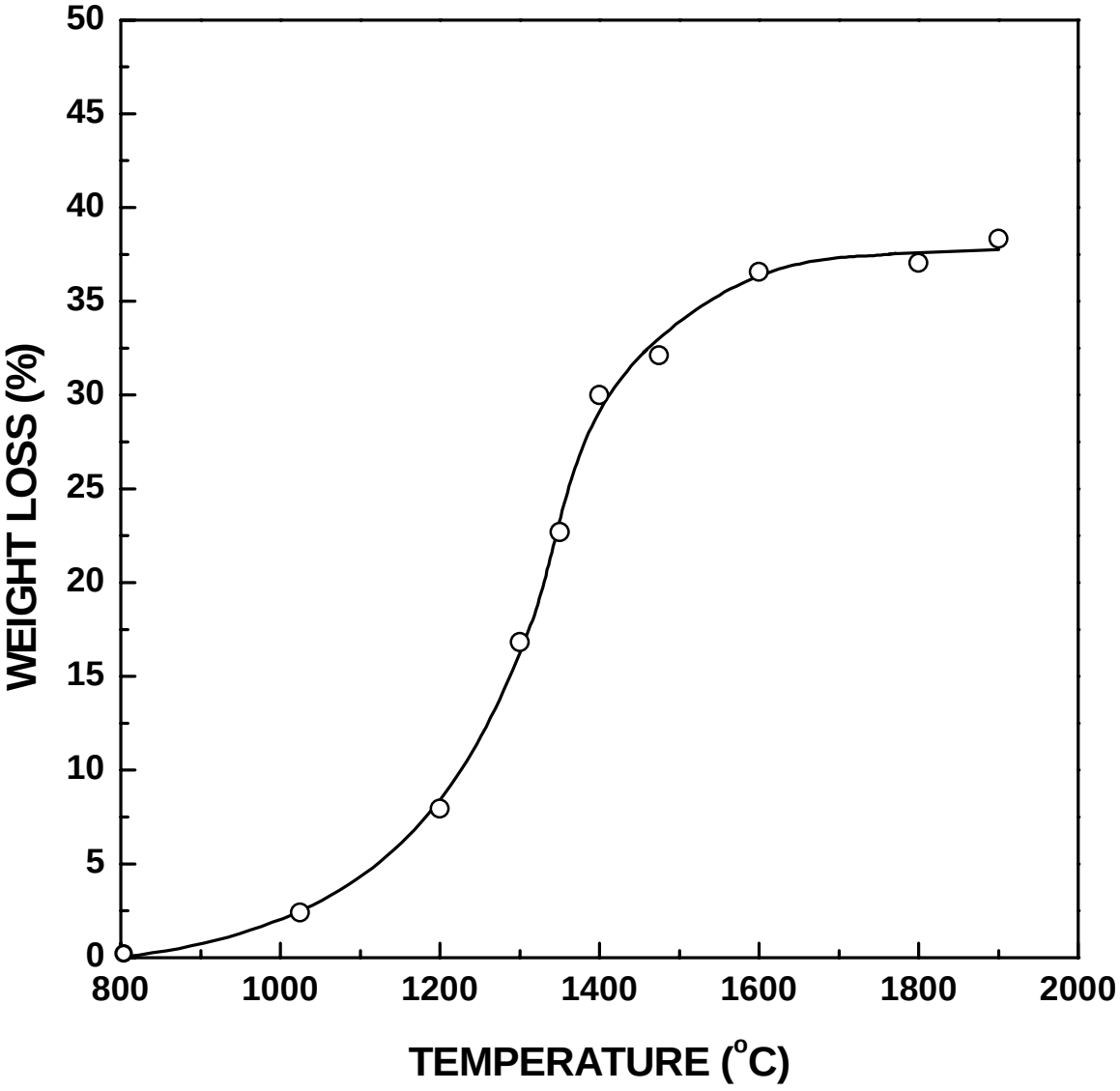

Figure 5.24 Plot of weight loss vs. temperature for 800°C-pyrolyzed ZrPM-59 sample.

be noted that these samples were prepared using a "ZrC"-based substrate, instead of a carbon (Graphoil®) substrate.) The residual oxygen concentration in the 1800°C ZrPM-59 sample was higher than the concentration that was observed in the 1800°C ZrPM-45 sample (i.e., ~0.1 wt%, Table 5.13). This indicates that it was more difficult to remove oxygen from the zirconium oxycarbide phase when "free" carbon was not present. Recall that the 1475°C ZrPM-45 sample still had ~2.32 wt% "free" carbon that was available to react with the dissolved oxygen in the lattice. The CTR reaction was mostly completed by 1600°C in ZrPM-45 samples, as indicated by the weight loss behavior shown in Figure 5.12 and Table 5.14. In contrast, the 1475°C ZrPM-59 sample had a higher residual oxygen concentration than the 1475°C ZrPM-45 sample, as well as a carbon-deficient composition (Table 5.23). Therefore, the CTR weight losses continued until higher temperatures. Figure 5.24 and Table 5.25 show that small weight losses were observed in the ZrPM-59 samples at least up through the 1900°C heat treatment.

Table 5.25 Weight loss data of ZrPM-59 samples heat treated at various temperatures for 2 h.

Temperature (°C)	Weight Loss (%)
1200	8.0
1300	16.8
1350	22.7
1400	30.0
1475	32.1
1600	36.6
1800	37.1
1900	38.3

There may be more than one CTR reaction responsible for the weight losses and the removal of oxygen from the ZrPM-59 samples at elevated temperatures (e.g., >1475°C). The reaction shown in equation 5-2 is only possible when free carbon is present in the sample. Table 5.23 shows that free carbon was not present in ZrPM-59 samples that were heat treated at or above 1475°C. However, as noted earlier, the reaction shown in equation 5-2 could have occurred in ZrPM-59 samples which were heat treated on carbon substrates. In contrast, this reaction would not be expected to occur for samples heat treated on ZrC-based substrates. Therefore, the decrease in oxygen concentrations shown in Table 5.23 for the samples heat treated to 1800°C and 2000°C must be explained by other reactions than the one given by equation 5-2. Two possible CTR reactions are shown in equations 5-3 and 5-4 below:

$$ZrO_{y-2}C_{2(1-x)+y\ (s)} + ZrO_{2\ (s)} = 2ZrC_{1-x\ (s)} + yCO_{\ (g)} \quad (5\text{-}3)$$

$$ZrO_yC_{(1-x)+y\ (s)} = ZrC_{1-x\ (s)} + yCO_{\ (g)} \quad (5\text{-}4)$$

The first reaction (equation 5-3) would only be possible to limited extent because free zirconia is required. Hence, this reaction might be possible in the 1475°C ZrPM-59 sample (or, more likely, in samples at even lower temperatures). In contrast, the second reaction (equation 5-4) could account for weight losses and decreases in oxygen concentration upon heat treatment (at higher temperatures) of samples which do not contain free zirconia.

There is a problem with applying equations 5-3 and 5-4 to the results obtained with the ZrPM-59 samples. According to these reactions, the carbon and oxygen concentrations in the sample should both decrease with increasing heat treatment

temperature (i.e., as the reaction proceeds to a greater extent). However, Table 5.23 shows that there was no significant change in the carbon concentration for ZrPM-59 samples which were heat treated in the range of 1475-1800°C. The most likely explanation for this observation is that the carbon concentrations are "incorrect" for the 1600°C and 1800°C samples because those samples were heat treated on a carbon substrate. Hence, there was some reaction between the powder and substrate (according to equation 5-2) which removed oxygen from the zirconium oxycarbide, but allowed the carbon concentration to be maintained. (According to equation 5-2, carbon is removed during the reaction as part of the volatile CO, but carbon is also added in the process of converting the carbon-deficient zirconium oxycarbide reactant to a stoichiometric (or near-stoichiometric) ZrC product.) Another explanation for the essentially constant carbon concentrations for the 1475°C, 1600°C, and 1800°C ZrPM-59 samples is that oxygen was removed from the zirconium oxycarbide lattice as molecular oxygen (equation 5-5) or as a combination of ZrO and CO volatiles (equation 5-6), as shown in the reactions below:

$$ZrC_xO_{y\,(s)} = ZrC_{x\,(s)} + (y/2)O_{2\,(g)} \quad (5\text{-}5)$$

$$ZrC_xO_{2y\,(s)} = yZrO_{(g)} + yCO_{(g)} + Zr_{1-y}C_{x-y\,(s)} \quad (5\text{-}6)$$

where x is <1.

This explanation seems less likely because the vapor pressures of molecular oxygen and ZrO vapor are probably rather low at the heat treatment temperatures used in this study.[11]

Table 5.24 shows the zirconium carbide lattice parameters for ZrPM59 samples that were heat treated at temperatures in the range of 1300 to 2000°C for 2 h. Figure 5.25

shows a plot of lattice parameter vs. heat treatment temperatures for these samples. The lattice parameter value for the 1300°C sample was 0.4690 nm. This value is smaller than the lattice parameter values usually reported for stoichiometric ZrC (see section 2.1[1,2,3,11,23]). This suggests that either some oxygen had already dissolved in the zirconium carbide lattice or that there was direct formation of a zirconium oxycarbide phase during the CTR reaction at 1300°C. The lattice parameter was also slightly smaller than that observed in the corresponding ZrPM-45 sample (Table 5.15), so it is possible that more oxygen was dissolved in the lattice for the ZrPM-59 sample. However, there is no convincing evidence for this because the lattice parameter values for the 1350°C and 1400°C ZrPM-59 samples were essentially the same as the value observed for a ZrPM-45 sample that had been heat treated at 1400°C.

The lattice parameter decreased to 0.4686 nm for the 1475°C ZrPM-59 sample. One explanation for this decrease is that additional zirconia dissolved in the zirconium carbide lattice at the higher heat treatment temperature. Another explanation is that the lattice parameter decreased due to the development of a carbon-deficient composition (i.e., ZrC_{1-x} or ZrO_yC_{1-x}), as discussed in section 2.3. There is evidence to support both oxygen dissolution and carbon deficiency as the reasons for the decrease in the lattice parameter upon heat treatment from 1400°C to 1475°C. The latter effect is suggested by the low carbon content (9.0 wt%) measured in the 1475°C sample (Table 5.23). The former effect is suggested by the decrease in the ZrO_2 peak intensity in the XRD patterns upon heat treatment from 1400°C to 1475°C (Figure 5.21).

The lattice parameter decreased from 0.4686 nm to 0.4675 nm upon heat treatment from 1475°C to 1600°C. This decrease may again reflect both effects discussed

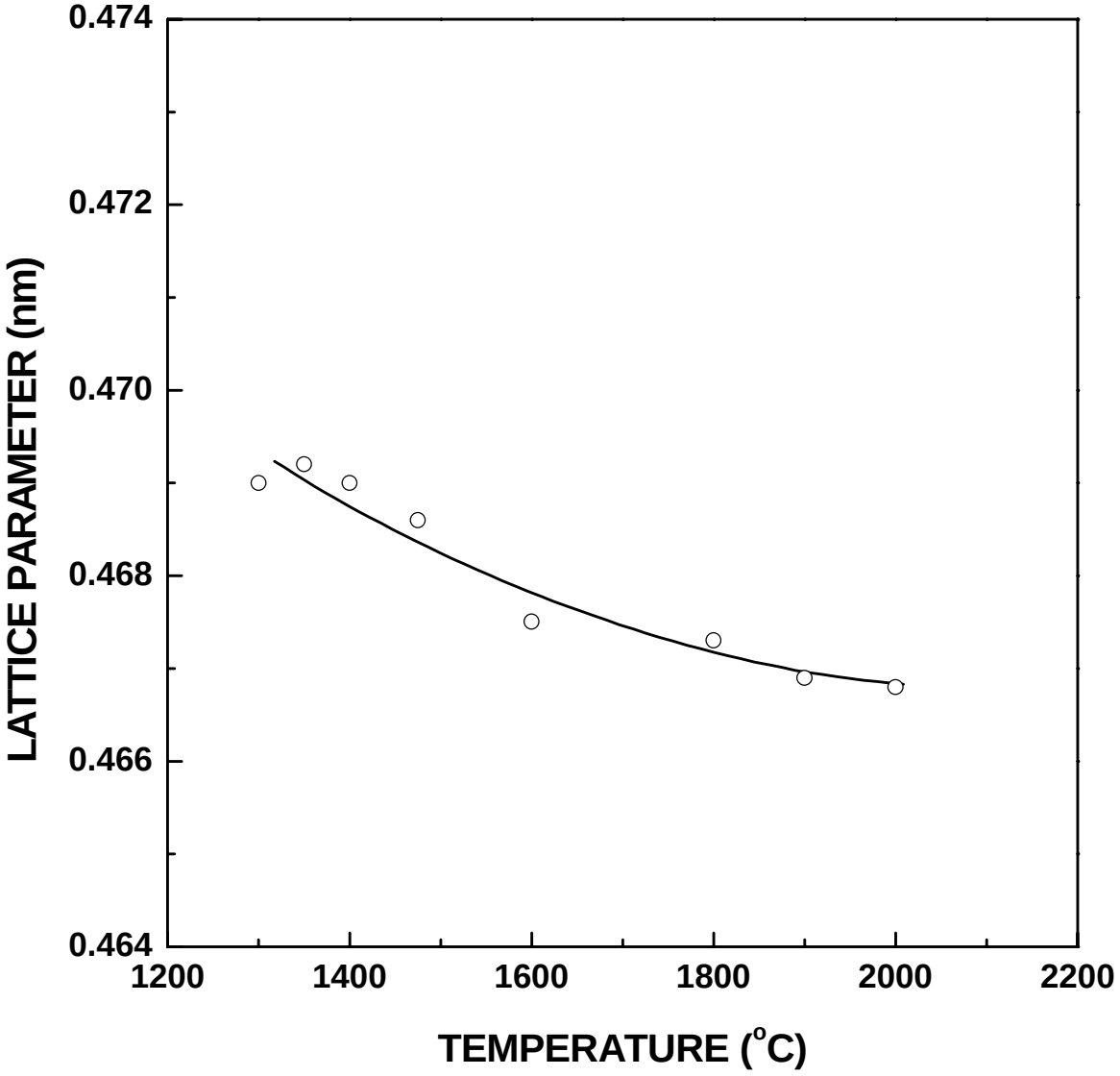

Figure 5.25 Plot of lattice parameter vs. temperature for carbothermally reduced ZrPM-59 samples.

above, i.e., increased oxygen dissolution and increased carbon deficiency in the ZrC lattice. The former effect is possible based on the absence of ZrO_2 in the XRD pattern in the 1600°C sample (Figure 5.22). In contrast, the latter effect is not supported by the carbon analysis results in Table 5.23. However, it was noted previously that the carbon content values for the samples heat treated at higher temperature samples (>1475°C) may be inaccurately high because of a reaction between the sample and the Graphoil® substrate.

The lattice parameter continued to decrease with increasing heat treatment temperature, e.g., from 0.4675 nm for the 1600°C sample to 0.4668 nm for the 2000°C sample. Figure 5.24 and Table 5.25 show that weight losses are relatively small in this temperature range. Table 5.23 shows that the oxygen concentration decreased from 1.0 wt% for the 1800°C sample to 0.56 wt% for the 2000°C sample. Figure 5.22 shows that there is no free ZrO_2 in the samples heat treated in the range of 1600-2000°C. In combination, these results indicate that the decrease in lattice parameter from 1600°C to 2000°C was due to an increased carbon deficiency in the ZrC lattice. The only problem with this interpretation is that the carbon concentration showed essentially no change for the samples heat treated at higher temperatures. However, as discussed earlier, this is probably because a reaction occurred between the sample and the Graphoil® substrate.

Figure 5.26 shows the average crystallite sizes for each phase (i.e., ZrC, t-ZrO_2, and m-ZrO_2) as a function of heat treatment temperature. (Data from Tables 5.20 and 5.26 have been combined for these plots.) The crystallite size increased rapidly with the onset of carbothermal reduction reaction at temperatures >1100°C. The crystallite sizes of both t-ZrO_2 and m-ZrO_2 increased from ~35-40 nm at 1200°C to ~100-120 nm at 1350°C

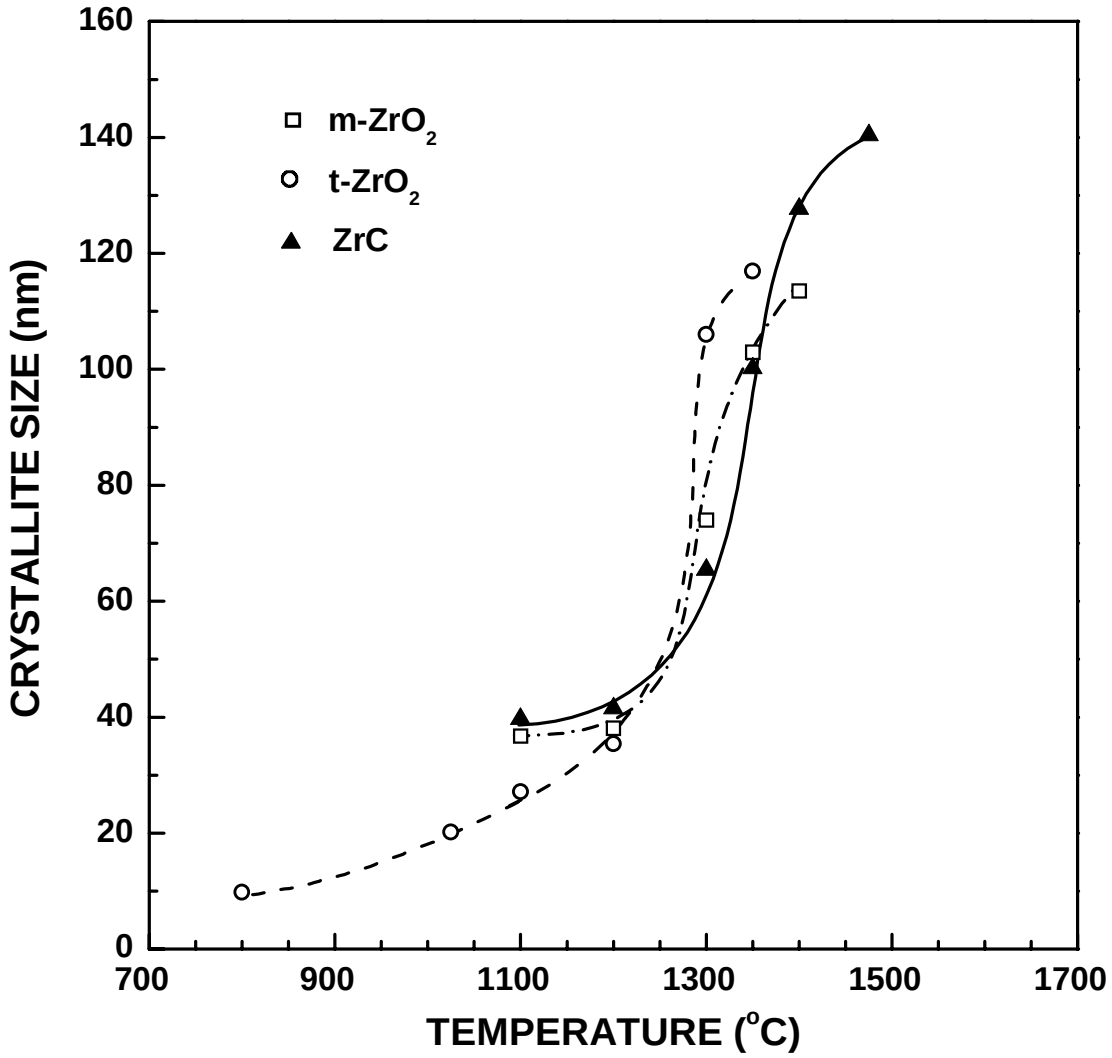

Figure 5.26 Plot of the t-ZrO_2, m-ZrO_2, and ZrC crystallite sizes (determined from XRD line broadening measurements) vs. heat treatment temperature for ZrPM-59 samples.

Table 5.26 Crystallite sizes for the phases observed by XRD in ZrPM-59 samples after heat treatment at various temperatures for 2 h.

Heat treatment Temperature (^{o}C)	Crystallite Size (nm)		
	t-ZrO_2	m-ZrO_2	ZrC
1200	35	38	42
1300	106	74	65
1350	117	103	100
1400	-	114	128
1475	-	-	140

during carbothermal reduction reaction. The ZrC crystallite sizes also increased from ~40 nm at 1200^{o}C to ~140 nm in the sample heat treated at 1475^{o}C. The crystallite size growth of the ZrC and two ZrO_2 phases was similar to that observed for ZrPM-45 samples and was also consistent with certain aspects of the reaction mechanism suggested by Maitre et al.,[11] as discussed in section 5.2.1.3.

Figure 5.27 shows a plot of specific surface area vs. temperature for samples heat treated in the range of 800 to 1475^{o}C for 2 h. Tables 5.21 and 5.27 show the data used to plot Figure 5.27. The specific surface area initially increased with increasing heat treatment temperature and reached a maximum value of ~219 m^2/g for the 1200^{o}C sample. The calculated specific surface area using equation 5-1 would be in the range of 22 to 28 m^2/g. This range of specific surface areas was determined using the following crystallite sizes and densities: 35.4 nm and 5.95 g/cm^3 for t-ZrO_2, 35.4 nm and 5.82 g/cm^3 for m-ZrO_2, and 41.5 nm and 6.6 g/cm^3 for ZrC. (See Tables 5.20 and 5.26 for the crystallite sizes.) As discussed in section 5.2.1.3, the fact that the measured specific

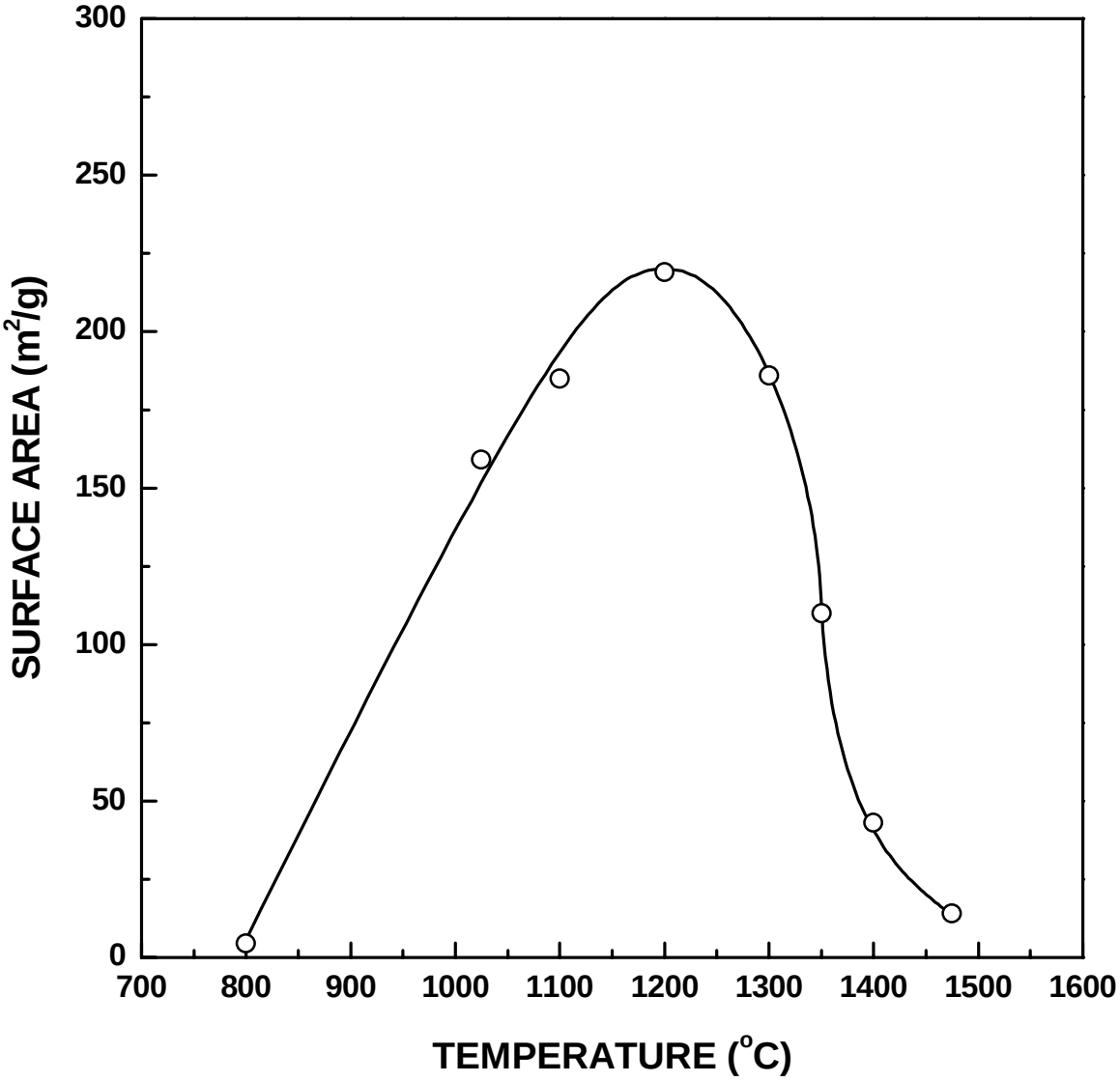

Figure 5.27 Plot of specific surface area vs. temperature for pyrolyzed and carbothermally reduced ZrPM-59 samples.

Table 5.27 Specific surface areas and other gas adsorption results for ZrPM-59 samples heat treated at various temperatures for 2 h.

Temperature (°C)	BET	*C*	r_L	Langmuir	*b*	r_L
1200	**219**	**211**	**0.9999**	319	0.035	0.9972
1300	**186**	**220**	**0.9999**	270	0.033	0.9974
1350	**110**	**142**	**0.9999**	160	0.037	0.9967
1400	**42**	**105**	**0.9999**	62	0.041	0.9961
1475	**9**	**42**	**0.9997**	14	0.062	0.9935

surface area is higher than the values calculated from equation 5-1 indicates that fine porosity (i.e., finer than the ZrC and ZrO_2 crystallite sizes) is present in the samples.

Figure 5.27 shows that the specific surface area decreased with increasing temperature above 1200°C. This indicates that finer pores underwent coarsening and/or were eliminated. Based on equation 5-1 and the crystallite sizes in Table 5.26, specific surface areas in the range of 9 to 14 m^2/g and 8 to 10 m^2/g were calculated for the 1300°C and 1350°C samples, respectively. The measured values were ~186 m^2/g and ~110 m^2/g, respectively.

Based on equation 5-1 and the crystallite sizes in Table 5.26, specific surface areas in the range of 7 to 9 m^2/g and 7 m^2/g were calculated for the 1400°C and 1475°C samples, respectively. The measured values were ~42 m^2/g and ~9 m^2/g, respectively. The measured specific surface area values were closer to the calculated values as the heat

treatment temperature increased. The decrease in the measured specific surface areas with increasing temperature was consistent with the decrease in carbon concentration. As noted previously, carbon is believed to be associated with the development of fine pores in the heat treated samples. (The presence of fine pores would, in turn, be the reason for increased specific surface areas. The fine pores could be present within the carbon regions themselves or in regions between the phases in the carbon/zirconium carbide/zirconia sample.) The good agreement between the measured specific surface area (~9 m^2/g) and the calculated specific surface (~6.5 m^2/g) for the 1475°C ZrPM-59 sample suggests that there is no free carbon in the sample. This is consistent with the results in Table 5.23 which show that the 1475°C sample has a carbon-deficient composition (i.e., compared to stoichiometric ZrC).

The changes in specific surface area as a function of temperature are similar for the ZrPM-45 and ZrPM-59 samples at temperatures ≤1400°C. The specific surface areas are very similar for the two 1400°C samples (i.e., ~39 m^2/g and ~42 m^2/g for the ZrPM-45 and ZrPM-59 samples, respectively). However, the specific surface areas are considerably different for the 1475°C samples. The values are ~23 m^2/g and ~9 m^2/g for the ZrPM-45 and ZrPM-59 samples, respectively. This difference is attributed to the presence of free carbon in the ZrPM-45 sample. This conclusion was based on the following considerations: (1) The ZrC crystallite sizes are similar for the two samples, i.e., ~127 nm and ~140 nm for the 1475°C ZrPM-45 and ZrPM-59 samples, respectively. The calculated specific surface areas using these crystallite sizes and equation 5.1 (and assuming a ZrC density of 6.6 g/cm^3) are 7.2 m^2/g and 6.5 m^2/g, respectively. Therefore, the difference in the measured specific surface areas cannot be attributed to the

differences in the ZrC crystallite sizes. (2) The XRD patterns (Figures 5.11 and 5.21) show that the 1475°C ZrPM-45 has no free zirconia and the 1475°C ZrPM-59 has only a trace of m-ZrO_2. The m-ZrO_2 crystallite size was not measured for the 1475°C ZrPM-59 sample, but the value should be comparable to or slightly greater than the ZrC crystallite size based on the data (in Figure 5.26 and Table 5.26) for the 1400°C ZrPM-59 sample. Therefore, the difference in the measured specific surface areas cannot be attributed to differences in the free zirconia content. (3) As discussed in section 5.2.1.3, the 1475°C ZrPM-45 sample has two phases present, i.e., zirconium oxycarbide and "free" carbon. The amount of "free" carbon was estimated with reasonable accuracy because the overall carbon and oxygen concentrations in the sample were known. It was determined that the sample had ~2.3 wt% "free" carbon. In contrast, the 1475°C ZrPM-59 sample probably does not have any "free" carbon based on the carbon-deficient composition (i.e., relative to stoichiometric ZrC) shown in Table 5.23. As shown in section 5.2.1.3, the specific surface area associated with the "free" carbon phase alone (i.e., a 100% carbon sample) was estimated to be ~630 m^2/g.

The particle size distributions for the milled ZrPM-45 and ZrPM-59 samples have both similarities and differences, as shown by direct comparison plots of the data in Figure 5.28. The ZrPM-59 sample is similar to the ZrPM-45 sample in that a bimodal particle size distribution is observed. The volume fraction of particles in each mode differs for the two samples, but size distributions in each mode are similar. First consider the mode associated with the smallest particles (~0.04 - 0.10 μm). The distribution of particle sizes for this mode is extremely similar for the two powders. As noted earlier, the mode for the smaller particles in the distribution represents the primary particles (and

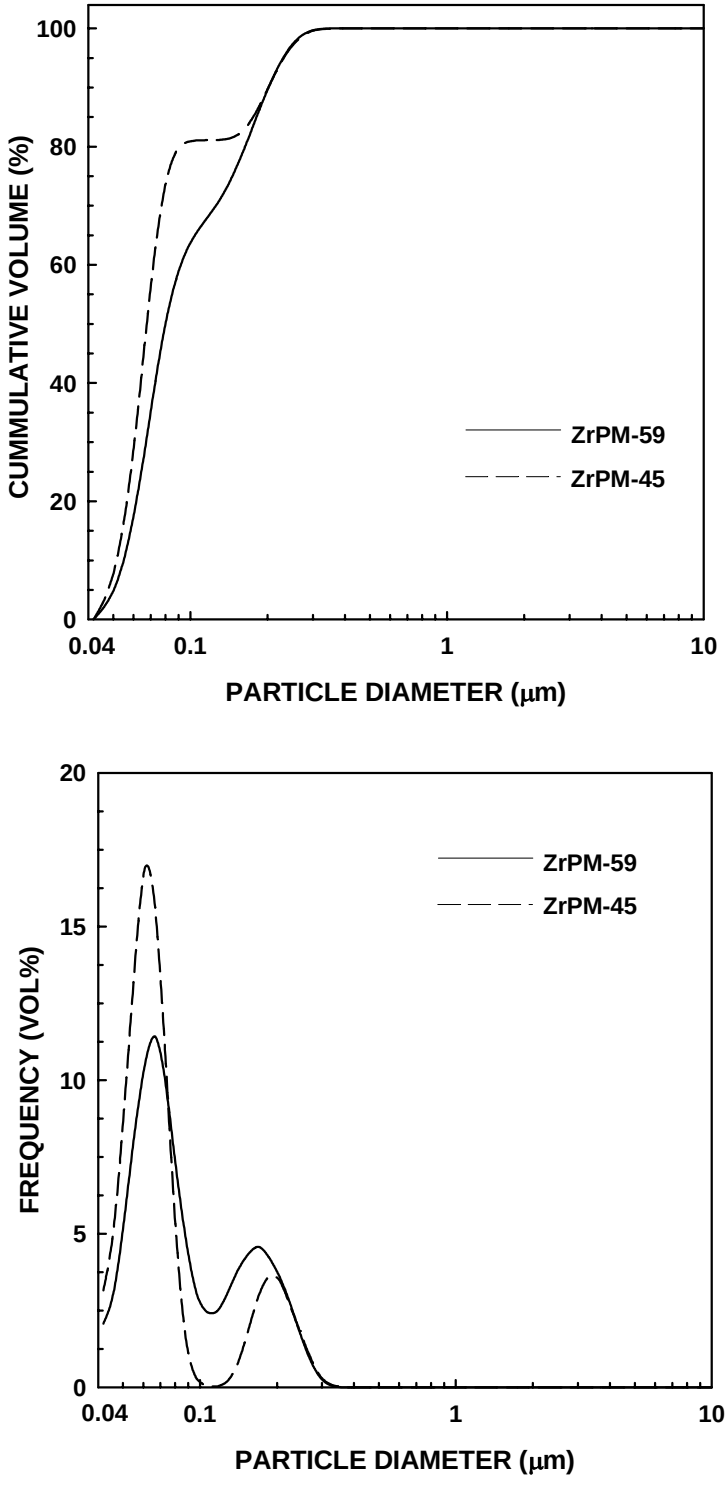

Figure 5.28 Combined particle size distribution plots for the 10 min-milled 1475°C ZrPM-59 and 1475°C ZrPM-45 samples: cumulative distribution plot (top) and relative frequency plot (bottom).

Table 5.28 Particle size distribution data for the 10 min-milled 1475°C ZrPM-59 powder sample.

	Diameter (μm)
Mean	0.10
Modes*	0.07, 0.17
D_{90}	0.19
D_{50}	0.08
D_{10}	0.05
Standard Deviation	0.06

* Mode values are listed for each distinct peak in the accompanying relative frequency plot.

possibly some very small aggregates of primary particles) which could be dispersed in the suspension used for the size measurement. As expected from the XRD line broadening measurements, there are only small differences in the sizes of the primary particles for the ZrPM-45 and ZrPM-59 samples. In contrast, the amount of particles associated with the mode for the smaller particles is smaller for the ZrPM-59 sample (68 vol%) compared to the ZrPM-45 sample (81 vol%). This indicates that the primary particles are more aggregated for the ZrPM-59 sample. Of course, this is also indicated by the fact that the amount of particles associated with the mode for larger particles (~0.1-0.3 μm) is 32 vol% for the ZrPM-59 sample and 19 vol% for the ZrPM-45 sample. The larger particles are mostly aggregates of primary particles that were not broken down

by the milling process. The question arises as to why there was a difference in the extent of aggregation in the two samples. It is speculated that the reason is associated with the higher free carbon content and/or the absence of ZrO_2 in the 1475°C ZrPM-45. It is well-known that extensive sintering will occur in fine-sized ZrO_2 powders at temperatures in the range of interest in this study.[87,89] Hence, the formation of aggregates via neck growth between individual crystallites might be promoted in the ZrPM-59 sample by the presence of either ZrO_2 crystallites and/or oxide-rich surface layers on zirconium oxycarbide particles. In contrast, it is also well-known that high concentrations of free carbon will inhibit sintering processes in refractory carbide materials (e.g., SiC, ZrC, etc.).[52,90] Hence, the formation of aggregates via neck growth between individual zirconium oxycarbide crystallites might be inhibited in the ZrPM-45 samples by the presence of a significant amount of free carbon.

5.3 Effect of CTR Heat Treatment Conditions on Powder Properties

5.3.1 Batch Size and Powder Packing

The characteristics (i.e., particle size distribution, surface area, crystallite size, phase composition, etc.) of CTR powders depended upon the batch size of the powder sample (i.e., amount of powder used for CTR) and how the powder was packed during CTR. Powder samples were loaded into containers for the CTR reaction using two different "packing" methods. In the first method, powder was loaded into the containers and lightly compacted. In the second method, powder was loaded into the containers and channels were made in the powder as discussed in Chapter IV section 4.1.5. These two types of packing will be referred to as "dense packing" and "loose packing", respectively.

The powders were spread over a much larger surface area in case of “loose packing” as compared to “dense packing.”

When a batch with larger size (i.e. ≥2 g) with dense packing was reacted with similar conditions as used for a batch with smaller size (i.e. ≤2 g), the yield for the larger sample was much higher than that obtained for smaller batch size. This indicated that the CTR reaction for the larger sample was less complete. For example, the yield obtained by using a 0.4 g ZrPM-59-800-pyrolyzed sample after heat treatment at 1400^{o}C (2 h) was ~70 wt%, while the yield obtained by using a 2.2 g sample was ~83 wt%. (The gas flow rate used during heat treatment was 100 ml/min.)

The effect of powder packing was investigated using powder batches with different sizes. ZrPM-45-800-pyrolyzed samples were heat treated at 1400^{o}C (2 h) using batch sizes of 0.4 g and 3.0 g and a "loose packing" arrangement in a Graphoil tray. (The gas flow rate used during heat treatment was 100 ml/min.) The yields for the two samples were 66.4 wt% and 68.1 wt%, respectively. The fact that the yields were very similar in this case (i.e., compared to the first case described above) indicates the packing density was a dominant factor in these experiments. This was further confirmed by heat treatment of a 4.5 g sample of ZrPM-45-800 at 1400^{o}C (2 h) using a "dense packing" arrangement. The yield in this case was much higher (87.5 wt%). Figure 5.29 shows the XRD patterns for the three 1400^{o}C heat-treated samples. It is evident that a similar extent of reaction occurred for the samples with “loose packing” arrangement, while the extent of reaction was less for the sample with “dense packing” arrangement.

Table 5.29 shows similar results were obtained using other batches. Samples with different batch sizes and a "loose packing" arrangement were heat treated at 1425^{o}C (2 h)

using a gas (argon) flow rate of ~500 ml/min and a heating rate of 5°C/min. The batch size had negligible effect on the yield when the loose packing arrangement was used. (Appendix G (Figures G29-G30) contains the XRD patterns for the samples listed in Table 5.29.)

Table 5.29 Yields of various samples heat treated at 1425°C for 2 h using different batch sizes.

Sample	Amount of Sample (g)	Batch Size	Yield (wt%)
ZrPM-87-800-1-1425-1	0.37	Small	68.32
ZrPM-87-800-1-1425-2	7.8	Large	68.51
ZrPM-91-800-1-1425-1	0.37	Small	72.76
ZrPM-91-800-1-1425-4	7.0	Large	71.07
ZrPM-95-800-1-1425-1	0.37	Small	67.48
ZrPM-95-800-1-1425-2	2.0	Large	67.00

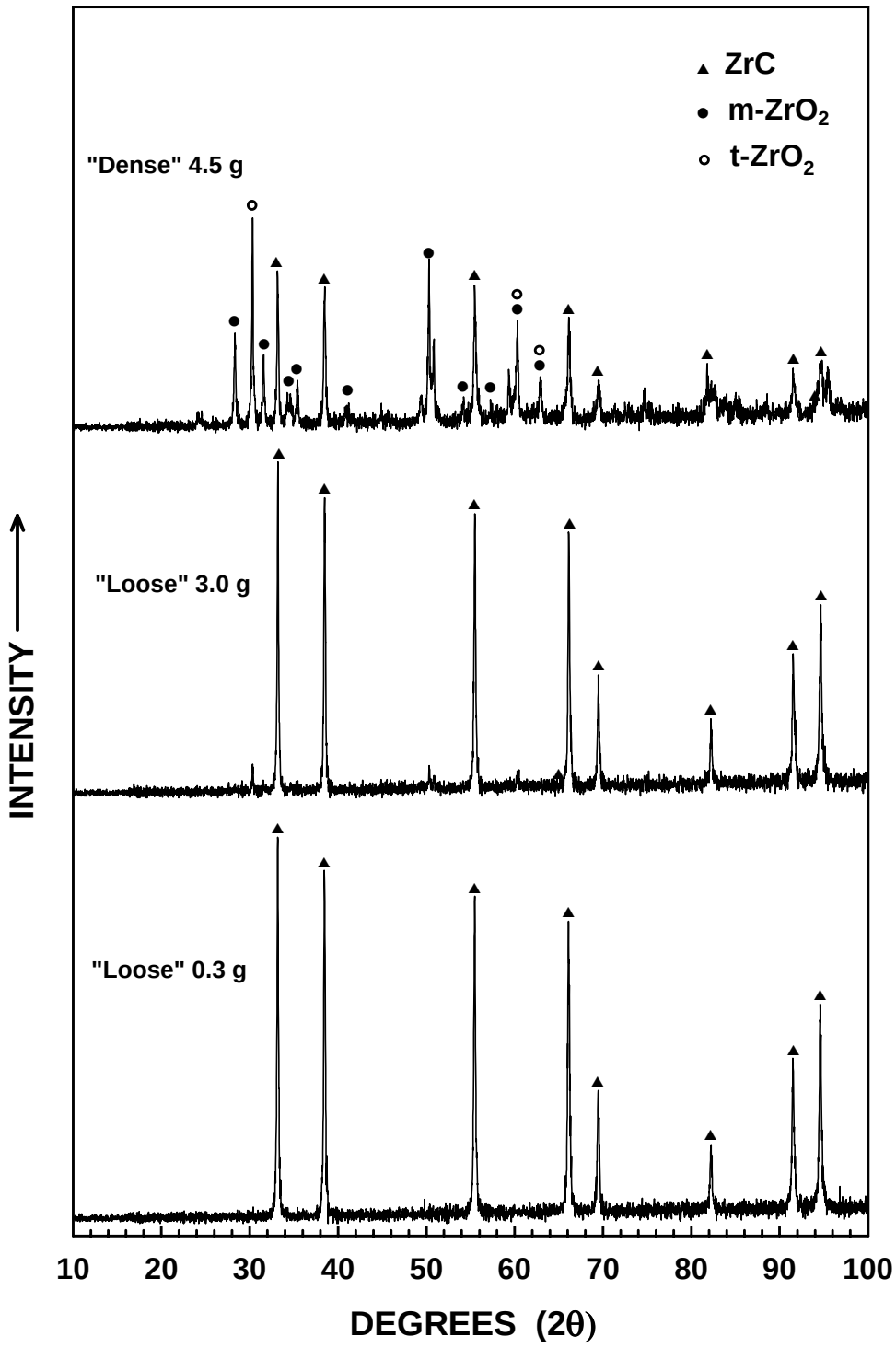

Figure 5.29 XRD patterns for ZrPM-45 samples heat treated at 1400°C using "loose packing" and "dense packing" arrangements.

In summary, there is an apparent increase in reaction rate for samples with a "loose packing" arrangement and for samples with smaller batch size (i.e., in samples with the "dense packing" arrangement). Both of these effects presumably reflect the influence of sample size and packing arrangement on the diffusion and removal of CO from the sample during CTR. The ideal CTR reaction is represented by the reaction:

$$ZrO_{2\,(s)} + 3C_{(s)} = ZrC_{(s)} + 2CO_{(g)} \qquad (5\text{-}7)$$

It is evident from LeChatelier's principle that a high CO concentration in the surrounding atmosphere would tend to impede the formation of ZrC. The removal of CO from the reaction zone will be impeded if the volatiles must travel through porosity with a longer, more tortuous path or through pores that have finer diameters. An increase in sample size would increase the diffusion distance that would be required for the CO volatile to be removed from the reaction zone. The same thing would be true for the case of the "dense packing" arrangement used in this study. It should be noted that the two "packing arrangements" probably did not have much difference in the actual powder packing density (and the corresponding size and volume fraction of pore within the packed powder). Instead, the powder was spread out over a much larger area in the "loose-packing" arrangement and this resulted in a much smaller depth of the powder layer. Hence, the so-called "packing" effect was probably due mostly to the difference in the length of the egress path for the CO.

5.3.2 Gas Flow Rate

The effect of gas flow rate was investigated using samples with different batch sizes and using the "loose packing" arrangement. Two different flow rates were used: 100 ml/min and 500 ml/min. The first experiment was carried out with a gas flow rate of 100 ml/min using ZrPM-58-dried material with batch sizes of 1 and 20 g. The CTR heat treatment was carried at 1300^{o}C for 48 h. As expected, the yield was much higher for the larger sample, i.e., 47.4 wt% as compared to 38.4 wt% for smaller sample. Figure 5.30.a shows the XRD patterns for the two 1300^{o}C heat-treated samples. It is evident that the extent of reaction was less for the larger sample.

The batch size effect was much smaller when a high gas flow rate was used. ZrPM-61-350-800-pyrolyzed material with batch sizes of 0.9 and 19.5 g were heat treated at 1300^{o}C for 48 h using a gas flow rate of 500 ml/min. The yields for the two samples were 30.8 wt% and 33.5 wt%, respectively. The fact that the yields were very similar in this case (i.e., compared to the first experiment described above) indicates that the gas flow rate was a dominant factor in these experiments. Figure 5.30.b also shows the XRD patterns for the two 1300^{o}C heat-treated samples. It is evident that the extent of reaction was similar for the two samples.

Based on the results in sections 5.3.1 and 5.3.2, the following conditions were used to process larger samples (>2 g) starting with batch ZrPM-65: a loose-packing arrangement in a Graphoil tray and a 500 ml/min gas flow rate.

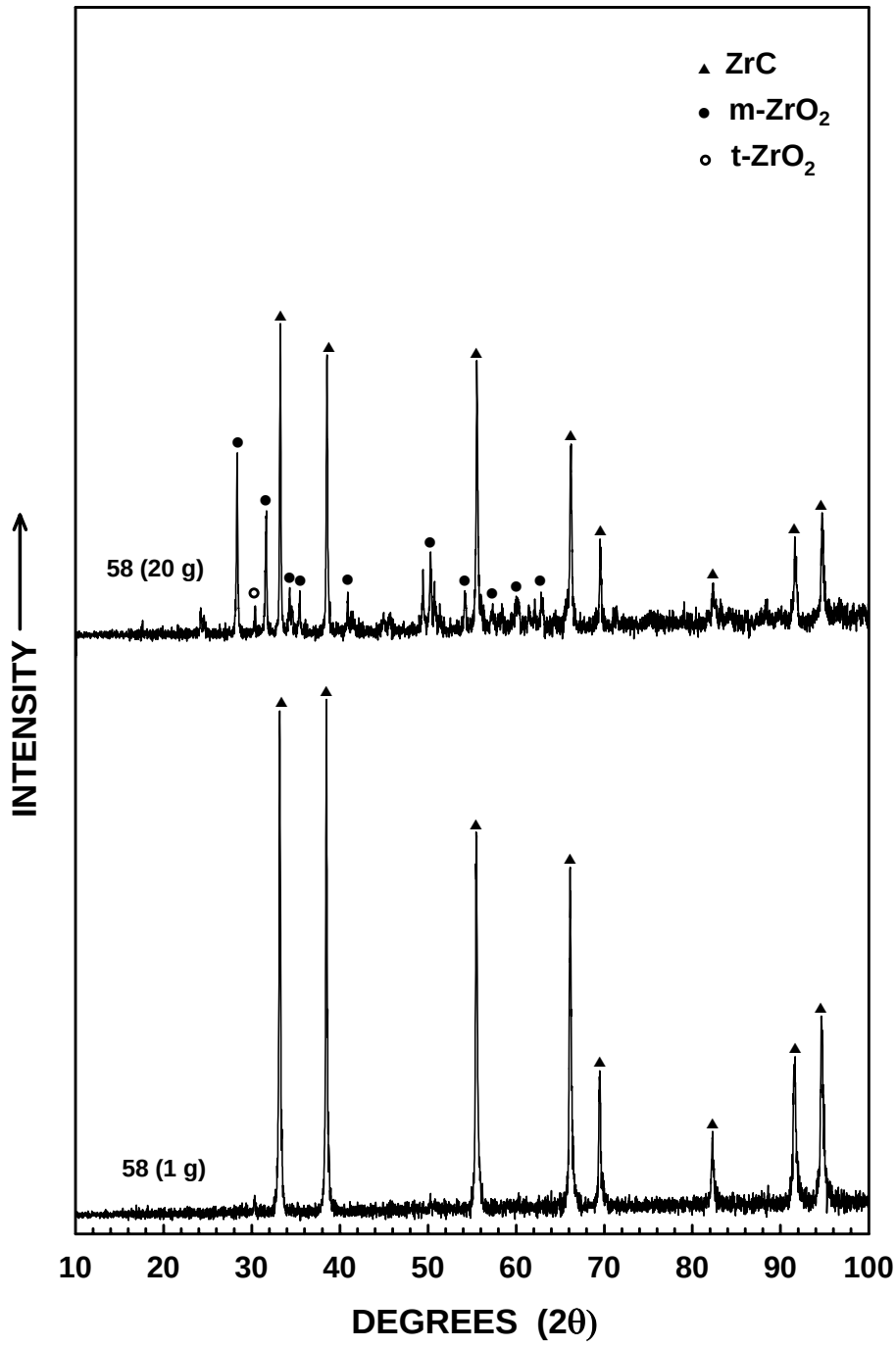

Figure 5.30.a XRD patterns for ZrPM-58 samples with different batch sizes that were heat treated at 1300°C using a gas flow rate of 100 ml/min.

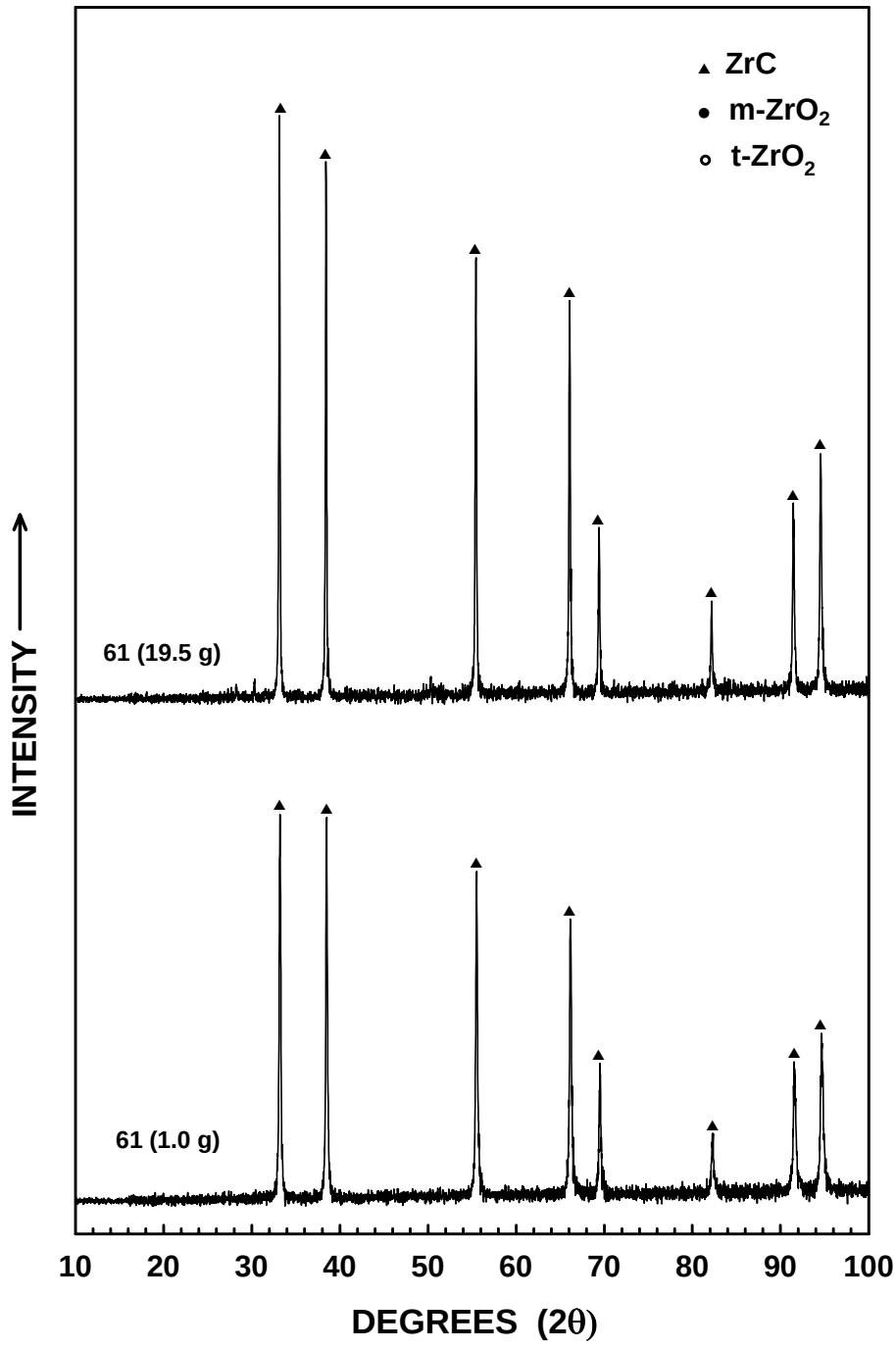

Figure 5.30.b XRD patterns for ZrPM-61 samples with different batch sizes that were heat treated at 1300°C using a gas flow rate of 500 ml/min.

5.4 Powder Grinding Investigation

Table 5.30 shows particle size distribution data for an unmilled ZrPM-90-800-pyrolyzed powder which had been heat treated at 1475°C for 2 h. The mean diameter was ~18 μm. Figure 5.31 shows particle size distribution plots for this sample. These plots showed that particles as large as 50 μm were present in the sample. Table 5.31 shows particle size distribution data after milling the same material for 10 min. The corresponding particle size distribution plots are shown in Figure 5.32. The particle size distribution for the milled sample had a mean diameter of ~0.46 μm and all the particles were <3 μm. Thus, a significant reduction in particle size was obtained after milling the powder for 10 min. Such rapid size reduction suggests that the milling operation was primarily breaking down relatively weak powder aggregates.

Table 5.32 and Figure 5.33 show particle size distribution data for a ZrPM-69-76-85-800-1400 powder which was milled for 10 min. (This sample was prepared by first mixing together separate 800°C-pyrolyzed samples of ZrPM-69, ZrPM-76, and ZrPM-85 samples and then heating the mixture at 1400°C for 2 h.) The mean diameter for this sample was ~0.44 μm. Table 5.33 and Figure 5.34 show particle size distribution data for a ZrPM-69-76-85-800-1400 powder which was milled for 20 minutes. The mean diameter for this sample was ~0.37 μm. Comparison of Table 5.32 vs. Table 5.33 and Figure 5.33 vs. 5.34 shows that there was only a limited amount of particle size reduction during the additional 10 minutes of milling. Since longer milling times would be expected to contribute more contamination to the powder batch, it was decided that the total milling time would 10 minutes for most batches prepared in this study.

Table 5.30 Particle size distribution data for the unmilled ZrPM-90-800-1475 powder sample.

	Diameter (μm)
Mean	18.0
Mode	28.7
D_{90}	35.7
D_{50}	16.6
D_{10}	2.6
Standard Deviation	12.5

Table 5.31 Particle size distribution data for the 10 min-milled ZrPM-90-800-1475 powder sample.

	Diameter (μm)
Mean	0.46
Modes*	0.07, 0.17, 1.32
D_{90}	1.38
D_{50}	0.13
D_{10}	0.06
Standard Deviation	0.56

* Mode values are listed for each distinct peak in the accompanying relative frequency plot.

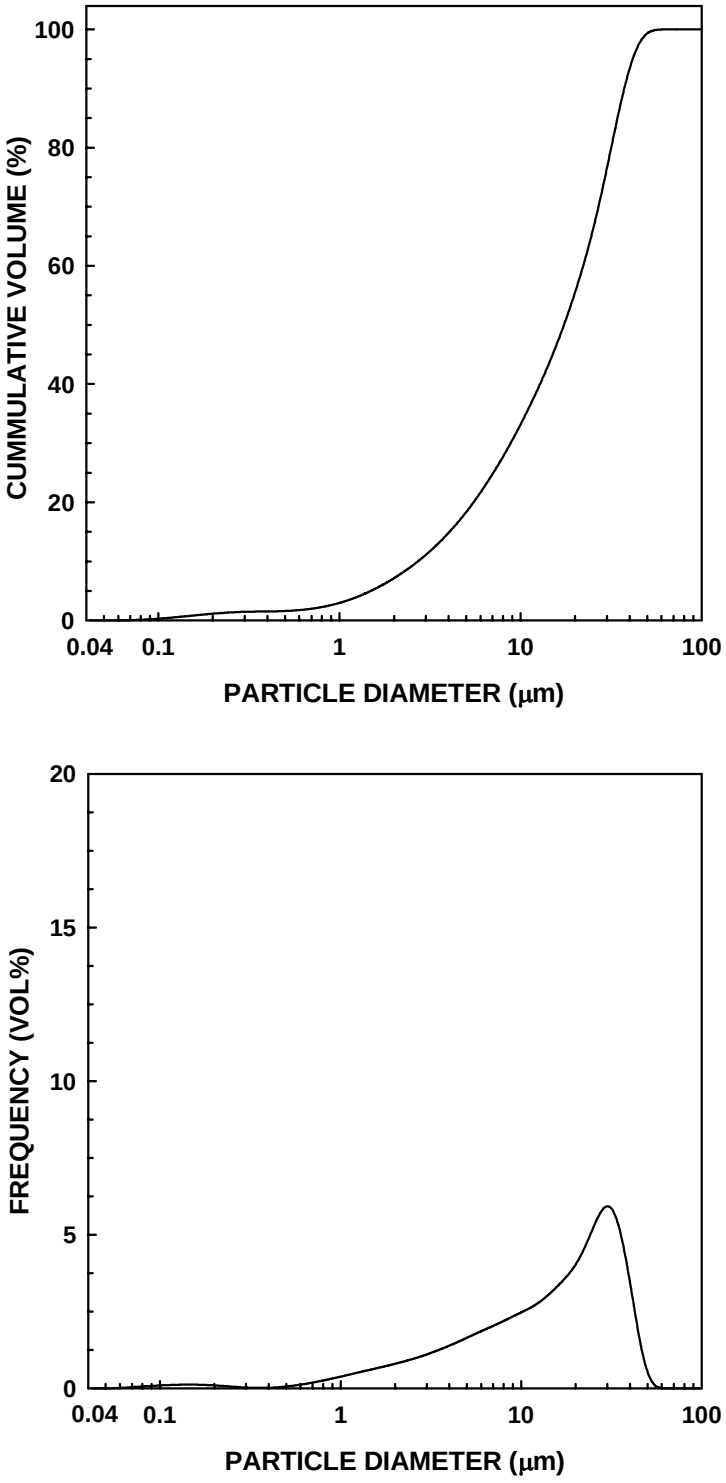

Figure 5.31 Particle size distribution plots for the unmilled ZrPM-90-800-1475 sample: cumulative frequency plot (top) and relative frequency plot (bottom).

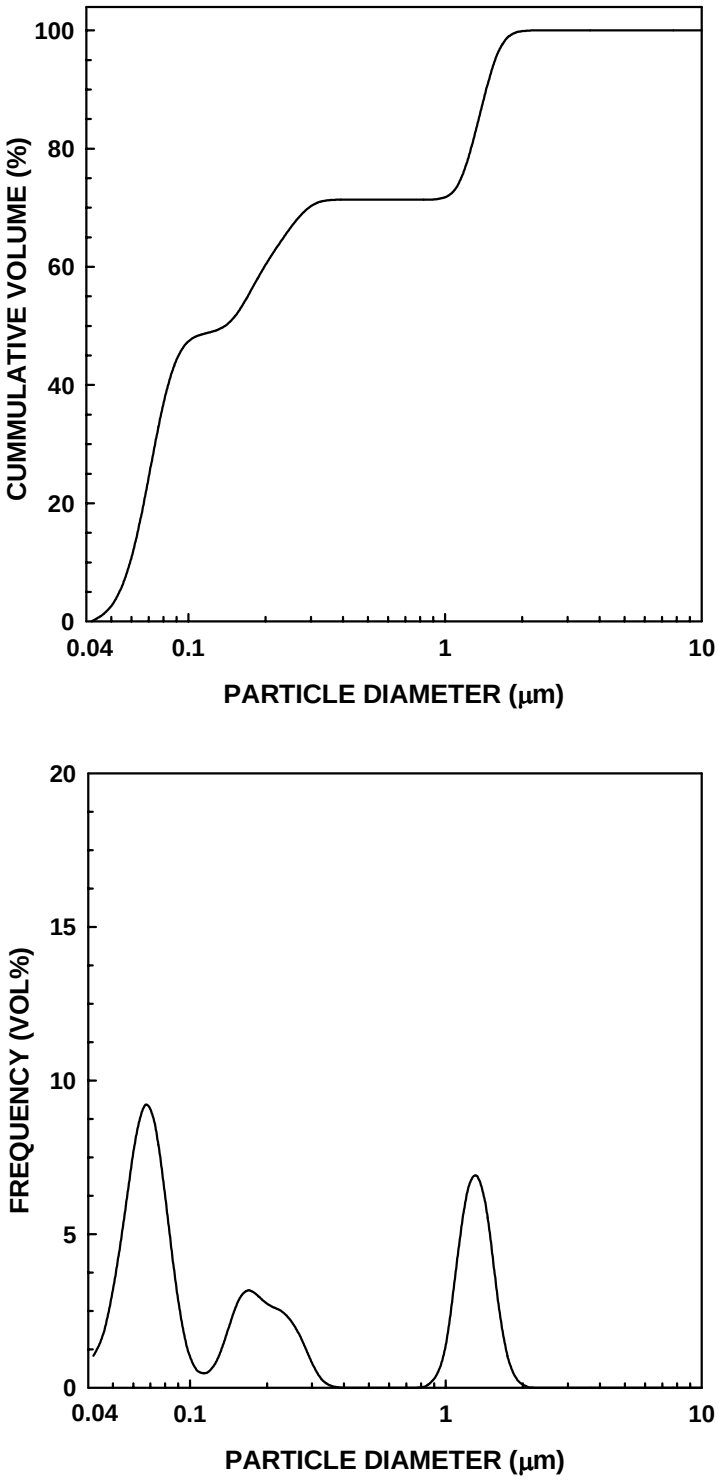

Figure 5.32 Particle size distribution plots for the 10 min-milled ZrPM-90-800-1475 sample: cumulative frequency plot (top) and relative frequency plot (bottom).

Table 5.32 Particle size distribution data for the 10 min-milled ZrPM-69-76-85-800-1475 powder sample.

	Diameter (μm)
Mean	0.44
Modes*	0.067, 0.19, 0.47, 1.45
D_{90}	1.54
D_{50}	0.08
D_{10}	0.05
Standard Deviation	0.61

* Mode values are listed for each distinct peak in the accompanying relative frequency plot.

Table 5.33 Particle size distribution data for the 20 min-milled ZrPM-69-76-85-800-1400 powder sample.

	Diameter (μm)
Mean	0.37
Modes*	0.06, 0.19, 0.47, 1.59
D_{90}	1.60
D_{50}	0.07
D_{10}	0.05
Standard Deviation	0.59

* Mode values are listed for each distinct peak in the accompanying relative frequency plot.

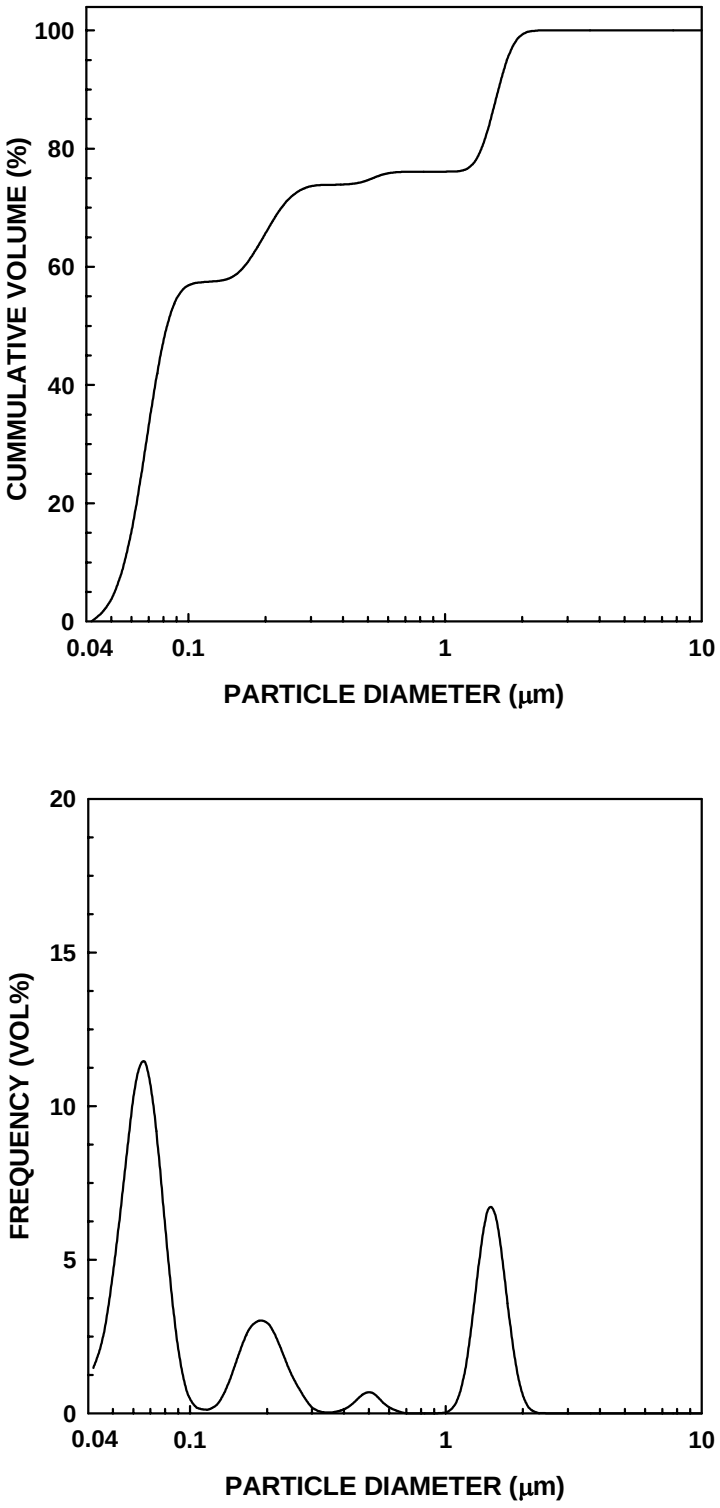

Figure 5.33 Particle size distribution plots for the 10 min-milled ZrPM-69-76-85-800-1400 sample: cumulative frequency plot (top) and relative frequency plot (bottom).

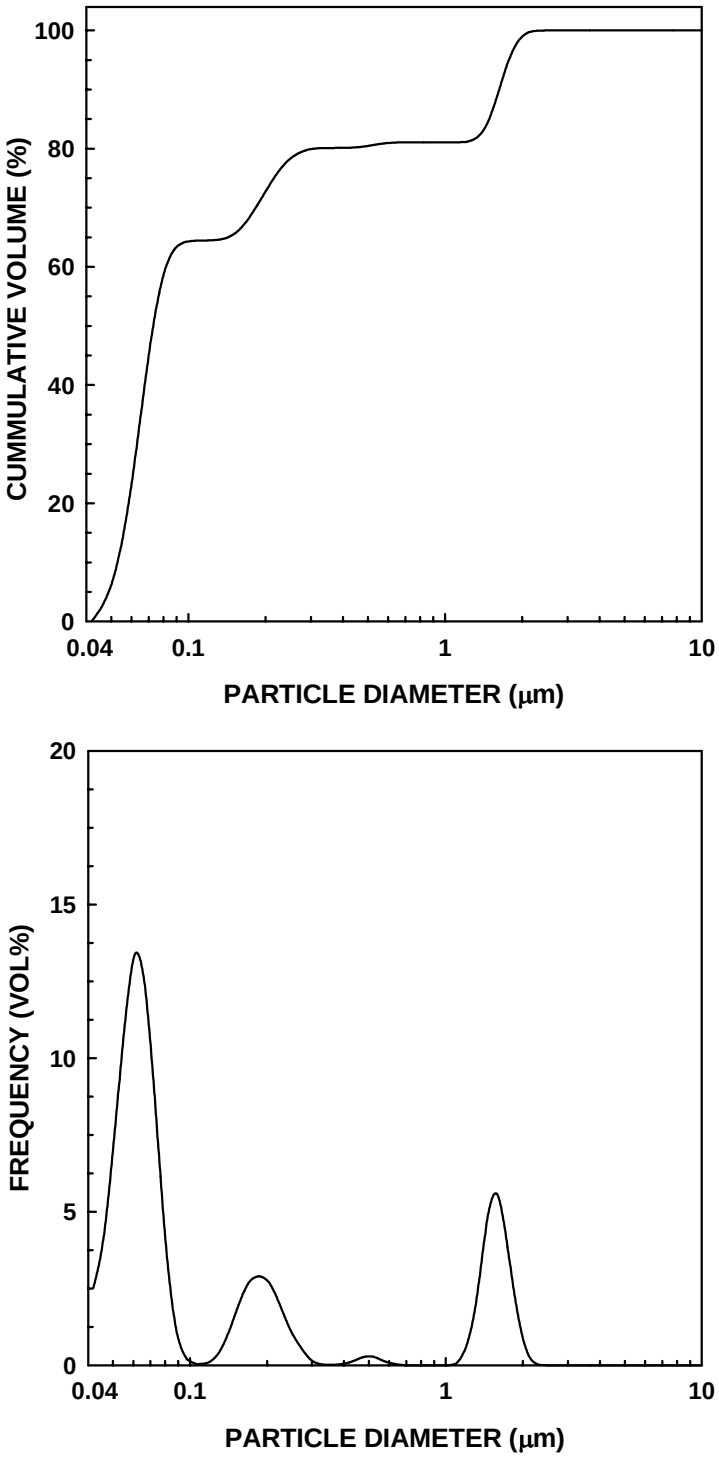

Figure 5.34 Particle size distribution plots for the 20 min-milled ZrPM-69-76-85-800-1400 sample: cumulative frequency plot (top) and relative frequency plot (bottom).

Table 5.34 Specific surface areas of CTR samples before and after milling.

Sample	Specific Surface Area (m^2/g)	
	Before Milling	After Milling
ZrPM-45-800-1350-1400	48	46
ZrPM-61-800-1300-1475	40	45
ZrPM-99-800-1400	19	17

The effect of milling on specific surface area was also studied for some samples. Table 5.34 shows the specific surface areas of some CTR samples before and after the milling. The specific surface area did not vary significantly before and after the milling and differences observed are probably within the range of experimental error. It should be noted that the milling operation primarily broke down large porous powder aggregates into smaller units (i.e., to smaller aggregates and primary particles). In contrast, milling was not expected to change the size of the dense primary particles. Hence, the milling operation would not produce any significant change in the solid surface area available from the gas adsorption measurements.

5.5 Effect of Powder Characteristics on Powder Compact Density

Table 5.35 shows the relative densities of dry pressed samples that were prepared from various batches. The estimated true solid densities used to calculate the relative densities are included. (The densities were calculated with the same type of assumptions

Table 5.35 Information on processing conditions, powder characteristics, and powder compact relative densities (RD) for different ZrPM samples.

ZrPM Sample	Mill time (min)	Pyrolyzed Carbon Content (wt%)	C/Zr Molar Ratio	CTR			CTR yield (wt%)	ZrO_2 Content	Surface Area (m^2/g)	Mean Dia. (µm)	RD (%)	Assum. S.D. (g/cm^3)
				Sample Size (g)	Packing	Gas Flow Rate (ml/min)						
58-1300(57)-1-1350(16)-1	10	17.9[a]	2.2	7.0	Loose	500	41.0[d]	31	18	0.56	55.8	6.36
91-800-1-1425-2	n.a.	18.5[b]	2.3	0.4	Loose	500	72.4	15	13	n.a.	n.a.	n.a.
91-800-1-1425-4	10	18.5[b]	2.3	8.0	Loose	500	71.1	13	20	0.32	48.6	6.50
87-800-1-1425-1	n.a.	18.9[b]	2.4	0.4	Loose	500	68.3	15	16	n.a.	n.a.	n.a.
87-800-1-1425-2	10	18.9[b]	2.4	8.0	Loose	500	68.5	11	24	0.28	47.4	6.54
59-800-2-1400-1	40	19.4[a]	2.5	2.0	Dense	100	83.0	n.a.	n.a.	n.a.	37.5	6.53
69+76+85-800-1-1400-1	10	n.a.	2.5[c]	7.0	Loose	500	74.9	24	7	0.44	54.3	6.32
100-800-1-1425-1	n.a.	21.3[b]	2.8	2.0	Loose	500	67.7	n.a.	41	n.a.	n.a.	n.a.
100-800-2-1450-1	10	21.3[b]	2.8	8.0	Loose	500	68.2	4	20	0.87	46.2	6.55
94-800-1-1425-1	n.a.	21.8[b]	2.9	0.5	Loose	500	668	n.a.	50	n.a.	n.a.	n.a.
94-800-3-1475-1	10	21.8[b]	2.9	8.0	Loose	500	66.5	n.a.	16	0.09	46.8	6.59
95-800-1-1425-1	n.a.	22.4[b]	3.0	0.5	Loose	500	67.5	n.a.	67	n.a.	n.a.	n.a.
95-800-3-1475-1	10	22.4[b]	3.0	8.0	Loose	500	64.7	n.a.	13	0.09	45.5	6.60
45-800-2-1400-1	25	23.3[a]	3.1	4.5	Dense	100	87.5	60	232	n.a.	30.6	6.44
45-800-1-1350-1400-3	40	23.3[a]	3.1	3.0	Loose	100	68.1	n.a.	48	0.16	52.1	6.44
98-800-1-1425-1	n.a.	23.3[b]	3.1	2.0	Loose	500	66.4	2.5	29	n.a.	n.a.	n.a.
98-800-1-1450-1	10	23.3[b]	3.1	8.0	Loose	500	64.0	n.a.	21	0.09	46.5	6.39
99-800-1-1425-2	n.a.	23.7[b]	3.2	0.5	Loose	500	66.5	n.a.	36	n.a.	n.a.	n.a.
99-800-1-1475-1	10	23.7[b]	3.2	8.0	Loose	500	62.9	n.a.	n.a.	0.09	47.7	6.25
97-800-1-1475-1	n.a.	24.1[b]	3.3	2.0	Loose	500	65.4	n.a.	56	n.a.	n.a.	n.a.
97-800-1-1500-1	10	24.1[b]	3.3	8.0	Loose	500	62.3	n.a.	30	0.08	44.6	6.14
79+82-800-1-1425-1	10	n.a.	3.4[c]	7.0	Loose	500	66.0	n.a.	20	0.27	45.3	6.40
61-350-1-1300(48)-2-1300(8)-1	10	27.1[a]	3.8	10.0	Loose	500	48.2[e]	n.a.	112	0.09	36.3	5.51

Table 5.35 continued.

ZrPM Sample	Mill time (min)	Pyrolyzed Carbon Content (wt%)	C/Zr Molar Ratio	CTR			CTR yield (wt%)	ZrO_2 Content	Surface Area (m^2/g)	Mean Dia. (µm)	RD (%)	Assum. S.D. (g/cm^3)
				Sample Size (g)	Packing	Gas Flow Rate (ml/min)						
61-350-1-1300(48)-2-1300(8)-1-1475-1	10	27.1[a]	3.8	2.0	Loose	100	45.1[e]	n.a.	40	0.09	52.5	5.51
61-350-1-800-1-1475-1	n.a.	27.1[a]	3.8	2.0	Loose	100	50.4[e]	n.a.	207	n.a.	n.a.	n.a.
61-350-1-800-1-1350(8)-1-1400-1	n.a.	27.1[a]	3.8	0.4	Loose	100	67.2	n.a.	183	n.a.	n.a.	n.a.

[a] Analysis by Sherry Laboratories of a 1025°C-pyrolyzed sample.
[b] Analysis by Leco Corp. of a 1025°C-pyrolyzed sample.
[c] Based on the carbon content determined by oxidation (using the pyrolysis furnace) of a 1100°C-pyrolyzed sample.
[d] Reported yield is for pyrolysis (from the dried powder) and CTR.
[e] The reported yield is for pyrolysis (from the 350°C powder) and CTR.

made in calculating the solid densities for the CTR samples in section 5.6.) Table 5.35 includes some information on the CTR processing conditions and some measured powder characteristics (pyrolyzed and CTR) of the samples. (Appendix G gives the complete particle size distributions for the samples which have mean diameters listed in Table 5.35. XRD patterns for the samples are also given in the same appendix.) Table 5.35 also includes similar information for some CTR samples which were not dry pressed, but which were prepared from the same ZrPM batch used for the samples that were pressed.

It is difficult to draw clear associations between the powder characteristics and the compact densities because many different characteristics (C/Zr ratio, phase composition, particle size distribution, surface area, etc.) varied simultaneously. However, the results shown in Table 5.35 and Figure 5.35 indicate that the powder specific surface area was one of the most important variables affecting the compact relative density. Although there is significant scatter of the data, Figure 5.35 shows that the relative density tends to increase as the specific surface area of the powder decreases.

The dominant effect of specific surface area on compact density is also shown clearly be comparing the results for the ZrPM-61-350-1-1300(48)-2-1300(8)-1 and ZrPM-61-350-1-1300(48)-2-1300(8)-1-1475-1 samples. These two samples had specific surface areas of 112 m^2/g and 40 m^2/g, respectively, and relative densities of 36.3 and 55.5, respectively. Other powder properties for the two powders were similar. For example, the XRD patterns were similar for the samples, as shown in Figures F21 and F23, respectively. (The ZrPM-61-350-1-1300(48)-2-1300(8)-1 sample did have a small amount of residual ZrO_2 and the yield upon heat treatment (from 350^oC) was somewhat lower (Table 5.35). This indicated that the reaction was less complete compared to the

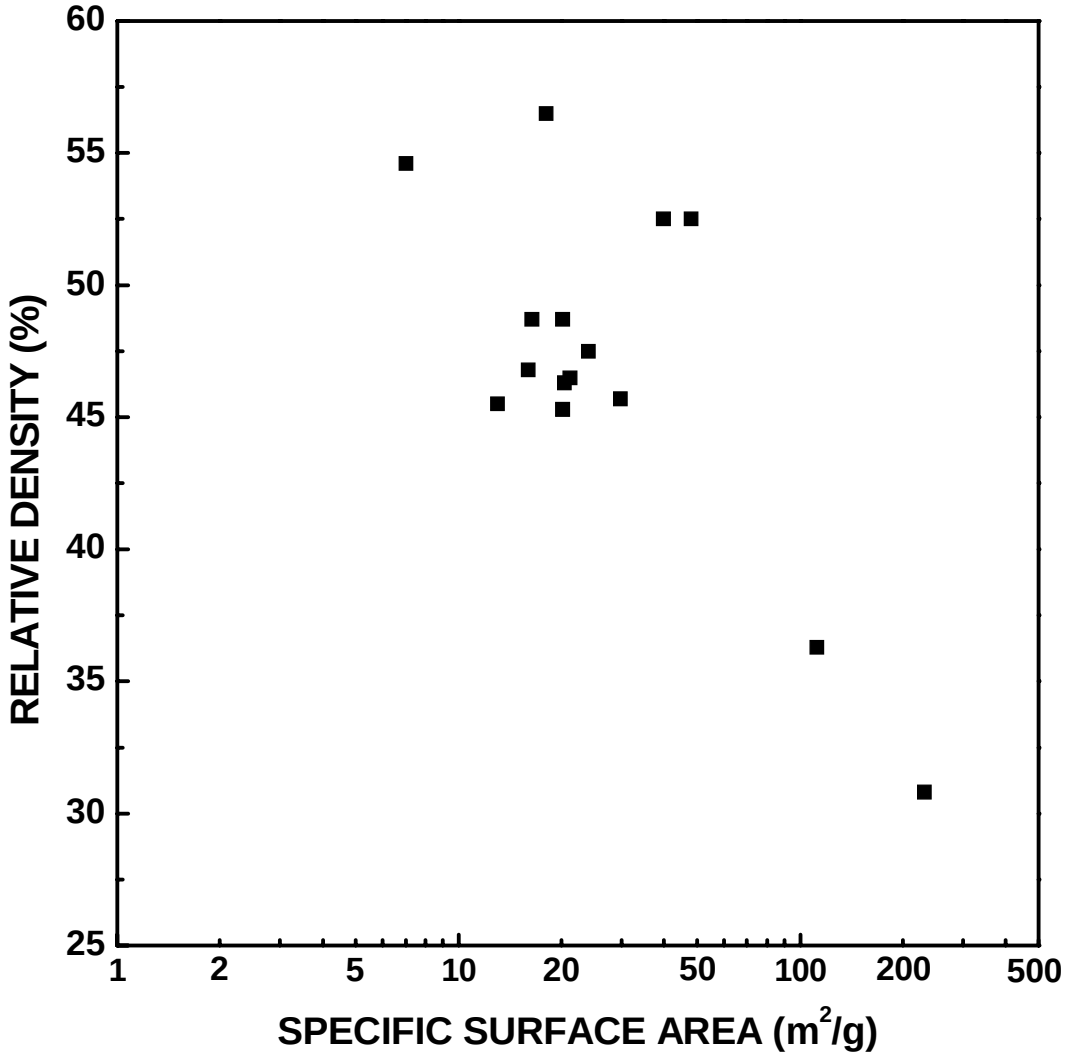

Figure 5.35 Plot of specific surface area vs. relative density for various ZrC-based samples.

ZrPM-61-350-1-1300(48)-2-1300(8)-1-1475-1 sample. However, the difference in the extent of reaction was relatively minor.) In addition, the particle size distributions for these samples were very similar, as shown in Figures F20 and F22, respectively. The size distribution measurements are presumably dominated by the sizes of the ZrC primary particles and aggregates. These sizes apparently did not change substantially for the different CTR conditions used for these two samples. In contrast, the rapid decrease in specific surface area for the ZrPM-61-350-1-1300(48)-2-1300(8)-1-1475-1 sample presumably reflects the coarsening and/or elimination of small, accessible pores associated with the carbon regions. (This effect was discussed previously in section 5.2.1.3 for the ZrPM-45 samples.)

The specific mechanism(s) responsible for the higher relative density in the ZrPM-61-350-1-1300(48)-2-1300(8)-1-1475-1 sample are not entirely clear. Two possible reasons include the following: (1) Lower specific surface area powders have less tendency to form agglomerates compared to higher specific surface area powders. Hence, there may have been improved powder flow and/or reduced agglomerate formation in the ZrPM-61-350-1-1300(48)-2-1300(8)-1-1475-1sample during the various processing steps that were used to form the compacts (i.e., binder additions, powder screening, die filling, and pressing). (2) Some porosity associated with the carbon regions might have been eliminated by the higher heat treatment temperature in the ZrPM-61-350-1-1300(48)-2-1300(8)-1-1475-1 sample.

5.6 Sintering Behavior

5.6.1 Preliminary Sintering Experiments

Some preliminary sintering experiments were carried out to develop the procedure that would be used in the sintering study. These experiments were called "preliminary sintering experiments" primarily because certain procedures were being studied, such as the amount of binders added to the powder, the method of mixing the binder and the powder, the dry pressing conditions (e.g., maximum pressure used), the binder burnout conditions, etc. The amount of powders processed for these experiments was enough to prepare only 1-2 pellets. Thus, detailed sintering studies could not be done on these samples.

5.6.1.1 ZrPM-45

5.6.1.1.1 Processing Before Sintering

Dried powder was sieved through a 150-mesh screen and pyrolyzed at 800^{o}C for 2 h. The C/Zr molar ratio of a sample pyrolyzed at 1025^{o}C for 2 h was 3.1. (This was estimated from the carbon content of 23.3 wt% measured by Sherry Laboratories.) A pyrolyzed sample (~3 g) was heat treated first at 1350^{o}C for 2 h and then at 1400^{o}C (2 h) in a flowing argon (~100 ml/min) atmosphere in the 3-zone lindberg furnace (Model 54259). The specific surface area of the CTR powder was 48 m^2/g. (See Appendix D for details.) XRD (Figure 5.36) showed only zirconium carbide in the pattern. However, it is expected from the results in section 5.3 that the sample has some dissolved oxygen and free (amorphous) carbon. Table 5.36 shows some particle size distribution data for a 40-

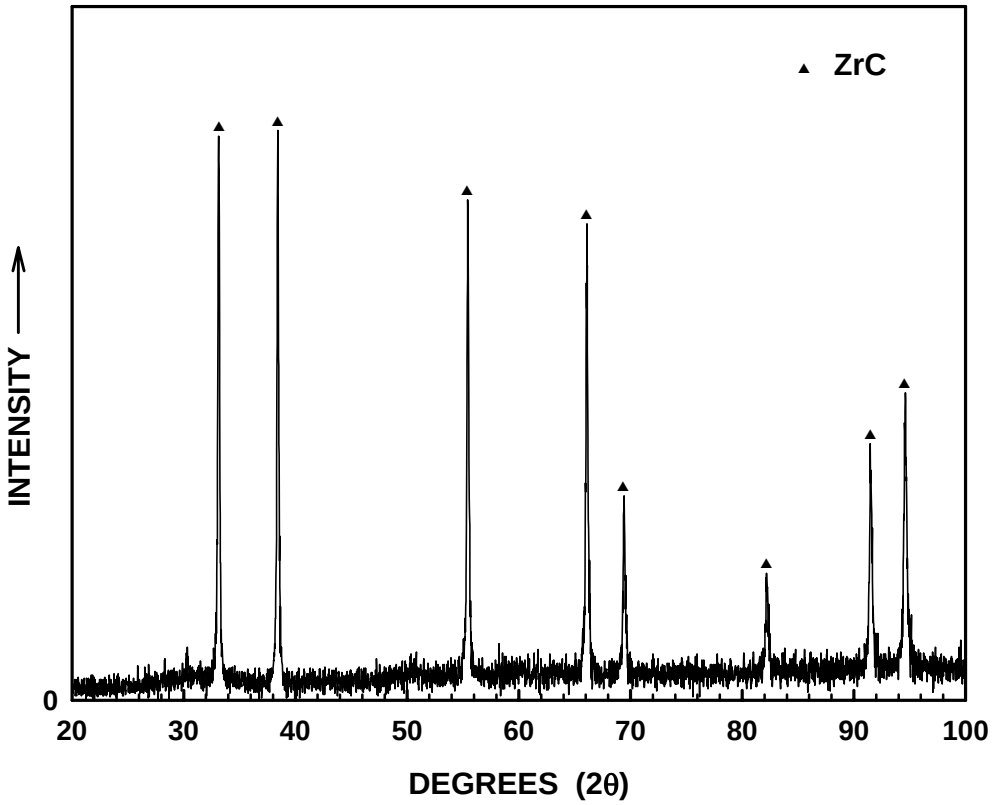

Figure 5.36 X-ray diffraction pattern for a ZrPM-45-800 pyrolyzed sample that was heat treated at 1350°C (2 h) and then at 1400°C (2 h).

Table 5.36 Particle size distribution data for the 40 min-milled ZrPM-45-800-1350-1400 powder sample.

	Diameter (μm)
Mean	0.16
Modes*	0.06, 0.19, 1.92
D_{90}	0.20
D_{50}	0.07
D_{10}	0.05
Standard Deviation	0.38

* Mode values are listed for each distinct peak in the accompanying relative frequency plot.

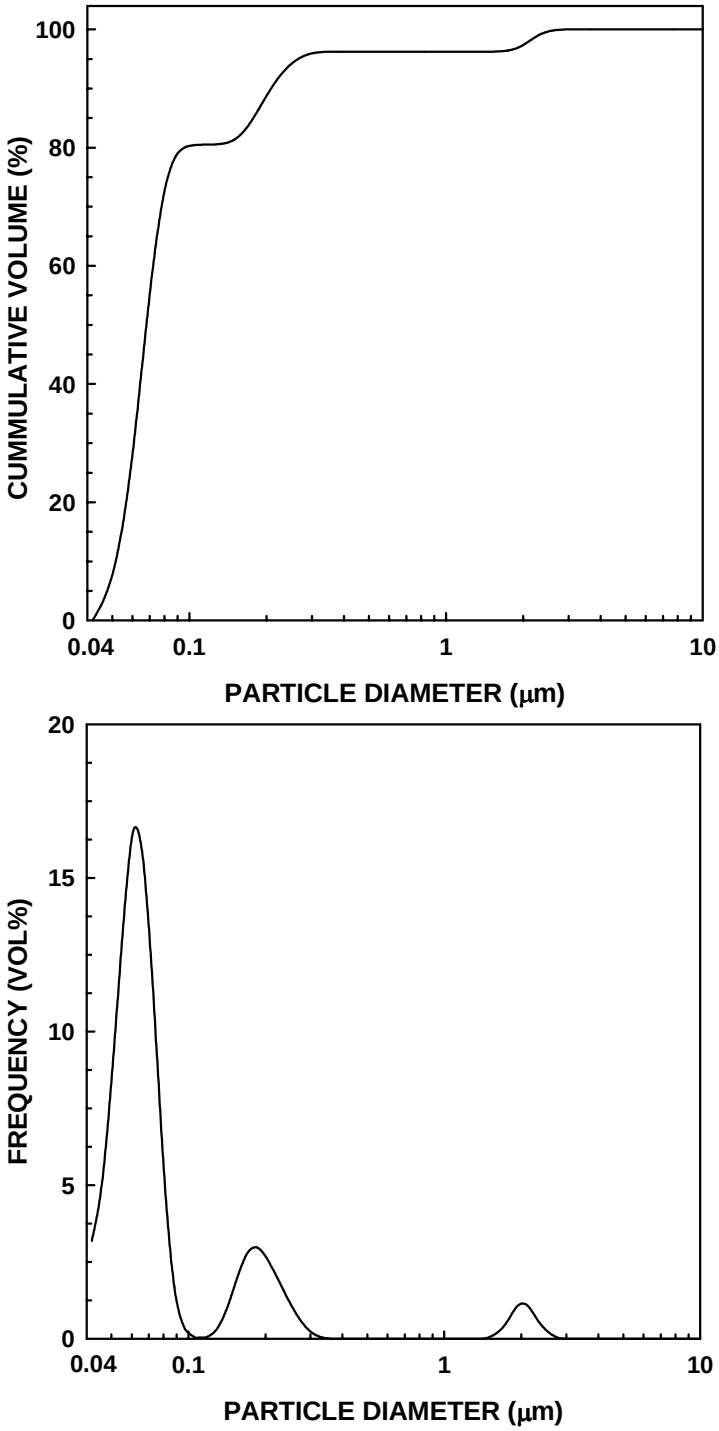

Figure 5.37 Particle size distribution plots for the 40 min-milled ZrPM-45-800-1350-1400 powder sample: cumulative frequency plot (top) and relative frequency plot (bottom).

min milled sample. The specific surface area of the milled powder was 46 m^2/g. Particle size distribution plots for the milled sample are shown in Figure 5.37.

In section 5.2.1.3, it was noted that samples prepared at temperatures in the range of 1400-1475^oC consisted of zirconium carbide (with dissolved oxygen) and "free" carbon. In the present case, it was assumed that the overall carbon and oxygen concentrations (in the ZrPM-45-800-1350-1400) were the same as listed in Table 5.13 for the ZrPM-45-800-1475 sample. (This was done because data was not available for samples heat treated at 1400^oC.) The Zr content was obtained by difference, i.e., 100 - (carbon wt% + oxygen wt%). In order to partition the overall carbon amount into the amount of free carbon and the amount of carbon that was part of the zirconium carbide, it was assumed for this part of the calculation that the latter material was stoichiometric ZrC. Hence, using the Zr content obtained by difference, the amount of carbon in the ZrC was determined. The weight percent of "free" carbon was then determined by difference. (This value was reported as 2.3 wt% in section 5.2.1.3.) The rest of the material was then assumed to be zirconium oxycarbide (ZrC with all the oxygen in the sample dissolved in the lattice).

The solid density used for the zirconium oxycarbide was calculated by using an estimated y and x values in the chemical formula ZrO_yC_x. The y and x values were estimated using the oxygen (3.3 wt%) and carbon (13.3 wt%) concentrations that were measured for the 1475^oC ZrPM-45 sample (Table 5.13) and the estimated free carbon concentration of 2.3 wt%. (The oxygen was assumed to be entirely dissolved in the zirconium oxycarbide lattice.) The carbon concentration in the zirconium oxycarbide lattice was assumed to be 11 wt% (i.e., the difference between the overall carbon content

of 13.3 wt% and the estimated "free" carbon concentration of 2.3 wt%). Hence, the composition of the zirconium oxycarbide phase was estimated to be $ZrO_{0.21}C_{0.92}$. In Table 5.15 (section 5.2.1.3), a lattice parameter value of 0.4691 nm is given for the ZrPM-45-800-1400 sample. Using this value and the estimated chemical composition, the solid density of the zirconium oxycarbide phase ($ZrO_{0.21}C_{0.92}$) was calculated using the following equation:

$$\frac{4(1\times 91.224 + 0.92\times 12.01 + 0.21\times 16)}{(0.4691)^3 \times\ 6.022\times 10^{23}} \times 10^{21} = 6.80\ g/cm^3 \qquad (5\text{-}8)$$

where 91.224 is the atomic mass of Zr, 12.01 is the atomic mass of C, and 16 is the atomic mass of O. Note that zirconium oxycarbide has a cubic crystal structure.

The overall solid density of the ZrPM-45-800-1350-1400 sample was calculated by using the above value (i.e., 6.80 g/cm^3) for the solid density of the zirconium oxycarbide phase and an assumed value of 2 g/cm^3 for the free carbon. The solid density is given by:

$$\text{density of ZrPM-45-800-1350-1400} = \frac{100}{\frac{97.7}{6.80}+\frac{2.3}{2}} = 6.44\ g/cm^3 \qquad (5\text{-}9)$$

The milled powder was mixed with 10 vol% polymer binder and plasticizer as described in section 4.3.1.1. Two powder compacts were uniaxially dry-pressed in a 15.4 mm diameter die at 200 MPa. The bulk densities of these samples, determined from

geometric dimensions, are listed in Table 5.37. (The relative densities were calculated using the solid density value calculated in equation 5-9.)

The compacts were heat treated or "pre-sintered" at 1490^{o}C for 4 h under flowing argon (~100 ml/min) in 3-zone lindberg furnace (Model 54259). This resulted in burnout of the binder, additional CTR reaction, and partial sintering of the compacts. As noted in section 4.3.1.2 the "pre-sintering" was carried out to more completely react the powders so that less weight loss (due to evolution of gases) occurred during subsequent sintering heat treatments. The percentage weight loss due to binder burnout and carbothermal reduction reaction is listed in Table 5.37. (The weight loss expected due to the binder burnout alone was 1.84 wt%, i.e., based on the amount of binder that was added to the powder. This suggests that most of the weight loss was due to additional CTR reaction at 1490^{o}C for 4 h. However, this amount of weight loss is much larger than expected from the CTR yield data in Table 5.35 for the ZrPM-45-800-1-1350-1400-3 sample and from the weight loss data shown in Table 5.14. Therefore, it is concluded that there may be an experimental error (e.g., in recording the sample weights) associated with the weight loss values listed in Table 5.37.)

The bulk densities after pre-sintering, determined from geometric dimensions, are also listed in Table 5.37. To calculate the relative density, it was assumed that the 1490^{o}C (4 h) heat treatment produced a material that was nearly single phase stoichiometric ZrC. Thus, the density of powder was calculated using a lattice parameter of 0.4696 nm for ZrC and assuming that free carbon and dissolved oxygen were not present :

Density of ZrPM-45-800-1350-1400-1490

$$= \frac{4(1 \times 91.224 + 1 \times 12.01)}{(0.4696)^3 \times 6.022 \times 10^{23}} \times 10^{21} = 6.62\ g/cm^3 \qquad (5\text{-}10)$$

Table 5.37 Compact densities after dry-pressing and "pre-sintering" and weight loss after "pre-sintering" for ZrPM-45-800-1350-1400 samples.

Pellet #	As-Dry Pressed		Weight (As-Dry Pressed) (g)	After Pre-sintering		Weight Loss (%)
	Bulk Density (g/cm^3)	Relative Density (%)		Bulk Density (g/cm^3)	Relative Density (%)	
1	3.45	53.6	0.6729	4.08	61.6	11.7
2	3.26	50.6	0.6623	4.09	61.8	11.7
Average	3.36	52.2	-	4.09	61.7	11.7

Table 5.37 shows the calculated relative densities for the "pre-sintered" samples. It is evident that some densification occurred during this heat treatment.

5.6.1.1.2 Sintering/Heat Treatment

The pre-sintered samples were sintered at temperatures in the range of 1600-1900^{o}C (see Table 5.38). The two pellets were used for repeated sequential heat treatments. The first pellet was sintered at 1800^{o}C for times in the range of 1-16 h. (The times indicated in Table 5.38 are cumulative sintering times.) The second pellet was heat treated sequentially at 1600^{o}C, 1700^{o}C, and 1800^{o}C for 1 h each. The sample was then sintered for an additional 3 h and 12 h at 1800^{o}C. This was followed by sintering at 1900^{o}C for 1 h.

Relative densities were calculated using the same solid density that was determined using equation 5-9. For the "pre-sintered samples," it was highly questionable to assume that the reaction had been completed and that the material was single-phase, oxygen-free, stoichiometric ZrC after heat treatment at only 1490^{o}C (for 4 h). However,

the assumption becomes more reasonable as the heat treatment temperature increases. Based on the fact that weight losses for ZrPM-45 samples were small after heat treatment at 1600°C (see Table 5.14 in section 5.2), the assumed solid density seems reasonable even for the samples sintered at 1600°C. (In addition, the fact that weight losses were small during heat treatment at ≥1600°C was confirmed again during this sintering study, as shown in Table 5.38.)

The bulk densities and relative densities (determined from geometric measurements) are shown in Table 5.38. This table also shows the percentage shrinkage in the diameter and thickness of the samples at various heat treatment temperatures. The weight losses observed during heat treatments at temperatures in the range of 1600-1900°C are also shown in the table.

Higher densities were obtained for pellet #1 compared to pellet #2. The reason is not known, but it might be due to the higher "green" (initial) density for the former sample. It is also not known why some heat treatments resulted in substantial shrinkage anisotropy, while others did not. Substantial shrinkage anisotropy was observed for most of the sintering heat treatments for pellet #2.

Figure 5.38 shows plots of bulk density and relative density vs. sintering time for the pellet #1 samples. It is evident that the densification rate slows substantially after the first hour of sintering at 1800°C.

Table 5.38 Densities (bulk and relative), percent shrinkages, and percent weight losses for sintered samples.

Pellet #	Temperature(°C)/ Time (h)	Shrinkage (%)		Bulk Density+ (g/cm^3)	Relative Density (%)	Weight Loss (wt%)*
		Diameter	Thickness			
Avg.	1490/4	-	-	4.09	61.7	-
1	1800/1	10.04	9.38	5.51	83.2	1.08
1	1800/4	11.52	14.45	5.99	90.5	0.25
1	1800/16	14.50	13.48	6.35	95.9	0.36
2	1600/1	3.36	3.65	4.53	68.4	0.22
2	1700/1	6.72	4.04	4.88	73.7	0.34
2	1800/1	8.96	4.04	5.12	77.3	0.53
2	1800/4	11.94	7.50	5.64	85.2	1.01
2	1800/16	12.69	11.44	5.97	90.2	1.40
2	1900/1	13.43	10.26	5.99	90.5	1.38

* Weight losses listed are for individual runs
+ Determined from the sample geometric dimensions.

Table 5.39 shows open porosity, bulk density, and relative density values, determined by the Archimedes method, for some of the same samples listed in Table 5.38. The density values showed significant differences from those calculated from the geometric measurements. It was difficult to obtain accurate results for both types of measurements because of the small sample sizes. This is also reflected by an obvious problem with some of values obtained by the Archimedes method, i.e., the summation of the open porosity and the relative density exceeded 100%. This indicates that either there was an error in the assumed solid density value used to calculate the relative density or there was an error in the open porosity measurement.

Table 5.39 Densities (bulk and relative) and percentage open porosity for sintered samples.

Pellet #	Temperature (^{o}C)/ Time (h)	Open Porosity* (%)	Bulk Density* (g/cm^3)	Relative Density (%)
1	1800/1	12.5	5.85	88.4
1	1800/4	9.9	6.17	93.2
1	1800/16	8.4 (8.31, 8.46)	6.19 (6.21, 6.17)	93.5 (93.8, 93.2)

* Determined by the Archimedes method. When more than one measurement was made, the individual values are listed in the parentheses.

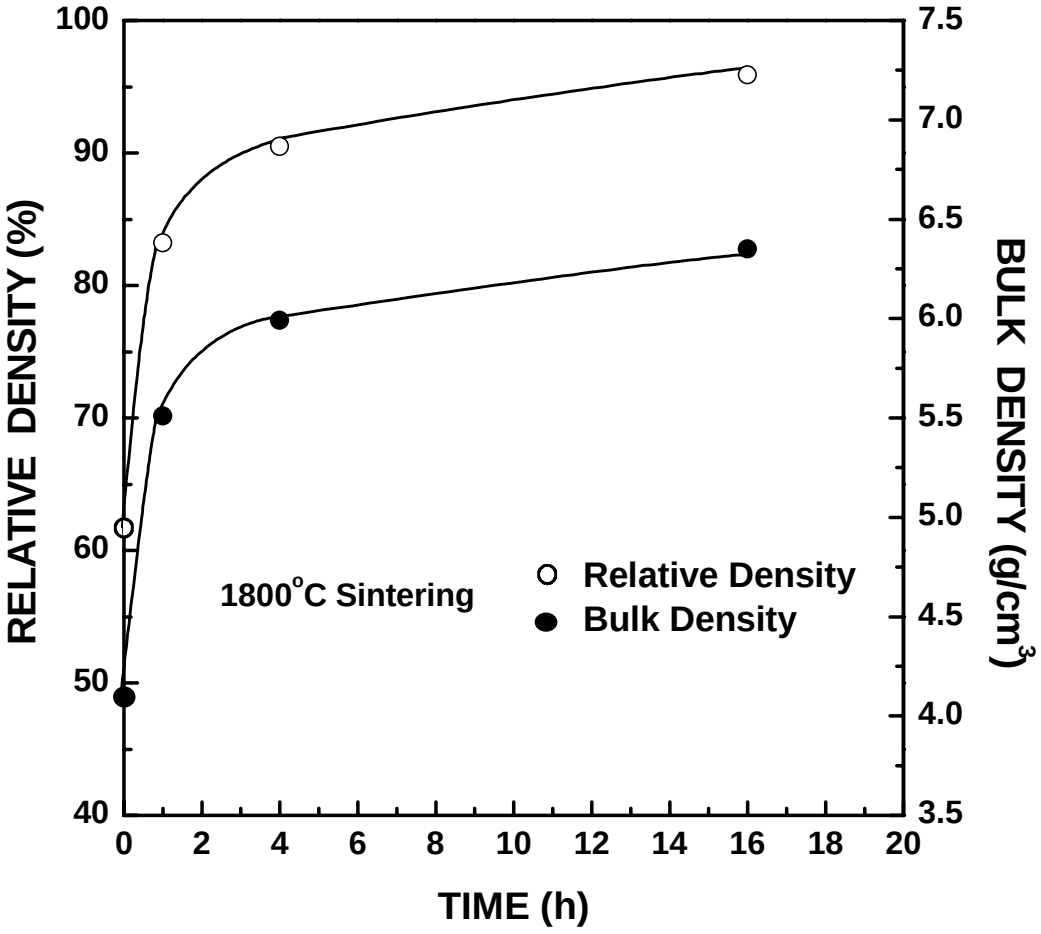

Figure 5.38 Plots of bulk density and relative density vs. sintering time at 1800^{o}C for a ZrC powder compact.

5.6.1.2 ZrPM-58

5.6.1.2.1 Processing Before Sintering

Dried powder was sieved exactly as described in section 5.6.1.1.1. The C/Zr molar ratio of a sample pyrolyzed at 1025°C for 2 h was 2.23. (It was estimated from the carbon content of 17.86 wt%, measured by Sherry Laboratories.) A dried sample (~7 g) was heat treated first at 1300°C for 57 h and then at 1350°C (16 h) in flowing argon (~100 ml/min) atmosphere in the 3-zone lindberg furnace (Model 54259). The powder was further heat treated at 1300°C (8 h) in flowing argon (500 ml/min) atmosphere. The specific surface area of CTR powder was ~18 m^2/g. XRD (Figure 5.39) showed phases of t-ZrO_2, m-ZrO_2, and zirconium carbide in the pattern. Table 5.40 shows some particle size distribution data for a 10-min milled sample. Particle size distribution plots for the milled sample are shown in Figure 5.40.

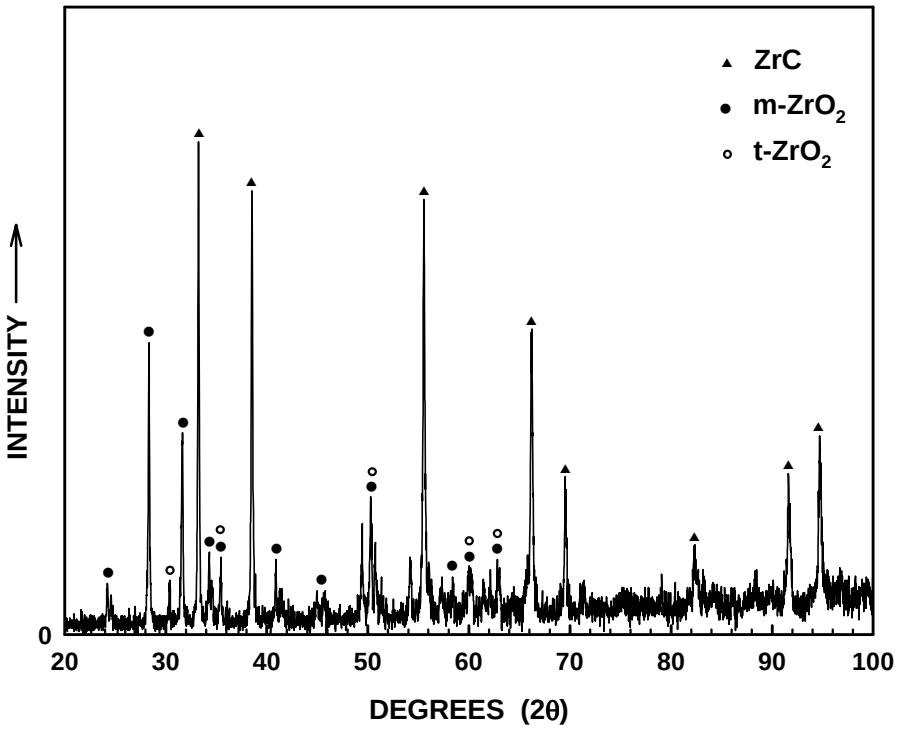

Figure 5.39 X-ray diffraction pattern for a ZrPM-58 dried powder that was heat treated at 1300°C (57 h), then at 1350°C (16 h), and then at 1300°C (8 h).

Table 5.40 Particle size distribution data for the 10 min-milled ZrPM-58-1300(57)-1350(16)-1300(8) powder sample.

	Diameter (μm)
Mean	0.56
Modes*	0.07, 0.17, 1.20
D_{90}	1.47
D_{50}	0.17
D_{10}	0.06
Standard Deviation	0.66

* Mode values are listed for each distinct peak in the accompanying relative frequency plot.

Since the lattice parameters for ZrPM-58 were not measured, they were assumed to be similar to ZrPM-87 samples (see section 5.6.2.2) because of similar carbon concentration in the pyrolyzed material. (See Appendix E for details.) A calculation was made for the solid density of the ZrPM-58-1300(57)-1350(16)-1300(8) sample, but it should be noted that the value was even more of an estimate than the value calculated for the ZrPM-45-800-1350-1400 sample in section 5.6.1.1.1. This is because the ZrPM-58-1300(57)-1350(16)-1300(8) was a multiphase sample with substantial amounts of ZrO_2 and ZrC. Furthermore, the zirconia contained both the monoclinic and tetragonal phases. The zirconium carbide presumably had dissolved oxygen and it is not known if free carbon was present in the sample. To make an estimate of the solid density, the relative

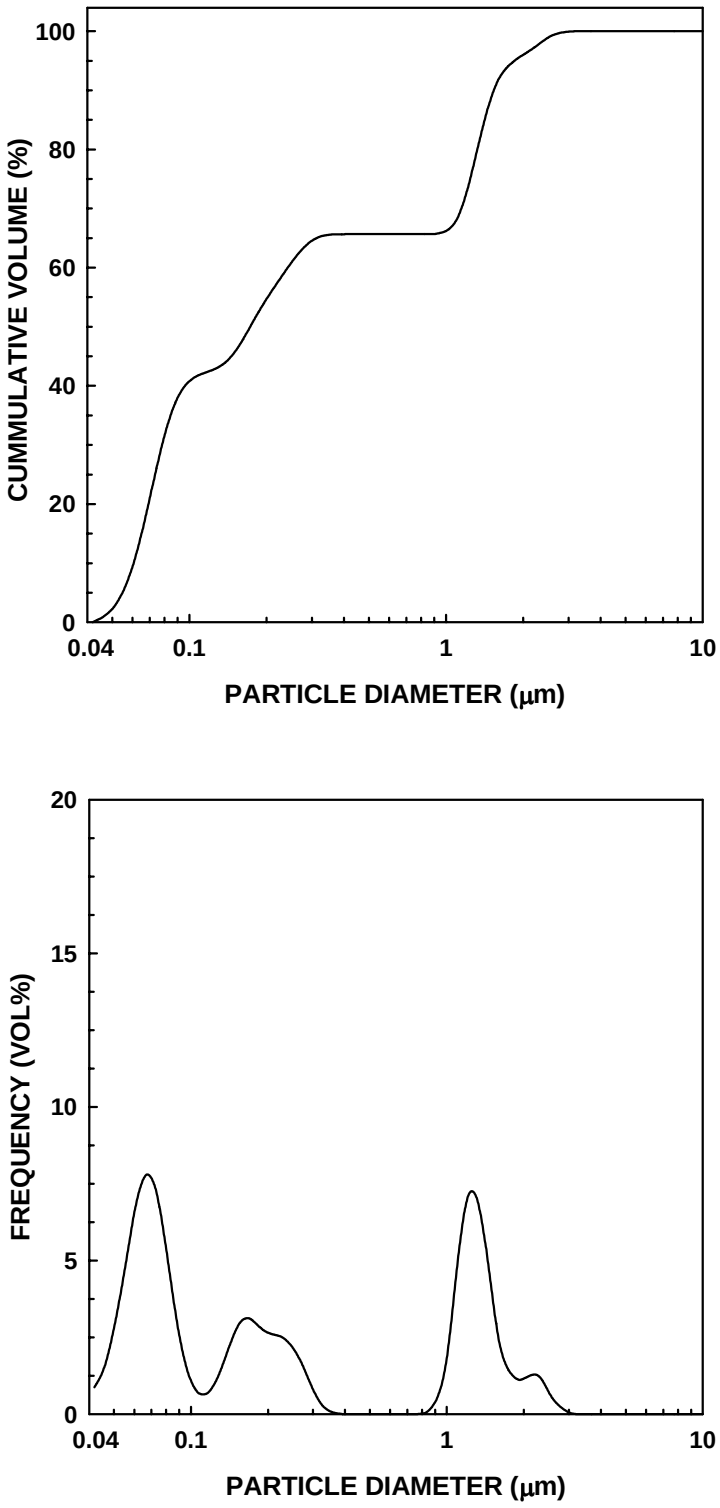

Figure 5.40 Particle size distribution plots for the 10 min-milled ZrPM-58-1300(57)-1350(16)-1300(8) powder sample: cumulative frequency plot (top) and relative frequency plot (bottom).

amounts of ZrO_2 and ZrC in the sample were very crudely estimated from the background-corrected, integrated intensities in the XRD pattern (Figure 5.34) for the highest intensity peaks of the m-ZrO_2 and ZrC phases. (The t-ZrO_2 phase in the sample was neglected.) The procedure used to obtain the integrated intensities is described in Appendix H. For sample ZrPM-58-1300(57)-1350(16)-1300(8), the estimated composition was ~31 wt% ZrO_2/~69 wt% ZrC. Therefore, the solid density of ZrPM-58-1300(57)-1350(16)-1300(8) sample is given by :

$$\frac{100}{\frac{68.8}{6.64}+\frac{31.2}{5.82}} = 6.36\ g/cm^3 \qquad (5\text{-}11)$$

where 5.82 g/cm^3 was used as the solid density for m-ZrO_2 and 6.64 g/cm^3 was used as the density of the zirconium oxycarbide phase. The latter value was calculated for a ZrPM-87-800-1425 sample (see section 5.6.2.2.1).

The milled powder was mixed with binder and the powder compact was processed exactly as discussed in section 5.6.1.1.1. The bulk density of the sample, determined from geometric dimensions, is listed in Table 5.41. (The relative density was calculated using the solid density value in equation 5-11.)

The compact was "pre-sintered" at 1490^{o}C (4 h) for the same reasons as discussed in section 5.6.1.1.1. The percentage weight loss due to binder burnout and any additional carbothermal reduction reaction is listed in the Table 5.41. The weight loss due to additional CTR (at 1490^{o}C, 4 h) is much less for this sample compared to the weight loss for the ZrPM-45-800-1350-1400 sample in section 5.6.1.1.1. This reinforces the earlier conclusion that the high weight losses in Table 5.37 may have been due to an experimental error. The bulk density after pre-sintering, determined from geometric

Table 5.41 Compact density after dry-pressing and "pre-sintering" and weight loss after "pre-sintering" for ZrPM-58-1300(57)-1350(16)-1300(8) sample.

Pellet #	As-Dry Pressed		Weight (As-Dry Pressed) (g)	After Pre-sintering		Weight Loss (%)
	Bulk Density (g/cm^3)	Relative Density (%)		Bulk Density (g/cm^3)	Relative Density (%)	
1	3.55	55.8	0.6685	4.26	67.0	2.88

dimensions, is also listed in Table 5.41. It is evident that some densification occurred during "pre-sintering."

5.6.1.2.2 Sintering/Heat Treatment

The pre-sintered ZrPM-58-1300(57)-1350(16)-1300(8)-1490 sample was sintered at temperatures in the range of 1600-1900^{o}C. The pellet was heat treated sequentially at 1600^{o}C, 1700^{o}C, and 1800^{o}C for 1 h each. The pellet was then sintered for an additional 3 h and 12 h at 1800^{o}C. This was followed by sintering at 1900^{o}C for 1 h. Relative densities were calculated using the same solid density that was determined for ZrPM-87-800-1900 sample (section 5.6.2.2.2).

The bulk densities and relative densities (determined from geometric measurements) are shown in Table 5.42. This table also shows the percentage shrinkage in the diameter and thickness at various heat treatment temperatures. The weight losses observed during heat treatments at temperatures in the range of 1600-1900^{o}C are also shown in the table. It should be noted that the shrinkages are more isotropic at most temperatures compared to the samples in section 5.6.1.1.2.

Table 5.43 shows open porosity, bulk density, and relative density values, determined by the Archimedes method, for some of the same samples listed in Table 5.42.

Table 5.42 Densities (bulk and relative), percent shrinkages, and percent weight losses for sintered samples.

Pellet #	Temperature (^{o}C)/ Time (h)	Shrinkage (%)		Bulk Density^{+} (g/cm^{3})	Relative Density (%)	Weight Loss (wt%)*
		Diameter	Thickness			
1	1490 /4	-	-	4.26	67.0	-
1	1600/1	0.71	1.01	4.36	66.5	0.19
1	1700/1	4.29	-	4.63	70.6	0.29
1	1800/1	9.29	9.02	5.65	86.1	0.66
1	1800/4	10.71	9.72	5.83	88.9	0.82
1	1800/16	11.43	10.03	5.97	91.0	-
1	1900/1	11.43	10.33	5.98	91.4	-

* Weight losses listed are for individual runs
+ Determined from the sample geometric dimensions.

Table 5.43 Densities (bulk and relative) and percentage open porosity for sintered samples.

Pellet #	Temperature (^{o}C)/ Time (h)	Open Porosity* (%)	Bulk Density* (g/cm^{3})	Relative Density (%)
1	1800/4	3.80 (4.1, 3.5)	5.91 (5.73, 6.09)	90.1 (87.3, 92.8)
1	1900/1	1.07	6.19	94.4

* Determined by the Archimedes method. When more than one measurement was made, the individual values are listed in the parentheses.

5.6.1.3 ZrPM-61

5.6.1.3.1 Processing Before Sintering

Dried powder was sieved and pyrolyzed exactly as described in section 5.6.1.1.1. The C/Zr molar ratio was 3.8 for a sample that was initially dried at 120^{o}C and pyrolyzed at 1025^{o}C for 2 h. (This was estimated from the carbon content of 27.1 wt% measured by Sherry Laboratories.)

Some as-dried ZrPM-61 powder was initially heat treated at 350^{o}C (2 h). Approximately 10 g of this powder was then heat treated at 1300^{o}C for 48 h in a flowing argon (~100 ml/min) atmosphere in the 3-zone lindberg furnace (Model 54259). This was followed by an additional 8 h of heat treatment under the same conditions.

The specific surface area of the CTR powder was 112 m^2/g. XRD (Figure 5.41) showed only zirconium carbide in the pattern. However, based on the carbon concentration in (27.1 wt%) the 1025^{o}C-pyrolyzed material, it is expected that a significant amount of "free" carbon was in the CTR sample. This was confirmed by analysis of the carbon concentration for a sample which was heat treated at 1475^{o}C for 2 h. Appendix E shows that the ZrPM-61-350-800-1475 sample had a carbon concentration of 19.4 wt%, i.e., well above the carbon content of 11.6 wt% in phase-pure stoichiometric ZrC.

Table 5.44 shows some particle size distribution data for a 10 min-milled sample. Particle size distribution plots for the milled sample are shown in Figure 5.42.

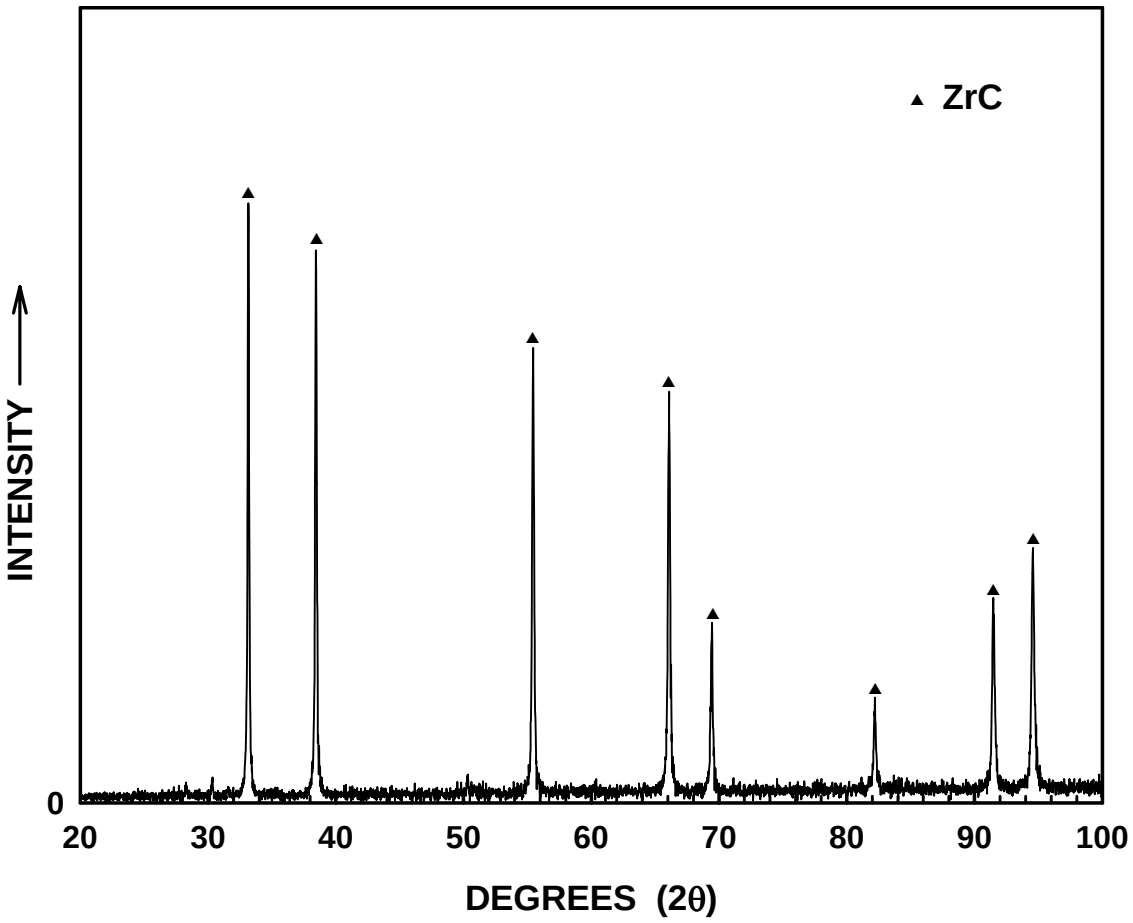

Figure 5.41 X-ray diffraction pattern for a ZrPM-61-350 sample that was heat treated at 1300°C (48 h) and then at 1300°C (8 h).

Table 5.44 Particle size distribution data for the 10 min-milled ZrPM-61-350-1-1300(48)-2-1300(8)-1 powder sample.

	Diameter (μm)
Mean	0.09
Modes*	0.06, 0.19
D_{90}	0.19
D_{50}	0.06
D_{10}	0.05
Standard Deviation	0.06

* Mode values are listed for each distinct peak in the accompanying relative frequency plot.

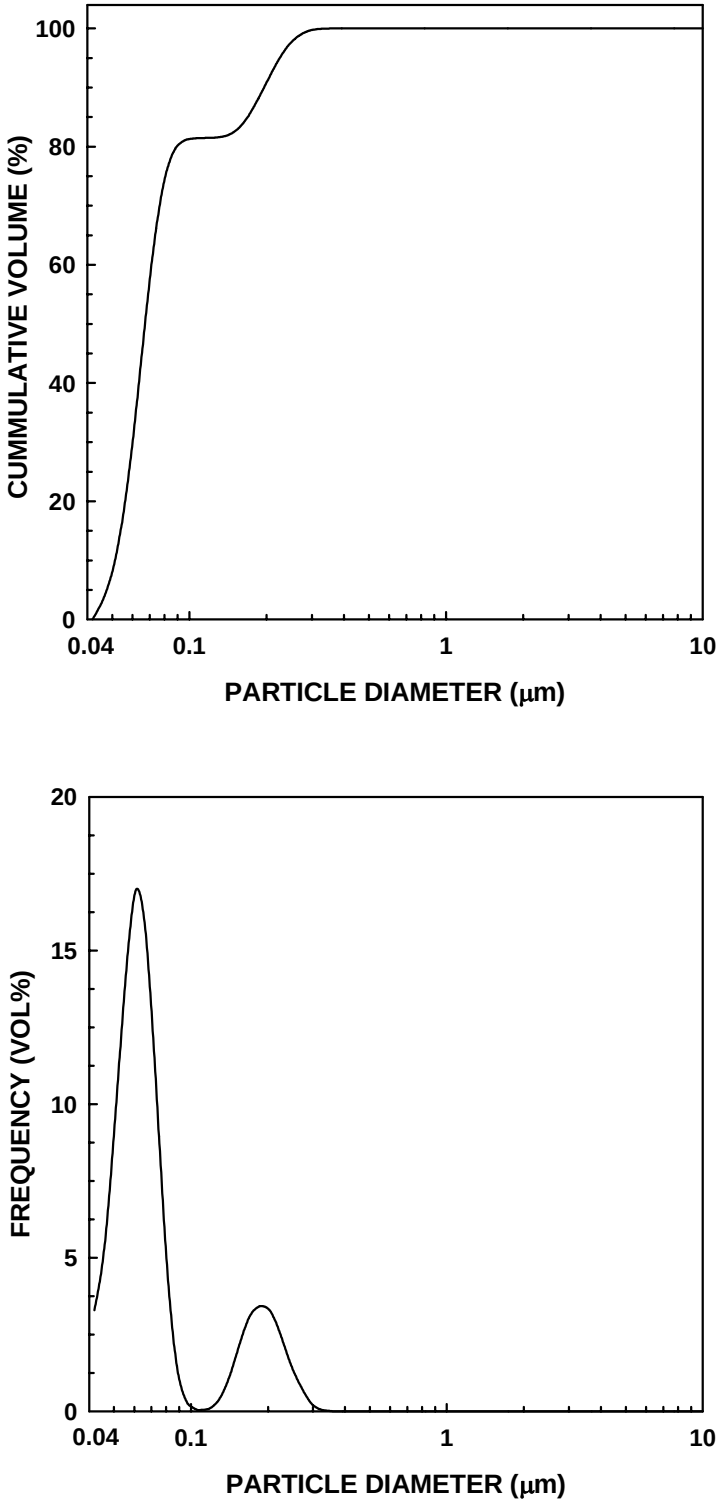

Figure 5.42 Particle size distribution plots for the 10 min-milled ZrPM-61-350-1-1300(48)-2-1300(8)-1 powder sample: cumulative frequency plot (top) and relative frequency plot (bottom).

The lattice parameter of zirconium carbide phase for the ZrPM-61-350-1-1300(48)-2-1300(8)-1 sample was not measured, but it could be assumed to be close to stoichiometric value of 0.4696 nm (as for ZrPM-45-800-1800, Table 5.15) because of the highly carbon-rich composition. Therefore, the density of the zirconium carbide phase in the sample is given by :

$$density\ of\ \mathrm{ZrC} = \frac{4(1\times 91.224 + 1\times 12.01)}{(0.4696)^3 \times 6.022\times 10^{23}}\times 10^{21} = 6.62\ g/cm^3 \qquad (5\text{-}12)$$

The amounts of ZrC and "free" carbon in the ZrPM-61-350-1-1300(48)-2-1300(8)-1 sample were estimated by using the measured carbon concentration of 19.4 wt% for the ZrPM-61-350-800-1475 sample. This carbon concentration gives 91.3 wt% stoichiometric ZrC and 8.7 wt% "free" carbon. Therefore, the overall solid density of the ZrPM-61-350-1-1300(48)-2-1300(8)-1 is given by:

$$\frac{100}{\frac{91.3}{6.62}+\frac{8.7}{2}} = 5.51\ g/cm^3 \qquad (5\text{-}13)$$

The milled powder was mixed with binder and the powder compact was processed exactly as discussed in section 5.6.1.1.1. The bulk density of the sample, determined from geometric dimensions, is shown in Table 5.45. (The relative density was calculated using the solid density value calculated using equation 5-13.) The green density value in Table 5.45 is consistent with the results discussed in section 5.5 (Table 5.35); low green density values are obtained when powders with high specific surface areas are used.

The compact was "pre-sintered" at 1490°C (4 h) for the same reasons as discussed in section 5.6.1.1.1. The percentage weight loss due to binder burnout and carbothermal reduction reaction is listed in the Table 5.45. The weight loss upon heat treatment of the ZrPM-61-350-1-1300(48)-2-1300(8)-1 sample at 1490°C (4 h) is higher than expected. Table 5.35 shows that the CTR yield increased only 3.1 wt% when a ZrPM-61-350-1-1300(48)-2-1300(8)-1 sample was heat treated for an additional 2 h at 1475°C. Binder burnout would contribute another ~2 wt% during the 1490°C (4 h) heat treatment. This would give a weight loss of ~5 wt% for additional heat treatment at 1475°C (2 h), while ~8.4 wt% weight loss was observed during the additional heat treatment at 1490°C (4 h).

The bulk density after pre-sintering, determined from geometric dimensions, is also shown in Table 5.45. The point to note is that the densification during "pre-sintering", for this sample, was much less compared to the ZrPM-45 and ZrPM-58 samples discussed in sections 5.6.1.1.1 and 5.6.1.2.1.

Table 5.45 Compact density after dry-pressing and "pre-sintering" and weight loss after "pre-sintering" for ZrPM-61-350-1-1300(48)-2-1300(8)-1 sample.

Pellet #	As-Dry Pressed		Weight (As-Dry Pressed) (g)	After Pre-sintering		Weight Loss (%)
	Bulk Density (g/cm^3)	Relative Density (%)		Bulk Density (g/cm^3)	Relative Density (%)	
1	2.00	36.3	0.6796	2.18	39.6	8.42

5.6.1.3.2 Sintering/Heat Treatment

The pre-sintered sample was sintered sequentially at 1700°C and 1800°C for 1 h each. The pellet was then sintered for an additional 3 h at 1800°C.

The lattice parameter for the ZrC phase in the 1800°C-sintered sample was assumed to be 0.4696 nm for the same reasons as discussed in section 5.6.1.3.1. The "free" carbon concentration in the 1800°C-sintered sample was estimated to be 6.7 wt%. In other words, it was assumed that the "free" carbon concentration decreased 2 wt% from the 8.7 wt% value that was assumed for the starting CTR powder and the "pre-sintered" sample. This estimated decrease in the "free" carbon concentration was based on the difference in overall concentration that was observed for ZrPM-45 samples that had been heat treated at 1475°C (13.3 wt% carbon) and 1800°C (11.3 wt% carbon) as shown in Table 5.13. Therefore, the solid density of the 1800°C-sintered ZrPM-61 sample was estimated from the following equation:

$$\frac{100}{\frac{93.3}{6.62}+\frac{6.7}{2}} = 5.73\ g/cm^3 \qquad (5\text{-}14)$$

The bulk densities and relative densities (determined from geometric measurements) are shown in Table 5.46. (The relative densities were calculated using the solid density values calculated using equation 5-14.) This table also shows the percentage shrinkages in the diameter and thickness of the samples at various heat treatment temperatures. The weight losses observed upon heat treatments at temperatures in the range of 1700-1800°C are also shown in the table. Substantial shrinkage anisotropy was observed for the sintered samples.

Table 5.46 Densities (bulk and relative), percent shrinkages, and percent weight losses for sintered samples.

Pellet #	Temperature(°C) /Time (h)	Shrinkage (%)		Bulk Density+ (g/cm^3)	Relative Density (%)	Weight Loss* (wt%)
		Diameter	Thickness			
1	1490 /4	-	-	2.18	39.8	-
1	1700/1	5.67	8.24	2.62	45.7	1.94
1	1800/1	7.80	11.50	2.82	49.2	2.88
1	1800/4	13.48	17.19	3.40	59.3	3.49

* Weight losses listed are for individual runs
+ Determined from the sample geometric dimensions.

Table 5.47 shows that relatively little densification occurred in the ZrPM-61 sample after sintering at 1800°C for 4 h. The relative density was only ~59%. In contrast, the value for the corresponding ZrPM-45 sample (Table 5.38, section 5.6.1.1.2) and ZrPM-58 sample (Table 5.42, section 5.6.1.2.2) was ~91%. The main reason for the poor densification in the ZrPM-61 sample is presumably because the "free" carbon content is very high. Solid-state diffusion would be significantly inhibited if the ZrC crystallites were surrounded by carbon surface layers. The low initial density of the ZrPM-61 sample is also another factor that would contribute to the low sintered density obtained after the 1800°C heat treatment.

Table 5.47 shows open porosity, bulk density, and relative density values, determined by the Archimedes method, for the same sample (1800°C/4 h) listed in Table 5.46. The bulk density determined by the Archimedes method (4.41 g/cm^3) is extremely

Table 5.47 Densities (bulk and relative) and percentage open porosity for sintered samples.

Pellet #	Temperature(^{o}C) /Time (h)	Open Porosity (%)	Bulk Density (g/cm^3)	Relative Density (%)
1	1800/4	32.8 (34.4, 32.4, 31.6)	4.41 (4.60, 4.39, 4.24)	77.0 (80.3, 76.6, 74.0)

* Determined by the Archimedes method. Individual values are listed in the parentheses.

different from the value (3.40 g/cm^3) obtained from the geometric measurements. Based on the precision of the diameter and thickness measurements used in the geometric determination of the density, it must be concluded that the Archimedes measurements are extremely inaccurate in this case. (This is also supported by the observation that the summation of the open porosity + relative density far exceeds 100%.) The Archimedes measurements might be inaccurate due to incomplete penetration of water into the open pores.

5.6.2 Effect of Composition on Sintering Behavior

5.6.2.1 Introduction

ZrC-based batches with varying C/Zr molar ratios were prepared for a sintering study. The detailed synthesis procedures for these batches (i.e., ZrPM-87, 94, 97, and 99) are given in Appendix B. Measured carbon contents (measured by Leco Corp.) and calculated C/Zr molar ratios are shown in Table 5.48 for the samples heat treated at temperatures in the range of 1025^{o}C-1900^{o}C. Carbon contents for samples heat treated at 1900^{o}C (2 h) varied from 12.6 wt% for the ZrPM-97 sample (above the value of 11.6

wt% for single-phase, stoichiometric ZrC) to 7.7 wt% for the ZrPM-87 sample. The 1900°C ZrPM-97 sample had a carbon-rich composition, so it contained some "free" carbon. In contrast, the 1900°C ZrPM-87 sample not only had a highly carbon-deficient composition, but it also contained a small amount of zirconia, as will be shown later by XRD. The 1900°C ZrPM-99 sample had a carbon content (~10.8 wt%) that was closest to the stoichiometric value, but it was still slightly carbon-deficient. The 1900°C ZrPM-94 sample had a carbon content (~9.4 wt%) that was between the amounts for the 1900°C ZrPM-87 and ZrPM-99 samples.

The main purpose of this study was to determine the effect of composition on the densification behavior. Thus, an attempt was made to keep the other powder and powder compact characteristics (e.g., particle size, surface area, compact bulk density, etc.) similar for the four batches. However, the starting composition governed the phase and structural development of the powders during the CTR heat treatments required to produce ZrC-based powders. Hence, it was not possible to obtain powders, for the four batches, that were exactly the same in their characteristics or the characteristics of the compacts produced from the powders.

Powder compacts were pressed by the author. The pressureless sintering heat treatments and lattice parameter measurements were made by Dr. Zhaohui Yang and Ms. Yanli Xie of the Georgia Institute of Technology.

Table 5.48 Measured carbon contents and calculated C/Zr molar ratios for samples heat treated at the indicated temperatures.

Sample	Heat Treatment Temperature (^{o}C)	Carbon Content (wt%)	C/Zr Molar Ratio
ZrPM-87	1025	18.9	2.4
ZrPM-87	1800*	7.6	0.6
ZrPM-87	1900*	7.7	0.6
ZrPM-94	1025	21.8	2.9
ZrPM-94	1800*	10.5	0.9
ZrPM-94	1900*	9.4	0.8
ZrPM-97	1025	24.1	3.3
ZrPM-97	1800*	12.6	1.1
ZrPM-97	1900*	12.6	1.1
ZrPM-99	1025	23.7	3.2
ZrPM-99	1800*	11.0	0.9
ZrPM-99	1900*	10.8	0.9

* Sample was pyrolyzed at 800^{o}C prior to heat treatment at the indicated temperature.

5.6.2.2 ZrPM-87

5.6.2.2.1 Processing Before Sintering

Dried powder was sieved through a 150-mesh screen and pyrolyzed at 800^{o}C for 2 h. The C/Zr molar ratio was 2.38 for a sample (initially dried at 120^{o}C) that was pyrolyzed at 1025^{o}C for 2 h. (This ratio was estimated from the carbon content of 18.9 wt%, measured by Leco Corp.) The pyrolyzed sample (~7.8 g) was heat treated at 1425^{o}C for 2 h in a flowing argon (~500 ml/min) atmosphere in the 3-zone lindberg furnace. The specific surface area of the CTR powder was 24 m^2/g. XRD (Figure 5.43) showed phases of zirconium carbide, t-ZrO_2, and m-ZrO_2 in the pattern. Table 5.49

shows some particle size distribution data for a 10 min-milled sample. Particle size distribution plots for the milled sample are shown in Figure 5.44.

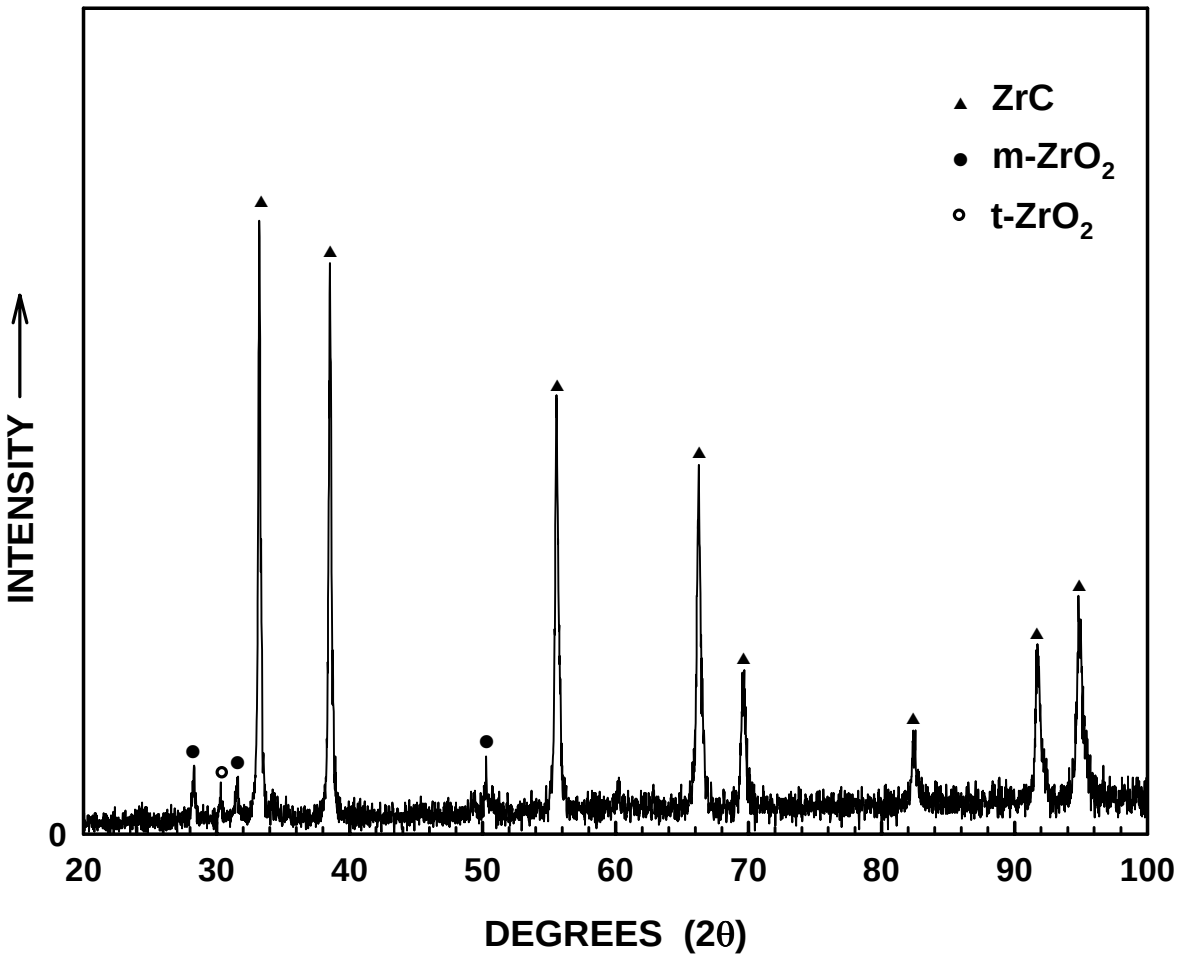

Figure 5.43 X-ray diffraction pattern for a ZrPM-87-800 pyrolyzed sample that was heat treated at 1425°C (2 h).

Table 5.49 Particle size distribution data for the 10 min-milled ZrPM-87-800-1425 powder sample.

	Diameter (μm)
Mean	0.28
Modes*	0.07, 0.17, 1.59
D_{90}	1.40
D_{50}	0.08
D_{10}	0.05
Standard Deviation	0.51

* Mode values are listed for each distinct peak in the accompanying relative frequency plot.

The measured lattice parameter for the ZrPM-87-800-1425 sample was 0.4688 nm. (See Appendix F for details.) It was assumed that the zirconium carbide phase in the ZrPM-87-800-1425 sample was carbon-deficient and had some oxygen dissolved in its lattice, i.e., it can be described by the formula ZrC_xO_y (where x is <1). The composition of the ZrC_xO_y phase was estimated to be $ZrC_{0.85}O_{0.1}$ using data reported from the literature in Figure 2.7. (The carbon amount was obtained by drawing a line parallel to the x-axis (i.e., C/Zr molar ratio) in Figure 2.7 at a lattice parameter (y-axis) value of 0.4688. The x-axis value at which this line intersected the plotted data set was used to determine the carbon amount. The same procedure was used to determine the oxygen amount.) The solid density of the zirconium oxycarbide phase is given by:

$$\frac{4\left[\left(N_{Zr}\times A_{Zr}\right)+\left(N_C\times A_C\right)+\left(N_O\times A_O\right)\right]}{(a)^3\times N} \tag{5-15}$$

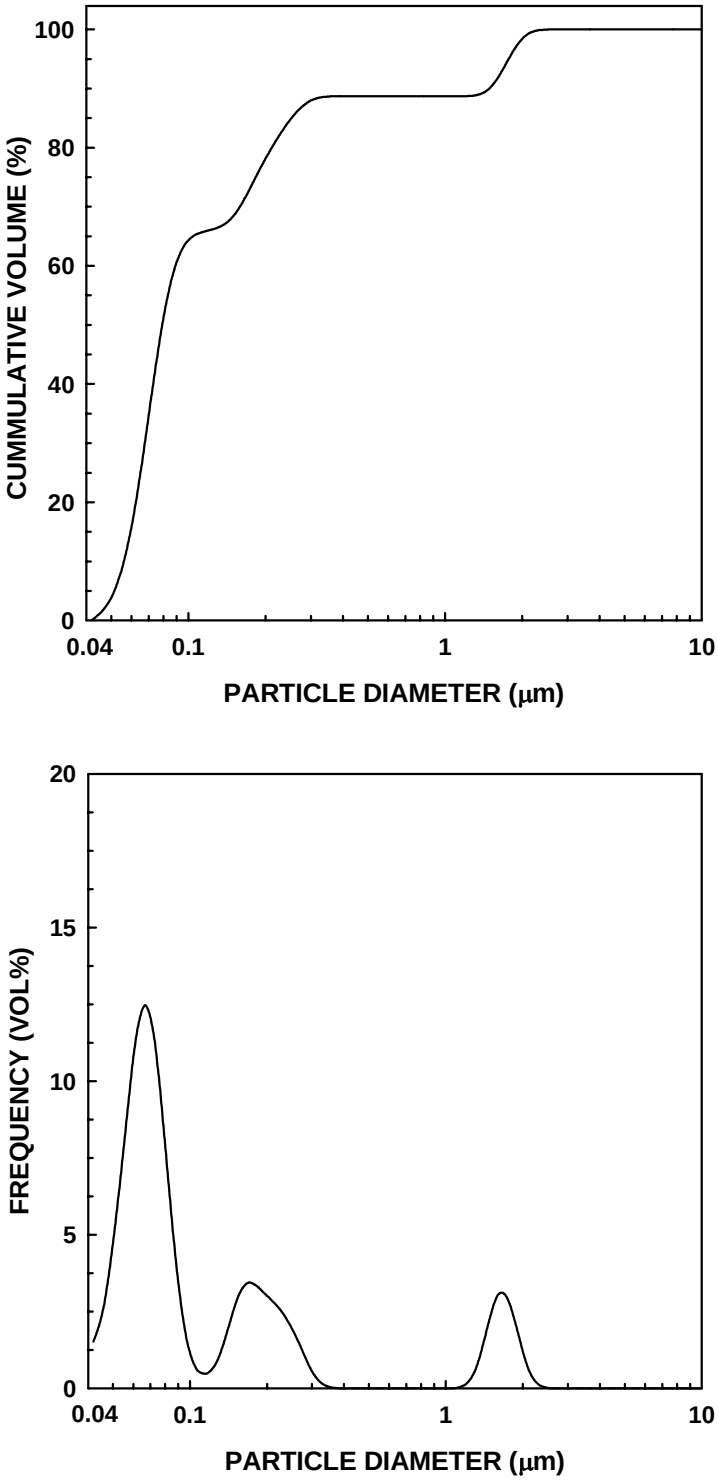

Figure 5.44 Particle size distribution for the 10 min-milled ZrPM-87-800-1425 powder sample: cumulative frequency plot (top) and relative frequency plot (bottom).

where N_{Zr}, N_C, and N_O are the number of moles of zirconium, carbon, and oxygen, respectively, in the zirconium oxycarbide; A_{Zr}, A_C, and A_O are the atomic weights of zirconium, carbon, and oxygen, respectively; a is the lattice parameter of the zirconium oxycarbide and N is the Avogadro's number. Therefore, the solid density of $ZrC_{0.85}O_{0.1}$ is given by :

$$\frac{4(1\times 91.224 + 0.85\times 12.01 + 0.1\times 16)}{(0.4688)^3 \times\ 6.022\times 10^{23}} \times 10^{21} \quad = 6.64\ g/cm^3 \tag{5-16}$$

The estimated amounts of t-ZrO_2 and m-ZrO_2 remaining in the ZrPM-87-800-1425 sample were ~3.4 wt% and ~7.6 wt%, respectively. (The rest of the material was assumed to be zirconium oxycarbide.) These amounts were determined from the XRD pattern (Figure 5.44), based on the relative integrated intensities of the highest peaks for the t-ZrO_2, m-ZrO_2, and zirconium oxycarbide. The solid density used for the latter material was that calculated according to equation 5-16. The solid density values of t-ZrO_2 and m-ZrO_2 were assumed to be 5.95 g/cm^3 and 5.82 g/cm^3, respectively. The solid density for the powder mixture containing zirconium oxycarbide and zirconia is given by:

$$density\ of\ \ powder = \frac{100}{\frac{100-(a+b)}{\rho_{ZrC_xO_y}} + \frac{a}{\rho_{t-ZrO_2}} + \frac{b}{\rho_{m-ZrO_2}}} \tag{5-17}$$

where a is the amount (wt%) of t-ZrO_2, b is the amount (wt%) of m-ZrO_2, and [100 - (a+b)] is the amount (wt%) of zirconium oxycarbide phase; ρ_{ZrCxOy} is the solid

density of ZrC_xO_y and $\rho_{t\text{-}ZrO2}$ and $\rho_{m\text{-}ZrO2}$ are the solid densities of t-ZrO_2 and m-ZrO_2, respectively. Therefore, the solid density of ZrPM-87-800-1425 is given by :

$$\frac{100}{\frac{89}{6.64}+\frac{7.6}{5.82}+\frac{3.4}{5.95}} = 6.54\ g/cm^3 \qquad (5\text{-}18)$$

Although, the above calculation is considered the best estimate of the solid density, some other values were used in the calculation in order to give a rough idea of the range of error that might be expected. As an extreme case, it was assumed that the zirconium carbide phase in the ZrPM-87-800-1425 sample which was carbon-deficient and oxygen-free (i.e., ZrC_{1-x}). It was also assumed, arbitrarily, that the amounts of t-ZrO_2 and m-ZrO_2 in the sample were 7 wt% and 15 wt%, respectively (i.e., approximately twice the amounts used in equation 5-18). The ZrC_{1-x} composition was estimated as $ZrC_{0.85}$ by using Figure 2.7 and the lattice parameter value of 0.4688 nm. The solid density of $ZrC_{0.85}$, calculated using equation 5-15, is 6.54 g/cm^3. Therefore, the solid density of ZrPM-87-800-1425, calculated using equation 5-17, is 6.45 g/cm^3. This solid density value is 1.4% lower than the solid density value given by equation 5-18.

The milled powder was mixed with 10 vol% polymer binder and plasticizer as described in section 5.6.1.1.1. Five powder compacts were uniaxially dry-pressed in a 6.4 mm diameter die at 250 MPa. The bulk densities of these samples, determined from geometric dimensions, are shown in Table 5.50. (The relative densities were calculated using the solid density value given in equation 5-18.) The compacts were heat treated at 1150^{o}C for 2 h under flowing argon (~100 ml/min) in a tube furnace (Model 55031). This

Table 5.50 Compact densities after dry pressing and compact density and weight loss after 1150°C heat treatment.

Pellet #	As-Dry Pressed		Weight (g) (As-Dry Pressed)	After 1150°C (2 h)		% Weight Loss
	Bulk Density (g/cm^3)	Relative Density (%)		Bulk Density (g/cm^3)	Relative Density (%)	
1	3.09	47.2	0.4151	3.05	46.6	2.4
2	3.07	46.9	0.4180	3.07	46.9	2.2
3	3.11	47.6	0.4116	3.08	47.1	2.1
4	3.09	47.2	0.4161	3.06	46.8	1.8
5	3.12	47.7	0.4181	3.08	47.1	1.9
Average	3.10	47.4	-	3.07	46.9	2.1

resulted in burnout of the binder that was added to the powder. The percentage weight loss due to binder burnout is also shown in Table 5.50. The weight losses were close to the value expected (1.84 wt%) based on the amount of binder originally added to the powder. (The small differences from the expected value were probably due to some adsorbed moisture in the samples.) Bulk density and relative density values after binder burnout, determined from geometric dimensions, are also shown in Table 5.50.

5.6.2.2.2 Sintering/Heat Treatment

Figures 5.45 and 5.46 show XRD patterns for the ZrPM-87-800-1425 powder and for samples sintered at temperatures in the range of 1600°C to 1950°C. As indicated in the previous section, the XRD pattern of the 1425°C sample showed zirconium carbide was the predominant phase, although m-ZrO_2 and t-ZrO_2 were also present. XRD of

samples heat treated at temperatures ≥1600°C showed some residual of m-ZrO_2, while the predominant phase was zirconium carbide.

The solid density for the 1900°C ZrPM-87 sample was calculated using three different approaches:

(1) It was assumed that the zirconium carbide phase was actually a zirconium oxycarbide, i.e., ZrC_xO_y. The measured lattice parameter of a ZrPM-87-800 pyrolyzed powder that was subsequently heat treated at 1900°C (2 h) was 0.4664 nm. The molar carbon value, x, was estimated using the carbon content of 7.72 wt% reported in Table 5.48 for the ZrPM-87-800-1900 sample. This yields a value of x = 0.64 if it is assumed that the samples consisted of Zr and C only. The oxygen value, y, was estimated to be 0.25 by using Figure 2.7, as described in section 5.6.2.2.1. Thus, the composition of ZrC_xO_y was estimated to be $ZrC_{0.64}O_{0.25}$. The solid density of $ZrC_{0.64}O_{0.25}$, calculated using equation (5-14), is 6.73 g/cm^3. The XRD pattern for the 1900°C ZrPM-87 sample (Figure 5.46) shows the presence of a trace amount of m-ZrO_2. The amount of m-ZrO_2 was determined to be ~4 wt%, based on the XRD integrated (peak area) intensities. Therefore, the density of the ZrPM-87-800-1900 sample is given by:

$$\frac{100}{\frac{96}{6.64}+\frac{4}{5.82}} = 6.60\ g/cm^3 \qquad (5\text{-}19)$$

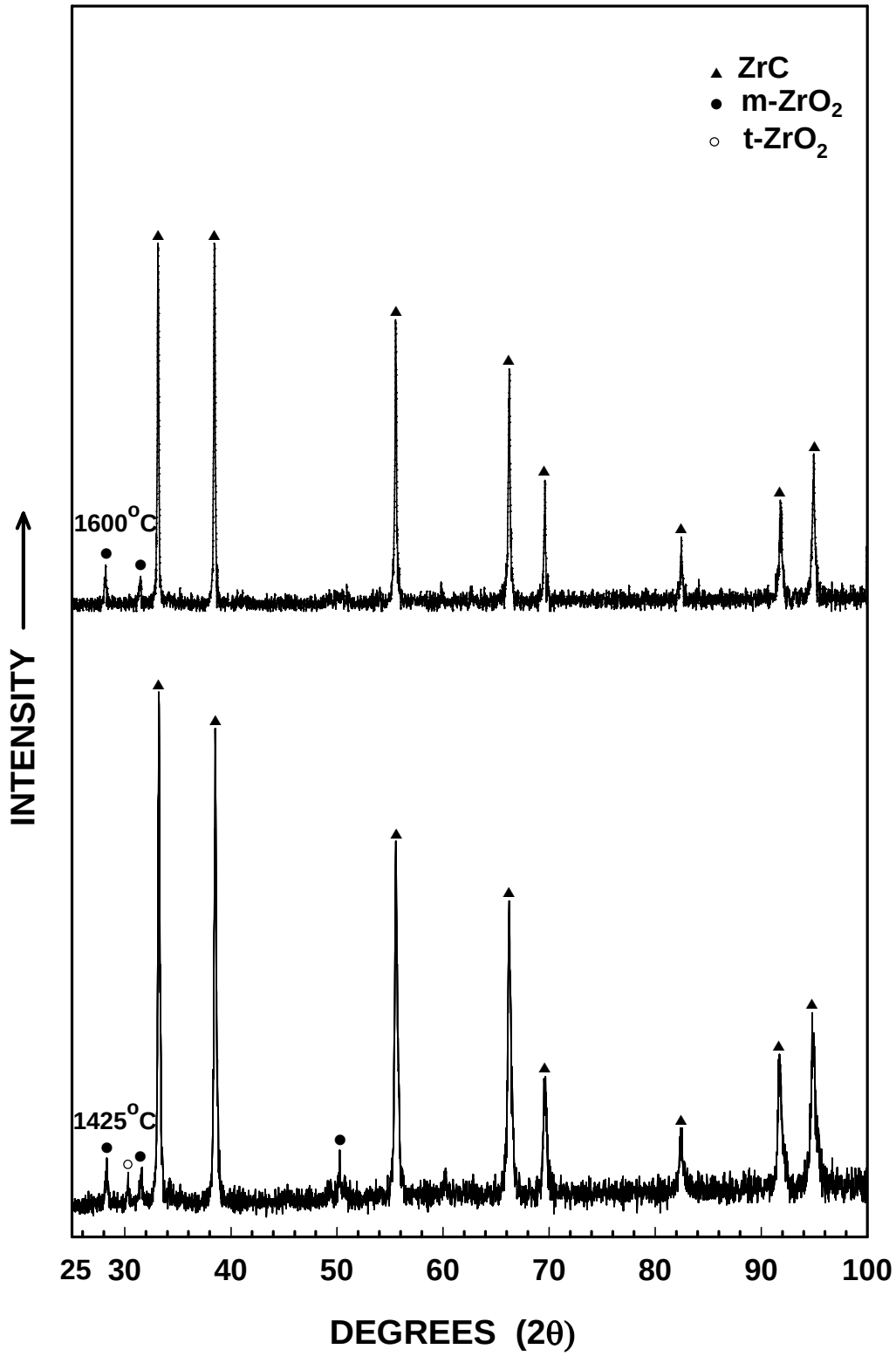

Figure 5.45 X-ray diffraction patterns for ZrPM-87 samples heat treated at 1425°C and 1600°C.

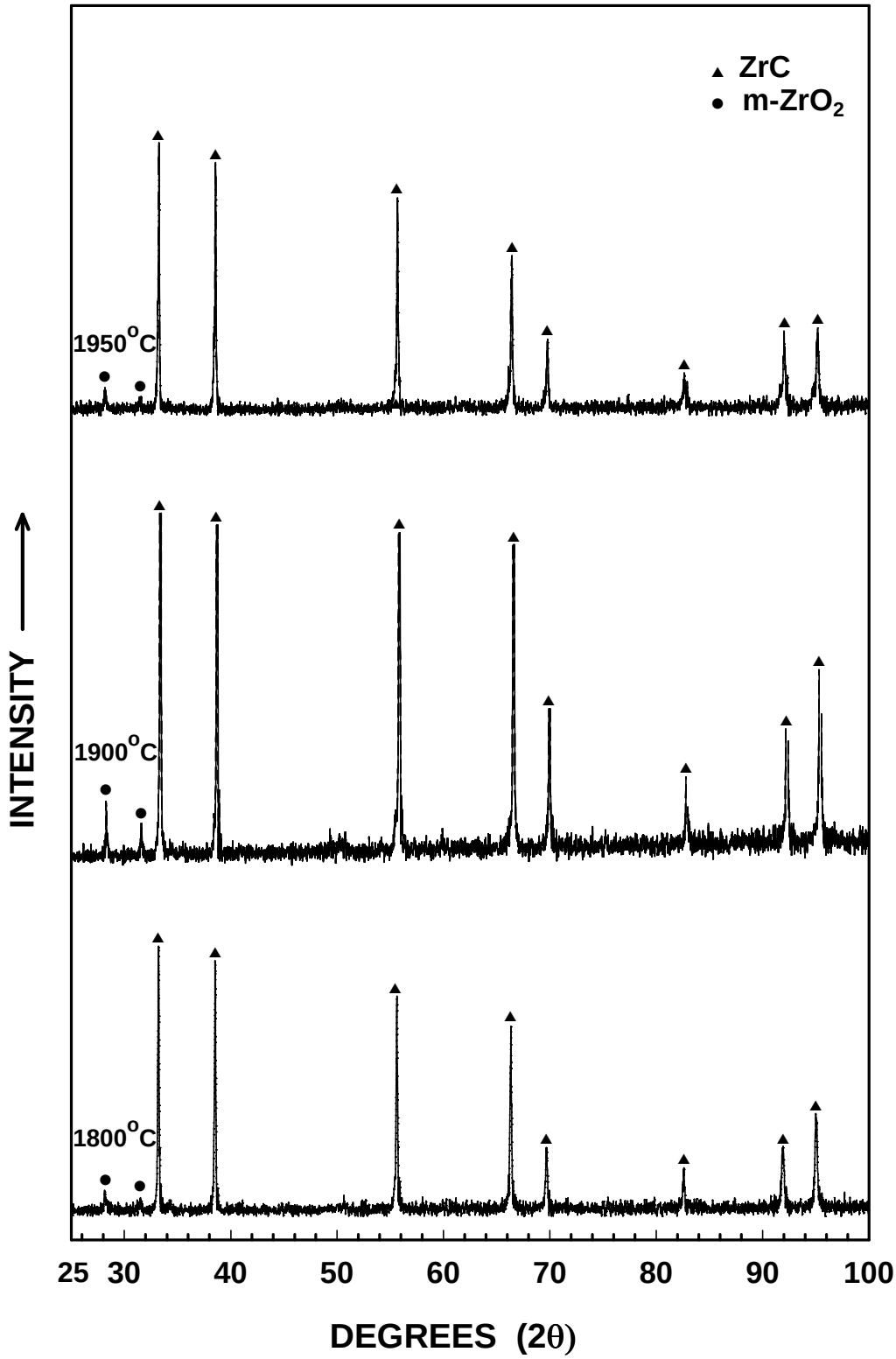

Figure 5.46 X-ray diffraction patterns for ZrPM-87 samples heat treated at temperatures in the range of 1800 to 1950°C.

However, the assumption that 0.25 moles of oxygen were dissolved in each mole of zirconium carbide for the 1900°C ZrPM-87 sample does not seem reasonable. This is because the weight losses upon heat treatment of ZrPM-87 samples above 1600°C were relatively small (see Table 5.51). To remove all the oxygen from a sample with composition $ZrC_{0.64}O_{0.25}$ would mean that an additional weight loss of ~7 wt% would be required (assuming oxygen was removed as CO). This is unlikely considering the total weight loss between 1600-1950°C was only 4.4 wt%.

(2) It was assumed that the zirconium carbide phase was carbon-deficient and oxygen-free, i.e., $ZrC_{0.64}$. The solid density for this phase was calculated (as $\rho = 6.47$ g/cm^3) using equation 5-15. The solid density for the ZrPM-87-800-1900 sample was then calculated from equation 5-17, by using the $ZrC_{0.64}$ density, the amount of m-ZrO_2 in the material (i.e., ~4 wt%), and the measured lattice parameter value of 0.4664 nm. The calculated value is 6.44 g/cm^3. However, the assumption that all the oxygen would be removed from the zirconium carbide lattice at 1900°C is not correct because small weight losses were observed upon heat treatment of ZrPM-87 samples at temperatures ≥1800°C (Table 5.51). Furthermore, the oxygen contents determined for ZrPM-59-800-1800 and ZrPM-59-800-2000 samples were 1.0 wt% and 0.56 wt%, respectively (Table 5.23). (ZrPM-59 had a carbon content of 19.4 wt% for a sample pyrolyzed at 1025°C, so it was not quite as carbon-deficient (relative to the stoichiometric amount for equation 5-7) as in the corresponding ZrPM-87 pyrolyzed sample.)

(3) It was assumed that the solid density of the zirconium carbide phase was between the two extremes of $ZrC_{0.64}O_{0.25}$ and $ZrC_{0.64}$, i.e., 6.6 g/cm^3. Therefore, the density of the ZrPM-87-800-1900 sample, calculated using equation 5-17, is 6.56 g/cm^3. (The amount

of m-ZrO_2 was assumed to be ~4 wt%.) This density was used to calculate the percentage relative density of samples heat treated at temperatures ≥1600°C. In fact, the solid density will vary over the range of sintering temperatures used in this study (1600-1950°C). However, the actual variation in solid density values is probably well within the range of the error associated with the calculations that have been described in this section.

Table 5.51 shows the bulk density values, determined from geometric measurements, and the corresponding calculated relative density values for the samples sintered at temperatures in the range of 1600-1950°C. The table also lists the percentage shrinkage in the diameter and thickness and the percentage weight loss for each sample. The weight losses were also corrected for adsorbed moisture. (The weight loss due to adsorbed moisture was measured separately. The average value of 1.5 wt% was applied as the correction for all samples.) Figure 5.47 shows a plot of weight loss (corrected for adsorbed moisture) vs. sintering temperature. The significant weight loss (~2.9 wt%) for the 1600°C sintered sample was consistent with the decreased amount of zirconia in the XRD pattern (Figure 5.45, i.e., compared to the 1425°C ZrPM-87 sample). The small weight losses observed when samples were sintered at temperatures >1600°C were again consistent with the slight decrease in the zirconia amount indicated in the XRD patterns (Figures 5.45 and 5.46). Figure 5.48 shows plots of the diameter and thickness shrinkages vs. sintering temperature. The shrinkage behavior in the range of 1600-1950°C was almost isotropic.

Table 5.51 Densities (bulk and relative), percent shrinkages, and percent weight losses for sintered samples.

Pellet #	Temperature (^{o}C)	Shrinkage (%)		Bulk Density^{+} (g/cm^{3})	Relative Density (%)	Weight Loss (wt%)	Corrected Weight Loss (wt%)
		Diameter	Thickness				
2	1600	11.47	11.78	4.29	65.4	4.41	2.91
4	1725	18.46	18.66	5.47	83.4	4.78	3.28
5	1800	21.01	21.62	6.02	91.8	5.24	3.74
3	1900	22.92	22.85	6.42	97.9	5.54	4.04
1	1950	23.42	24.17	6.54	99.7	5.87	4.37

+ Determined from the sample geometric dimensions.

Figure 5.49 shows plots of bulk density and relative density vs. sintering temperature based on measurements made from the geometric dimensions of the samples. The relative density value of the sample sintered at 1950^{o}C was ~100%. However, this value was based on a solid density calculated by making some assumptions that were discussed earlier in the section 5.6.2.2.1. Nevertheless, the actual value is expected to be within a few percent of the one reported.

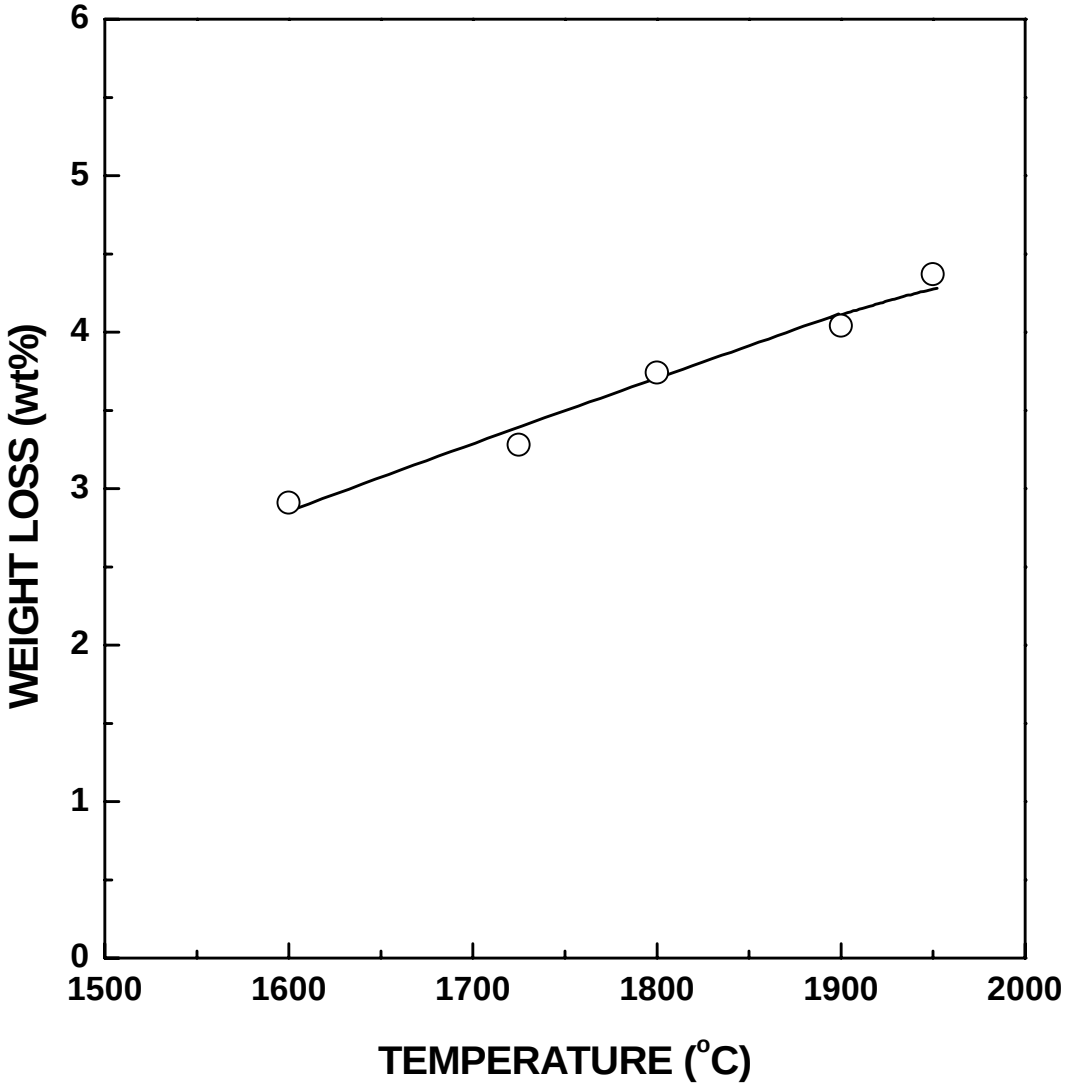

Figure 5.47 Plot of corrected weight loss vs. sintering temperature for ZrPM-87 powder compacts that were initially heat treated at 1150°C (2 h). The compacts were prepared with ZrPM-87-800-1425 powder.

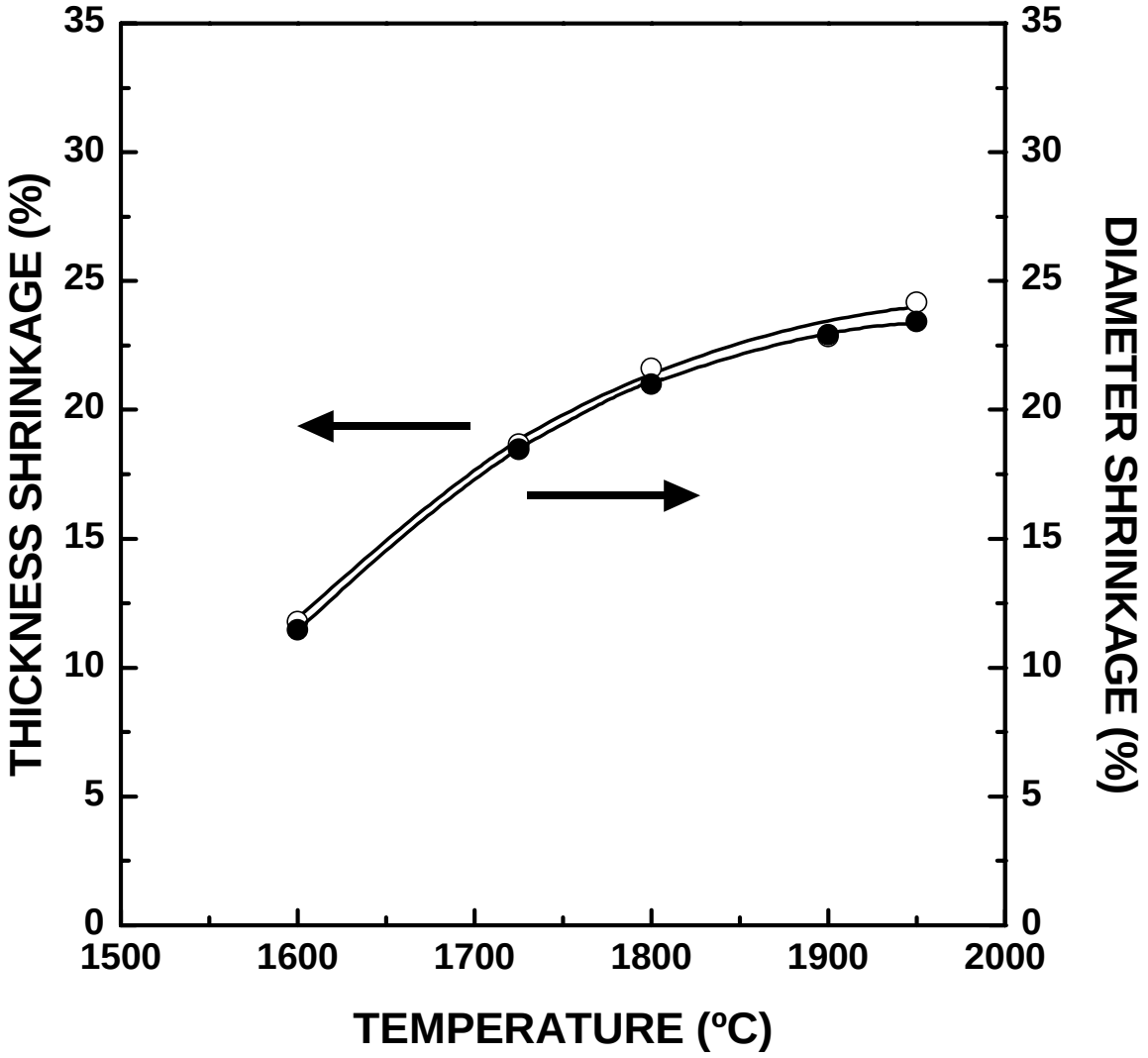

Figure 5.48 Plots of thickness and diameter shrinkage vs. sintering temperature for ZrPM-87 powder compacts that were initially heat treated at 1150°C (2 h). The compacts were prepared with ZrPM-87-800-1425 powder.

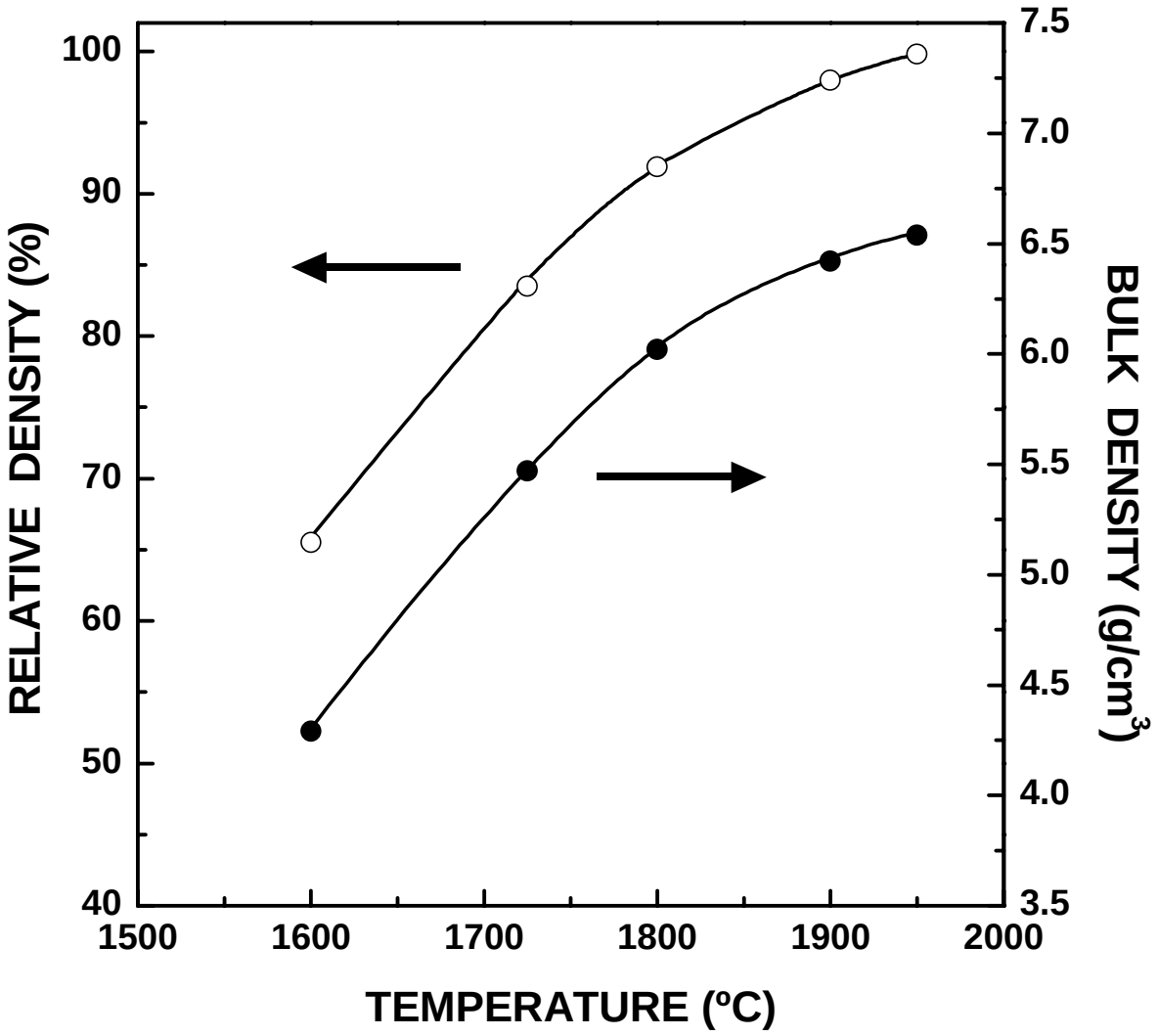

Figure 5.49 Plots of relative density and bulk density vs. sintering temperature for ZrPM-87 powder compacts that were initially heat treated at 1150°C (2 h). Bulk densities were determined by measurements of the sample dimensions.

Table 5.52 shows open porosity, bulk density, and relative density values, determined by the Archimedes method, for some of the same samples shown in Table 5.51. The measurements for each sample were repeated at least twice. The individual and average values are listed in Table 5.52.

The open porosity measured for the 1600^{o}C sintered sample was ~20%. The summation of the open porosity and relative density (i.e., ~86%) implies that there should be ~14% closed porosity in the sample. However, this amount of closed porosity is highly unlikely for a sample that has such low relative density.[91] This suggests that there was problem with penetration of water into the pores for the 1600^{o}C sample. Hence, the open porosity value is considered unreliable. In contrast to the 1600^{o}C sample, the measured open porosity was zero for samples sintered at temperatures ≥1800^{o}C. This is consistent with the high relative densities of the samples.

Table 5.52 Densities (bulk and relative) and percentage open porosity for sintered samples.

Pellet #	Temperature (^{o}C)	Open Porosity* (%)	Bulk Density* (g/cm^3)	Relative Density (%)
2	1600	19.6 (20.1, 19.3, 19.4)	4.35 (4.36, 4.34, 4.35)	66.3 (66.5, 66.2, 66.3)
5	1800	0.0 (0.0, 0.0)	6.05 (6.08, 6.03)	92.3 (92.7, 92.0)
3	1900	0.0 (0.0, 0.0, 0.0, 0.0)	6.45 (6.48, 6.45, 6.46, 6.42)	98.4 (98.8, 98.4, 98.5, 97.9)
1	1950	0.0 (0.0, 0.0)	6.59 (6.60, 6.57)	100.0 (100.0, 100.0)

* Determined by the Archimedes method. When more that one measurement was made, the individual values are listed in the parenthesis.

Figure 5.50 shows plots of the bulk density (determined by the Archimedes method) and the calculated relative density as a function of sintering temperature for the ZrPM-87 samples. The calculated relative density value was ~100% for the sample sintered at 1950^{o}C. (However, as indicated previously, the solid density used to calculate this relative density is based on some assumptions that may not be valid.) Figure 5.51 shows plots comparing the bulk density values (for various sintering temperatures) that were determined from the Archimedes and geometric measurement methods. The two methods gave similar bulk density values at each sintering temperature.

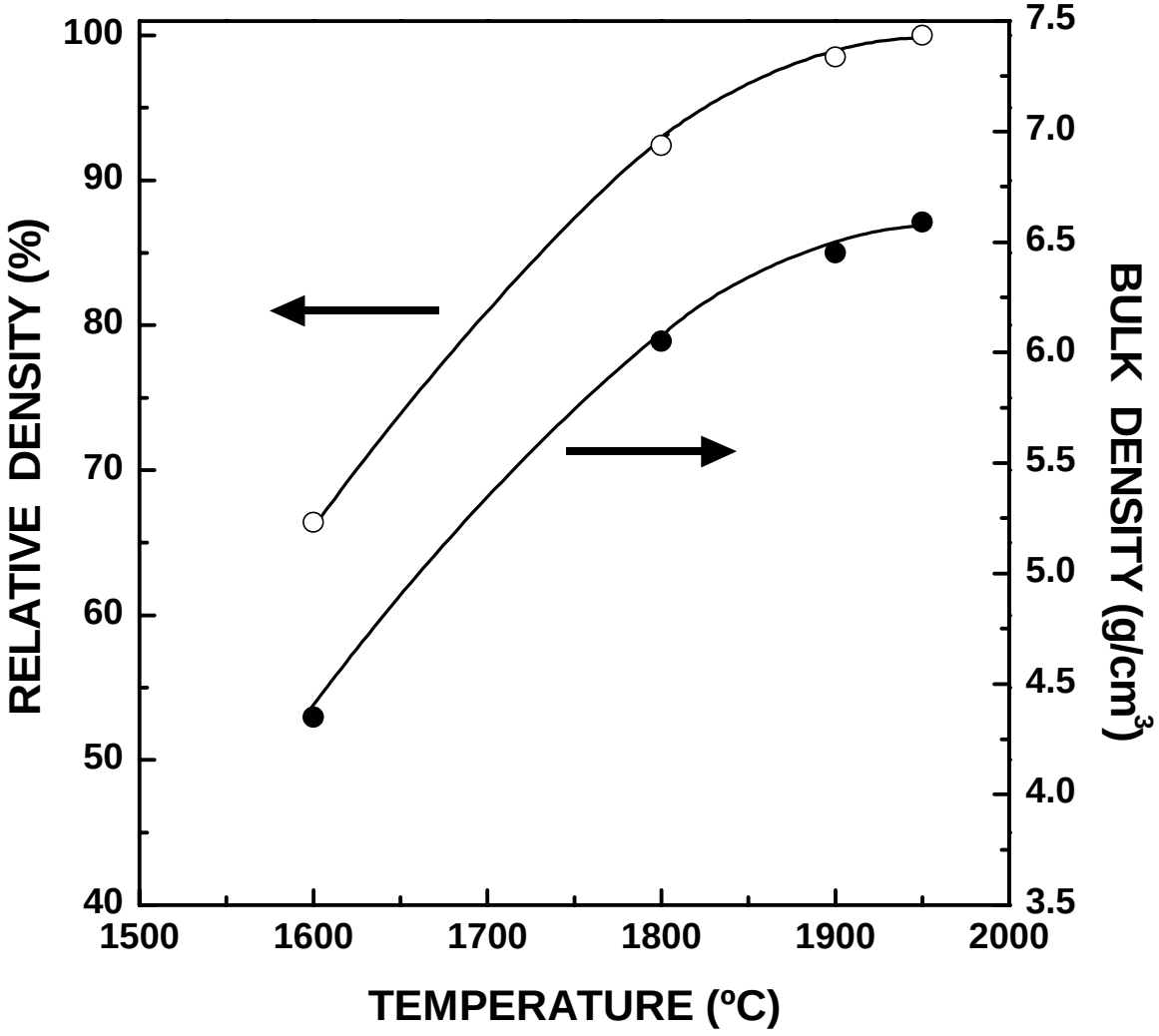

Figure 5.50 Plots of relative density and bulk density vs. sintering temperature for ZrPM-87 powder compacts that were initially heat treated at 1150°C (2 h). Bulk densities were determined by the Archimedes method.

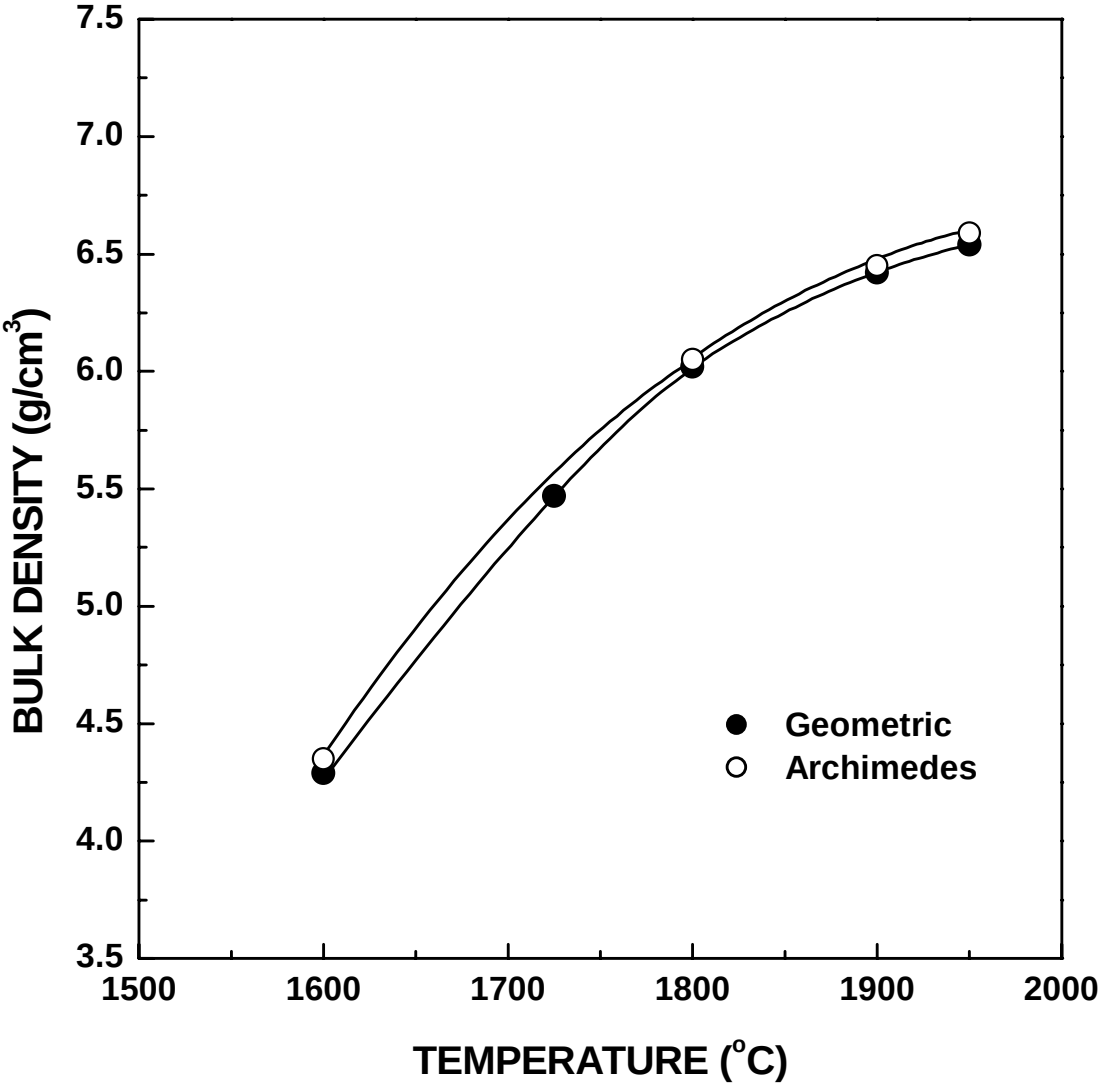

Figure 5.51 Plots of bulk density vs. sintering temperature for ZrPM-87 powder compacts that were initially heat treated at 1150°C (2 h). Bulk densities were determined by the geometric and Archimedes methods.

5.6.2.3 ZrPM-94

5.6.2.3.1 Processing Before Sintering

Dried powder was sieved and pyrolyzed exactly as described in section 5.6.2.2.1. The C/Zr molar ratio was 2.85 for a sample (initially dried at 120^{o}C) that was pyrolyzed at 1025^{o}C for 2 h. (This ratio was estimated from the carbon content of 21.8 wt% measured by Leco Corp.) The pyrolyzed sample (~8 g) was heat treated at 1475^{o}C for 2 h in a flowing argon (~500 ml/min) atmosphere in the 3-zone lindberg furnace. The specific surface area of the CTR powder was 16 m^2/g. XRD (see Figure 5.52) showed phases of zirconium carbide, t-ZrO_2, and m-ZrO_2 in the pattern.

Table 5.53 shows some particle size distribution data for a 10-min milled sample. Particle size distribution plots for the milled sample are shown in Figure 5.53. Comparison of the particle size distributions in Figures 5.44 and 5.53 shows that the milled 1425^{o}C ZrPM-87 sample has more aggregates compared to the milled 1475^{o}C ZrPM-94 sample. (This is particularly evident from the mode for particles in the size range of ~1 - 2.5 μm in the ZrPM-87 sample.) A similar, but less pronounced, difference in particle size distributions was observed for milled ZrPM-45 and ZrPM-59 powders (see Figure 5.28). As discussed in section 5.2.2.3, the difference in the extent of aggregation in the samples may be due to compositional differences (i.e., in which "oxide-rich" compositions show more aggregation compared to "carbon-rich" compositions). The results in Figures 5.44 and 5.53 are consistent with the previous results in that the sample with the more oxide-rich composition is more aggregated.

Table 5.53 Particle size distribution data for the 10 min-milled ZrPM-94-800-1475 powder sample.

	Diameter (μm)
Mean	0.09
Modes*	0.07, 0.19, 0.47
D_{90}	0.20
D_{50}	0.07
D_{10}	0.05
Standard Deviation	0.07

* Mode values are listed for each distinct peak in the accompanying relative frequency plot.

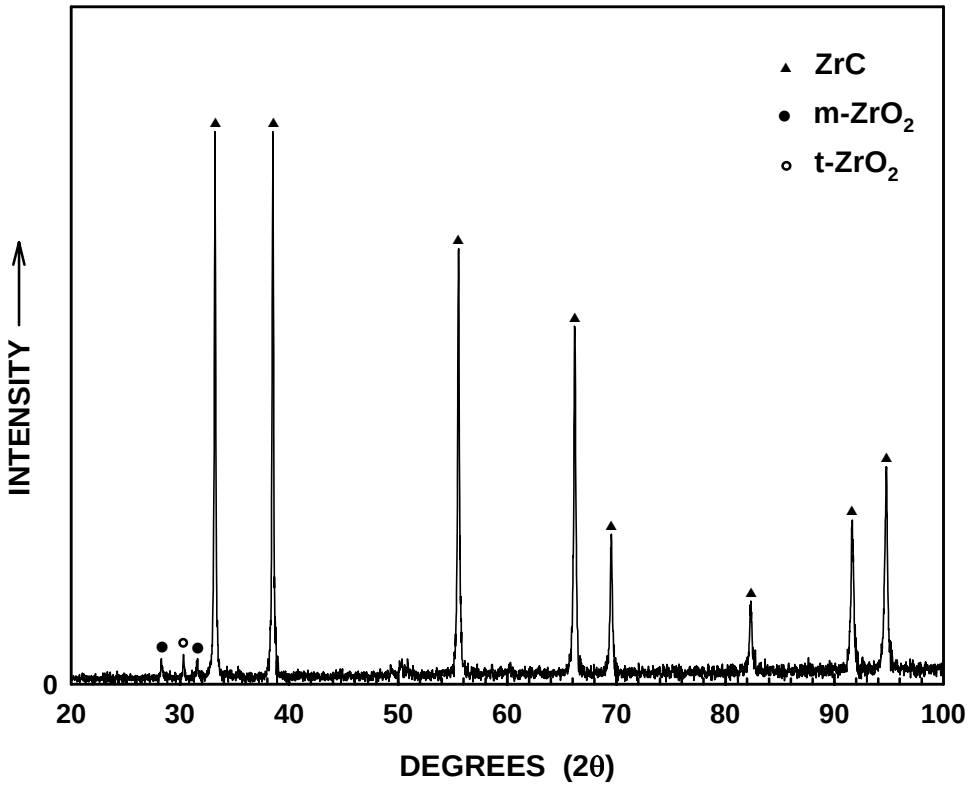

Figure 5.52 X-ray diffraction pattern for ZrPM-94-800 pyrolyzed sample that was heat treated at 1475°C (2 h).

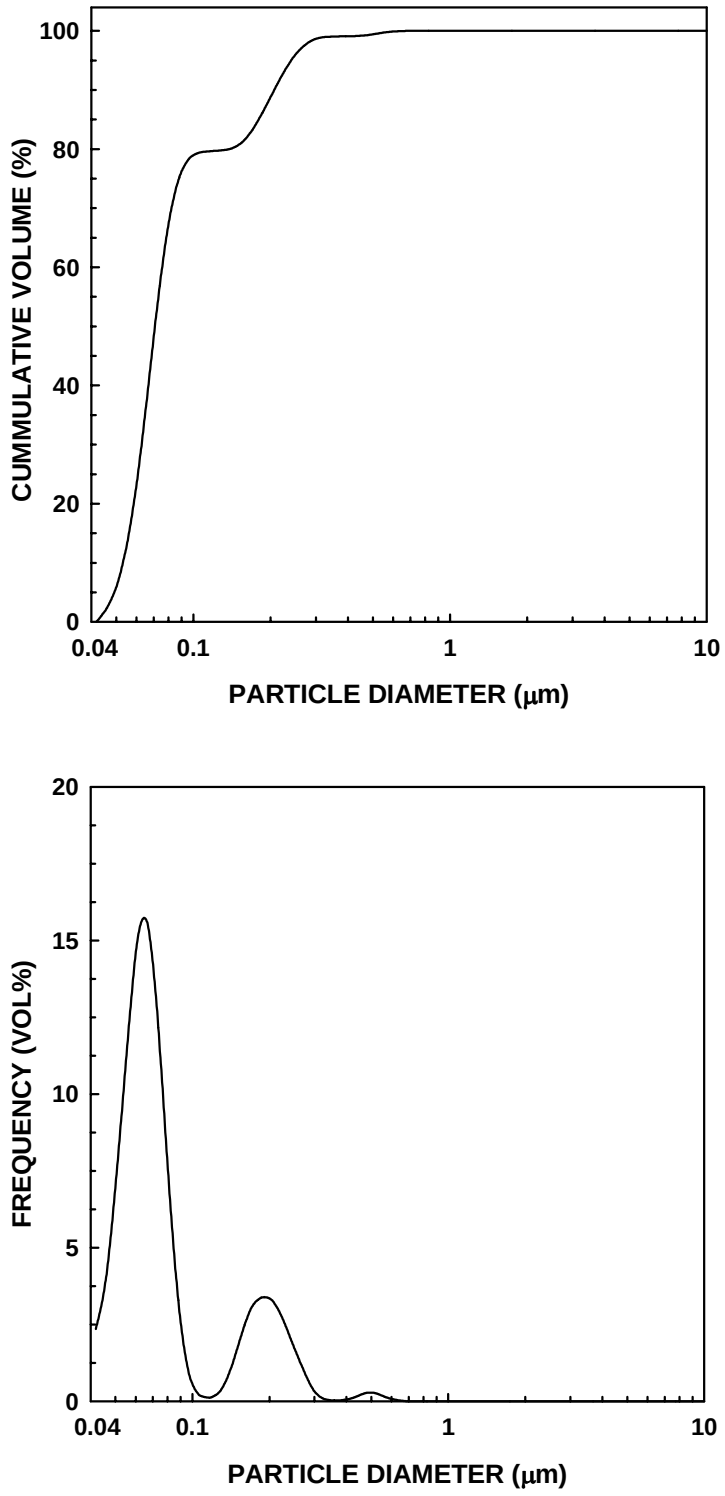

Figure 5.53 Particle size distribution plots for the 10 min-milled ZrPM-94-800-1475 powder sample: cumulative frequency plot (top) and relative frequency plot (bottom).

The measured lattice parameter for the ZrPM-94-800-1475 sample was 0.4688 nm. (See Appendix F for details.) It was assumed that the zirconium carbide phase in this sample was carbon-deficient (based on the C/Zr molar ratio in the pyrolyzed material) and that some oxygen was dissolved in its lattice. It was also assumed that composition of the ZrC_xO_y phase was the same as in the ZrPM-87-800-1425 sample, i.e., $ZrC_{0.85}O_{0.1}$ (see section 5.6.2.2.1). The solid density of $ZrC_{0.85}O_{0.1}$ was calculated in section 5.6.2.2.1 using equations 5-15 and 5-16. The calculated value was 6.64 g/cm^3. The estimated amounts of t-ZrO_2 and m-ZrO_2 remaining in the ZrPM-94-800-1475 sample were ~2 wt% and ~3 wt%, respectively. These amounts were determined from the XRD pattern (Figure 5.52), based on the relative integrated intensities of the highest peaks for the t-ZrO_2, m-ZrO_2, and zirconium oxycarbide. Based on the above information, the solid density of ZrPM-94-800-1475 sample was calculated using the following equation:

$$\frac{100}{\frac{95}{6.64}+\frac{3}{5.82}+\frac{2}{5.95}} = 6.59\ g/cm^3 \qquad (5\text{-}20)$$

The pressing and processing conditions for the powder compacts were exactly same as described in section 5.6.2.2.1. The bulk densities of these samples, determined from geometric dimensions, are shown in Table 5.54. (The relative densities were calculated using the solid density value given in equation 5-20.) The percentage weight losses due to binder burnout are also shown in Table 5.54. The weight losses due to the binder burnout were essentially the same as observed for the ZrPM-87 samples (section

Table 5.54 Compact densities after dry pressing and compact density and weight loss after 1150°C heat treatment.

Pellet #	As-Dry Pressed		Weight (g) (As-Dry Pressed)	After 1150°C (2 h)		% Weight Loss
	Bulk Density (g/cm^3)	Relative Density (%)		Bulk Density (g/cm^3)	Relative Density (%)	
1	3.09	46.8	0.4150	3.03	45.9	1.7
2	3.09	46.8	0.4153	3.04	46.1	1.8
3	3.09	46.8	0.4180	3.05	46.2	1.9
4	3.08	46.7	0.4191	3.08	46.7	2.0
5	3.08	46.7	0.4198	3.05	46.2	1.8
Average	3.09	46.8	-	3.05	46.2	1.8

5.6.2.2.1). Bulk density and relative density values after binder burnout, determined from geometric dimensions, are also shown in Table 5.54.

5.6.2.3.2 Sintering/Heat Treatment

Figures 5.54 and 5.55 show XRD patterns for the ZrPM-94-800-1475 powder and for samples sintered at temperatures in the range of 1600°C to 1950°C. As indicated in the previous section, the XRD pattern of the 1475°C sample showed zirconium carbide was the predominant phase, although m-ZrO_2 and t-ZrO_2 were also present. Zirconium carbide and a small amount of m-ZrO_2 were observed in the XRD pattern for the 1600°C ZrPM-94 sample (Figure 5.55). Zirconium carbide was the only crystalline phase observed in the sample heat treated at temperatures >1600°C.

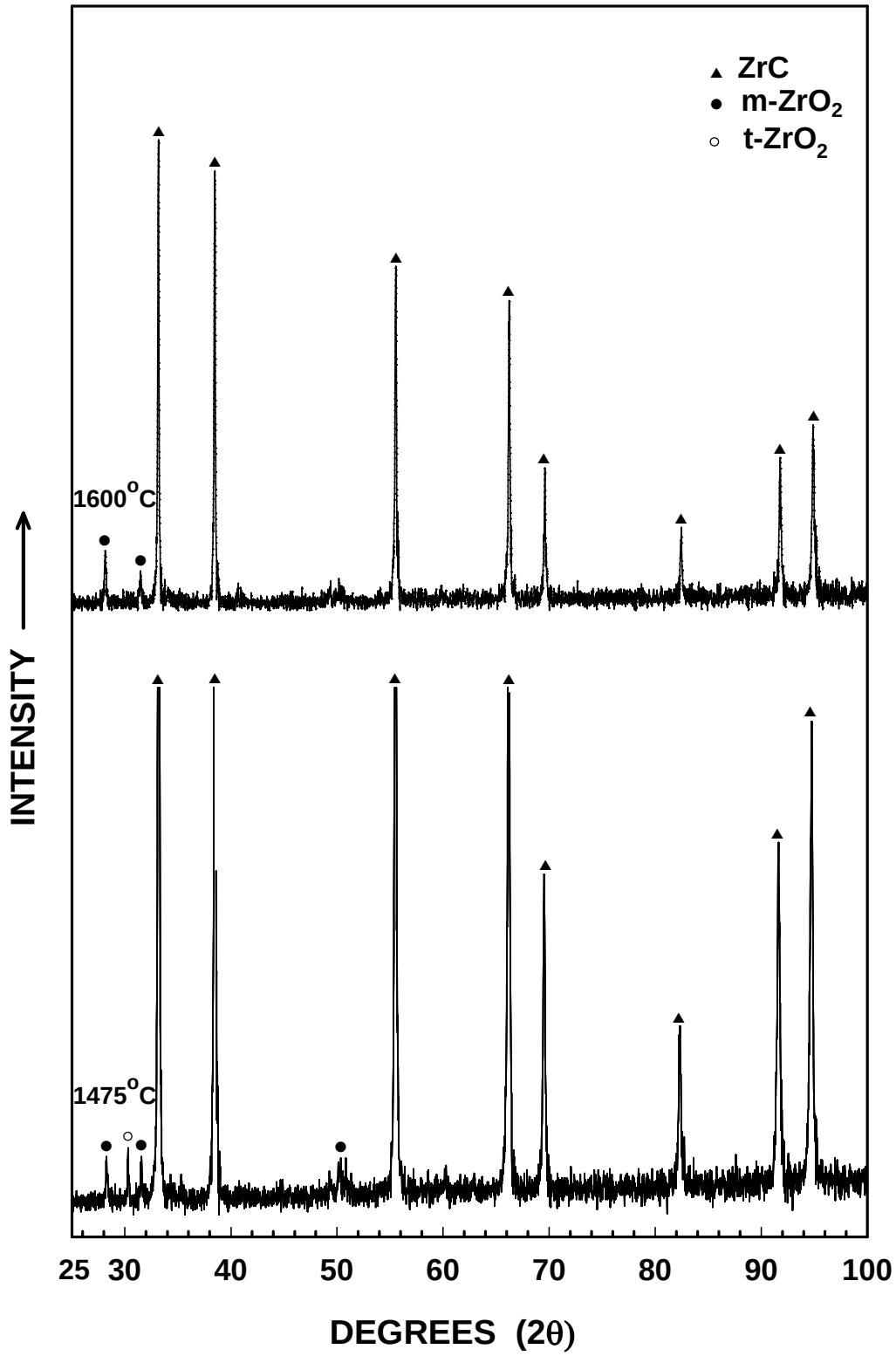

Figure 5.54 X-ray diffraction patterns for ZrPM-94 samples heat treated at 1475°C and 1600°C.

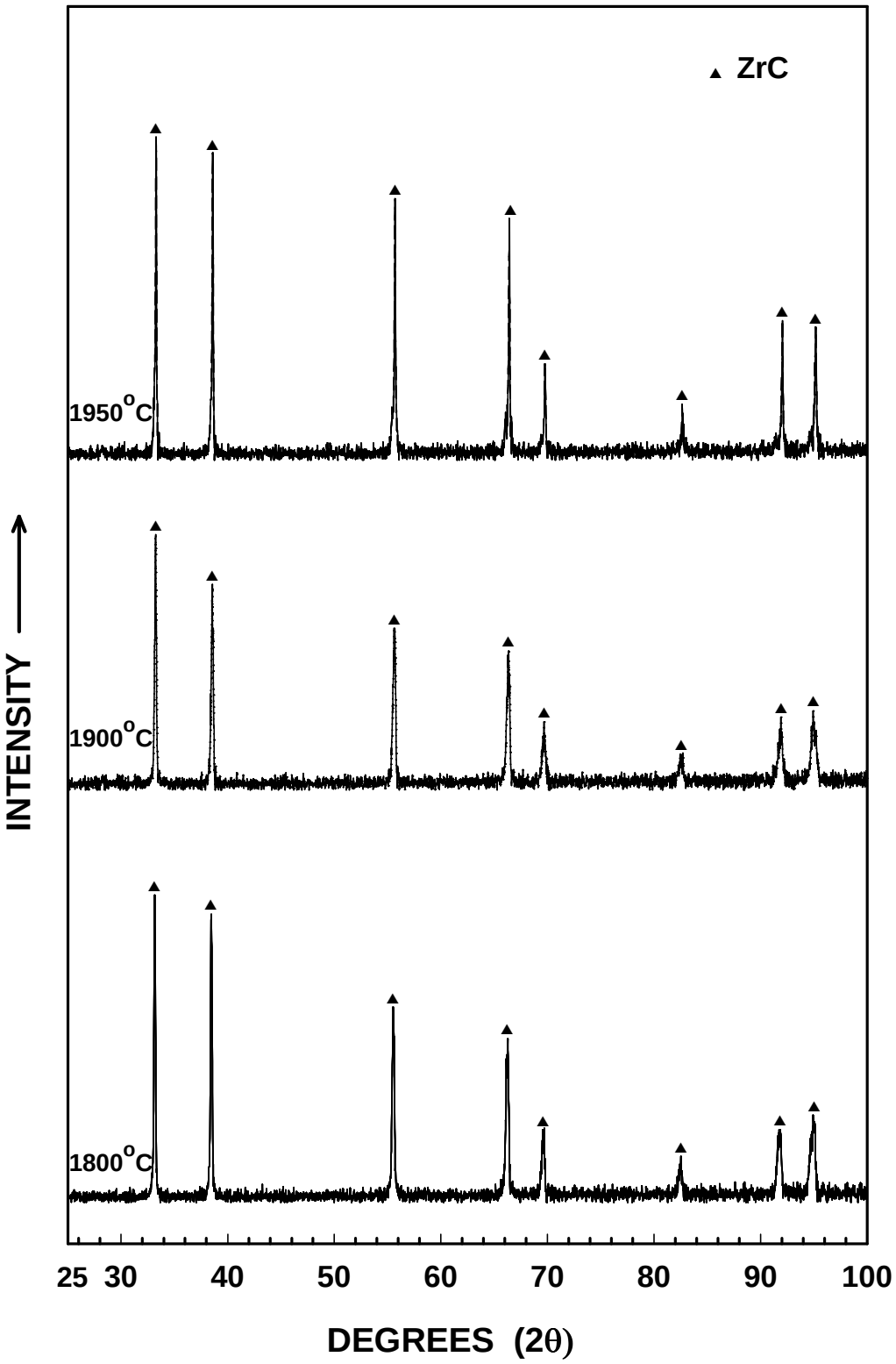

Figure 5.55 X-ray diffraction patterns for ZrPM-94 samples heat treated at temperatures in the range of 1800 to 1950°C.

Table 5.55 lists percentage weight losses for ZrPM-94-800-1475 powder compacts which were sintered at temperatures in the range of 1600-1950^{o}C. The table also shows weight loss values which were corrected for adsorbed moisture by applying the same correction factor (i.e., 1.5 wt%) that was used for the ZrPM-87 samples discussed in section 5.6.2.2.1. Figure 5.56 shows a plot of the corrected weight loss vs. sintering temperature for the samples. The weight loss of ~1.4 wt% for the 1600^{o}C ZrPM-94 sample was consistent with the decreased amount of zirconia observed in the XRD pattern (Figure 5.54), i.e., compared to the XRD pattern for the ZrPM-94-800-1475 powder. An additional ~0.9 wt% loss occurred after the 1800^{o}C heat treatment. This is consistent with the disappearance of the zirconia peaks in the 1800^{o}C ZrPM-94 sample (Figure 5.55). The small weight losses (<0.3 wt%) that occurred during heat treatments at temperatures above 1800^{o}C were presumably associated with CTR reactions that removed small amounts of residual oxygen from the zirconium carbide lattice.

An estimated value of the solid density of the ZrPM-94-800-1475-1900 sample was used to calculate relative densities for samples sintered in the temperature range of 1600-1950^{o}C. This was done because the CTR reaction was substantially completed after the 1600^{o}C heat treatment. Although it is obvious from the XRD patterns and the weight loss data that some limited CTR reactions still occurred at higher temperatures, the solid densities values were not expected to vary substantially for samples sintered over the range of the 1600-1950^{o}C. As noted in section 5.6.2.2.1, the actual variation in solid density values in this temperature range was probably well within the range of the error associated with the estimation of the solid density value for the 1900^{o}C ZrPM-94 sample. The solid density for this sample was estimated by assuming it was an oxygen-

free, carbon-deficient zirconium carbide, i.e., ZrC_x (where x <1). Table 5.48 shows that the carbon concentration for the ZrPM-94-800-1900 sample was 9.35 wt%. Assuming that the sample consists only of Zr and C, the calculated value for x is 0.78, i.e., the estimated formula for the carbon-deficient zirconium carbide is $ZrC_{0.78}$. The measured lattice parameter for the ZrPM-94-800-1900 sample was 0.4667 nm. (See Appendix F for details.) Using the above information, the solid density for the ZrPM-94-800-1900 sample is given by:

$$density\ of\ ZrC_{0.78} = \frac{4(1 \times 91.224 + 0.78 \times 12.01)}{(0.4667)^3 \times 6.022 \times 10^{23}} \times 10^{21} = 6.57\ g/cm^3 \quad (5\text{-}21)$$

Table 5.55 shows the bulk density values, determined from geometric measurements, and the corresponding calculated relative density values for the ZrPM-94 samples sintered at temperatures in the range of 1600-1950^{o}C. The table also lists the percentage shrinkage in the diameter and thickness for each sample. Figure 5.57 shows plots of the diameter and thickness shrinkages vs. sintering temperature for the ZrPM-94 samples. The shrinkage behavior in the range of 1600-1950^{o}C was relatively isotropic, especially for samples sintered in the range of 1800-1950^{o}C. Figures 5.58 shows plots of bulk density and relative density vs. sintering temperature based on measurements made from the geometric dimensions of the samples. The relative density value of the sample sintered at 1950^{o}C was ~ 99%.

Table 5.55 Densities (bulk and relative), percent shrinkages, and percent weight losses for sintered samples.

Pellet #	Temperature (^{o}C)	Shrinkage (%)		Bulk Density* (g/cm^{3})	Relative Density (%)	Weight Loss (wt%)	Corrected Weight Loss (wt%)
		Diameter	Thickness				
1	1600	9.89	10.73	4.11	62.6	2.87	1.37
4	1725	17.28	18.30	5.33	81.1	3.25	1.75
2	1800	19.59	20.24	5.74	87.4	3.75	2.25
3	1900	21.74	22.40	6.25	95.1	3.90	2.40
5	1950	22.78	23.47	6.49	98.8	4.02	2.52

* Determined from the sample geometric dimensions.

Table 5.56 shows open porosity, bulk density, and relative density values, determined by the Archimedes method, for some of the same samples shown in Table 5.55. The measurements for each sample were repeated at least twice. The individual and average values are listed in Table 5.56.

The open porosity values for the 1600^{o}C ZrPM-94 sintered sample is considered highly unreliable for the same reason discussed in section 5.6.2.2.2 (for the sintered 1600^{o}C ZrPM-87 sample). (The summation of the relative density and the open porosity is ~79 % which implies that the sample contains 21 % closed porosity. This is highly unlikely for a sample in the early stage of sintering.)[91] In contrast, the open porosity forthe 1800^{o}C sintered sample is more reasonable. (The summation of the open porosity and the relative density is ~96.5 %.) The reason for the apparent improvement in the ability of water to penetrate the pores in the 1800^{o}C sample compared to the 1600^{o}C

sample was not determined. However, one possibility is that coarsening of the pores (and grains) occurred at the higher temperature. Water penetration might have been enhanced in the 1800°C sample if pores with larger diameters were present. The open porosity decreased to zero for the 1900°C and 1950°C samples. This is consistent with the high relative densities of these samples.

Figure 5.59 shows plots of the bulk density (determined by the Archimedes method) and the calculated relative density as a function of sintering temperature for the ZrPM-94 samples. The calculated relative density value was ~99% for the sample sintered at 1950°C. Figure 5.60 shows plots comparing the bulk density values (for various sintering temperatures) that were determined from the Archimedes and geometric measurement methods. The two methods gave similar bulk density values at each sintering temperature.

Table 5.56 Densities (bulk and relative) and percentage open porosity for sintered samples.

Pellet #	Temperature (°C)	Open Porosity* (%)	Bulk Density* (g/cm^3)	Relative Density (%)
1	1600	14.9 (13.2, 15.7, 15.8)	4.21 (4.23, 4.21, 4.18)	64.1 (64.4, 64.1, 63.6)
2	1800	8.8 (10.9, 7.4, 8.2)	5.75 (5.79, 5.75, 5.70)	87.5 (88.1, 87.5, 86.8)
3	1900	0.0 (0.0, 0.0, 0.0)	6.23 (6.21, 6.25, 6.24)	94.8 (94.5, 95.1, 95.0)
5	1950	0.0 (0.0, 0.0)	6.47 (6.48, 6.46)	98.5 (98.6, 98.3)

* Determined by the Archimedes method. When more that one measurement was made, the individual values are listed in the parenthesis.

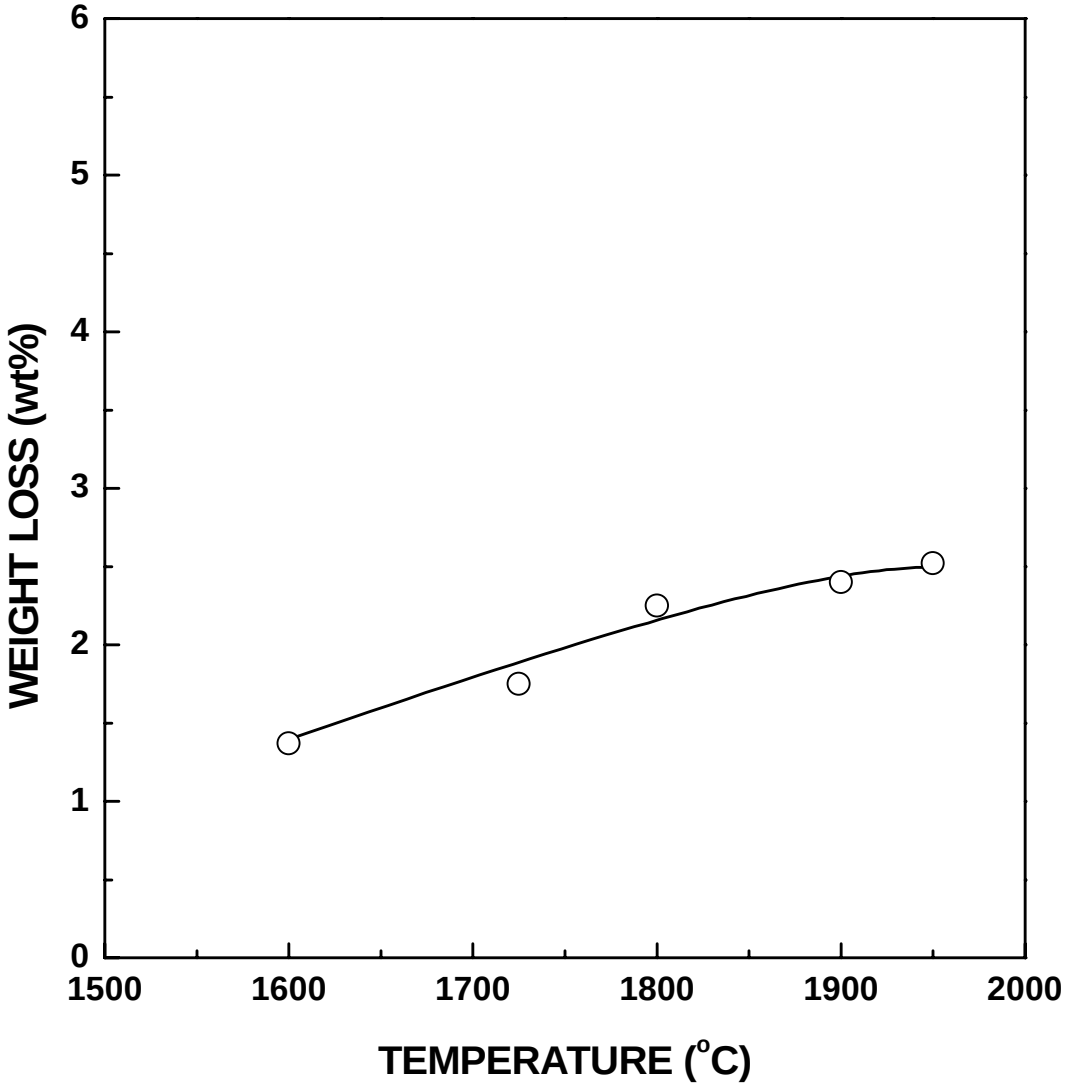

Figure 5.56 Plot of corrected weight loss vs. sintering temperature for ZrPM-94 powder compacts that were initially heat treated at 1150°C (2 h). The compacts were prepared with ZrPM-94-800-1475 powder.

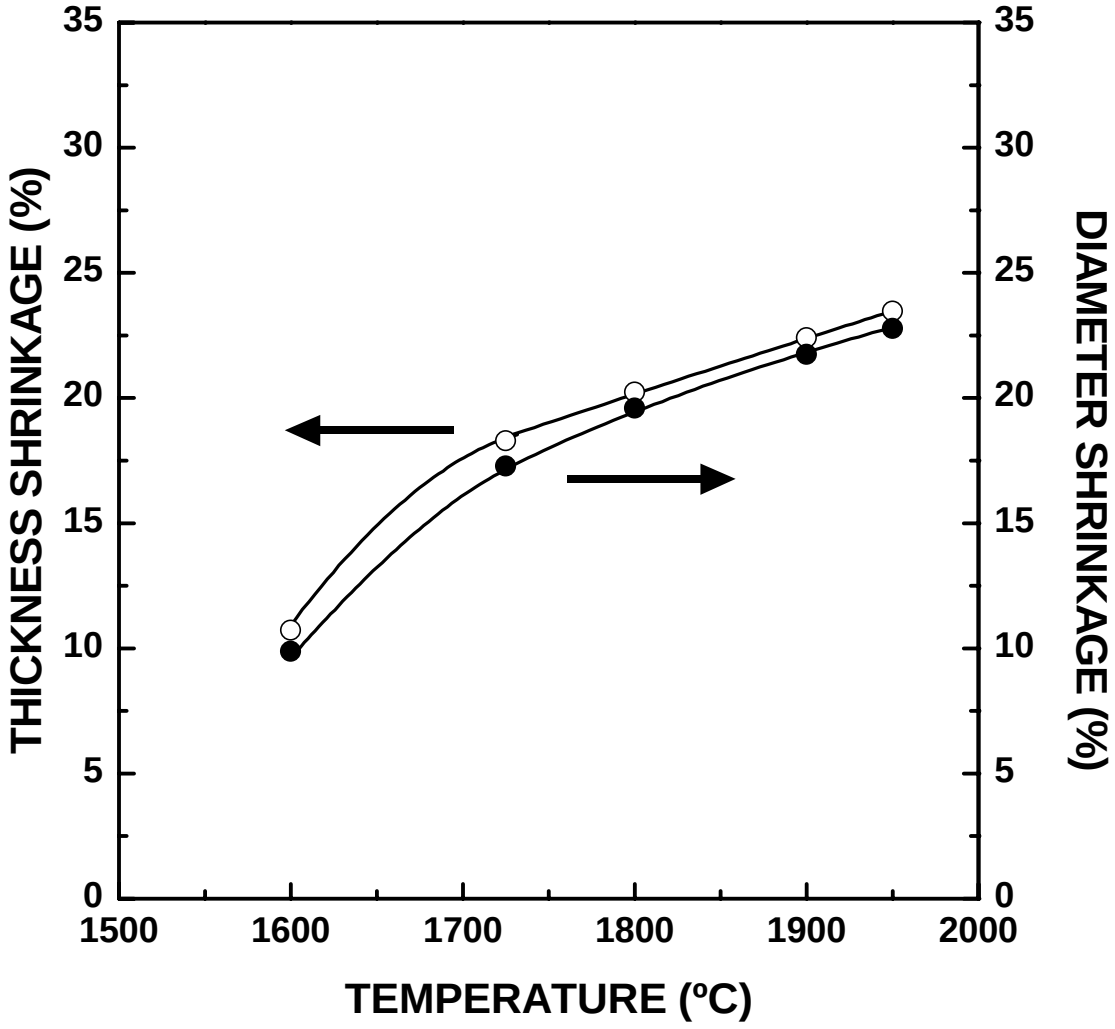

Figure 5.57 Plots of thickness and diameter shrinkage vs. sintering temperature for ZrPM-94 powder compacts that were initially heat treated at 1150°C (2 h). The compacts were prepared with ZrPM-94-800-1475 powder.

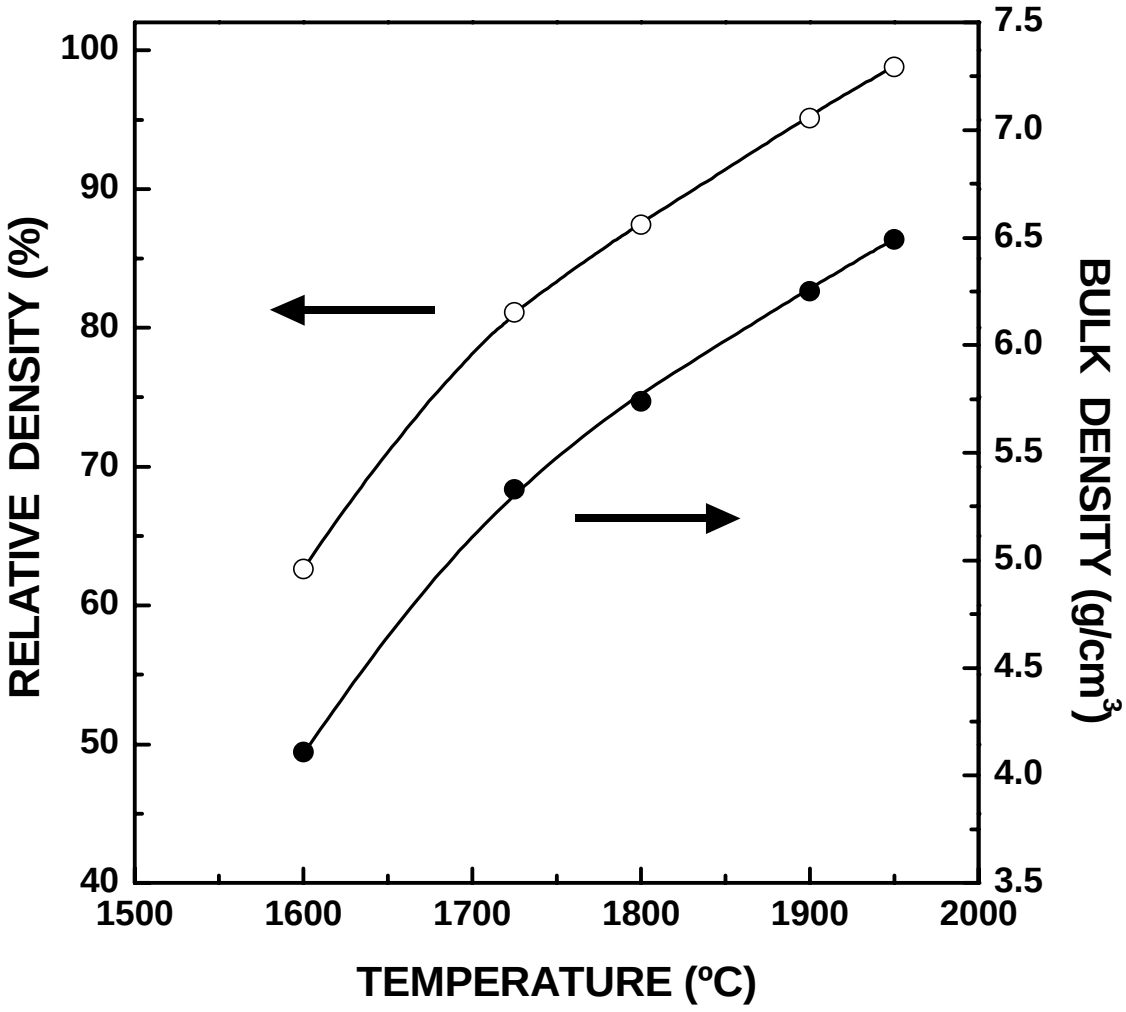

Figure 5.58 Plots of relative density and bulk density vs. sintering temperature for ZrPM-94 powder compacts that were initially heat treated at 1150°C (2 h). Bulk densities were determined by measurements of the sample dimensions.

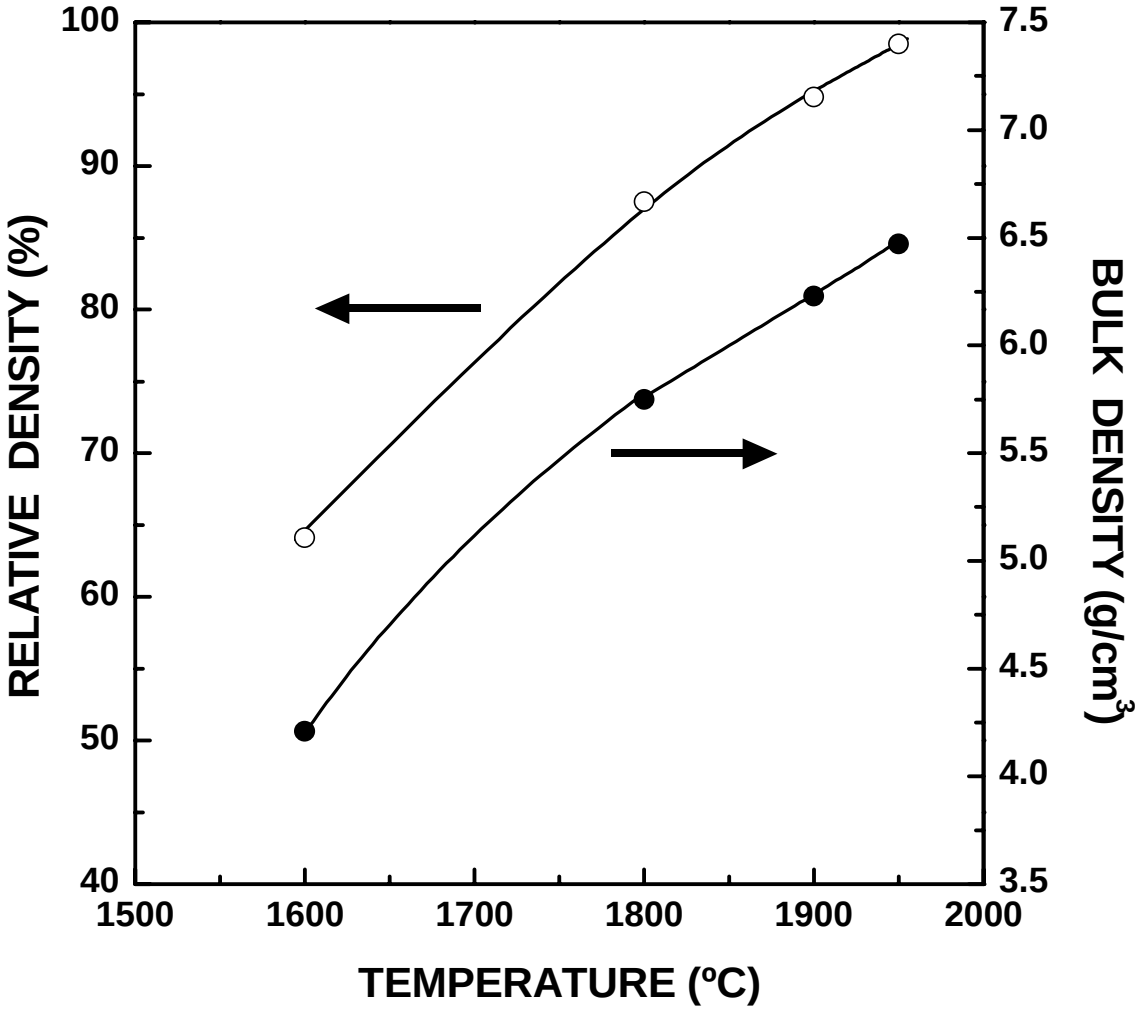

Figure 5.59 Plots of relative density and bulk density vs. sintering temperature for ZrPM-94 powder compacts that were initially heat treated at 1150°C (2 h). Bulk densities were determined by the Archimedes method.

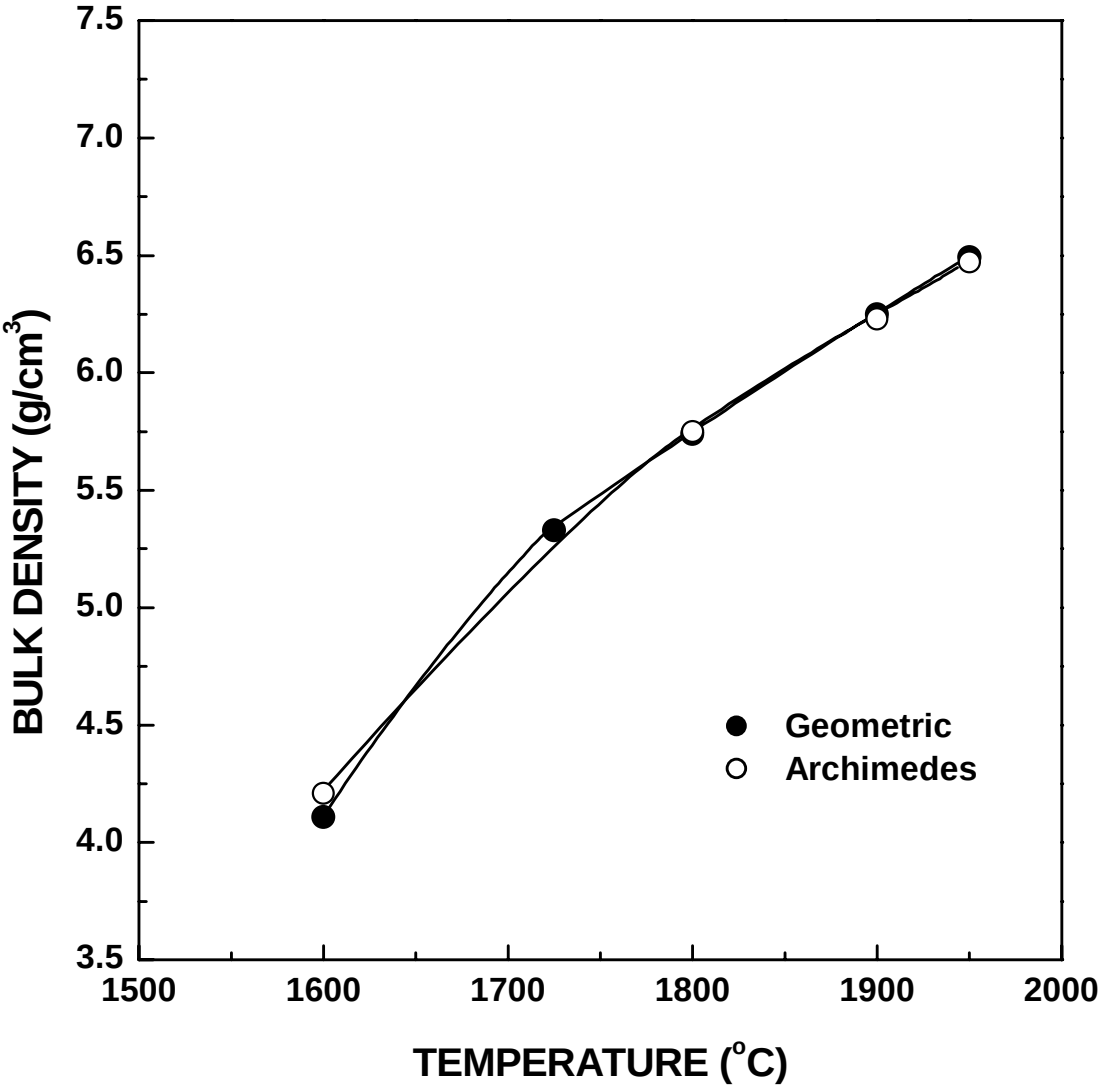

Figure 5.60 Plots of bulk density vs. sintering temperature for ZrPM-94 powder compacts that were initially heat treated at 1150°C (2 h). Bulk densities were determined by the geometric and Archimedes methods.

5.6.2.4 ZrPM-99

5.6.2.4.1 Processing Before Sintering

Dried powder was sieved and pyrolyzed exactly as described in section 5.6.2.2.1. The C/Zr molar ratio was 3.19 for a sample (initially dried at 120^{o}C) that was pyrolyzed at 1025^{o}C for 2 h. (This ratio was estimated from the carbon content of 23.7 wt% measured by Leco Corp.) The pyrolyzed sample (~8 g) was heat treated at 1475^{o}C for 2 h in a flowing argon (~500 ml/min) atmosphere in the 3-zone lindberg furnace. The specific surface area of the CTR powder was 16 m^2/g. The specific surface areas were essentially the same for the 1475^{o}C ZrPM-94 and the 1475^{o}C ZrPM-99 samples. These two samples had the same CTR heating schedule and their carbon concentrations after pyrolysis and after high temperature heat treatment (1800^{o}C and 1900^{o}C) were similar (Table E1 Appendix E).

Table 5.57 shows particle size distribution data for the 10 min-milled ZrPM-99-800-1475 powder. Particle size distribution plots are shown in Figure 5.61. The results are consistent with those discussed in section 5.6.2.3.1 in that the "carbon-rich" ZrPM-99 sample shows less aggregation compared to the corresponding "oxide-rich" ZrPM-87 (Figure 5.43) and ZrPM-94 (Figure 5.52) samples. It was suggested in section 5.2.2.3 that sintering of primary particles is inhibited in samples with more “free” carbon and/or it is promoted in samples with more “free” zirconia.

Figure 5.62 shows the XRD pattern for the ZrPM-99-800-1475 sample. The only crystalline phase present was ZrC. However, this sample should also have “free” (amorphous) carbon based on the carbon concentration (23.7 wt%) in the 1025^{o}C-pyrolyzed material. The carbon concentration for the ZrPM-99-800-1475 sample was not

measured. However, it was estimated using the measured concentrations for two other carbon-rich samples, i.e., ZrPM-45-800-1475 and ZrPM-61-350-800-1475. Table 5.58 shows that a value of 13.9 wt% carbon was estimated (by interpolation) for the ZrPM-99-800-1475 sample. Using this value and assuming that the sample consisted only of Zr and C, the estimated free carbon concentration was ~2.6 wt%.

Table 5.57 Particle size distribution data for the 10 min-milled ZrPM-99-800-1475 powder sample.

	Diameter (μm)
Mean	0.09
Modes*	0.06, 0.19
D_{90}	0.19
D_{50}	0.06
D_{10}	0.05
Standard Deviation	0.06

* Mode values are listed for each distinct peak in the accompanying relative frequency plot.

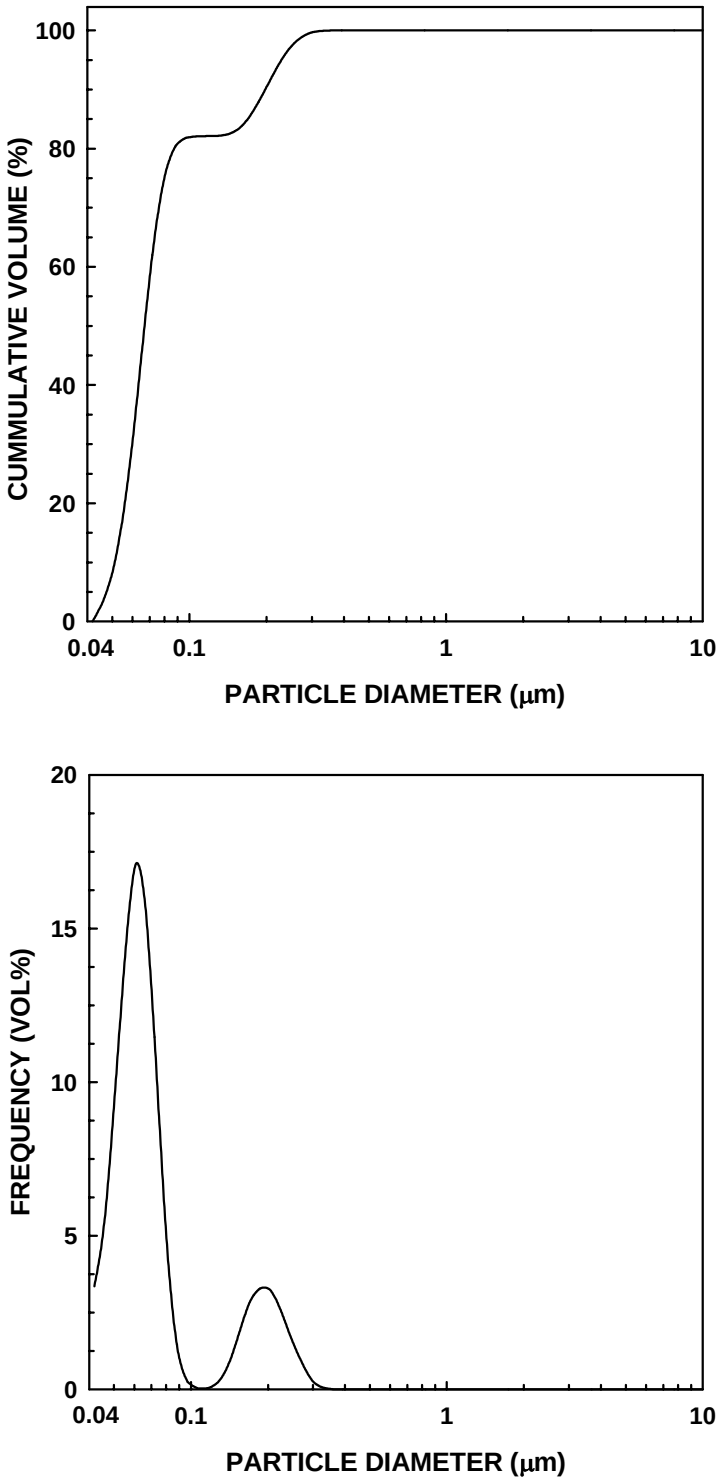

Figure 5.61 Particle size distribution for the 10 min-milled ZrPM-99-800-1475 powder sample: cumulative frequency plot (top) and relative frequency plot (bottom).

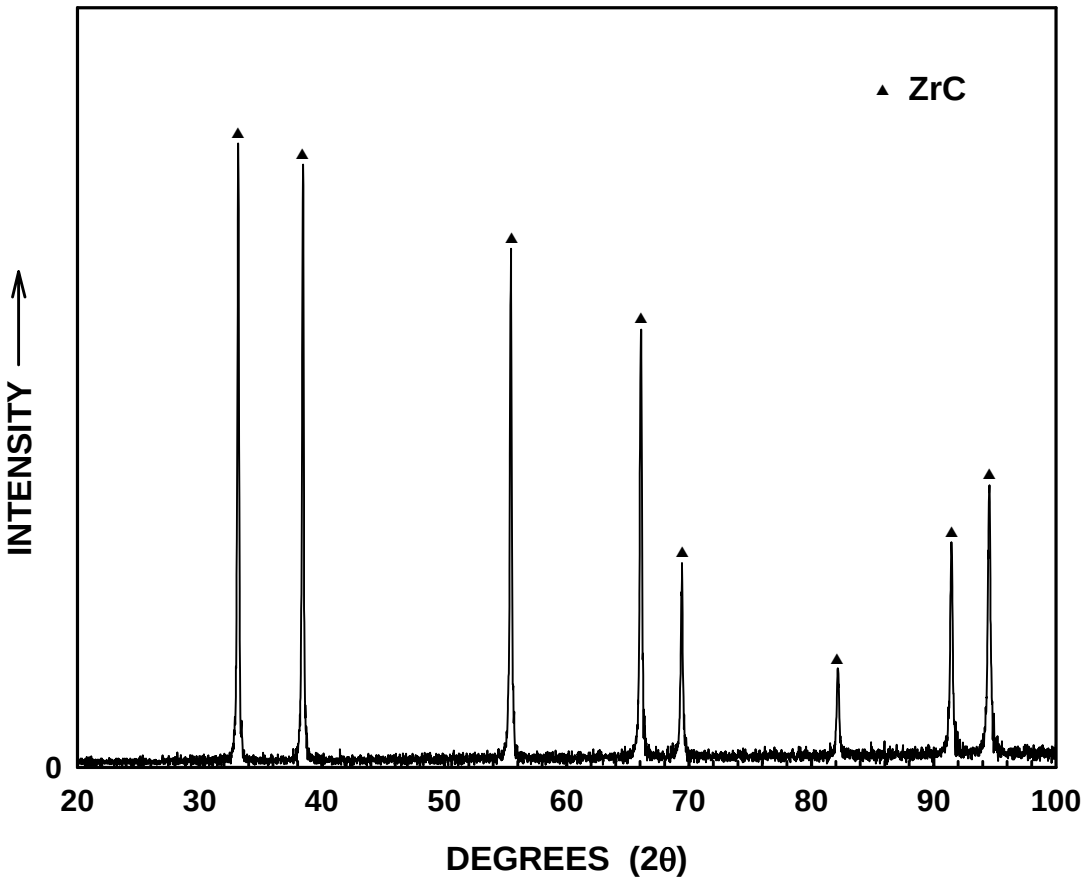

Figure 5.62 X-ray diffraction pattern for ZrPM-99-800 pyrolyzed sample that was heat treated at 1475°C (2 h).

Table 5.58 Carbon concentrations of ZrPM-45, ZrPM-61, and ZrPM-97 pyrolyzed and CTR powders.

Sample	Temperature (°C)	Total Carbon (wt%)
ZrPM-45	1025	23.3
ZrPM-99	1025	23.7
ZrPM-61-350	1025	27.1
ZrPM-45-800	1475	13.3
ZrPM-99-800	1500	13.9 (interpolated)
ZrPM-61-350-800	1475	19.4

The measured lattice parameter for ZrPM-99-800-1475 sample was 0.4697 nm. (See Appendix F for details.) The value of the lattice parameter is close to the stoichiometric value reported for ZrC. Assuming that there was no dissolved oxygen in the lattice, the solid density of ZrC is given by:

$$\frac{4(1\times 91.224+1\times 12.01)}{(0.4697)^3\times\ 6.022\times 10^{23}}\times 10^{21}\ = 6.62\ g/cm^3 \qquad (5\text{-}22)$$

The solid density of the ZrPM-99-800-1475 sample was estimated with the following assumptions: (i) The zirconium carbide phase was oxygen-free and had the stoichiometric composition. The solid density of the ZrC phase was given by equation 5-22. (ii) The "free" carbon concentration was 2.6 wt% and the carbon density was 2 g/cm^3. Based on these assumptions, the solid density of the ZrPM-99-800-1475 powder is given by:

$$\frac{100}{\frac{97.4}{6.62}+\frac{2.6}{2}}\ = 6.25\ g/cm^3 \qquad (5\text{-}23)$$

The pressing and processing conditions for powder compacts were exactly same as described in section 5.6.2.2.1. The bulk densities of these samples, determined from geometric dimensions, are shown in Table 5.59. (The relative densities were calculated using the solid density value given in equation 5-23.) The percentage weight losses due to binder burnout are also shown in Table 5.59. The weight losses due to the binder burnout

Table 5.59 Compact densities after dry pressing and compact density and weight loss after 1150°C heat treatment.

Pellet #	As-Dry Pressed		Weight (g) (As-Dry Pressed)	After 1150°C (2 h)		% Weight Loss
	Bulk Density (g/cm^3)	Relative Density (%)		Bulk Density (g/cm^3)	Relative Density (%)	
1	2.97	47.5	0.4118	2.92	46.7	1.7
2	2.99	47.8	0.4127	2.93	46.9	2.1
3	2.98	47.7	0.4199	2.92	46.7	2.0
4	2.98	47.7	0.4131	2.92	46.7	2.2
5	2.99	47.8	0.4153	2.94	47.0	2.1
Average	2.98	47.7	-	2.93	46.9	2.0

were essentially the same as observed for the ZrPM-87 and ZrPM-94 samples (sections 5.6.2.2.1 and 5.6.2.3.1). Bulk density and relative density values after binder burnout, determined from geometric dimensions, are also shown in Table 5.59.

5.6.2.4.2 Sintering/Heat Treatment

Figures 5.63 and 5.64 show XRD patterns for the ZrPM-99-800-1475 powder and for samples sintered at temperatures in the range of 1600°C to 1950°C. Zirconium carbide was the only crystalline phase observed in the samples heat treated at temperatures ≥1475°C.

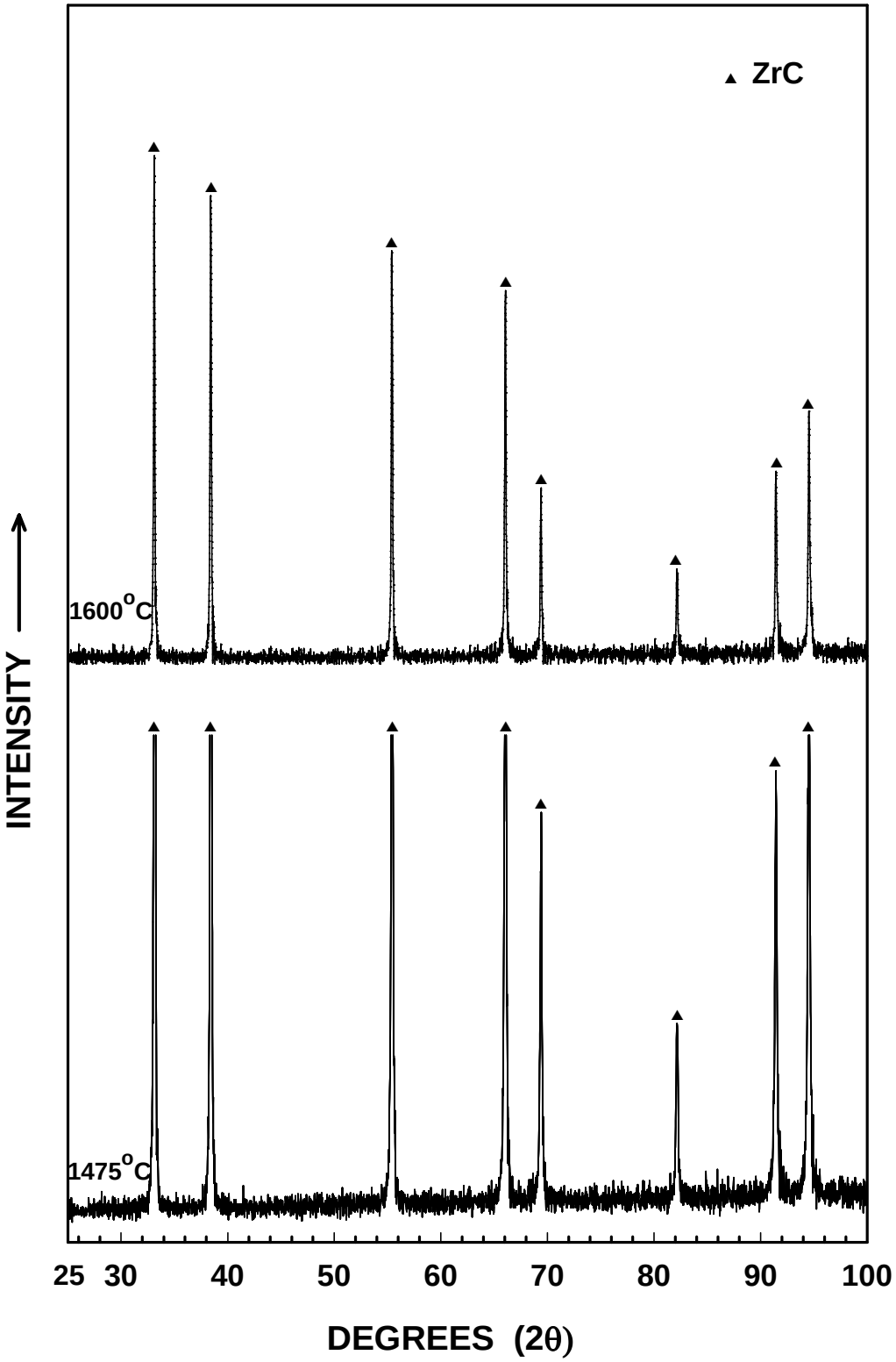

Figure 5.63 X-ray diffraction patterns for ZrPM-99 samples heat treated at temperatures in the range of 1475 to 1600°C.

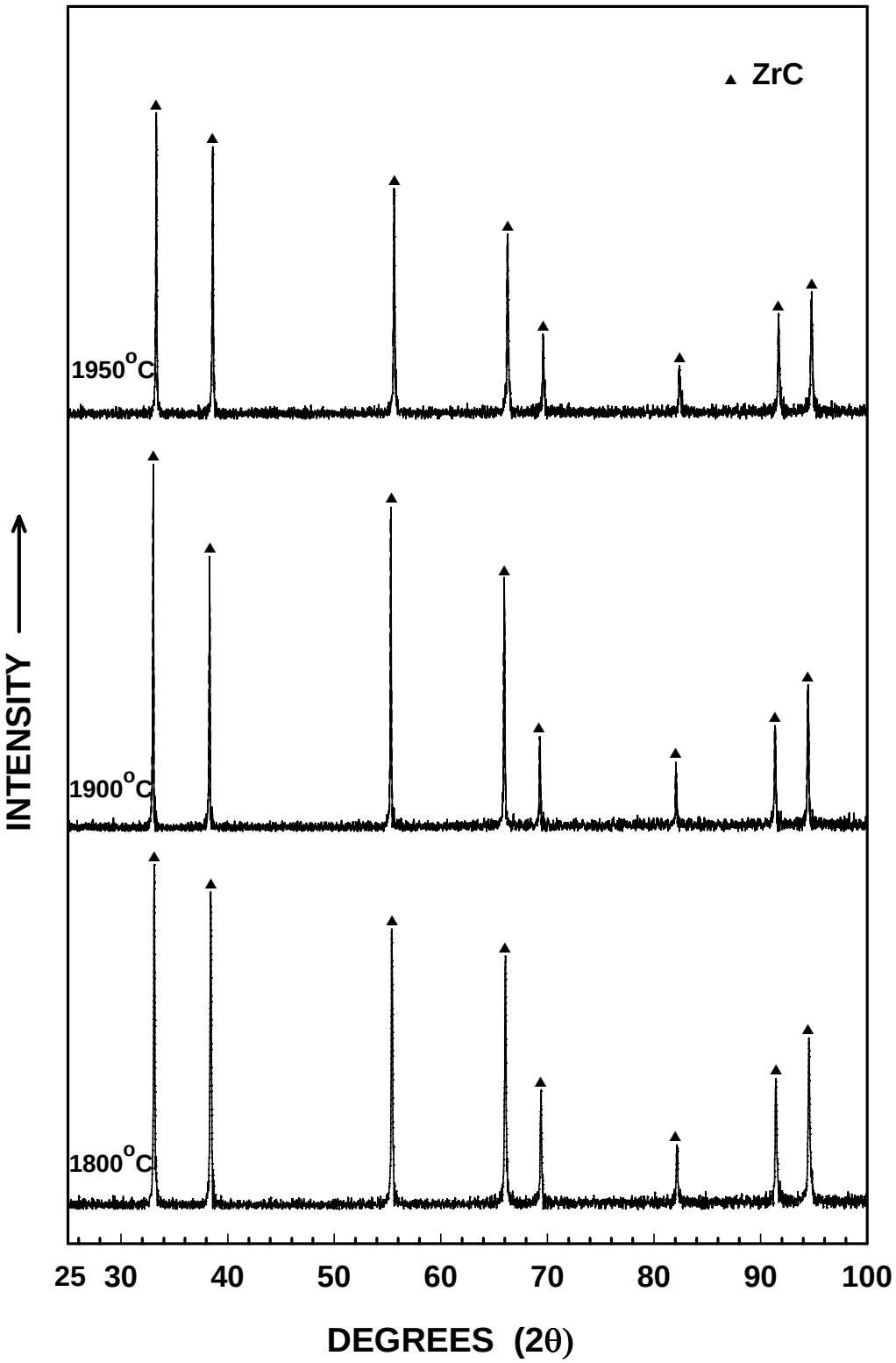

Figure 5.64 X-ray diffraction patterns for ZrPM-99 samples heat treated at temperatures in the range of 1800 to 1950°C.

Table 5.60 lists percentage weight losses for ZrPM-99-800-1475 powder compacts which were sintered at temperatures in the range of 1600-1950°C. The table also shows weight loss values which were corrected for adsorbed moisture by applying the same correction factor (i.e., 1.5 wt%) that was used for the ZrPM-87 samples discussed in section 5.6.2.2.1. Figure 5.65 shows a plot of the corrected weight loss vs. sintering temperature for the samples. The weight loss of ~2.5 wt% for the 1600°C ZrPM-99 was presumably due to CTR reactions in which oxygen dissolved the ZrC lattice was removed. The small additional weight losses (~0.8 wt%) that occurred for heat treatments above 1600°C were also presumably associated with the same type of CTR reactions. The high temperature weight loss behavior is similar to that observed in a sample with similar pyrolyzed composition, i.e., ZrPM-45-800-1475 (section 5.2.1.3), in that most of the weight loss was completed after the 1600°C heat treatment.

An estimated value of the solid density of the ZrPM-99-800-1475-1900 sample was used to calculate relative densities for samples sintered in the temperature range of 1600-1950°C. This was done because the CTR reaction was substantially completed after the 1600°C heat treatment. Although the weight loss data show that some limited CTR reactions still occurred at higher temperatures, the solid densities values were not expected to vary substantially for samples sintered over the range of the 1600-1950°C. As noted in section 5.6.2.2.2, the actual variation in solid density values in this temperature range was probably well within the range of the error associated with the estimation of the solid density value for the 1900°C ZrPM-99 sample. The solid density for this sample was estimated by assuming it was an oxygen-free, carbon-deficient

zirconium carbide, i.e., ZrC_x (where x <1). Table 5.48 shows that the carbon concentration for the ZrPM-94-800-1900 sample was 10.8 wt%. Assuming that the sample consisted only of Zr and C, the calculated value for x is 0.92, i.e., the estimated formula for the carbon-deficient zirconium carbide is $ZrC_{0.92}$. The measured lattice parameter for the ZrPM-99-800-1900 sample was 0.4696 nm. (See Appendix F for details.) Using the above information, the solid density for the ZrPM-94-800-1900 sample is given by:

$$\frac{4(1\times 91.224 + 0.92\times 12.01)}{(0.4696)^3 \times\ 6.022\times 10^{23}} \times 10^{21} = 6.56\ g/cm^3 \qquad (5\text{-}24)$$

Table 5.60 shows the bulk density values, determined from geometric measurements, and the corresponding calculated relative density values for the ZrPM-99 samples sintered at temperatures in the range of 1600-1950^{o}C. The table also lists the percentage shrinkage in the diameter and thickness for each sample. Figure 5.66 shows plots of the diameter and thickness shrinkages vs. sintering temperature. The shrinkage behavior in the range of 1600-1950^{o}C showed some anisotropy, especially for the 1900^{o}C and 1950^{o}C samples. This behavior was consistent with the results in sections 5.6.1.1.2 (Table 5.38) and 5.6.1.3.2 (Table 5.42) in that more shrinkage anisotropy was observed in samples with "carbon-rich" compositions. Figure 5.67 shows plots of bulk density and relative density vs. sintering temperature, based on measurements from geometric dimensions, of the samples. The relative density value of the sample sintered at 1950^{o}C was close to 100%.

Table 5.60 Densities (bulk and relative), percent shrinkages, and percent weight losses for sintered samples.

Pellet #	Temperature (^{o}C)	Shrinkage (%)		Bulk Density* (g/cm^{3})	Relative Density (%)	Weight Loss (wt%)	Corrected Weight Loss (wt%)
		Diameter	Thickness				
3	1600	10.47	12.15	4.04	61.6	3.95	2.45
4	1725	18.01	19.56	5.24	79.9	4.13	2.63
1	1800	22.20	22.98	6.06	92.4	4.58	3.08
2	1900	23.15	25.98	6.50	99.1	4.70	3.20
5	1950	23.14	26.16	6.53	99.5	4.71	3.21

* Determined from the sample dimensions.

Table 5.61 shows open porosity, bulk density, and relative density values, determined by the Archimedes method, for the some of the samples shown in Table 5.60 The measurements for each sample were repeated at least twice. The individual and average values are listed in Table 5.61.

The open porosity value for the 1600^{o}C ZrPM-99 sintered sample is considered unreliable for the same reason discussed in section 5.6.2.2.2. (The summation of the relative density and the open porosity is ~91% which implies that the sample contains 9% closed porosity. This does not seem likely for a sample in the early stage of sintering.)[91] The open porosity value for the sample sintered at 1800^{o}C is more reasonable. However, it is somewhat surprising that the calculated closed porosity (i.e., ~0.4%) is so low in a sample sintered to ~91% relative density. (The calculated closed porosity is given by: [100 - relative density - open porosity].) If the open porosity value

is accurate, this suggests that the estimated solid density used to calculate the relative density may have been too low. The open porosity decreased to zero for the 1900°C and 1950°C sintered samples. This is consistent with the high relative densities for these samples.

Figure 5.68 shows plots of the bulk density (determined by the Archimedes method) and the calculated relative density as a function of sintering temperature for the ZrPM-97 samples. The calculated relative density value was ~100% for the sample sintered at 1950°C. However, as noted earlier, the solid density used for the relative density calculation may have been too low. Nevertheless, it is still clear that high relative densities were obtained in these samples. Figure 5.69 shows plots comparing the bulk density values (for various sintering temperatures) that were determined from the Archimedes and geometric measurement methods. The two methods gave similar bulk density values for samples sintered at temperatures in the range of 1725-1950°C.

Table 5.61 Densities (bulk and relative) and percentage open porosity for sintered samples.

Pellet #	Temperature (°C)	Open Porosity* (%)	Bulk Density* (g/cm^3)	Relative Density (%)
3	1600	26.4 (25.7, 26.9, 26.6)	4.22 (4.22, 4.33, 4.10)	64.3 (64.3, 66.0, 62.5)
1	1800	8.6 (9.2, 7.9)	5.97 (6.00, 5.94)	91.0 (91.5, 90.5)
2	1900	0.0 (0.0, 0.0)	6.53 (6.53, 6.53)	99.5 (99.5, 99.5)
5	1950	0.0 (0.0, 0.0)	6.55 (6.54, 6.55)	99.8 (99.7, 99.8)

* Determined by the Archimedes method. When more that one measurement was made, the individual values are listed in the parenthesis.

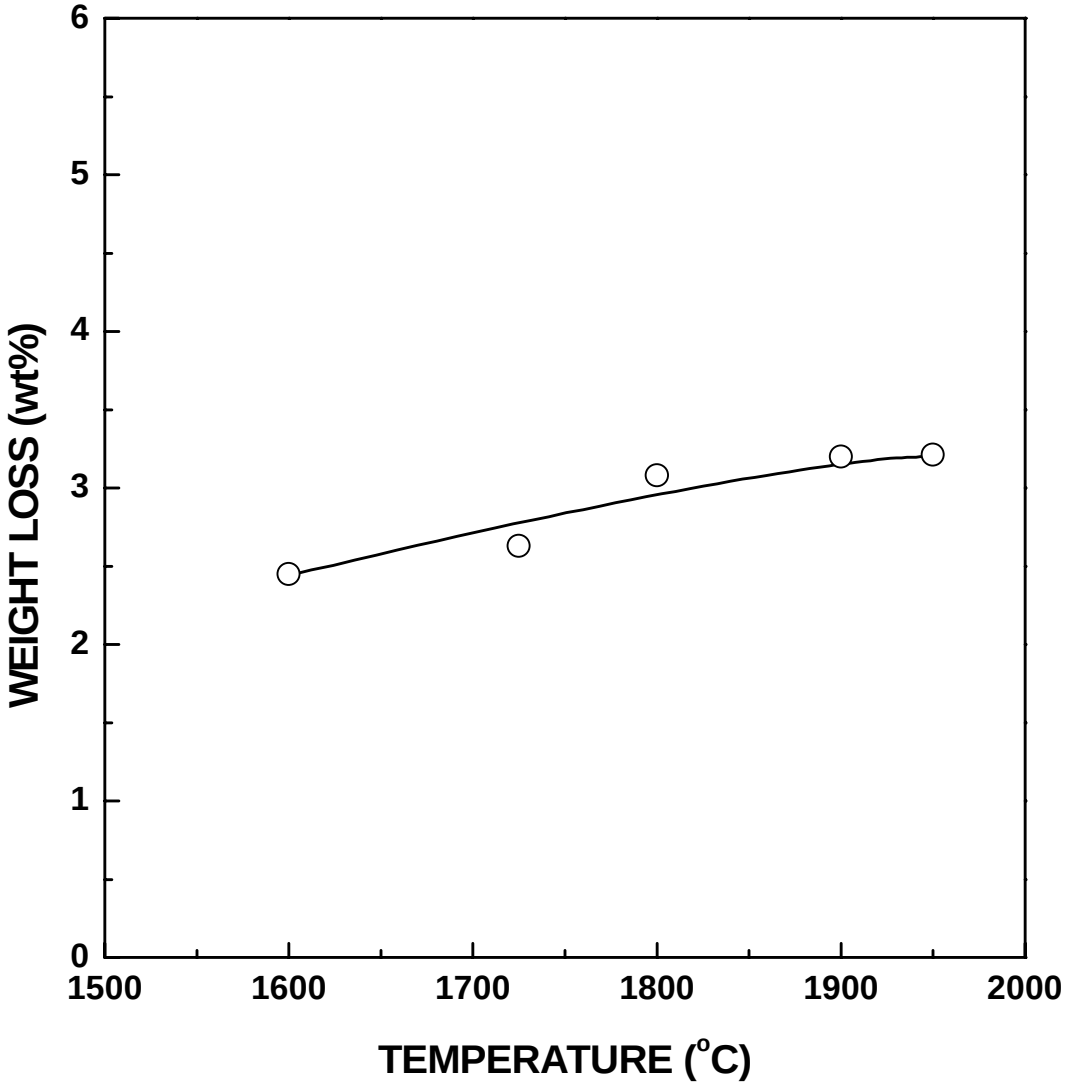

Figure 5.65 Plot of corrected weight loss vs. sintering temperature for ZrPM-99 powder compacts that were initially heat treated at 1150°C (2 h). The compacts were prepared with ZrPM-99-800-1475 powder.

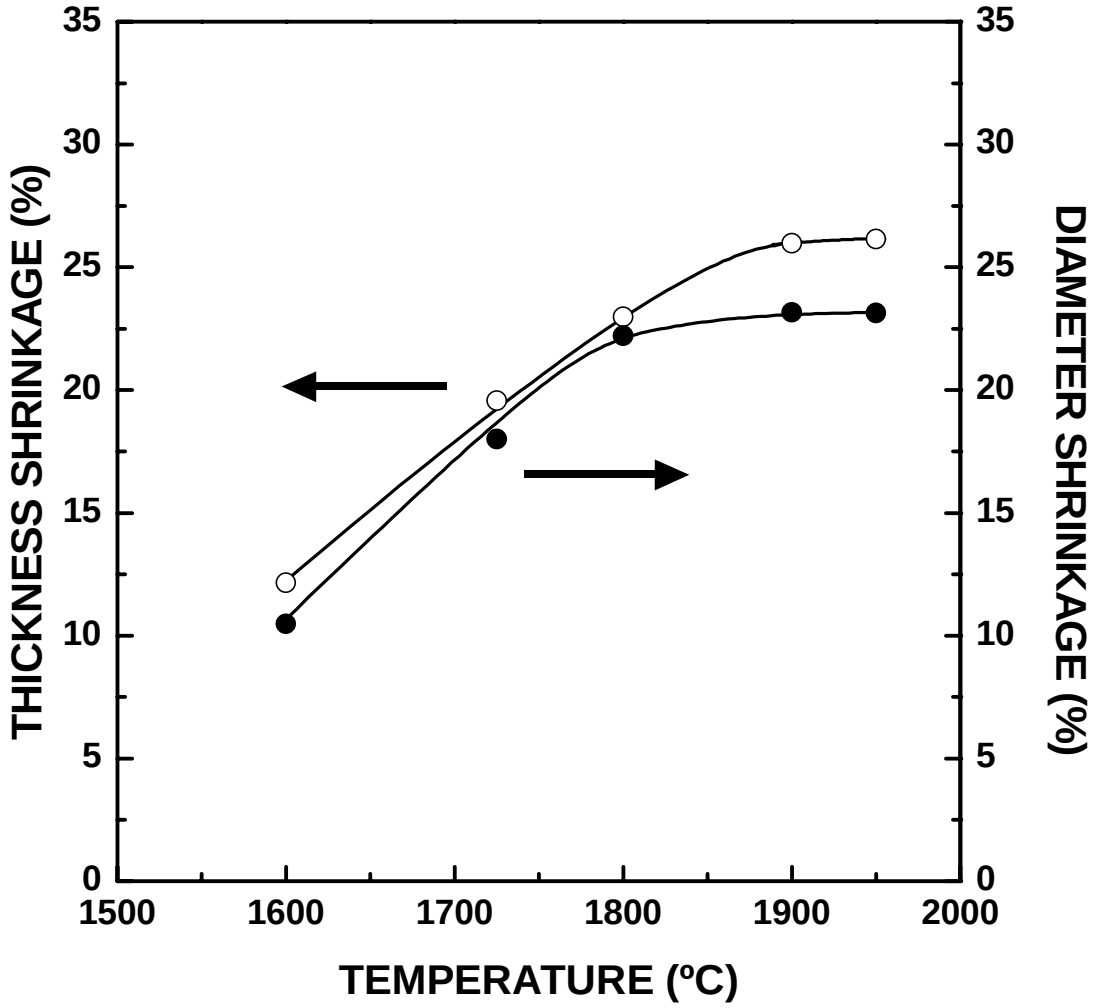

Figure 5.66 Plots of thickness and diameter shrinkage vs. sintering temperature for ZrPM-99 powder compacts that were initially heat treated at 1150°C (2 h). The compacts were prepared with ZrPM-99-800-1475 powder.

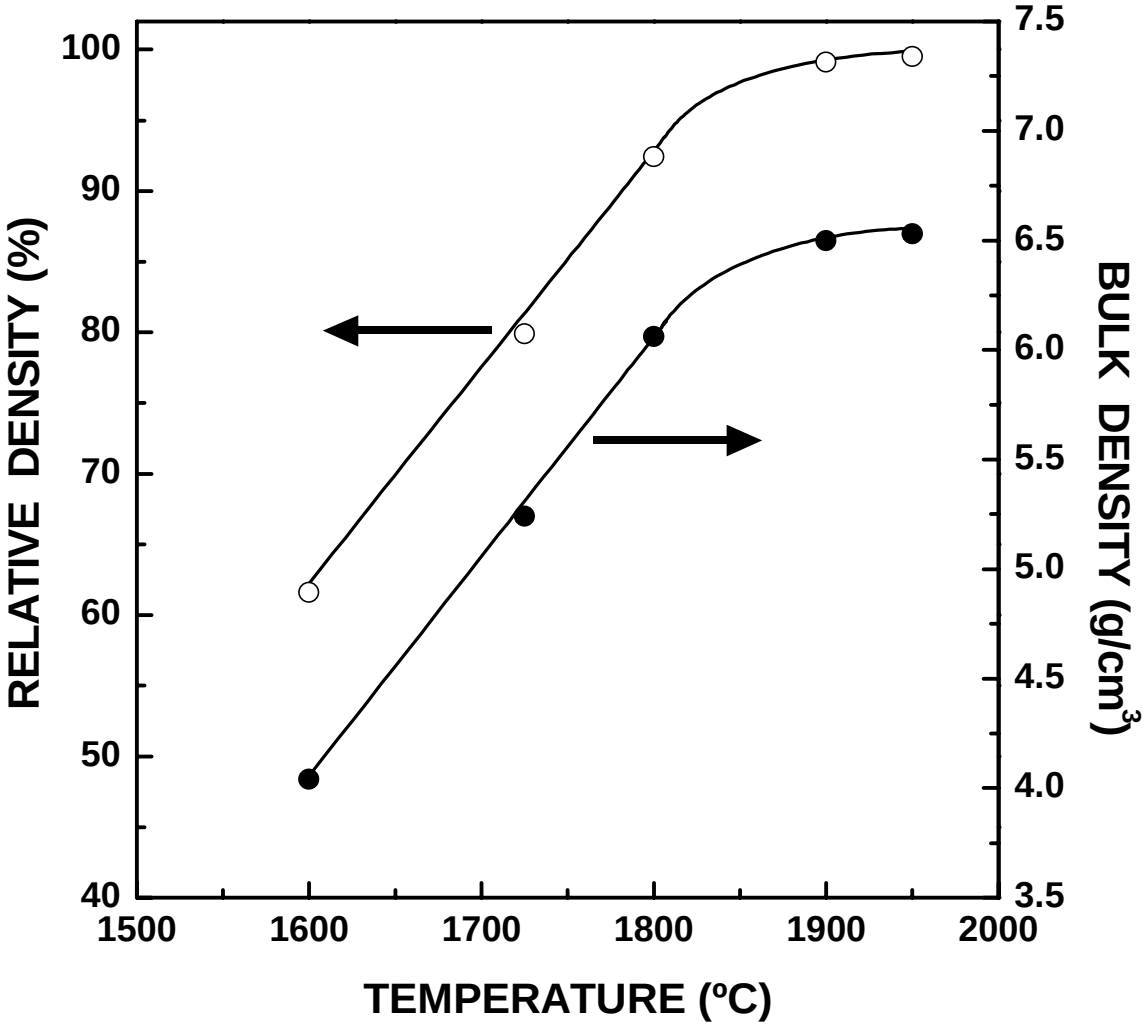

Figure 5.67 Plots of relative density and bulk density vs. sintering temperature for ZrPM-99 powder compacts that were initially heat treated at 1150°C (2 h). Bulk densities were determined by measurements of the sample dimensions.

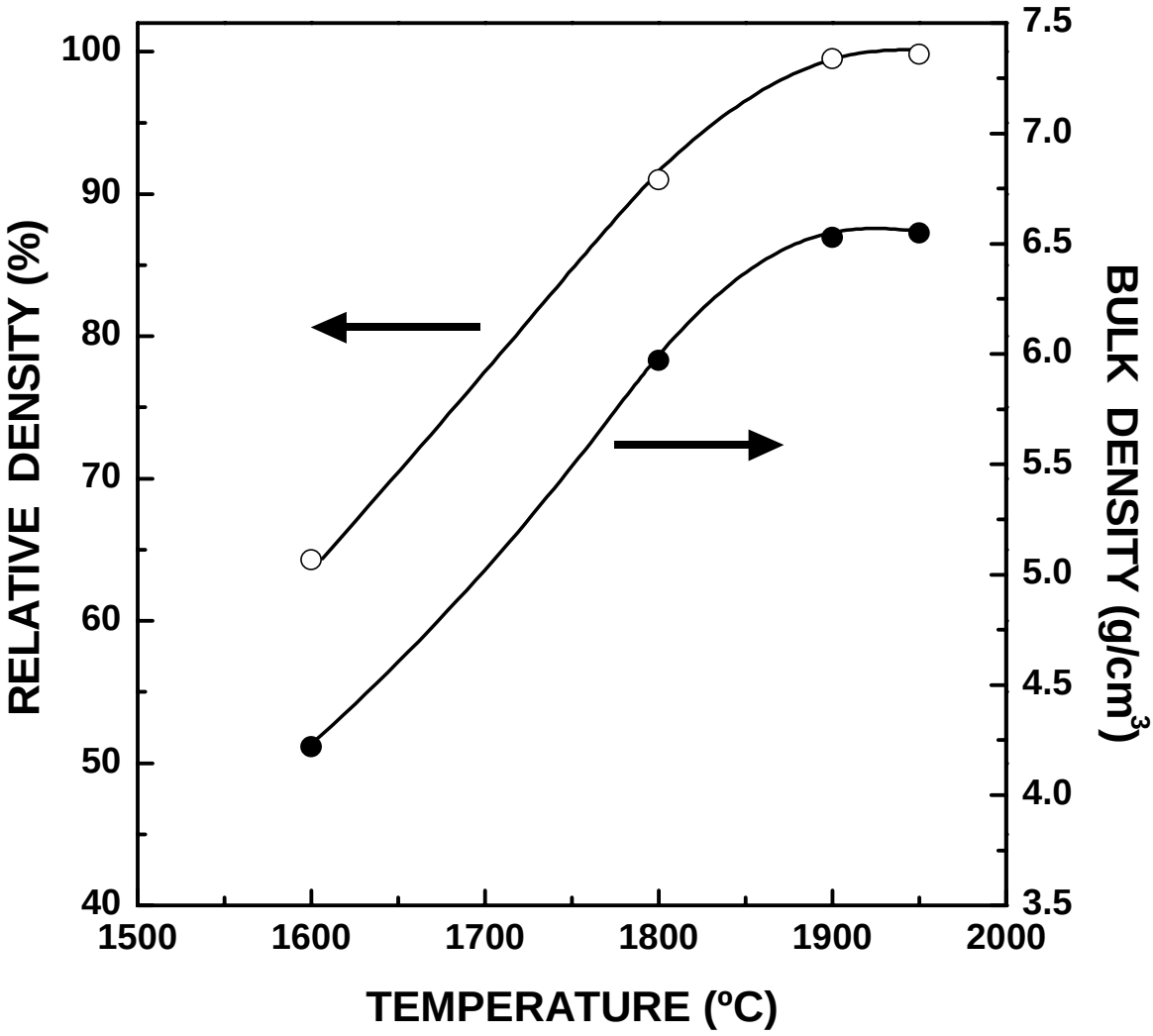

Figure 5.68 Plots of relative density and bulk density vs. sintering temperature for ZrPM-99 powder compacts that were initially heat treated at 1150°C (2 h). Bulk densities were determined by the Archimedes method.

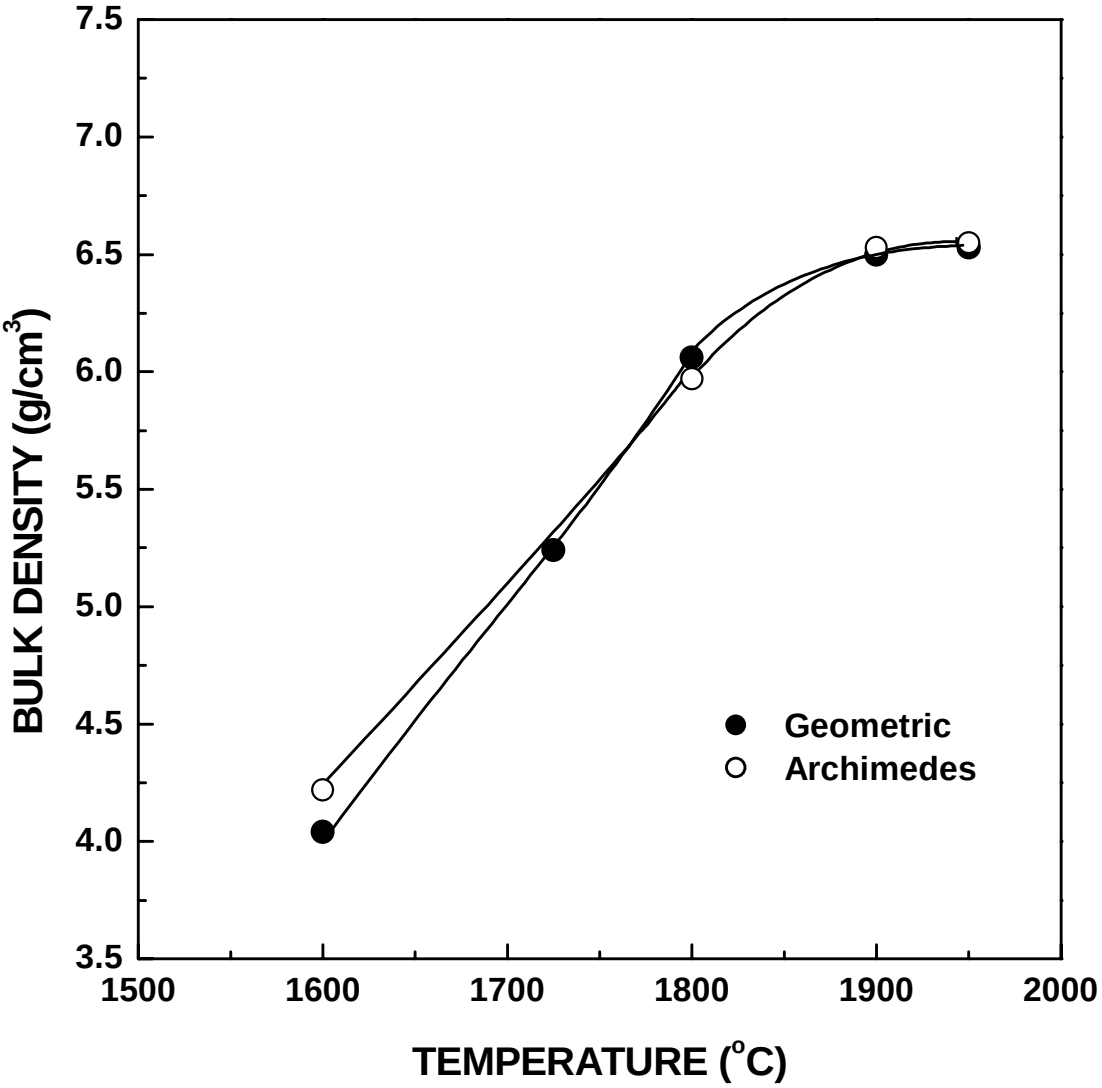

Figure 5.69 Plots of bulk density vs. sintering temperature for ZrPM-99 powder compacts that were initially heat treated at 1150°C (2 h). Bulk densities were determined by the geometric and Archimedes methods.

5.6.2.5 ZrPM-97

5.6.2.5.1 Processing Before Sintering

Dried powder was sieved and pyrolyzed exactly as described in section 5.6.2.2.1. The C/Zr molar ratio was 3.25 for a sample (initially dried at 120^{o}C) that was pyrolyzed at 1025^{o}C for 2 h. (This ratio was estimated from the carbon content of 24.1 wt% measured by Leco Corp.) The pyrolyzed sample (~8 g) was heat treated at 1500^{o}C for 2 h in a flowing argon (~500 ml/min) atmosphere in the 3-zone lindberg furnace. The specific surface area of the CTR powder was 30 m^2/g.

The ZrPM-97-800-1500 sample had higher specific surface area than the ZrPM-87-800-1425 (24 m^2/g), ZrPM-94-800-1475 (16 m^2/g), and ZrPM-99-800-1475 (16 m^2/g) samples even though the CTR temperature was the highest among the four samples (i.e., 1500^{o}C vs. 1425-1475^{o}C). This is attributed to the carbon-rich composition of the ZrPM-97 sample. It is expected that the ZrPM-97 sample had more “free” carbon compared to the other samples.

Table 5.62 shows particle size distribution data for the 10 min-milled ZrPM97-800-1500 powder. Particle size distribution plots are shown in Figure 5.70. The results are consistent with those discussed in section 5.6.2.3.1 in that the "carbon-rich" ZrPM-97 sample shows less aggregation compared to the corresponding "oxide-rich" ZrPM-87 (Figure 5.44) and ZrPM-94 (Figure 5.53) samples. It was suggested in section 5.2.2.3 that sintering of primary particles is inhibited in samples with more “free” carbon and/or it is promoted in samples with more free zirconia.

Figure 5.71 shows the XRD pattern for the ZrPM-97-800-1500 sample. The only crystalline phase present was ZrC. However, this sample should also have “free”

(amorphous) carbon based on the carbon concentration (24.1 wt%) in the 1025°C-pyrolyzed material. The carbon concentration for the ZrPM-97-800-1500 sample was not measured. However, it was estimated using the measured concentrations for two other carbon-rich samples, i.e., ZrPM45-800-1475 and ZrPM61-350-800-1475. Table 5.63 shows that a value of 14.6 wt% carbon was estimated (by interpolation) for the ZrPM-97-800-1500 sample. Using this value and assuming that the sample consisted only of Zr and C, the estimated "free" carbon concentration was ~3.4 wt%.

Table 5.62 Particle size distribution data for milled ZrPM-97-800-1500 powder sample.

	Diameter (μm)
Mean	0.08
Modes*	0.06, 0.19
D_{90}	0.18
D_{50}	0.06
D_{10}	0.05
Standard Deviation	0.06

* Mode values are listed for each distinct peak in the accompanying relative frequency plot.

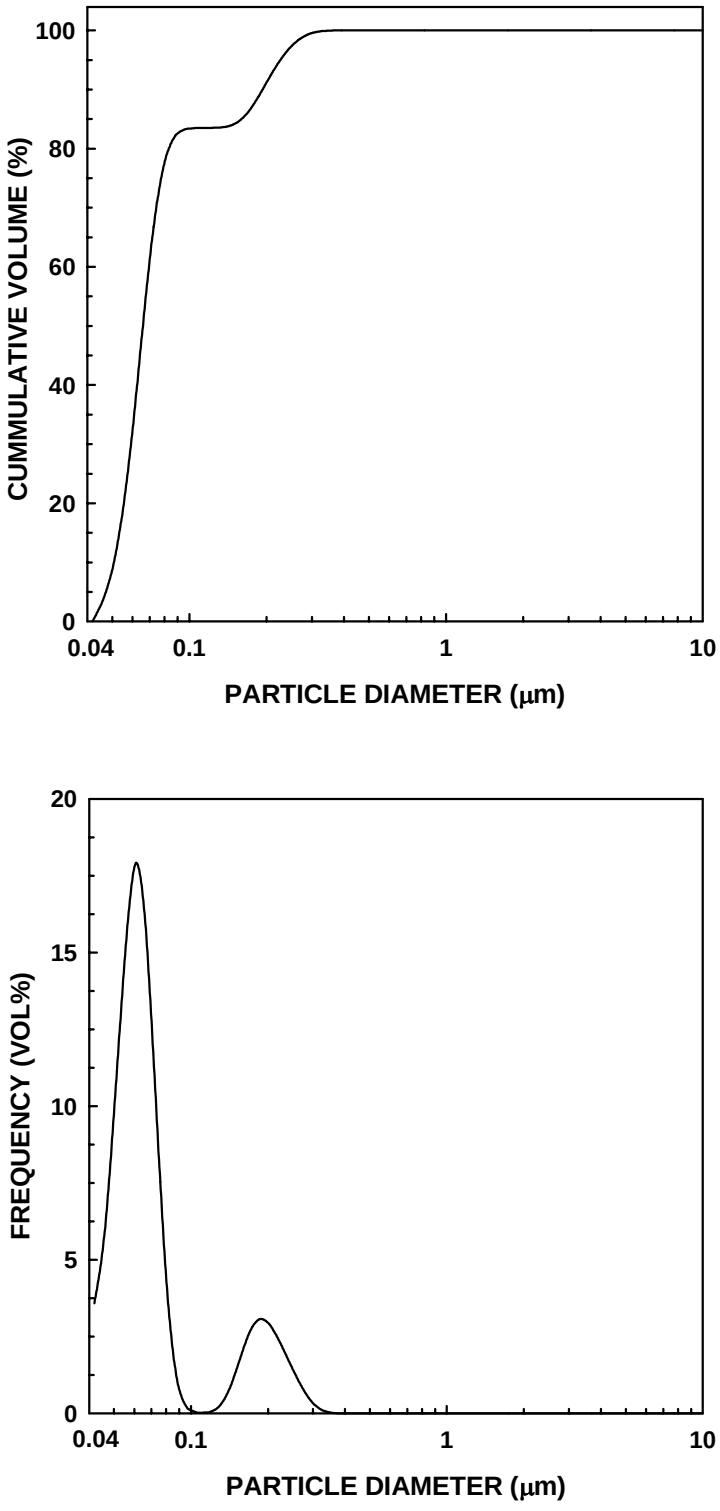

Figure 5.70 Particle size distribution plots for the 10 min-milled ZrPM-97-800-1500 powder sample: cumulative frequency plot (top) and relative frequency plot (bottom).

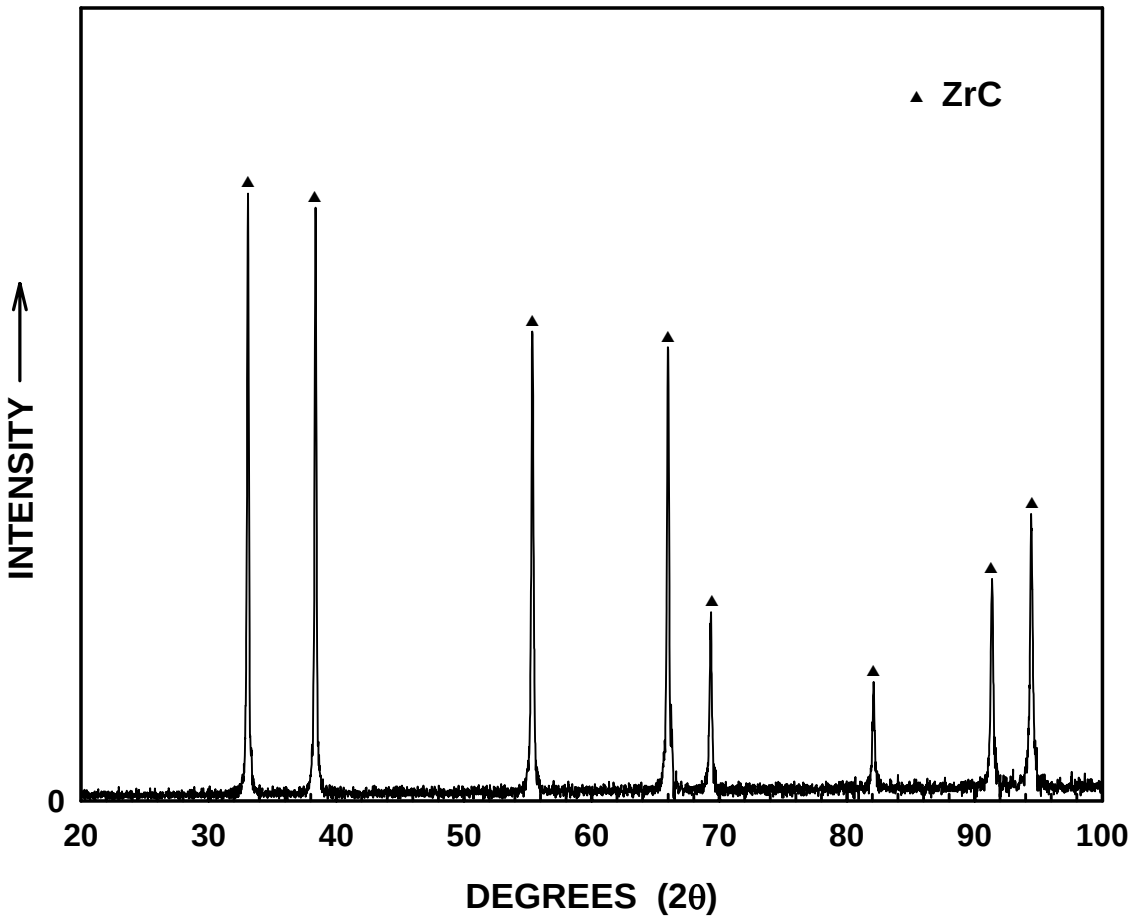

Figure 5.71 X-ray diffraction pattern for a ZrPM-97-800 pyrolyzed sample that was heat treated at 1500°C (2 h).

The measured lattice parameter for the ZrPM-97-800-1500 sample was 0.4697 nm. (See Appendix F for details.) The value of the lattice parameter is close to the stoichiometric value reported for ZrC. Assuming that there was no dissolved oxygen in the lattice, the solid density of the ZrC is given by:

$$\frac{4(1\times 91.224 + 1\times 12.01)}{(0.4697)^3 \times\ 6.022\times 10^{23}}\times 10^{21} = 6.62\ g/cm^3 \qquad (5\text{-}25)$$

The solid density of the ZrPM-97-800-1500 sample was estimated with the following assumptions: (i) The zirconium carbide phase was oxygen-free and had a stoichiometric (ZrC) composition. The solid density of the ZrC phase was given by equation 5-25. (ii) The "free" carbon concentration was 3.4 wt% and the carbon density was 2 g/cm^3. Therefore, the solid density of ZrPM-97-800-1500 material is given by:

$$\frac{100}{\frac{96.6}{6.62}+\frac{3.4}{2}} = 6.14\ g/cm^3 \qquad (5\text{-}26)$$

The pressing and processing conditions for the powder compacts were exactly same as described in section 5.6.2.2.1. The bulk densities of these samples, determined from geometric dimensions, are shown in Table 5.64. (The relative densities were calculated using the solid density value given in equation 5-26.) The percentage weight

Table 5.63. Carbon concentrations of ZrPM-45, ZrPM-61, and ZrPM-97 pyrolyzed and CTR powders.

Sample	Temperature (^{o}C)	Total Carbon (wt%)
ZrPM-45	1025	23.3
ZrPM-97	1025	24.1
ZrPM-61-350	1025	27.1
ZrPM-45-800	1475	13.3
ZrPM-97-800	1500	14.6 (interpolated)
ZrPM-61-350-800	1475	19.4

Table 5.64 Compact densities after dry pressing and compact density and weight loss after 1150°C heat treatment.

Pellet #	As-Dry Pressed		Weight (g) (As-Dry Pressed)	After 1150°C (2 h)		% Weight Loss
	Bulk Density (g/cm^3)	Relative Density (%)		Bulk Density (g/cm^3)	Relative Density (%)	
1	2.74	44.6	0.4140	2.57	41.9	2.4
2	2.73	44.5	0.4127	2.58	42.0	2.3
3	2.73	44.5	0.4140	2.58	42.0	2.3
4	2.73	44.5	0.4127	2.60	42.3	2.0
5	2.75	44.8	0.4192	2.61	42.5	2.0
Average	2.74	44.6	-	2.59	42.2	2.2

losses due to binder burnout are also shown in Table 5.64. The weight losses due to the binder burnout were essentially the same as observed for the corresponding ZrPM-87, ZrPM-94, and ZrPM-99 samples: (sections 5.6.2.2.1-5.6.2.4.1). Bulk density and relative density values after binder burnout, determined from geometric dimensions, are also shown in Table 5.64.

5.6.2.5.2 Sintering/Heat Treatment

Figures 5.72 and 5.73 show XRD patterns for the ZrPM-97-800-1500 powder and for samples sintered at temperatures in the range of 1600°C to 1950°C. Zirconium carbide was the only crystalline phase observed in the samples heat treated at temperatures ≥1500°C.

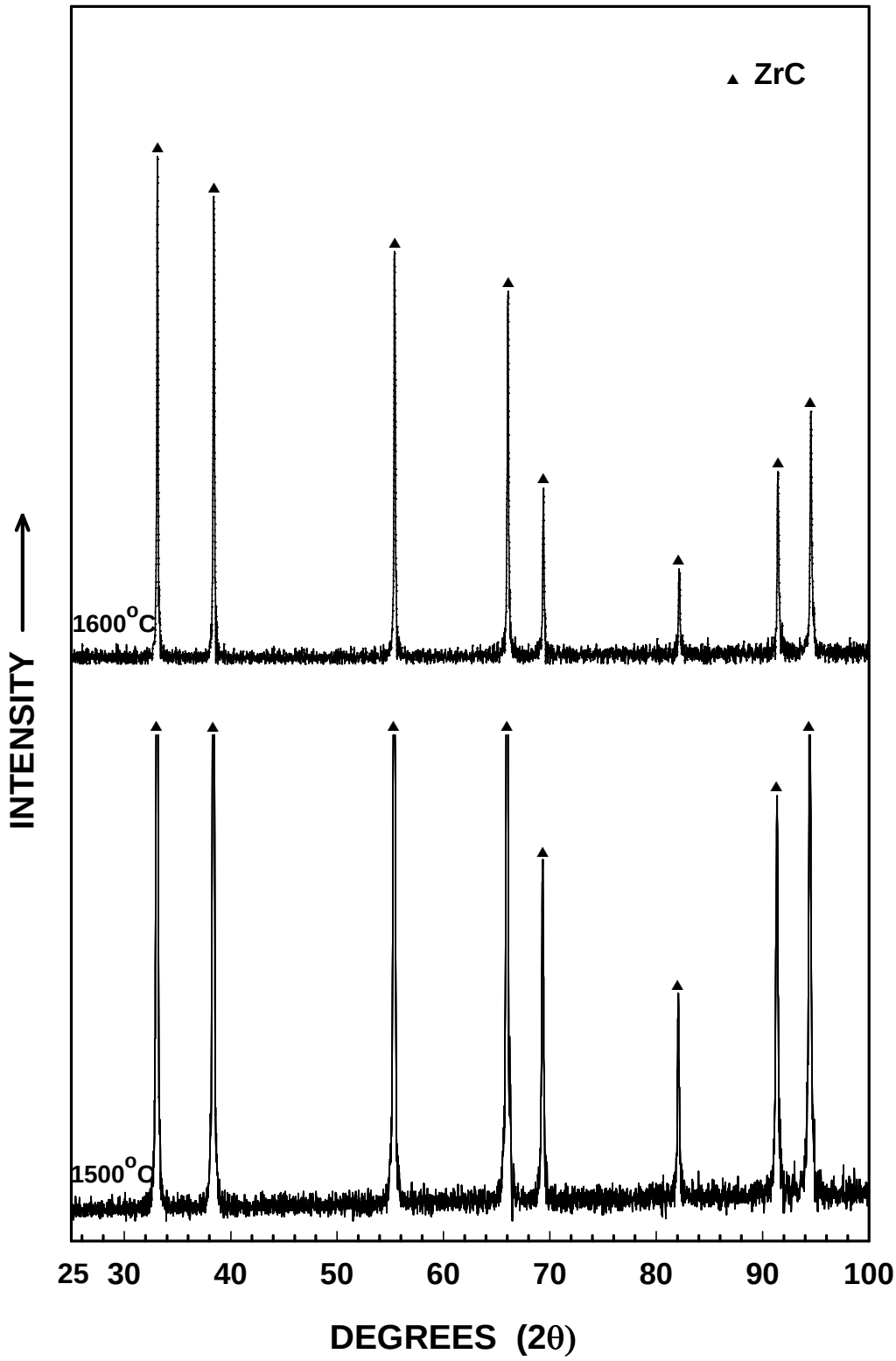

Figure 5.72 X-ray diffraction patterns for ZrPM-97 samples heat treated at 1500°C and 1600°C.

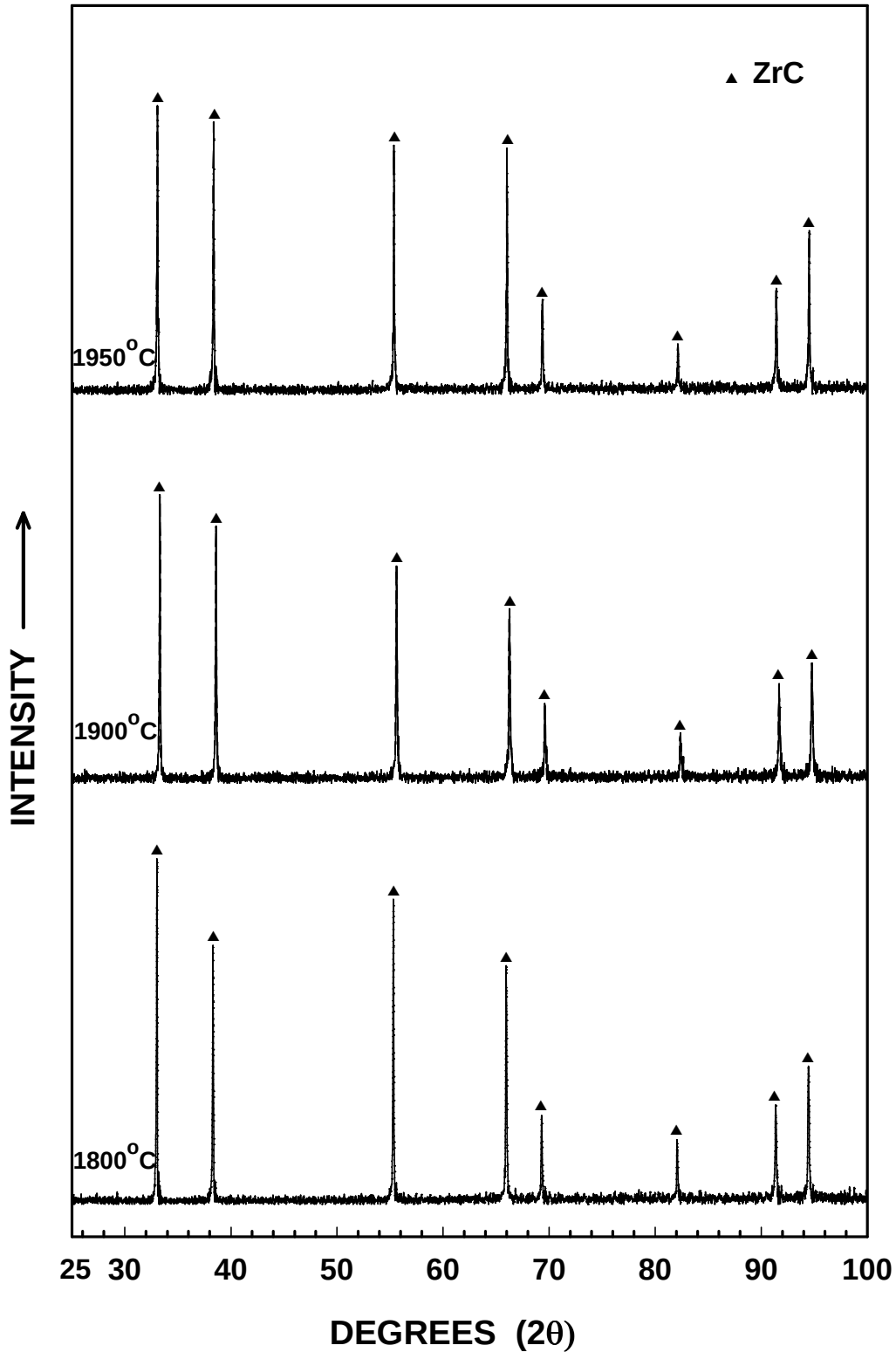

Figure 5.73 X-ray diffraction patterns for ZrPM-97 samples heat treated at temperatures in the range of 1800 to 1950°C.

Table 5.65 lists percentage weight losses for ZrPM-97-800-1500 powder compacts which were sintered at temperatures in the range of 1600-1950^{o}C. The table also shows weight loss values which were corrected for adsorbed moisture by applying the same correction factor (i.e., 1.5 wt%) that was used for the ZrPM-87 samples discussed in section 5.6.2.2.1. Figure 5.74 shows a plot of the corrected weight loss vs. sintering temperature for the samples. The corrected weight loss of ~5.1 wt% for the 1600^{o}C ZrPM-97 is larger than the weight losses observed in the corresponding ZrPM-87, ZrPM-94, and ZrPM-99 samples. This is rather surprising considering the higher carbon concentration for the ZrPM-97 samples and the fact that there was essentially no difference in the XRD patterns for the ZrPM-97-800-1500 and ZrPM-97-800-1600 samples. The reason for this behavior is not understood. One speculative suggestion is that more moisture was adsorbed in the ZrPM-97 sample (i.e., more than the assumed value of 1.5 wt%) because it had a higher specific surface area (and presumably a larger percentage of fine pores) compared to the other samples.

An estimated value of the solid density of the ZrPM-97-800-1500-1900 sample was used to calculate relative densities for samples sintered in the temperature range of 1600-1950^{o}C. This was done because the CTR reaction was substantially completed after the 1600^{o}C heat treatment. This was indicated by the observation that only small weight losses occurred for heat treatments at temperatures >1600^{o}C (Figure 5.74). In addition, the XRD patterns showed essentially no changes (Figures 5.72 and 5.73) for samples heat treated in the range of 1600-1950^{o}C. As noted in section 5.6.2.2.1, the actual variation in solid density values in this temperature range was probably well within the range of the error associated with the estimation of the solid density value for the

1900°C ZrPM-97 sample. The solid density of the ZrPM-97-800-1900 sample was estimated with the following assumptions:

(1) The zirconium carbide phase was oxygen-free and had the stoichiometric composition. The solid density of the ZrC phase was calculated using the measured lattice parameter of 0.4696 nm (Appendix F):

$$\frac{4(1\times 91.224+1\times 12.01)}{(0.4696)^3\times\ 6.022\times 10^{23}}\times 10^{21}\ = 6.62\ g/cm^3 \qquad (5\text{-}27)$$

(2) The amount of "free" carbon in the ZrPM-97-800-1900 sample was estimated based on the overall carbon concentration. Table 5.48 shows that the measured carbon concentration was 12.6 wt% (determined by Leco Corp.). Using this value and assuming that the sample consisted only of Zr and C, the estimated free carbon concentration was ~1.1 wt%.

Using the above information, the solid density for the ZrPM-94-800-1900 sample is given by:

$$\frac{100}{\frac{98.9}{6.62}+\frac{1.1}{2}}\ = 6.46\ g/cm^3 \qquad (5\text{-}28)$$

Table 5.65 shows the bulk density values, determined from geometric measurements, and the corresponding calculated relative density values for the samples sintered at temperatures in the range of 1600-1950°C. The table also lists the percentage shrinkage in the diameter and thickness for each sample.

Table 5.65 Densities (bulk and relative), percent shrinkages, and percent weight losses for sintered samples.

Pellet #	Temperature (^{o}C)	Shrinkage (%)		Bulk Density* (g/cm^{3})	Relative Density (%)	Weight Loss (wt%)	Corrected Weight Loss (wt%)
		Diameter	Thickness				
1	1600	13.23	16.32	3.87	59.9	6.63	5.13
4	1725	21.80	24.70	5.30	82.0	7.21	5.71
2	1800	23.38	26.21	5.40	83.6	8.21	6.71
5	1900	25.24	30.26	6.26	96.9	7.55	6.05
3	1950	26.16	30.68	6.33	98.0	7.73	6.23

* Determined from the sample geometric dimensions.

Figure 5.75 shows plots of the diameter and thickness shrinkages vs. sintering temperature. The shrinkage behavior in the range of 1600-1950^{o}C showed significant anisotropy. The reason for the shrinkage anisotropy is not understood. However, it is apparent that the effect is more significant in carbon-rich samples (i.e., samples with more free carbon). Significant shrinkage anisotropy was observed for the "carbon-rich" ZrPM-45 and ZrPM-61 samples described in sections 5.6.1.1.2 (Table 5.38) and 5.6.1.3.2 (Table 5.42). In contrast, there was less shrinkage anisotropy for the "oxide-rich" samples ZrPM-58 (section 5.6.1.2.2, Table 5.46), ZrPM-87 (section 5.6.2.2.2, Table 5.51 and Figure 5.48), and ZrPM-94 (section 5.6.2.3.2, Table 5.55 and Figure 5.57).

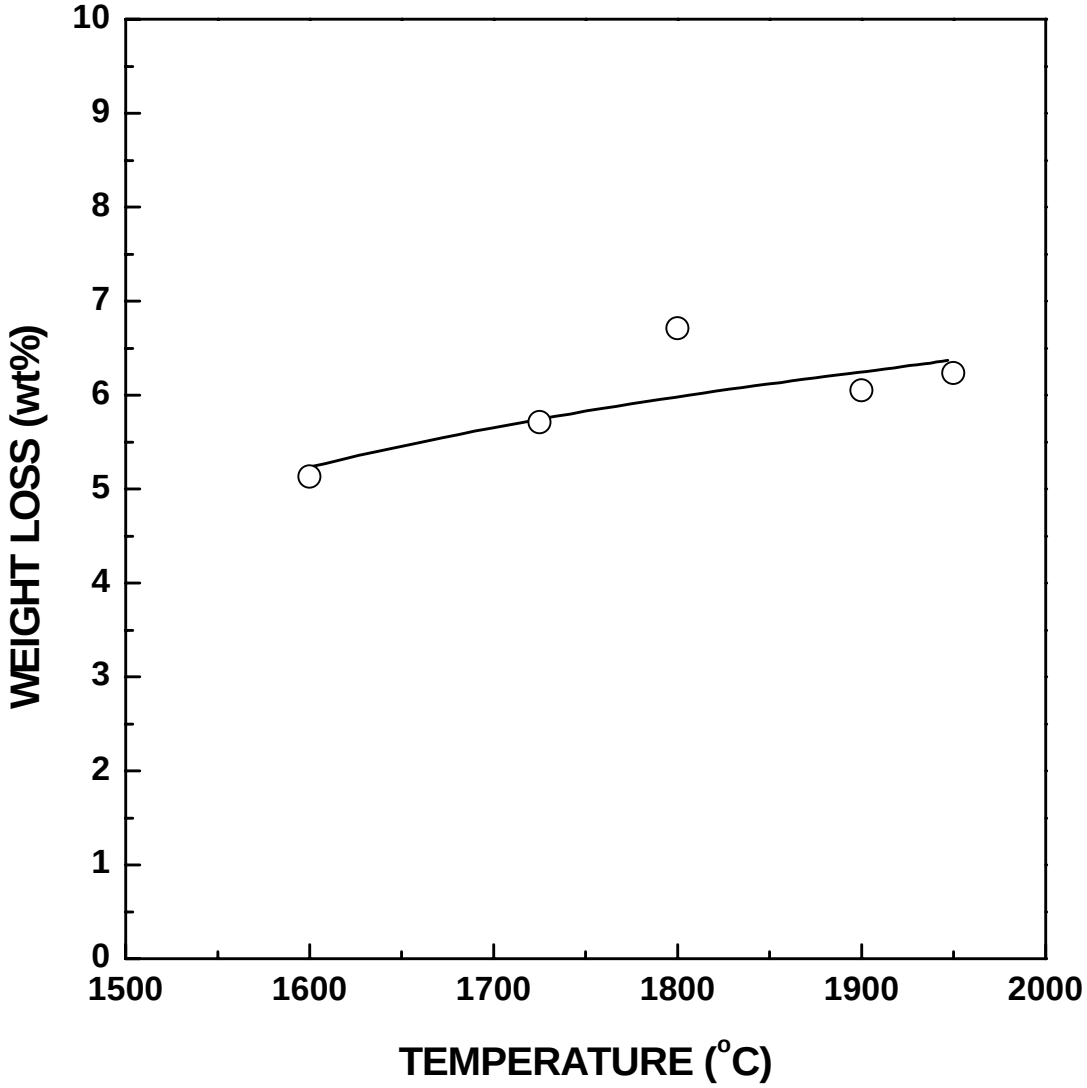

Figure 5.74 Plot of corrected weight loss vs. sintering temperature for ZrPM-97 powder compacts that were initially heat treated at 1150°C (2 h). The compacts were prepared with ZrPM-97-800-1500 powder.

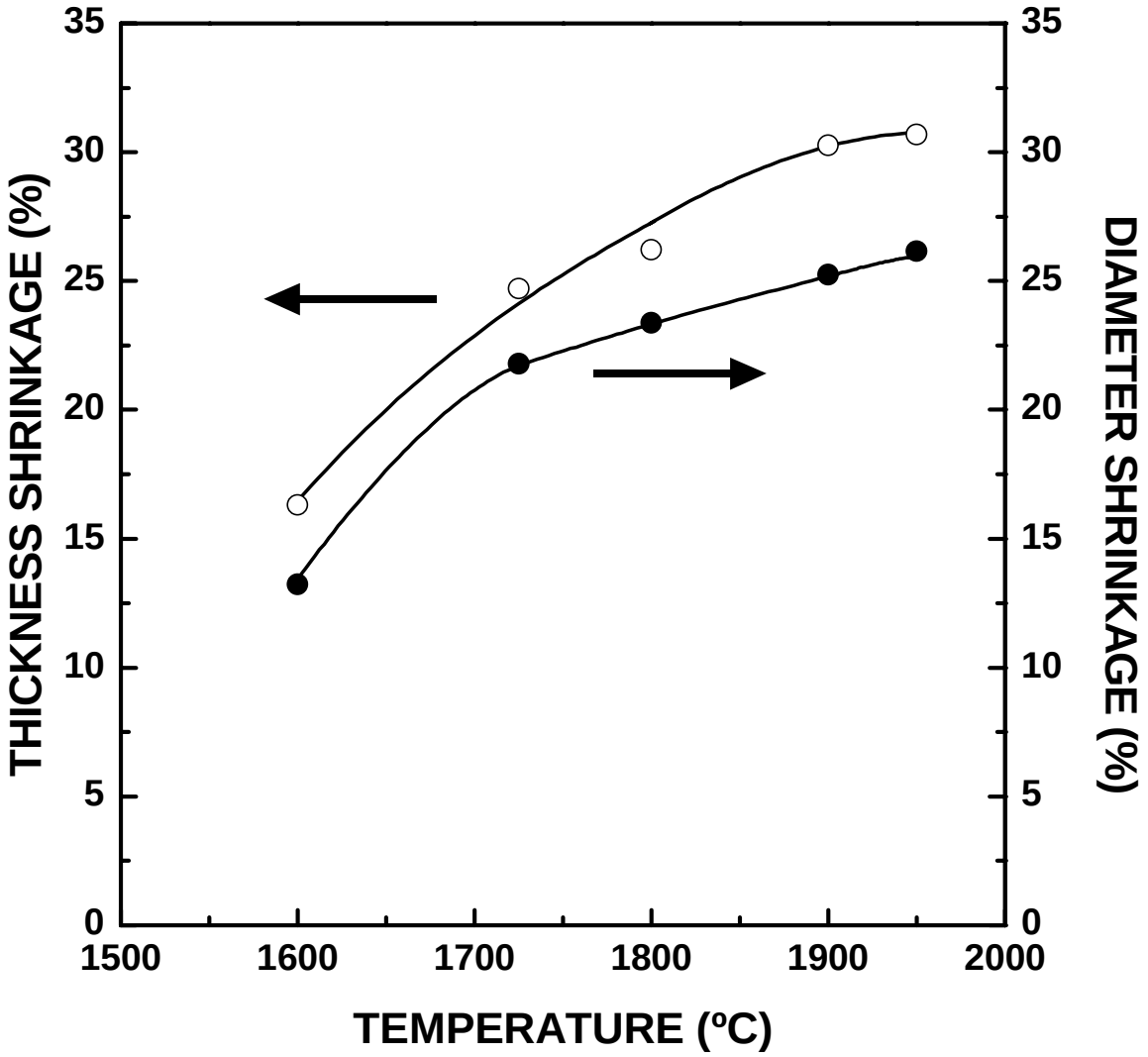

Figure 5.75 Plots of thickness and diameter shrinkage vs. sintering temperature for ZrPM-97 powder compacts that were initially heat treated at 1150°C (2 h). The compacts were prepared with ZrPM-97-800-1500 powder.

Figures 5.76 shows plots of bulk density and relative density vs. sintering temperature, based on measurements from the geometric dimensions of the samples. The relative density value of the sample sintered at 1950^{o}C was ~98%. The 1800^{o}C data point does not follow well the trend exhibited by the other data points. It is possible that a piece broke off from the sample. This would have resulted in an overestimation of the sample volume (which was calculated from the diameter and thickness by assuming a perfect cylindrical shape). In turn, this would have resulted in a low bulk density value. The loss of a piece of the sample is also suggested by the anomalously high weight loss for the 1800^{o}C sample, as shown in Table 5.65 and Figure 5.74.

Table 5.66 shows open porosity, bulk density, and relative density values, determined by the Archimedes method, for the some of the samples shown in Table 5.65. The measurements for each sample were repeated at least twice. The individual and average values are listed in Table 5.66. Figure 5.77 shows plots of the bulk density (determined by the Archimedes method) and the calculated relative density as a function of sintering temperature for the ZrPM-97 samples.

The open porosity values for the 1600^{o}C sintered sample is considered unreliable for the same reason discussed in section 5.6.2.2.2. It is also possible that the open porosity values for the 1800-1950^{o}C samples are unreliable. This is because the summation of the open porosity (OP) and relative density (RD) values at each temperature exceeded 100%. Although the open porosity measurement could be inaccurate, another possibility is that the assumed value for the solid density was too low. This is suggested because the problem (of OP+RD > 100%) was not observed in the corresponding ZrPM-87, ZrPM-94, and ZrPM-99 sintered samples. In any case, the error

seems to be relatively small because the summation of the open porosity and relative density values was in the range of 101-102% for all the samples.

The ZrPM-97 samples were the only ones in the series (i.e., ZrPM-87, -94, -97, and -99) in which open porosity was detected in the 1900°C and 1950°C sintered samples (see Tables 5.52, 5.56, 5.61, and 5.66). If the open porosities are accurate, then the relative densities for the 1900°C and 1950°C ZrPM-97 samples are really no higher than 97.2% and 98.1%, respectively. It seems reasonable that the "final" relative densities in the ZrPM-97 samples would be lower compared to the other samples. This is because the ZrPM-97 samples are apparently the only ones in which free carbon remains after heat treatment at 1900°C and 1950°C. Previous investigations with SiC have shown that the addition of small amounts of “free” carbon is highly beneficial for densification of powder compacts.[92,93] However, addition of larger amounts of carbon is detrimental for densification of SiC powder compacts.[90] It has also been shown that densification of ZrC is inhibited by carbon additions in the range of 5-10 wt%.[52] In the present study, the calculated amount of free carbon in the ZrPM-97-800-1900 sample was ~1.1 wt%. Although this may seem like a small amount of carbon, it should be recognized that the amount is more significant when the difference in carbon and zirconium carbide densities are considered. Using the density values assumed earlier in this section, the amounts of carbon and zirconium carbide in the sample on a volume basis are 3.6 vol% and 96.4%, respectively.

Table 5.66 Densities (bulk and relative) and percentage open porosity for sintered samples.

Pellet #	Temperature (^oC)	Open Porosity* (%)	Bulk Density* (g/cm^3)	Relative Density (%)
1	1600	27.9 (29.1, 27.2, 27.3)	3.94 (3.93, 3.97, 3.92)	61.0 (60.8, 61.5, 60.8)
2	1800	9.8 (10.7, 9.6, 9.2)	5.92 (5.90, 5.93, 5.94)	91.6 (91.3, 91.8, 92.0)
5	1900	2.8 (3.1, 2.7, 2.5)	6.38 (6.37, 6.38, 6.39)	98.8 (98.6, 98.8, 98.9)
3	1950	1.9 (1.5, 2.2)	6.41 (6.42, 6.40)	99.2 (99.4, 99.1)

* Determined by the Archimedes method. When more that one measurement was made, the individual values are listed in the parenthesis.

Figure 5.78 shows plots comparing the bulk density values (for various sintering temperatures) that were determined from the Archimedes and geometric measurement methods. The large difference in values observed for the 1800^{o}C ZrPM-97 sample presumably reflects a major error in the geometric measurement, as discussed earlier in this section. However, it is still noted that the difference between the bulk density values determined by the two methods for the 1900^{o}C and 1950^{o}C ZrPM-97 samples is slightly larger than observed for the corresponding ZrPM-87, ZrPM-94, and ZrPM-99 samples (see sections 5.6.2.2.2 (Figure 5.51), 5.6.2.3.2 (Figure 5.60), and 5.6.2.4.2 (Figure 5.69), respectively). One possible explanation is that there was some difficulty in achieving complete penetration of water into the pores in the ZrPM-97 samples. (The ZrPM-87, ZrPM-94, and ZrPM-99 samples showed zero open porosity after the 1900^{o}C and 1950^{o}C heat treatments, while the ZrPM-97 samples still showed ~2% open porosity.)

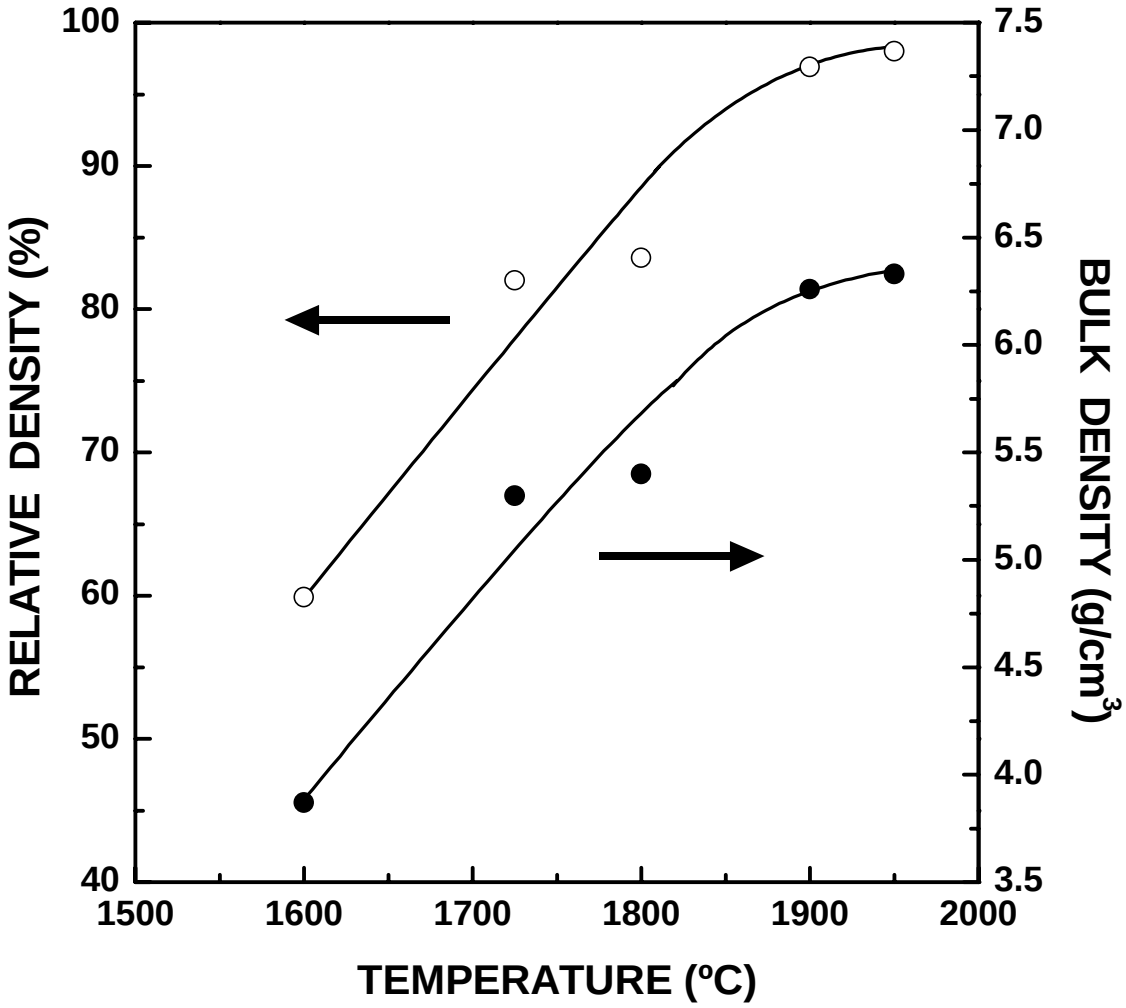

Figure 5.76 Plots of relative density and bulk density vs. sintering temperature for ZrPM-97 powder compacts that were initially heat treated at 1150°C (2 h). Bulk densities were determined by measurements of the sample dimensions.

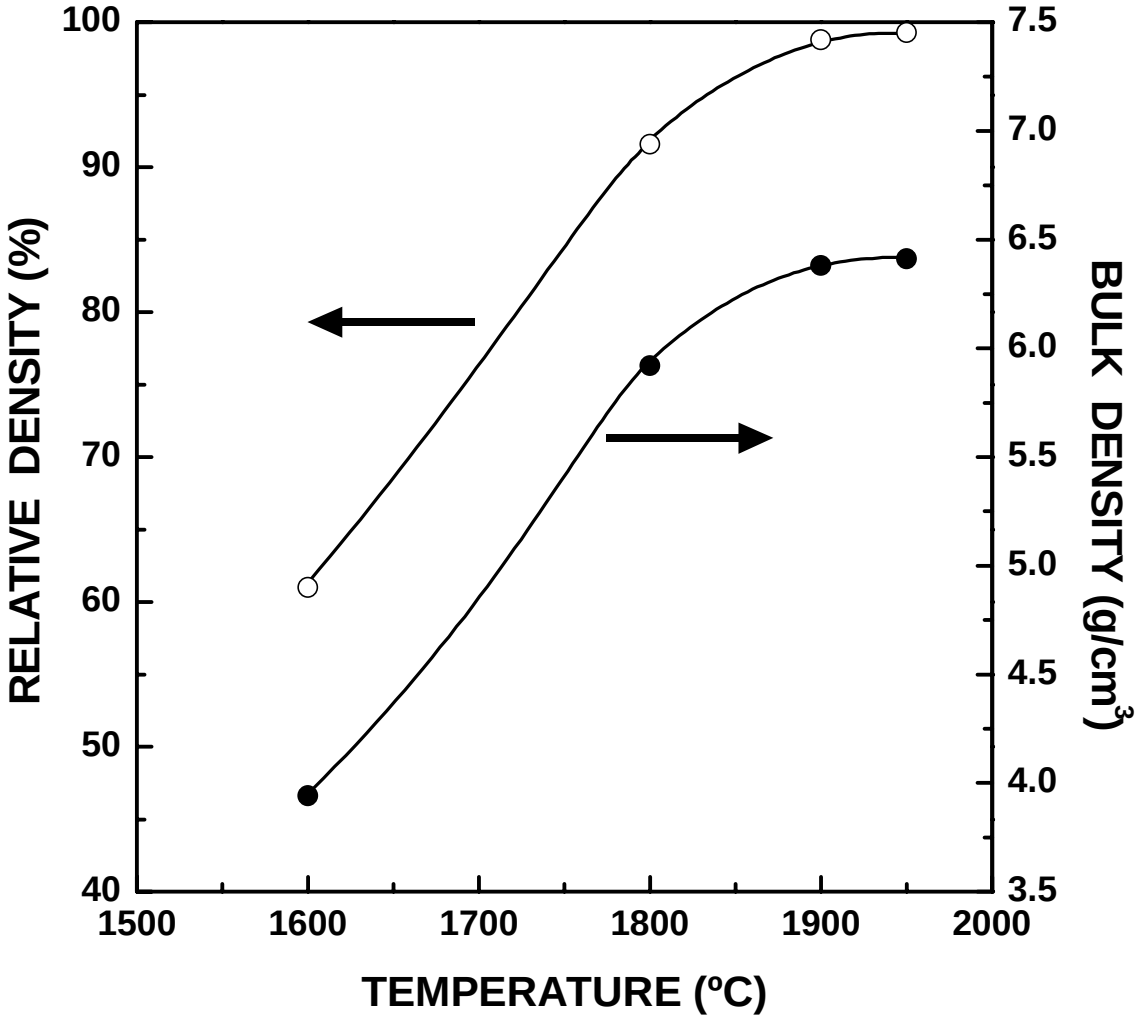

Figure 5.77 Plots of relative density and bulk density vs. sintering temperature for ZrPM-97 powder compacts that were initially heat treated at 1150°C (2 h). Bulk densities were determined by the Archimedes method.

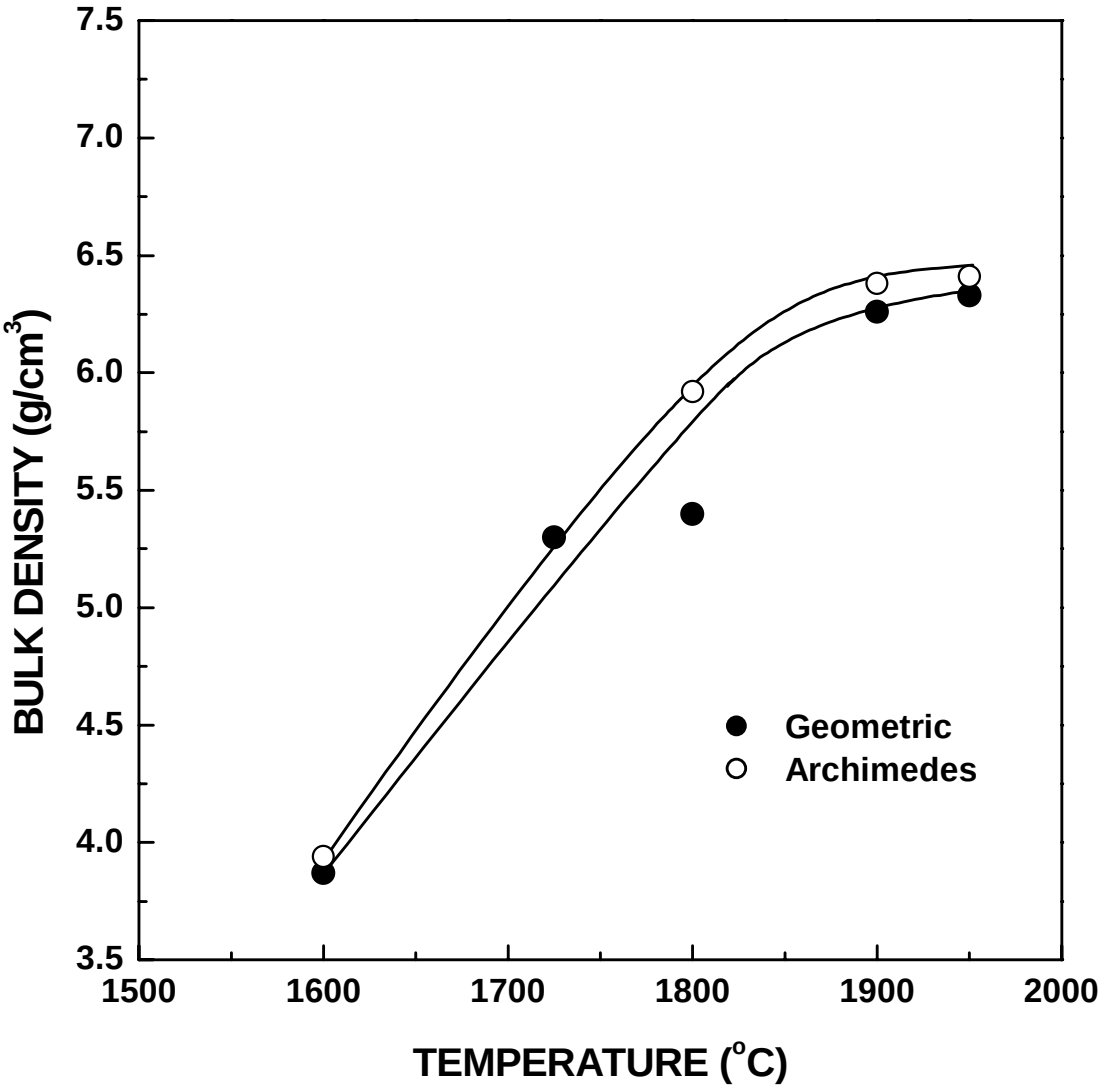

Figure 5.78 Plots of bulk density vs. sintering temperature for ZrPM-97 powder compacts that were initially heat treated at 1150°C (2 h). Bulk densities were determined by the geometric and Archimedes methods.

5.6.2.6 Comparison of ZrPM-87, 94, 97, and 99

Figures 5.79 and 5.80 show plots of bulk density, determined by the geometric and Archimedes measurement methods, respectively, as a function of sintering temperature for the ZrPM-87, ZrPM-94, ZrPM-97, and ZrPM-99 samples. These plots show that the overall trend in densification is similar for all samples. However, it was not possible to draw any significant conclusions regarding differences in the densification behavior that might be due to compositional differences. This is because the samples have different solid densities.

Figure 5.81 shows a plot of relative density, calculated from the bulk density data using the geometric measurements, as a function of sintering temperature for the ZrPM-87, ZrPM-94, ZrPM-97, and ZrPM-99 samples. Although there is substantial uncertainty in the calculation of the relative densities, the results in Figure 5.81 suggest that composition has relatively little effect on densification behavior, i.e., for the range of compositions investigated in this study. There does appear to be a small enhancement of the densification rate for the "oxide-rich" ZrPM-87 samples. This is consistent with results reported by Min-Haga et al.[54]

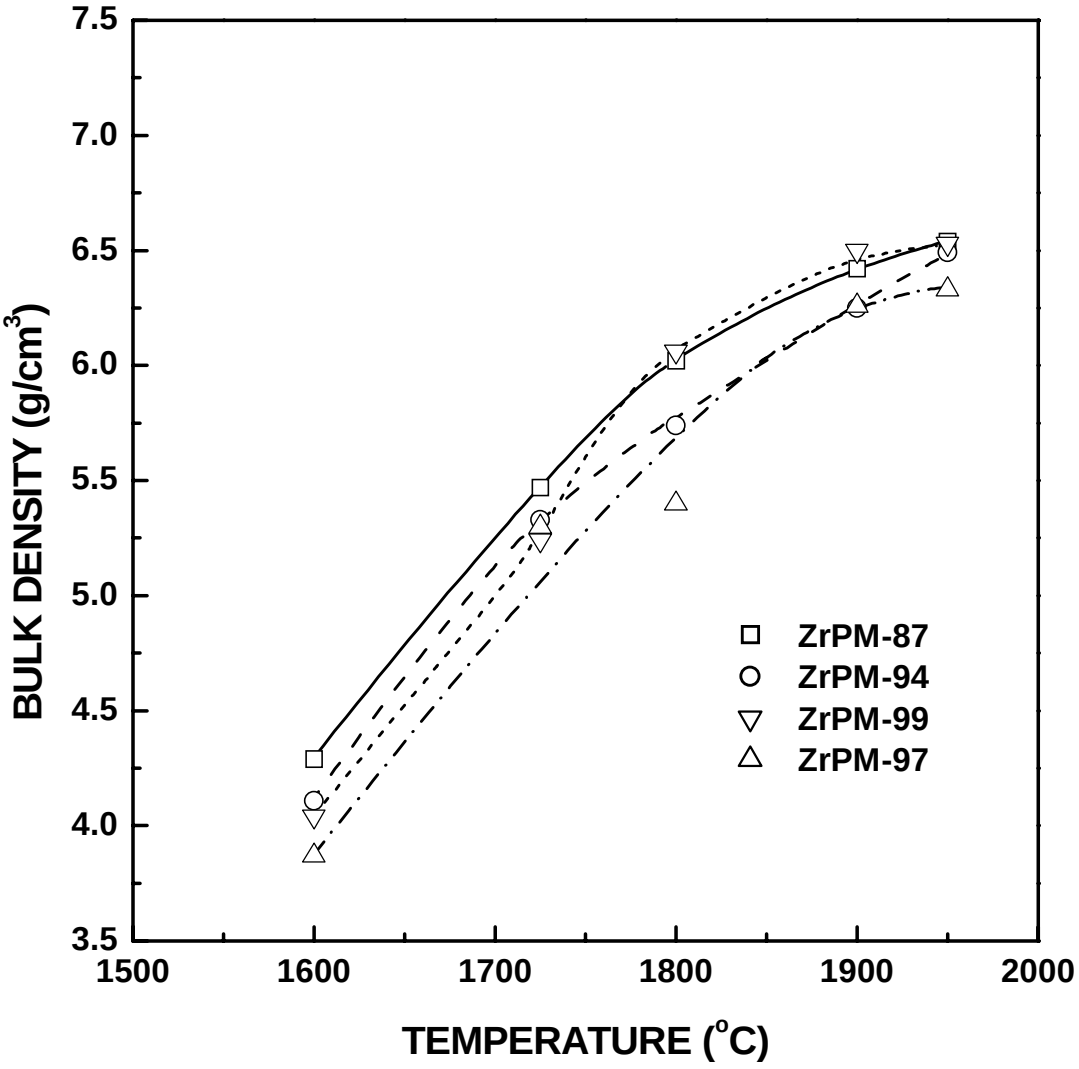

Figure 5.79 Plots of bulk density (determined by geometric measurements) vs. sintering temperature for ZrC-based powder compacts.

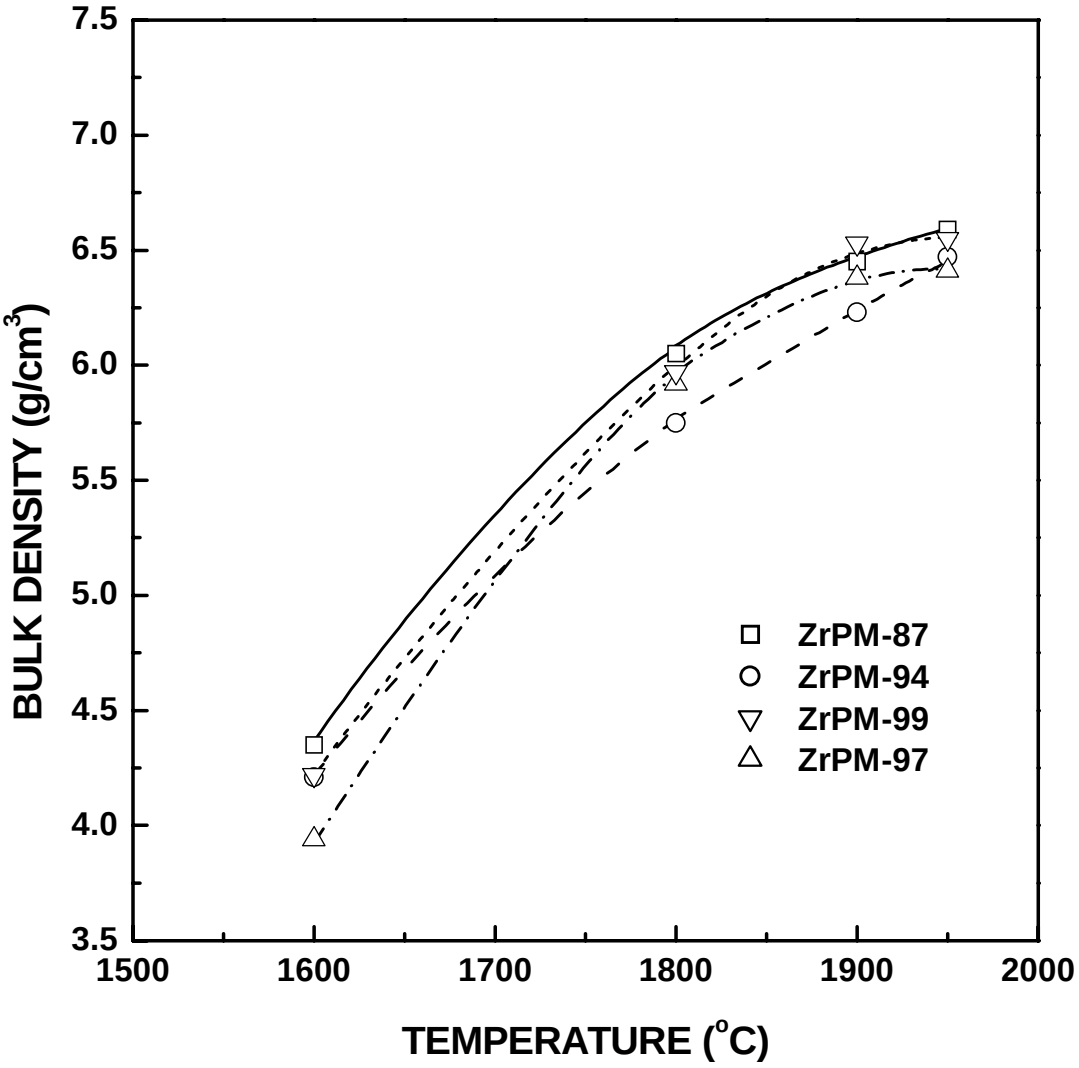

Figure 5.80 Plots of bulk density (determined by the Archimedes method) vs. sintering temperature for ZrC-based powder compacts.

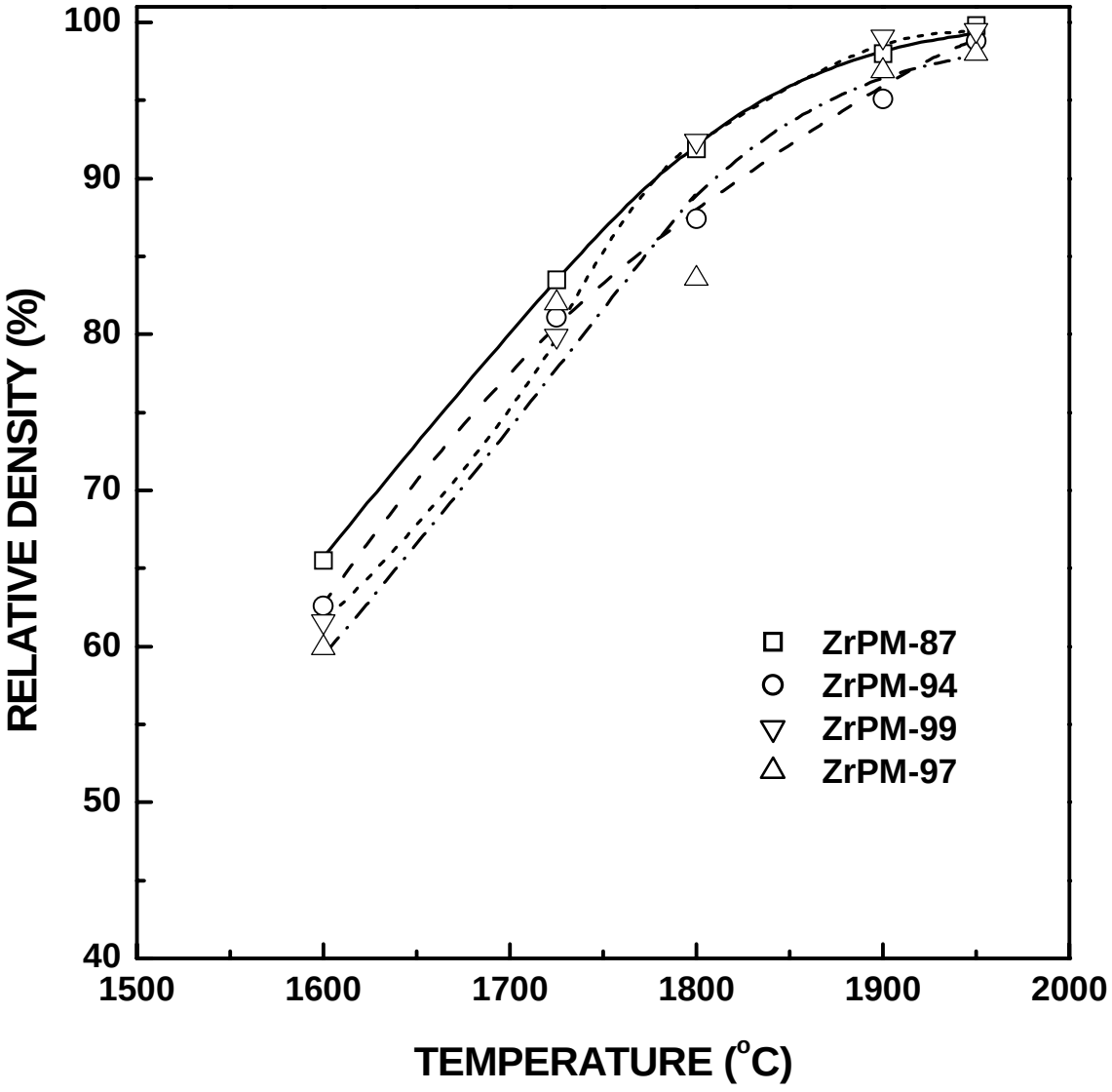

Figure 5.81 Plots of relative density (based on using geometric measurements) vs. sintering temperature for ZrC-based powder compacts.

Figure 5.82 shows plots of the shrinkage in sample diameter (determined from geometric measurements) as a function of sintering temperature for the ZrPM-87, ZrPM-94, ZrPM-97, and ZrPM-99 samples. The differences in the diameter shrinkage are very similar for the ZrPM-87, ZrPM-94, and ZrPM-99 samples, while the ZrPM-97 sample shows larger shrinkages. The larger shrinkages for the latter sample are presumably associated with the lower relative densities for the starting samples (as-dry pressed and 1150^{o}C powder compacts). The diameter shrinkage at 1600^{o}C for each sample in a given series (ZrPM-87, ZrPM-94, ZrPM-97, and ZrPM-99) was subtracted from the corresponding shrinkage at each temperature in the range from 1600-1950^{o}C. The difference in shrinkage was plotted as a function of temperature. Figure 5.83 shows the results for each series of samples. There was relatively little difference in shrinkage behavior during sintering at temperatures above 1600^{o}C. The ZrPM-99 and ZrPM-97 samples tended to have slightly higher values than the ZrPM-87 and ZrPM-94 samples.

Figure 5.84 shows plots of the shrinkage in sample thickness (determined from geometric measurements) as a function of sintering temperature for the ZrPM-87, ZrPM-94, ZrPM-97, and ZrPM-99 samples. The ZrPM-87 and ZrPM-94 samples showed very similar thickness shrinkages over the entire range of temperatures, while the ZrPM-99 samples showed slightly larger shrinkages at the higher temperatures and the ZrPM-97 sample shows considerably larger shrinkages for all temperatures. As noted earlier, the larger shrinkages for the ZrPM-97 samples are presumably related to the lower starting relative density. The larger shrinkage for the ZrPM-99 sample (compared to the ZrPM-87 and ZrPM-94 samples) at the highest temperature (1950^{o}C) was unexpected because the calculated relative densities of the starting materials were very similar for the ZrPM-87,

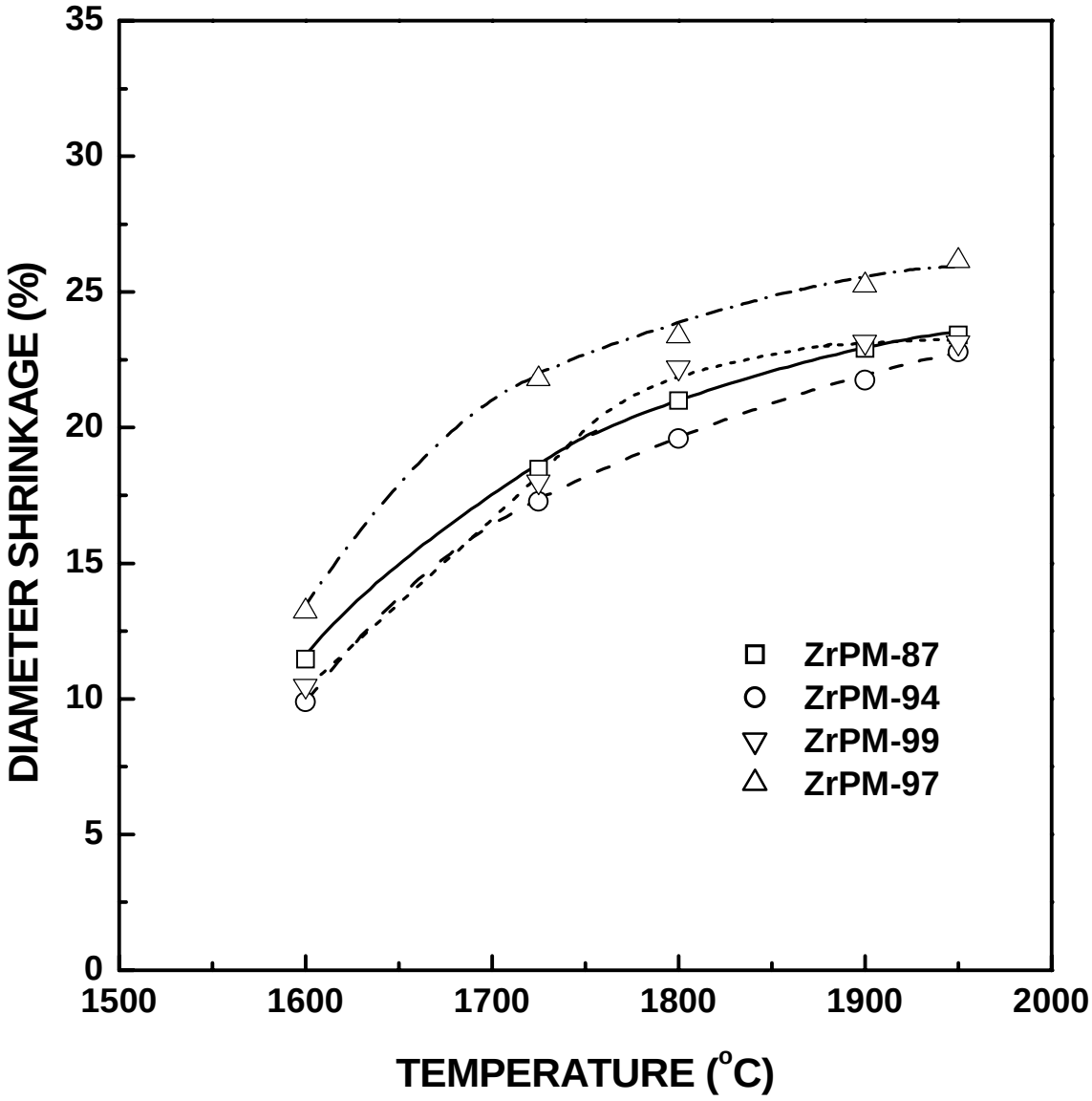

Figure 5.82 Plots of diameter shrinkage vs. sintering temperature for ZrC-based powder compacts.

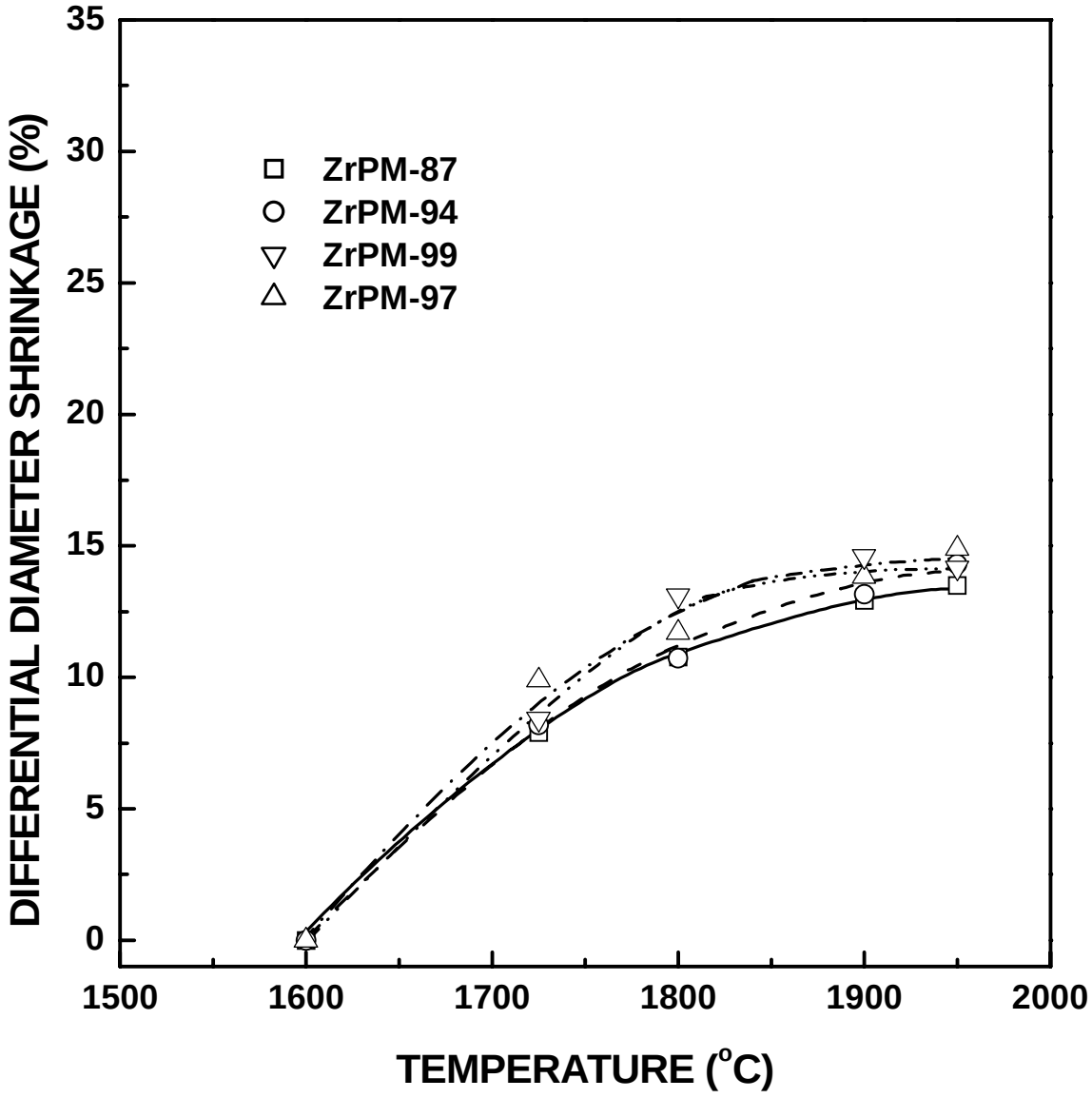

Figure 5.83 Plots of the difference in diameter shrinkage vs. sintering temperature for ZrC-based powder compacts.

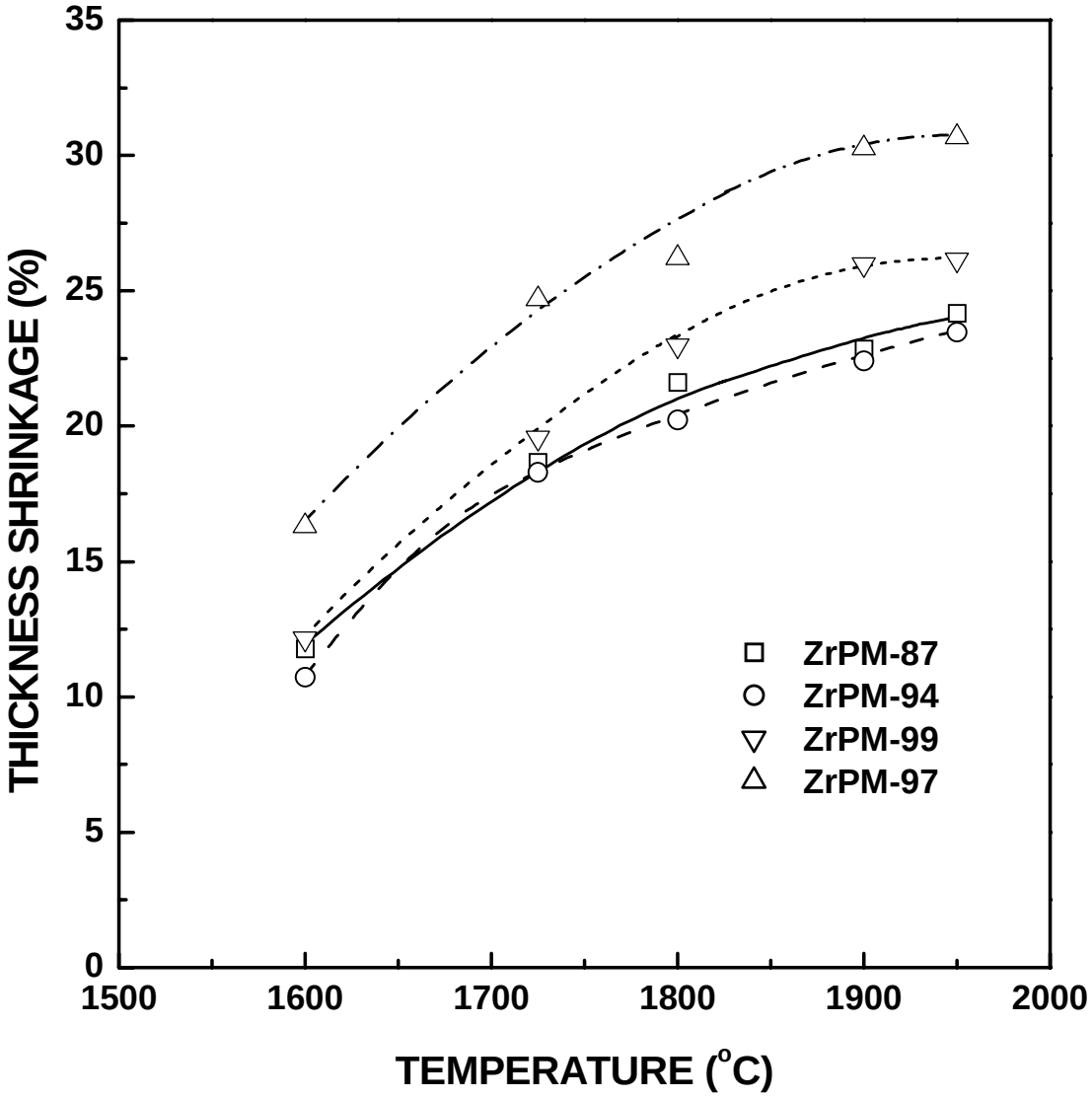

Figure 5.84 Plots of thickness shrinkage vs. sintering temperature for ZrC-based powder compacts.

ZrPM-94, and ZrPM-99 samples. This result suggests that there were errors in the estimated starting relative densities of the samples. This is suggested because there is no evidence indicating that the "final" (1950°C) relative density for the ZrPM-99 sample was significantly different from the "final" relative densities of the ZrPM-87 and ZrPM-94 samples.

The thickness shrinkage at 1600°C for each sample in a given series (ZrPM-87, ZrPM-94, ZrPM-97, and ZrPM-99) was subtracted from the corresponding shrinkage at each temperature in the range from 1600-1950°C. The difference in shrinkage was plotted as a function of temperature. Figure 5.85 shows the results for each series of samples. The ZrPM-97 and ZrPM-99 samples showed somewhat larger differences in shrinkage at most temperatures compared to the ZrPM-87 and ZrPM-94 samples, especially at the higher temperatures. As indicated earlier, the result for the ZrPM-97 samples is attributed to the lower starting density. In contrast, the higher values for the ZrPM-99 samples are more likely due to some errors in calculating the starting densities (i.e., either for the ZrPM-99 sample and/or for the ZrPM-87 and ZrPM-94 samples.)

Figure 5.86 shows plots of the weight loss as a function of sintering temperature for the ZrPM-87, ZrPM-94, ZrPM-97, and ZrPM-99 samples. The weight loss at 1600°C for each sample in a given series (ZrPM-87, ZrPM-94, ZrPM-97, and ZrPM-99) was subtracted from the corresponding weight loss at each temperature in the range from 1600-1950°C. The difference in weight loss was plotted as a function of temperature. Figure 5.87 shows the results for each series of samples. (Note that the y-axis scale has been expanded for this plot.) Figures 5.86 and 5.87 illustrate that most of the differences in weight loss between the different samples had occurred during the 1600°C heat

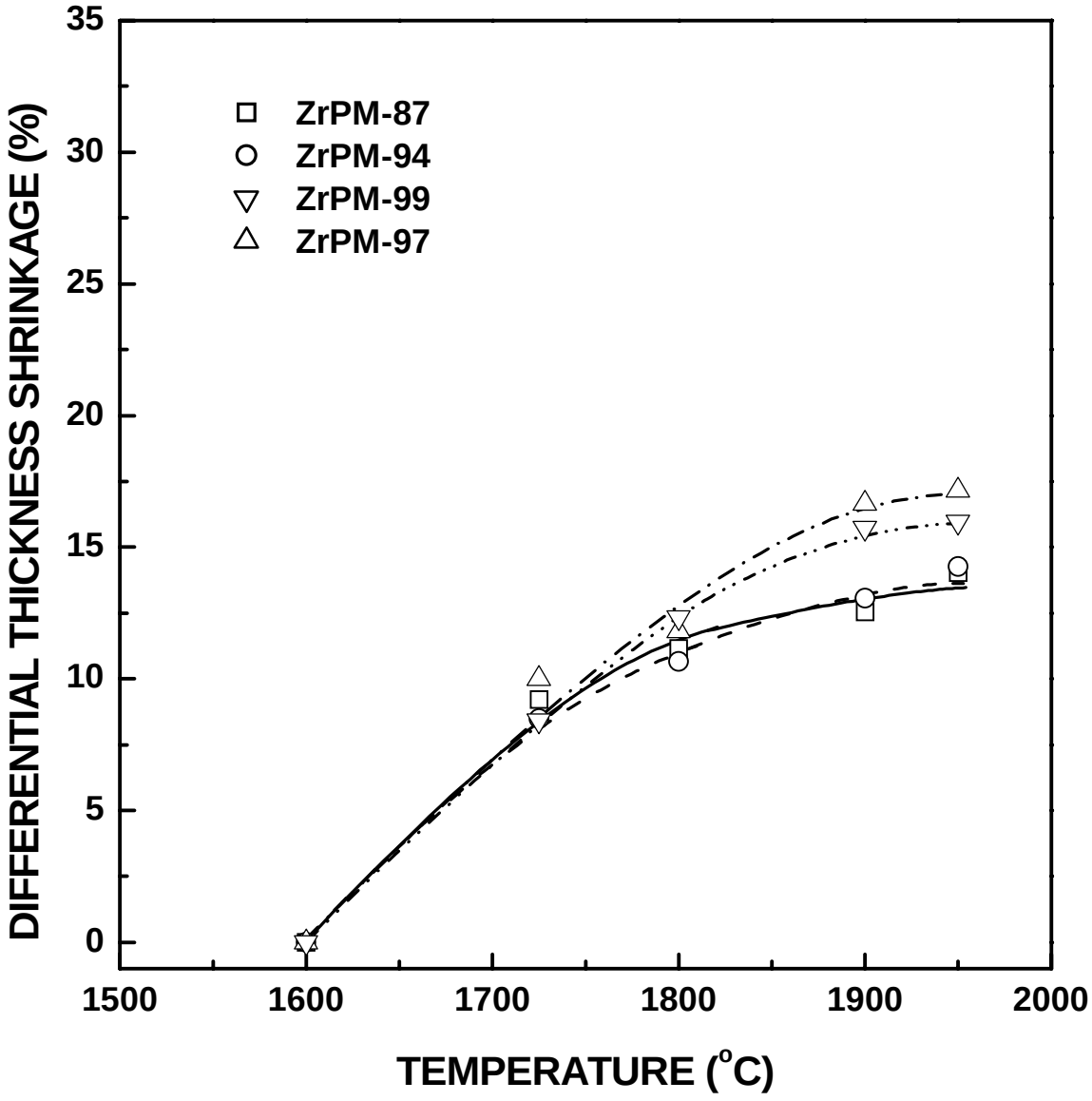

Figure 5.85 Plots of the difference in thickness shrinkage vs. sintering temperature for ZrC-based powder compacts.

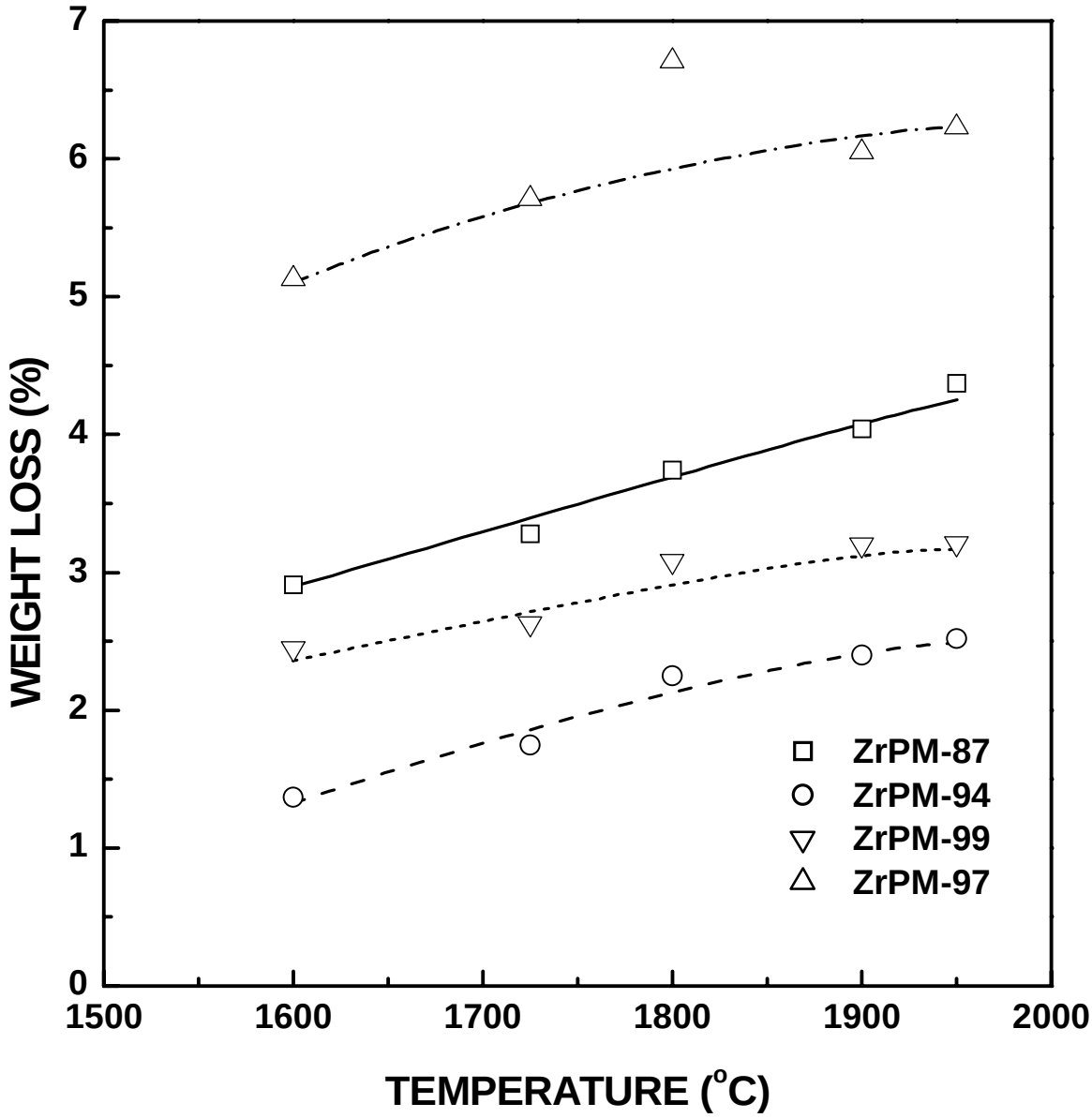

Figure 5.86 Plots of weight loss vs. sintering temperature for ZrC-based powder compacts.

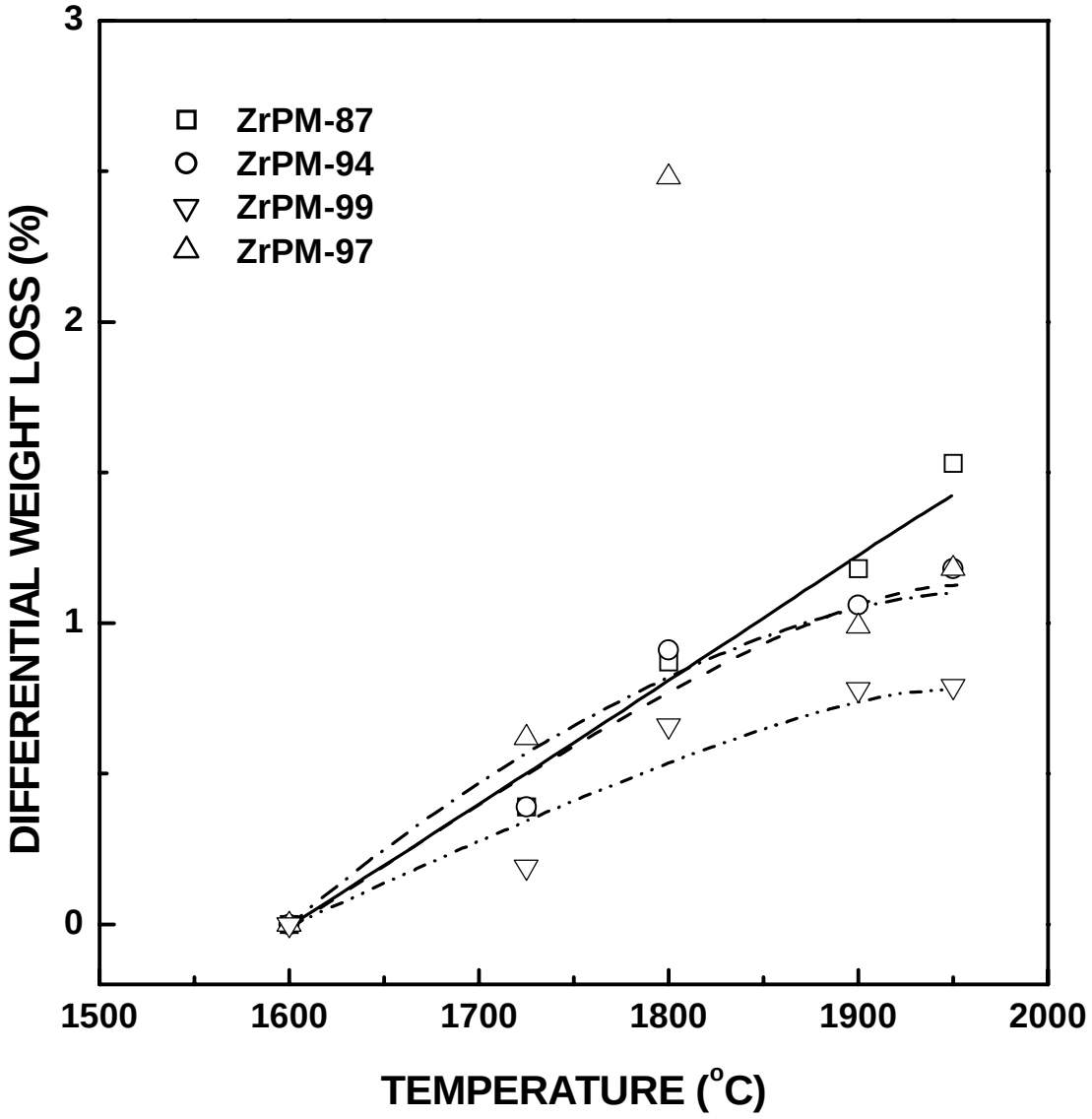

Figure 5.87 Plots of the difference in weight loss vs. sintering temperature for ZrC-based powder compacts.

treatment. The reasons for the large differences during this heat treatment are not understood. The relatively high weight loss at 1600°C for the ZrPM-87 sample was anticipated because the original CTR temperature was lower compared to the other samples (1425°C). In contrast, the high weight loss at 1600°C for the ZrPM-97 was surprising since the original CTR temperature was 1500°C. Figure 5.87 illustrates that the weight loss differences for the various samples were relatively small during heat treatment at temperatures >1600°C. (As noted previously, the anomalous result at 1800°C for the ZrPM-97 sample was probably due to a piece of the sample breaking off.) However, it is noted that the weight losses are leveling off more at the highest temperatures for the ZrPM-94, ZrPM-97, and ZrPM-99 samples compared to the ZrPM-87 sample. This difference is attributed to the highly "oxide-rich" composition of the ZrPM-87 sample. As shown in section 5.6.2.2.2 (Figures 5.45 and 5.46), the ZrPM-87 samples still contained a small amount of ZrO_2 after heat treatment at each temperature. Hence, small weight losses would be expected to occur with continued high temperature heat treatment until the zirconia is removed, either by reaction with the zirconium carbide or by direct volatilization.

5.6.3 Dilatometry

5.6.3.1 Processing Before Sintering

Dilatometry experiments were carried out using powder from batch ZrPM-45. Dried powder was sieved through a 150-mesh screen and pyrolyzed at 800°C for 2 h. The C/Zr molar ratio was 3.1 for a sample (initially dried at 120°C) that was pyrolyzed at 1025°C, as discussed in section 5.6.1.1.1. A pyrolyzed sample (~4 g) was heat treated first at 1400°C (2 h) and then at 1475°C (2 h) in flowing argon (~100 ml/min) atmosphere in the 3-zone lindberg furnace.

The specific surface area for the ZrPM-45-800-1400-1475 sample was 13 m^2/g. This value is lower than the value of 48 m^2/g that was reported in section 5.6.1.1 for the ZrPM-45-800-1350-1400 sample. This is attributed to the higher maximum CTR reaction temperature for the ZrPM-45-800-1400-1475 sample. The specific surface area for this sample is also lower than the value of 23 m^2/g that was reported in section 5.2.1.3 for the ZrPM-45-800-1475 sample. This is probably due to the additional heat treatment time at 1400°C for the ZrPM-45-800-1400-1475 sample.

Table 5.67 shows particle size distribution data for a 10 min-milled ZrPM-45-800-1400-1475 powder. Particle size distribution plots are shown in Figure 5.88. The particle size distribution is similar to the distribution reported in section 5.6.1.1 for the ZrPM-45-800-1350-1400 sample (Figure 5.37). However, the latter sample contains ~3.8 vol% of larger aggregated particles with sizes in the range of ~1.5 – 2.8 μm, while the former sample contains only ~1.1 vol% of smaller aggregated particles with sizes in the range of ~0.4 - 0.6 μm. This difference is probably due to a difference in the milling procedure. The ZrPM-45-800-1400-1475 sample was milled using the "5 x 2 min"

method described in Chapter 4 (section 4.1.6). The ZrPM-45-800-1350-1400 sample was milled sequentially for periods of 5, 5, 10 and 20 min (i.e., total time of 40 min). However, the walls of the milling vial were never scraped, to remove adhered powder, between each milling step. Despite the much longer milling time, the latter method was much less efficient because powder tended to cling to the walls of the vial and agglomerates were not broken down effectively.

The particle size distribution for the 10 min-milled ZrPM-45-800-1400-1475 powder (Figure 5.88) is even more similar to the distribution reported in section 5.2.1.3 for the ZrPM-45-800-1475 sample (Figure 5.17). A minor difference is that the distribution for the latter sample does not contain the aggregated particles with sizes in the range of ~0.4 - 0.6 μm. It is speculated that this reflects a difference in the initial degree of aggregation in the two powders, i.e., before milling. The ZrPM-45-800-1400-1475 powder had the additional heat treatment at 1400°C, so it may have been more aggregated before milling. (The lower surface specific surface for this sample is consistent with this speculation.)

Table 5.67 Particle size distribution data for the 10 min-milled ZrPM-45-800-1400-1475 powder sample.

	Diameter (μm)
Mean	0.10
Modes*	0.07, 0.19, 0.47
D_{90}	0.20
D_{50}	0.07
D_{10}	0.05
Standard Deviation	0.07

* Mode values are listed for each distinct peak in the accompanying relative frequency plot.

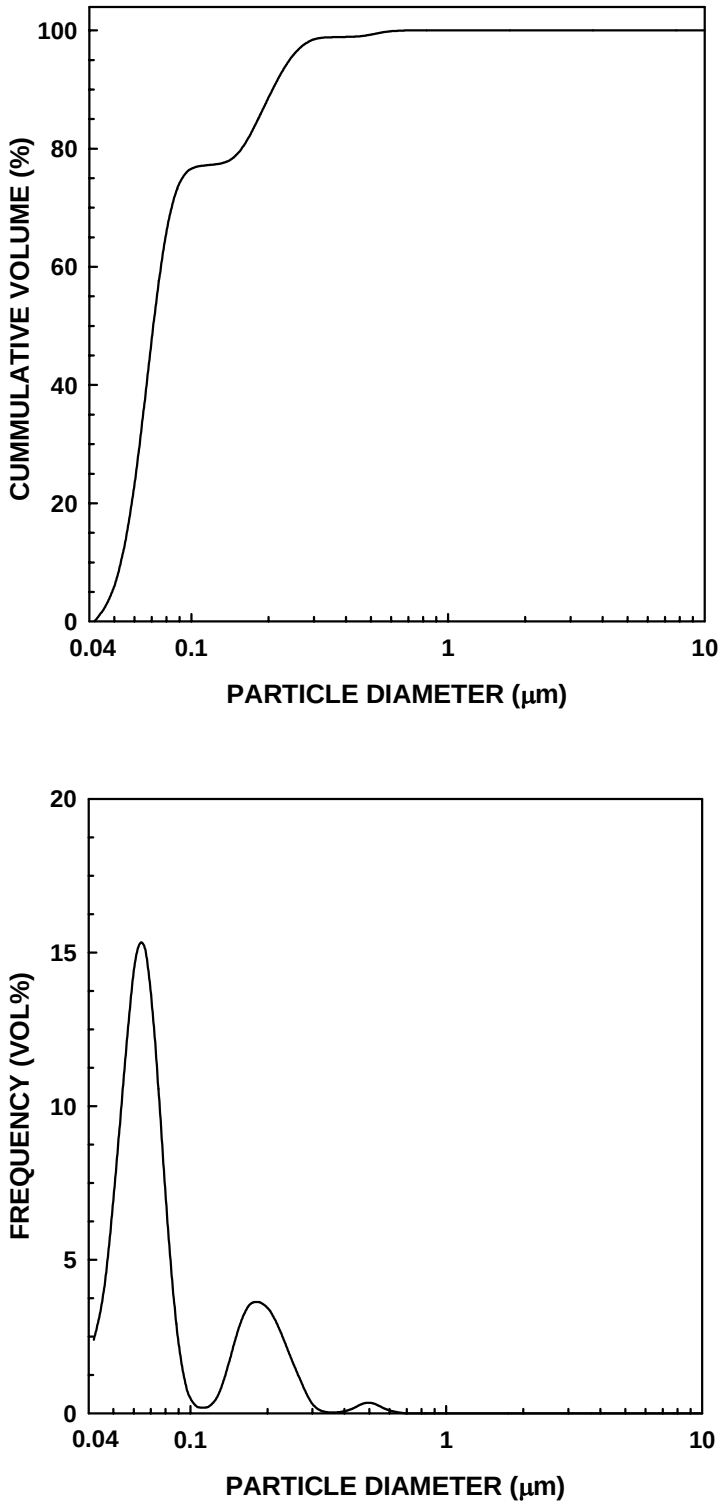

Figure 5.88 Particle size distribution plots for the 10 min-milled ZrPM-45-800-1400-1475 powder sample: cumulative frequency plot (top) and relative frequency plot (bottom).

The milled powder was mixed with 10 vol% polymer binder and plasticizer as described in section 4.3.1.1. Six powder compacts were uniaxially dry-pressed in a 6.4 mm diameter die at 250 MPa. The bulk densities and relative densities of these samples, determined from the geometric dimensions, are shown in Table 5.68. (The relative densities were evaluated using the same solid density value of 6.44 g/cm^3 determined (using equation 5-9) in section 5.6.1.1.1 for the ZrPM-45-800-1350-1400 sample.) The reason for the lower green density for pellets #2 and #3 (i.e., compared to pellet #'s 4-6) is not known. The result was surprising because the pellets were prepared from the same milled powder. It is noted, however, that the powders were mixed with binder and dry pressed at different times. The green densities for the ZrPM-45-800-1400-1475 samples (Table 5.68) were mostly lower than the green densities for the ZrPM-45-800-1350-1400 samples (Table 5.37). The reason for this difference is not understood. The result was very surprising because the specific surface area was considerably higher for the ZrPM-45-800-1350-1400 sample.

The as-pressed compacts were heat treated at 1150^{o}C for 2 h under flowing argon (100 ml/min) in a tube furnace (Model 55031). This resulted in burnout of the binder that was added to the powder. The percentage weight losses due to binder burnout are also shown in Table 5.68. The weight losses were close to the value expected (~1.8 wt%), as discussed in section 5.6.2.2.1. Bulk density and relative density values after binder burnout, determined from the geometric dimensions, are also shown in Table 5.68.

The pellets were then heat treated or "pre-sintered" at 1490^{o}C for 4 h exactly as discussed in section 5.6.1.1.1. The percentage weight losses during "pre-sintering" are shown in Table 5.68. The bulk density and relative density values for the "pre-sintered"

Table 5.68 Compact densities after dry pressing and compact density and weight loss after 1150°C heat treatment.

Pellet #	As-Dry Pressed		After 1150°C (2 h)		% Weight Loss (1150°C)	After Pre-sintering		% Weight Loss (1490°C)
	Bulk Density* (g/cm^3)	Relative Density (%)	Bulk Density* (g/cm^3)	Relative Density (%)		Bulk Density* (g/cm^3)	Relative Density (%)	
2	2.98	46.3	-	-	2.3	3.77	56.9	2.8
3	2.97	46.1	-	-	2.1	3.45	52.1	2.9
4	3.27	50.8	3.28	50.9	1.9	3.90	58.9	1.1
5	3.21	49.8	3.10	48.1	2.4	3.95	59.7	0.5
6	3.22	50.0	3.19	49.5	2.5	4.13	62.4	0.7

* Determined from the sample geometric dimensions.

samples, determined from the geometric dimensions, are also shown in Table 5.68. (The relative densities were calculated using the solid density value (6.62 g/cm^3) given in equation 5-10, section 5.6.1.1.1.)

5.6.3.2 Sintering/Heat Treatment

The "pre-sintered" samples were sintered in the dilatometer, as described in Chapter 4 (section 4.3.1.3.2). The samples were heated at 5°C/min to temperatures in the range of 1900-2200°C and then held at the maximum temperature for times in the range of 0-15 h.

Table 5.69 shows the bulk density values, determined from geometric measurements, and the corresponding calculated relative density values for the samples sintered at temperatures in the range of 1900-2200°C. (The relative densities were

Table 5.69 Densities (bulk and relative), percent shrinkages, and percent weight losses for sintered samples.

Pellet #	Temperature (°C)/ Time (h)	Shrinkage (%)		Bulk Density* (g/cm^3)	Relative Density (%)	Weight Loss (wt%)
		Diameter	Thickness			
2	2150/1	16.10	16.50	6.20	93.7	3.26
3	2000/5	16.75	17.50	6.34	95.8	2.68
4	2200/0	16.47	15.87	6.51	98.3	1.95
5	1900/15	15.03	15.00	6.31	95.3	1.94
6	2200/0	14.09	13.50	6.33	95.6	2.06

* Determined from the geometric dimensions.

calculated using the solid density (6.62 g/cm^3 given in equation 5-10, section 5.6.1.1.2). The table also lists the percentage shrinkage in the diameter and thickness and the percentage weight loss for each sample.

Table 5.70 shows open porosity, bulk density, and relative density values, determined by the Archimedes method, for the same samples shown in Table 5.69. Tables 5.69 and 5.70 show that there were significant differences in the densities obtained by the two measurements methods. (In most cases, these differences are considerably larger than observed in other samples, such as the ZrPM-87, ZrPM-94, ZrPM-97, and ZrPM-99 samples in section 5.6.2.) The reason for the large differences is not understood.

Table 5.70 Densities (bulk and relative) and percentage open porosity for sintered samples.

Pellet #	Temperature (^{o}C)/ Time (h)	Open Porosity* (%)	Bulk Density* (g/cm^{3})	Relative Density (%)
2	2150/1	n.a.	n.a.	n.a.
3	2000/5	1.39	6.62	100
4	2200/0	0.33	6.66	100
5	1900/15	0.17	6.52	98.5
6	2200/0	0.34	6.65	100

* Determined by the Archimedes method. When more that one measurement was made, the individual values are listed in the parenthesis.

As described in Chapter 4 (section 4.3.1.3.2), the use of dilatometry for sintering studies requires a knowledge of the changes in thermal expansion (or contraction) that occur in the solid material during heating. This information is used to extract the portion of the overall dimensional change of the sample that is due to any shrinkage (i.e., densification) that occurs during sintering. Sintered pellet #4 (Tables 5.69 and 5.70) was used to study thermal expansion behavior in this study. This sample was chosen for two reasons. First, ZrPM-45 samples heat treated at or above 1900^{o}C were expected to be nearly single-phase, nearly stoichiometric ZrC. Second, pellet #4 had the highest relative density (lowest porosity) of all the sintered ZrPM-45 samples.

Figure 5.89 shows plots of the fractional change in length (ΔL/Lo) vs. temperature (over the range 1600-2000^{o}C) for four independent heat treatments using pellet #4. Figure 5.90 shows corresponding plots of the thermal expansion coefficient vs.

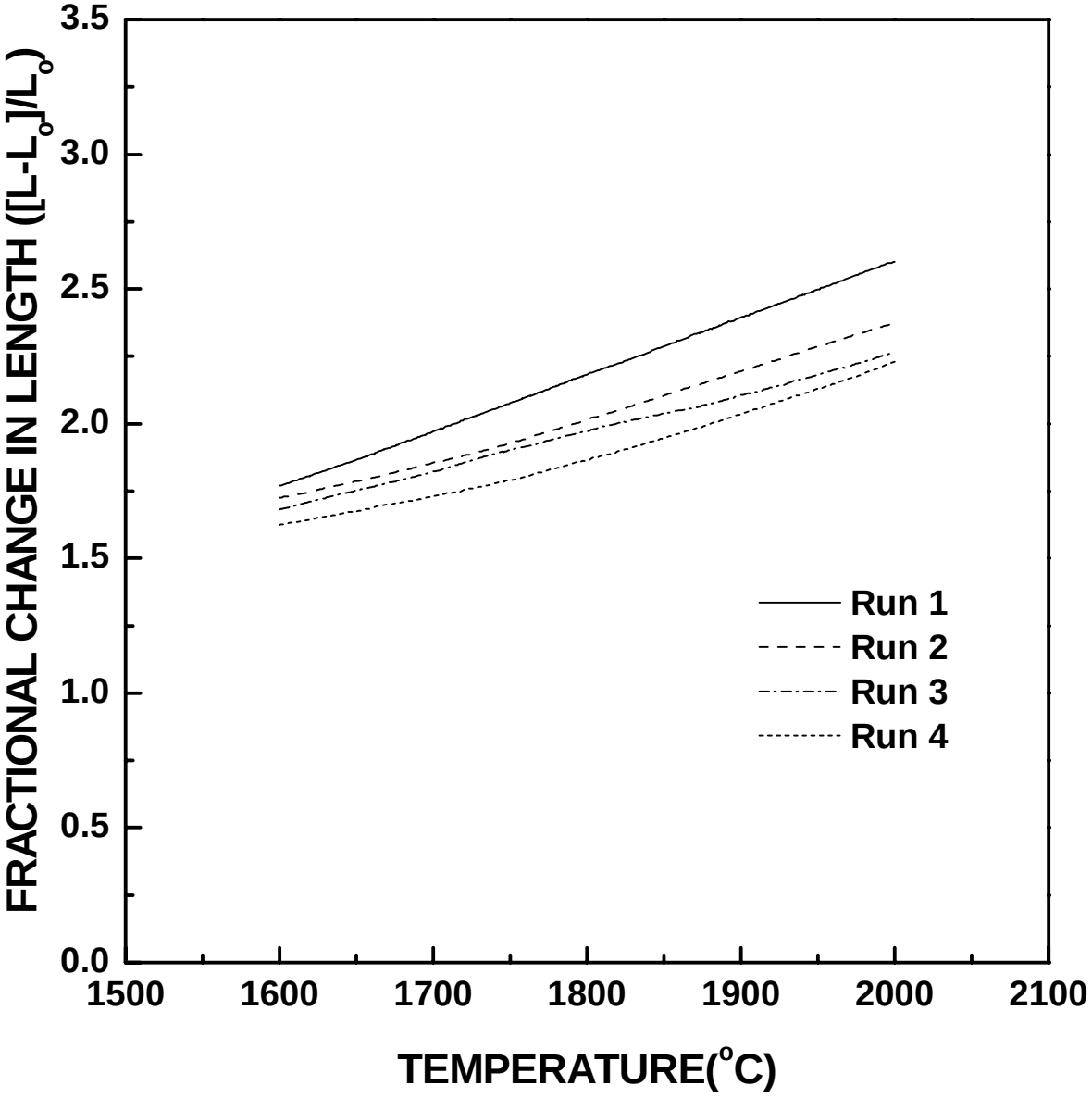

Figure 5.89 Plot of fractional change in length vs. temperature for four independent dilatometer experiments using a ZrPM-45-800-1400-1475-1490-2200 sample which had a near-stoichiometric ZrC composition and a high relative density (~98 %).

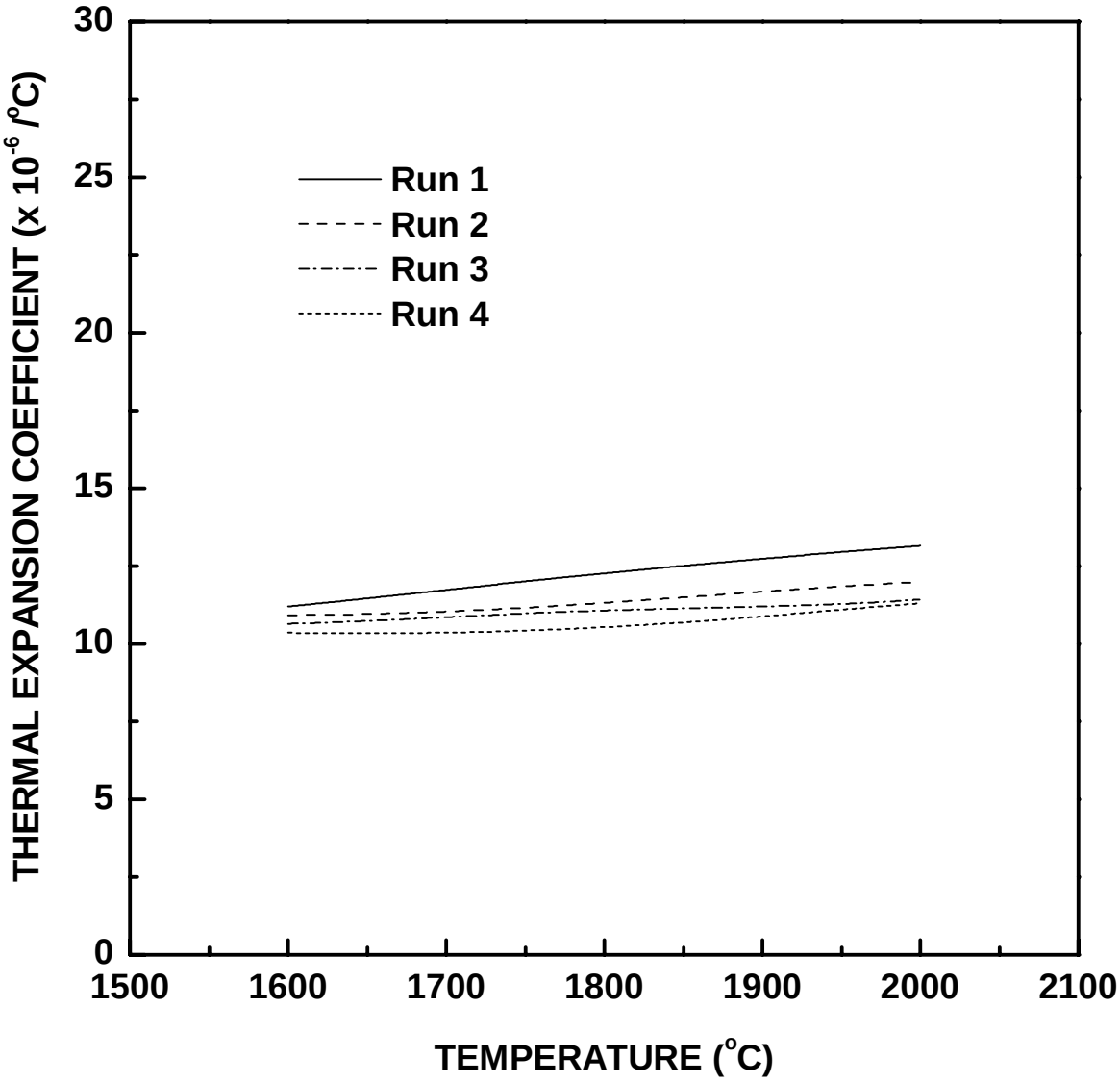

Figure 5.90 Plot of thermal expansion coefficient vs. temperature for four independent dilatometer experiments using a ZrPM-45-800-14001475-1490-2200 sample which had a near-stoichiometric ZrC composition and a high relative density (~98 %).

temperature (1600-2000°C) which was calculated from the data in Figure 5.89. Figure 5.91 shows a plot of the average thermal expansion coefficient vs. temperature (1600-2000°C) which was determined by averaging the four independent runs in Figure 5.90. Table 5.71 lists the average thermal expansion coefficients and standard deviations at specific temperatures in the range of 1600-2000°C, as well as the average value and standard deviation for the entire temperature range.

The thermal expansion coefficient data obtained in this study was compared with data reported by Houska.[93] Figure 5.92 shows plots of the thermal expansion coefficient vs. temperature for the ZrPM-45-800-1400-1475-1490-2200 sample and for the data from reference 93. It is evident that the ZrPM-45 sample had much higher thermal expansions coefficients over the entire range of temperatures that were used. The reason for the difference in the thermal expansion coefficients in the two studies is not known. However, the values obtained in this study are high relative to those reported by other investigators for several refractory carbides (i.e., ZrC, HfC, SiC, TiC).[3,23] Therefore, the data obtained in this study may not be reliable.

Figure 5.93 shows plots of the fractional change in length (ΔL/Lo) vs. sintering temperature for pellets 5 and 6 (from Table 5.69). Note that pellet 5 was heated to a maximum temperature of only 1900°C and then held for 15 h at this temperature, while pellet 6 was heated to a maximum temperature of 2200°C (with no hold time at 2200°C). Figure 5.94 shows plots of the percentage linear shrinkage vs. sintering temperature for pellets 5 and 6 after applying a correction for the average thermal expansion coefficient data shown in Figure 5.91. The two samples show significant differences in the shrinkage behavior over the range of temperatures (1500-1900°C) in which the heating

Table 5.71 Average thermal expansion coefficient data for a ZrPM-45-800-1400-1475-1490-2200 sample which had a near-stoichiometric ZrC composition and a high relative density (~98 %).

Temperature (^{o}C)	Thermal Expansion Coefficient (x 10^{-6} /^{o}C)	Standard Deviation (x 10^{-6} /^{o}C)
1600	11	0.4
1650	11	0.5
1700	11	0.6
1750	11	0.7
1800	11	0.7
1850	12	0.8
1900	12	0.8
1950	12	0.8
2000	12	0.9
Average (1600-2000^{o}C)	11	0.4

Table 5.72 Bulk density and percent shrinkages from geometric measurements and dilatometry.

Pellet	Shrinkage (%)			Bulk Density (g/cm^3)	
	Geometric Measurements (GM)		Dilatometry	GM	Dilatometry
	Diameter	Thickness	Thickness		
5	15.0	15.0	16.1	6.31	6.55
6	14.1	13.5	16.0	6.33	6.81

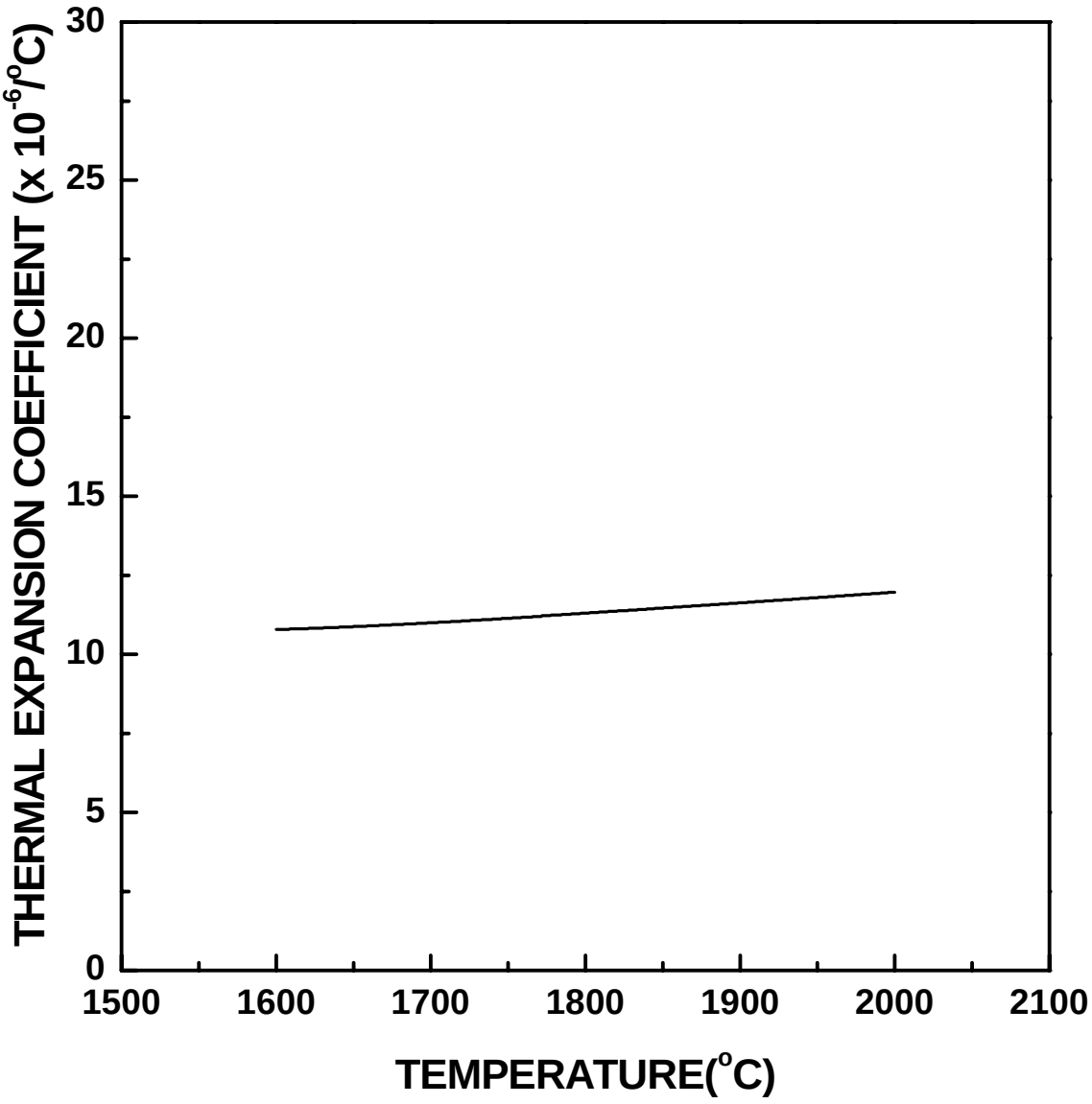

Figure 5.91 Plot of average thermal expansion coefficient vs. temperature for a ZrPM-45-800-1400-1475-1490-2200 sample which had a near-stoichiometric ZrC composition and a high relative density (~98 %). The average value was obtained from the four independent experiments shown in Figure 5.90.

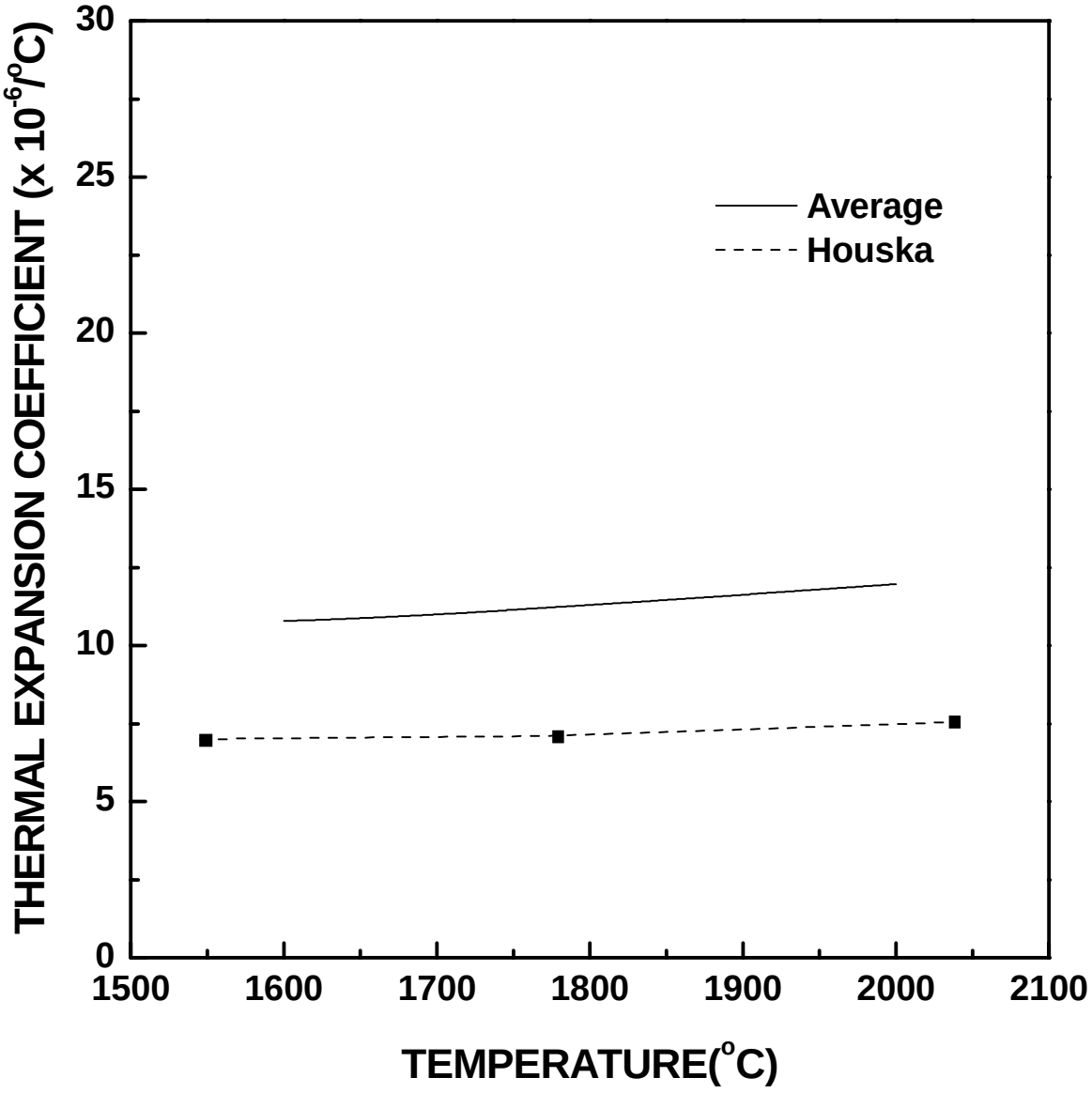

Figure 5.92 Plot of average thermal expansion coefficient vs. temperature for a ZrPM-45-800-1400-1475-1490-2200 sample and data from the reference 106.

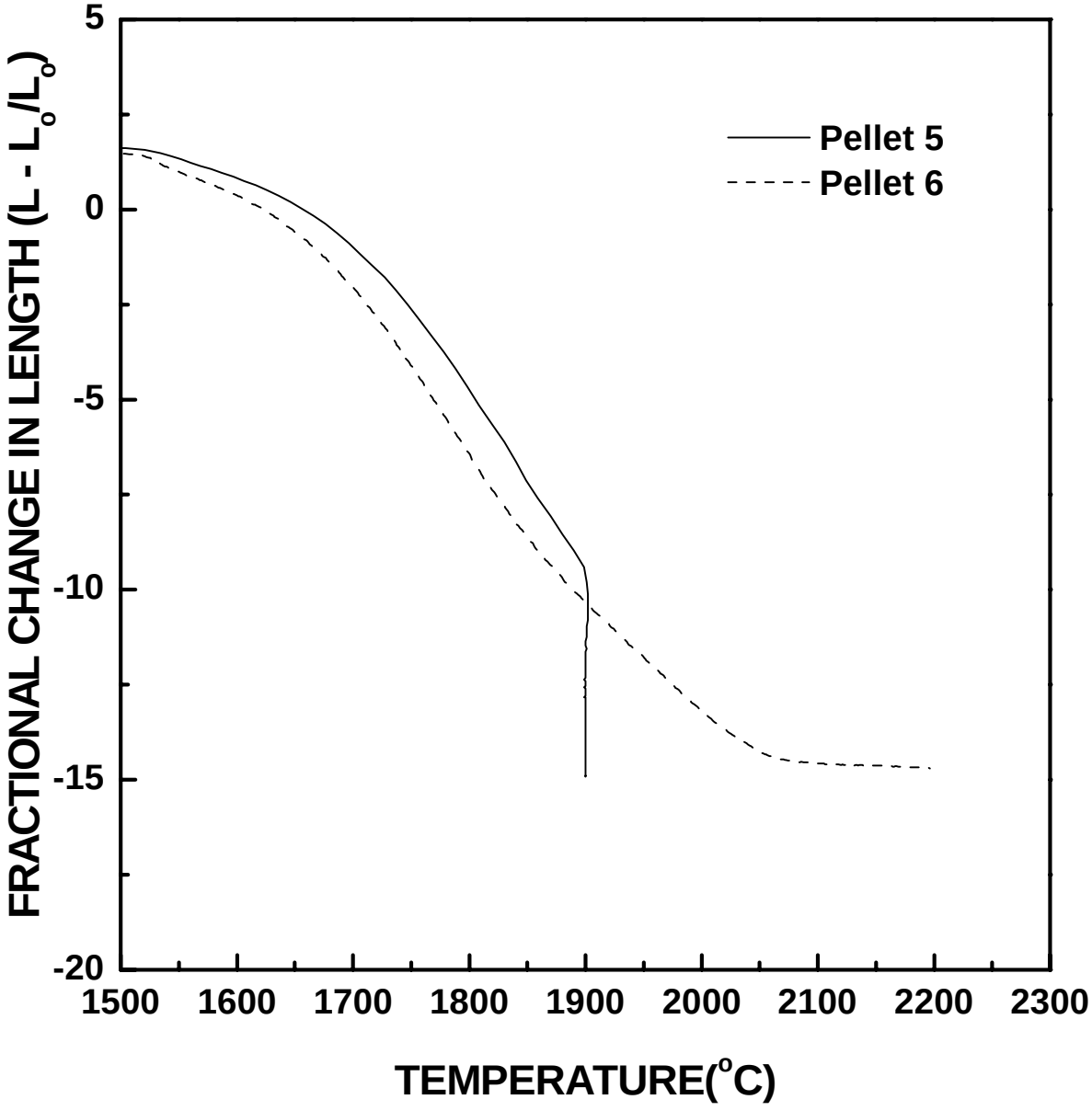

Figure 5.93 Plot of fractional change in length vs. temperature for two different ZrC-based powder compacts.

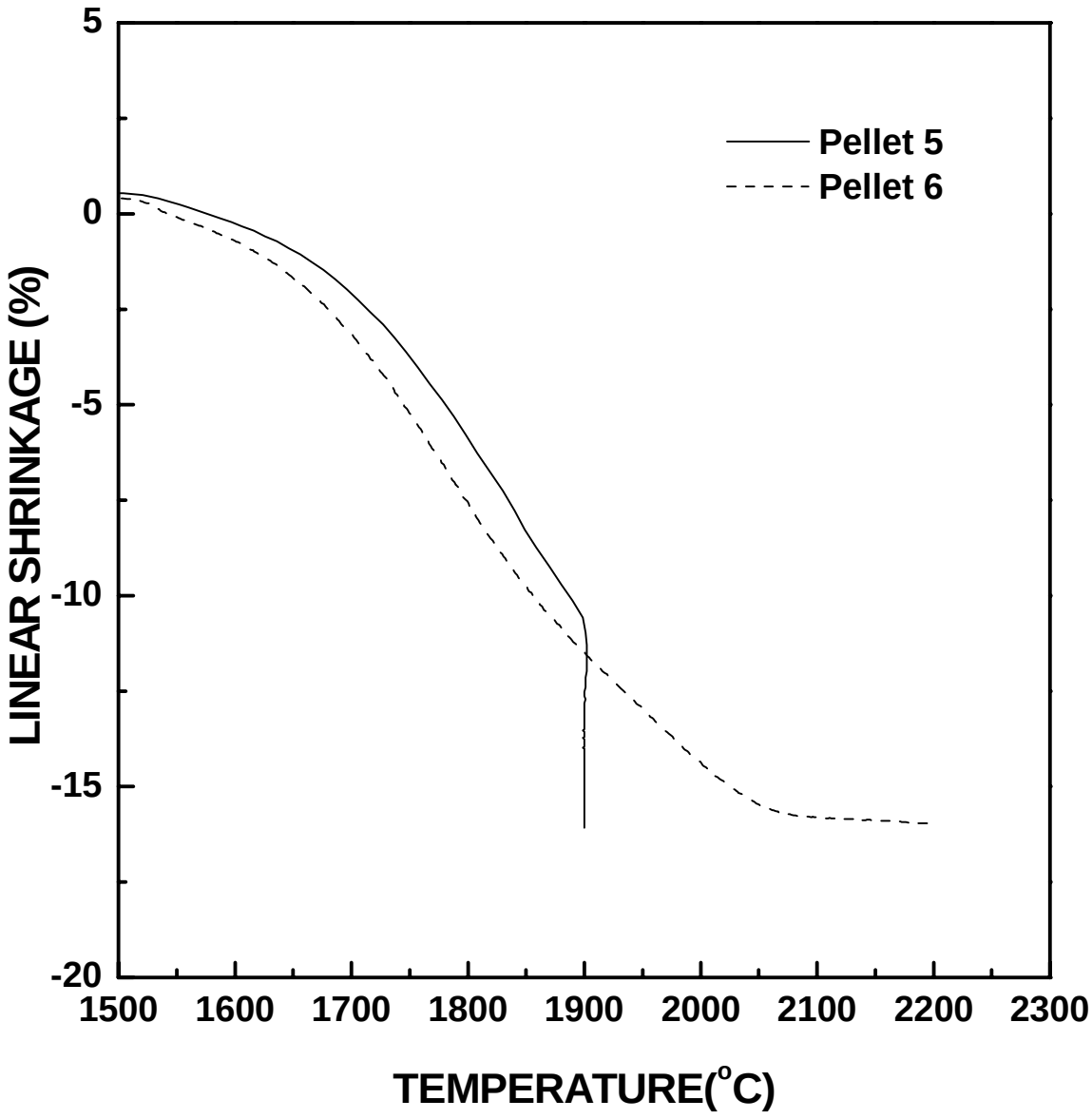

Figure 5.94 Plot of corrected fractional change in length vs. temperature for two different ZrC-based powder compacts.

conditions were the same. It is not clear if these differences are due to instrumental considerations or due to differences in the characteristics of the initial powder compacts. In regard to the latter issue, Table 5.68 shows that the two samples had essentially the same densities after dry pressing. However, the densities after the 1150^{o}C and 1490^{o}C heat treatments showed more significant differences. The relative density of the 1490^{o}C pellet 6 sample was almost 3% higher than the 1490^{o}C pellet 5 sample.

The bulk density of pellets 5 and 6 were calculated based on the final (and maximum) linear shrinkage that was observed in Figure 5.94. In order to make this calculation, it was necessary to assume that the shrinkage was isotropic. Table 5.72 shows the linear shrinkages (corrected for thermal expansion) and the calculated bulk density values. The table also includes the diameter and thickness shrinkages that were determined by measuring (with calipers) the sample dimensions before and after the heat treatment in the dilatometer. Table 5.72 shows that the thickness shrinkages determined by the dilatometer were larger than the corresponding shrinkages determined by measuring the dimensions with the calipers. As a result, the calculated bulk densities were much higher also. The bulk density value obtained for pellet 6 (6.81 g/cm^3) is higher than true solid density value for the sample, so the result is clearly in error. The error may be due to instrumental inaccuracy and/or the assumption of isotropic shrinkage. The measurements of the thickness and diameter of the sample using the calipers shows that there was some anisotropic shrinkage for pellet 6 (see Table 5.72). However, the diameter shrinkage was greater than the thickness shrinkage. If this result was applied to the dilatometry data, then the calculated bulk density value would be even higher.

Therefore, the major source of the error appears to be related to instrumental inaccuracies.

Based on the experiments described in this section, it was decided that the dilatometer would not be used for further investigations. It was originally intended that dilatometry would be used to investigate the effect of sample composition (i.e., C/Zr ratio) on densification kinetics. However, based on the results in Figures 5.89 and 5.94 and Tables 5.71 and 5.72, it was concluded that the data was not reliable or reproducible enough to obtain meaningful results.

CHAPTER VI

Summary

Zirconium carbide (ZrC) powders were produced by carbothermal reduction reactions using fine-scale carbon/metal oxide mixtures as the starting materials. The reactant mixtures were prepared by pyrolytic decomposition of solution-derived precursors.

The first step in the solution process involved refluxing zirconium alkoxide with 2,4 pentanedione ("acacH") in order to partially or fully convert the zirconium alkoxy groups to a chelated zirconium diketonate structure ("zirconium acac"). This was followed by the addition of water (under acidic conditions) in order to promote hydrolysis/condensation reactions. Precursors with variable carbon/metal ratios were produced by varying the concentrations of the solution reactants (i.e., the zirconium alkoxide, "acacH," water, and acid concentrations.) It was necessary to add a secondary soluble carbon source (i.e., phenolic resin or glycerol) during solution processing in order to obtain a C/Zr molar ratio close to or above 3 in the pyrolyzed powders. A C/Zr molar ratio of 3 was required to produce a stoichiometric (or near-stoichiometric) zirconium carbide.

The phase development during carbothermal reduction was investigated in detail using pyrolyzed powders with carbon/metal oxide molar ratio of ~3.1 and ~2.5. The pyrolyzed powders initially consisted of fine-scale mixtures of the tetragonal phase of ZrO_2 (~ 15-20 nm) and amorphous carbon. The tetragonal phase transformed to the monoclinic phase during heat treatment at or above 1100^{o}C. The initial formation of ZrC was clearly evident after heat treatment at 1200^{o}C and the reaction was substantially, but not fully, completed after heat treatments in the range of ~1400-1500^{o}C for powders with C/Zr molar

ratio ~3.1. For the pyrolyzed powder with C/Zr molar ratio ~2.5, some m-ZrO_2 phase could be observed after ~1500°C heat treatment. However, no zirconia phase was observed when the powder was heat treated at 1600°C, suggesting that the material developed a carbon-deficient and/or oxygen-rich ZrC lattice.

ZrC crystallite sizes (determined by XRD line broadening) were ~130-140 nm for powders produced at 1475°C. Weight loss measurements, lattice parameter measurements, and elemental analyses of the carbon and oxygen concentrations showed that the 1475°C sample with starting C/Zr molar ratio ~3.1 consisted of zirconium carbide with some oxygen dissolved in the lattice and some residual free carbon. Heat treatment at higher temperatures (>1600°C) was required to produce near-stoichiometric zirconium carbide with low oxygen content for this material. In contrast, non-stoichiometric ZrC_{1-x} (with small amounts of dissolved oxygen) was obtained using the pyrolyzed powder with C/Zr molar ratio ~2.5 after heat treatments above 1600°C.

ZrC powders, with varying C/Zr molar ratios (~2.4 to ~3.3) in the pyrolyzed material, were dry-pressed to form "green" compacts with relative density in the range of ~45 to ~48 %. The compacts were sintered at temperatures in the range of 1600-1950°C (2 h). The samples prepared from pyrolyzed materials with C/Zr molar ratios up to ~3.2 had zero open porosity and relative densities in the range of ~98-100% after sintering at 1950°C for 2 h. A sample with higher carbon concentration (C/Zr molar ratio of ~3.3 in the pyrolyzed material) ~2 % open porosity and ~98 % relative density after sintering at 1950°C for 2 h.

APPENDIX A

ELECTROPHORETIC MOBILITY DATA AND CALCULATED ZETA POTENTIAL VALUES

Table A1 Electrophoretic mobility data and calculated zeta potential values for the suspension of 10 min-milled ZrPM-45-800-1350-1400 sample in deionized water (pH = 2.9, 7, and 10).

pH	Mobility* (μm·cm/V·s)			Zeta Potential** (mV)		
	Angle (^{o})	Upper Level	Lower Level	Angle (^{o})	Upper Level	Lower Level
2.9	8.9	2.67 ± 1.76	2.72 ± 1.20	8.9	32.3	32.9
2.9	17.6	2.16 ± 1.59	2.41 ± 1.36	17.6	26.1	29.2
2.9	26.3	1.99 ± 1.65	2.27 ± 1.50	26.3	24.0	27.4
2.9	35.2	1.80 ± 1.80	2.28 ± 1.65	35.2	21.7	27.6
	Average	2.16 ± 1.7	2.42 ± 1.42	Average	26.1 ± 3.9	29.2 ± 2.2
7.0	8.9	-1.92 ± 0.79	-1.99 ± 0.68	8.9	-23.2	-24.0
7.0	17.6	-2.17 ± 0.84	-2.28 ± 0.73	17.6	-26.2	-27.6
7.0	26.3	-2.11 ± 0.91	-2.16 ± 0.79	26.3	-25.5	-26.1
7.0	35.2	-1.82 ± 0.99	-2.01 ± 0.85	35.2	-22.0	-24.3
	Average	-2.01 ± 0.88	-2.11 ± 0.76	Average	-24.3 ± 1.7	-25.5 ± 1.4

Table A1 continued.

pH	Mobility* (µm·cm/V·s)			Zeta Potential** (mV)		
	Angle (^{o})	Upper Level	Lower Level	Angle (^{o})	Upper Level	Lower Level
10.0	8.9	-2.75 ± 2.05	-3.90 ± 1.32	8.9	-33.2	-47.1
10.0	17.6	-3.21 ± 2.05	-4.44 ± 1.40	17.6	-38.8	-53.6
10.0	26.3	-3.34 ± 2.21	-4.68 ± 1.56	26.3	-40.3	-56.5
10.0	35.2	-3.21 ± 2.50	-5.10 ± 1.77	35.2	-38.8	-61.6
	Average	-3.13 ± 2.2	-4.53 ± 1.51	Average	-37.8 ± 2.7	-54.7 ± 5.2

* Averages and standard deviation values are reported.

** Zeta potential values were calculated using the Helmholtz-Smoluchowski equation. Measurements were made at 25.2^{o}C. At this temperature, the viscosity of water is 0.0089 N·s/m^2 and permittivity of water is 6.94 x 10^{-8} Farad/cm.

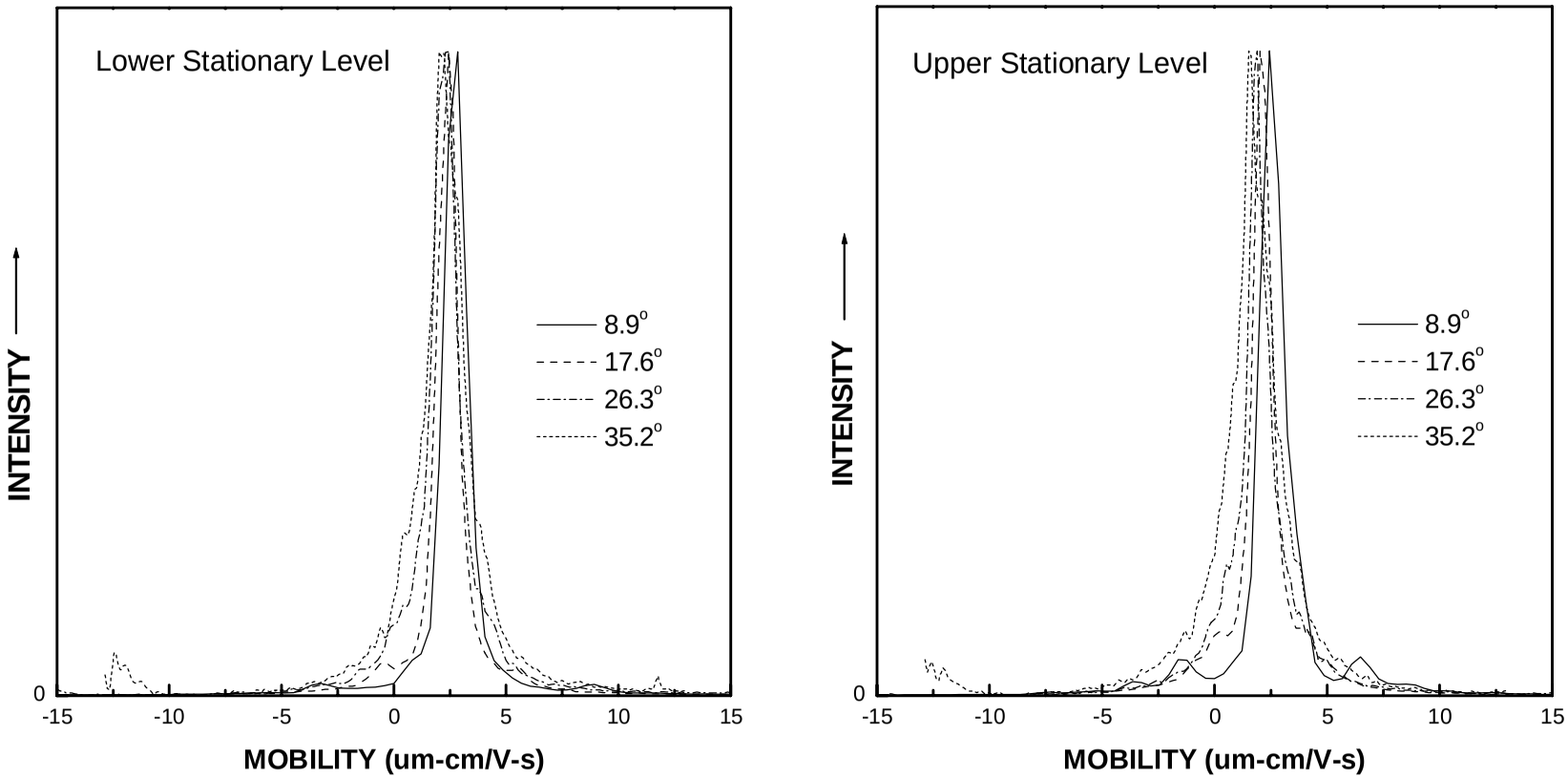

Figure A1 Electrophoretic mobility distribution plots for the suspension of 10 min-milled ZrPM-45-800-1350-1400 sample in deionized water (pH = 3).

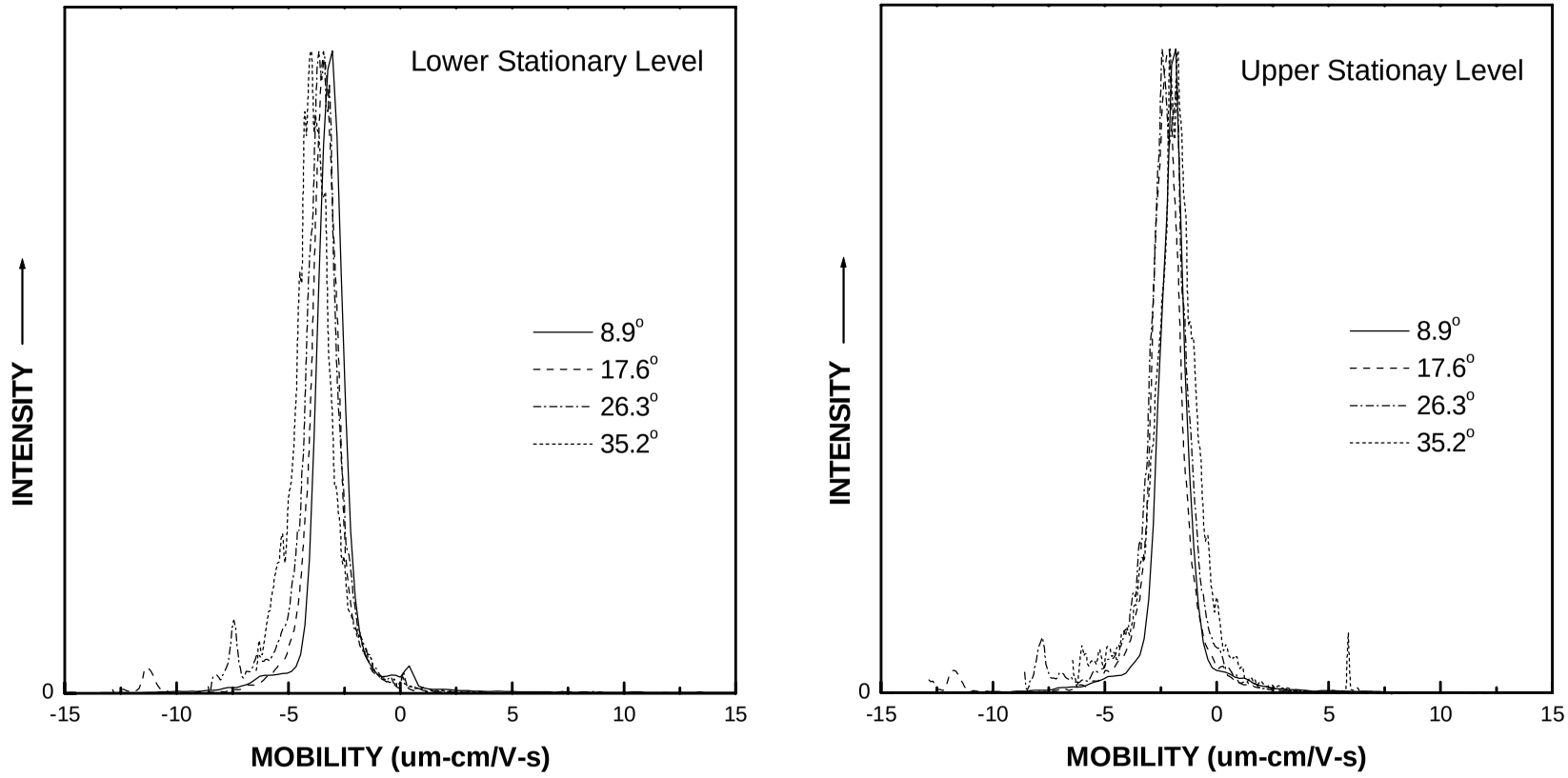

Figure A2 Electrophoretic mobility distribution plots for the suspension of 10 min-milled ZrPM-45-800-1350-1400 sample in deionized water (pH = 7).

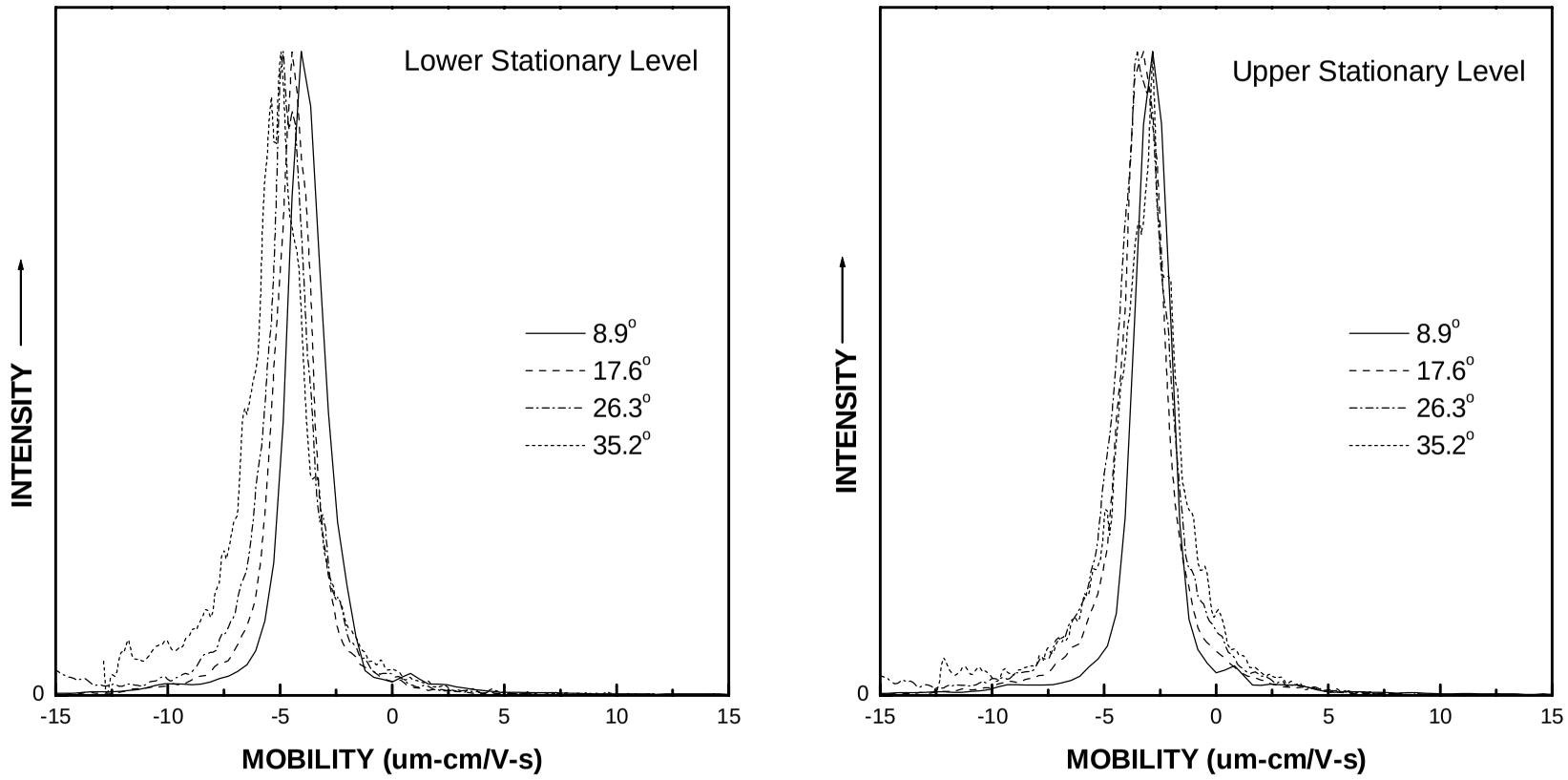

Figure A3 Electrophoretic mobility distribution plots for the suspension of 10 min-milled ZrPM-45-800-1350-1400 sample in deionized water (pH = 10).

APPENDIX B

DETAILED SYNTHESIS PROCEDURE FOR SPECIFIC ZrPM BATCHES

This section gives the detailed step-by-step procedures for synthesis of some specific ZrPM batches. The overall procedure followed was same as described in section 4.1.2.2.

ZrPM-45

1. 73.000 g (0.156 mol) of zirconium propoxide (ZP) solution was weighed into a two-liter round bottom flask. 657.0 g of distilled ethanol was added and the flask was shaken manually to mix the contents. The total concentration of ZP was 10 wt%. The whole procedure was done in a glove box.
2. The flask was taken out of the glove box and attached to the Schlenk apparatus. The procedure followed was same as described in section 4.1.2.2.2.
3. 62.40 g of acac was mixed with 249.6 g of distilled ethanol in a 500 ml flask in a fume hood. The total concentration of acac was 20 wt%. The flask was shaken manually to mix the contents. This solution was then transferred to the Schlenk apparatus and added to the ZP solution. The procedure followed was same as described in section 4.1.2.2.2. The time taken to add acac solution was ~ 4 – 5 min.
4. 5 ml of distilled ethanol was used to rinse the funnel walls as described in section 4.1.2.2.2.
5. The solution was refluxed at 130^{o}C for 2 h using a heating mantle with a variac.

6. After the solution was refluxed it was allowed to cool. The flask was left attached to the Schlenk apparatus for ~18 h before the next processing step.

7. The flask was then removed from the Schlenk apparatus and attached to a rotary evaporator ("rotovap"). The solution was partially concentrated. The temperature of the water bath was maintained in the range of 40–45^{o}C. The weights of the solution before and after the evaporation were not recorded. The amount of solution left after concentration was assumed to be 30 – 35 wt% of the initial amount.

8. The flask was removed from the rotovap and 1000 ml of distilled ethanol was added to the flask in ~15 – 30 sec. A magnetic stirrer was used to mix the solutions for ~5 min. The color of the solution was greenish yellow and the pH of the solution was 8.8.

9. 140 drops of 20 wt% nitric acid (HNO_3) solution in 80 wt% distilled ethanol was then added to the above solution. The time taken to add the acid solution was ~ 3 min. The solution was simultaneously stirred with a magnetic stirrer. The pH recorded after the addition was acid was 6.85. The amount of acid added (calculated later) corresponded to an HNO_3/Zr molar ratio of 0.04. The amount of water (from the nitric acid solution) corresponded to an H_2O/Zr molar ratio of 0.01.

10. 336.96 g of 20 wt% deionized (DI) water in 80 wt% distilled ethanol was then added to the solution under constant magnetic stirring. The conductivity of DI water was not measured. The water solution was added in ~ 6 – 7 min. The amount of water from this step corresponded to an H_2O/Zr molar ratio of 24.

11. The flask was sealed and then placed in an air oven at 50^{o}C for 2 h.

12. The flask was then taken out of the oven and allowed to cool for ~30 min. The pH of the solution was 4.64.

13. 4.21 g of phenolic resin was mixed with distilled ethanol to form a 20 wt% solution. This 20 wt% solution of phenolic resin was then added to the solution in step 12. The solution was mixed by a magnetic stirrer for ~10 min and then left for an additional 20 min prior to the next processing step.

14. The flask was then attached to the rotovap. The solution was concentrated until solvent loss was no longer obvious visually. The temperature of the water bath was maintained in the range of 35 – 40^{o}C. After concentration, the material can be described as a highly viscous yellow liquid.

15. The flask was then sealed with aluminum foil that was perforated in order to allow removal of small amounts of residual solvent. The flask was put in a vacuum oven and heated to 120^{o}C for 3 h. The weights of the material before and after drying were 68.83 g and 44.26 g, respectively. The material was a homogeneous dark yellow powder.

ZrPM-58

1. 73.000 g (0.156 mol) of zirconium propoxide (ZP) solution was weighed into a two-liter round bottom flask. 657.0 g of distilled ethanol was added and the flask was shaken manually to mix the contents. The total concentration of ZP was 10 wt%. The whole procedure was done in a glove box.

2. The flask was taken out of the glove box and attached to the Schlenk apparatus. The procedure followed was same as described in section 4.1.2.2.2.
3. 46.80 g of acac was mixed with 187.20 g of distilled ethanol in a 500 ml flask in a fume hood. The total concentration of acac was 20 wt%. The flask was shaken manually to mix the contents. This solution was then transferred to the Schlenk apparatus and added to the ZP solution. The procedure followed was same as described in section 4.1.2.2.2. The time taken to add acac solution was ~ 4 – 5 min.
4. 5 ml of distilled ethanol was used to rinse the funnel walls as described in section 4.1.2.2.2.
5. The solution was refluxed at 195^{o}C for 3 h using a heating mantle with a variac.
6. After the solution was refluxed it was allowed to cool. The flask was left attached to the Schlenk apparatus for ~15 h before the next processing step.
7. The flask was then removed from the Schlenk apparatus and attached to a rotary evaporator ("rotovap"). The solution was partially concentrated. The temperature of the water bath was maintained in the range of 40 – 45^{o}C. The weights of the solution before and after the evaporation were not recorded. The amount of solution left after concentration was assumed to be 30 wt% of the initial amount.
8. The flask was removed from the rotovap and 1000 ml of distilled ethanol was added to the flask in ~15 – 30 sec. A magnetic stirrer was used to mix the solutions for ~5 min. The color of the solution was greenish yellow.
9. 14.784 g of glycerol was added to the solution in ~3 min. The solution was shaken manually for ~30 sec and was stirred for additional ~5 min with a

magnetic stirrer. The amount of glycerol added in this step corresponded to a glycerol/Zr molar ratio of 1.03.

10. 270 drops of 20 wt% nitric acid (HNO_3) solution in 80 wt% distilled ethanol was then added to the above solution. The time taken to add the acid solution was ~ 3 min. The solution was simultaneously stirred with a magnetic stirrer. The pH recorded after the addition was acid was 5.8. The amount of acid (calculated later) added corresponded to an HNO_3/Zr molar ratio of 0.077. The amount of water (from the nitric acid solution) corresponded to an H_2O/Zr molar ratio of 0.49.
11. 336.96 g of 20 wt% deionized (DI) water in 80 wt% distilled ethanol was then added to the solution under constant magnetic stirring. The water solution was added in ~ 10 – 12 min. The amount of water from this step corresponded to an H_2O/Zr molar ratio of 24.
12. The flask was sealed and then placed in an air oven at 50^oC for 2 h.
13. The flask was then taken out of the oven and allowed to cool for ~30 min.
14. The flask was then attached to the rotovap. The solution was concentrated until solvent loss was no longer obvious visually. The temperature of the water bath was maintained in the range of 35 – 40^oC. After concentration, the material can be described as a highly viscous yellow liquid.
15. The flask was then sealed with aluminum foil that was perforated in order to allow removal of small amounts of residual solvent. The flask was put in a vacuum oven and heated to 120^oC for 3 h. The material was a homogeneous fractured powder cake and was yellow in color.

ZrPM-59

1. 73.000 g (0.156 mol) of zirconium propoxide (ZP) solution was weighed into a two-liter round bottom flask. 657.0 g of distilled ethanol was added and the flask was shaken manually to mix the contents. The total concentration of ZP was 10 wt%. The whole procedure was done in a glove box.
2. The flask was taken out of the glove box and attached to the Schlenk apparatus. The procedure followed was same as described in section 4.1.2.2.2.
3. 46.80 g of acac was mixed with 187.20 g of distilled ethanol in a 500 ml flask in a fume hood. The total concentration of acac was 20 wt%. The flask was shaken manually to mix the contents. This solution was then transferred to the Schlenk apparatus and added to the ZP solution. The procedure followed was same as described in section 4.1.2.2.2. The time taken to add acac solution was ~ 4 – 5 min.
4. 5 ml of distilled ethanol was used to rinse the funnel walls as described in section 4.1.2.2.2.
5. The solution was refluxed at 195^{o}C for 3 h using a heating mantle with a variac.
6. After the solution was refluxed it was allowed to cool. The flask was left attached to the Schlenk apparatus for ~15 h before the next processing step.
7. The flask was then removed from the Schlenk apparatus and attached to a rotary evaporator ("rotovap"). The solution was partially concentrated. The temperature of the water bath was maintained in the range of 40 – 45^{o}C. The weights of the solution before and after the evaporation were not recorded. The amount of solution left after concentration was assumed to be 30 wt% of the initial amount.

8. The flask was removed from the rotovap and 1000 ml of distilled ethanol was added to the flask in ~15 – 30 sec. A magnetic stirrer was used to mix the solutions for ~5 min. The color of the solution was greenish yellow.

9. 24.656 g of glycerol was added to the solution in ~3 min. The solution was shaken manually for ~30 sec and was stirred for additional ~5 min with a magnetic stirrer. The amount of glycerol added in this step corresponded to a glycerol/Zr molar ratio of 1.72.

10. 304 drops of 20 wt% nitric acid (HNO_3) solution in 80 wt% distilled ethanol was then added to the above solution. The time taken to add the acid solution was ~ 3 min. The solution was simultaneously stirred with a magnetic stirrer. The pH recorded after the addition was acid was 5.6. The amount of acid (calculated later) added corresponded to an HNO_3/Zr molar ratio of 0.087. The amount of water (from the nitric acid solution) corresponded to an H_2O/Zr molar ratio of 0.15.

11. 336.96 g of 20 wt% deionized (DI) water in 80 wt% distilled ethanol was then added to the solution under constant magnetic stirring. The water solution was added in ~ 10 – 12 min. The amount of water from this step corresponded to an H_2O/Zr molar ratio of 24.

12. The flask was sealed and then placed in an air oven at 50^{o}C for 2 h.

13. The flask was then taken out of the oven and allowed to cool for ~30 min.

14. The flask was then attached to the rotovap. The solution was concentrated until solvent loss was no longer obvious visually. The temperature of the water bath was maintained in the range of 35 – 40^{o}C. After concentration, the material can be described as a highly viscous yellow liquid.

15. The flask was then sealed with aluminum foil that was perforated in order to allow removal of small amounts of residual solvent. The flask was put in a vacuum oven and heated to 120^{o}C for 3 h. The material was a homogeneous fractured powder cake and was dark yellow in color.

ZrPM-67

1. 15.000 g (0.032 mol) of zirconium propoxide (ZP) solution was weighed into a half-liter round bottom flask. 135.0 g of distilled ethanol was added and the flask was shaken manually to mix the contents. The total concentration of ZP was 10 wt%. The whole procedure was done in a glove box.
2. The flask was taken out of the glove box and attached to the Schlenk apparatus. The procedure followed was same as described in section 4.1.2.2.2.
3. 9.62 g of acac was mixed with 38.64 g of distilled ethanol in a 500 ml flask in a fume hood. The total concentration of acac was 20 wt%. The flask was shaken manually to mix the contents. This solution was then transferred to the Schlenk apparatus and added to the ZP solution. The procedure followed was same as described in section 4.1.2.2.2. The time taken to add acac solution was ~ 4 – 5 min.
4. 5 ml of distilled ethanol was used to rinse the funnel walls as described in section 4.1.2.2.2.
5. The solution was refluxed at 195^{o}C for 2 h using a heating mantle with a variac.
6. After the solution was refluxed it was allowed to cool. The flask was left attached to the Schlenk apparatus for 16 h before the next processing step.

7. The flask was then removed from the Schlenk apparatus and attached to a rotary evaporator ("rotovap"). The solution was partially concentrated. The temperature of the water bath was maintained in the range of 40 – 45^{o}C. The weights of the solution before and after the evaporation were 231.96 g and 119.09 g, respectively. This was equivalent to ~51 wt% solution left after evaporation.

8. The flask was removed from the rotovap and 300 ml of distilled ethanol was added to the flask in ~10 – 15 sec. A magnetic stirrer was used to mix the solutions for ~5 min. The color of the solution was greenish yellow and the pH of the solution was 9.51.

9. 5.5 g (6.3 ml) of 10 wt% nitric acid (HNO_3) solution in 90 wt% distilled ethanol was then added to the above solution. The time taken to add the acid solution was ~ 2 min. The solution was simultaneously stirred with a magnetic stirrer. The pH recorded after the addition was acid was 4.51. The amount of acid added corresponded to an HNO_3/Zr molar ratio of 0.27. The amount of water (from the nitric acid solution) corresponded to an H_2O/Zr molar ratio of 0.47.

10. 138.45 g of 10 wt% deionized (DI) water in 90 wt% distilled ethanol was then added to the solution under constant magnetic stirring. The water solution was added in ~ 5 – 7 min and the pH recorded after water addition was 5.26. The amount of water from this step corresponded to an H_2O/Zr molar ratio of 24.

11. The flask was sealed and then placed in an air oven at 50^{o}C for 2 h.

12. The flask was then taken out of the oven and allowed to cool for ~30 min. The pH of the solution was 4.2.

13. The flask was then attached to the rotovap. The solution was concentrated until solvent loss was no longer obvious visually. The temperature of the water bath was maintained in the range of 35 – 40^{o}C. After concentration, the material can be described as a yellow gel.

14. The flask was then sealed with aluminum foil that was perforated in order to allow removal of small amounts of residual solvent. The flask was put in a vacuum oven and heated to 120^{o}C for 3 h. The weights of the material before and after drying were 10.12 g and 8.42 g, respectively. The material was a homogeneous fractured powder cake and was light yellow in color.

ZrPM-79

1. 15.000 g (0.032 mol) of zirconium propoxide (ZP) solution was weighed into a half-liter round bottom flask. 135.0 g of distilled ethanol was added and the flask was shaken manually to mix the contents. The total concentration of ZP was 10 wt%. The whole procedure was done in a glove box.

2. The flask was taken out of the glove box and attached to the Schlenk apparatus. The procedure followed was same as described in section 4.1.2.2.2.

3. 9.62 g of acac was mixed with 38.64 g of distilled ethanol in a 500 ml flask in a fume hood. The total concentration of acac was 20 wt%. The flask was shaken manually to mix the contents. This solution was then transferred to the Schlenk apparatus and added to the ZP solution. The procedure followed was same as described in section 4.1.2.2.2. The time taken to add acac solution was ~ 4 – 5 min.

4. 5 ml of distilled ethanol was used to rinse the funnel walls as described in section 4.1.2.2.2.

5. The solution was refluxed at 195^{o}C for 2 h using a heating mantle with a variac.

6. After the solution was refluxed it was allowed to cool. The flask was left attached to the Schlenk apparatus for 15 h before the next processing step.

7. The flask was then removed from the Schlenk apparatus and attached to a rotary evaporator ("rotovap"). The solution was partially concentrated. The temperature of the water bath was maintained in the range of 40 – 45^{o}C. The weights of the solution before and after the evaporation were 232.17 g and 111.52 g, respectively. This was equivalent to ~48 wt% solution left after evaporation.

8. The flask was removed from the rotovap and 300 ml of distilled ethanol was added to the flask in ~10 – 15 sec. A magnetic stirrer was used to mix the solutions for ~5 min. The color of the solution was greenish yellow and the pH of the solution was 9.49.

9. 1.86 g of glycerol was added to the solution in ~1 min. The solution was shaken manually for ~30 sec and was stirred for an additional ~5 min with a magnetic stirrer. The amount of glycerol added in this step corresponded to a glycerol/Zr molar ratio of 0.63.

10. 5.5 g (6.4 ml) of 10 wt% nitric acid (HNO_3) solution in 90 wt% distilled ethanol was then added to the above solution. The time taken to add the acid solution was ~ 3 min. The solution was simultaneously stirred with a magnetic stirrer. The pH recorded after the addition was acid was 5.78. The amount of acid added

corresponded to an HNO_3/Zr molar ratio of 0.272. The amount of water (from the nitric acid solution) corresponded to an H_2O/Zr molar ratio of 0.47.

11. 138.46 g of 10 wt% deionized (DI) water in 90 wt% distilled ethanol was then added to the solution under constant magnetic stirring. The conductivity of DI water was measured to be 0.33 μS/cm. The water solution was added in ~ 5 – 7 min and the pH recorded after water addition was 5.39. The amount of water from this step corresponded to an H_2O/Zr molar ratio of 24.
12. The flask was sealed and then placed in an air oven at 50°C for 2 h.
13. The flask was then taken out of the oven and allowed to cool for ~30 min. The pH of the solution was 4.98.
14. The flask was then attached to the rotovap. The solution was concentrated until solvent loss was no longer obvious visually. The temperature of the water bath was maintained in the range of 35 – 40°C. After concentration, the material can be described as a yellow gel.
15. The flask was then sealed with aluminum foil that was perforated in order to allow removal of small amounts of residual solvent. The flask was put in a vacuum oven and heated to 120°C for 3 h. The weights of the material before and after drying were 11.46 g and 9.74 g, respectively. The material was a homogeneous fractured powder cake and was light yellow in color.

ZrPM-87

1. 75.000 g (0.160 mol) of zirconium propoxide (ZP) solution was weighed into a three-liter round bottom flask. 675.0 g of distilled ethanol was added and the flask

was shaken manually to mix the contents. The total concentration of ZP was 10 wt%. The whole procedure was done in a glove box.

2. The flask was taken out of the glove box and attached to the Schlenk apparatus. The procedure followed was same as described in section 4.1.2.2.2.
3. 48.07 g of acac was mixed with 193.20 g of distilled ethanol in a 500 ml flask in a fume hood. The total concentration of acac was 20 wt%. The flask was shaken manually to mix the contents. This solution was then transferred to the Schlenk apparatus and added to the ZP solution. The procedure followed was same as described in section 4.1.2.2.2. The time taken to add acac solution was ~ 4 – 5 min.
4. 5 ml of distilled ethanol was used to rinse the funnel walls as described in section 4.1.2.2.2.
5. The solution was refluxed at 195^{o}C for 2 h using a heating mantle with a variac.
6. After the solution was refluxed it was allowed to cool. The flask was left attached to the Schlenk apparatus for 16 h before the next processing step.
7. The flask was then removed from the Schlenk apparatus and attached to a rotary evaporator ("rotovap"). The solution was partially concentrated. The temperature of the water bath was maintained in the range of 40 – 45^{o}C. The weights of the solution before and after the evaporation were 986.77 g and 371.69 g, respectively. This was equivalent to ~38 wt% solution left after evaporation.
8. The flask was removed from the rotovap and 1500 ml of distilled ethanol was added to the flask in ~15 – 30 sec. A magnetic stirrer was used to mix the

solutions for ~5 min. The color of the solution was greenish yellow and the pH of the solution was 10.3.

9. 3.5 g of glycerol was added to the solution in ~1 min. The solution was shaken manually for ~30 sec and was stirred for additional ~5 min with a magnetic stirrer. The pH of the solution was 10.14. The amount of glycerol added in this step corresponded to a glycerol/Zr molar ratio of 0.238.

10. 27.5 g (32.5 ml) of 10 wt% nitric acid (HNO_3) solution in 90 wt% distilled ethanol was then added to the above solution. The time taken to add the acid solution was ~ 3 min. The solution was simultaneously stirred with a magnetic stirrer. The pH recorded after the addition was acid was 5.31. The amount of acid added corresponded to an HNO_3/Zr molar ratio of 0.272. The amount of water (from the nitric acid solution) corresponded to an H_2O/Zr molar ratio of 0.46.

11. 345.21 g of 20 wt% deionized (DI) water in 80 wt% distilled ethanol was then added to the solution under constant magnetic stirring. The conductivity of DI water was measured to be 0.30 μS/cm. The water solution was added in ~ 6 – 7 min and the pH recorded after water addition was 6.2. The amount of water from this step corresponded to an H_2O/Zr molar ratio of 24.

12. The flask was sealed and then placed in an air oven at 50^{o}C for 2 h.

13. The flask was then taken out of the oven and allowed to cool for ~30 min. The pH of the solution was 5.29.

14. The flask was then attached to the rotovap. The solution was concentrated until solvent loss was no longer obvious visually. The temperature of the water bath

was maintained in the range of 35 – 40^{o}C. After concentration, the material can be described as a yellow gel with some liquid remaining.

15. The flask was then sealed with aluminum foil that was perforated in order to allow removal of small amounts of residual solvent. The flask was put in a vacuum oven and heated to 120^{o}C for 3 h. The weights of the material before and after drying were 56.43 g and 44.81 g, respectively. The material was a homogeneous fractured powder cake and was light yellow in color.

ZrPM-94

1. 75.000 g (0.160 mol) of zirconium propoxide (ZP) solution was weighed into a three-liter round bottom flask. 675.0 g of distilled ethanol was added and the flask was shaken manually to mix the contents. The total concentration of ZP was 10 wt%. The whole procedure was done in a glove box.
2. The flask was taken out of the glove box and attached to the Schlenk apparatus. The procedure followed was same as described in section 4.1.2.2.2.
3. 48.07 g of acac was mixed with 193.20 g of distilled ethanol in a 500 ml flask in a fume hood. The total concentration of acac was 20 wt%. The flask was shaken manually to mix the contents. This solution was then transferred to the Schlenk apparatus and added to the ZP solution. The procedure followed was same as described in section 4.1.2.2.2. The time taken to add acac solution was ~ 4 – 5 min.
4. 5 ml of distilled ethanol was used to rinse the funnel walls as described in section 4.1.2.2.2.

5. The solution was refluxed at 195^{o}C for 2 h using a heating mantle with a variac.

6. After the solution was refluxed it was allowed to cool. The flask was left attached to the Schlenk apparatus for 15 h before the next processing step.

7. The flask was then removed from the Schlenk apparatus and attached to a rotary evaporator ("rotovap"). The solution was partially concentrated. The temperature of the water bath was maintained in the range of 40 – 45^{o}C. The weights of the solution before and after the evaporation were 989.19 g and 413.09 g, respectively. This was equivalent to ~42 wt% solution left after evaporation.

8. The flask was removed from the rotovap and 1500 ml of distilled ethanol was added to the flask in ~15 – 30 sec. A magnetic stirrer was used to mix the solutions for ~5 min. The color of the solution was greenish yellow and the pH of the solution was 9.94.

9. 7.46 g of glycerol was added to the solution in ~2 min. The solution was shaken manually for ~30 sec and was stirred for additional ~5 min with a magnetic stirrer. The pH of the solution was 9.52. The amount of glycerol added in this step corresponded to a glycerol/Zr molar ratio of 0.506.

10. 27.5 g (32.5 ml) of 10 wt% nitric acid (HNO_3) solution in 90 wt% distilled ethanol was then added to the above solution. The time taken to add the acid solution was ~ 3 min. The solution was simultaneously stirred with a magnetic stirrer. The pH recorded after the addition was acid was 5.83. The amount of acid added corresponded to an HNO_3/Zr molar ratio of 0.272. The amount of water (from the nitric acid solution) corresponded to an H_2O/Zr molar ratio of 0.46.

11. 692.11 g of 10 wt% deionized (DI) water in 90 wt% distilled ethanol was then added to the solution under constant magnetic stirring. The conductivity of DI water was measured to be 0.32 μS/cm. The water solution was added in ~ 10 – 12 min and the pH recorded after water addition was 5.98. The amount of water from this step corresponded to an H_2O/Zr molar ratio of 24.
12. The flask was sealed and then placed in an air oven at 50°C for 2 h.
13. The flask was then taken out of the oven and allowed to cool for ~30 min. The pH of the solution was 5.2.
14. The flask was then attached to the rotovap. The solution was concentrated until solvent loss was no longer obvious visually. The temperature of the water bath was maintained in the range of 35 – 40°C. After concentration, the material can be described as a yellow gel with some liquid remaining.
15. The flask was then sealed with aluminum foil that was perforated in order to allow removal of small amounts of residual solvent. The flask was put in a vacuum oven and heated to 120°C for 3 h. The weights of the material before and after drying were 58.58 g and 49.68 g, respectively. The material was a homogeneous fractured powder cake and was light yellow in color.

ZrPM-97

1. 75.000 g (0.160 mol) of zirconium propoxide (ZP) solution was weighed into a three-liter round bottom flask. 675.0 g of distilled ethanol was added and the flask was shaken manually to mix the contents. The total concentration of ZP was 10 wt%. The whole procedure was done in a glove box.

2. The flask was taken out of the glove box and attached to the Schlenk apparatus. The procedure followed was same as described in section 4.1.2.2.2.

3. 48.07 g of acac was mixed with 193.20 g of distilled ethanol in a 500 ml flask in a fume hood. The total concentration of acac was 20 wt%. The flask was shaken manually to mix the contents. This solution was then transferred to the Schlenk apparatus and added to the ZP solution. The procedure followed was same as described in section 4.1.2.2.2. The time taken to add acac solution was ~ 4 – 5 min.

4. 5 ml of distilled ethanol was used to rinse the funnel walls as described in section 4.1.2.2.2.

5. The solution was refluxed at 195^{o}C for 2 h using a heating mantle with a variac.

6. After the solution was refluxed it was allowed to cool. The flask was left attached to the Schlenk apparatus for 15 h before the next processing step.

7. The flask was then removed from the Schlenk apparatus and attached to a rotary evaporator ("rotovap"). The solution was partially concentrated. The temperature of the water bath was maintained in the range of 40 – 45^{o}C. The weights of the solution before and after the evaporation were 989.60 g and 378.40 g, respectively. This was equivalent to ~38 wt% solution left after evaporation.

8. The flask was removed from the rotovap and 1500 ml of distilled ethanol was added to the flask in ~15 – 30 sec. A magnetic stirrer was used to mix the solutions for ~5 min. The color of the solution was greenish yellow and the pH of the solution was 9.93.

9. 27.5 g (32.5 ml) of 10 wt% nitric acid (HNO_3) solution in 90 wt% distilled ethanol was then added to the above solution. The time taken to add the acid solution was ~ 3 min. The solution was simultaneously stirred with a magnetic stirrer. The pH recorded after the addition was acid was 4.86. The amount of acid added corresponded to an HNO_3/Zr molar ratio of 0.272. The amount of water (from the nitric acid solution) corresponded to an H_2O/Zr molar ratio of 0.46.

10. 692.11 g of 10 wt% deionized (DI) water in 90 wt% distilled ethanol was then added to the solution under constant magnetic stirring. The conductivity of DI water was measured to be 0.27 μS/cm. The water solution was added in ~ 6 – 7 min and the pH recorded after water addition was 5.26. The amount of water from this step corresponded to an H_2O/Zr molar ratio of 24.

11. The flask was sealed and then placed in an air oven at 50^oC for 2 h.

12. The flask was then taken out of the oven and allowed to cool for ~30 min. The pH of the solution was 4.38.

13. 4.66 g of phenolic resin was mixed with distilled ethanol to form a 20 wt% solution. This 20 wt% solution of phenolic resin was then added to the solution in step 12. The solution was mixed by a magnetic stirrer for ~10 min and then left for an additional 20 min prior to the next processing step. The pH of the solution was 4.25.

14. The flask was then attached to the rotovap. The solution was concentrated until solvent loss was no longer obvious visually. The temperature of the water bath was maintained in the range of 35 – 40^oC. After concentration, the material can be described as a yellow gel.

15. The flask was then sealed with aluminum foil that was perforated in order to allow removal of small amounts of residual solvent. The flask was put in a vacuum oven and heated to 120^{o}C for 2 h. The weights of the material before and after drying were 53.23 g and 43.63 g, respectively. The material was homogeneous fractured powder cake and was yellow in color.

ZrPM-99

1. 75.000 g (0.160 mol) of zirconium propoxide (ZP) solution was weighed into a three-liter round bottom flask. 675.0 g of distilled ethanol was added and the flask was shaken manually to mix the contents. The total concentration of ZP was 10 wt%. The whole procedure was done in a glove box.
2. The flask was taken out of the glove box and attached to the Schlenk apparatus. The procedure followed was same as described in section 4.1.2.2.2.
3. 48.07 g of acac was mixed with 193.20 g of distilled ethanol in a 500 ml flask in a fume hood. The total concentration of acac was 20 wt%. The flask was shaken manually to mix the contents. This solution was then transferred to the Schlenk apparatus and added to the ZP solution. The procedure followed was same as described in section 4.1.2.2.2. The time taken to add acac solution was ~ 4 – 5 min.
4. 5 ml of distilled ethanol was used to rinse the funnel walls as described in section 4.1.2.2.2.
5. The solution was refluxed at 195^{o}C for 2 h using a heating mantle with a variac.
6. After the solution was refluxed it was allowed to cool. The flask was left attached to the Schlenk apparatus for 18 h before the next processing step.

7. The flask was then removed from the Schlenk apparatus and attached to a rotary evaporator ("rotovap"). The solution was partially concentrated. The temperature of the water bath was maintained in the range of 40 – 45^{o}C. The weights of the solution before and after the evaporation were 988.75 g and 407.75 g, respectively. This was equivalent to ~41 wt% solution left after evaporation.
8. The flask was removed from the rotovap and 1500 ml of distilled ethanol was added to the flask in ~15 – 30 sec. A magnetic stirrer was used to mix the solutions for ~5 min. The color of the solution was greenish yellow and the pH of the solution was 9.91.
9. 27.5 g (32.5 ml) of 10 wt% nitric acid (HNO_3) solution in 90 wt% distilled ethanol was then added to the above solution. The time taken to add the acid solution was ~3 min. The solution was simultaneously stirred with a magnetic stirrer. The pH recorded after the addition was acid was 5.09. The amount of acid added corresponded to an HNO_3/Zr molar ratio of 0.272. The amount of water (from the nitric acid solution) corresponded to an H_2O/Zr molar ratio of 0.46.
10. 692.11 g of 10 wt% deionized (DI) water in 90 wt% distilled ethanol was then added to the solution under constant magnetic stirring. The conductivity of DI water was measured to be 0.26 μS/cm. The water solution was added in ~ 6 – 7 min and the pH recorded after water addition was 5.75. The amount of water from this step corresponded to an H_2O/Zr molar ratio of 24.
11. The flask was sealed and then placed in an air oven at 50^{o}C for 2 h.
12. The flask was then taken out of the oven and allowed to cool for ~30 min. The pH of the solution was 4.64.

13. 4.25 g of phenolic resin was mixed with distilled ethanol to form a 20 wt% solution. This 20 wt% solution of phenolic resin was then added to the solution in step 12. The solution was mixed by a magnetic stirrer for ~10 min and then left for an additional 20 min prior to the next processing step. The pH of the solution was 4.53.
14. The flask was then attached to the rotovap. The solution was concentrated until solvent loss was no longer obvious visually. The temperature of the water bath was maintained in the range of 35 – 40^{o}C. After concentration, the material can be described as a yellow gel with some liquid remaining.
15. The flask was then sealed with aluminum foil that was perforated in order to allow removal of small amounts of residual solvent. The flask was put in a vacuum oven and heated to 120^{o}C for 3 h. The weights of the material before and after drying were 59.86 g and 46.91 g, respectively. The material was a homogeneous fractured powder cake and was light yellow in color.

APPENDIX C

CRYSTALLITE SIZE DATA FOR ZrPM-45 AND ZrPM-59 SAMPLES

Table C1 Crystallite size data for ZrPM-45 samples.

Phase	Temperature (^{o}C)	XRD Peak Information		Crystallite Size (nm)	
		2θ	hkl	Individual Values	Average/Standard Deviation
t-ZrO_2	600	30.243	111	3	
t-ZrO_2	800	30.206	111	6	
t-ZrO_2	900	30.126	111	10	
t-ZrO_2	1100	30.429 63.302 95.574	111 222 005	21 15 14	17 (3.9)
t-ZrO_2	1200	30.307	111	30	
t-ZrO_2	1300	30.325	111	69	
t-ZrO_2	1350	30.191	111	127	
m-ZrO_2	1200	28.373	111	45	
m-ZrO_2	1300	28.312 31.577	-111 111	90 92	91 (1.4)
m-ZrO_2	1350	28.321 31.600	-111 111	125 105	115 (14.1)
ZrC	1200	33.141 38.431 55.572 66.270	111 200 220 311	44 39 46 37	42 (4.2)

Table C1 continued.

Phase	Temperature (^{o}C)	XRD Peak Information		Crystallite Size (nm)	
		2θ	hkl	Individual Values	Average/Standard Deviation
ZrC	1300	33.115	111	69	56 (6.4)
		38.421	200	57	
		55.429	220	54	
		66.030	311	51	
		69.415	222	49	
		91.435	331	57	
		94.548	420	57	
ZrC	1350	33.161	111	103	96 (7.2)
		38.453	200	95	
		55.443	220	104	
		66.094	311	101	
		69.426	222	93	
		82.221	400	82	
		91.470	331	95	
		94.567	420	93	
ZrC	1400	33.174	111	110	115 (10.2)
		38.472	200	105	
		55.471	220	117	
		66.100	311	111	
		69.453	222	107	
		82.223	400	112	
		91.509	331	128	
		94.599	420	133	
ZrC	1475	33.029	111	108	127 (11.0)
		38.325	200	112	
		55.317	220	133	
		65.956	311	127	
		69.926	222	129	
		82.045	400	140	
		91.341	331	131	
		94.436	420	133	

Table C2 Crystallite size data for ZrPM-59 samples.

Phase	Temperature (^{o}C)	XRD Peak Information		Crystallite Size (nm)	
		2θ	hkl	Individual Values	Average/Standard Deviation
t-ZrO2	800	30.084	111	10	
t-ZrO_2	1025	30.255	111	20	
t-ZrO_2	1100	30.291 63.054	111 222	26 28	27 (1.8)
t-ZrO_2	1200	30.352	111	35	
t-ZrO_2	1300	30.297	111	106	
t-ZrO_2	1350	30.361	111	117	
m-ZrO_2	1100	28.209	-111	37	
m-ZrO_2	1200	28.361	-111	38	
m-ZrO_2	1300	28.297 31.558	-111 111	80 68	74 (8.5)
m-ZrO_2	1350	28.371 31.611	-111 111	115 91	103 (17.3)
m-ZrO_2	1400	28.332	-111	114	
ZrC	1200	33.214 55.689 66.278	111 220 311	57 25 21	42 (22.0)
ZrC	1300	33.151 38.467 55.443 66.092 91.504 94.697	111 200 220 311 331 420	82 63 61 66 78 42	65 (14.1)
ZrC	1350	33.206 38.493 55.487 66.121 69.446 82.215 91.462 94.596	111 200 220 311 222 400 331 420	115 118 110 99 83 125 78 74	100 (19.8)

Table C2 continued.

Phase	Temperature (^{o}C)	XRD Peak Information		Crystallite Size (nm)	
		2θ	hkl	Individual Values	Average/Standard Deviation
ZrC	1400	33.210	111	129	128 (18.0)
		38.509	200	129	
		55.509	220	160	
		66.147	311	105	
		69.472	222	129	
		82.247	400	144	
		91.556	331	117	
		94.627	420	109	
ZrC	1475	33.248	111	133	140 (23.2)
		38.549	200	135	
		55.568	220	157	
		66.222	311	148	
		69.570	222	110	
		82.356	400	186	
		91.675	331	124	
		94.758	420	131	

APPENDIX D

BET AND LANGMUIR SPECIFIC SURFACE AREA VALUES

Table D1 Specific surface areas, other gas adsorption results, and some CTR processing conditions for various ZrC-based samples.

Sample	CTR Processing Variables			SA_{BET} (m^2/g)	C	$r_{L\text{-}BET}$	$SA_{Langmuir}$ (m^2/g)	b	$r_{L\text{-}Langmuir}$
	Sample Size (g)	Gas Flow Rate (ml/min)	Sample Packing						
ZrPM-45-800	20.0	100	Loose	1.2	4.2	0.9883	4	0.87	0.9347
ZrPM-45-800-900	0.4	100	Loose	106	-96	0.9981	**149**	**0.01**	**0.9999**
ZrPM-45-800-1100	0.4	100	Loose	**206**	**244**	**0.9995**	297	0.03	0.9985
ZrPM-45-800-1200	0.5	100	Loose	**232**	**231**	**0.9998**	337	0.03	0.9979
ZrPM-45-800-1300	0.5	100	Loose	**184**	**208**	**0.9999**	268	0.04	0.9971
ZrPM-45-800-1350	0.4	100	Loose	**124**	**127**	**0.9999**	180	0.04	0.9963
ZrPM-45-800-1400	0.5	100	Loose	**39**	**100**	**0.9999**	55	0.03	0.9983
ZrPM-45-800-1475	0.5	100	Loose	**23**	**65**	**0.9999**	34	0.05	0.9950
ZrPM-45-800-1350-1400	3.0	100	Loose	**48**	**111**	**0.9999**	70	0.06	0.9962
ZrPM-45-800-1350-1400-M[a]	3.0	100	Loose	**46**	**150**	**0.9999**	67	0.04	0.9975
ZrPM-45-800-2-1400-1	4.5	100	Dense	**232**	**176**	**0.9999**	338	0.04	0.9969
ZrPM-58-800-1475	0.4	100	Loose	**10**	**51**	**0.9998**	15	0.06	0.9939
ZrPM-58-1300(57)-1350(16)-1300(8)	7.0	100	Loose	**19**	**167**	**0.9999**	27	0.04	0.9966

Table D1 continued.

Sample	CTR Processing Variables			SA_{BET} (m^2/g)	C	$r_{L\text{-}BET}$	$SA_{Langmuir}$ (m^2/g)	b	$r_{L\text{-}Langmuir}$
	Sample Size (g)	Gas Flow Rate (ml/min)	Sample Packing						
ZrPM-59-800	16.0	100	Loose	18	2	0.7734	-108	3.01	-0.4489
ZrPM-59-800-1025	0.4	100	Loose	**159**	**135**	**0.9997**	229	0.03	0.9985
ZrPM-59-800-1100	0.4	100	Loose	**186**	**475**	**0.9998**	270	0.03	0.9980
ZrPM-59-800-1200	0.4	100	Loose	**219**	**211**	**0.9999**	319	0.04	0.9972
ZrPM-59-800-1300	0.4	100	Loose	**186**	**239**	**0.9999**	270	0.03	0.9974
ZrPM-59-800-1350	0.4	100	Loose	**110**	**142**	**0.9999**	160	0.04	0.9967
ZrPM-59-800-1400	0.4	100	Loose	**42**	**104**	**0.9999**	62	0.04	0.9961
ZrPM-59-800-1475	0.6	100	Loose	**9**	**42**	**0.9997**	14	0.06	0.9935
ZrPM-61-350-1-800-1-1350(8)-1-1400-1	3.0	100	Loose	**183**	**155**	**0.9999**	266	0.04	0.9968
ZrPM-61-350-1-1300(48)-1	20.0	500	Loose	**160**	**158**	**0.9999**	233	0.04	0.9965
ZrPM-61-350-1-1300(48)-3	1.0	100	Loose	**107**	**140**	**0.9999**	157	0.04	0.9968
ZrPM-61-350-1-1300(48)-2-1300(8)-1	10.0	500	Loose	**112**	**125**	**0.9999**	164	0.04	0.9964
ZrPM-61-350-1-800-1-1475-1	2.0	100	Loose	**207**	**146**	**0.9999**	303	0.04	0.9965
ZrPM-61-350-1-800-1-1475-1-M[a]	2.0	100	Loose	**225**	**148**	**0.9999**	329	0.04	0.9965
ZrPM-61-350-1-1300(48)-2-1300(8)-1-1475-1	2.0	100	Loose	**40**	**102**	**0.9999**	58	0.04	0.9954

Table D1 continued.

Sample	CTR Processing Variables			SA_{BET} (m^2/g)	C	$r_{L\text{-}BET}$	$SA_{Langmuir}$ (m^2/g)	b	$r_{L\text{-}Langmuir}$
	Sample Size (g)	Gas Flow Rate (ml/min)	Sample Packing						
ZrPM-61-350-1-1300(48)-2-1300(8)-1-1475-1-M[a]	2.0	100	Loose	**45**	**110**	**0.9999**	65	0.04	0.9956
ZrPM-79+82-800-1425	7.0	500	Loose	**25**	**118**	**0.9999**	36	0.04	0.9964
ZrPM-69+76+85-800-1400	7.0	500	Loose	**7**	**64**	**0.9999**	11	0.05	0.9952
ZrPM-80-800-1425	0.4	500	Loose	**57**	**164**	**0.9999**	83	0.04	0.9971
ZrPM-80-1100-1425	0.4	500	Loose	**51**	**149**	**0.9999**	75	0.04	0.9969
ZrPM-87-800-1-1425-1	0.4	500	Loose	**16**	**52**	**0.9997**	24	0.06	0.9939
ZrPM-87-800-1-1425-2	8.0	500	Loose	**25**	**127**	**0.9999**	36	0.04	0.9957
ZrPM-90-800-1-1400-1	0.4	500	Loose	**11**	**62**	**0.9998**	17	0.05	0.9933
ZrPM-90-800-1-1400-2	8.0	500	Loose	**19**	**8**	**0.9999**	29	0.05	0.9954
ZrPM-91-800-1-1425-1	0.4	500	Loose	**13**	**56**	**0.9996**	20	0.05	0.9925
ZrPM-91-800-1-1425-4	8.0	500	Loose	**20**	**91**	**0.9999**	30	0.04	0.9960
ZrPM-92-800-1-1425-1	1.0	500	Loose	**24**	**102**	**0.9999**	35	0.04	0.9963
ZrPM-92-800-1-1450-1	8.0	500	Loose	**8**	**64**	**0.9999**	12	0.05	0.9953
ZrPM-94-800-1-1425-1	0.5	500	Loose	**50**	**124**	**0.9999**	73	0.04	0.9965
ZrPM-94-800-3-1475-1	8.0	500	Loose	**14**	**65**	**0.9999**	20	0.05	0.9952

Table D1 continued.

Sample	CTR Processing Variables			SA_{BET} (m^2/g)	C	$r_{L\text{-}BET}$	$SA_{Langmuir}$ (m^2/g)	b	$r_{L\text{-}Langmuir}$
	Sample Size (g)	Gas Flow Rate (ml/min)	Sample Packing						
ZrPM-95-800-1-1425-1	0.4	500	Loose	**67**	**171**	**0.9999**	97	0.04	0.9971
ZrPM-95-800-1-1425-2	2.0	500	Loose	**46**	**142**	**0.9999**	68	0.04	0.9968
ZrPM-95-800-3-1475-1	8.0	500	Loose	**18**	**66**	**0.9999**	27	0.05	0.9951
ZrPM-97-1100-1-1425-1	0.4	500	Loose	**167**	**160**	**0.9999**	243	0.04	0.9970
ZrPM-97-800-1-1475-1	2.0	500	Loose	**59**	**120**	**0.9999**	86	0.04	0.9950
ZrPM-97-800-1-1500-1	8.0	500	Loose	**40**	**112**	**0.9999**	58	0.04	0.9950
ZrPM-98-800-1-1425-1	2.0	500	Loose	**29**	**94**	**0.9999**	43	0.04	0.9957
ZrPM-98-800-1-1450-1	8.0	500	Loose	**21**	**80**	**0.9999**	31	0.04	0.9954
ZrPM-99-800-1-1475-1	8.0	500	Loose	**19**	**46**	**0.9995**	29	0.06	0.9916
ZrPM-99-800-1-1425-2	0.5	500	Loose	**36**	**110**	**0.9999**	53	0.04	0.9961
ZrPM-100-800-1-1425-1	2.0	500	Loose	**41**	**110**	**0.9999**	59	0.04	0.9957
ZrPM-100-800-2-1450-1	8.0	500	Loose	**20**	**84**	**0.9999**	30	0.05	0.9960

[a] Sample was milled using a spex mill.

APPENDIX E

CARBON AND OXYGEN CONTENTS OF VARIOUS ZrC-BASED SAMPLES

Table E1 Carbon (from Sherry Laboratories and Leco Corp.) and oxygen (from Leco Corp.) contents of various ZrC-based samples.

Sample	Carbon* (wt%)	C/Zr Molar Ratio	Oxygen* (wt%)
ZrPM-45-1025	23.26	3.1	16.25 (15.2, 17.3)
ZrPM-45-800-1475	13.36	1.3	3.32 (average of #1, #2) #1: 3.8 #2: 2.85 (2.83, 2.86)
ZrPM-45-800-1800	11.25	1.1	0.107 (0.103, 0.111)
ZrPM-58-1025	17.86	2.2	n.a.
ZrPM-58-800-1475	8.05	0.8	n.a.
ZrPM-59-1025	19.40	2.5	n.a.
ZrPM-59-800-1475	8.99	0.9	4.48 (4.41, 4.55)
ZrPM-59-800-1800	9.38	0.9	1.02 (average of #1, #2) #1: 1.15 (1.22, 1.07) #2: 0.89 (0.91, 0.87)
ZrPM-59-800-2000	8.94	0.8	0.56 (average of #1, #2) #1: 0.42 #2: 0.70 (0.71, 0.69)
ZrPM-61-350-1025	27.10	3.8	n.a.
ZrPM-61-350-800-1475	19.35	2.1	n.a.
ZrPM-86-1025	18.30 (18.20, 18.40)	2.3	n.a.
ZrPM-87-1025	18.85 (19.0, 18.70)	2.4	n.a.
ZrPM-87-800-1800	7.60	0.6	n.a.
ZrPM-87-800-1900	7.72 (7.85, 7.59)	0.6	n.a.
ZrPM-88-1025	17.90 (17.90, 17.90)	2.2	n.a.
ZrPM-89-1025	15.60 (15.60, 15.60)	1.9	n.a.
ZrPM-90-1025	14.75 (14.70, 14.80)	1.8	n.a.
ZrPM-91-1025	18.50 (18.40, 18.60)	2.3	n.a.
ZrPM-94-1025	21.75 (21.60, 21.90)	2.9	n.a.

Table E1 continued.

Sample	Carbon* (wt%)	C/Zr Molar Ratio	Oxygen* (wt%)
ZrPM-94-800-1800	10.50 (10.50, 10.50)	0.9	n.a.
ZrPM-94-800-1900	9.35 (9.43, 9.27)	0.8	n.a.
ZrPM-95-1025	22.40 (22.40, 22.4)	3.0	n.a.
ZrPM-95-800-1800	10.90 (11.00, 10.80)	0.9	n.a.
ZrPM95-800-1900	9.71 (9.76, 9.66)	0.8	n.a.
ZrPM-97-1025	24.05 (24.00, 24.10)	3.3	n.a.
ZrPM-97-800-1800	12.60 (12.50, 12.70)	1.1	n.a.
ZrPM-97-800-1900	12.60 (12.60, 12.60)	1.1	n.a.
ZrPM-98-1025	23.30 (23.30, 23.30)	3.1	n.a.
ZrPM-98-800-1800	10.75 (10.70, 10.80)	0.9	n.a.
ZrPM-98-800-1900	10.10 (10.00, 10.20)	0.9	n.a.
ZrPM-99-1025	23.70 (23.90, 23.50)	3.2	n.a.
ZrPM-99-800-1800	11.00 (11.00, 11.00)	0.9	n.a.
ZrPM-99-800-1900	10.75 (10.80, 10.70)	0.9	n.a.
ZrPM-100-1025	21.30 (21.20, 21.40)	2.8	n.a.
ZrPM-100-800-1800	10.70 (10.60, 10.80)	0.9	n.a.
ZrPM-100-800-1900	8.60 (8.49, 8.71)	0.7	n.a.

* The values in the parentheses are individual measurements. The number in the larger font is the average value.

APPENDIX F

LATTICE PARAMETER CALCULATIONS FOR VARIOUS ZrC-BASED SAMPLES

In section 5.2.2.3, XRD patterns with peak splitting were observed for "oxide-rich" ZrPM-59 samples which had been heat treated at temperatures in the range of 1800-2000^{o}C (Figure 5.22). This was attributed to reaction between the powder sample and the carbon substrate that was used during the heat treatment. This explanation was confirmed in experiments carried out with "oxide-rich" ZrPM-87 and ZrPM-94 samples. ZrPM87-800-pyrolyzed and ZrPM-94-800-pyrolyzed samples were heat treated at 1900^{o}C using two different substrates -- a carbon (Graphoil®) substrate and a ZrC-based substrate. (The latter substrate is the same as described in section 4.1.5.) Figures F1 and F2 shows the XRD patterns for the 1900^{o}C ZrPM-87 and ZrPM-94 samples, respectively. It is evident from these figures that peak splitting had occurred for both samples when the carbon substrate was used. (This is consistent with the results described in section 5.2.2.3 for the heat treated ZrPM-59 samples.) In contrast, peak splitting did not occur when the samples were heat treated using the ZrC-based substrate. Tables F19 and F23 shows the calculated lattice parameters for the 1900^{o}C ZrPM-87 and 1900^{o}C ZrPM-94 samples, respectively. These lattice parameters were obtained from the XRD patterns shown in Figures 5.46 and 5.55, respectively. The lattice parameter calculations were made for both the "right peak" and "left peak" for the cases in which peak splitting was observed. Tables F20 and F24 show that the lattice parameters calculated from the “right peaks” agree very closely with the lattice parameters calculated from the corresponding XRD patterns which did not show peak splitting (i.e., for the corresponding samples heat

treated on the ZrC-based substrates). These lattice parameters have relatively low values, as would be expected for carbon-deficient zirconium oxycarbides (i.e., ZrO_yC_x where x <1). Tables F21 and F25 also show that the lattice parameters calculated from the “left peaks” (in the XRD patterns with peak splitting) have values that would be expected for a zirconium carbide with stoichiometric (or near-stoichiometric) composition (i.e., ZrC). This is consistent with the explanation presented in section 5.2.2.3, i.e., that the "oxide-rich" zirconium oxycarbide samples reacted with the carbon substrate and thereby formed stoichiometric (or near-stoichiometric) ZrC.

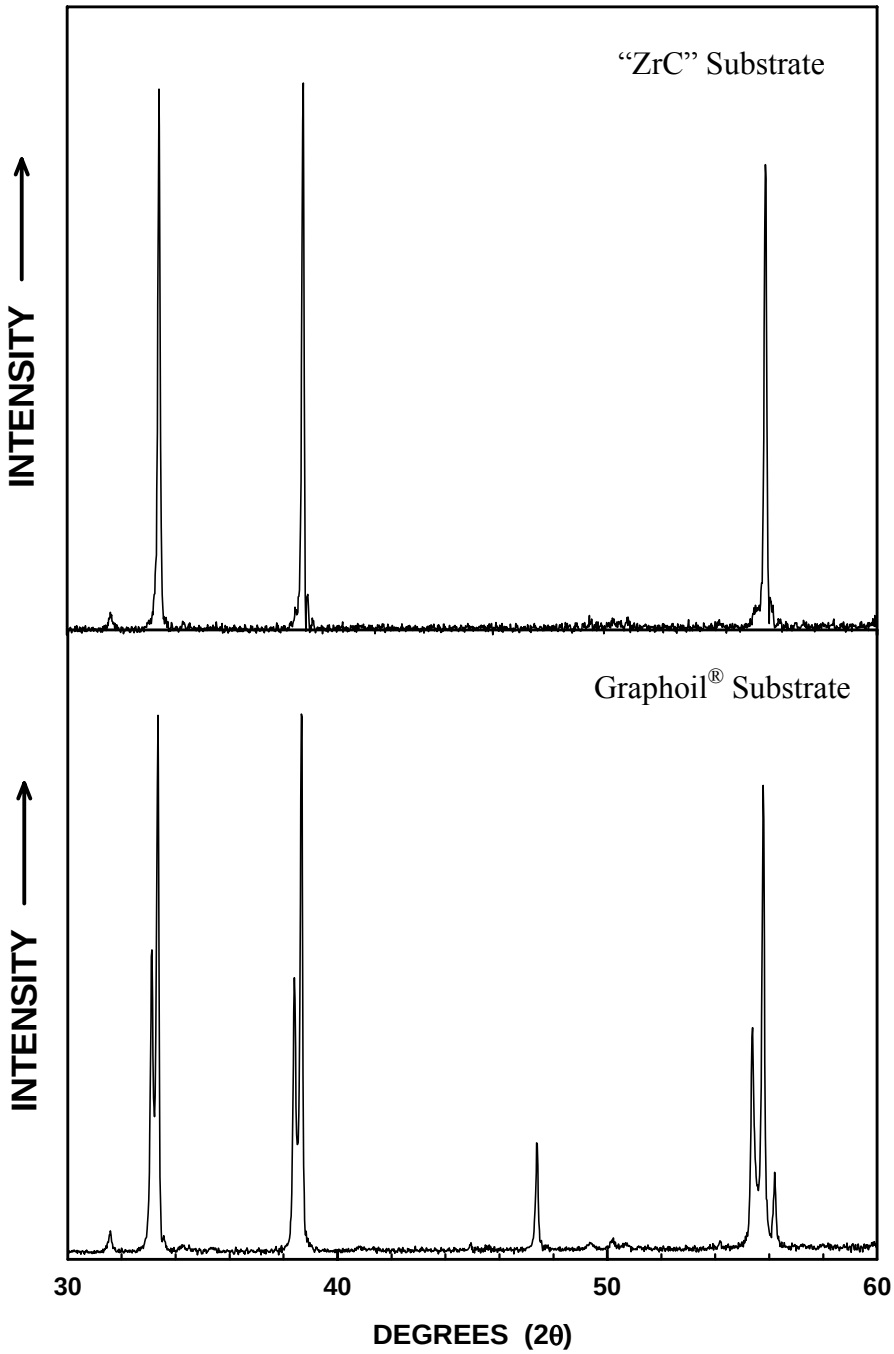

Figure F1a Combined XRD graphs of ZrPM-87-800-pyrolyzed powder sample heat treated at 1900°C using "ZrC" and Graphoil® substrates (30-60°).

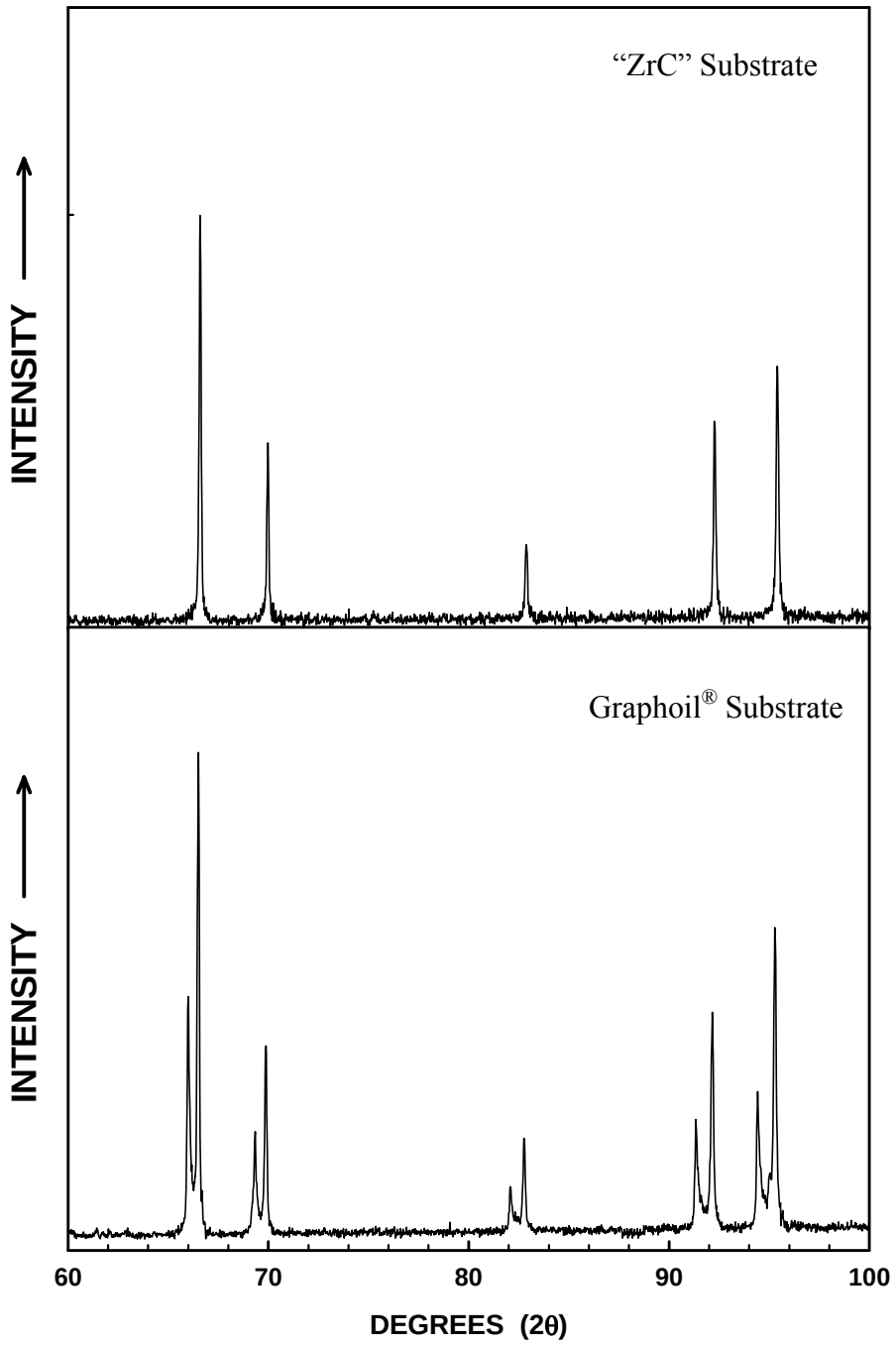

Figure F1b Combined XRD graphs of ZrPM-87-800-pyrolyzed powder sample heat treated at 1900°C using "ZrC" and Graphoil® substrates (60-100°).

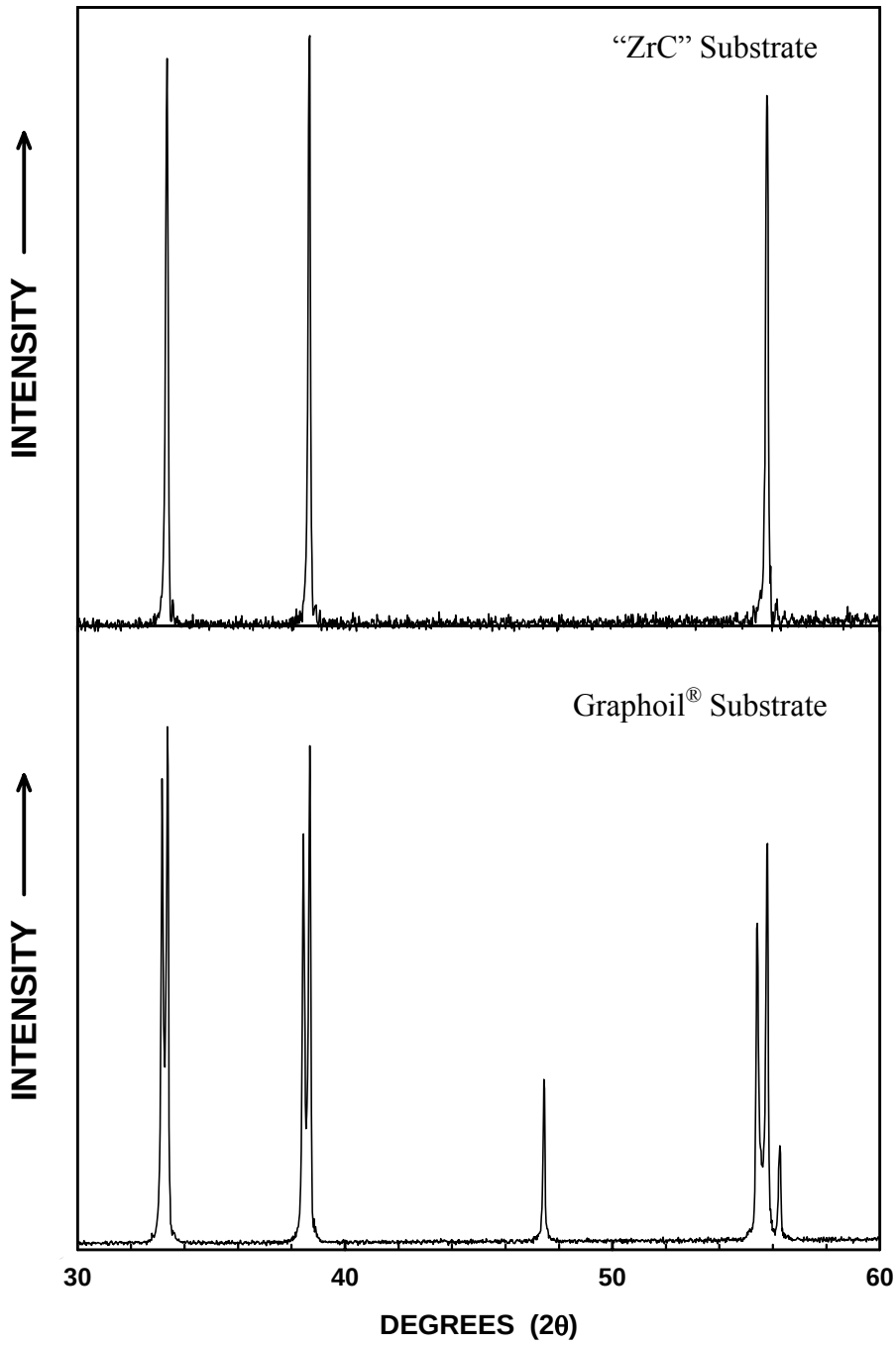

Figure F2a Combined XRD graphs of ZrPM-94-800-pyrolyzed powder sample heat treated at 1900°C using "ZrC" and Graphoil® substrates (30-60°).

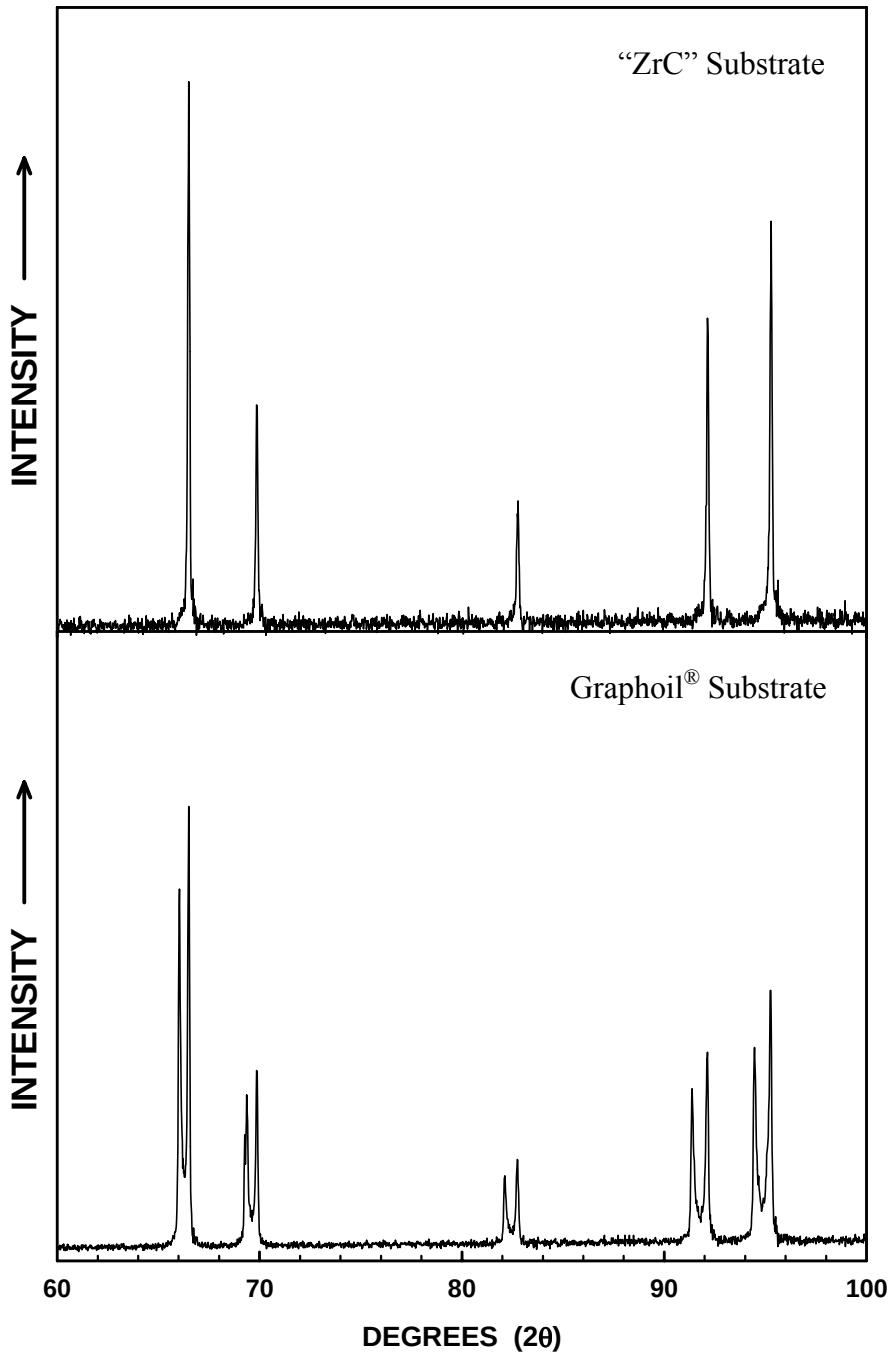

Figure F2b Combined XRD graphs of ZrPM-94-800-pyrolyzed powder sample heat treated at 1900°C using "ZrC" and Graphoil® substrates (60-100°).

ZrPM-45-800-1300

***a* = 0.4693 nm**

Table F1 Measured and corrected ZrC 2θ values and corresponding Si values used for correction.

Si (hkl)	Measured Si 2θ	NBS Si 2θ		ZrC (hkl)	Measured ZrC 2θ	Corrected ZrC 2θ
111	28.632	28.443		111	33.239	33.048
220	47.500	47.303		200	38.530	38.337
311	56.304	56.123		220	55.524	55.337
400	n.a.	69.131		311	66.125	65.945
331	76.551	76.377		400	82.209	82.029
422	88.187	88.032		331	91.520	91.368
511	95.067	94.954		420	94.616	94.486

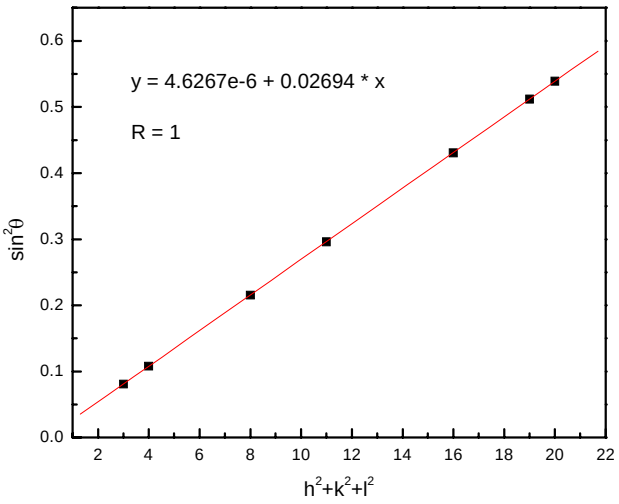

Figure F3 Plot of $\sin^2\theta$ vs. $h^2+k^2+l^2$ for calculating the lattice parameter.

ZrPM-45-800-1350

***a* = 0.4693 nm**

Table F2 Measured and corrected ZrC 2θ values and corresponding Si values used for correction.

Si (hkl)	Measured Si 2θ	NBS Si 2θ		ZrC (hkl)	Measured ZrC 2θ	Corrected ZrC 2θ
111	28.600	28.443		111	33.130	32.972
220	47.465	47.303		200	38.423	38.264
311	56.280	56.123		220	55.393	55.236
400	n.a.	69.131		311	66.022	65.875
331	76.515	76.377		400	82.128	81.997
422	88.155	88.032		331	91.391	91.269
511	95.075	94.954		420	94.462	94.341

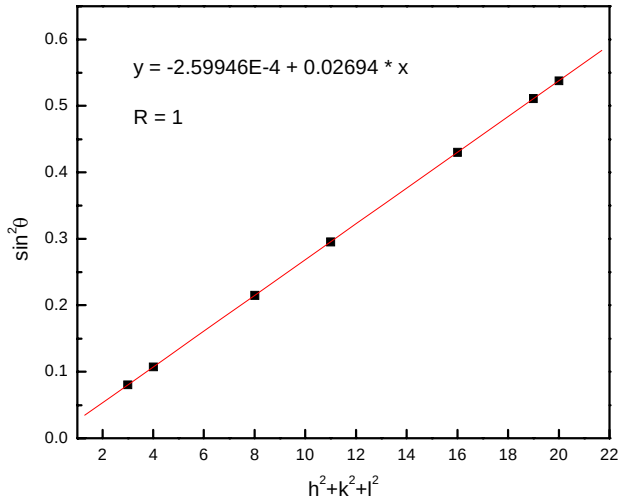

Figure F4 Plot of $\sin^2\theta$ vs. $h^2+k^2+l^2$ for calculating the lattice parameter.

ZrPM-45-800-1400

***a* = 0.4691 nm**

Table F3 Measured and corrected ZrC 2θ values and corresponding Si values used for correction.

Si (hkl)	Measured Si 2θ	NBS Si 2θ		ZrC (hkl)	Measured ZrC 2θ	Corrected ZrC 2θ
111	28.553	28.443		111	33.153	33.045
220	47.403	47.303		200	38.447	38.342
311	56.224	56.123		220	55.450	55.349
400	n.a.	69.131		311	66.090	66.002
331	76.450	76.377		400	82.195	82.122
422	88.105	88.032		331	91.470	91.397
511	n.a.	94.954		420	94.570	94.497

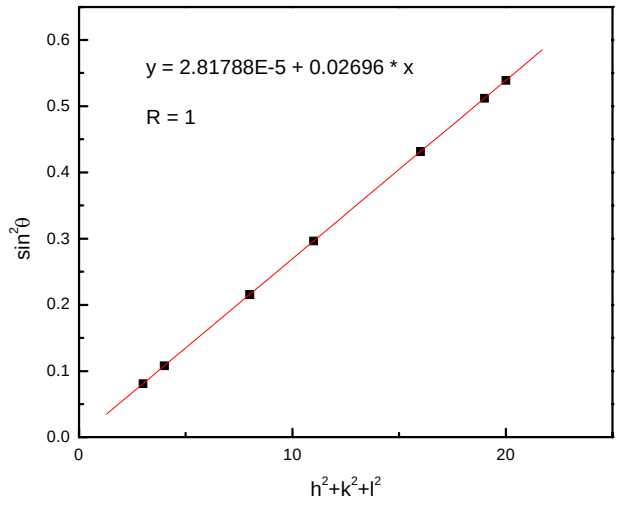

Figure F5 Plot of $\sin^2\theta$ vs. $h^2+k^2+l^2$ for calculating the lattice parameter.

ZrPM-45-800-1475

***a* = 0.4691 nm**

Table F4 Measured and corrected ZrC 2θ values and corresponding Si values used for correction.

Si (hkl)	Measured Si 2θ	NBS Si 2θ		ZrC (hkl)	Measured ZrC 2θ	Corrected ZrC 2θ
111	28.605	28.443		111	33.21	33.048
220	47.465	47.303		200	38.495	38.333
311	n.a.	56.123		220	55.48	55.319
400	n.a.	69.131		311	66.135	65.976
331	76.535	76.377		400	82.26	82.119
422	88.155	88.032		331	91.55	91.437
511	n.a.	94.954		420	94.575	94.471

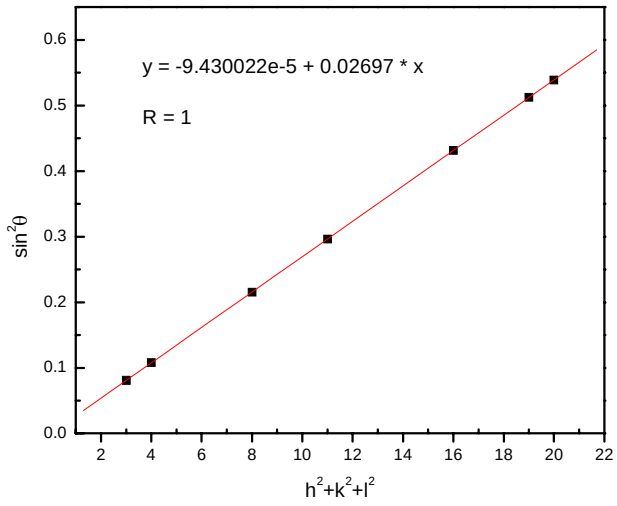

Figure F6 Plot of $\sin^2\theta$ vs. $h^2+k^2+l^2$ for calculating the lattice parameter.

ZrPM-45-800-1600

***a* = 0.4696 nm**

Table F5 Measured and corrected ZrC 2θ values and corresponding Si values used for correction.

Si (hkl)	Measured Si 2θ	NBS Si 2θ		ZrC (hkl)	Measured ZrC 2θ	Corrected ZrC 2θ
111	28.543	28.443		111	33.130	33.028
220	47.408	47.303		200	38.423	38.320
311	n.a.	56.123		220	55.393	55.297
400	n.a.	69.131		311	66.022	65.938
331	76.450	76.377		400	82.128	82.052
422	88.111	88.032		331	91.391	91.312
511	n.a.	94.954		420	94.462	94.383

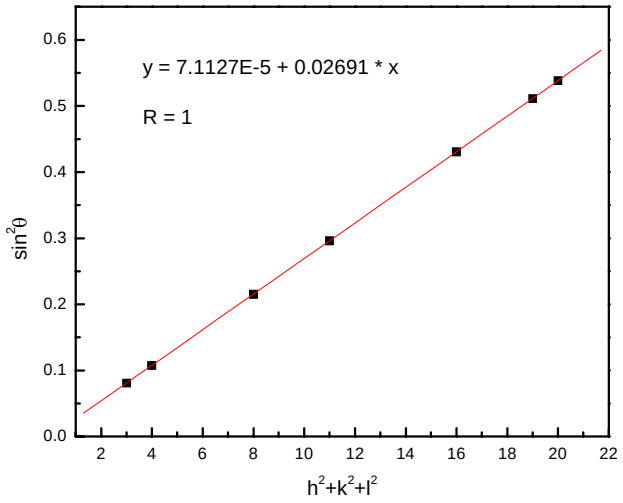

Figure F7 Plot of $\sin^2\theta$ vs. $h^2+k^2+l^2$ for calculating the lattice parameter.

ZrPM-45-800-1800

***a* = 0.4696 nm**

Table F6 Measured and corrected ZrC 2θ values and corresponding Si values used for correction.

Si (hkl)	Measured Si 2θ	NBS Si 2θ		ZrC (hkl)	Measured ZrC 2θ	Corrected ZrC 2θ
111	28.596	28.443		111	33.177	33.027
220	47.445	47.303		200	38.462	38.315
311	56.267	56.123		220	55.437	55.318
400	n.a.	69.131		311	66.062	65.927
331	76.502	76.377		400	82.144	82.028
422	88.139	88.032		331	91.411	91.307
511	95.054	94.954		420	94.493	94.392

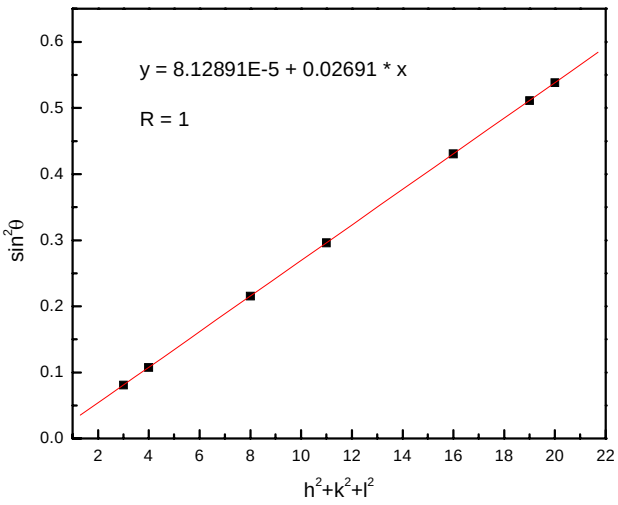

Figure F8 Plot of $\sin^2\theta$ vs. $h^2+k^2+l^2$ for calculating the lattice parameter.

ZrPM-59-800-1300

***a* = 0.4690 nm**

Table F7 Measured and corrected ZrC 2θ values and corresponding Si values used for correction.

Si (hkl)	Measured Si 2θ	NBS Si 2θ		ZrC (hkl)	Measured ZrC 2θ	Corrected ZrC 2θ
111	28.600	28.443		111	33.175	33.041
220	47.410	47.303		200	38.440	38.310
311	56.220	56.123		220	55.440	55.325
400	n.a.	69.131		311	66.095	65.989
331	76.475	76.377		400	82.240	82.147
422	88.145	88.032		331	91.420	91.335
511	95.025	94.954		420	94.555	94.473

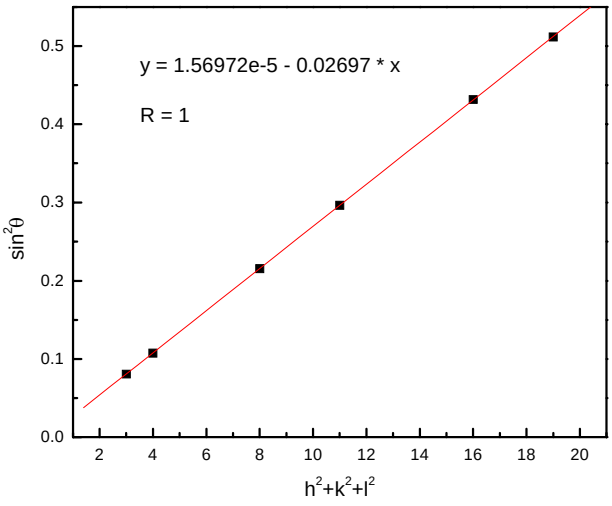

Figure F9 Plot of $\sin^2\theta$ vs. $h^2+k^2+l^2$ for calculating the lattice parameter.

ZrPM-59-800-1350

***a* = 0.4692 nm**

Table F8 Measured and corrected ZrC 2θ values and corresponding Si values used for correction.

Si (hkl)	Measured Si 2θ	NBS Si 2θ		ZrC (hkl)	Measured ZrC 2θ	Corrected ZrC 2θ
111	28.57	28.443		111	33.18	33.054
220	47.41	47.303		200	38.455	38.331
311	56.255	56.123		220	55.475	55.358
400	n.a.	69.131		311	66.075	65.962
331	76.5	76.377		400	82.23	82.124
422	88.115	88.032		331	91.42	91.317
511	95.06	94.954		420	94.575	94.474

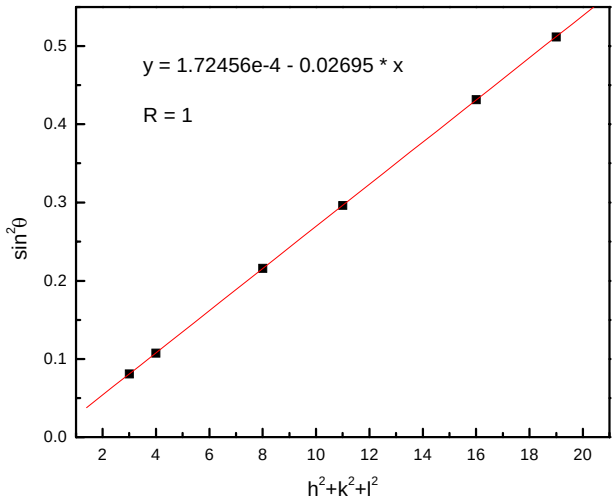

Figure F10 Plot of $\sin^2\theta$ vs. $h^2+k^2+l^2$ for calculating the lattice parameter.

ZrPM-59-800-1400

***a* = 0.4690 nm**

Table F9 Measured and corrected ZrC 2θ values and corresponding Si values used for correction.

Si (hkl)	Measured Si 2θ	NBS Si 2θ		ZrC (hkl)	Measured ZrC 2θ	Corrected ZrC 2θ
111	28.572	28.443		111	33.2	33.071
220	47.431	47.303		200	38.4885	38.359
311	56.250	56.123		220	55.4919	55.365
400	n.a.	69.131		311	66.1502	66.033
331	76.484	76.377		400	82.2464	82.144
422	88.129	88.032		331	91.5359	91.438
511	n.a.	94.954		420	94.6258	94.528

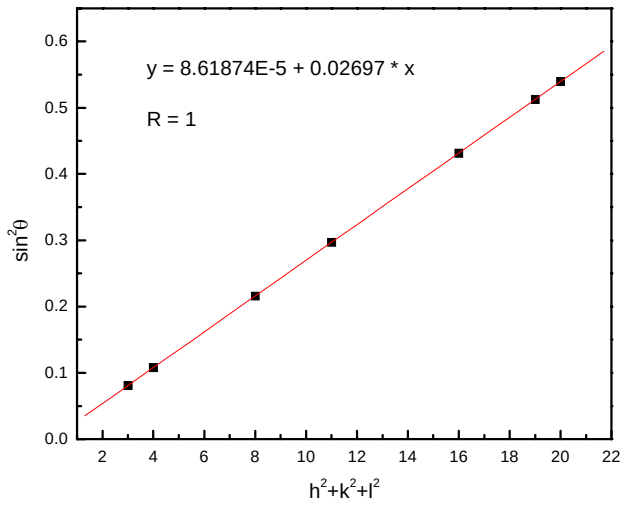

Figure F11 Plot of $\sin^2\theta$ vs. $h^2+k^2+l^2$ for calculating the lattice parameter.

ZrPM-59-800-1475

***a* = 0.4686 nm**

Table F10 Measured and corrected ZrC 2θ values and corresponding Si values used for correction.

Si (hkl)	Measured Si 2θ	NBS Si 2θ		ZrC (hkl)	Measured ZrC 2θ	Corrected ZrC 2θ
111	28.582	28.443		111	33.26	33.116
220	47.461	47.303		200	38.564	38.415
311	56.264	56.123		220	55.580	55.438
400	n.a.	69.131		311	66.223	66.087
331	76.509	76.377		400	82.388	82.267
422	88.142	88.032		331	91.692	91.583
511	n.a.	94.954		420	94.777	94.668

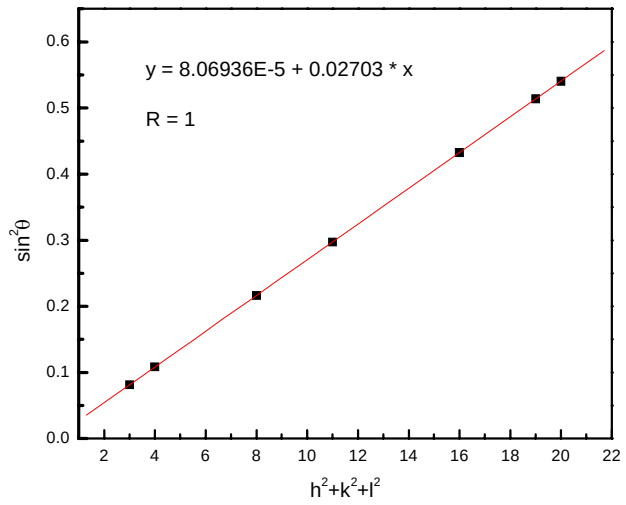

Figure F12 Plot of $\sin^2\theta$ vs. $h^2+k^2+l^2$ for calculating the lattice parameter.

ZrPM-59-800-1600

***a* = 0.4675 nm**

Table F11 Measured and corrected ZrC 2θ values and corresponding Si values used for correction.

Si (hkl)	Measured Si 2θ	NBS Si 2θ		ZrC (hkl)	Measured ZrC 2θ	Corrected ZrC 2θ
111	28.626	28.443		111	33.350	33.171
220	47.469	47.303		200	38.655	38.481
311	n.a.	56.123		220	55.720	55.556
400	n.a.	69.131		311	66.415	66.255
331	76.534	76.377		400	82.565	82.418
422	88.169	88.032		331	91.950	91.813
511	n.a.	94.954		420	94.695	94.558

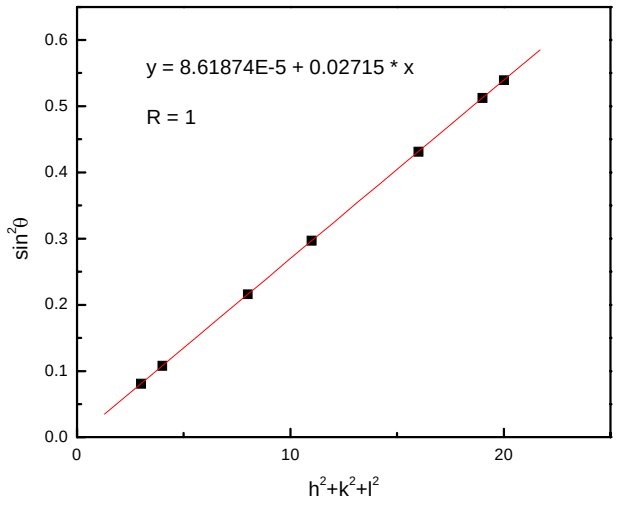

Figure F13 Plot of $\sin^2\theta$ vs. $h^2+k^2+l^2$ for calculating the lattice parameter.

ZrPM-59-1800 ("Right peaks")

***a* = 0.4673 nm**

Table F12 Measured and corrected ZrC 2θ values and corresponding Si values used for correction.

Si (hkl)	Measured Si 2θ	NBS Si 2θ		ZrC (hkl)	Measured ZrC 2θ	Corrected ZrC 2θ
111	28.616	28.443		111	33.382	33.210
220	47.471	47.303		200	38.691	38.520
311	56.290	56.123		220	55.787	55.620
400	n.a.	69.131		311	66.484	66.320
331	76.537	76.377		400	82.674	82.530
422	88.160	88.032		331	91.998	91.870

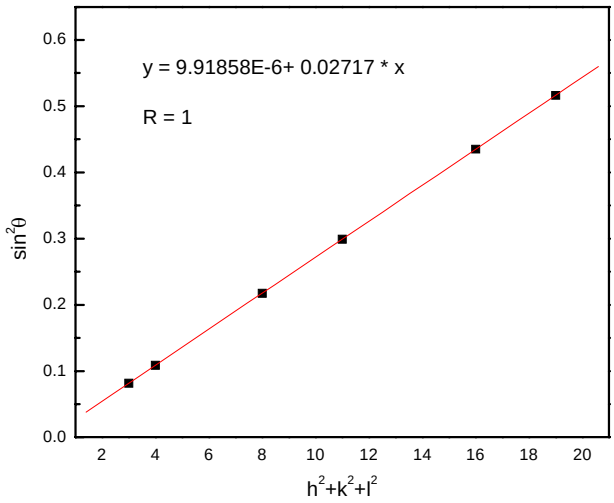

Figure F14 Plot of $\sin^2\theta$ vs. $h^2+k^2+l^2$ for calculating the lattice parameter.

ZrPM-59-800-1800 ("Left peaks")

***a* = 0.4693 nm**

Table F13 Measured and corrected ZrC 2θ values and corresponding Si values used for correction.

Si (hkl)	Measured Si 2θ	NBS Si 2θ		ZrC (hkl)	Measured ZrC 2θ	Corrected ZrC 2θ
111	28.616	28.443		111	33.222	33.050
220	47.471	47.303		200	38.521	38.350
311	56.290	56.123		220	55.517	55.350
400	n.a.	69.131		311	66.144	65.980
331	76.537	76.377		400	82.264	82.120
422	88.160	88.032		331	91.478	91.350

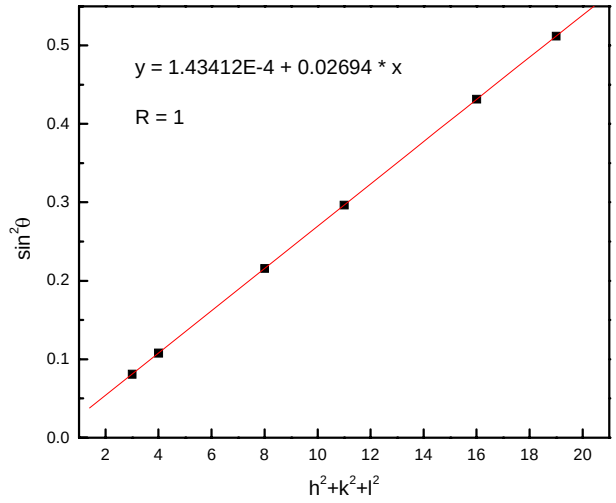

Figure F15 Plot of $\sin^2\theta$ vs. $h^2+k^2+l^2$ for calculating the lattice parameter.

ZrPM-59-800-1900 ("Right peaks")

***a* = 0.4669 nm**

Table F14 Measured and corrected ZrC 2θ values and corresponding Si values used for correction.

Si (hkl)	Measured Si 2θ	NBS Si 2θ		ZrC (hkl)	Measured ZrC 2θ	Corrected ZrC 2θ
111	28.652	28.443		111	33.4329	33.219
220	47.527	47.303		200	38.7549	38.537
311	56.312	56.123		220	55.8583	55.666
400	n.a.	69.131		311	66.5607	66.382
331	76.544	76.377		400	82.7749	82.602
422	88.208	88.032		331	92.1688	91.992

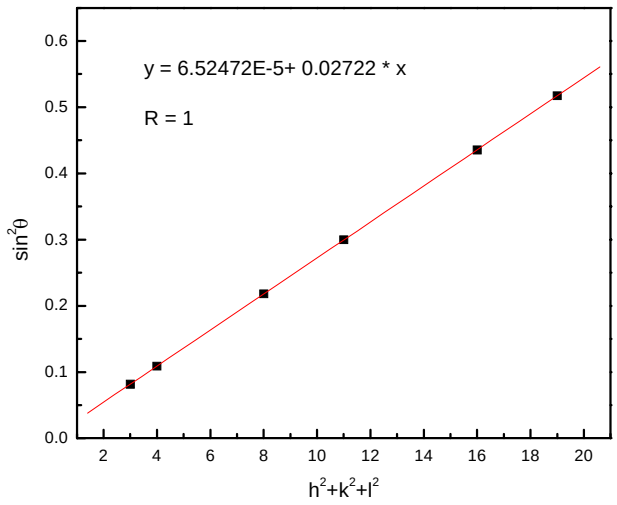

Figure F16 Plot of $\sin^2\theta$ vs. $h^2+k^2+l^2$ for calculating the lattice parameter.

ZrPM-59-800-1900 ("Left peaks")

***a* = 0.4699 nm**

Table F15 Measured and corrected ZrC 2θ values and corresponding Si values used for correction.

Si (hkl)	Measured Si 2θ	NBS Si 2θ		ZrC (hkl)	Measured ZrC 2θ	Corrected ZrC 2θ
111	28.652	28.443		111	33.234	33.020
220	47.527	47.303		200	38.528	38.310
311	56.312	56.123		220	55.482	55.290
400	n.a.	69.131		311	66.089	65.910
331	76.544	76.377		400	82.212	82.040
422	88.208	88.032		331	91.367	91.190

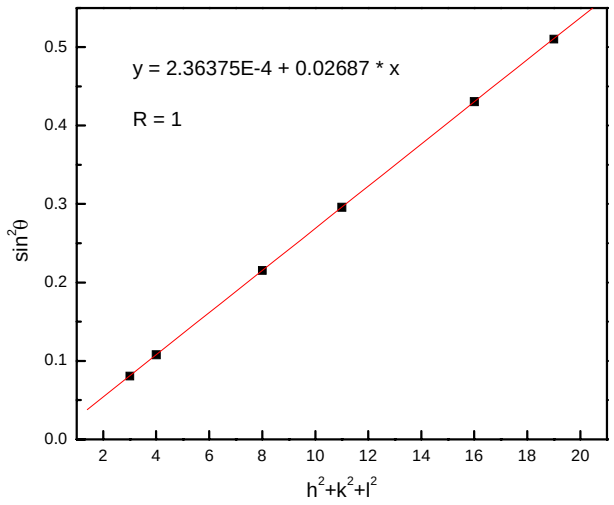

Figure F17 Plot of $\sin^2\theta$ vs. $h^2+k^2+l^2$ for calculating the lattice parameter.

ZrPM-59-800-2000 ("Right peaks")

***a* = 0.4668 nm**

Table F16 Measured and corrected ZrC 2θ values and corresponding Si values used for correction.

Si (hkl)	Measured Si 2θ	NBS Si 2θ		ZrC (hkl)	Measured ZrC 2θ	Corrected ZrC 2θ
111	28.543	28.443		111	33.328	33.225
220	47.414	47.303		200	38.645	38.539
311	56.212	56.123		220	55.747	55.656
400	n.a.	69.131		311	66.459	66.364
331	76.470	76.377		400	82.707	82.620
422	88.107	88.032		331	92.073	91.998

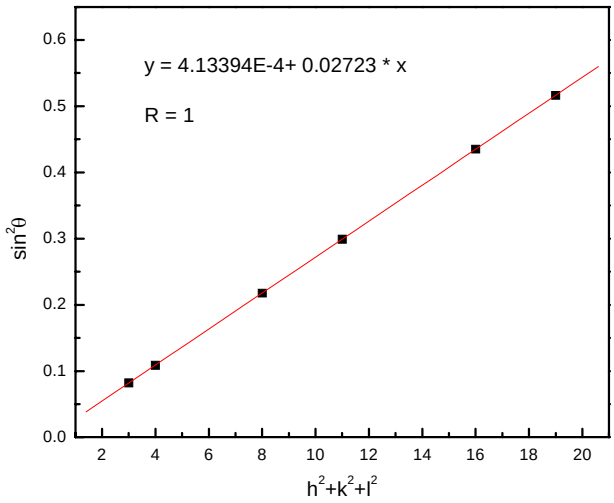

Figure F18 Plot of $\sin^2\theta$ vs. $h^2+k^2+l^2$ for calculating the lattice parameter.

ZrPM-59-800-2000 ("Left peaks")

***a* = 0.4696 nm**

Table F17 Measured and corrected ZrC 2θ values and corresponding Si values used for correction.

Si (hkl)	Measured Si 2θ	NBS Si 2θ		ZrC (hkl)	Measured ZrC 2θ	Corrected ZrC 2θ
111	28.543	28.443		111	33.124	33.017
220	47.414	47.303		200	38.458	38.346
311	56.212	56.123		220	55.344	55.216
400	n.a.	69.131		311	66.058	65.920
331	76.470	76.377		400	82.108	81.955
422	88.107	88.032		331	91.436	91.274

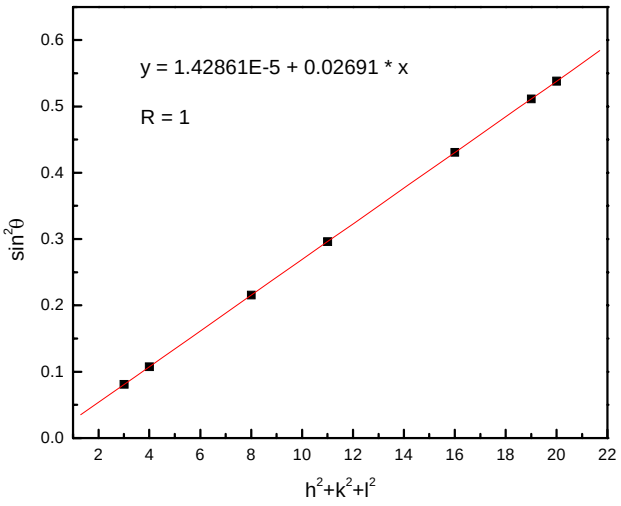

Figure F19 Plot of $\sin^2\theta$ vs. $h^2+k^2+l^2$ for calculating the lattice parameter.

ZrPM-87-800-1425

***a* = 0.4688 nm**

Table F18 Measured and corrected ZrC 2θ values and corresponding Si values used for correction.

Si (hkl)	Measured Si 2θ	NBS Si 2θ		ZrC (hkl)	Measured ZrC 2θ	Corrected ZrC 2θ
111	28.605	28.443		111	33.245	33.083
220	47.465	47.303		200	38.525	38.363
311	56.265	56.123		220	55.535	55.393
400	n.a.	69.131		311	66.190	66.045
331	76.525	76.377		400	82.320	82.180
422	88.155	88.032		331	91.600	91.479
511	95.075	94.954		420	94.695	94.575

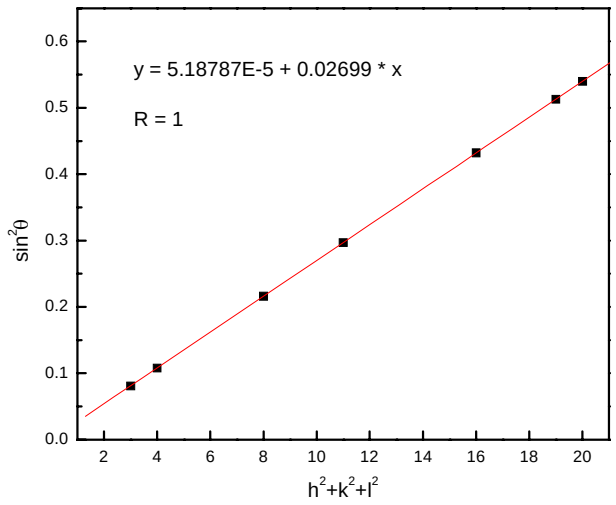

Figure F20 Plot of $\sin^2\theta$ vs. $h^2+k^2+l^2$ for calculating the lattice parameter.

ZrPM-87-800-1900 ("ZrC" substrate)

***a* = 0.4664 nm**

Table F19 Measured and corrected ZrC 2θ values and corresponding Si values used for correction.

Si (hkl)	Measured Si 2θ	NBS Si 2θ		ZrC (hkl)	Measured ZrC 2θ	Corrected ZrC 2θ
111	28.520	28.443		111	33.3450	33.264
220	47.395	47.303		200	38.6700	38.584
311	56.210	56.123		220	55.7850	55.697
400	n.a.	69.131		311	66.5150	66.437
331	76.445	76.377		400	82.7700	82.707
422	88.090	88.032		331	92.1650	92.108

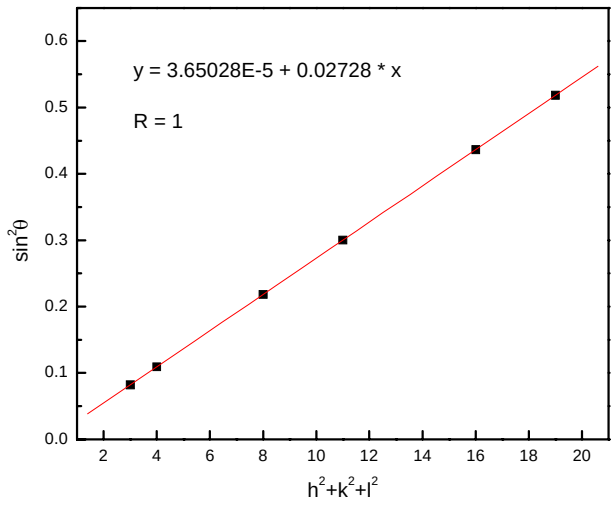

Figure F21 Plot of $\sin^2\theta$ vs. $h^2+k^2+l^2$ for calculating the lattice parameter.

ZrPM-87-800-1900 (“Right peaks”; “Graphoil” substrate)

***a* = 0.4664 nm**

Table F20 Measured and corrected ZrC 2θ values and corresponding Si values used for correction.

Si (hkl)	Measured Si 2θ	NBS Si 2θ		ZrC (hkl)	Measured ZrC 2θ	Corrected ZrC 2θ
111	28.645	28.443		111	33.340	33.140
220	47.495	47.303		200	38.650	38.453
311	56.315	56.123		220	55.815	55.623
400	n.a.	69.131		311	66.530	66.350
331	76.545	76.377		400	82.865	82.708
422	88.180	88.032		331	92.260	92.113

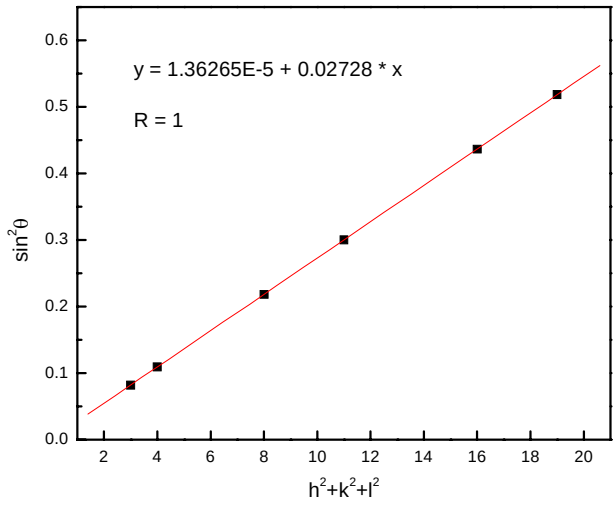

Figure F22 Plot of $\sin^2\theta$ vs. $h^2+k^2+l^2$ for calculating the lattice parameter.

ZrPM-87-80-1900 ("Left peaks"; "Graphoil" substrate)

***a* = 0.4696 nm**

Table F21 Measured and corrected ZrC 2θ values and corresponding Si values used for correction.

Si (hkl)	Measured Si 2θ	NBS Si 2θ		ZrC (hkl)	Measured ZrC 2θ	Corrected ZrC 2θ
111	28.645	28.443		111	33.240	33.040
220	47.495	47.303		200	38.525	38.328
311	56.315	56.123		220	55.515	55.323
400	n.a.	69.131		311	66.140	65.960
331	76.545	76.377		400	82.235	82.077
422	88.180	88.032		331	91.530	91.383

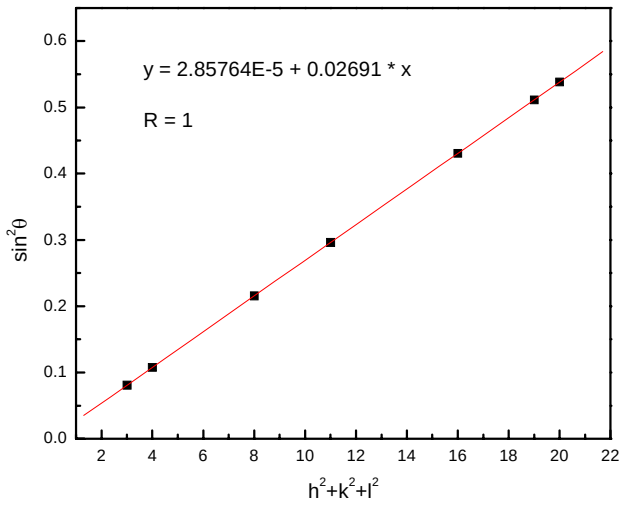

Figure F23 Plot of $\sin^2\theta$ vs. $h^2+k^2+l^2$ for calculating the lattice parameter.

ZrPM-94-800-1475

***a* = 0.4688 nm**

Table F22 Measured and corrected ZrC 2θ values and corresponding Si values used for correction.

Si (hkl)	Measured Si 2θ	NBS Si 2θ		ZrC (hkl)	Measured ZrC 2θ	Corrected ZrC 2θ
111	28.605	28.443		111	33.255	33.095
220	47.460	47.303		200	38.550	38.392
311	56.285	56.123		220	55.565	55.401
400	n.a.	69.131		311	66.240	66.095
331	76.50	76.377		400	82.405	82.282
422	88.150	88.032		331	91.690	91.573
511	95.075	94.954		420	94.765	94.647

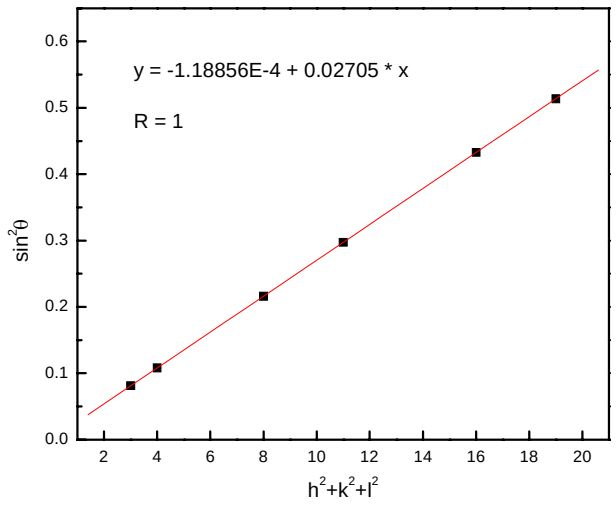

Figure F24 Plot of $\sin^2\theta$ vs. $h^2+k^2+l^2$ for calculating the lattice parameter.

ZrPM-94-800-1900 ("ZrC" substrate)

***a* = 0.4662 nm**

Table F23 Measured and corrected ZrC 2θ values and corresponding Si values used for correction.

Si (hkl)	Measured Si 2θ	NBS Si 2θ		ZrC (hkl)	Measured ZrC 2θ	Corrected ZrC 2θ
111	28.585	28.443		111	33.3900	33.248
220	47.445	47.303		200	38.7100	38.568
311	56.245	56.123		220	55.8200	55.698
400	n.a.	69.131		311	66.5400	66.414
331	76.505	76.377		400	82.7900	82.679
422	88.13	88.032		331	92.1700	92.063
511	95.06	94.954		420	95.3000	95.189

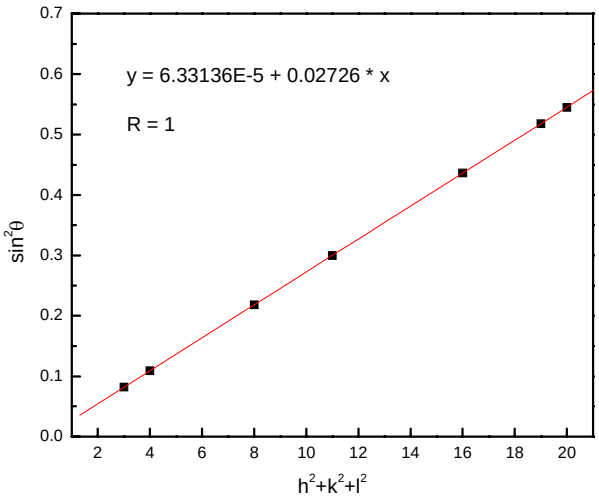

Figure F25 Plot of $\sin^2\theta$ vs. $h^2+k^2+l^2$ for calculating the lattice parameter.

ZrPM-94-800-1900 ("Right peaks"; "Graphoil" substrate)

***a* = 0.4667 nm**

Table F24 Measured and corrected ZrC 2θ values and corresponding Si values used for correction.

Si (hkl)	Measured Si 2θ	NBS Si 2θ		ZrC (hkl)	Measured ZrC 2θ	Corrected ZrC 2θ
111	28.580	28.443		111	33.370	33.232
220	47.445	47.303		200	38.690	38.550
311	56.265	56.123		220	55.790	55.648
400	n.a.	69.131		311	66.510	66.380
331	76.495	76.377		400	82.745	82.627
422	88.150	88.032		331	92.130	92.012

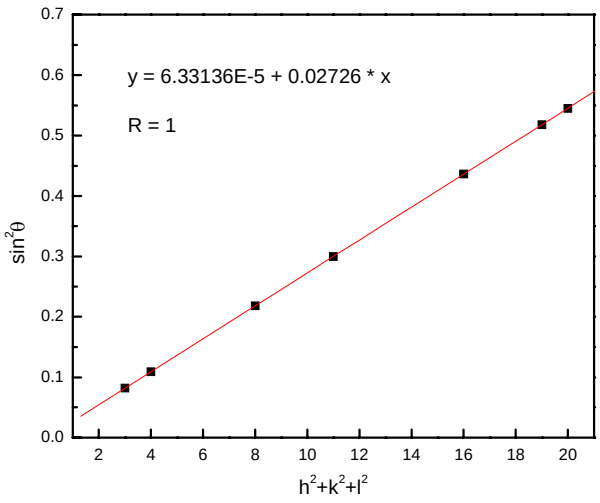

Figure F26 Plot of $\sin^2\theta$ vs. $h^2+k^2+l^2$ for calculating the lattice parameter.

ZrPM-94-800-1900 (“Left peaks”; “Graphoil” substrate)

***a* = 0.4695 nm**

Table F25 Measured and corrected ZrC 2θ values and corresponding Si values used for correction.

Si (hkl)	Measured Si 2θ	NBS Si 2θ		ZrC (hkl)	Measured ZrC 2θ	Corrected ZrC 2θ
111	28.580	28.443		111	33.336	33.198
220	47.445	47.303		200	38.663	38.523
311	56.265	56.123		220	55.779	55.637
400	n.a.	69.131		311	66.501	66.371
331	76.495	76.377		400	82.761	82.643
422	88.150	88.032		331	92.144	92.026

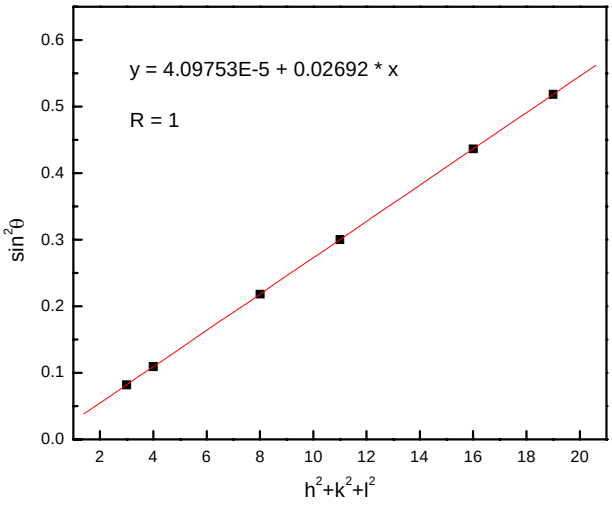

Figure F27 Plot of $\sin^2\theta$ vs. $h^2+k^2+l^2$ for calculating the lattice parameter.

ZrPM-97-800-1500

***a* = 0.4697 nm**

Table F26 Measured and corrected ZrC 2θ values and corresponding Si values used for correction.

Si (hkl)	Measured Si 2θ	NBS Si 2θ		ZrC (hkl)	Measured ZrC 2θ	Corrected ZrC 2θ
111	28.605	28.443		111	33.190	33.030
220	47.460	47.303		200	38.465	38.306
311	56.275	56.123		220	55.445	55.294
400	n.a.	69.131		311	66.075	65.930
331	76.515	76.377		400	82.175	82.045
422	88.150	88.032		331	91.445	91.246
511	95.065	94.954		420	94.505	94.307

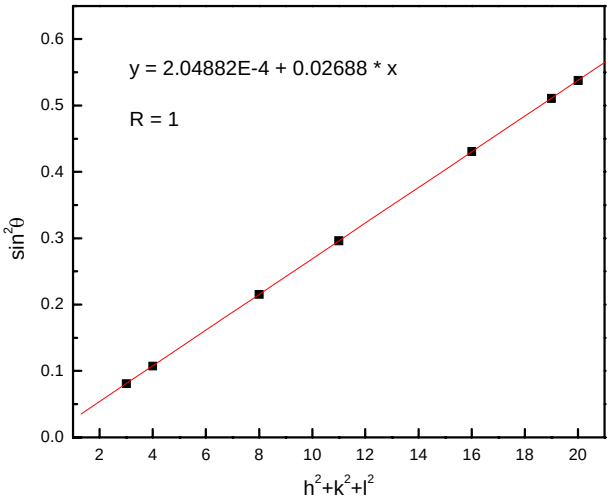

Figure F28 Plot of $\sin^2\theta$ vs. $h^2+k^2+l^2$ for calculating the lattice parameter.

ZrPM-97-800-1900

***a* = 0.4696 nm**

Table F27 Measured and corrected ZrC 2θ values and corresponding Si values used for correction.

Si (hkl)	Measured Si 2θ	NBS Si 2θ		ZrC (hkl)	Measured ZrC 2θ	Corrected ZrC 2θ
111	28.605	28.443		111	33.185	33.012
220	47.510	47.303		200	38.470	38.284
311	56.275	56.123		220	55.440	55.282
400	n.a.	69.131		311	66.065	65.934
331	76.485	76.377		400	82.140	82.022
422	88.160	88.032		331	91.405	91.285
511	95.065	94.954		420	94.490	94.377

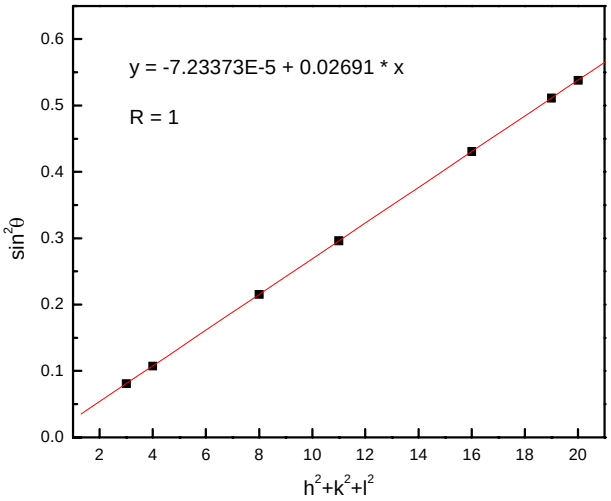

Figure F29 Plot of $\sin^2\theta$ vs. $h^2+k^2+l^2$ for calculating the lattice parameter.

ZrPM-99-800-1475

***a* = 0.4697 nm**

Table F28 Measured and corrected ZrC 2θ values and corresponding Si values used for correction.

Si (hkl)	Measured Si 2θ	NBS Si 2θ		ZrC (hkl)	Measured ZrC 2θ	Corrected ZrC 2θ
111	28.600	28.443		111	33.200	33.044
220	47.450	47.303		200	38.495	38.342
311	56.255	56.123		220	55.470	55.336
400	n.a.	69.131		311	66.115	65.982
331	76.510	76.377		400	82.170	82.045
422	88.150	88.032		331	91.565	91.449
511	95.060	94.954		420	94.505	94.394

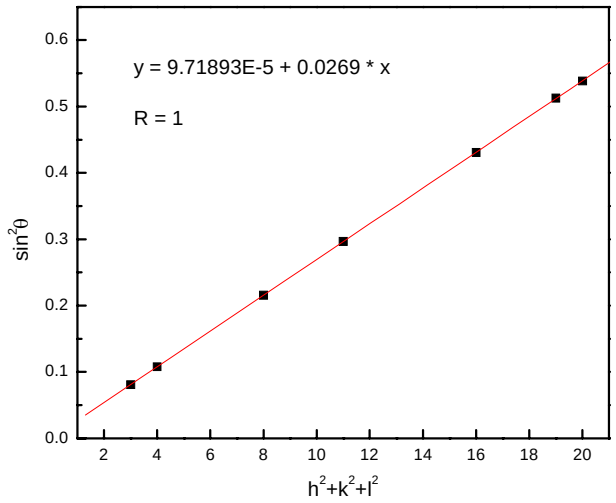

Figure F30 Plot of $\sin^2\theta$ vs. $h^2+k^2+l^2$ for calculating the lattice parameter.

ZrPM-99-800-1900

***a* = 0.4696 nm**

Table F29 Measured and corrected ZrC 2θ values and corresponding Si values used for correction.

Si (hkl)	Measured Si 2θ	NBS Si 2θ		ZrC (hkl)	Measured ZrC 2θ	Corrected ZrC 2θ
111	28.525	28.443		111	33.105	33.023
220	47.385	47.303		200	38.395	38.313
311	56.205	56.123		220	55.375	55.293
400	n.a.	69.131		311	66.000	65.924
331	76.445	76.377		400	82.085	82.017
422	88.100	88.032		331	91.365	91.297
511	95.020	94.954		420	94.445	94.378

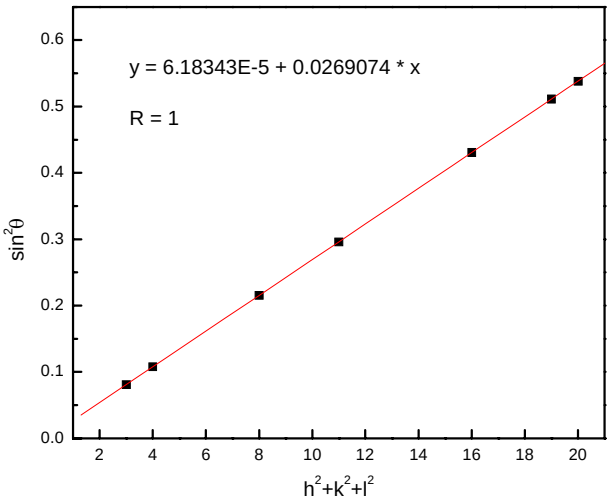

Figure F31 Plot of $\sin^2\theta$ vs. $h^2+k^2+l^2$ for calculating the lattice parameter.

APPENDIX G

PARTICLE SIZE DISTRIBUTION PLOTS FOR SAMPLES LISTED IN TABLE 5.35 AND XRD GRAPHS FOR SAMPLES LISTED IN TABLE 5.29 and TABLE 5.35

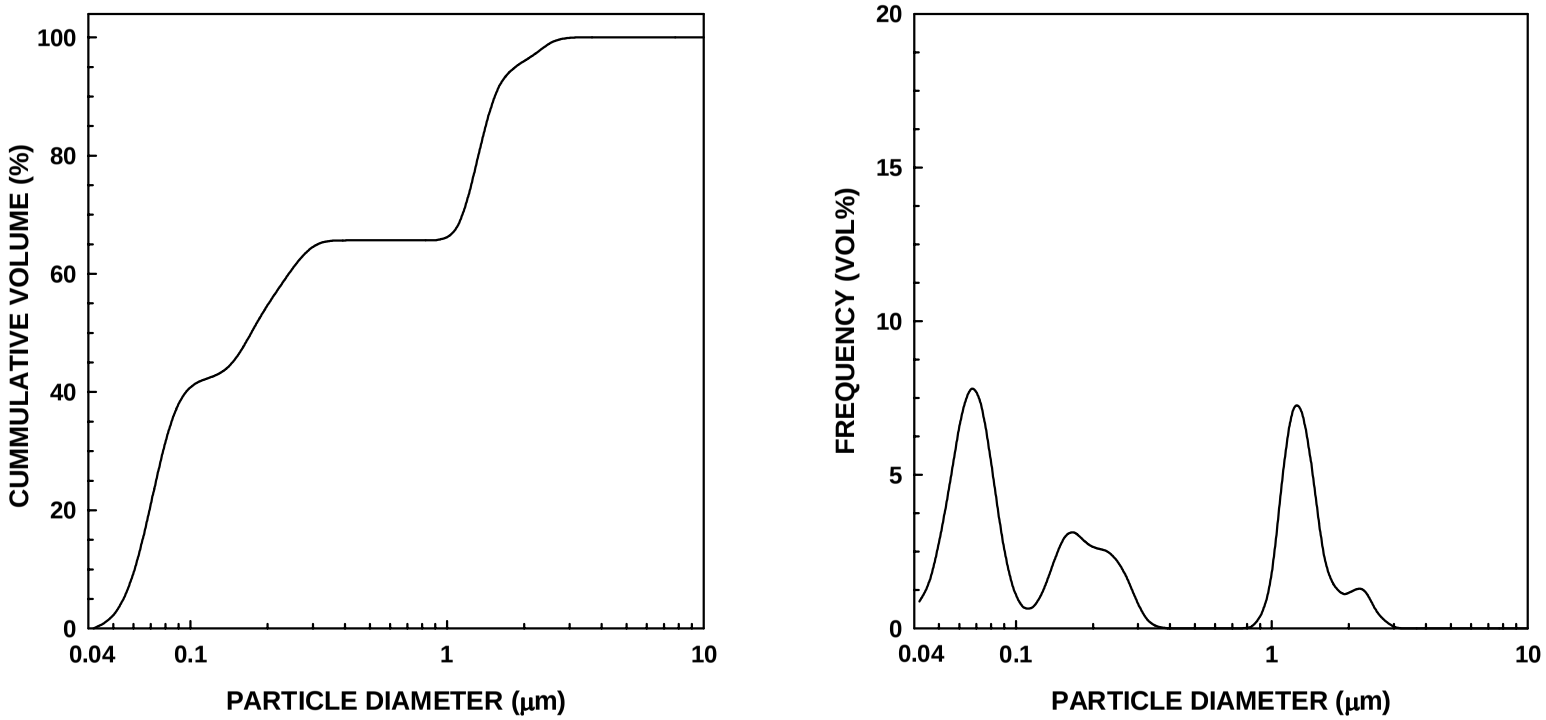

Figure G1 Particle size distribution plots for the 10 min-milled ZrPM-58-1300-1350-1300 powder sample: cumulative frequency plot (left) and relative frequency plot (right).

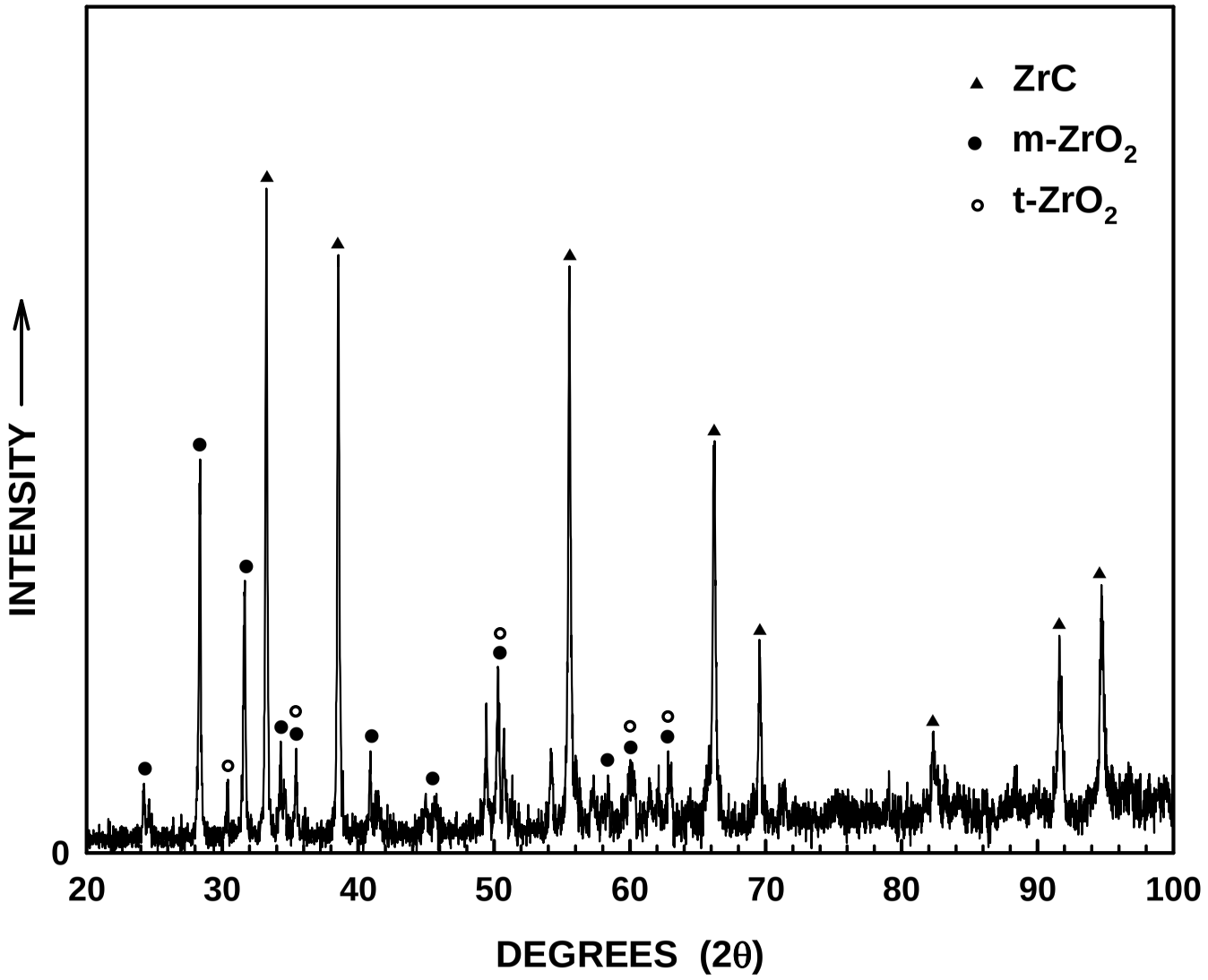

Figure G2 XRD graph of ZrPM-58-1300-1350-1300 powder sample.

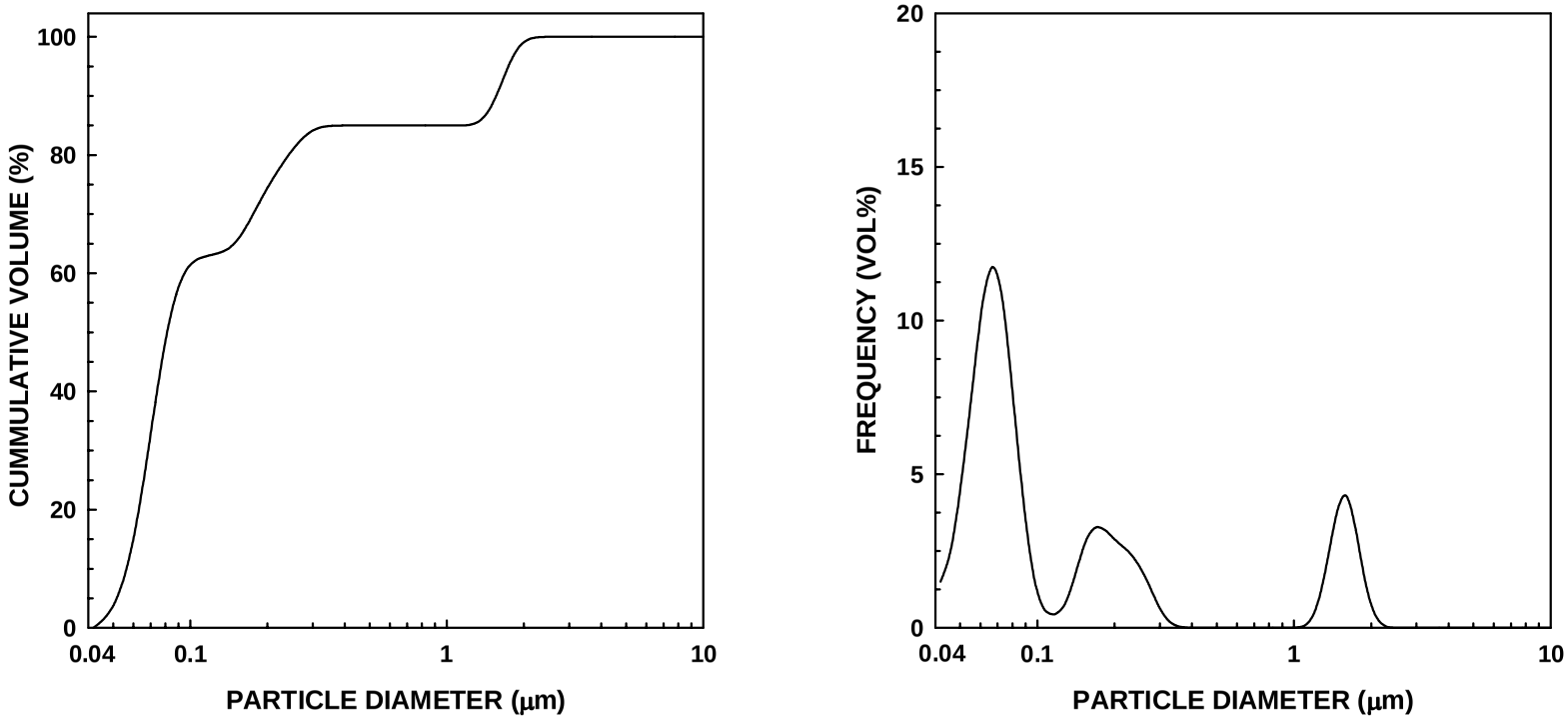

Figure G3 Particle size distribution plots for the 10 min-milled ZrPM-91-800-1425-4 powder sample: cumulative frequency plot (left) and relative frequency plot (right).

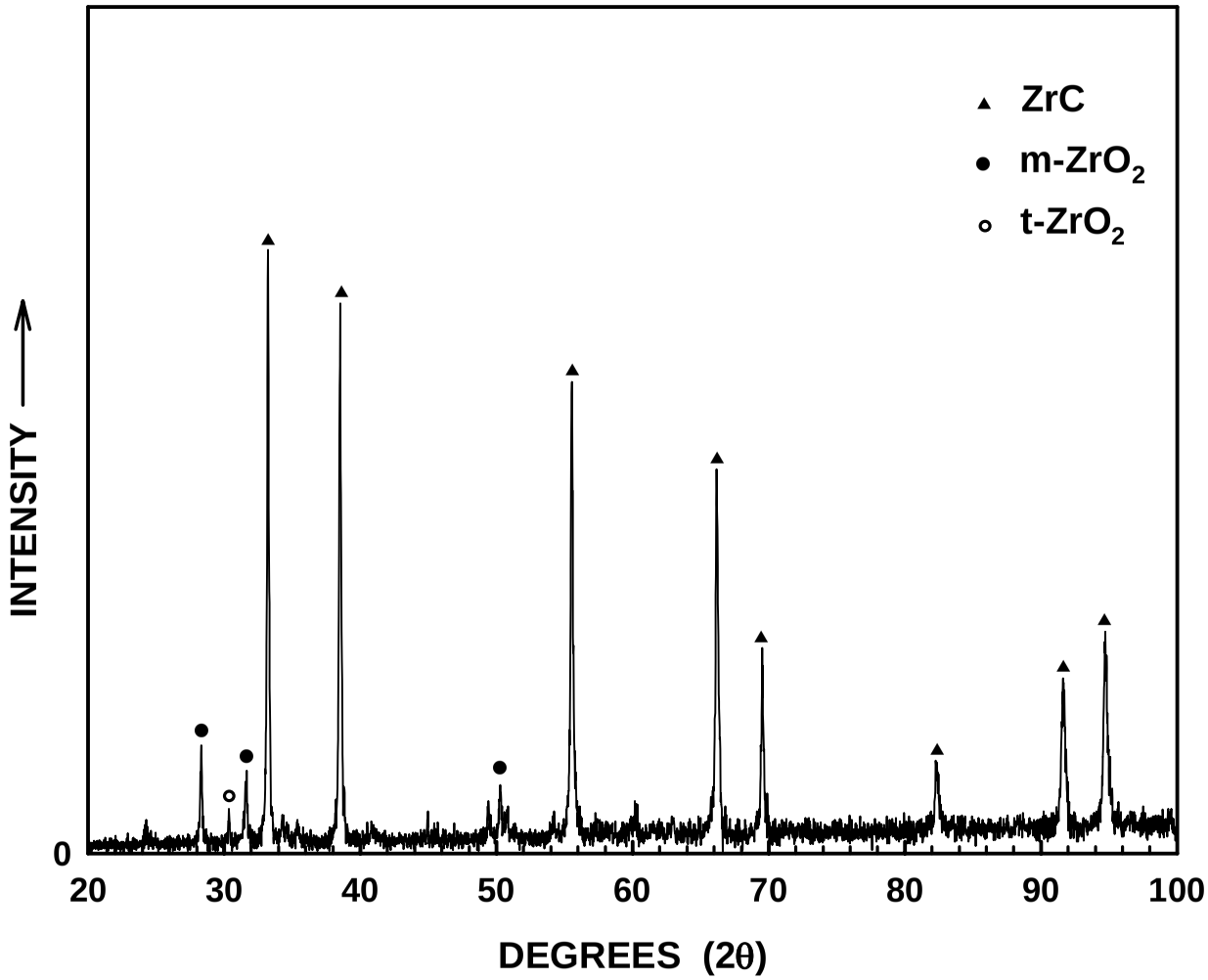

Figure G4 XRD graph of ZrPM-91-800-1425-4 powder sample.

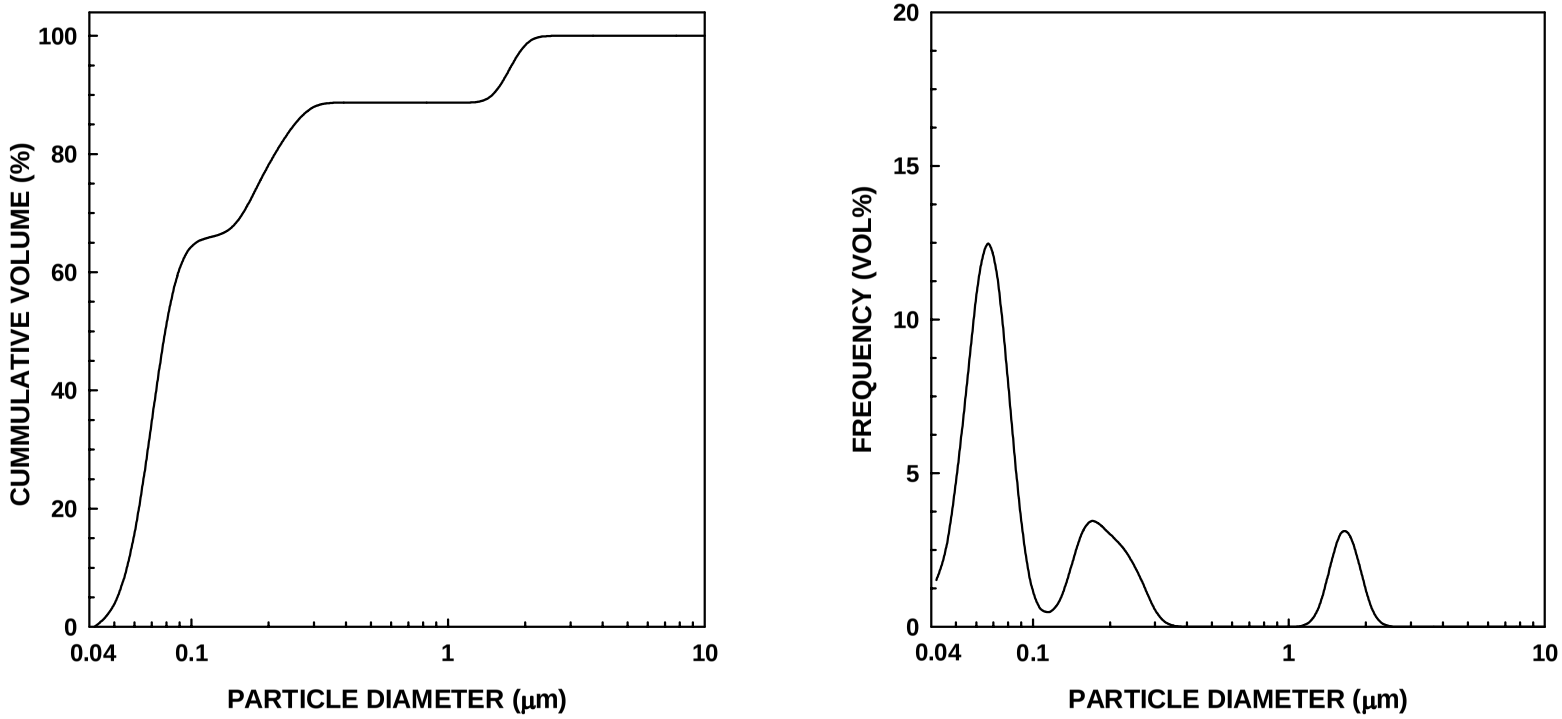

Figure G5 Particle size distribution plots for the 10 min-milled ZrPM-87-800-1-1425-2 powder sample: cumulative frequency plot (left) and relative frequency plot (right).

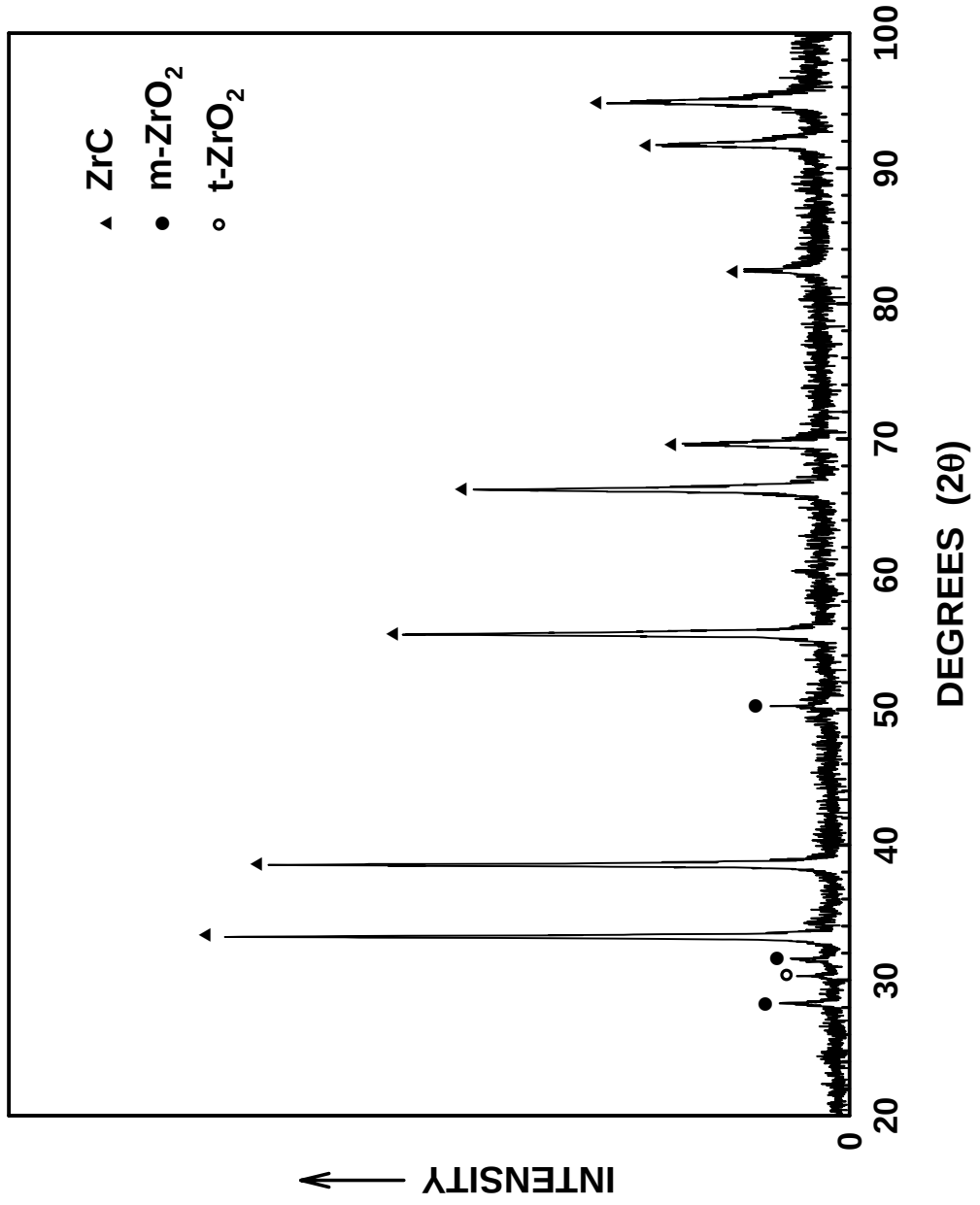

Figure G6 XRD graph of ZrPM-87-800-1-1425-2 powder sample.

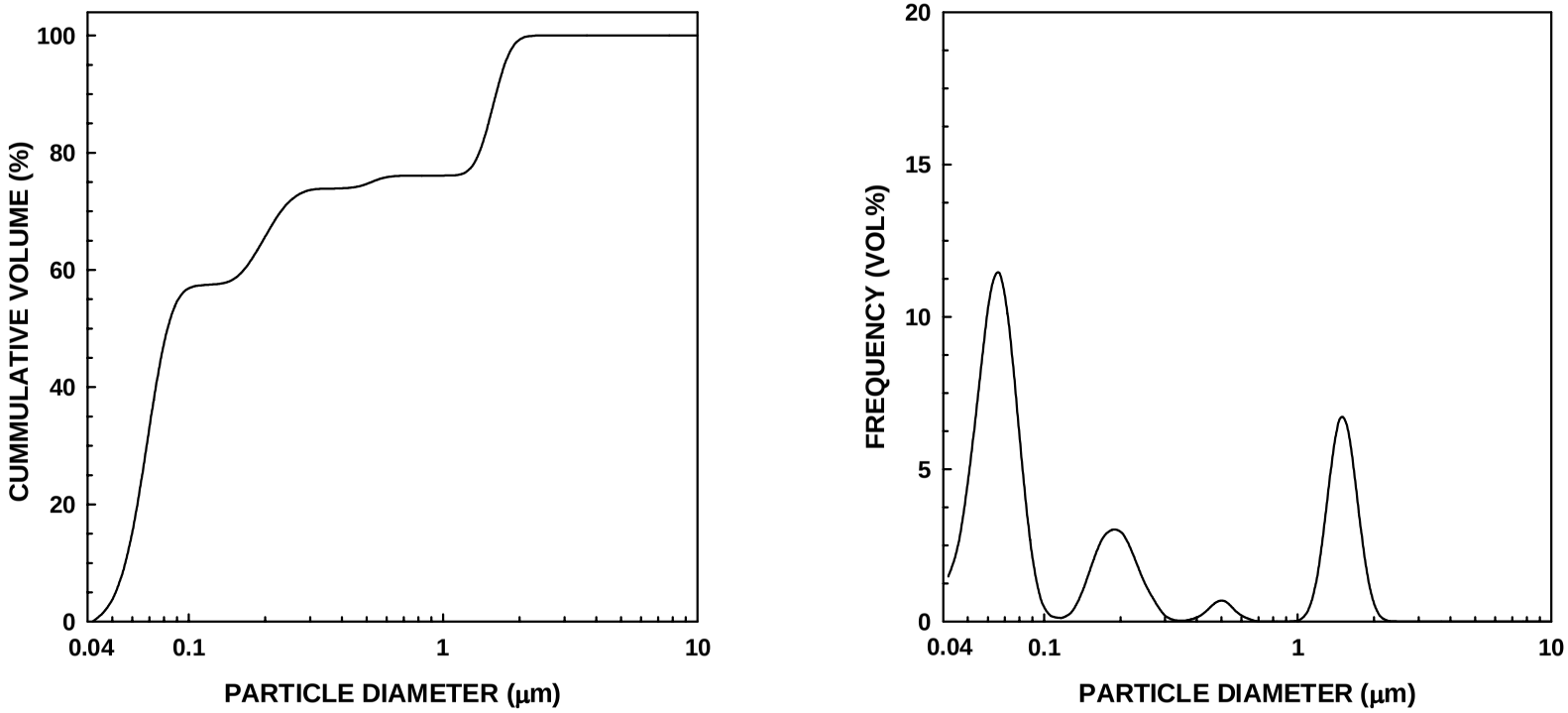

Figure G7 Particle size distribution plots for the 10 min-milled ZrPM-69+76+85-800-1-1400-1 powder sample: cumulative frequency plot (left) and relative frequency plot (right).

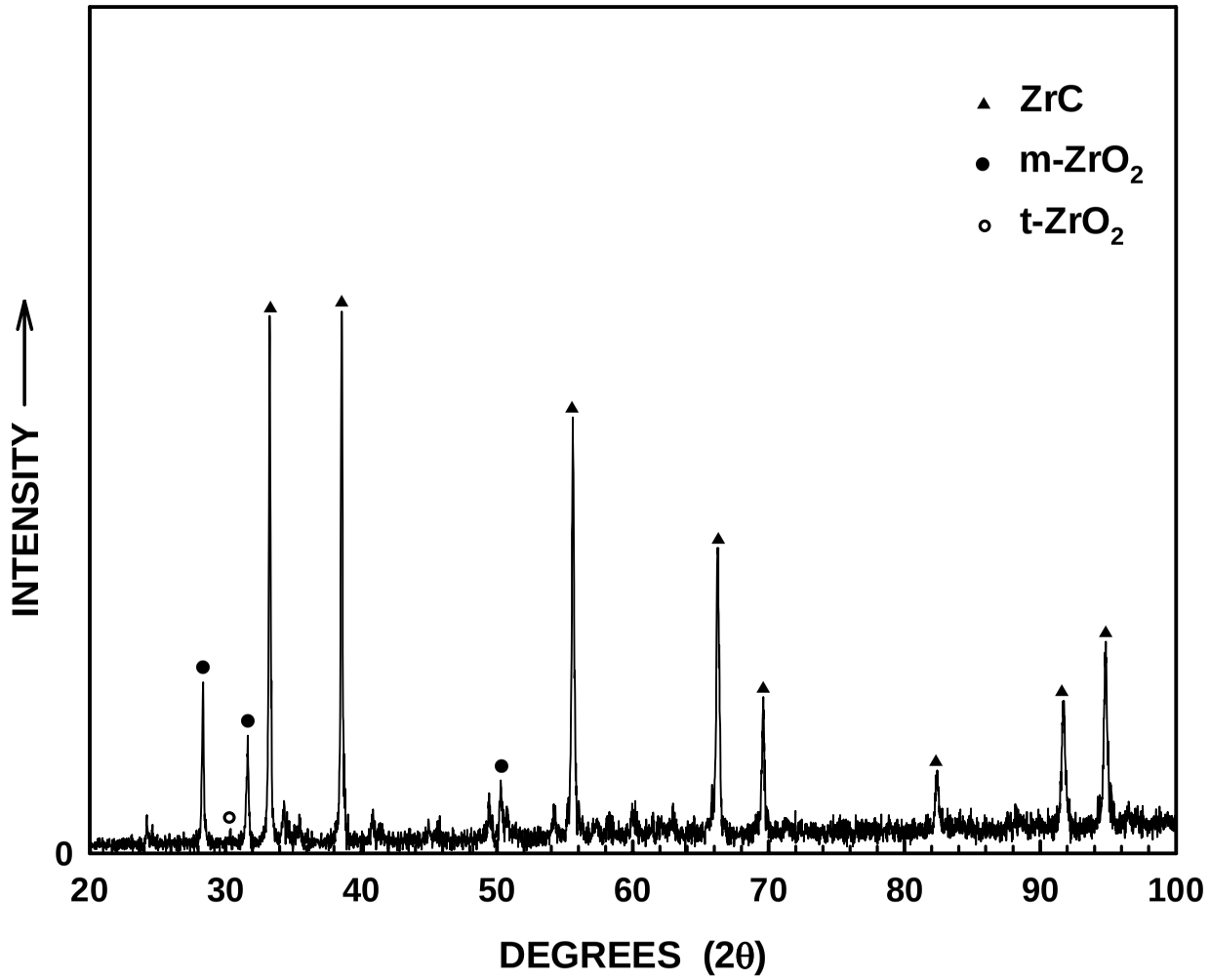

Figure G8 XRD graph of ZrPM-69+76+85-800-1-1400-1 powder sample.

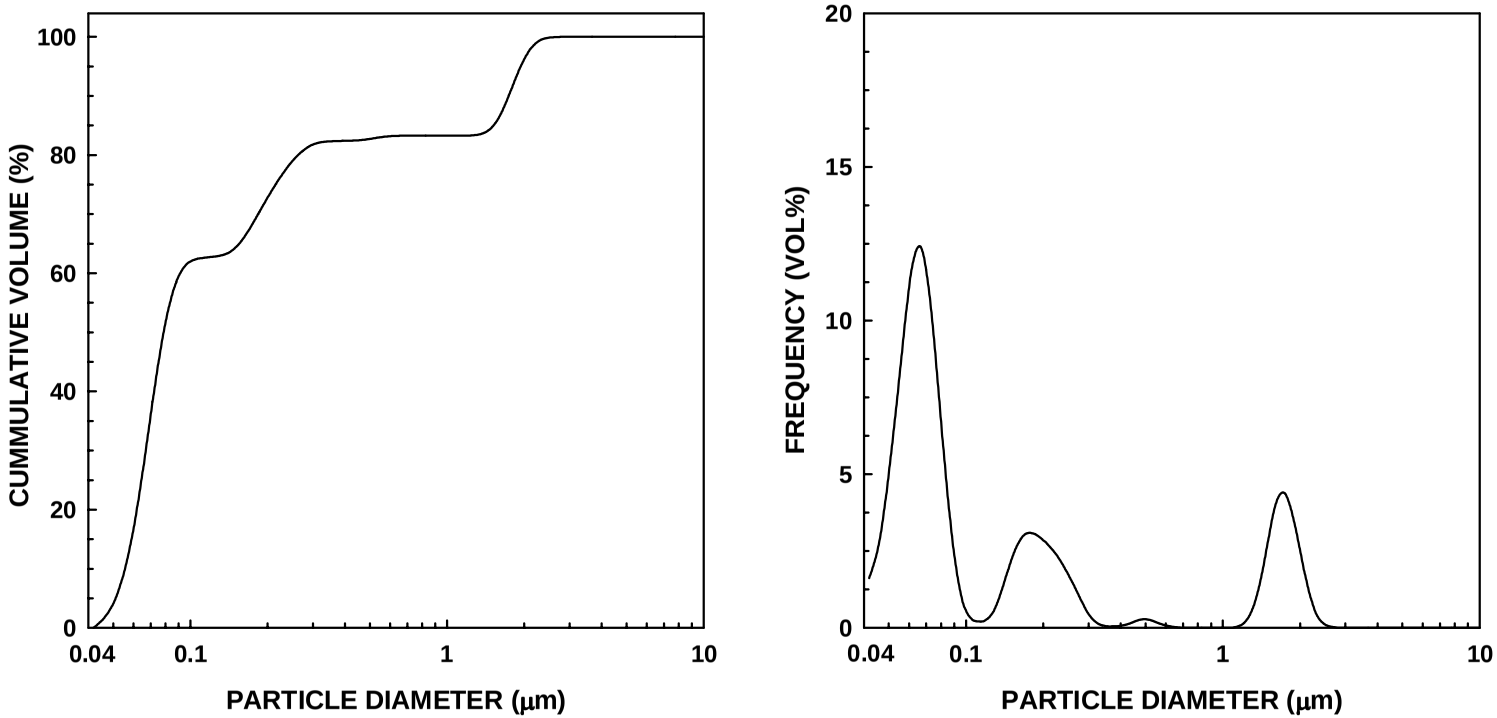

Figure G9 Particle size distribution plots for the 10 min-milled ZrPM-100-800-2-1450-1 powder sample: cumulative frequency plot (left) and relative frequency plot (right).

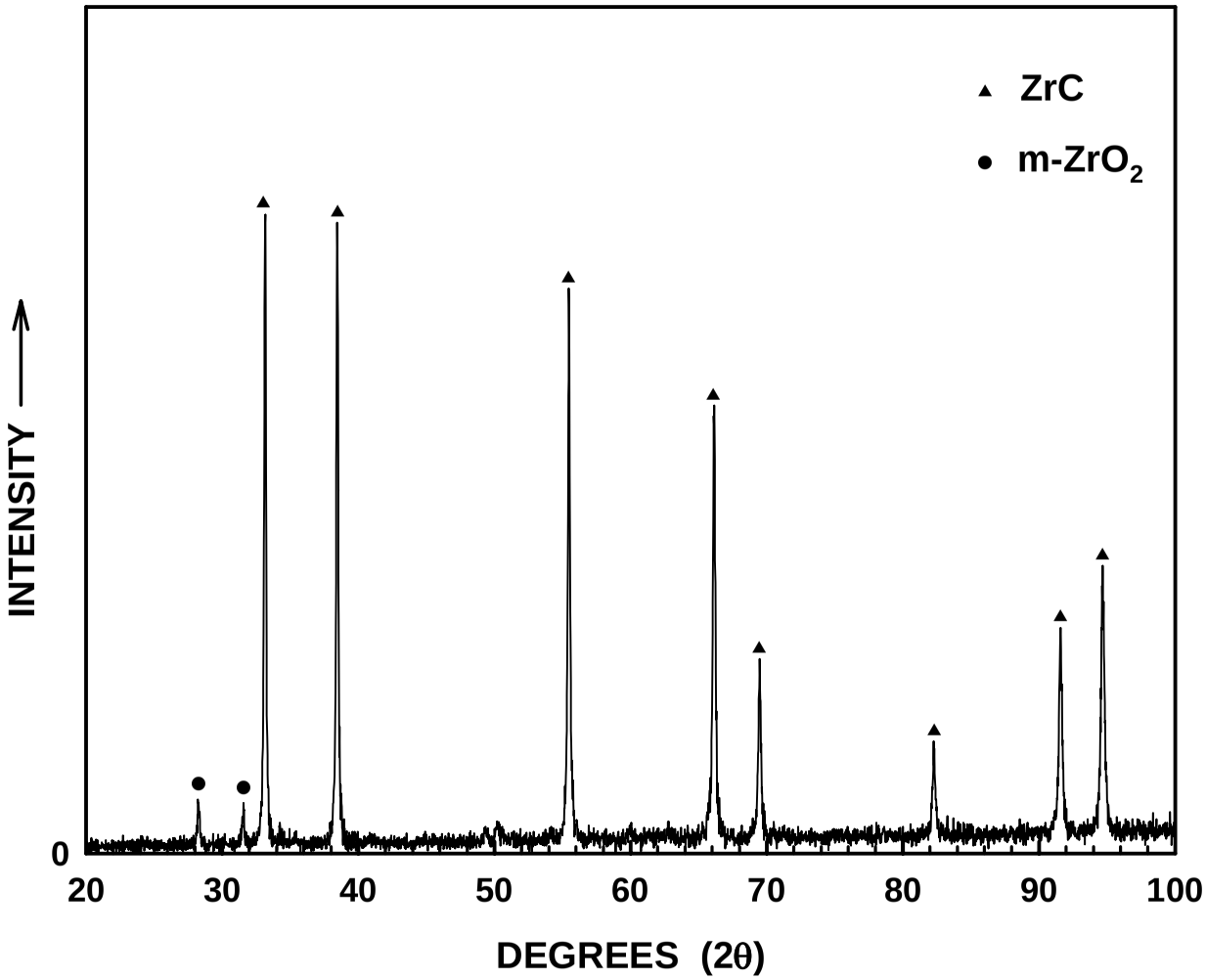

Figure G10 XRD graph of ZrPM-100-800-2-1450-1 powder sample.

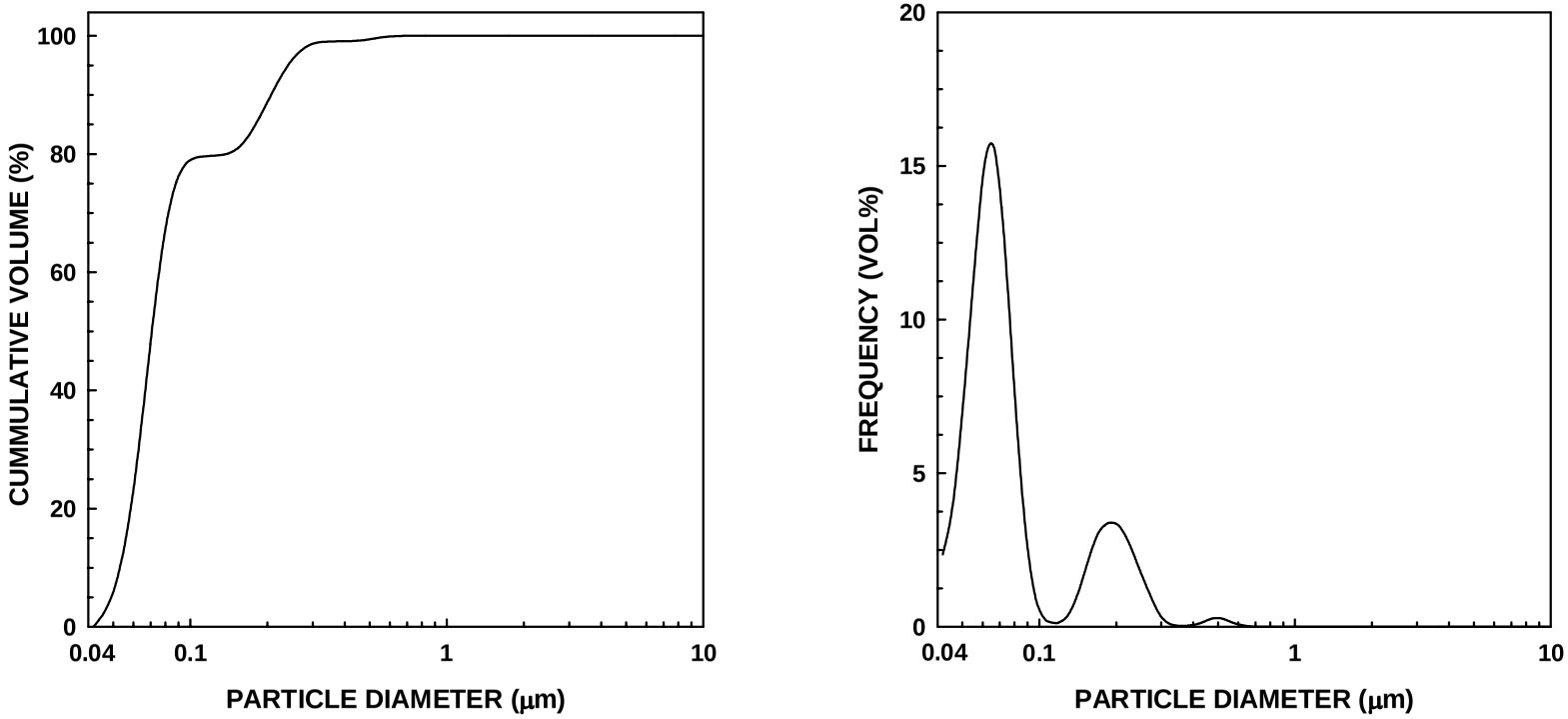

Figure G11 Particle size distribution plots for the 10 min-milled ZrPM-94-800-3-1475-1 powder sample: cumulative frequency plot (left) and relative frequency plot (right).

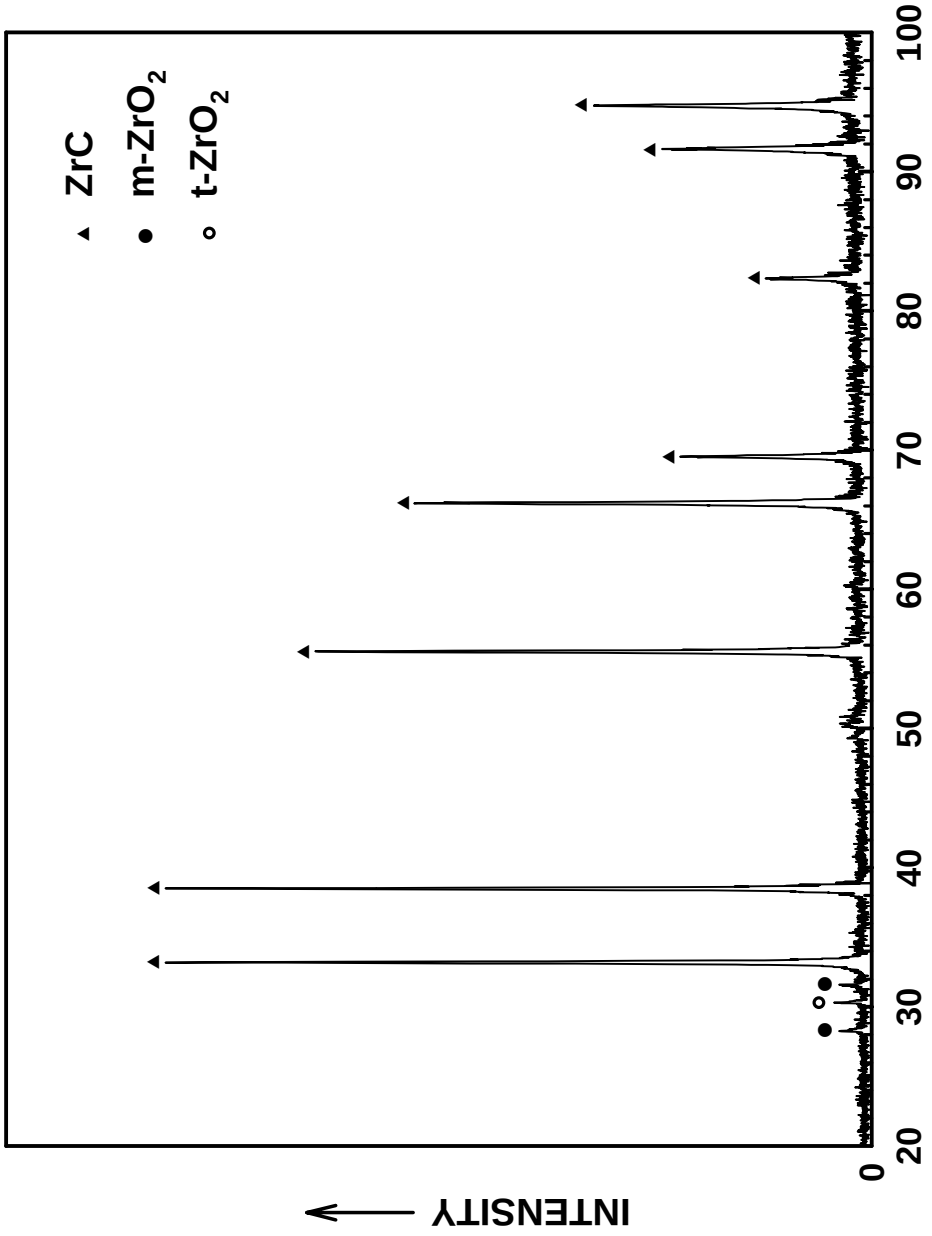

Figure G12 XRD graph of ZrPM-94-800-3-1475-1 powder sample.

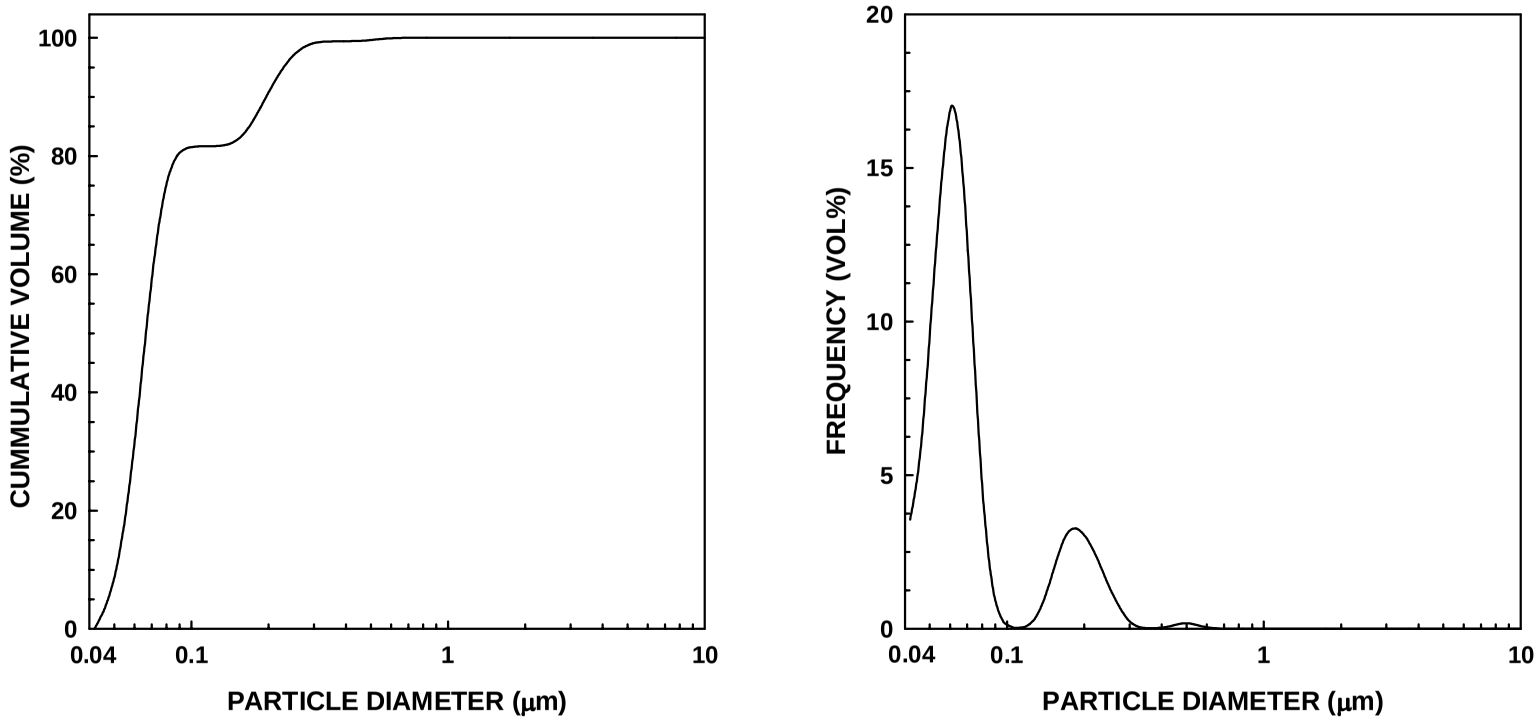

Figure G13 Particle size distribution plots for the 10 min-milled ZrPM-95-800-3-1475-1 powder sample: cumulative frequency plot (left) and relative frequency plot (right).

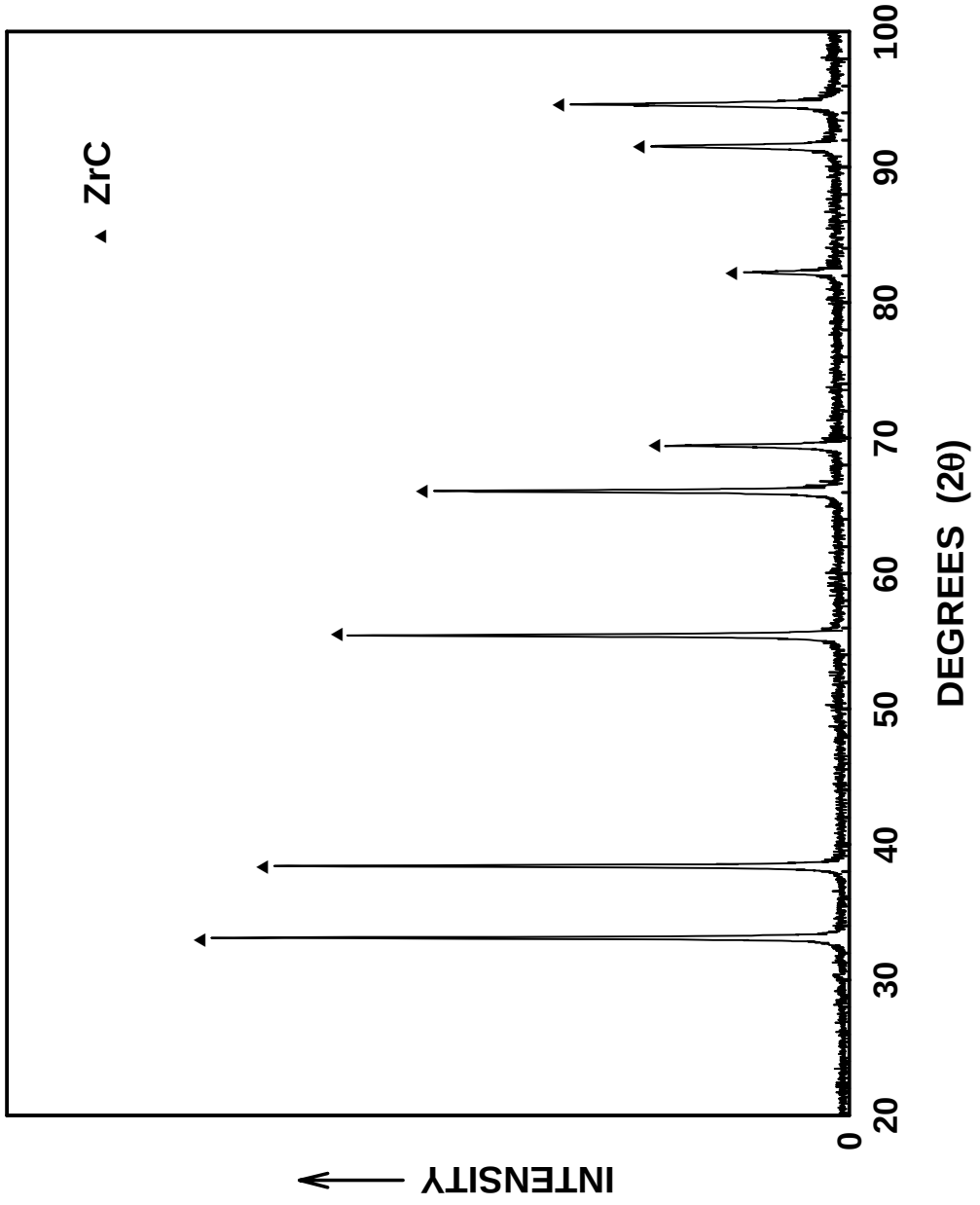

Figure G14 XRD graph of ZrPM-95-800-3-1475-1 powder sample.

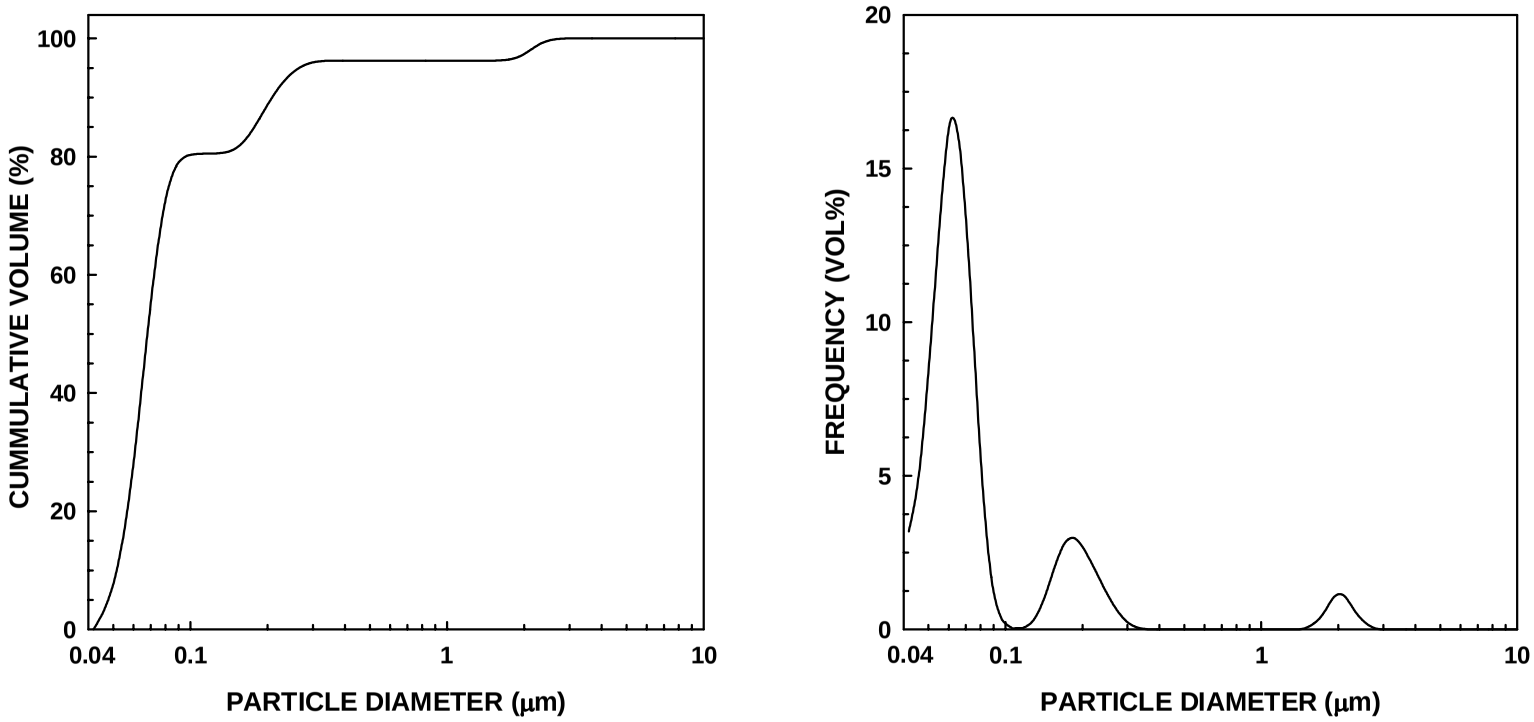

Figure G15 Particle size distribution plots for the 10 min-milled ZrPM-45-800-1-1350-1400-3 powder sample: cumulative frequency plot (left) and relative frequency plot (right).

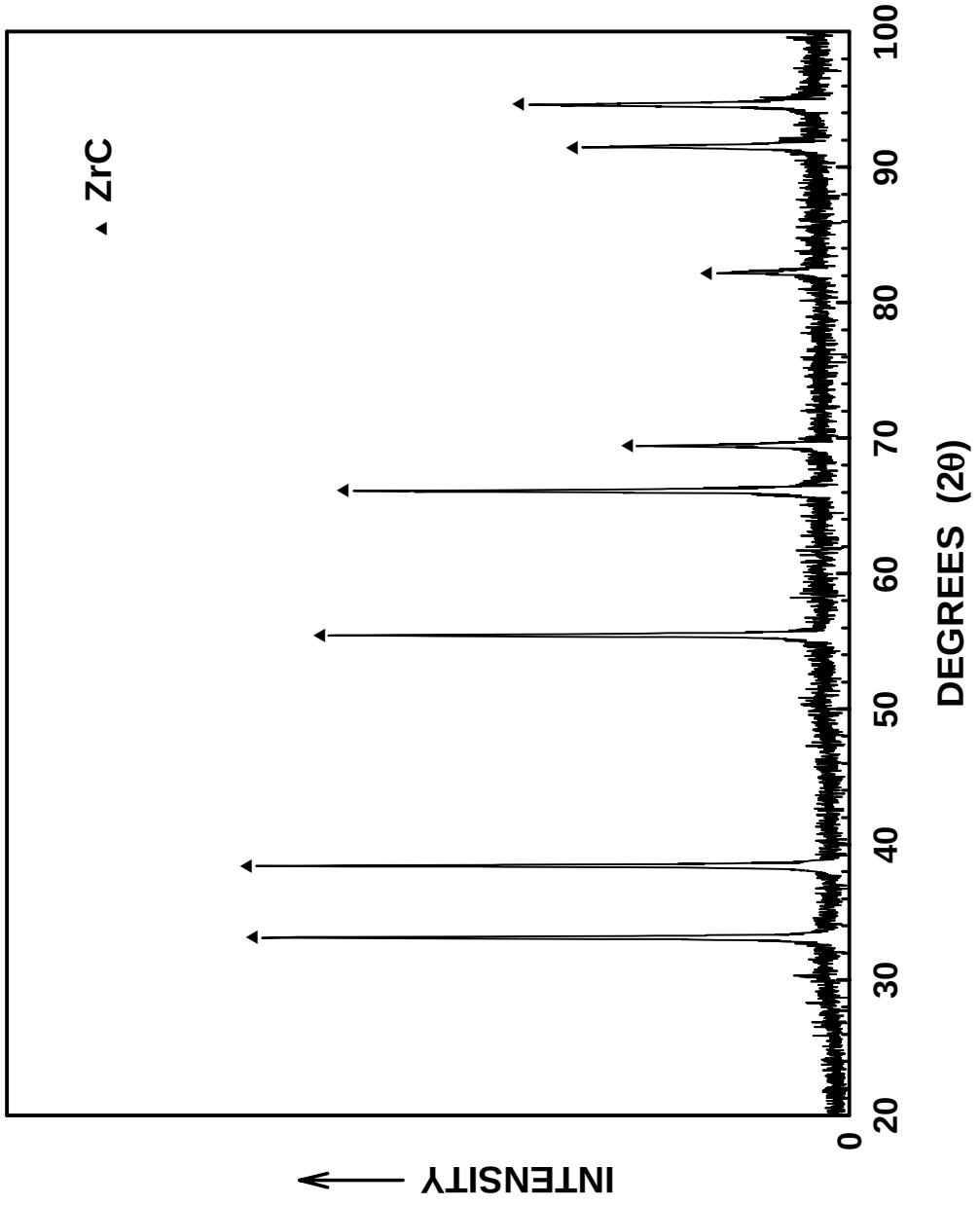

Figure G16 XRD graph of ZrPM-45-800-1-1350-1400-3 powder sample.

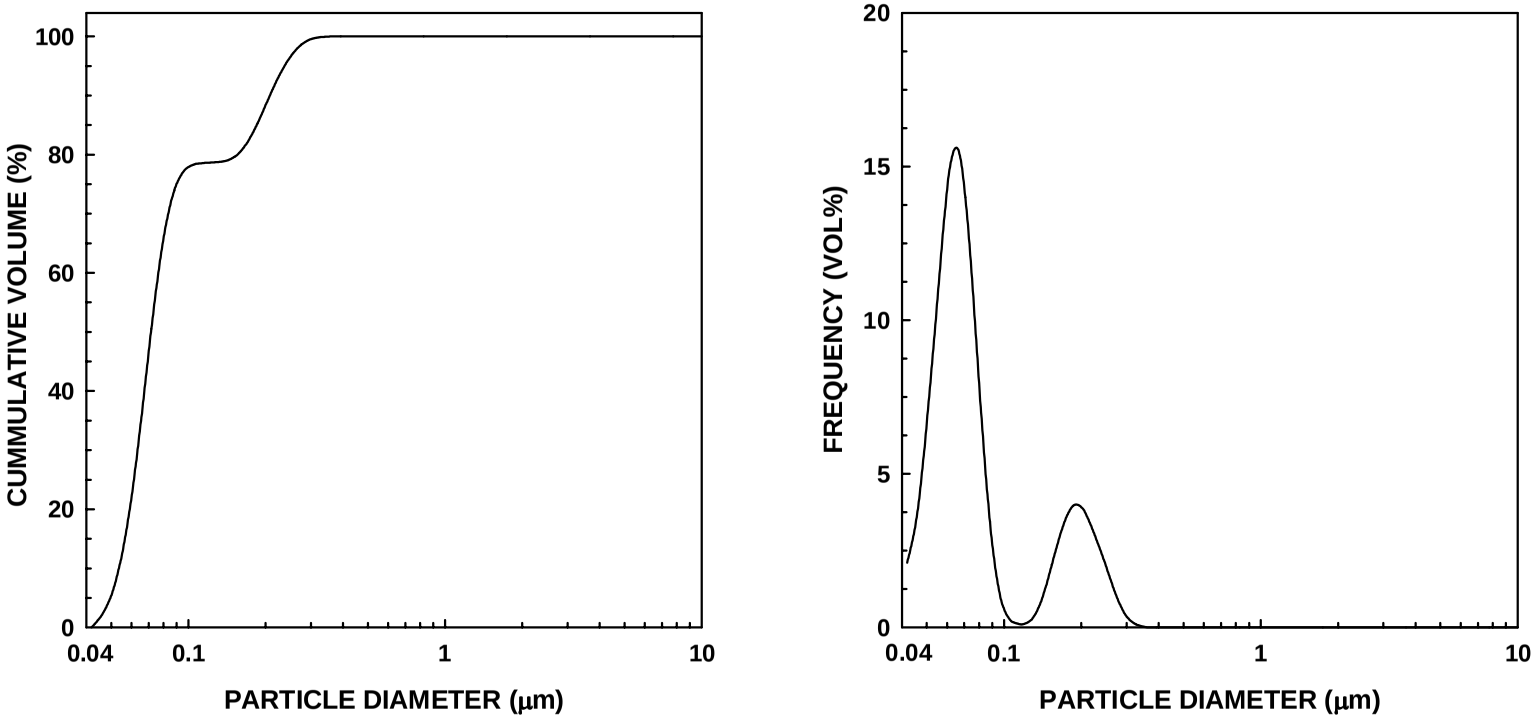

Figure G17 Particle size distribution plots for the 10 min-milled ZrPM-98-800-1-1450-1 powder sample: cumulative frequency plot (left) and relative frequency plot (right).

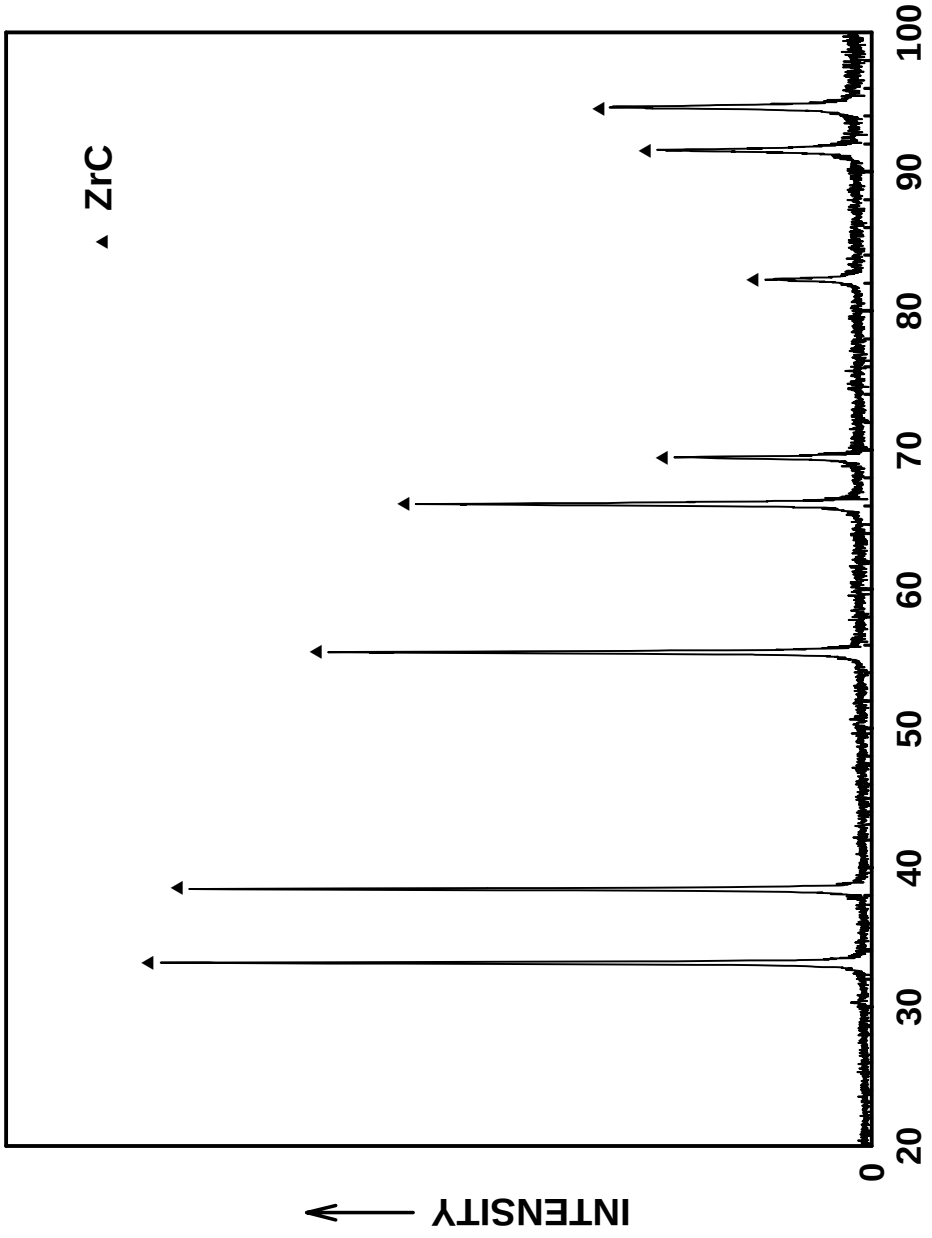

Figure G18 XRD graph of ZrPM-98-800-1-1450-1 powder sample.

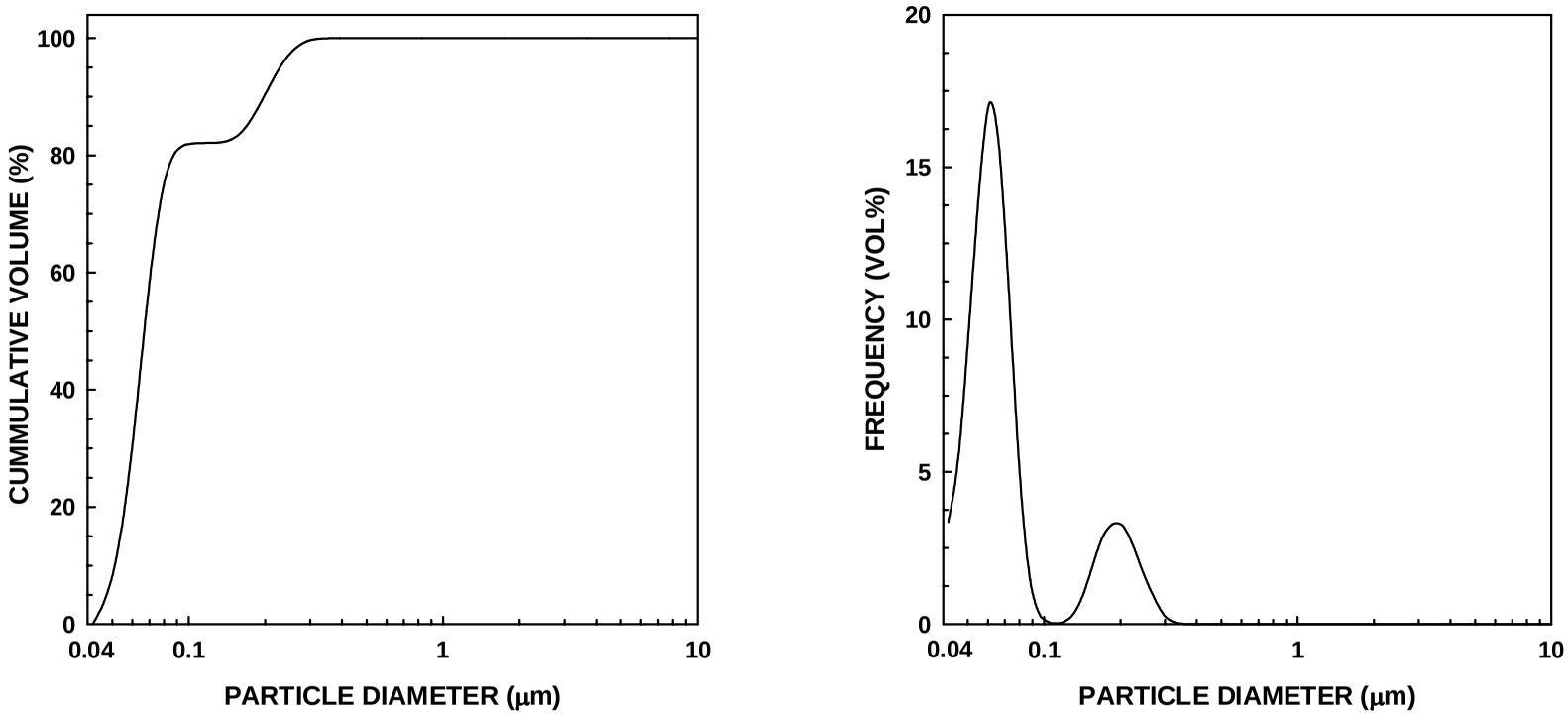

Figure G19 Particle size distribution plots for the 10 min-milled ZrPM-99-800-1-1475-1 powder sample: cumulative frequency plot (left) and relative frequency plot (right).

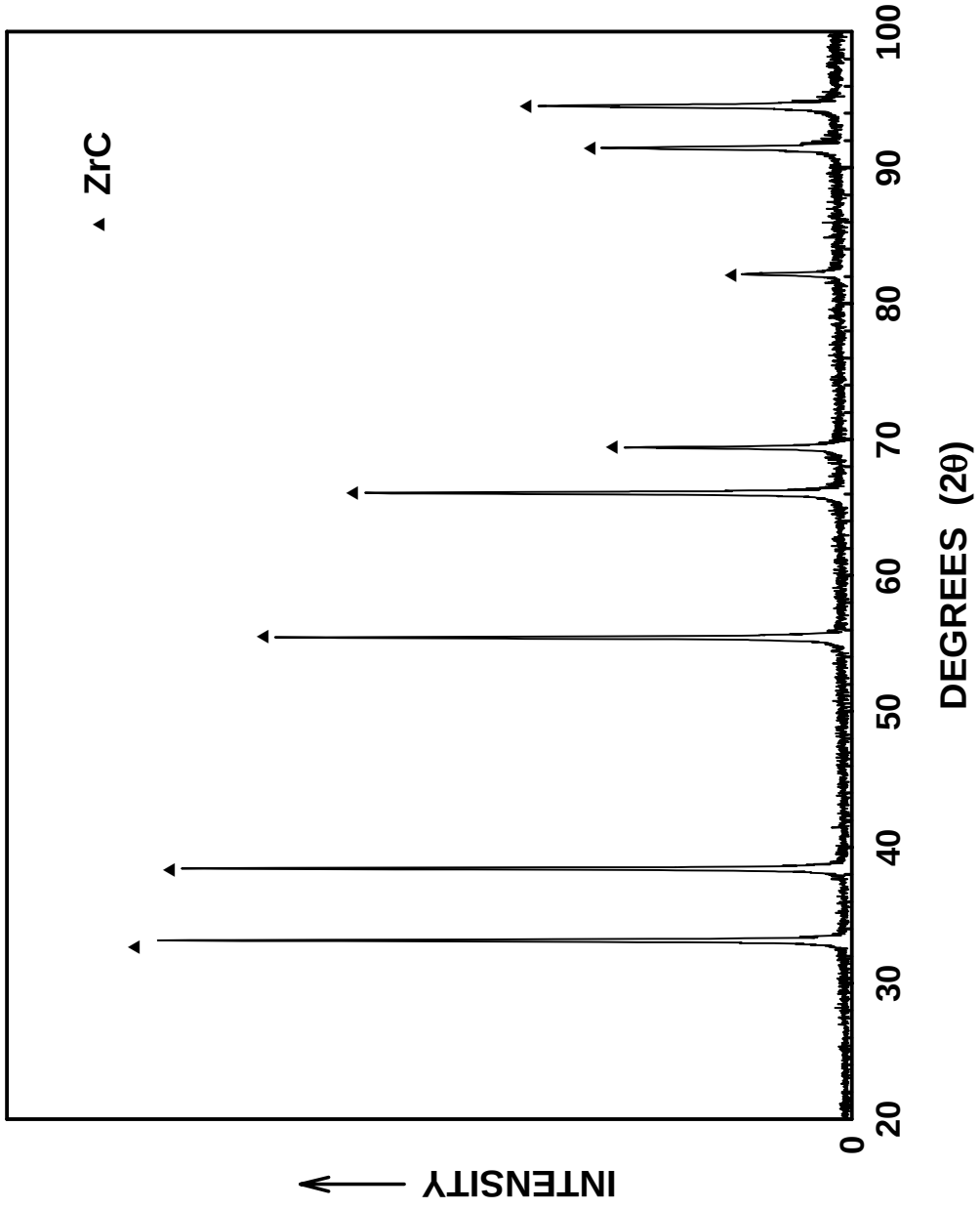

Figure G20 XRD graph of ZrPM-99-800-1-1475-1 powder sample.

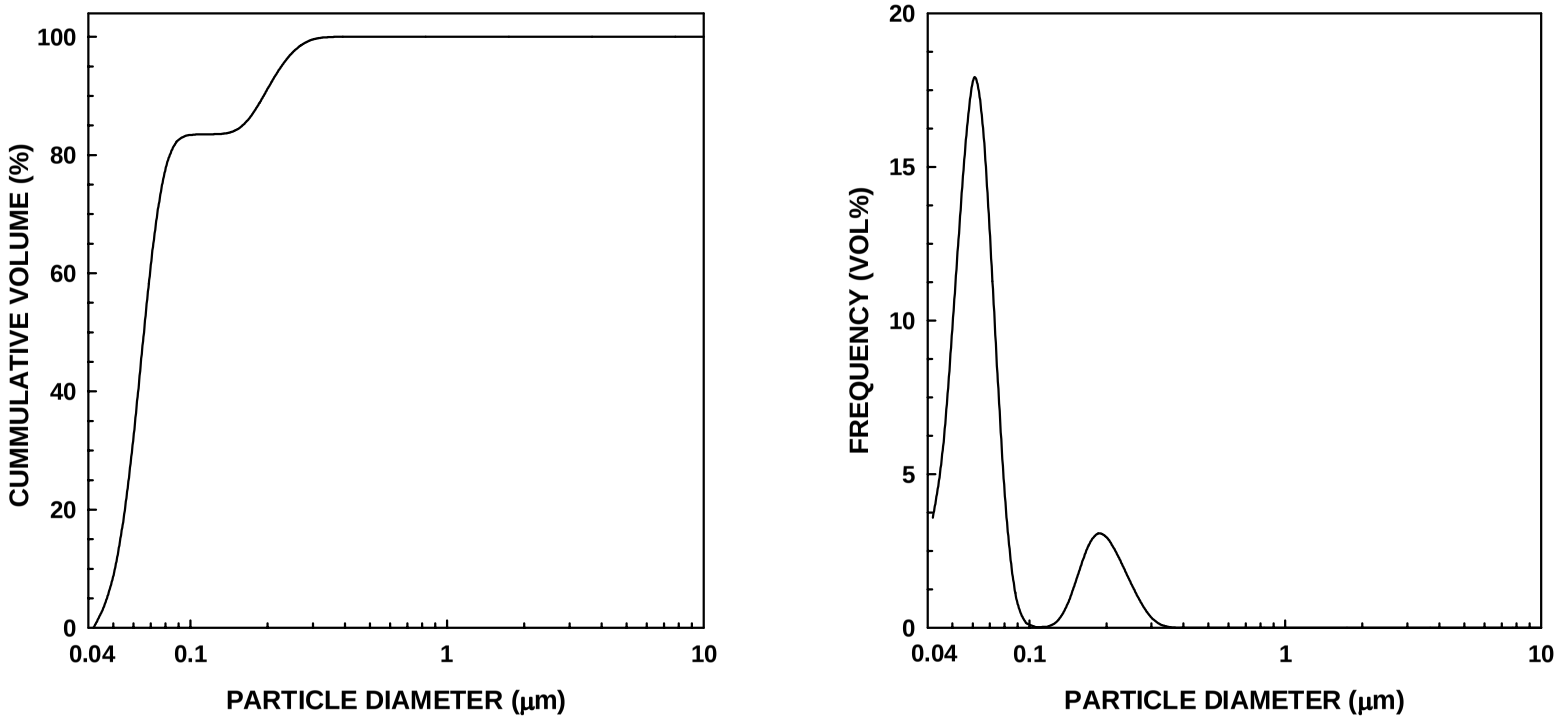

Figure G21 Particle size distribution plots for the 10 min-milled ZrPM-97-800-1-1500-1 powder sample: cumulative frequency plot (left) and relative frequency plot (right).

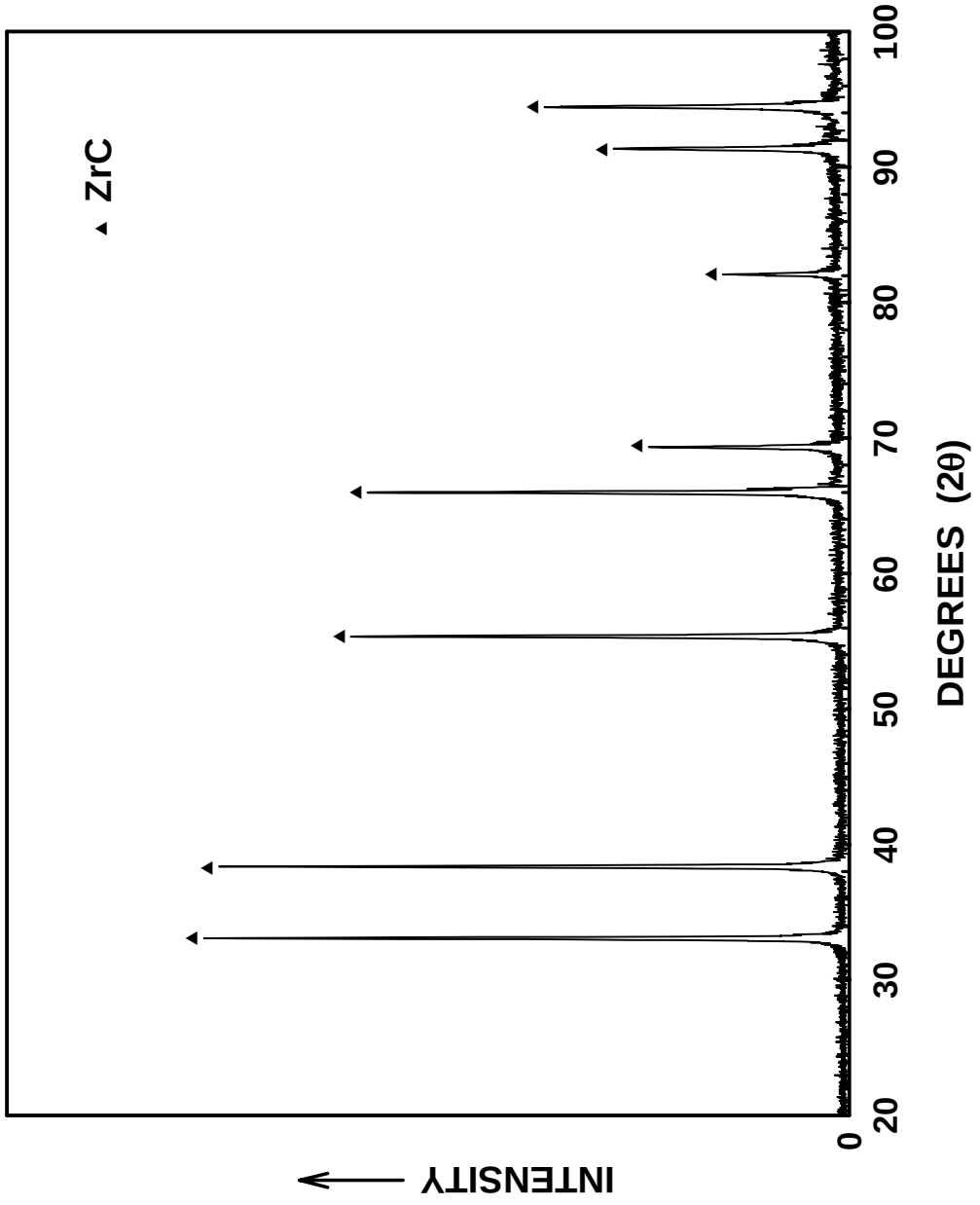

Figure G22 XRD graph of ZrPM-97-800-1-1500-1 powder sample.

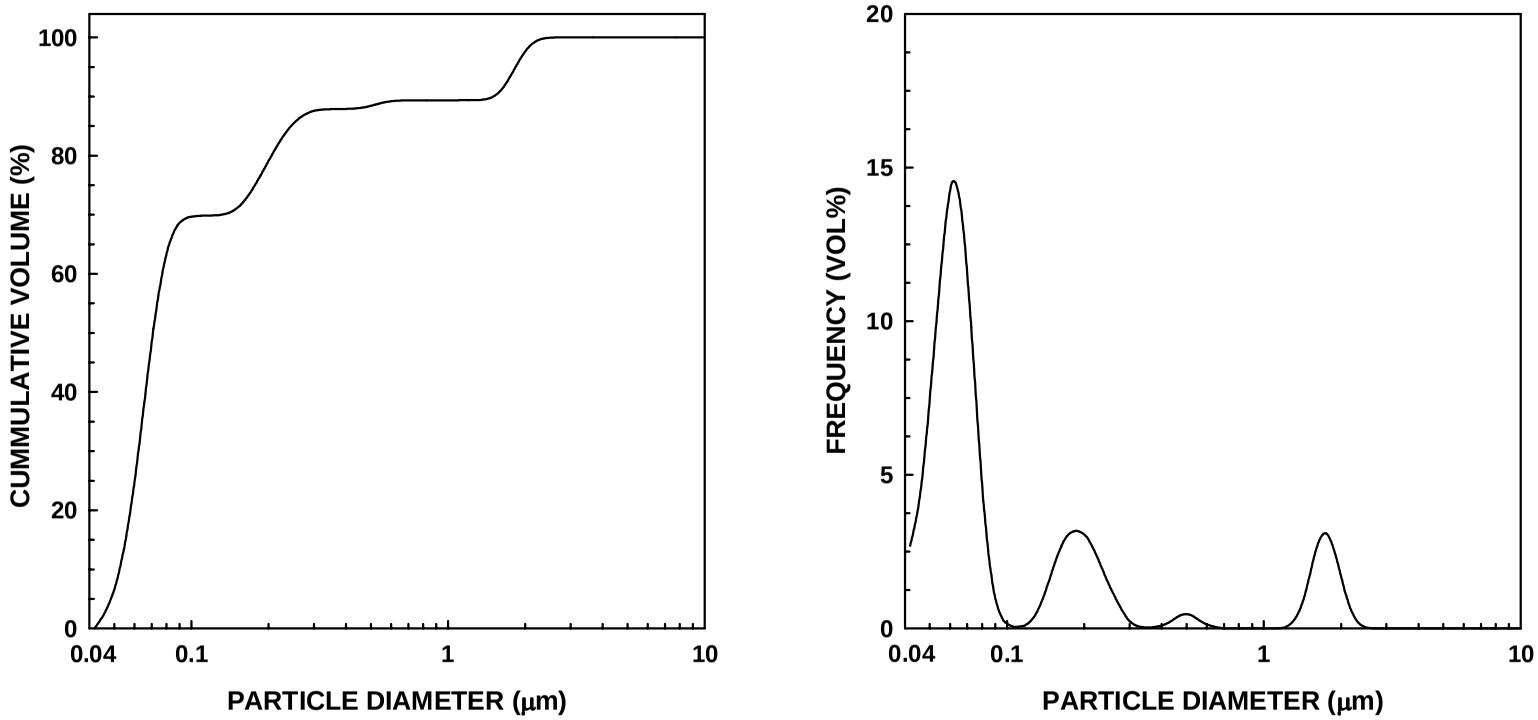

Figure G23 Particle size distribution plots for the 10 min-milled ZrPM-79+82-800-1-1425-1 powder sample: cumulative frequency plot (left) and relative frequency plot (right).

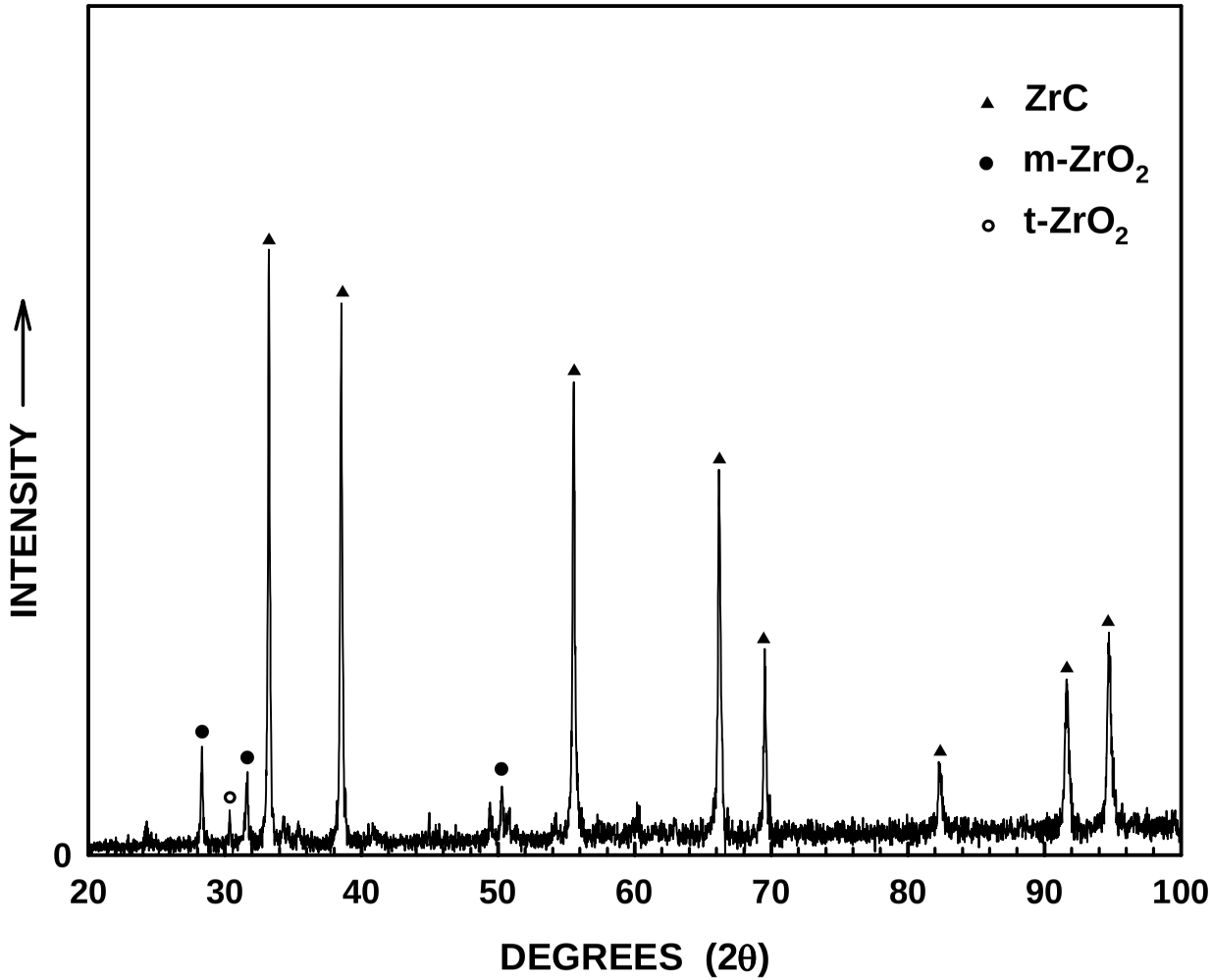

Figure G24 XRD graph of ZrPM-79+82-800-1-1425-1 powder sample.

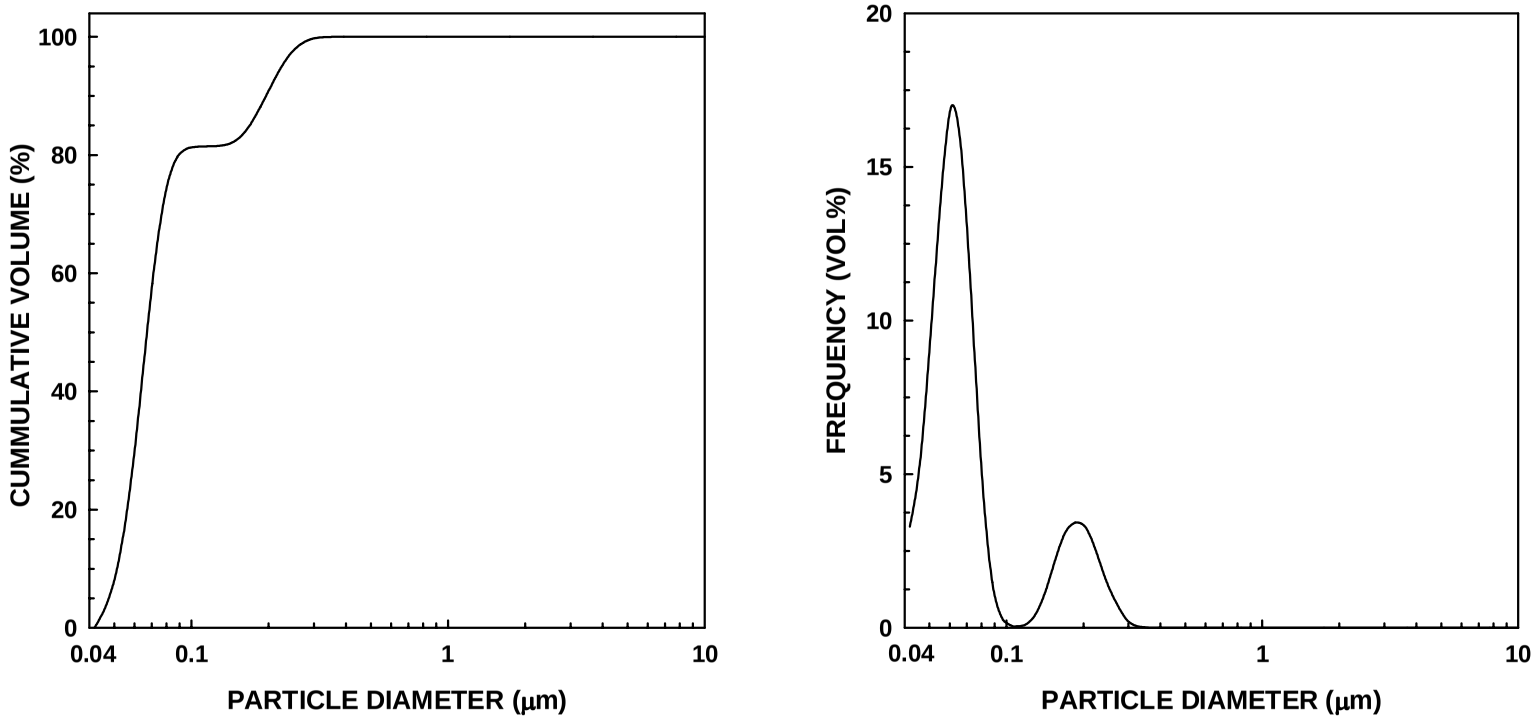

Figure G25 Particle size distribution plots for the 10 min-milled ZrPM-61-350-1-1300(48)-2-1300(8)-1 powder sample: cumulative frequency plot (left) and relative frequency plot (right).

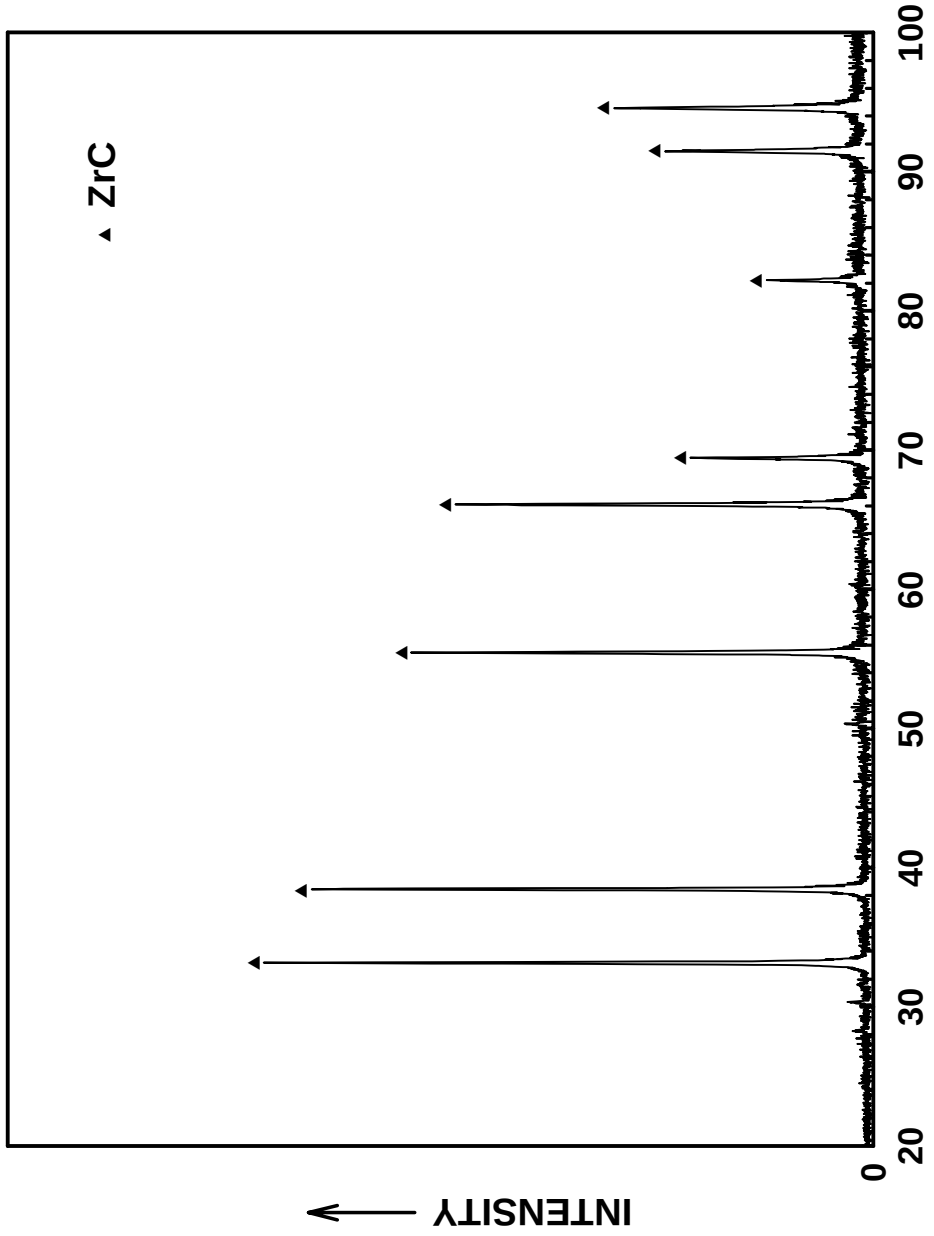

Figure G26 XRD graph of ZrPM-61-350-1-1300(48)-2-1300(8)-1 powder sample.

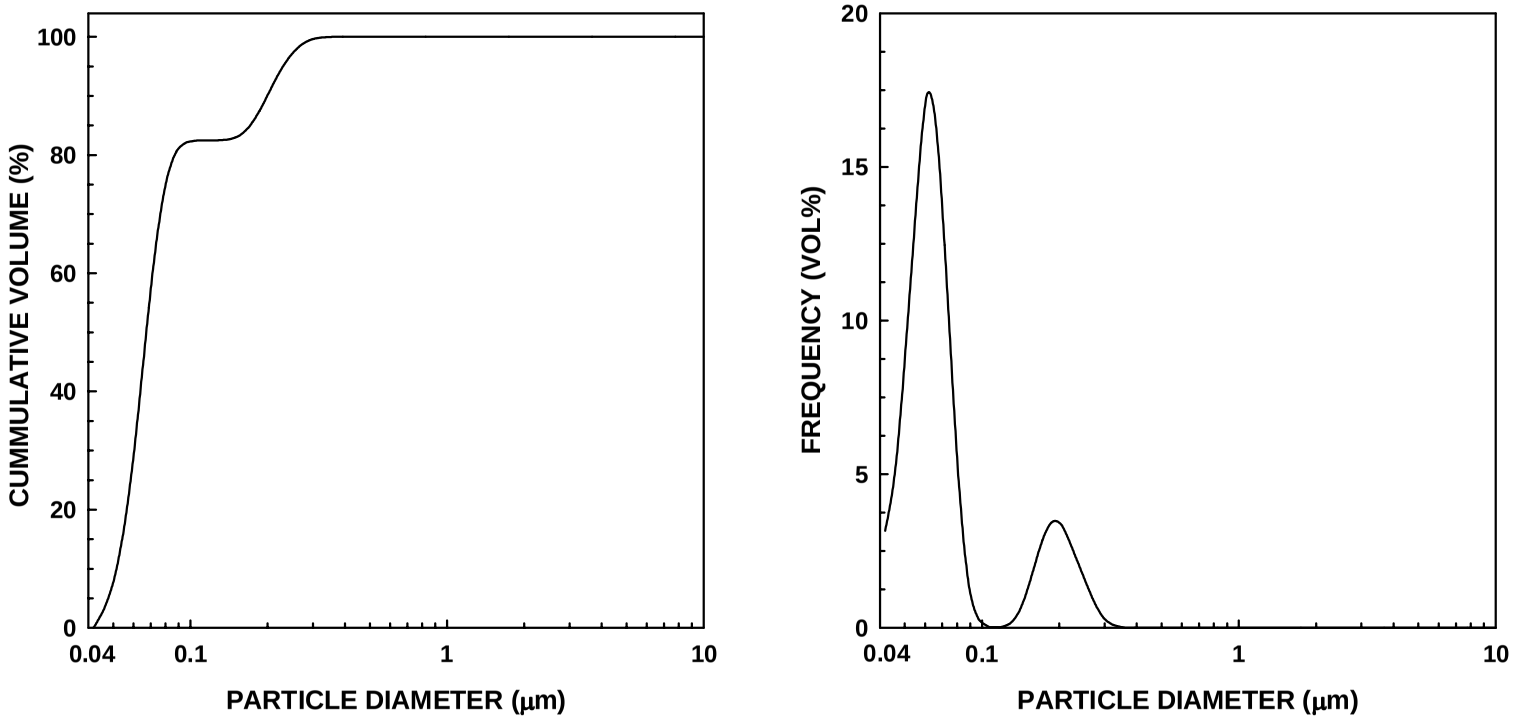

Figure G27 Particle size distribution plots for the 10 min-milled 61-350-1-1300(48)-2-1300(8)-1-1475-1 powder sample: cumulative frequency plot (left) and relative frequency plot (right).

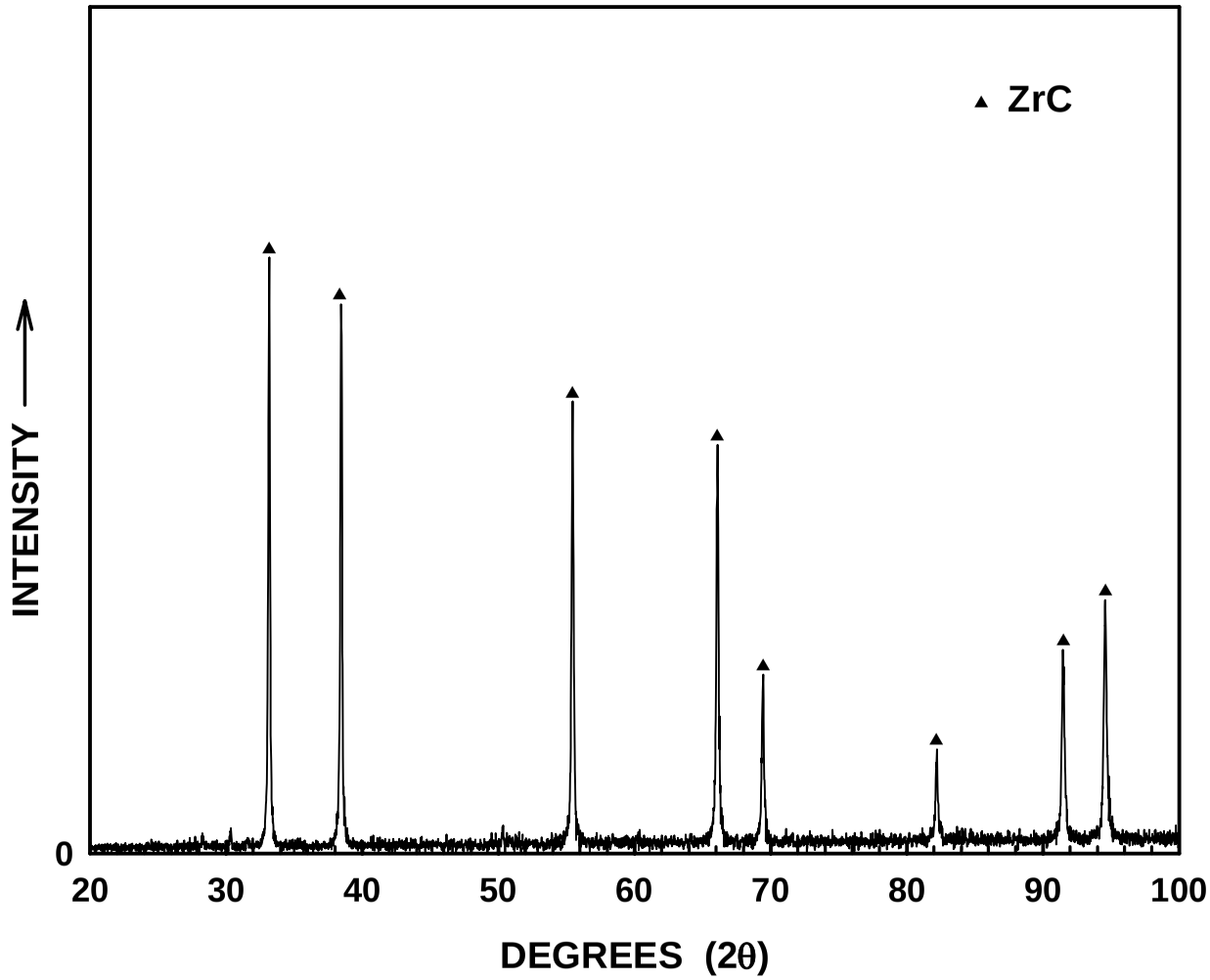

Figure G28 XRD graph of 61-350-1-1300(48)-2-1300(8)-1-1475-1 powder sample.

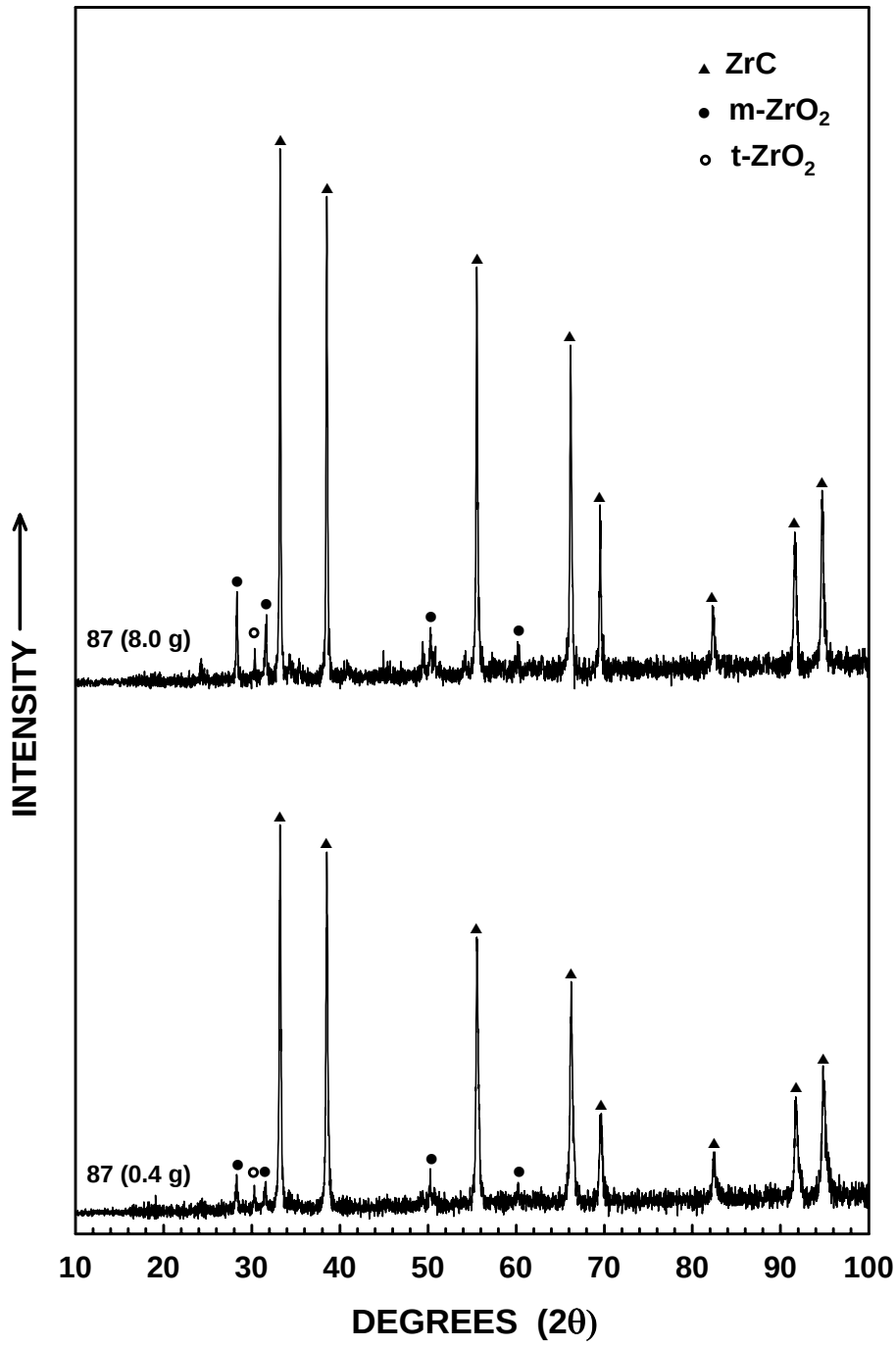

Figure G29 XRD patterns for ZrPM-87 samples with different batch sizes that were heat treated at 1425°C using a gas flow rate of 500 ml/min.

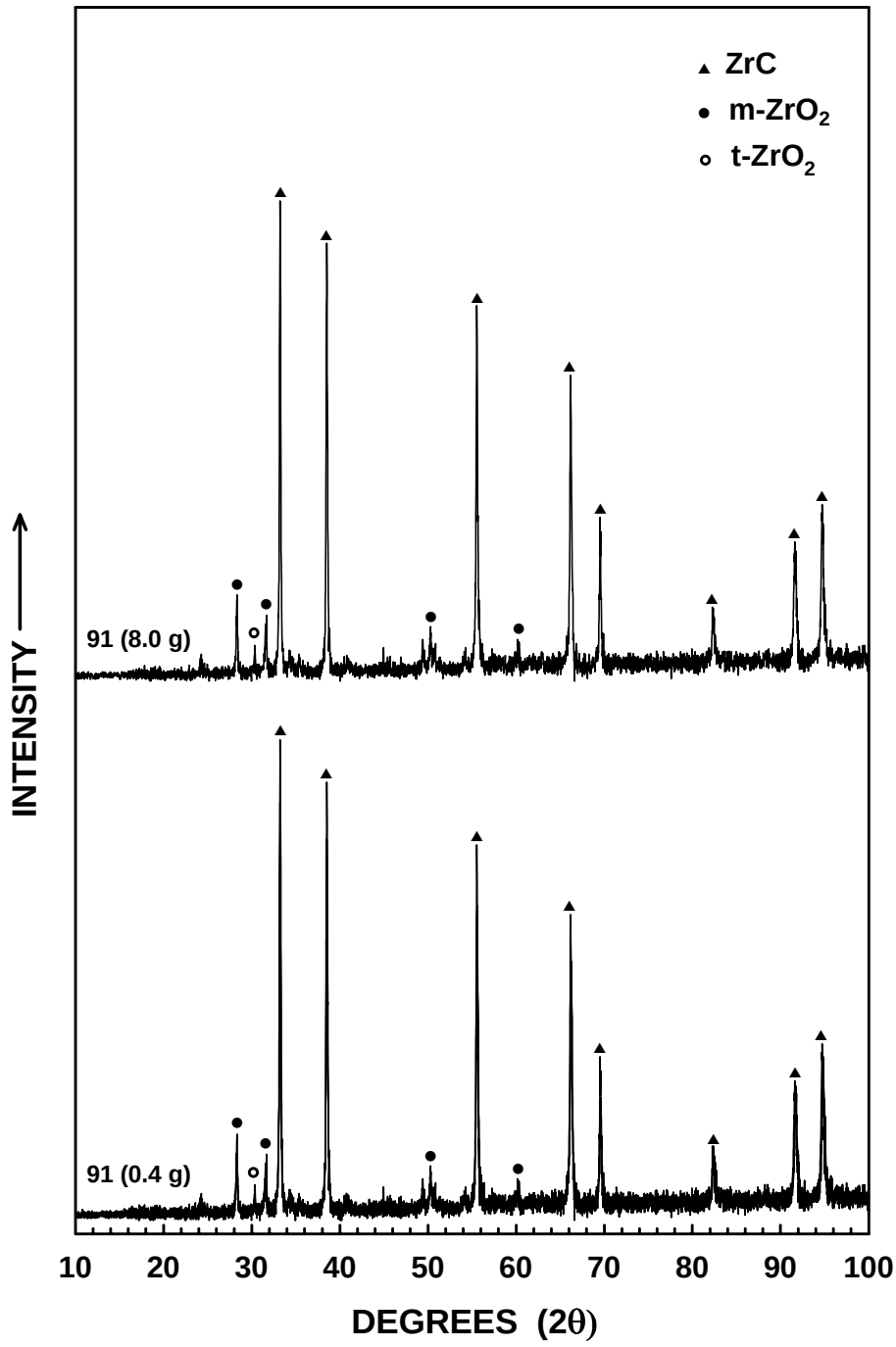

Figure G30 XRD patterns for ZrPM-91 samples with different batch sizes that were heat treated at 1425°C using a gas flow rate of 500 ml/min.

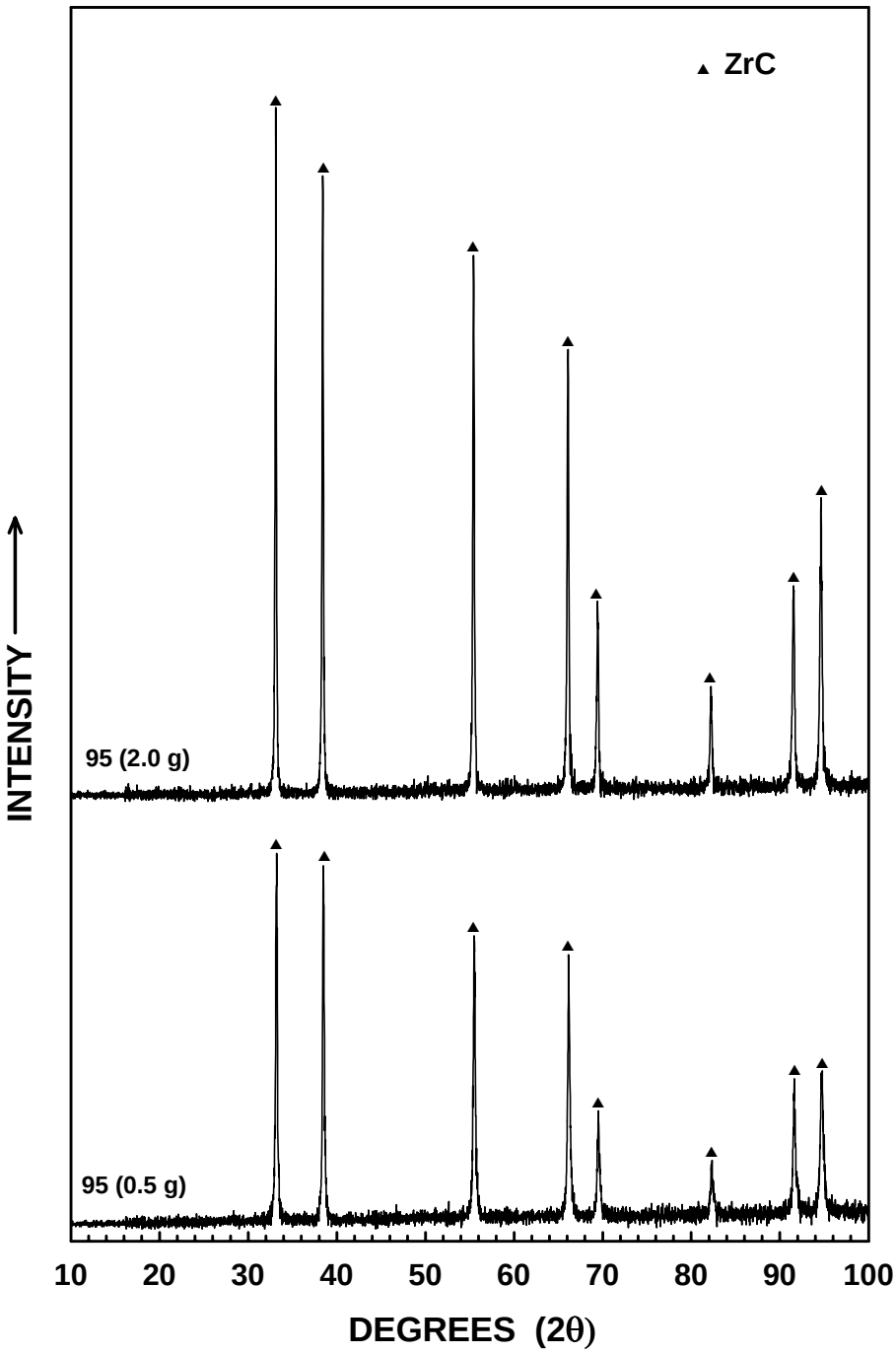

Figure G31 XRD patterns for ZrPM-95 samples with different batch sizes that were heat treated at 1425°C using a gas flow rate of 500 ml/min.

APPENDIX H

PROCEDURE TO OBTAIN THE AMOUNTS OF VARIOUS PHASES FROM INTEGRATED INTENSITIES OF PEAKS

The amounts of each crystalline phase present in the sample (i.e., t-ZrO_2, m-ZrO_2, and/or ZrC) were roughly determined from integrated intensities of the highest intensity peaks in the XRD pattern. The highest intensity peak for each of the phases was from the 111 plane. To measure the integrated intensity of the peak, a 2θ-angle range was chosen by selecting two 2θ angles (one on each side of the peaks) where the peak started to flatten out and merge with the baseline. This is shown in Figure G1. A line was drawn (using the Philips PC-APD instrument software, version 3.6, Philips Analytical, Netherlands) through the baseline such that the integrated intensity of the background "noise" was zero. The integrated intensity of the peak was then calculated using the instrument software. This procedure was repeated for all phases present in the sample. The amount of a particular phase was then calculated by taking the ratio of the integrated intensity of its peak to the sum of integrated intensities of the corresponding peaks for all of the phases present.

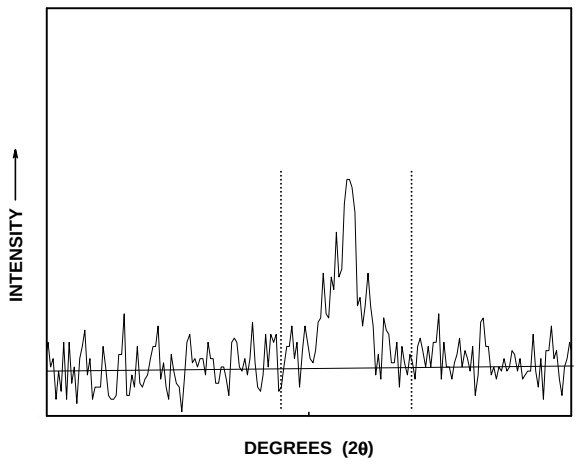

Figure G1 XRD pattern to illustrate measurement of integrated intensity.

LIST OF REFERENCES

1. H. O. PIERSON, in "Handbook of Refractory Carbides and Nitrides : Properties, Characteristics, Processing, and Applications" (Noyes Publication, New Jersey, 1996.)

2. E. K. STORMS, in "The Refractory Carbides" (Academic Press, New York, 1971.)

3. P. SCHWARZKOFF, R. KIEFFER, W. LESZYNSKI, and F. BENESOVSKY, in "Refractory Hard Metals : Borides, Carbides, Nitrides, and Silicides" (The Macmillan Company, New York, 1953.)

4. XIAO-MING HE, and L. SHU, HAI-BO LI, and D. WENG, J. Mater. Res., 14(2) (1999) 615. High corrosion resistant ZrC films synthesized by ion-beam-assisted deposition.

5. G. H. REYNOLDS, J. C. JANVIER, J. L. KAAE, and J. P. MORLEVAT, J. Nuc. Mat., 62 (1976) 9. Irradiation behavior of experimental fuel particles containing chemically vapor deposited zirconium carbide coatings.

6. J. R. SHEATS, W. A. MACKIE, S. ANZ, and T. XIE, SPIE 3148 (1997) 219. Polymer electroluminescent devices with zirconium carbide cathodes.

7. F. M. CHARBONNIER, W. A. MACKIE, R. L. HARTMAN, and TIANBAO XIE, J. Vac. Sci. Technol. B, 19 (2001) 1064. Robust high current field emitter tips and arrays for vacuum microelectronics devices.

8. B. V. COCKERAM, D. P. MEASURES, and A. J. MUELLER, Thin Solids Films 355-356 (1999) 17. The development and testing of emissivity enhancement coatings for thermophotovoltaic (TPV) radiator applications.

9. B. V. COCKERAM, and J. L. HOLLENBECK, Surface and Coatings Technol., 157 (2002) 274. The spectral emittance and long-term thermal stability of coatings for thermophotovoltaic (TPV) radiator applications.

10. K. MINATO, T. OGAWA, and K. SAWA, A. ISHIKAWA, T. TOMITA, S. IIDA, and H. SEKINO, Nuclear Technol., 130 (2000) 272. Irradiation experiment on ZrC-coated fuel particles for high-temperature gas-cooled reactors.

11. A. MAITRE, and P. LEFORT, Solid State Ionics, 104 (1997) 109. Solid-state reaction of zirconia with carbon.

12. T. TSUCHIDA, M. KAWAGUCHI, and K. KODAIRA, Solid State Ionics, 101-103 (1997) 149. Synthesis of ZrC and ZrN in air from mechanically activated Zr-C powder mixtures.

13. S. K. SARKAR, A. D. MILLER, and J. I. MUELLER, J. Am. Ceram. Soc., 55(1) (1972) 628. Solubility of oxygen in ZrC.

14. Y. KUROKAWA, H. OTA, T. SATO, J. Mater. Sci. Letters, 13 (1994) 516. Preparation of carbide fibers by thermal decomposition of cellulose-metal (Ti, Zr) alkoxide gel fibers.

15. Y. KUROKAWA, S. KOBAYASHI, M. SUZUKI, M. SHIMAZAKI, and M. TAKAHASHI, J. Mater. Res., 13(3) (1998) 760. Preparation of refractory carbide fibers by thermal decomposition of transition metal (Ti, Zr, Hf, Nb, Ta) alkoxide-cellulose precursor gel fibers.

16. I. HASEGAWA, Y. FUKUDA, and M. KAJIWARA, Ceram. International, 25 (1999) 523. Inorganic-organic hybrid route to synthesis of ZrC and Si-Zr-C fibers.

17. H. PREISS, E. SCHIERHORN, and K. W. BRZEZINKA, J. Mater. Sci., 33 (1998) 4697. Synthesis of polymeric titanium and zirconium precursors and preparation of carbide fibers and films.

18. E. L. SHAM, E. M. FARFAN-TORRES, S. BRUQUE-GAMEZ, and J. J. RODRIGUEZ-JIMENEZ, Solid State Ionics, 63-65 (1993) 45. Synthesis of ZrC/ZrO_2 by pyrolysis of modified zirconium alkoxide precursors.

19. A. JAIN, M. D. SACKS, and CHANG-AN WANG, Cer. Trans. 154 (2003) 37. Preparation of nanocrystalline zirconium carbide powders by carbothermal reduction.

20. A. JAIN, M. D. SACKS, CHANG-AN WANG, M. MIDDLEMAS, and Z. CHENG, Ceram. Eng. Sci. Proc., 24 (3) (2003) 41. Processing of nanocrystalline zirconium carbide powders.

21. Z. HU, M. D. SACKS, G. A. STAAB, CHANG-AN WANG, and A. JAIN, Ceram. Eng. Sci. Proc., 23(4) (2002) 711. Solution-based processing of nanocrystalline ZrC.

22. M. D. SACKS, CHANG-AN WANG, Z. YANG, and A. JAIN, J. Mater. Sci. (submitted). Carbothermal reduction synthesis of nanocrystalline zirconium carbide and hafnium carbide powders using solution-derived precursors.

23. L. E. TOTH, in "Transition Metal Carbides and Nitrides" (Academic Press, New York, 1967.)

24. W. A. MACKIE and C.H. HINRICHS, J. Cryst. Growth 87 (1988) 101. Preparation of zirconium carbide (ZrC_x) single crystals by an arc melting floating zone technique.

25. T. OGAWA, K. FUKUDA, S. KASHIMURA, T. TOBITA, F. KOBAYASHI, S. KADO, H.MIYANISHI, I. TAKAHASHI, and T. KIKUCHI, J. Am. Ceram. Soc., 75, 2985 (1992). Performance of ZrC-coated particle fuel in irradiation and postirradiation heating tests.

26. T. OGAWA and K. IKAWA, High Temp. Sci., 22, 179 (1986). Reactions of Pd with SiC and ZrC.

27. T. OGAWA and K. FUKUDA, "ZrC Coated Particle Fuel Development," Proc. 4th Int. Symp. Advanced Nuclear Energy Research, Mito, Japan, Feb. 5-7, 1992, JAERI-M 92-207, p. 554, Japan Atomic Energy Research Institute (Dec. 1992)

28. T. OGAWA, K. IKAWA, K. FUKUDA, S. KASHIMURA, and K. IWAMOTO, Nuclear Fuel Performance, p. 163, British Nuclear Energy Society, London (1985) Research and development of ZrC-coated UO_2 particle fuel at Japan Atomic Energy Research Institute.

29. www.kyoceraadvancedceramics.com

30. O. RUFF and R. WALLSTEIN, Z. Anorg. Allg. Chem. 128, (1923) 96; German Patent 286,054 (1914)

31. E. FRIEDERICH and L. SITTIG, Z. Anorg. Allg. Chem. 144, (1925) 169.

32. J. DONG, W. SHEN, X. LIU, X. HU, B. ZHANG, F. KANG, J. GU, D. LI, and N. CHEN, Mater. Res. Bull., 36 (2001) 933-938. A new method synthesizing the encapsulated ZrC with graphitic layers.

33. Y. ANDO and R. UYEDA, J. Crys. Growth, 52 (1981) 178-181. Preparation of ultrafine particles of refractory metal carbides by gas-evaporation method.

34. J. T. NORTON and R. K. LEWIS, Advanced Metals Research Corp., N63-18389 (1963).

35. A. A. BORISOV, L. D. LUCA, and A. MERZHANOV, in "Self-Propagating High-Temperature Synthesis of Materials". (Taylor and Francis, New York, 2002.)

36. C. LI, X. YANG, Z. ZHAO, and Y. QIAN, Chem. Lett. (2002) 1088-1089. A co-reduction-carburization route to synthesize nanocrystalline ZrC.

37. G. SHEN, D. CHEN, Y. LIU, K. TANG, and Y. QIAN, J. Crys. Growth, 262 (2004) 277-280. Synthesis of ZrC hollow nanospheres at low temperature.

38. Y-H. CHANG, C-W. CHIU, Y-C. CHEN, C-C. WU, C-P. TSAI, J-L. WANG, and H-T. CHIU, J. Mater. Chem., 12 (2002) 2189-2191. Synthesis of nano-sized cubic phase early transition metal carbides from metal chlorides and n-butyllithium.

39. H. KOBYASHI, K. SHIMOSAKA, M. SAITOH, and T. MITAMURA, J. Am. Ceram. Soc., 76 [9] (1993) 2389-92. Low-temperature synthesis of ZrC powder by cyclic reaction of Mg in ZrO_2-Mg-CH_4.

40. S. MOTOJIMA, H. ASANO, and H. IWANAGA, J. Eur. Ceram. Soc., 16 (1996) 989-993. Preparation of micro-coiled ZrC fibers by vapour phase metallizing of micro-coiled carbon fibers.

41. N. I. BAKLANOVA, V. N. KULYUKIN, M. A. KORCHAGIN, and N. Z. LYAKHOV, J. Mat. Syn. Process., 6 (1) (1998) 15-20. Formation of carbide coatings on nicalon fiber by gas-phase transport reactions.

42. G. H. REYNOLDS, J. Nucl. Mater., 50 (1974) 215-216. Chemical vapor deposition of ZrC on pyrocarbon-coated fuel particles.

43. P. WAGNER, L. A. WAHMAN, R. W. WHITE, C. M. HOLLABAUGH, and R. D. REISWIG, J. Nucl. Mater., 62 (1976) 221-228. Factors influencing the chemical vapor depostion of ZrC.

44. C. M. HOLLABAUGH, L. A. WAHMAN, R. D. REISWIG, and R. W. WHITE, Nucl. Tech., 35 (1977) 527-535. Chemical vapor deposition of ZrC made by reactions of $ZrCl_4$ with CH_4 and with C_3H_6.

45. K. HANKO, G. VASS, and L. SZEPES, J. Organometallic Chem., 492 (1995) 235-239. Arene-transition metal complexes as precursors of hard coatings prepared by the chemical vapour deposition technique.

46. M. D. HEALY, D. C. SMITH, R. R. RUBIANO, R. W. SPRINGER, and J. E. PARMETER, The organometallic chemical vapor deposition of transition metal carbide: The use of homoleptic alkyls.

47. A. M. NARTOWSKI, I. P. PARKIN, M. MACKENZIE, A. J. CRAVEN, and I. MACLEOD, J. Mater. Chem., 9 (1999) 1275-1281. Solid state metathesis routes to transition metal carbides.

48. S. I. ALYAMOVSKII, Y. G. ZAINULIN, G. P. SCHVEIKIN, and P. V. GELD, Rus. J. Inorg. Chem., 16 [1] (1971) 3- 6. Concentration range corresponding to the stability of the cubic (NaCl type) zirconium oxide carbide and the degree of filling of its unit cell.

49. P. BARNIER, C. BRODHAD, and F. THEVENOT, J. Mater. Sci., 21 (1986) 2547. Hot-pressing kinetics of zirconium carbide.

50. A. OUENSANGA, A. PIALOUX, and M. DODE, Rev. Int. Hautes Temp. Refract., 11 (1974) 289.

51. K. CONSTANT, R. KIEFFER, and P. ETTMAYER, Monatshefte fur Chemie, 106 (1975) 823. About the pseudoternary system ZrO-ZrN-XrC.

52. L. B. NEZHEVENKO, I. I. SPIVAK, P. V. GERASIMOV, B. D. GUREVICH, and V. N. RYSTSOV, Poroshkovaya Metallurgiya, 212(8) (1980) 23. Sintering of zirconium and niobium carbides with carbon additions.

53. V. P. BULYCHEV, R. A. ANDRIEVSKII, and L. B. NEZHEVENKO, Poroshkovaya Mettallurgiya, 172(4) (1977) 38. Theory and technology of sintering, thermal, and chemicothermal treatment processes.

54. EUNGI MIN-HAGA, WILLIAM D. SCOTT, J. Mater. Sci., 23 (1988) 2865. Sintering and mechanical properties of ZrC-ZrO_2 composites.

55. A. G. LANIN, E. V. MARCHEV, and S. A. PRITCHIN, Ceramics International, 17 (1991) 301. Non-isothermal sintering parameters and their influence on the structure and properties of zirconium carbide.

56. D. C. BRADLEY, R. C. MEHROTRA, and D. P. GAUR, in "Metal Alkoxides", p 209-217. (Academic Press, New York, 1978.)

57. R. L. DAVID, "Handbook of Chemistry and Physics", 84th ed. (2003-04), CRC Press.

58. S. OHE, http://www.s-ohe.com/Ethanol_cal.html

59. http://www.s-ohe.com/vp_data.html

60. M. D. SACKS, private communication.

61. A. C. PIERRE, in "Introduction to Sol-Gel Processing", p 205-247. (Kluwer Academic Publishers, Boston, 1998.)

62. www.spexcsp.com

63. Z. CHENG, Master Thesis.

64. S. J. GREGG and K. S. W. SING, "Adsorption, Surface Area and Porosity." (Academic Press, London, 1982.)

65. N. Dragoe, J. Appl. Crystallography, 34[4] (2001) , p 235. PowderV2. A suite of applications for powder x-ray diffraction calculations.

66. B.D. CULLITY, in “Elements of X-ray Diffraction” (Addison-Wesley Publishing Co., Reading, MA, 1967).

67. Delsa 440X User Manual, Beckman Coulter.

68. LS 13320 User Manual, Beckman Coulter.

69. T. KOIDE, T. SHIDARA, H. FUKUTANI, A. FUJIMORI, S. OTANI, and Y. ISHIZAWA, Jpn. J. Appl. Phys., 32 (1993) Pt. 1, No. 3A, 1130-1134. Optical constants of $TiC_{0.95}$, $VC_{0.86}$ and $NbC_{0.93}$ from 0.8 to 80 eV.

70. W. J. CHOYKE, Z. C. FENG, and J. A. POWELL, J. Appl. Phys. 64 [6] (1988) 3163. Low-temperature photoluminescence studies of chemical-vaopr-deposition-grown 3C-SiC on Si.

71. L. PATRICK and W. J. CHOYKE, Physical Review, 186 [3] (1969) 775. Optical absorption in n-type cubic SiC.

72. H. T. M. PHAM, T. AKKAYA, C. BOER, C. C. G. VISSER and P. M. SARRO, Proceedings of SeSens 2002-Workshop on Semiconductor Sensors, (2002). Electrical and optical properties of PECVD SiC thin film for surface micromachined devices.

73. M. BOULOUZ, F. TCHELIEBOU, and A. BOYER, J. European Ceram. Soc., 17 (1997), 1741-1748. Electrical and optical properties of magnetron-sputtered Y_2O_3 stabilized ZrO_2 thin films.

74. R. THIELSCH, A. GATTO, J. HEBER, and N. KAISER, Thin Solid Films, 410 (2002) 86-93. A comparative study of the UV optical and structural properties of SiO_2, Al_2O_3, and HfO_2 single layers deposited by reactive evaporation, ion-assisted deposition, and plasma ion-assisted deposition.

75. Z. W. ZHAO, B. K. TAY, S. P. LAU, and G. Q. YU, J. Crystal Growth, 268 (2004) 543-546. Optical properties of titania films prepared by off-plane filtered cathodic vacuum arc.

76. Z. W. ZHAO, B. K. TAY, S. P. LAU, and C. Y. XIAO, J. Vac. Sci. Technol., A 21(4) (2003) 906-910. Microstructural and optical properties of aluminum oxide thin films prepared by off-plane filtered cathodic vacuum arc system.

77. D. PILLOUD, A. S. DEHLINGER, J. F. PIERSON, A. ROMAN, and L. PICHON, Surface Coatings Technol., 174-175 (2003) 338-344. Reactively sputtered zirconium nitride coatings: structural, mechanical, optical, and electrical characteristics.

78. J. S. REED, in “Principles of Ceramics Processing”, p 172-200. (A Wiley-Interscience Publication, New York, 1995.)

79. H. LEE and R. F. SPEYER, J. Am. Ceram. Soc., 86 [9] (2003) 1468-73. Pressureless sintering of boron carbide.

80. D. B. FISCHBACH and M. E. RORABAUGH, High Temp.-High Pres., 9 (1977) 199-205. Glassy carbon graphitization: density change.

81. T-H. KO, W-S. KUO, and Y-H CHANG, J. App. Polymer Sci., 81 (2001) 1084-1089. Microstructural changes of phenolic resin during pyrolysis.

82. K. KAWAMURA, S. OZAWA, and H. ENDO, Carbon 41 (2003) 179-198. Volume expansion of glass-like carbon upon high temperature heat treatment.

83. T. FURUTA, Y. SANADA, and H. HONDA, Carbon 7 (1969) 512-513. Pore structure of phenol-formaldehyde resin carbons.

84. M. ENDO, Y. A. KIM, T. HAYASHI, K. NISHIMURA, T. MATUSITA, K. MIYASHITA, and M. S. DRESSELHAUS, Carbon 39 (2001) 1287-1297. Vapor-grown carbon fibers (VGCFs) Basic properties and their battery applications.

85. G. G. TIBBETTS, G. L. DOLL, D. W. GORKIEWICZ, J. J. MOLESKI, T. A. PERRY, C. J. DASCH, and M. J. BALOGH, Carbon 31(7) (1993) 1039-1047. Physical properties of vapor-grown carbon fibers.

86. Z. YANG and M.D. SACKS, private communication.

87. JCPDS card 17-0923.

88. JCPDS card 37-1484.

89. G. SKANDAN, H. HAHN, M. RODDY, and W. R. CANNON, J. Am. Ceram. Soc., 77[7] (1994) 1706-1710. Ultrafine-grained dense monoclinic and tetragonal zirconia.

90. J. HOJO, K. MIYACHI, Y. OKABE, and A. KATO, J. Am. Ceram. Soc., 66[7] (1983) C114-115. Effect of Chemical Composition on the Sinterability of Ultrafine SiC Powders.

91. J. S. REED, in “Principles of Ceramics Processing”, p 583-624. (A Wiley-Interscience Publication, New York, 1995.)

92. S. PROCHAZKA and R. M. SCANLAN, J. Am. Ceram. Soc., 58[1-2] (1975) p 72. Effect of boron and carbon on sintering of SiC.

93. W. RIJSWIJK and D. J. SHANEFIELD, J. Am. Ceram. Soc., 73[1] (1990) p 148-149. Effects of carbon as a sintering aid in silicon carbide.

94. C. R. HOUSKA, J. Phys. Chem. Solids, 25 (1964) p 359-366. Thermal Expansion and Atomic Vibration Amplitudes for TiC, TiN, ZrC, ZrN, and Pure Tungsten.